Proceedings of the

Helmholtz International School

Physics of Heavy Quarks and Hadrons

(HQ2013)

July 15-28, 2013
BLTP, JINR, Dubna, Russia

Impressum

Proceedings of the Helmholtz International School
Physics of Heavy Quarks and Hadrons (HQ2013)

July 15-28, 2013, BLTP, JINR, Dubna, Russia

Preface

The Helmholtz International Summer School: Physics of Heavy Quarks and Hadrons (HQ-2013), was held at the Bogoliubov Laboratory of Theoretical Physics (BLTP) of the Joint Institute for Nuclear Research (JINR), Dubna, Russia, in the period July 15-28, 2013. It was co-organized by Ahmed Ali (DESY, Hamburg), Mikhail Ivanov (BLTP, JINR, Dubna) and Klaus Peters (GSI, Darmstadt), and was attended by 70 participants (faculty + students), not counting the JINR physicists who attended some lectures as non-registered participants. The school HQ-2013 continued the HISS-series, with the earlier schools on the same topic held at JINR, Dubna, in 2002, 2005, and 2008.

The scientific program of HQ-2013 consisted of five regular (one-hour long) lectures in the morning and afternoon sessions, with two contributed talks given by younger participants (students and post-docs), each half-hour long, in the late afternoons. Altogether, we had fifty lectures by the faculty and 14 contributed talks. Being also a part of the series called Dubna International Advanced School on Theoretical Physics (DIAS-Th), the main emphasis of the HQ-2013 school was on the theoretical techniques and calculational frameworks, such as the heavy quark effective theories, soft collinear effective theories, perturbative QCD, Lattice QCD, QCD sum rules, and QCD-inspired quark models. The lectures ranged from pedagogical introductions to the state-of-the-art applications at the frontier of the heavy quark and hadron physics. The interaction between theory and experiment is particularly strong in our field. This aspect was also reflected in the HQ-2013 scientific program, as we heard the latest experimental results on the heavy quark and quarkonia physics from the four LHC collaborations (ALICE, ATLAS, CMS, and LHCb) and the Belle collaboration at the Japanese laboratory KEK. In addition, two lectures were devoted to review the experimental exotic quarkonia sector, which covered the existing experiments (CLEO, BaBar, Belle, CDF, D0 and the LHC experiments), and the planned experiment PANDA at the FAIR facility in Darmstadt, Germany, and Belle-II at the Super-B factory at KEK, which are expected to start taking data in several years from now. The scientific program also included a joint session on the experimental and theoretical aspects of the Higgs physics, which was conducted as part of the JINR Colloquium on particle physics. These talks were given by Fernando Barreiro (ATLAS collboration), Guenakh Mitselmacher (CMS) and Dmitri Kazakov (Theory, BLTP, JINR, Dubna).

HISS series of schools have played an important role in bringing together an international faculty and young physicists (Ph.D. and postdocs), mostly from Russia and Germany, to participate in two-week long intense scientific discussions, which followed dedicated lectures on selected topics covering the foundation and the frontiers of high energy physics and cosmology. These schools were held on a particular topic with a frequency of once in three years, though the present school had a gap of five years, with the previous school on heavy quarks and hadrons, held in 2008. In a fast developing field, where a number of experimental facilities started to operate, foremost the LHC, we had a wealth of new data and advances in theoretical calculations to match the experimental progress, presented at our school. The scientific program was necessarily dense and detailed and required some effort to digest. However, the two coffee breaks and a lunch interval provided an opportunity to follow up on some of the lectures in a more relaxed atmosphere. The HQ-2013 school was also used by several collaborating theoretical groups, whose members were participating, to discuss intensely their ongoing research projects, and this

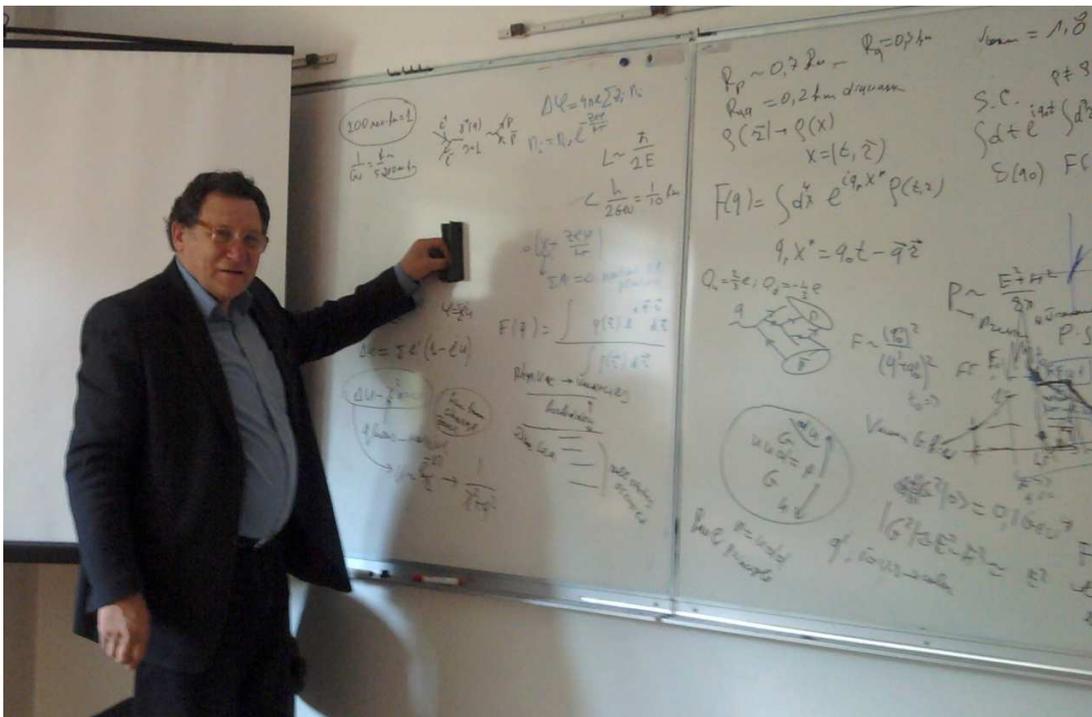is also an aspect of the HISS program we wish to emphasize.

Co-editors:
Ahmed Ali, Yury Bystritskiy, Mikhail Ivanov

Eduard Alekseevich Kuraev

(*Krasnodar: 17 October, 1940   †Dubna: 4 March, 2014)

In Memoriam:
Eduard Alekseevich Kuraev

Eduard Alekseevich Kuraev sadly passed away on March 4, 2014, in Dubna, Russia. It is an invaluable loss for the high energy physics community, in particular for his colleagues, and for us, for whom he was a mentor, collaborator and friend.

Eduard was born on 17 October 1940 in a village Tblisskaya in the Knarsnodarsk region of the former Soviet Union. He graduated from the University of Kharkov in 1962, under the supervision of the well-known physicists Alexander Il'ch Akhiezer and Dmitrij Vasil'evich Volkov. Thereafter he started his career as a theoretical physicist at the Kharkov Institute of Physics and Technology (KIPT), now in Ukraine. He was from the start very much interested in QED; in particular, he helped Alexander Il'ch in the second addition of the well-known book on Quantum Electrodynamics by Akhiezer and Berestetsky in that he wrote a chapter about double-logarithmic asymptotics in QED. At Kharkov, he wrote several papers, among others on the photon-photon scattering in QED. Attracted by the excellent theoretical physics group at the Leningrad (now St. Petersburg) Institute of Nuclear Physics (INP) in Gatchina, Eduard was a frequent visitor to INP, and started his collaboration with Lev Lipatov, which was also the beginning of a life-long friendship between the two of them. In 1974 Eduard moved to the Budker Institute of Nuclear Physics in Novosibirsk, earning his higher doctoral degree (D. Sc.) in the Physical-Mathematical Sciences in 1986 from Novosibirsk. In 1992, Eduard joined the Bogoliubov Laboratory for Theoretical Physics, JINR, Dubna, as a leading scientific researcher, where he worked until his death.

Eduard Kuraev was a prolific writer! His earliest published papers date back to the mid sixties. A representative paper from this earlier epoch is "Interference between coulomb and strong interactions at high energies ", JETP 60 (1971) 1211, written in collaboration with Lev Lipatov and collaborators (V.G. Gorshkov and M.M. Nesterov). His last paper was on the high energy quark (electron)-proton peripheral collisions, written with Azad Inshalla Ahmadov, which appeared at the end of January 2014 (arxiv: 1401.7746). In between these two, he co-authored some 350 scientific papers, according to the high energy physics database InSPIRE. They were mostly about the applications of QED and QCD in high energy reactions, in particular, electron-positron annihilation, deep inelastic lepton-nucleon scatterings, proton-proton (antiproton) collisions, Drell-Yan production, and parton evolution processes involving both high-Q^2 and low x domains, using techniques based on the renormalization groups. His work on radiative corrections in e^+e^- annihilation, often carried out in collaboration with Victor Fadin, provides a standard theoretical framework used in the experimental analysis of data, and is still very much *en vogue*. However, he will be best remembered for his renowned papers on multi-Reggeon processes in Non-abelian gauge theories and on the Pomeranchuk singularities. Written in collaboration with Lev Lipatov and Victor Fadin, during 1975 - 1977, they have climbed steadily in their popularity and impact, and are now considered as classic papers in gauge theories. They are invaluable in a quantitative understanding of deep inelastic phenomena in the small Bjoken-x region as well as in elucidating the behaviour of strong interactions in the Regge limit. We list some of them below to celebrate these scientific milestone.

- The Pomeranchuk Singularity in Nonabelian Gauge Theories, E.A. Kuraev, L.N. Lipatov, and Victor S. Fadin, Sov.Phys.JETP 45 (1977) 199, Zh.Eksp.Teor.Fiz. 72 (1977) 377.

- Multi - Reggeon Processes in the Yang-Mills Theory, E.A. Kuraev, L.N. Lipatov, and Victor S. Fadin, Sov.Phys.JETP 44 (1976) 443-450, Zh.Eksp.Teor.Fiz. 71 (1976) 840, Erratum-ibid. 45 (1977) 199.

- On the Pomeranchuk Singularity in Asymptotically Free Theories, Victor S. Fadin, E.A. Kuraev, and L.N. lipatov, Phys. Lett. B60 (1975) 50.

The second of the above listed papers, together with a subsequent one by Ian Balitsky and Lev Lipatov [Sov. J. Nucl. Phys. 28 (1978) 822], are collectively called the BFKL papers. They initiated an entire field of high energy physics, associated with the BFKL pomeron and the BFKL parton evolution equation.

Eduard Kuraev had a penchant for solving calculationally difficult problems. This was, and has remained since then, a hallmark of a dedicated group of particle theorists in the former Soviet Union, which excelled in combining intuitive ideas with an extraordinary technical ability and astonishing energy for hard work, personified, among others, by Eduard. He had a passion for sharing his ideas, discoveries and results, and in teaching and educating young researchers. Often equipped with nothing more than a black board and chalks, and his encyclopedic knowledge of QED and QCD, he was ready to listen and discuss with anyone who came by and knocked at his office door. He took great pleasure in collaborating with other fellow physicists and students, without any prejudice or hierarchy, which is amply reflected in his list of publications. According to InSPIRE, he collaborated with well over a hundred fellow physicists - an unusually high number for a theorist.

At a personal level, Eduard was an extremely modest person, to the extent of self-denial, and an exceedingly caring one, who would share with others whatever he had. Oblivious of the administrative constraints to which most of the scientists are subjected, Eduard was completely absorbed in his science and other intellectual pursuits. Being oriented towards science, in particular physics and mathematics, but also very much interested in the literature, novels, poems, history and science fiction, he was an avid reader. Curious about new ideas and unexplained phenomena in nature, he was often a source of creative conjectures and brilliant explanations. With Eduard's death, we have lost an exceptional physicist and a great human being, who combined professional excellence with remarkable kindness and humility. He remained an enthusiastic supporter of the Dubna schools on theoretical physics, including the Helmholtz summer school on the physics of the heavy quarks and hadrons, held during July 15 -28, 2013, in which he lectured. These proceedings are dedicated to his cherished memory.

Contents

x

Higgs boson production and couplings with the ATLAS detector

Fernando Barreiro[1],

[1] Universidad Autónoma de Madrid, Madrid, Spain

I briefly review the status of Higgs boson production and couplings with the ATLAS detector at the LHC.

1 Introduction

The Higgs boson is the last missing piece in the Standard model. The Higgs boson is necessary to tame the singularities appearing in the amplitudes for elastic longitudinally polarized W_L and Z_L's as well as to avoid infinities in loops involving them. With the Higgs, the calculability of gauge theories is recovered, and for that it is necessary that the tree level Higgs boson couplings to fermions and gauge bosons take precise values, namely: a) $H \to WW, ZZ : gM_W, \frac{gM_Z}{cos\theta_W}$ and b) $H \to f\bar{f} : \frac{gM_f}{2M_W}$.

Without a Higgs boson the validity of the Standard Model would extend up to scales of the order of $1\ TeV$. With a light Higgs i.e. m_H in the range between $100 - 170\ GeV$, the Standard Model can make consistent predictions up to scales close to the Planck scale i.e. $10^{19}\ GeV$.
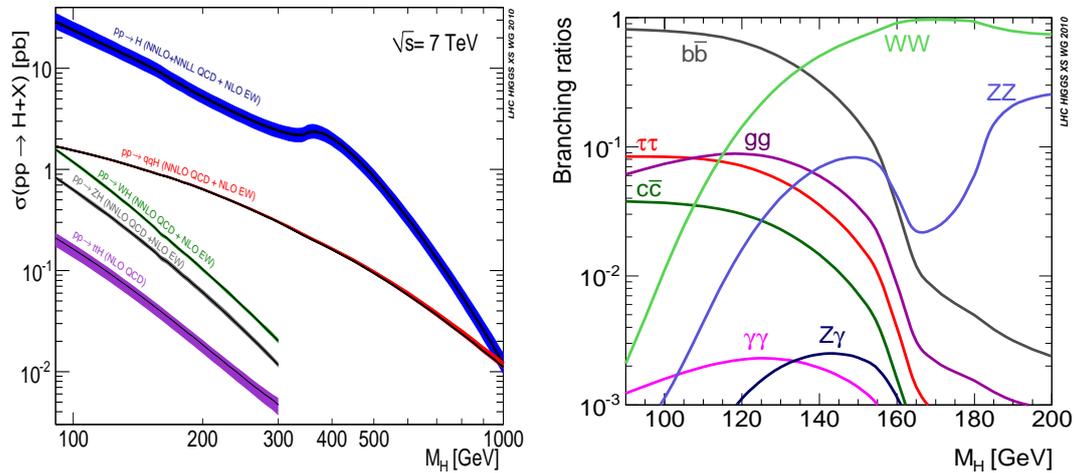
Figure 1: The cross sections for Higgs production (left) via $ggF - VBF - (W,Z)H - (t\bar{t})H$ from top to bottom, and the Higgs boson branching ratios (right) in the SM.

In $p - p$ collisions at $7\ TeV$, the production cross-sections for a Higgs boson with a mass in

the range 100 GeV to 1 TeV are shown on the left hand side of Fig. 1. Clearly, the dominant production process is gg fusion, suppressed by an order of magnitude is vector boson fusion (VBF) and Higgs strahlung (VH, V=W,Z). The production in association with $t\bar{t}$ (ttH) is marginal at present energies/luminosities. The branching ratios for Higgs boson decays into gauge bosons and fermion pairs are shown on the right hand side.

Thus, searching for the Higgs boson is essentially searching for a handful of events sometimes in the presence of huge backgrounds. It is therefore imperative to check that not only QCD multijet processes are measured with enough accuracy, but also those with smaller cross-sections, like boson pair and $t\bar{t}$ production, and to check that they agree with SM predictions, as illustrated in Fig. 2.
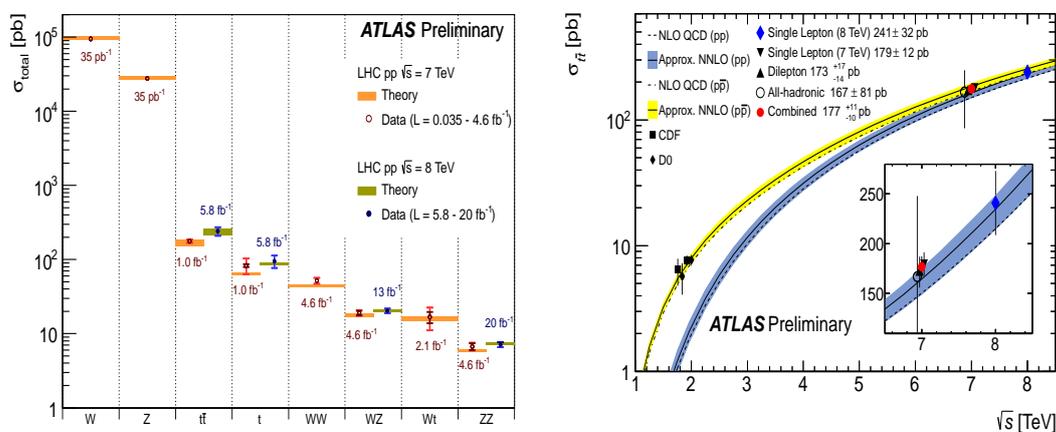
Figure 2: The cross sections for several SM processes (left) and for top production (right).

The search for Higgs has been made possible by the excellent performance of the ATLAS detector and most important the LHC machine which has delivered approximately 5 pb^{-1} at 7 TeV in 2011 and 20 pb^{-1} at 8 TeV in 2012, Fig. 3.

2 Production and couplings

It is now well over a year since the discovery of a Higgs-like particle, by the ATLAS and CMS Collaborations, was announced at CERN. At that time, July 2012, no conclusive evidence i.e. 5σ effect, had been observed in any given particular channel. The purpose of this talk is to review the progress made since then.

SM Higgs boson production processes as well as background production processes are modelled with detailed MC programmes including detector effects, as shown in Table 1, see [1] for more details.

2.1 The channel $H \rightarrow \gamma\gamma$

This channel is particularly sensitive to physics BSM since the decay proceeds via loops. Events are required to have *two isolated high p_T photons* with invariant mass in the range $100-160\,GeV$.
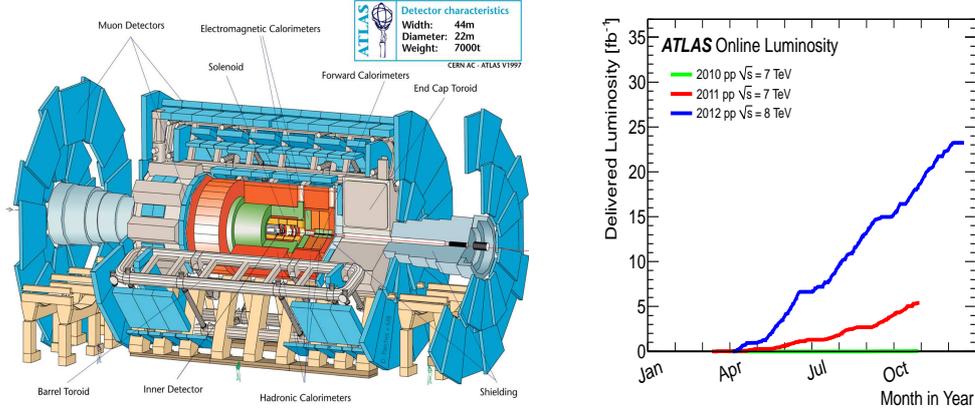
Figure 3: The ATLAS detector (left) and the delivered integrated luminosity (right).

Table 1: Event generators used to model the signal and the main background processes.

Process	Generator
ggF, VBF	POWHEG+PYTHIA
WH, ZH, $t\bar{t}H$	PYTHIA
$H \to ZZ \to 4l$ decay	PROPHECY4f
W+jets, Z/γ^*+jets	ALPGEN+HERWIG
	POWHEG+PYTHIA, SHERPA
$t\bar{t}$, tW, tb	MC@NLO+HERWIG
tqb	AcerMC+PYTHIA6
$q\bar{q} \to WW$	POWHEG+PYTHIA6
$gg \to WW$	gg2WW+HERWIG
$q\bar{q} \to ZZ^*$	POWHEG+PYTHIA
$gg \to ZZ^*$	gg2ZZ+HERWIG
WZ	MadGraph+PYTHIA6, HERWIG
$W\gamma$+jets	ALPGEN+HERWIG
$W\gamma^*$	MadGraph+PYTHIA6 for $m_{\gamma^*} < 7$ GeV
	POWHEG+PYTHIA for $m_{\gamma^*} > 7$ GeV
$q\bar{q}/gg \to \gamma\gamma$	SHERPA

The main background is continuum $\gamma\gamma$ production, with smaller contributions from $\gamma + jet$ and dijet production. The selected events are separated into 14 mutually exclusive categories in order to increase sensitivity to the overall Higgs signal as well as to specific VBF and VH production modes. This is done by demanding that the two isolated photons are accompanied by two forward jets, by leptons, E_T^{miss}, or by two low mass jets. These extra requirements are designed to enhance the sensitivity to a given production mechanism. The left hand side of Fig. 4 shows for instance how one can select VBF candidates with the help of a BDT algorithm. On the right hand side we show the photon pair invariant mass. A clear peak is observed at $m_H = 126.8 \pm 0.2(stat.) \pm 0.7(syst)$ GeV over a smooth background. The observed significance is 7.4σ with 4.3σ expected from the SM.
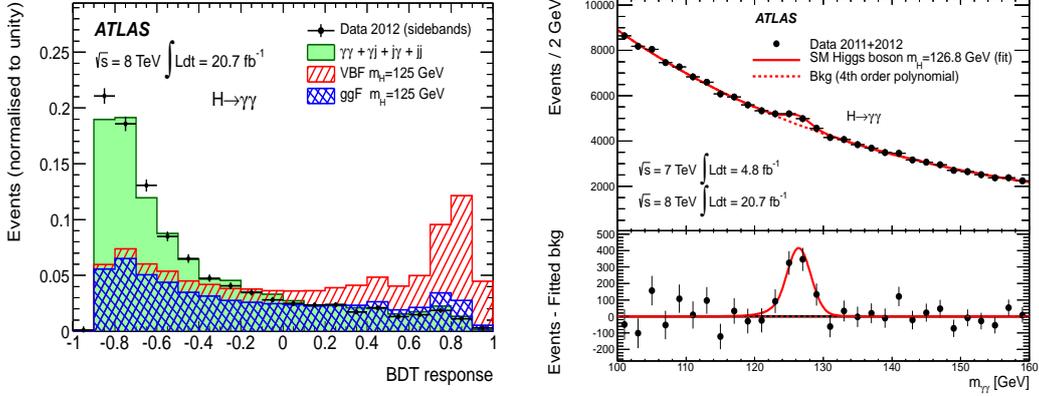
Figure 4: Selecting VBF with a BDT algorithm, left, and the diphoton invariant mass (right).

2.2   The channel $H \to 4l$

Despite the small branching ratio, this channel provides sensitivity to the Higgs coupling to Z bosons because of the large signal to background ratio. Events are required to have *two pairs of same flavour, opposite charge, high p_T isolated leptons*. The main backgrounds are ZZ^* continuum production, top pair and $Z + b\bar{b}$ production. The $4l$ invariant mass is shown on the left hand side of Fig. 5. From it one can extract $m_H = 124.3 \pm 0.6(stat.) \pm 0.5(syst.)$ GeV. The observed significance is 6.6σ with 4.4σ expected in the SM.
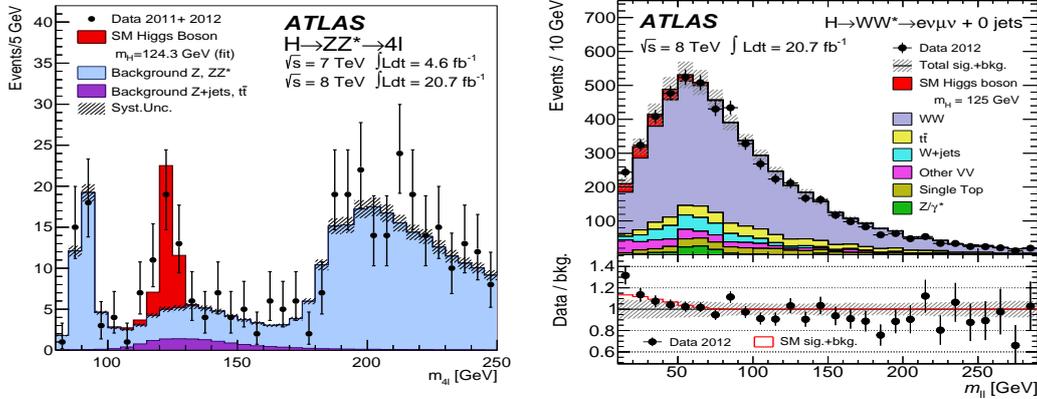
Figure 5: The distributions in m_{4l}, left, and m_{ll}, right, in the $H \to ZZ^* \to 4l$ and $H \to WW^* \to l\nu l\nu$ modes.

2.3   The channel $H \to WW^* \to l\nu l\nu$

This channel is interesting because it is sensitive to the Higgs boson coupling to W bosons. It has a large rate, but due to the production of neutrinos in the W decays, it is not possible to reconstruct the W pair invariant mass. The selection criteria require *two high p_T opposite*

charge isolated leptons plus E_T^{miss}. Dominant backgrounds are WW^* continuum production, top pair and Wt production and Drell-Yan. The selected events are classified into different categories depending on the associated jet multiplicity. The dilepton mass for $e\mu$ events with $N_{jet} = 0$ is shown on the right hand side of Fig. 5. A clear excess of events for masses below $\sim 50\,GeV$ is observed which can be attributed to $H \to WW \to e\nu\mu\nu$.

2.4 Higgs boson mass and production strengths

To derive a combined mass measurement one uses the profile likelihood method $\Lambda(m_H)$ with the individual strengths $\mu_{\gamma\gamma}$ and μ_{4l} as nuissance parameters. The combined mass is measured to be

$$m_H = 125.5 \pm 0.2\,(\text{stat})\,^{+0.5}_{-0.6}\,(\text{sys})\ GeV \tag{1}$$

In order to measure the production strength, μ, one uses the profile likelihood $\Lambda(\mu)$ method for the previously determined mass. The result are shown on the left hand side of Fig. 6. The overall signal production strength is:

$$\mu = 1.33 \pm 0.14\,(\text{stat}) \pm 0.15\,(\text{sys}) \tag{2}$$

To test the sensitivity to VBF production alone, the data are also fitted with $\mu_{\text{VBF}}/\mu_{\text{ggF}+ttH}$ as a free parameter, obtaining

$$\mu_{\text{VBF}}/\mu_{\text{ggF}+ttH} = 1.4^{+0.4}_{-0.3}\,(\text{stat})\,^{+0.6}_{-0.4}\,(\text{sys}) \tag{3}$$

from the combination of the three channels, see the right hand side of Fig. 6.
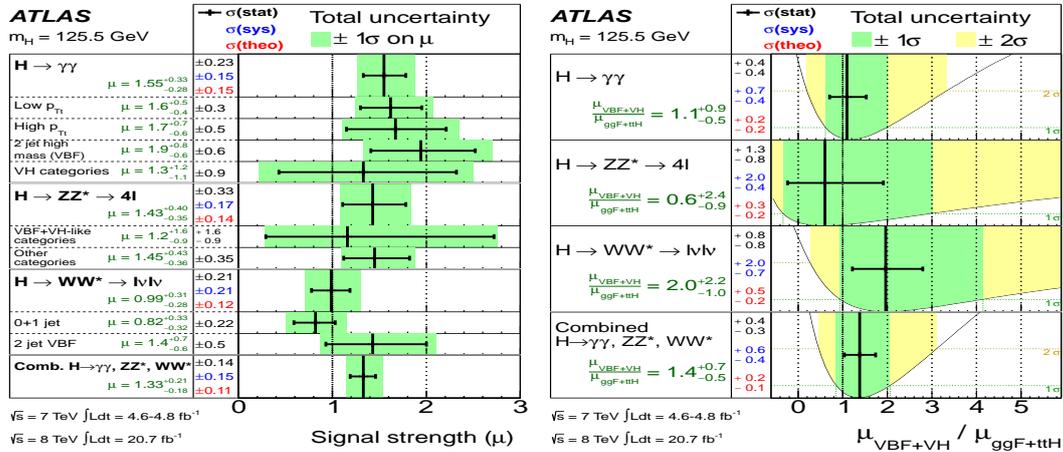
Figure 6: The fitted signal strengths for various channels.

2.5 Coupling measurements

The coupling scale factors κ_j are defined in such a way that the cross sections σ_j and the partial decay widths Γ_j associated with the SM particle j scale with κ_j^2 compared to the SM

prediction. It is assumed that the signals observed in the different channels come from a single Higgs resonance with narrow width.

Results are extracted from fits to the data using the profile likelihood ratio $\Lambda(\vec{\kappa})$, where the κ_j couplings are treated either as parameters of interest or as nuisance parameters, depending on the measurement.

The first benchmark considered here assumes one coupling scale factor for fermions, κ_F, and one for bosons, κ_V; in this scenario, the $H \to \gamma\gamma$ and $gg \to H$ loops and the total Higgs boson width depend only on κ_F and κ_V, with no contributions from physics beyond the Standard Model (BSM). The strongest constraint on κ_F comes indirectly from the $gg \to H$ production loop. The results are shown on the left hand side of fig. 7. The 68% CL intervals of κ_F and κ_V, obtained by profiling over the other parameter, are:

$$
\begin{aligned}
\kappa_F &\in& [0.76, 1.18] &\quad (4) \\
\kappa_V &\in& [1.05, 1.22] &\quad (5)
\end{aligned}
$$

with similar contributions from the statistical and systematic uncertainties.

Many BSM physics scenarios predict the existence of new heavy particles, which can contribute to loop-induced processes such as $gg \to H$ production and $H \to \gamma\gamma$ decay. In the approach used here, it is assumed that the new particles do not contribute to the Higgs boson width and that the couplings of the known particles to the Higgs boson have SM strength (*i.e.* $\kappa_i=1$). Effective scale factors κ_g and κ_γ are introduced to parameterise the $gg \to H$ and $H \to \gamma\gamma$ loops. The results of their measurements from a fit to the data are shown on the r.h.s of Fig. 7. The best-fit values when profiling over the other parameters are:

$$
\begin{aligned}
\kappa_g &=& 1.04 \pm 0.14 &\quad (6) \\
\kappa_\gamma &=& 1.20 \pm 0.15 &\quad (7)
\end{aligned}
$$
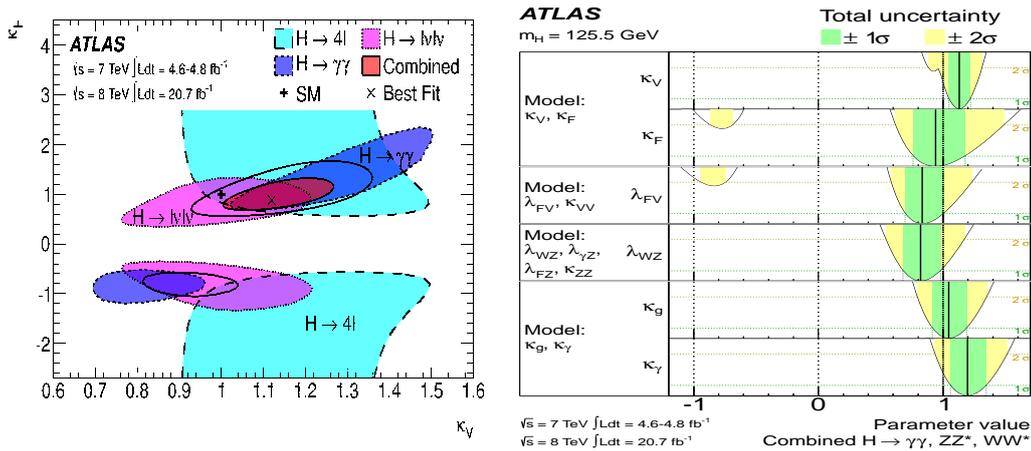
Figure 7: Determination of coupling scale factors.

3 Higgs spin-parity measurements

Evidence for the spin 0 nature of the newly discovered Higgs boson is presented in [2]. The $J^P = 0^+$ hypothesis of the SM is compared to several alternative hypotheses with $J^P = 0^-$, 1^+, 1^-, 2^+. The measurements are based on the kinematic properties of the three final states $H \to \gamma\gamma$, $H \to ZZ \to 4l$ and $H \to WW \to l\nu l\nu$. To improve the sensitivity to different spin–parity hypotheses, several final states are combined. To test the $J^P = 0^-$ spin–parity hypothesis, only the $H \to 4l$ decay mode is used, while for the $J^P = 1^+, 1^-$ hypotheses the $H \to ZZ, WW$ are combined. For the $J^P = 2^+$ study, all three decay modes are combined. A likelihood function $\mathcal{L}(J^P, \mu, \vec{\theta})$ that depends on the spin–parity assumption of the signal is constructed as a product of conditional probabilities over binned distributions of the discriminant observables in each channel:

$$\mathcal{L}(J^P, \mu, \vec{\theta}) = \prod_j^{N_{\text{chann.}}} \prod_i^{N_{\text{bins}}} P\big(N_{i,j} \mid \mu_j \cdot S_{i,j}^{(J^P)}(\vec{\theta}) + B_{i,j}(\vec{\theta})\big) \times \mathcal{A}_j(\vec{\theta}) \tag{8}$$

where μ_j represents the nuisance parameter associated with the signal rate in each channel j. The symbol $\vec{\theta}$ represents all other nuisance parameters. The likelihood function is therefore a product of Poisson distributions P corresponding to the observation of $N_{i,j}$ events in each bin i of the discriminant observable(s), given the expectations for the signal, $S_{i,j}^{(J^P)}(\vec{\theta})$, and for the background, $B_{i,j}(\vec{\theta})$. Some of the nuisance parameters are constrained by auxiliary measurements through the functions $\mathcal{A}_j(\vec{\theta})$.
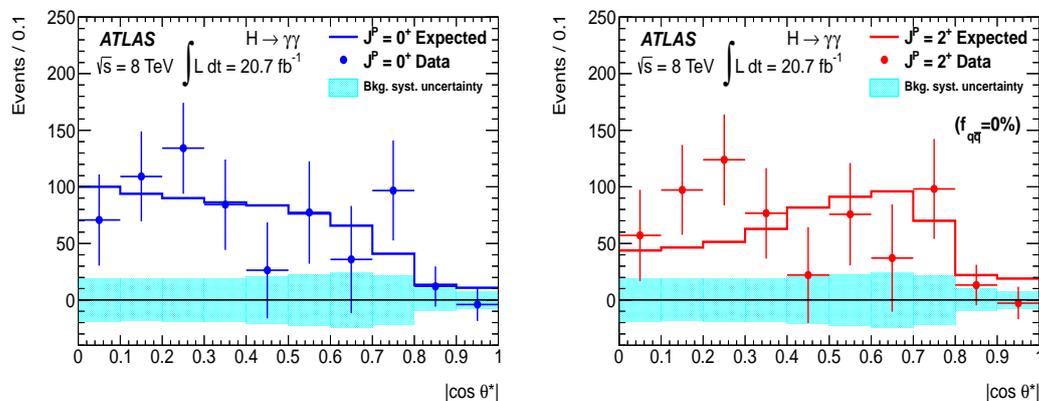
Figure 8: The background subtracted $|cos\theta^*|$ for the channel $H \to \gamma\gamma$ compared with expectations from 0^+ and 2^+ hypotheses.

The test statistic q used to distinguish between the two signal spin–parity hypotheses is based on a ratio of likelihoods:

$$q = \log \frac{\mathcal{L}(0^+, \hat{\hat{\mu}}_{0^+}, \hat{\hat{\vec{\theta}}}_{0^+})}{\mathcal{L}(J^P, \hat{\hat{\mu}}_{JP}, \hat{\hat{\vec{\theta}}}_{JP})} , \tag{9}$$

where $\mathcal{L}(0^+, \hat{\hat{\mu}}_{0^+}, \hat{\hat{\theta}}_{0^+})$ is the maximum likelihood estimator, evaluated under the 0^+ hypothesis and J^P stands for an alternative spin–parity assumption.

3.1 $H \to \gamma\gamma$

This decay mode is sensitive to the spin of the Higgs boson through the measurement of the polar angle distribution of the photons in the Higgs rest frame. For this channel ths SM spin hypothesis ia compared only to the $J^P = 2^+$, as shown in Fig. 8 where background subtracted distributions are presented.
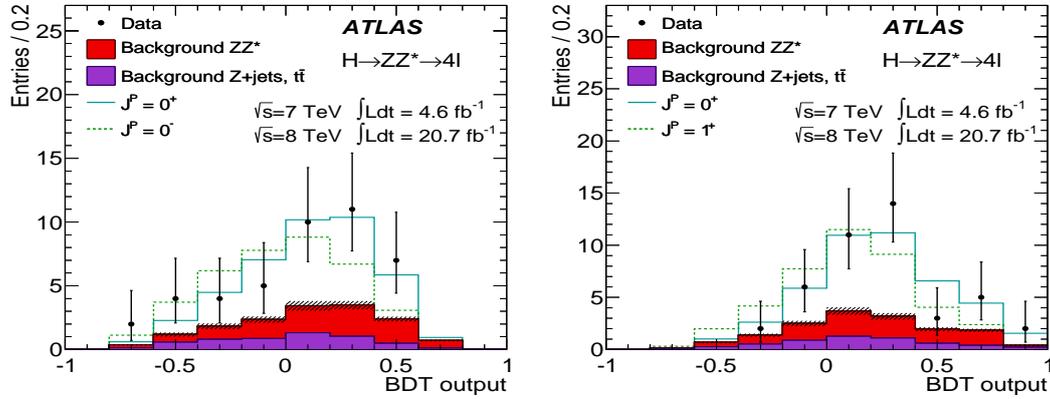
Figure 9: BDT response compared to the expectations for the SM and $J^P = 0^-, 1^+$ hypothesis.

3.2 $H \to ZZ^* \to 4l$

The two lepton pair masses as well as the five angles needed to describe the decay are fed into a BDT algorithm. The BDT response is shown in Fig. 9.

3.3 $H \to WW^* \to e\nu\mu\nu + 0 - jets$

Two variables found to be sensitive to the spin hypothesis are fed into a MVA, i.e. the lepton pair invariant mass, m_{ll} and their azimuthal separation, $\Delta\phi_{ll}$.

3.4 Summary on spin results

To illustrate the exclusion results obtained from the previous analysis we show two figures. In the left hand side of Fig. 10 we show the q distribution for the 0^+ and 0^- hypotheses from the $H \to ZZ^* \to 4l$ channel. The data, vertical black line, are in agreement with the SM and exclude the 0^- hypothesis at 97.8% CL. On the right hand side we show a summary of the exclusion limits obtained upon combining the information from all three channels.
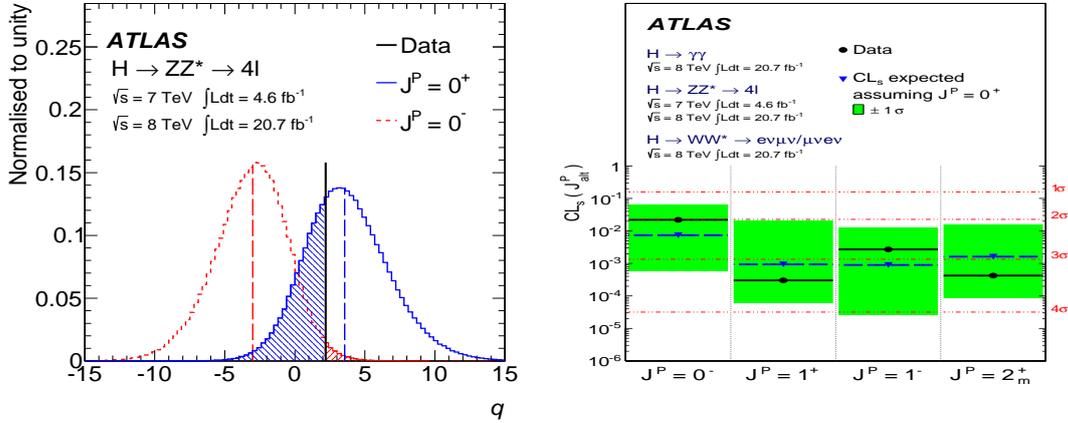
Figure 10: The q distributions for the 0^+ and 0^- hypotheses, left, and obtained exclusion limits for non SM J^P assignments, right.

4   Direct searches for Higgs decays to fermion pairs

No convincing signals have been observed yet in the decay modes $H \to \tau\tau$ and $H \to b\bar{b}$. For the latter the most promising production mechanism is Higgsstrahlung. In the l.h.s. of Fig. 11 we show the mass distribution of the $b\bar{b}$ pair, produced in association with a vector boson, with all backgrounds subtracted but for VV production. No clear signal at $\sim 125~GeV$. The fitted production strength is, see the r.h.s. of Fig.11, $\mu = 0.2 \pm 0.5(stat) \pm 0.4(syst)~GeV$, [3].
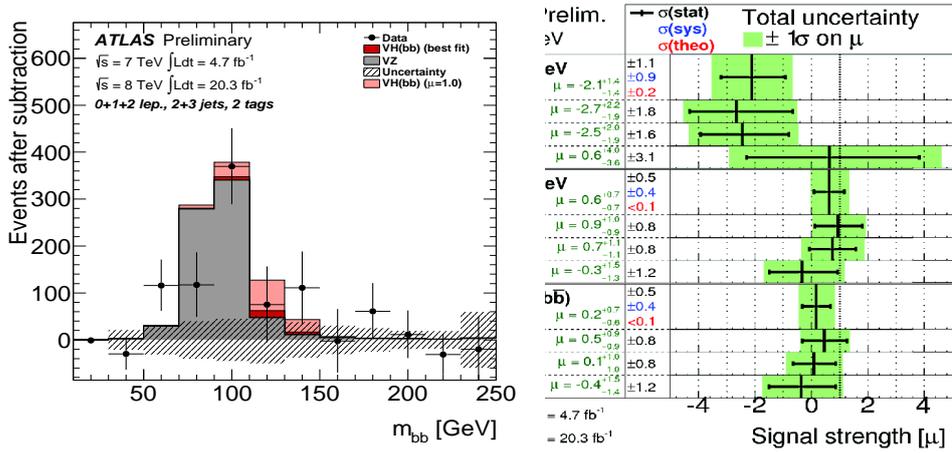
Figure 11: The background subtracted mass of the $b\bar{b}$ pair, left, and fitted production strength, right.

5 Search for charged Higgs bosons

To give a flavour of the kind of charged Higgs boson searches carried out by ATLAS, [4], we show results for light (i.e. below top quark mass) charged Higgs boson searches in the decay channel $H^+ \to c\bar{s}$. The mode is searched for in the top quark pair production channel where one top decays according to the dominant Wb mode, with the W decaying leptonically, and the second one decays via Hb. The final state consists of *one high p_T lepton, large mising transverse energy, two tagged b's and at least two high p_T additional jets*. The invariant mass of the dijet system, resulting from a kinematic fit to the full top quark pair, is shown in Fig. 12 left hand side. Good agreement with the SM is observed and limits are placed on possible H^+ signals assuming $BR(H^+ \to c\bar{s}) = 100\%$, right hand side of Fig. 12.
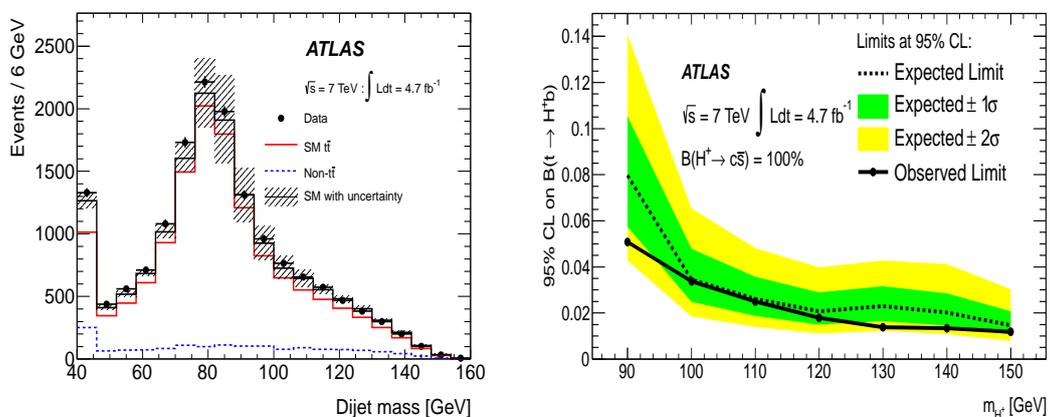
Figure 12: The dijet mass distribution for data and MC, left, and exclusion limits, right.

6 Conclusions

There is increasing evidence that the Higgs-like particle discovered a year ago, is the Higgs boson predicted in the SM. We look forward to the $14\,TeV$ run where we will be able to reduce the uncertainties in present coupling strength measurements, find direct evidence for $H \to \tau\tau$ and/or $H \to b\bar{b}$ and put more stringent limts on possible non SM Higgses.

7 Acknowledgments

I would like to thank the local organizers for their hospitality through this superb school.

References

[1] ATLAS Coll, G. Aad *et al.*, arXiv:1307.1427[hep-ex]

[2] ATLAS Coll, G. Aad *et al.*, arXiv:1307.1432[hep-ex]

[3] ATLAS Coll, G. Aad *et al.*, ATLAS-CONF-2013-079

[4] ATLAS Coll, G. Aad *et al.*, Eur. Phys. J. **C73** (2013) 12465.

Recent CMS Results on Heavy Quarks and Hadrons

Alice Bean for the CMS Collaboration

University of Kansas, Lawrence, KS 66045, United States

Using dedicated dimuon triggers with the CMS detector, several results are presented from data collected during 2010, 2011, and 2012. Polarization measurements are shown for the J/Ψ and Υ states. A search for states decaying to $\Upsilon(1S)\pi^+\pi^-$ is presented. The Λ_b^0 lifetime has been measured. An observation of the decay $B_S \rightarrow \mu^+\mu^-$ decay is presented.

1   Introduction

Studies of the b-quark are key to understanding the nature of the strong force.[1] The heavy-quark expansion model of nonperturbative quantum chromodynamics provides a framework for predicting properties of b-hadrons. Here, the heavy quarks in the meson move at non-relativistic speeds, so the relativistic corrections are small. The CMS Collaboration has previously published b-hadron production cross section results for: $pp \rightarrow \Lambda_b X \rightarrow J/\Psi\Lambda X$ [2], $pp \rightarrow B^+ X$ [3], $pp \rightarrow B^0 X$ [4], and $pp \rightarrow B_S X \rightarrow J/\Psi\phi X$ [5]. Figure 1 shows these results compared to Monte Carlo simulations using the Monte Carlo at Next to Leading Order (MC@NLO)/POWHEG [6] generator. The properties of quarkonia states such as J/Ψ, $J/\Psi(2S)$, and $\Upsilon(nS)$, have also been predicted with NRQCD [7].

The CMS Collaboration has recorded proton-proton data at the Large Hadron Collider during 2010, 2011, and 2012. During 2010 and 2011, the center of mass energy was 7 TeV and during 2012, data were taken at 8 TeV. The central feature of the CMS apparatus [8] is a superconducting solenoid of 6 m internal diameter. A tracker, consisting of silicon pixel and silicon strip layers, is immersed in a 3.8 T axial magnetic field of the superconducting solenoid. The pixel tracker consists of three barrel layers and two endcap disks at each barrel end. The strip tracker has 10 barrel layers and 12 endcap disks at each barrel end. The tracker provides an impact parameter resolution of $\sim 15\mu$m and a transverse momentum p_T resolution of about 1.5% for 100 GeV particles. Muons are measured in gas-ionisation detectors that are embedded in the steel return yoke outside the solenoid. In the barrel, there is a drift tube system interspersed with resistive plate chambers, and in the endcaps there is a cathode strip chamber system, also interspersed with resistive plate chambers. The CMS experiment uses a right-handed coordinate system, with the origin at the nominal interaction point, the x axis pointing towards the center of the LHC ring, the y axis pointing up (perpendicular to the plane of the LHC ring), and the z axis along the anticlockwise-beam direction. The polar angle θ is measured from the positive z axis and the pseudorapidity is defined by $\eta = -\ln[\tan(\theta/2)]$. The azimuthal angle ϕ is measured from the positive x axis in the plane perpendicular to the beam.

Decay channels with muons are measured well in the detector. For the results presented here, the muon triggers were used to select events. As the data-taking has progressed, the
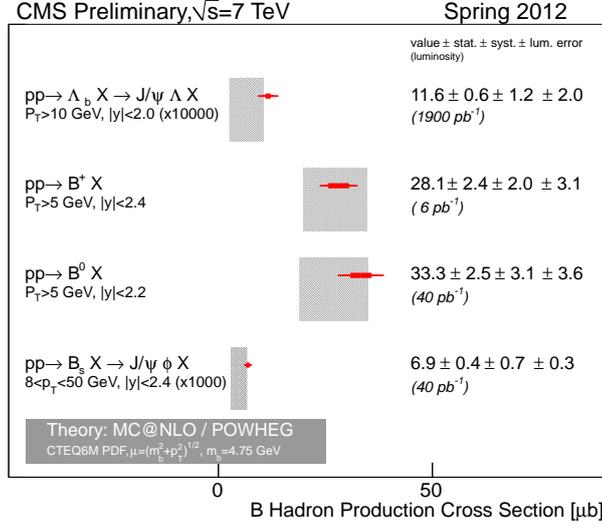
Figure 1: Summary of *b*-hadron cross section measurements performed by CMS with 7 TeV p-p collision at LHC. The inner error bars of the data points correspond to the statistical uncertainty, whil the outer (thinner) error bars correspond to the quadratic sum of statistical and systematic uncertainties. The outermost brackets correspond to the total error, including a luminosity uncertainty which is also added in quadrature.

collider has continued to improve on the luminosity and the earlier low values of the transverse muon momenta p_T for these triggers have been raised thus limiting the bandwidth for the later datasets for *B*-physics studies. For proton-proton collisions at a center of mass energy of 7 TeV, the $\Upsilon(1S)$, $\Upsilon(2S)$, and $\Upsilon(3S)$ cross sections are measured as a function of the dimuon transverse momentum and rapidity. A search for the decay $X_b \to \Upsilon(1S)\pi^+\pi^-$, with $\Upsilon(1S) \to \mu^+\mu^-$ is presented. The angular distributions are examined for the J/Ψ, $\Psi(2S)$, $\Upsilon(1S)$, $\Upsilon(2S)$, and $\Upsilon(3S)$ to determine their polarizations. The Λ_b^0 lifetime is measured. Finally, the $B_s \to \mu^+\mu^-$ branching ratio is measured.

2 Cross section measurements for $\Upsilon(nS)$ states

Quarkonium production in hadron collisions is still not well understood [9]. Using 35.8 ± 1.4 pb^{-1} of data taken at a center of mass energy of 7 TeV, the $\Upsilon(1S)$, $\Upsilon(2S)$, and $\Upsilon(3S)$ production cross sections were measured. Their decays to dimuons were used. The product of the $\Upsilon(nS)$ differential cross section and the dimuon branching fraction is determined from the signal yield determined from an extended unbinned maximum likelihood fit to the dimuon invariant mass spectrum, corrected by the acceptance and the efficiency. After integrating over the Υ transverse momentum range $p_T <$ 50 GeV/c and rapidity range $|y(\Upsilon)| < 2.4$, the $\Upsilon(nS)$ cross sections times dimuon branching fractions are found to be: $\sigma(pp \to \Upsilon(1S)X) \times B(\Upsilon(1S) \to \mu^+\mu^-) = (3.06 \pm 0.02^{+0.20}_{-0.18} \pm 0.12)$ nb, $\sigma(pp \to \Upsilon(2S)X) \times B(\Upsilon(1S) \to \mu^+\mu^-) = (0.910 \pm 0.011^{+0.055}_{-0.046} \pm 0.036)$ nb, and $\sigma(pp \to \Upsilon(3S)X) \times B(\Upsilon(3S) \to \mu^+\mu^-) = 0.490 \pm 0.010 \pm$

0.029 ± 0.020) nb. Here, the first uncertainty is statistical, the second is systematic and the third is associated with the integrated luminosity of the sample. Figure 2 shows that the cross sections are relatively flat as a function of rapidity until about 1.6 where they then fall quickly. The ratios of the differential cross sections for the $\Upsilon(nS)$ are also found to rise linearly as function of the transverse momentum of the Υ until about 20 GeV/c where they then become consistent with being constant. More information can be found in the reference [10].
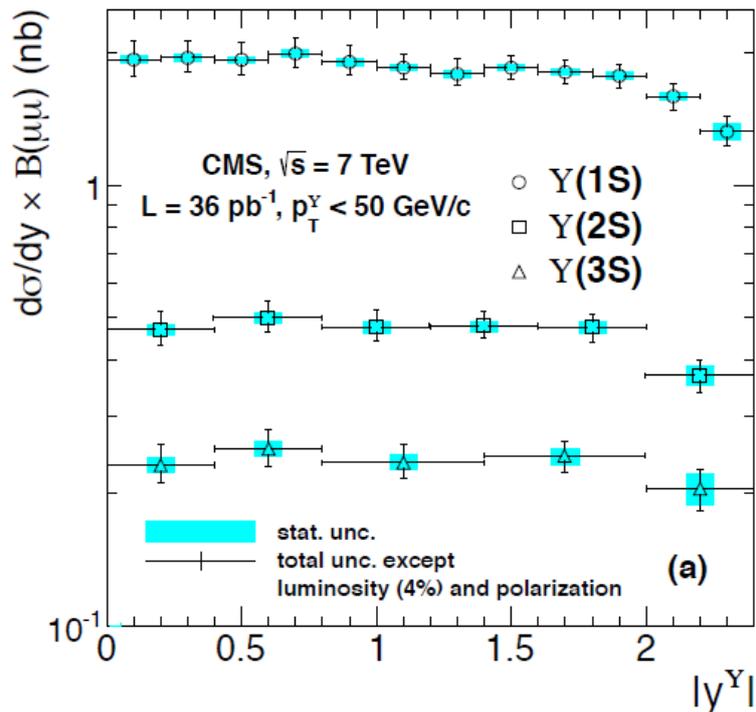
Figure 2: Acceptance-corrected differential production cross sections of the $\Upsilon(nS)$ as a function of rapidity. The bands represent the satistical uncertainty and the error bars represent the total uncertainty, except for those from the $\Upsilon(nS)$ polarization and integrated luminosity.

3   Search for a bottomonium state decaying to $\Upsilon(1S)\pi^+\pi^-$

An exotic charmonium state X(3872) has been observed by many including the CMS collaboration [11]. A theory for this state has not been established. Recently, the CMS collaboration has searched for the corresponding narrow bottomonium state (X_b) that would decay to $\Upsilon(1S)\pi^+\pi^-$ followed by $\Upsilon(1S) \to \mu^+\mu^-$ using a dataset of proton-proton collisions taken at a center of mass energy of 8 TeV that corresponds to an integrated luminosity of 20.65 fb^{-1}.

The reconstruction of the potential X_b meson and the normalization channel $\Upsilon(2S) \to \Upsilon(1S)\pi^+\pi^-$ starts with the reconstruction of the $\Upsilon(1S) \to \mu^+\mu^-$ and two oppositely charged pion candidates. Selection criteria are introduced that include the thresholds on transverse

momenta, a mass window for the $\Upsilon(1S)$, quality requirements on kinematic fits, and requiring the minimum distance in the pseudorapidity and azimuthal angles to be small for the pions with respect to the $\Upsilon(1S)$ candidate momentum. The study was conducted in the kinematic region $p_T[\Upsilon(1S)\pi^+\pi^-] > 7.2$ GeV/c and $y[\Upsilon(1S)\pi^+\pi^-] < 2.0$. No significant signal is seen and an upper limit on the ratio of $\sigma[pp \to X_b \to \Upsilon(1S)\pi^+\pi^-]/\sigma[pp \times \Upsilon(2S) \to \Upsilon(1S)\pi^+\pi^-]$ is set in the range of 0.008-0.046 at the 95% confidence level [12].

4   Polarization studies for J/Ψ and Υ states

So far, the polarization of J/Ψ mesons is not satisfactorily described in the context of NRQCD. Here, the perturbative color-singlet production is complemented by possible nonperturbative transitions from colored quark pairs to the observable bound states. The high p_T quarkonia S-wave states directly produced are predicted to be transversely polarized with respect to the direction of their own momentum [13]. The CMS collaboration has studied the polarizations from prompt $\Upsilon(1S)$, $\Upsilon(2S)$, $\Upsilon(3S)$, J/Ψ, and $\Psi(2S)$ decays using a data sample collected at a center of mass energy of 7 TeV with integrated luminosity of 4.9 fb^{-1}.

The polarization of the $J^{PC} = 1^-$ states is measured through a study of the angular distribution from the decay to $\mu^+\mu^-$ using $W(\cos\theta, \phi|\bar{\lambda}) \propto \frac{1}{(3+\lambda_\theta)}(1+\lambda_\theta \cos^2\theta + \lambda_\phi \sin^2\theta \cos 2\phi + \lambda_{\theta\phi} \sin 2\theta \cos \phi)$, where θ and ϕ are the polar and azimuthal angles, respectively, of the μ^+ with respect to the z axis of the chosen polarization frame. The three frame-dependent anisotropy parameters are extracted in three polarization frames and presented here for the center of helicity (HX) frame where the z axis coincides with the direction of the quarkonium momentum in the laboratory. Prompt decays are found by examining the proper time distribution. For the $\Upsilon(nS)$ states, Figure 3 shows for the rapidity range 0.0-0.6, one dimensional profiles of the polarization parameters as a function of the p_T of the Υ state and similar values are obtained for the 0.6-1.2 rapidity range [14]. Similarly, for the J/Ψ and $\Psi(2S)$ states, Figure 4 shows the distributions as a function of p_T for several $|y|$ bins [15]. All of the polarization parameters are compatible with zero or no transverse polarization. This is in disagreement with existing next-to-leading-order NRQCD theoretical expectations [16].

5   The Λ_b^0 lifetime

Using approximately 5 fb^{-1} of data collected in 2011, the Λ_b^0 lifetime was measured using the decay $\Lambda_b^0 \to J/\Psi\Lambda$ with $\Lambda \to p\pi^-$ and $J/\Psi \to \mu^+\mu^-$. Dimuon triggers optimised for selecting events with J/Ψ candidates were used. The four charged particles ($\mu^+\mu^-p\pi^-$) allow for a full reconstruction of the Λ_b^0 baryon. After particle quality cuts, kinematic vertex fits are used to find the Λ, the J/Ψ, and the proper decay time of the Λ_b^0 candidate. An unbinned extended maximum-likelihood fit is performed to determine the Λ_b^0 lifetime which uses the invariant mass of the Λ_b^0 candidate, the proper decay time and its uncertainty calculated per candidate. A projection of the invariant-mass and proper decay time distributions and the results of the fit is shown in Figure 5. Since the overall efficiency, determined through simulation, is consistent with being independent of the proper decay time, no efficiency correction is used. However, the largest systematic error is assigned to this source in addition to other systematic errors from alignment, event selection, and the fit model. The Λ_b^0 lifetime is found to be 1.503 ± 0.052 (stat.)± 0.031 (syst.) ps [17].
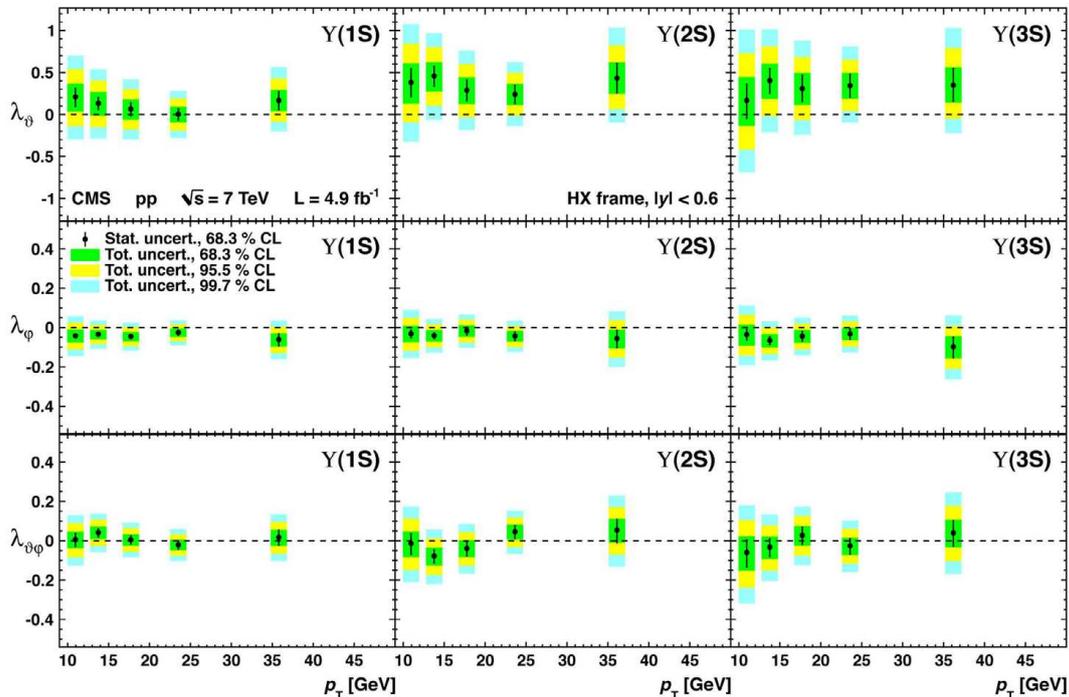
Figure 3: The λ_θ, λ_ϕ, and $\lambda_{\theta\phi}$ parameters (top to bottom) for the $\Upsilon(1S)$, $\Upsilon(2S)$, and $\Upsilon(3S)$ states (left to right), in the HX frame, for the rapidity < 0.6 range. The bands represent 68.3, 95.5 and 99.7% C.L. intervals, while the error bars indicate the 68.3% C.L. interval when neglecting systematic uncertainties.

6 Observation of the decay $B_S \to \mu^+\mu^-$

A search for the rare decays $B_S^0 \to \mu^+\mu^-$ and $B^0 \to \mu^+\mu^-$ in pp collisions at center of mass energies of 7 and 8 TeV, with data samples corresponding to integrated luminosities of 5 and 20 fb^{-1}, respectively [19] is performed. At tree-level, flavor-changing neutral-current decays are forbidden in the standard model. However, these decays may proceed through higher-order loop diagrams so small branching fractions are predicted of $B(B_S^0 \to \mu^+\mu^-) = (3.57 \pm 0.30) \times 10^{-9}$ and $B(B^0 \to \mu^+\mu^-) = (1.07 \pm 0.10) \times 10^{-10}$ [18].

The search for the $B \to \mu\mu$ signal, where B denotes either B_S^0 or B^0, is performed in the dimuon invariant mass regions around the respective masses. The signal region was kept blind until all selection criteria were established. Selection variables included those which constrained isolated muons to a common vertex. The final selection is performed using boosted decision trees trained to distinguish between signal and background candidates. The combinatorial background is evaluated by extrapolating the data in nearby mass sidebands to the signal
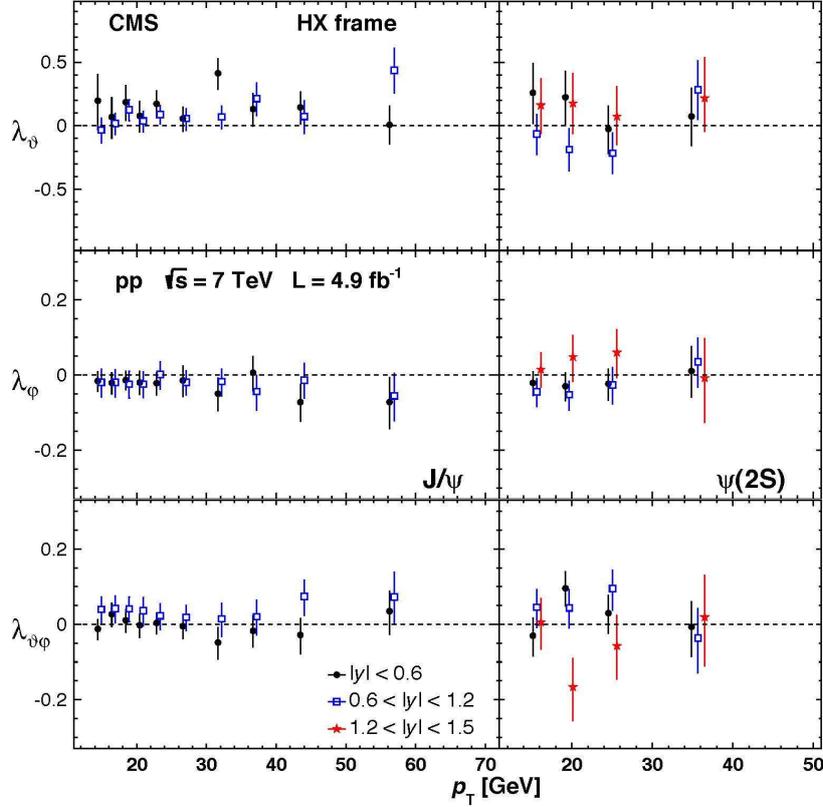
Figure 4: Measurements of the λ_θ, λ_ϕ, and $\lambda_{\theta\phi}$ parameters (top to bottom) for the J/Ψ (left) and $J/\Psi(2S)$ (right) in the HX frame, as a function of the $\Psi(nS)$ p_T for all rapidity ranges. The error bars represent the 68.3% C.L. total uncertainties.

region. Monte Carlo simulations are used to account for background from B and Λ_b decays. A normalization sample of $B^+ \to J/\Psi K^+ \to \mu^+\mu^- K^+$ decays is used. An unbinned maximum-likelihood fit to the dimuon invariant mass distribution gives a branching fraction $B(B_S^0 \to \mu^+\mu^-) = (3.0^{+1.0}_{-0.9}) \times 10^{-9}$, where the uncertainty includes both statistical and systematic contributions. An excess with respect to background of $B_S^0 \to \mu^+\mu^-$ is seen with a significance of 4.3 standard deviations. An upper limit at the 95% C.L. of $B(B^0 \to \mu^+\mu^-) < 1.1 \times 10^{-9}$ is determined. As can be seen from Figure 6, the results are in agreement with expectations from the standard model.

7   Acknowledgments

We congratulate our colleagues in the CERN accelerator departments for the excellent performance of the LHC and thank the technical and administrative staffs at CERN and at other CMS institutes for their contributions to the success of the CMS effort. In addition, we gratefully acknowledge the computing centres and personnel of the Worldwide LHC Computing Grid
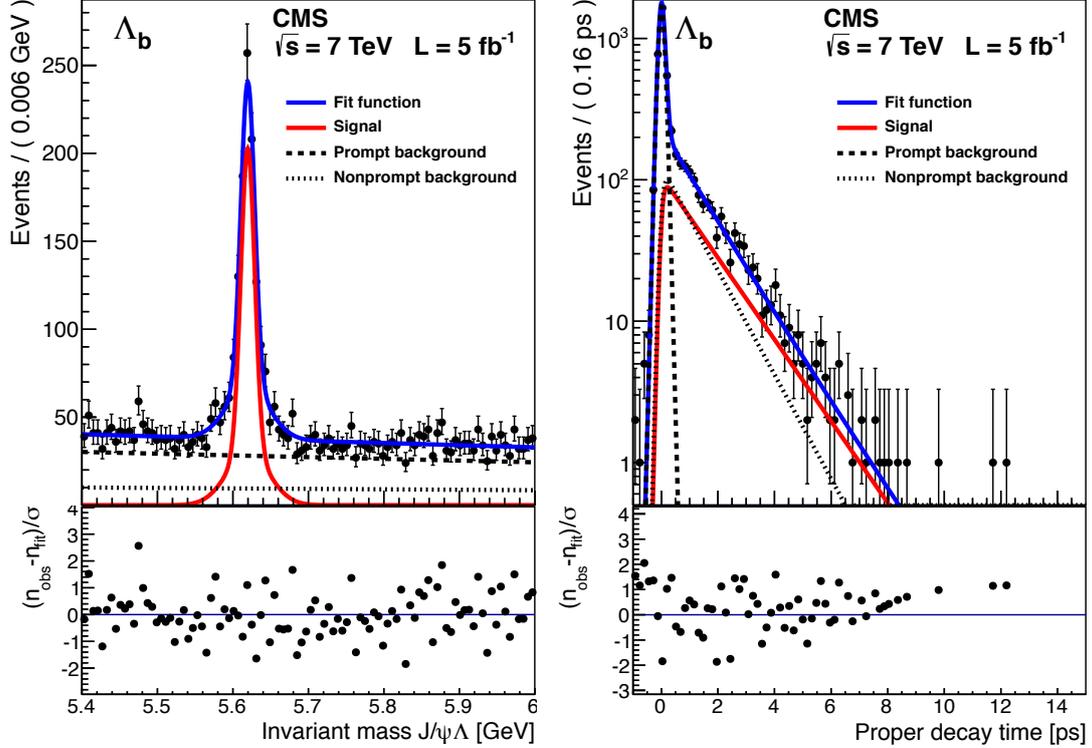
Figure 5: Projections of the invariant-mass and proper decay time distributions and the results of the fit are shown. The dark solid lines give the results of the overall fit to the data. The lighter solid lines are the signal contributions, and the dashed an dotted lines show the prompt and nonprompt background contributions, respectively.

Figure 6: Categorized boosted decision tree scan of the ratio of the joint likelihood $B(B_S^0 \to \mu^+\mu^-)$ and $B(B^0 \to \mu^+\mu^-)$. The insets show the likelihood ratio scan for each of the branching fractions when the other is profiled together with other nuisance parameters. The significance at which the background-only hypothesis is rejected is also shown.

References

[1] P. Nason, S. Dawson, and R.K. Ellis, Nucl. Phys. **B303** 607 (1988); M. Cacciari, M. Greco, and P. Nason, JEHP **05** 007 (1998); B.A. Kriehl, G. Kramer, I Schienbein *el al.*, Phys. Rev. **D77** 014011 (2008).

[2] CMS Collaboration, Phys. Lett. **B714** 136 (2011).

[3] CMS Collaboration, Phys. Rev. Lett. **106** 112001 (2011).

[4] CMS Collaboration, Phys. Rev. Lett. **106** 252001 (2011).

[5] CMS Collaboration, Phys. Rev. D **84** 052008 (2011).

[6] M Cacciari and M. Greco, Nucl. Phys. **B421** 530 (1994); M. Cacciari, M. Greco, and P. Nason, JHEP **05** 007 (1998); S. Alioli *et al.*, JHEP **06** 043 (2010); S. Frixione, P. Nason, and G. Ridolfi, JHEP **09** 126 (2007).

[7] G.T. Bodwin, E. Braaten, and G.P. Lepage, Phys. Rev. **D51** 1125 (1995).

[8] S. Chatrchyan *et al.* (CMS Collaboration), JINST **3** S08004 (2008).

[9] N. Brambilla *et al.*, Phys. J. **C71** 1534 (2011);

[10] CMS Colaboration, arXiv:1303.5900 (2013), to be published in Phys. Lett. B.

[11] CMS Collaboration, JHEP **04** 154 (2013).

[12] CMS Collaboration, arXiv:1309.0250 (2013), submitted to Phys. Lett. B.

[13] J.-P. Lansberg, Eur. Phys. J. **C61** 693 (2009); M. Beneke and M. Kramer, Phys. Rev. **D55** 5269 (1997); A.K. Leibovich, Phys. Rev. **D56** 4412 (1997); E. Braaten, B.A. Kniehl, and J. Lee, Phys. Rev. **D62** 094005 (2000).

[14] CMS Collaboration, Phys. Rev. Lett. **110** 0818022 (2013).

[15] CMS Collaboration, arXiv:1307.6070 (2013), to be published in Phys. Lett. B.

[16] B. Gong, J.-X. Wang, and H.-F. Zhang, Phys. Rev. **D83** 114021 (2011); P. Artoisenet, J. Campbell, J.P. Lansbert, F. Maltoni, and F. Tramontano, Phys. Rev. Lett **101** 152001 (2008); M. Butenschoen and B.A. Kniehl, Phys. Rev. Lett. **108** 172002 (2012); B. Gong, L.-P. Wan, and H.-F. Zhang, Phys. Rev. Lett. **110** 042002 (2013).

[17] CMS Collaboration, JHEP **07** (2013);

[18] A.J. Buras, J. Girrbach, D. Guadagnoli, and G. Isidori, Eur. Phys. J. **72** (2012); K. De-Bruyn *et al.*, Phys. Rev. Lett. **109** 041801 (2012).

[19] CMS Collaboration, Phys. Rev. Lett. **111** 101804 (2013).

Mesons with open charm and beauty: an overview

P. Colangelo[a], F. De Fazio[a], F. Giannuzzi[a,b] and S. Nicotri[a,b]

[a]Istituto Nazionale di Fisica Nucleare, Sezione di Bari, Italy
[b]Dipartimento di Fisica, Universitá degli Studi di Bari, Italy

The spectrum of mesons with open charm and beauty is analyzed using heavy quark symmetry arguments. A classification of the newly observed states is presented, together with predictions for several unobserved resonances.

1   Heavy meson doublets

A QCD framework for the analysis of hadrons containing a single heavy quark can be set up using the heavy quark (HQ) limit, and is formalized in the heavy quark effective theory (HQET) [1]. This is an effective theory of QCD formulated for N_f heavy quarks Q with mass $m_Q \gg \Lambda_{QCD}$, with the four-velocity of Q fixed. The theory displays heavy quark spin-flavour symmetries, i.e. the invariance under $SU(2N_f)$ transformations, which are symmetries of the QCD Lagrangian in the heavy quark limit. Within this framework, several heavy hadron properties can be studied, with important results represented, for instance, by the relations among semileptonic transition form factors in weak heavy hadron matrix elements [2]. The heavy meson spectrum can also be studied from the point of view of the heavy quark limit [3]: this is particularly interesting, due to the numerous recently discovered charm and beauty resonances needing to be recognized [4].

The classification of heavy $Q\bar{q}$ mesons (q is a light quark) in the HQ limit relies on the decoupling of the heavy quark spin s_Q from the spin of the light antiquark and gluons. The separate conservation in strong interaction processes of s_Q and of the total angular momentum s_ℓ of the light degrees of freedom permits a classification of the heavy mesons according to the value of s_ℓ. Mesons can be collected in doublets: the two states in each doublet (*spin partners*) have total spin $J = s_\ell \pm \frac{1}{2}$ and parity $P = (-1)^{\ell+1}$, with ℓ the orbital angular momentum of the light degrees of freedom and $\vec{s}_\ell = \vec{\ell} + \vec{s}_q$ (s_q is the light antiquark spin). Within each doublet the two states are degenerate in the HQ limit and, due to flavour symmetry, the properties of the states in a doublet can be related to those of the corresponding states differing for the heavy quark flavour. Corrections can be systematically included considering next-to-leading terms in an expansion in the inverse heavy quark mass.

We focus on the meson doublets with $\ell = 0, 1, 2$ ($s-$, $p-$ and $d-$wave states in the quark model), discussing their properties in the HQ limit and considering a few next-to-leading corrections. This allows us to study how the observed charmed and beauty mesons fit in the theoretical classification. Moreover, using data in the charm sector, the properties of the corresponding beauty mesons can be predicted.

Important information for a proper identification comes from the heavy meson decays to

light pseudoscalar mesons, whose features depend on the quantum numbers of the decaying resonances. An effective Lagrangian approach, with the heavy meson doublets represented by effective fields and the octet of light pseudo Goldstone mesons grouped in a single field, can be formulated imposing the invariance under heavy quark spin-flavour transformations and chiral transformations of the light pseudo Goldstone boson fields. This allows to infer the properties of the heavy meson doublets in the HQ limit, namely that the two degenerate states in a doublet have the same full width, that the sum of the partial widths of a state in a doublet to another heavy state in another doublet with emission of a light meson is the same for the two members of a doublet, that the ratios of partial decay widths for a given state are related, that the partial decay widths are independent of the heavy quark flavour [3].

The lightest $Q\bar{q}$ mesons correspond to $\ell = 0$, hence $s_\ell^P = \frac{1}{2}^-$. This doublet consists of two states with $J^P = (0^-, 1^-)$, denoted as (P, P^*). For $\ell = 1$ one has $s_\ell^P = \frac{1}{2}^+$ with $J^P = (0^+, 1^+)$ (the states are (P_0^*, P_1')), and $s_\ell^P = \frac{3}{2}^+$ with $J^P = (1^+, 2^+)$ $((P_1, P_2^*))$. $\ell = 2$ corresponds to either $s_\ell^P = \frac{3}{2}^-$ (states (P_1^*, P_2)) or $s_\ell^P = \frac{5}{2}^-$ ($(P_2'^*, P_3)$). An analogous notation holds for the radial excitations with $n = 2$ (denoted by a tilde: $\tilde{P}, \tilde{P}^*, ...$). The effective fields describing the various doublets in the HQ limit are listed below, with $a = u, d, s$ light flavour index. The fields, defined including a factor $\sqrt{m_Q}$, have dimension 3/2 and annihilate mesons of four velocity v which is conserved in strong interaction processes.

$$
\begin{aligned}
s_\ell^P = \frac{1}{2}^- : \quad & H_a = \frac{1 + \slashed{v}}{2} \left[P_{a\mu}^* \gamma^\mu - P_a \gamma_5 \right] \\[2mm]
s_\ell^P = \frac{1}{2}^+ : \quad & S_a = \frac{1 + \slashed{v}}{2} \left[P_{1a}'^\mu \gamma_\mu \gamma_5 - P_{0a}^* \right] \\[2mm]
s_\ell^P = \frac{3}{2}^+ : \quad & T_a^\mu = \frac{1 + \slashed{v}}{2} \left[P_{2a}^{\mu\nu} \gamma_\nu - P_{1a\nu} \sqrt{\frac{3}{2}} \gamma_5 \left[g^{\mu\nu} - \frac{1}{3} \gamma^\nu (\gamma^\mu - v^\mu) \right] \right] \\[2mm]
s_\ell^P = \frac{3}{2}^- : \quad & X_a^\mu = \frac{1 + \slashed{v}}{2} \left[P_{2a}^{*\mu\nu} \gamma_5 \gamma_\nu - P_{1a\nu}'^* \sqrt{\frac{3}{2}} \left[g^{\mu\nu} - \frac{3}{2} \gamma^\nu (\gamma^\mu + v^\mu) \right] \right] \\[2mm]
s_\ell^P = \frac{5}{2}^- : \quad & X_a'^{\mu\nu} = \frac{1 + \slashed{v}}{2} \left[P_{3a}^{\mu\nu\sigma} \gamma_\sigma - P_{2a}^{*'\alpha\beta} \sqrt{\frac{5}{3}} \gamma_5 \left[g_\alpha^\mu g_\beta^\nu - \frac{1}{5} \gamma_\alpha g_\beta^\nu (\gamma^\mu - v^\mu) - \frac{1}{5} \gamma_\beta g_\alpha^\mu (\gamma^\nu - v^\nu) \right] \right] .
\end{aligned}
\tag{1}
$$

The octet of light pseudoscalar mesons is introduced defining $\xi = e^{\frac{i\mathcal{M}}{f_\pi}}$ and $\Sigma = \xi^2$, with $\mathcal{M}$ incorporating the fields of π, K and η ($f_\pi = 132$ MeV):

$$
\mathcal{M} = \begin{pmatrix} \sqrt{\frac{1}{2}}\pi^0 + \sqrt{\frac{1}{6}}\eta & \pi^+ & K^+ \\ \pi^- & -\sqrt{\frac{1}{2}}\pi^0 + \sqrt{\frac{1}{6}}\eta & K^0 \\ K^- & \bar{K}^0 & -\sqrt{\frac{2}{3}}\eta \end{pmatrix} .
\tag{2}
$$

Imposing invariance under heavy quark spin-flavour and light quark chiral transformations, an effective QCD Lagrangian can be constructed [5, 6], with kinetic terms of the heavy meson

doublets and of the Σ field reading:

$$
\begin{aligned}
\mathcal{L} &= \frac{f_\pi^2}{8} Tr[\partial^\mu \Sigma \partial_\mu \Sigma^\dagger] + i\, Tr[\bar{H}_b v^\mu D_{\mu ba} H_a] \\
&+ Tr[\bar{S}_b\, (i\, v^\mu D_{\mu ba} - \delta_{ba}\, \Delta_S) S_a] + Tr[\bar{T}_b^\alpha\, (i\, v^\mu D_{\mu ba} - \delta_{ba}\, \Delta_T) T_{a\alpha}] \\
&+ Tr[\bar{X}_b^\alpha\, (i\, v^\mu D_{\mu ba} - \delta_{ba}\, \Delta_X) X_{a\alpha}] + Tr[\bar{X}_b^{\prime \alpha\beta}\, (i\, v^\mu D_{\mu ba} - \delta_{ba}\, \Delta_{X'}) X'_{a\alpha\beta}] ,
\end{aligned} \tag{3}
$$

with $D_{\mu ba} = -\delta_{ba}\partial_\mu + \mathcal{V}_{\mu ba} = -\delta_{ba}\partial_\mu + \frac{1}{2}\left(\xi^\dagger\partial_\mu\xi + \xi\partial_\mu\xi^\dagger\right)_{ba}$ and $\mathcal{A}_{\mu ba} = \frac{i}{2}\left(\xi^\dagger\partial_\mu\xi - \xi\partial_\mu\xi^\dagger\right)_{ba}$. The parameters Δ_F (with $F = S, T, X, X'$) correspond to the mass splittings between the higher mass doublets and the lightest one described by H:

$$
\Delta_F = \overline{M}_F - \overline{M}_H , \tag{4}
$$

with $\overline{M}_{(F)}$ the spin-averaged masses of the doublets:

$$
\begin{aligned}
\overline{M}_H &= \frac{3M_{P^*} + M_P}{4} , & \overline{M}_S &= \frac{3M_{P_1'} + M_{P_0^*}}{4} , & \overline{M}_T &= \frac{5M_{P_2^*} + 3M_{P_1}}{8} , \\
\overline{M}_X &= \frac{5M_{P_2} + 3M_{P_1^*}}{8} , & \overline{M}_{X'} &= \frac{7M_{P_3} + 5M_{P_2'^*}}{12} .
\end{aligned} \tag{5}
$$

Corrections to the heavy quark limit involve symmetry breaking terms suppressed by powers of $1/m_Q$ [7]. For instance, the Lagrangian terms

$$
\begin{aligned}
\mathcal{L}_{1/m_Q} &= \frac{1}{2m_Q}\Big\{\lambda_H Tr[\bar{H}_a \sigma^{\mu\nu} H_a \sigma_{\mu\nu}] + \lambda_S Tr[\bar{S}_a \sigma^{\mu\nu} S_a \sigma_{\mu\nu}] + \lambda_T Tr[\bar{T}_a^\alpha \sigma^{\mu\nu} T_a^\alpha \sigma_{\mu\nu}] \\
&\quad + \lambda_X Tr[\bar{X}_a^\alpha \sigma^{\mu\nu} X_{a\alpha} \sigma_{\mu\nu}] + \lambda_{X'} Tr[\bar{X}_a^{\prime \alpha\beta} \sigma^{\mu\nu} X_a^{\prime \alpha\beta} \sigma_{\mu\nu}]\Big\}
\end{aligned} \tag{6}
$$

break the mass degeneracy between the members of the various doublets. The constants λ_H, λ_S, λ_T, λ_X and $\lambda_{X'}$ are related to the hyperfine splittings:

$$
\begin{aligned}
\lambda_H &= \frac{1}{8}\left(M_{P^*}^2 - M_P^2\right) , & \lambda_S &= \frac{1}{8}\left(M_{P_1'}^2 - M_{P_0^*}^2\right) , & \lambda_T &= \frac{3}{16}\left(M_{P_2^*}^2 - M_{P_1}^2\right) , \\
\lambda_X &= \frac{3}{16}\left(M_{P_2}^2 - M_{P_1^*}^2\right) , & \lambda_{X'} &= \frac{5}{24}\left(M_{P_3}^2 - M_{P_2'^*}^2\right) .
\end{aligned} \tag{7}
$$

The transitions $F \to H M$ (with $F = H, S, T, X, X'$ and M a light pseudoscalar meson), at the leading order in the light meson momentum and heavy quark mass expansion, can be described by the Lagrangian interaction terms [5]:

$$
\begin{aligned}
\mathcal{L}_H &= g\, Tr\Big[\bar{H}_a H_b \gamma_\mu \gamma_5 \mathcal{A}_{ba}^\mu\Big] \\
\mathcal{L}_S &= h\, Tr\Big[\bar{H}_a S_b \gamma_\mu \gamma_5 \mathcal{A}_{ba}^\mu\Big] + h.c. \\
\mathcal{L}_T &= \frac{h'}{\Lambda_\chi} Tr\Big[\bar{H}_a T_b^\mu (iD_\mu \slashed{\mathcal{A}} + i\slashed{D}\mathcal{A}_\mu)_{ba}\gamma_5\Big] + h.c. \\
\mathcal{L}_X &= \frac{k'}{\Lambda_\chi} Tr\Big[\bar{H}_a X_b^\mu (iD_\mu \slashed{\mathcal{A}} + i\slashed{D}\mathcal{A}_\mu)_{ba}\gamma_5\Big] + h.c. \\
\mathcal{L}_{X'} &= \frac{1}{\Lambda_\chi^2} Tr\Big[\bar{H}_a X_b^{\prime \mu\nu}\big[k_1\{D_\mu, D_\nu\}\mathcal{A}_\lambda + k_2(D_\mu D_\lambda \mathcal{A}_\nu + D_\nu D_\lambda \mathcal{A}_\mu)\big]_{ba}\gamma^\lambda\gamma_5\Big] + h.c.;
\end{aligned} \tag{8}
$$

these terms involve the coupling constants g, h, h', k_i (we set $k = k_1 + k_2$, and the chiral symmetry-breaking scale Λ_χ to $\Lambda_\chi = 1$ GeV). $\mathcal{L}_S$ and $\mathcal{L}_T$ describe positive parity heavy meson transitions with the emission of light pseudoscalar mesons in $s-$ and $d-$ wave, respectively, $\mathcal{L}_X$ and $\mathcal{L}_{X'}$ the transitions of higher mass mesons of negative parity, belonging to the X and X' doublets, with the emission of light pseudoscalar mesons in $p-$ and $f-$ wave. At the same order in the expansion in the light meson momentum, the structure of the Lagrangian terms for radial excitations of the various doublets is unchanged, since it is dictated only by the spin-flavour and chiral symmetries, but the coupling constants are replaced by new ones, $\tilde{g}$, $\tilde{h}$, etc.

In this basic framework all data for mesons with open charm and beauty can be analyzed, and a classification scheme for the observed resonances can be elaborated. In Table 1 we propose the assignment for the observed charmed $c\bar{q}$, $c\bar{s}$, and beauty $b\bar{q}$, $b\bar{s}$ (with $q = u, d$) mesons to the various doublets [4], justified by the arguments presented below.[1]

Table 1: Observed open charm and open beauty mesons organized in HQ doublets. States denoted by ($\star$) have uncertain assignment; they are classified according to the scheme proposed in this study.

s_ℓ^P		J^P	$c\bar{q}$ (n=1)	$c\bar{q}$ (n=2)	$c\bar{s}$ (n=1)	$c\bar{s}$ (n=2)	$b\bar{q}$ (n=1)	$b\bar{s}$ (n=1)
H	$\frac{1}{2}^-$	0^-	$D(1869)$	$D(2550)$ $\star$	$D_s(1968)$		$B(5279)$	$B_s(5366)$
		1^-	$D^*(2010)$	$D^*(2600)$ $\star$	$D_s^*(2112)$	$D_{s1}^*(2700)$	$B^*(5325)$	$B_s^*(5415)$
S	$\frac{1}{2}^+$	0^+	$D_0^*(2400)$		$D_{s0}^*(2317)$			
		1^+	$D_1'(2430)$		$D_{s1}'(2460)$	$D_{sJ}(3040)$ $\star$		
T	$\frac{3}{2}^+$	1^+	$D_1(2420)$		$D_{s1}(2536)$	$D_{sJ}(3040)$ $\star$	$B_1(5721)$	$B_{s1}(5830)$
		2^+	$D_2^*(2460)$		$D_{s2}^*(2573)$		$B_2^*(5747)$	$B_{s2}^*(5840)$
X	$\frac{3}{2}^-$	1^-						
		2^-						
X'	$\frac{5}{2}^-$	2^-	$D(2750)$ $\star$					
		3^-	$D(2760)$ $\star$		$D_{sJ}(2860)$ $\star$			

2 Arguments for the classification

The analysis of the doublets with either $\ell = \frac{1}{2}^+, \frac{3}{2}^\pm, \ldots$, or $n > 1$ is based on the mass and width experimental data collected in Tables 2 and 3. The $s_\ell^P = \frac{3}{2}^+$ charmed doublets are filled by $(D_1(2420), D_2^*(2460))$ and $(D_{s1}(2536), D_{s2}^*(2573))$ in the non-strange and strange sector, respectively; their widths are quite narrow, as expected for mesons with d-wave decays.

$(D_0^*(2400), D_1'(2430))$ and $(D_{s0}^*(2317), D_{s1}'(2460))$ can be identified with the members of the $s_\ell^P = \frac{1}{2}^+$ charm doublet, although they present intriguing features. The non-strange states follow the expectation of being broad, due to their s-wave strong decays. After the first evidences of broad $c\bar{q}$ states [11], the separate identification of the two states and the measurement of their masses and widths is due to Belle [12]. On the contrary, the strange partners, first observed in 2003 [13], are very narrow: they are below the DK (for $D_{s0}^*(2317)$) and D^*K (for $D_{s1}'(2460)$) thresholds, their isospin-conserving decays are kinematically forbidden, and

---

[1]The recently observed structures $D_J(3000)$ and $D_J^*(3000)$, mentioned in the text, are not included in the Table.

Table 2: Measured mass and width of the observed excited open charm mesons, as reported by the PDG [8] (with the states denoted by † omitted from summary tables), excluding the data on $D^{*0,+}(2600)$, $D^0(2750)$ and $D^{*0,+}(2760)$ which are from BaBar [9]; new experimental results on these states have also been provided by LHCb [10]. The widths of $D^{*+}(2600)$ and $D^{*+}(2600)$ are kept fixed in the experimental BaBar analysis [9]. The bounds are at 95% CL.

$c\bar{q}$	mass (MeV)	Γ (MeV)	$c\bar{s}$	mass (MeV)	Γ (MeV)
$D_0^{*0}(2400)$	2318 ± 29	267 ± 40			
$D_0^{*\pm}(2400)^\dagger$	$2403 \pm 14 \pm 35$	$283 \pm 24 \pm 34$	$D_{s0}^*(2317)$	2317.8 ± 0.6	< 3.8
$D_1'^0(2430)^\dagger$	$2427 \pm 26 \pm 25$	$384 \pm_{75}^{107} \pm 74$			
			$D_{s1}'(2460)$	2459.6 ± 0.6	< 3.5
$D_1^0(2420)$	2421.4 ± 0.6	27.4 ± 2.5			
$D_1^\pm(2420)$	2423.2 ± 2.4	25 ± 6	$D_{s1}(2536)$	2535.12 ± 0.13	$0.92 \pm 0.03 \pm 0.04$
$D_2^{*0}(2460)$	2462.6 ± 0.6	49.0 ± 1.3			
$D_2^{*\pm}(2460)$	2464.3 ± 1.6	37 ± 6	$D_{s2}^*(2573)$	2571.9 ± 0.8	17 ± 4
$D^0(2550)^\dagger$	$2539.4 \pm 4.5 \pm 6.8$	$130 \pm 12 \pm 13$			
$D^{*0}(2600)$	$2608.7 \pm 2.4 \pm 2.5$	$93 \pm 6 \pm 13$			
$D^{*+}(2600)$	$2621.3 \pm 3.7 \pm 4.2$	93 (fixed)	$D_{s1}^*(2700)$	2709 ± 4	117 ± 13
$D^0(2750)$	$2752.4 \pm 1.7 \pm 2.7$	$71 \pm 6 \pm 11$			
$D^{*0}(2760)$	$2763.3 \pm 2.3 \pm 2.3$	$60.9 \pm 5.1 \pm 3.6$			
$D^{*+}(2760)$	$2769.7 \pm 3.8 \pm 1.5$	60.9 (fixed)	$D_{sJ}(2860)$	$2863.2\pm_{2.6}^{4.0}$	58 ± 11
			$D_{sJ}(3040)^\dagger$	$3044 \pm 8\pm_5^{30}$	$239 \pm 35\pm_{42}^{46}$

the observed strong decays $D_s\pi^0$ and $D_s^*\pi^0$ violate isospin conservation. Their identification with the doublet (D_{s0}^*, D_{s1}') is supported by analyses of the radiative decays [14] and by lattice QCD studies [15]. A puzzling aspect is the mass degeneracy between the strange states and their non-strange partners. Another issue is the possible mixing between the two 1^+ states: in the case of non-strange mesons, Belle has determined a small mixing angle: $\theta \simeq -0.10$ rad [12].

$D_{sJ}(2860)$ and $D_{s1}^*(2700)$ in Table 1 were observed in the DK final state at the B factories [16, 17], and confirmed in pp collisions at the LHC [18]. The spin-parity $J^P = 1^-$ of $D_{s1}^*(2700)$ has been established studying the production in B decays. $D_{s1}^*(2700)$ and $D_{sJ}(2860)$ are also seen to decay to D^*K [19], hence they have natural parity $J^P = 1^-, 2^+, 3^-, \cdots$; the D^*K mode excludes the assignment $J^P = 0^+$ for $D_{sJ}(2860)$. Additional information comes from the ratios of decay rates [19]

$$\frac{\mathcal{B}(D_{s1}^*(2700) \to D^*K)}{\mathcal{B}(D_{s1}^*(2700) \to DK)} = 0.91 \pm 0.13 \pm 0.12 , \quad \frac{\mathcal{B}(D_{sJ}(2860) \to D^*K)}{\mathcal{B}(D_{sJ}(2860) \to DK)} = 1.10 \pm 0.15 \pm 0.19 , \quad (9)$$

where $D^{(*)}K = D^{(*)0}K^+ + D^{(*)+}K_S^0$. As discussed below, for $D_{s1}^*(2700)$ the ratio coincides with the result in the heavy quark limit if $D_{s1}^*(2700)$ is identified with the first radial excitation of $D_s^*(2112)$ [20]. The classification of $D_{sJ}(2860)$ is more uncertain. The resonance decays to both DK and D^*K, hence it may be identified with the lowest lying $n = 1$ state with either $J_{s\ell}^P = 1_{3/2}^-$, i.e. D_{s1}^* in the X doublet, or $J_{s\ell}^P = 3_{5/2}^-$, i.e. the state D_{s3} in the X' doublet. Another possibility is the identification with the radial excitation with $n = 2$ and $J_{s\ell}^P = 2_{1/2}^+$, i.e. the state $\tilde{D}_{s2}^*$ in the $\tilde{T}$ doublet. Allowed decay modes are into DK, $D_s\eta$, D^*K and $D_s^*\eta$. Considering the ratios of strong decay rates in the three possible cases, the identification of

$D_{sJ}(2860)$ with D_{s3} was proposed [21], which explains the quite narrow width as due to the f-wave decays. On the other hand, D_{s1}^* and $\tilde{D}_{s2}^*$ decay in p- and d- wave, respectively; therefore, the first one is expected to be broader, while a larger mass, $M(\tilde{D}_{s2}^*) \simeq 3.157$ GeV, is predicted by the quark model for the second one [22]. We shall return below to $D_{sJ}(2860)$.

A broad structure in the D^*K distribution was also observed, $D_{sJ}(3040)$ [19]. Absence of signal in the DK distribution suggests unnatural parity $J^P = 1^+, 2^-, 3^+, \cdots$. The lightest not yet observed states with these quantum numbers are the two $J^P = 2^-$ states of the $\ell = 2$ doublets, D_{s2} with $s_\ell^P = \dfrac{3}{2}^-$ and $D_{s2}'^*$ with $s_\ell^P = \dfrac{5}{2}^-$. $J^P = 3^+$ corresponds to a doublet with $s_\ell^P = \dfrac{7}{2}^+$, the mass of which is expected to be larger. In the case of radial excitations, the identification with the states with $n = 2$, $J^P = 1^+$, and $s_\ell^P = \dfrac{1}{2}^+$ (the meson $\tilde{D}_{s1}'$) or $s_\ell^P = \dfrac{3}{2}^+$ (the meson $\tilde{D}_{s1}$) is possible. In the heavy quark limit, the two $J^P = 1^+$ are expected to be broader than the two $J^P = 2^+$ states, hence $D_{sJ}(3040)$ is likely to be identified with one of the two axial-vector mesons. This justifies the classification of $D_{sJ}(3040)$ as one of the two states with $J^P = 1^+$, $n = 2$, proposed in Table 1. The properties of the corresponding spin and non-strange partners can be predicted accordingly [23].

The last four states in Table 1 are the non-strange $c\bar{q}$ mesons discovered by BaBar in $e^+e^- \to c\bar{c} \to D^{(*)}\pi X$ [9], with measured mass and width in Table 2, recently confirmed by LHCb [10]. The ratios

$$\frac{\mathcal{B}(D^{*0}(2600) \to D^+\pi^-)}{\mathcal{B}(D^{*0}(2600) \to D^{*+}\pi^-)} = 0.32 \pm 0.02 \pm 0.09 \;, \;\; \frac{\mathcal{B}(D^{*0}(2760) \to D^+\pi^-)}{\mathcal{B}(D^{*0}(2750) \to D^{*+}\pi^-)} = 0.42 \pm 0.05 \pm 0.11 \tag{10}$$

measured by BaBar can be used for the classification. Moreover, for the $D^{*+}\pi^-$ mode, information comes from the $\cos\theta_H$ distribution, with θ_H the angle between the primary pion π^- and the slow pion π^+ from the D^{*+} decay. For $D^*(2600)$, this distribution suggests natural parity, consistent with the observation in both $D\pi$ and $D^*\pi$. The $\sim \cos^2\theta_H$ distribution for $D^0(2550)$ is compatible with a $J^P = 0^-$ state. Babar suggested that $(D(2550), D^*(2600))$ compose the $\tilde{H}$, $J^P = (0^-, 1^-)$ doublet of $n = 2$ radial excitations of (D, D^*) mesons, while $(D(2750), D^*(2760))$, can be identified with the $\ell = 2$, $n = 1$ states [9], mainly from comparison with quark model results [24]. Since there are two possible doublets with $\ell = 2$, the identification with the $J^P = (2^-, 3^-)$ doublet would come together with the assignment $D_{sJ}(2860) = D_{s3}$, and in this case $D_{sJ}(2860)$ and $D^*(2760)$ represent corresponding states with and without strangeness. Other classifications have been proposed [25] and discussed [4].

Finally, other broad states, denoted as $D_J(3000)$ and $D_J^*(3000)$, have been recently observed in the region around 3000 MeV by LHCb in the final states $D^{*+}\pi^-$, $D^+\pi^-$ and $D^0\pi^+$ [10]. They are not included in this overview, as their assignment deserves a dedicated study.

The masses and widths of the beauty excited states, observed at LEP [26], Tevatron [27] and LHCb [28], are collected in Table 3.

Table 3: Mass and width (in MeV) of the observed open beauty excited mesons [8].

$b\bar{q}$	mass	Γ	$b\bar{s}$	mass	Γ
$B_1^0(5721)$	5723.5 ± 2.0		$B_{s1}^0(5830)$	5828.7 ± 0.4	
$B_2^{*0}(5747)$	5743 ± 5	$22.7^{+3.8+3.2}_{-3.2-10.2}$	$B_{s2}^{*0}(5840)$	5839.7 ± 0.6	$1.56 \pm 0.13 \pm 0.47$

3   Mass parameters

The assignments proposed in Table 1 are supported by the values of the HQ parameters: the average masses $\overline{M}_F$ in Eq. (5), the mass splitting Δ_F and the hyperfine splitting λ_F parameters in Eq. (7) that we collect in Table 4. Flavour symmetry implies that the mass splitting Δ_F is the same regardless of the heavy quark flavour of the doublets, and that the mass splitting λ_F between spin partners in a doublet is independ of the heavy flavour. Indeed, from the Lagrangian (3) and (6), one has:

$$\Delta_F^{(c)} = \Delta_F^{(b)} \quad , \quad \lambda_F^{(c)} = \lambda_F^{(b)} \quad .$$

The observed deviations, due to both light flavour and heavy quark mass effects, suggest the size of the higher order symmetry breaking terms: as an example, the strange quark mass effect is visible in $\overline{M}_F$.

Table 4: Spin averaged masses $\bar{M}_F$ (in MeV), mass splittings Δ_F (in MeV) and hyperfine splitting parameters λ_F (in MeV^2) defined in Eq.(5) and (7).

	$c\bar{u}$	$c\bar{d}$	$c\bar{s}$	$b\bar{u}$	$b\bar{d}$	$b\bar{s}$
$\overline{M}_H$	1971.45 ± 0.12	1975.12 ± 0.10	2076.4 ± 0.4	5313.7 ± 0.3	5313.8 ± 0.3	5403 ± 2
$\overline{M}_{\tilde{H}}$	2591.4 ± 3.3					
$\overline{M}_S$	2400 ± 28		2424.1 ± 0.5			
$\overline{M}_T$	2447.1 ± 0.5	2449.0 ± 1.6	2558.1 ± 0.5		5735.7 ± 3.2	5834.7 ± 0.5
$\overline{M}_{X'}$	2758.8 ± 2.3					
Δ_S	429 ± 28		347.7 ± 0.6			
Δ_T	475.7 ± 0.5	473.9 ± 1.6	481.7 ± 0.6		421.9 ± 3.2	431.7 ± 2.1
$\Delta_{X'}$	787.4 ± 2.3					
λ_H	$(262.3 \pm 0.2)^2$	$(261.2 \pm 0.2)^2$	$(270.9 \pm 0.6)^2$	$(246.8 \pm 1.2)^2$	$(245.9 \pm 1.2)^2$	$(256.3 \pm 6.4)^2$
$\lambda_{\tilde{H}}$	$(211.2 \pm 13.4)^2$					
λ_S	$(254 \pm 54)^2$		$(290.9 \pm 0.9)^2$			
λ_T	$(195 \pm 2)^2$	$(193 \pm 7)^2$	$(187.7 \pm 2.1)^2$		$(205 \pm 28)^2$	$(149.9 \pm 6.7)^2$
$\lambda_{X'}$	$(112 \pm 24)^2$					

Using the input from Table 1, predictions can be worked out for the masses of unobserved states, namely the missing $n = 1$ and $n = 2$, $J_{s_\ell}^P = (0^-, 1^-)_{1/2}$ charmed mesons, see Table 5. Moreover, in the HQ limit and using charm data, the beauty meson properties can be computed. For $F = \tilde{H}, S, T, X'$ and $\tilde{T}$, with the data in Table 4 predictions for beauty doublets can be worked out, Table 6. Noticeably, B_{s0}^* and B_{s1}' turn out to be below the BK and B^*K thresholds; they are expected to be very narrow, with main $B_s\pi^0$ and $B_s^*\pi^0$ decay modes [29, 30]. The masses of the resonances recently observed by CDF [31] and LHCb [32] in the $B\pi$ channel follow the expectations.

Table 5: Predicted mass and width (in MeV) of two not yet observed charm mesons, together with their spin partners.

		$\tilde{D}_{(s)}$ $(0^-, n=2)$	$\tilde{D}_{(s)}^*$ $(1^-, n=2)$	$D_{(s)2}'^*$ (2^-)	$D_{(s)3}$ (3^-)
$c\bar{q}$		$D(2550)$	$D^*(2600)$	$D(2750)$	$D(2760)$
$c\bar{s}$	mass	2643 ± 13	$D_{s1}^*(2700)$	2851 ± 7	$D_{sJ}(2860)$
	Γ	33.5 ± 3.3		20.5 ± 2.4	

Table 6: Predicted mass and width (in MeV) of doublets of excited beauty mesons. For the decay widths of B_{s0}^* and B_{s1}' see the text.

		$\tilde{B}_{(s)}(0^-, n=2)$	$\tilde{B}_{(s)}^*(1^-, n=2)$	$B_{(s)0}^*(0^+)$	$B_{(s)1}'(1^+)$	$B_{(s)2}'^*(2^-)$	$B_{(s)3}(3^-)$
$b\bar{q}$	M	5911 ± 5	5941 ± 3	5708 ± 23	5753 ± 31	6098 ± 2	6103 ± 3
	Γ	149 ± 15	186 ± 18	269 ± 58	268 ± 70	103 ± 8	129 ± 10
$b\bar{s}$	M	5997 ± 6	6027 ± 8	5707 ± 1	5766 ± 1	6181 ± 5	6186 ± 5
	Γ	76 ± 9	118 ± 14			57 ± 6	78 ± 7

4 Strong decays

Two-body heavy meson decays in final states comprising a light pseudoscalar meson can be analyzed using the Lagrangian (8). A prime role is played by the effective strong coupling constants, for which the following information is available.

g governs the strong transition among states in the H doublet. The measurement $\Gamma(D^{*\pm}) = 96 \pm 4 \pm 22$ KeV [8], recently improved by BaBar: $\Gamma(D^{*\pm}) = 83.5 \pm 1.7 \pm 1.2$ KeV [33], corresponds to the value in Table 7; it is larger than a set of theoretical results in the HQ limit and at finite m_Q [34, 35, 36], and agrees with more recent calculations [37].

h controls the decays $S \to HM$, and can be obtained using data on the $c\bar{q}$ doublet S, with $q = u, d$. From the widths of $(D_0^*(2400), D_1'(2430))$ in Table 2, the value in Table 7 can be derived, which agrees with QCD sum rule [35] and lattice QCD determinations [36]. The predicted widths of the corresponding beauty mesons are in Table 6.

h' is involved in $T \to HM$ decays, and can be determined from Table 2. The obtained value in Table 7 translates into a prediction for the $D_{s1}(2536)$ decay width: $\Gamma(D_{s1}(2536)) = 0.305 \pm 0.002$ MeV. The BaBar determination in Table 2 [38], is larger than this result, a possible consequence of the mixing with the axial-vector state $D_{s1}'(2460)$ [39]. In the case of the beauty T doublet, the width of the B_2^{*0} meson has been measured, giving $h' = 0.36 \pm 0.09$, with a $\mathcal{O}(30\%)$ deviation form the charm value. The computed widths of the $s_\ell^P = 3/2^+$ beauty states are: $\Gamma(B_1) = 13.6 \pm 0.6$ MeV, $\Gamma(B_{s1}) = 0.016 \pm 0.002$ MeV and $\Gamma(B_{s2}^*) = 0.9 \pm 0.1$ MeV, the last one compatible with the recent LHCb result [28].

$\tilde{g}$ governs the decays $\tilde{H} \to HM$, with $\tilde{H}$ the radial excitations of H. Observed states that fit in such a doublet, with and without strangeness, are $D(2550)$, $D^*(2600)$ and the strange one $D_{s1}^*(2700)$. From their measured widths we obtain the value in Table 7. The predicted width of the spin partner of $D_{s1}^*(2700)$ using the mass fixed in Sec. 3, is in Table 5, and the expected widths of the corresponding beauty resonances are in Table 6.

k. In the classification of $D_{sJ}(2860)$ as the $J^P = 3^-$ state of the X' doublet, the resonances $(D(2750), D^*(2760))$ fill the corresponding non strange doublet. From their mass and width we obtain the coupling $k = k_1 + k_2$ in Table 7. This allows to predict the width of the $D_{s2}'^*$, the spin partner of $D_{sJ}(2860)$, and of the analogous beauty state, see Tables 5 and 6. The results from other assignments to $D_{sJ}(2860)$ are discussed in [4].

Information comes from ratios of decay rates in which the dependence on the strong cou-

Table 7: Coupling constants in the effective Lagrangian (8), obtained from the experimental data and using the classification in Table 1.

g	h	h'	$\tilde{g}$	k
0.64 ± 0.075	0.56 ± 0.04	0.43 ± 0.01	0.28 ± 0.015	0.42 ± 0.02

plings cancels out. For a meson $F_{(s)}$ decaying to $P_{(s)} M$ and $P_{(s)}^* M$, these ratios are relevant:

$$
\begin{aligned}
R_\pi^{(F)} &= \frac{\mathcal{B}(F \to D^*\pi)}{\mathcal{B}(F \to D\pi)} \ , \\
R_K^{(F_s)} &= \frac{\mathcal{B}(F_s \to D^*K)}{\mathcal{B}(F_s \to DK)} \ , \ R_\eta^{(F_s)} = \frac{\mathcal{B}(F_s \to D_s\eta)}{\mathcal{B}(F_s \to DK)} \ , \ R_\eta^{*(F_s)} = \frac{\mathcal{B}(F_s \to D_s^*\eta)}{\mathcal{B}(F_s \to DK)} \ .
\end{aligned} \quad (11)
$$

$D^{(*)}\pi(K)$ indicates $D^{(*)0}\pi^+(K^+) + D^{(*)+}\pi^0(K_S)$ for charged states and to $D^{(*)0}\pi^0(K_S) + D^{(*)+}\pi^-(K^-)$ for neutral ones. Table 8 reports the predictions for $D^*(2600)$ and $D_{s1}^*(2700)$, identified with $\tilde{D}^*$ and $\tilde{D}_s^*$, respectively; for $D_2^{*0}(2460)$ and $D_{s2}^*(2573)$, and for $D^*(2760)$ and $D_{sJ}(2860)$ identified with D_3 and D_{s3}. A detailed discussion is in [4]. Here we only mention a few issues.

- For $D_{s1}^*(2700)$, the results in Table 8 agree with the measurement in Eq.(9) [19], supporting the classification of this state as $\tilde{D}_{s1}^*$.

- Identifying $D^*(2760)$ with D_3 and $D(2750)$ with its spin partner $D_2'^*$, one obtains the ratio $\frac{\mathcal{B}(D^{*0}(2760) \to D^+\pi^-)}{\mathcal{B}(D^{*0}(2750) \to D^{*+}\pi^-)}\big|_{X'} = 0.660 \pm 0.001$. On the other hand, in the hypothesis that $(D(2750), D^*(2760))$ fill the $(\tilde{D}_1', \tilde{D}_2^*)$ doublet, the result is $\frac{\mathcal{B}(D^{*0}(2760) \to D^+\pi^-)}{\mathcal{B}(D^{*0}(2750) \to D^{*+}\pi^-)}\big|_{\tilde{T}} = 0.563 \pm 0.001$. The measurement (10) does not discriminate between the two possibilities.

- If $D_{sJ}(2860)$ is identified with D_{s3}, the ratios in Table 8 do not compare favorably with the measurement in Eq.(9) [21]. A possible reason is the existence of the spin partner with very close mass, $M(D_{s2}^{*\prime}) = 2851 \pm 7$ MeV, difficult to resolve in the common D^*K decay mode. If the signal measured to give Eq.(9) includes the decay $D_{s2}^{*\prime} \to D^*K$, the actual measurement is the $D^{(*)}K$ sample produced from both the states, hence

$$
\bar{R}(2860) = \frac{\Gamma(D_{sJ}(2860) \to D^*K) + \Gamma(D_{s2}^{*\prime}(2851) \to D^*K)}{\Gamma(D_{sJ}(2860) \to DK)} \ ,
$$

  whose prediction is: $\bar{R}(2860) = 0.99 \pm 0.05$, compatible with (9).

- For the beauty system, the computed ratio R_K for B_{s2}^* is confirmed by the LHCb measurement: $R_K = (9.1 \pm 1.3 \pm 1.2) \times 10^{-2}$ [28].

5   Conclusions

Using the heavy quark symmetry as a guideline, the observed $c\bar{q}$ and $b\bar{q}$ mesons can be classified in doublets. Of course, finite heavy quark mass effects, such as those inducing a mixing between states with the same J^P belonging to different doublets, could distort the picture: their

Table 8: Computed ratios $R_M^{(F)}$.

$c\bar{q}$	R_π	$c\bar{s}$	R_{K^0}	R_η	R_η^*
$D^{*0}(2600)$	1.22 ± 0.01	$D_{s1}^*(2700)$	0.91 ± 0.03	0.195 ± 0.006	0.05 ± 0.01
$D_2^{*0}(2460)$	0.440 ± 0.001	$D_{s2}^*(2573)$	0.086 ± 0.002	0.018 ± 0.001	-
$D^{*0}(2760)$	0.514 ± 0.004	$D_{sJ}(2860)$	0.39 ± 0.01	0.132 ± 0.003	0.025 ± 0.001
$b\bar{q}$	R_π	$b\bar{s}$	R_K	R_η	R_η^*
$\tilde{B}^*$	1.63 ± 0.005	$\tilde{B}_s^*$	1.43 ± 0.015	0.132 ± 0.008	0.11 ± 0.015
B_2^*	0.87 ± 0.01	B_{s2}^*	0.07 ± 0.005	-	-
B_3	0.92 ± 0.005	B_{s3}	0.815 ± 0.006	0.103 ± 0.002	0.063 ± 0.003
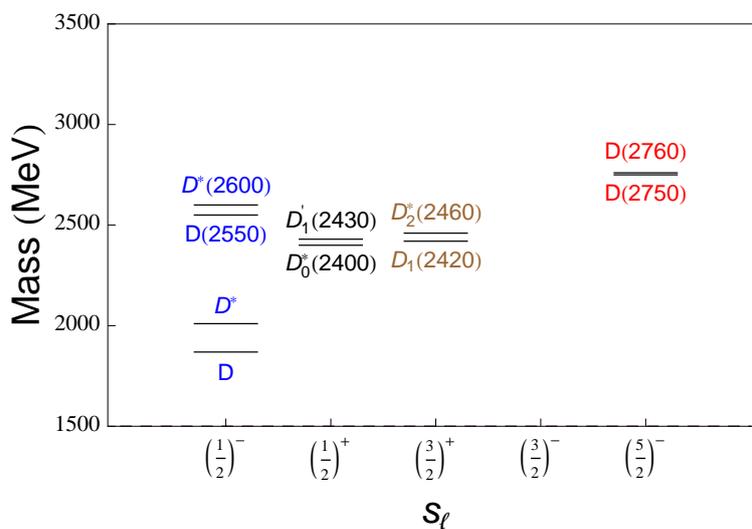
Figure 1: Spectrum of $c\bar{q}$ mesons organized in spin doublets. The structures denoted as $D_J(3000)^0$ and $D_J^*(3000)^0$ [10] are not included in the plot.

description in terms of the effective theory would require additional parameters. *A posteriori*, looking at data, one can estimate the size of such effects, and check the scaling rules and the main features determined by the heavy quark symmetry.

A comprehensive assignment is proposed in Table 1; in the case of charm, the spectrum is depicted in Figs.1 and 2. The properties of missing states are predicted accordingly. A wealth of new interesting information is expected from the ongoing experiments.

Acknowledgement
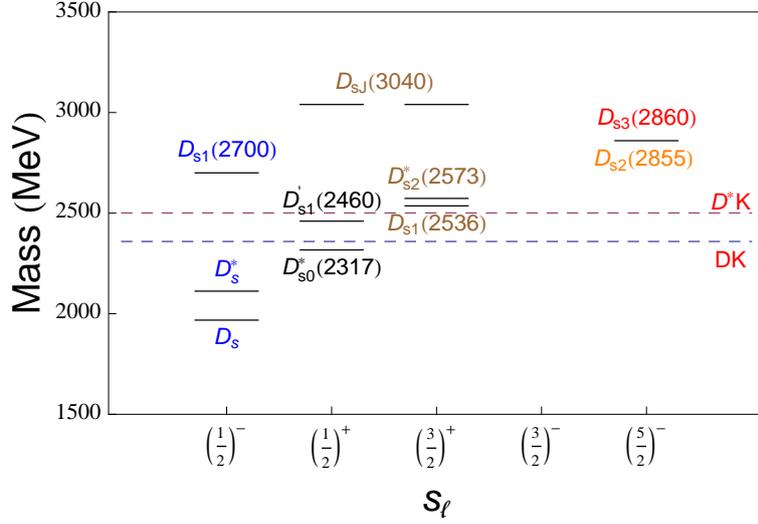
Figure 2: Spectrum of $c\bar{s}$ mesons organized in spin doublets. The horizontal dashed lines correspond to the DK and D^*K threshold. Two possible classifications for $D_{sJ}(3040)$ are shown. The predicted $D_{s2}(2855)$ is included in the plot.

References

[1] M. Neubert, Phys. Rept. **245**, 259 (1994); T. Mannel, In *St. Goar 1996, Heavy quarks at fixed target* 107-129; arXiv:hep-ph/9611411; F. De Fazio, in *At the Frontier of Particle Physics/Handbook of QCD*, ed. by M. Shifman (World Scientific, Singapore, 2001), page 1671, arXiv:hep-ph/0010007.

[2] N. Isgur and M. B. Wise, Phys. Lett. B **237**, 527 (1990).

[3] N. Isgur and M. B. Wise, Phys. Rev. Lett. **66**, 1130 (1991); M. Lu, M. B. Wise and N. Isgur, Phys. Rev. D **45**, 1553 (1992).

[4] P. Colangelo, F. De Fazio, F. Giannuzzi and S. Nicotri, Phys. Rev. D **86**, 054024 (2012).

[5] M. B. Wise, Phys. Rev. D **45**, 2188 (1992); G. Burdman and J. F. Donoghue, Phys. Lett. B **280**, 287 (1992); P. L. Cho, Phys. Lett. B **285**, 145 (1992); Phys. Rev. D **46**, 1148 (1992) [Erratum-ibid. D **55**, 5851 (1997)]; R. Casalbuoni, A. Deandrea, N. Di Bartolomeo, R. Gatto, F. Feruglio and G. Nardulli, Phys. Lett. B **299**, 139 (1993).

[6] A. V. Manohar and M. B. Wise, Camb. Monogr. Part. Phys. Nucl. Phys. Cosmol. **10**, 1 (2000).

[7] A. F. Falk and T. Mehen, Phys. Rev. D **53** (1996) 231.

[8] J. Beringer et al. (Particle Data Group), Phys. Rev. D **86**, 010001 (2012) and http://pdg.lbl.gov/.

[9] P. del Amo Sanchez *et al.* [The BABAR Collaboration], Phys. Rev. D **82**, 111101 (2010).

[10] R. Aaij *et al.* [LHCb Collaboration], JHEP **1309**, 145 (2013).

[11] S. Anderson *et al.* [CLEO Collaboration], Nucl. Phys. **A663**, 647 (2000); J. M. Link *et al.* [FOCUS Collaboration], Phys. Lett. **B586**, 11 (2004).

[12] K. Abe *et al.* [Belle Collaboration], Phys. Rev. D **69**, 112002 (2004).

[13] B. Aubert *et al.* [BABAR Collaboration], Phys. Rev. Lett. **90**, 242001 (2003); Y. Mikami *et al.* [Belle Collaboration], Phys. Rev. Lett. **92**, 012002 (2004); K. Abe *et al.*, Phys. Rev. Lett. **92**, 012002 (2004); D. Besson *et al.* [CLEO Collaboration], Phys. Rev. D **68**, 032002 (2003); L. Benussi [FOCUS Collaboration], Int. J. Mod. Phys. A **20**, 549 (2005); B. Aubert *et al.* [BABAR Collaboration], Phys. Rev. **D69**, 031101 (2004); P. Krokovny *et al.* [Belle Collaboration], Phys. Rev. Lett. **91**, 262002 (2003); P. Krokovny, AIP Conf. Proc. **717**, 475 (2004).

[14] P. Colangelo, F. De Fazio and A. Ozpineci, Phys. Rev. D **72**, 074004 (2005).

[15] D. Mohler, C. B. Lang, L. Leskovec, S. Prelovsek and R. M. Woloshyn, Phys. Rev. Lett. **111**, 222001 (2013).

[16] B. Aubert *et al.* [BABAR Collaboration], Phys. Rev. Lett. **97**, 222001 (2006).

[17] J. Brodzicka *et al.* [Belle Collaboration], Phys. Rev. Lett. **100**, 092001 (2008).

[18] R. Aaij *et al.* [LHCb Collaboration], arXiv:1207.6016 [hep-ex].

[19] B. Aubert *et al.* [BABAR Collaboration], Phys. Rev. D **80**, 092003 (2009).

[20] P. Colangelo, F. De Fazio, S. Nicotri and M. Rizzi, Phys. Rev. D **77**, 014012 (2008).

[21] P. Colangelo, F. De Fazio and S. Nicotri, Phys. Lett. B **642**, 48 (2006).

[22] M. Di Pierro and E. Eichten, Phys. Rev. D **64**, 114004 (2001).

[23] P. Colangelo and F. De Fazio, Phys. Rev. D **81**, 094001 (2010).

[24] S. Godfrey and N. Isgur, Phys. Rev. D **32**, 189 (1985).

[25] E. van Beveren and G. Rupp, Phys. Rev. D **81**, 118101 (2010); Z. G. Wang, Phys. Rev. D **83**, 014009 (2011).

[26] P. Abreu *et al.* [DELPHI Collaboration], Phys. Lett. B **345**, 598 (1995); D. Buskulic *et al.* [ALEPH Collaboration], Z. Phys. C **69**, 393 (1996); R. Barate *et al.* [ALEPH Collaboration], Phys. Lett. B **425**, 215 (1998); M. Acciarri *et al.* [L3 Collaboration], Phys. Lett. B **465**, 323 (1999); R. Akers *et al.* [OPAL Collaboration], Z. Phys. C **66**, 19 (1995).

[27] V. M. Abazov *et al.* [D0 Collaboration], Phys. Rev. Lett. **99**, 172001 (2007). T. Aaltonen *et al.* [CDF Collaboration], Phys. Rev. Lett. **102**, 102003 (2009). T. Aaltonen *et al.* [CDF Collaboration], Phys. Rev. Lett. **100**, 082001 (2008). V. M. Abazov *et al.* [D0 Collaboration], Phys. Rev. Lett. **100**, 082002 (2008).

[28] R. Aaij *et al.* [LHCb Collaboration], Phys. Rev. Lett. **110**, 151803 (2013).

[29] P. Colangelo and F. De Fazio, Phys. Lett. B **570**, 180 (2003).

[30] P. Colangelo, F. De Fazio and R. Ferrandes, Mod. Phys. Lett. A **19**, 2083 (2004); P. Colangelo, F. De Fazio and R. Ferrandes, Phys. Lett. B **634**, 235 (2006).

[31] T. A. Aaltonen *et al.* [CDF Collaboration], arXiv:1309.5961 [hep-ex].

[32] [LHCb Collaboration], LHCb-CONF-2011-053.

[33] J. P. Lees *et al.* [BaBar Collaboration], Phys. Rev. Lett. 111, **111801** (2013) [Phys. Rev. Lett. **111** (2013) 111801]; J. P. Lees *et al.* [BaBar Collaboration], Phys. Rev. D **88**, 052003 (2013).

[34] P. Colangelo, G. Nardulli, A. Deandrea, N. Di Bartolomeo, R. Gatto and F. Feruglio, Phys. Lett. B **339**, 151 (1994); P. Colangelo, F. De Fazio and G. Nardulli, Phys. Lett. B**334**, 175 (1994); V. M. Belyaev, V. M. Braun, A. Khodjamirian and R. Ruckl, Phys. Rev. D **51**, 6177 (1995); D. Becirevic, B. Blossier, E. Chang and B. Haas, Phys. Lett. B **679**, 231 (2009).

[35] P. Colangelo, F. De Fazio, G. Nardulli, N. Di Bartolomeo and R. Gatto, Phys. Rev. D **52** (1995) 6422; P. Colangelo and F. De Fazio, Eur. Phys. J. C **4** (1998) 503.

[36] D. Becirevic, E. Chang and A. L. Yaouanc, arXiv:1203.0167 [hep-lat].

[37] D. Becirevic and A. L. Yaouanc, JHEP **9903** (1999) 021; B. El-Bennich, M. A. Ivanov and C. D. Roberts, Phys. Rev. C **83**, 025205 (2011); K. U. Can, G. Erkol, M. Oka, A. Ozpineci and T. T. Takahashi, Phys. Lett. B **719**, 103 (2013); D. Becirevic and F. Sanfilippo, Phys. Lett. B **721**, 94 (2013).

[38] J. P. Lees *et al.* [The BABAR Collaboration], Phys. Rev. D **83**, 072003 (2011).

[39] V. Balagura *et al.* [Belle Collaboration], Phys. Rev. D **77**, 032001 (2008).

Lectures on new physics searches in $B \to D^{(*)}\tau\nu_\tau$

Svjetlana Fajfer[1,2], Ivan Nišandžić[2]

[1]Department of Physics, University of Ljubljana, Jadranska 19, 1000 Ljubljana, Slovenia
[2]J. Stefan Institute, Jamova 39, P. O. Box 3000, 1001 Ljubljana, Slovenia

The Standard model's predictions for the rates for $B \to D^*\tau\nu_\tau$ and $B \to D\tau\nu_\tau$ differ from the experimental results. The difference might be accounted by the presence of new physics. The understanding of the non-perturbative QCD dynamics in the meson transitions is crucial in order to refine the searches for new physics effects. We give short introduction to heavy quark effective theory (HQET) and then investigate the most general set of lowest dimensional effective operators leading to helicity suppressed modifications of $b \to c$ (semi)leptonic transitions. The contributions of these operators to $B \to D^{(*)}\tau\nu_\tau$ decay amplitudes can be found by determining the differential decay rate, longitudinal D^* polarization fraction, $D^* - \tau$ opening angle asymmetry and the τ helicity asymmetry. We identify the size of possible new physics contributions constrained by the present $B \to D^{(*)}\tau\nu_\tau$ rate measurements and find significant modifications are still possible in all these observables. Then we discuss few models of new physics scenarios which can contribute in both decay modes.

1 Introduction

In these lecture notes we present the short introduction to theoretical aspects of semileptonic decays [1] of B mesons, with an emphasis on the search for New physics (NP) in $B \to D^{(*)}\tau\nu_\tau$ processes. The semileptonic transitions are driven by the charged current interactions that originate from the exchange of the W boson in the Standard Model (SM). In theories beyond Standard Model (BSM), new particle could affect the physics of the decays as well. We explore these possibilities in subsequent sections.

The semileptonic decays have played significant role in the history of the particle physics, providing the basis for the construction of the SM. The four fermion interaction (Fermi's theory) was constructed as model of beta decays of nuclei. It has been further modified to include the parity violation through $V - A$ interactions [2], [3] and strangeness changing decays (Cabbibo mixing [4]). The theory breaks down at sufficiently high energies as it contains the dimensionful coupling parameter, and consequently a physical (electroweak) scale, v. The need for deeper, short distance understanding has been realized in a form of intermediate vector boson theory involving charged, massive spin one mediator. The developments that followed were leading towards the SM theory. The physics of the electroweak scale is currently probed at the Large Hadron Collider (LHC) experiments.

Following the observation of CP violation in weak interactions [5], Kobayashi and Maskawa (KM) [6] suggested that the CP violation can be explained with the introduction of the third generations of quarks. Consequently, the quark mixing matrix (known as Cabibbo-Kobayashi-

---

[1]involving lepton(s) and a hadron in the final state

Maskawa (CKM) matrix) can be parametrized in terms of three angles and one imaginary phase. The imaginary phase cannot be absorbed through the redefinitions of the quark fields and is source of all CP violation in the SM. This mechanism has been experimentally confirmed to be the dominant origin of the CP violation (see e.g. [7] and references therein), which led to the Nobel prize awarded to Kobayashi and Maskawa in 2008. The semileptonic decays are used for the extraction of the corresponding CKM elements, e.g. Wolfenstein's parameters λ and A [22] are precisely determined from the $K \to \pi\ell\nu$ and $b \to c\ell\nu$ transitions respectively. The underlying assumption is that these processes are fully described by the SM.

The CKM fits show impressive agreement with the KM mechanism, see e.g. [9], [10]. It is, however, worth to note that the fit gets significantly worse when the results of branching ratio of tauonic $B \to \tau\nu$ decay is included [1], [9], [10].

B physics provides some stringent tests of the SM at low energies. Recent measurements of $\mathcal{B}(B_s \to \mu^+\mu^-)$ and CP violation in $B_s \to J/\psi\phi$ decays considerably constrain contributions of NP to these observables. Semileptonic B decays play an important role in B physics, as their branching ratios are rather large and allow for extensive experimental studies. The decays are schematically represented by the diagram in the Fig. 1. The inclusive $B \to X_c\ell\nu$ and exclusive (with $D^{(*)}$ in the final state) processes are used for determination of V_{cb} matrix element. Inclusive determination uses the differential decay spectrum of final lepton's energy and hadronic, q^2 spectrum. It relies on operator product expansion (OPE) and Heavy Quark Effective Theory (HQET), [23], [24]. Average result of inclusive determinations is given in [1], $|V_{cb}| = (41.9 \pm 0.7) \cdot 10^{-3}$. Exclusive determinations also rely on HQET. In the infinite quark mass limit, all form factors are given by Isgur-Wise function, the function of product of four-velocities of B and $D^{(*)}$ mesons. Heavy Quark Symmetry defines normalization rate at $w = 1$ a point of maximal momentum transfer, $q^2 = (m_B - m_{D^{(*)}})^2$ and V_{cb} is obtained from extrapolation to $w = 1$. Exclusive determinations are less precise at the present and give [1] $|V_{cb}| = (39.6 \pm 0.9) \times 10^{-3}$.

Recently, there has been an increased interest in study of NP effects in semileptonic decays of B mesons involving tau leptons in the final state after the BaBar Colalboration published the results that show the excess in the following ratios [25]

$$\begin{align}
\mathcal{R}^*_{\tau/\ell} &= \mathcal{B}(B \to D^*\tau\nu)/\mathcal{B}(B \to D^*\ell\nu) = 0.332 \pm 0.030 \,, \tag{1} \\
\mathcal{R}_{\tau/\ell} &= \mathcal{B}(B \to D\tau\nu)/\mathcal{B}(B \to D\ell\nu) = 0.440 \pm 0.072 \,. \tag{2}
\end{align}$$

Both results are consistent with measurements previously performed by Belle Collaboration [26]. The BaBar's results turned out to be larger than the SM predictions $\mathcal{R}^{*,\text{SM}}_{\tau/\ell} = 0.252(3)$ [43] and $\mathcal{R}^{\text{SM}}_{\tau/\ell} = 0.296(16)$ [13], [43] with $3.4\,\sigma$ significance when the two observables are combined [42]. The eventual confirmation of these result might point to effects of NP in $b \to c\ell\nu$ transitions. We interpret these results as signs of the NP and correspondingly study the NP contributions through the effective field theory formalism. Consequently we discuss several specific models that can produce the specific effective higher dimensional operators.

Some of leading questions in the flavour physics are related to so called SM *flavour puzzle*. The flavour parameters (masses, mixing angles and a KM phase) are hierarchical; the quark masses span several orders of magnitude and are all (except the top's mass) much smaller than the electroweak scale. Since the *SM* can be taken as an effective description of physics at low energies, its Lagrangian may be supplemented with dimension six quark flavour changing operators that parametrize the FCNCs which appear at subleading order in the SM. If the NP has generic flavour structure such that the dimensionless couplings in these operators are of

order $\mathcal{O}(1)$ then the measurements of $FCNC$ observables constrain the scale of new physics to be bigger than $\sim 10^2 \cdots 10^4$ TeV [7]. However, the unnaturalness of the Higgs boson mass parameter is widely believed to be a problem which seeks for the resolution at the scale of around one TeV. Thus, if the new physics that solves the hierarchy problem exists at this scale, then it is constrained to have non-generic structure with couplings that resemble the SM. If this is the case, there is so called NP *flavour puzzle*.

There are several ways of dealing with the flavour violations in the NP models. One possibility is that of an Natural Flavour Conservation (NFC). As an example, the procedure of diagonalization of the mass matrices in the SM leaves the Yukawa couplings of quarks to Higgs boson flavour diagonal. Introduction of the second scalar doublet is theoretically well motivated for several reasons (see [12]). However it leads to appearance of two Yukawa matrices which are in general not simultaneously diagonalizable. Weinberg and Glashow [20] and Paschos [21] noted that if the quark of given helicity and charge has Yukawa interactions with only one Higgs doublet, FCNC Yukawa interactions are avoided at Lagrangian level. This can be achieved by the imposing the new discrete symmetries (for the most recent review of 2HDMs see e.g. [12]. The NP models in which all flavour and CP violation (in physical basis) originates from the CKM matrix belong to the class of models that satisfy Minimal Flavour Violation (MFV), [15], [16], see also lectures [17]. Within this criterion it is possible to relate the flavour violation for different sectors (e.g. FCNCs in processes involving B and K mesons [16]). We return to these scenarios through some specific examples later. The lectures are divided in the following sections: after introduction, sec. 2 describes parametrization of the amplitudes and form factors, sec. 3 introduces basic elements of heavy quark effective theory. In sec. 4 and 5 we consider the possible effects of the charged scalars from 2HDMs that couple more strongly to massive tau leptons and whose impact on the semileptonic processes involving the light lepton in final state is negligible. In sec. 6 we discuss the leptoquark model with the particular phenomenological ansatz for Yukawa couplings with leptons and quarks. The particular form of the ansatz can be consistently embedded into realistic GUT model.

2 Parametrization of the amplitudes and form factors

2.1 $B \to D\ell\nu_\ell$

The amplitude for the process $B \to D\ell\nu$ is given by product of matrix elements of the vector minus axial $(V - A)$ quark (hadronic) current $H_\mu \equiv \bar{c}\gamma_\mu(1 - \gamma_5)b$ between the B and D meson states and leptonic $V - A$ current, $L_\mu = \bar{l}\gamma_\mu(1 - \gamma_5)\nu_l$ between states of vacuum and $l - \nu$ pair,

$$\mathcal{A} = \frac{G_F}{\sqrt{2}}V_{cb}\langle l(k_1), \bar{\nu}_l|L_\mu|0\rangle \times \langle D(p')|H^\mu|\bar{B}(p)\rangle. \tag{3}$$

Both $\bar{B}(b\bar{q})$ and $D(c\bar{q})$ mesons are pseudoscalars ($J^P = 0^-$), so the the matrix element of the axial current between states B and D vanishes, due to the conservation of parity in QCD. It is easy to understand this fact if we note that the axial current changes sign under parity transformations, so that overall matrix element changes sign. The matrix element of the vector current needs a non-perturbative QCD evaluation. We may use the Lorentz covariance to parametrize it in terms of *form factors*

$$\langle D(p')|V^\mu|\bar{B}(p)\rangle = f_+(q^2)(p + p')^\mu + f_-(q^2)(p - p')^\mu, \tag{4}$$

where the squared transferred momentum varies in the range $m_l^2 \leq q^2 \leq (m_B - m_D)^2$. Alternatively, the matrix element can be parametrized by:

$$\langle D(p_D)|\bar{c}\gamma^\mu b|\bar{B}(p_B)\rangle = \left(p_B^\mu + p_D^\mu - \frac{m_B^2 - m_D^2}{q^2}q^\mu\right)f_+(q^2) + \frac{m_B^2 - m_D^2}{q^2}q^\mu f_0(q^2), \qquad (5)$$

and the form factor $f_0(q^2)$ is suppressed in the case of light lepton, as can be seen from the formula for the decay rate:

$$\begin{aligned}
\frac{d\Gamma}{dq^2}(B \to D\ell\bar{\nu}_\ell) =& \frac{G_F^2|V_{cb}|^2}{192\pi^3 m_B^3}\left(1 - \frac{m_l^2}{q^2}\right)^2\lambda^{1/2}\left[\lambda\left(1 + \frac{m_l^2}{2q^2}\right)f_+(q^2)^2\right. \\
& \left. + \frac{3}{2}\frac{m_l^2}{q^2}(m_B^2 - m_D^2)^2 f_0(q^2)^2\right],
\end{aligned} \qquad (6)$$

where function λ is given by $\lambda(m_B^2, m_D^2, q^2) = (m_B^2 - m_D^2 - q^2)^2 - 4m_D^2 q^2$. Also, in order to avoid the spurious pole at $q^2 = 0$, the kinematic constraint $f_+(0) = f_0(0)$ is implied.
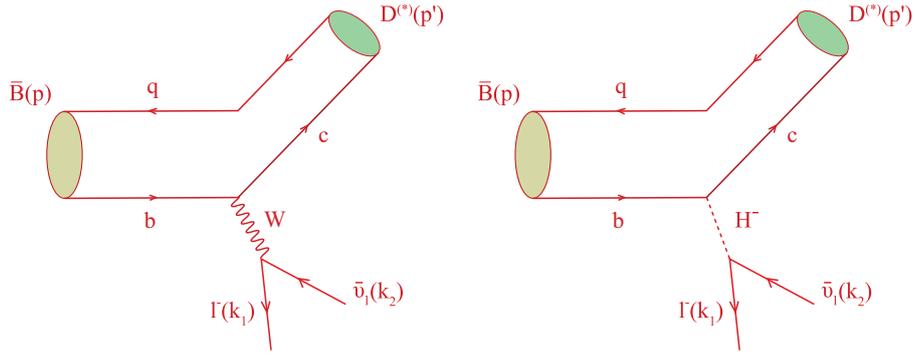
Figure 1: Diagrams contributing to the semileptonic B decays: SM exchange of W boson (left) and the exchange of the charged Higgs boson from the extended scalar sector (right)

In models that include charged scalar, the matrix element of scalar density is used $\langle D|\bar{c}b|B\rangle$. We may use the (anomalous Ward's) identity

$$q_\mu \langle D|\bar{c}\gamma^\mu b|B\rangle = (m_b - m_c)\langle D|\bar{c}b|B\rangle, \qquad (7)$$

to derive the formula for scalar density:

$$\langle D|\bar{c}b|B\rangle = \frac{m_B^2 - m_D^2}{m_b - m_c}f_0(q^2). \qquad (8)$$

In the formula for decay rate, this term is also suppressed by m_l^2/q^2, so that charged scalars do not influence the decays involving light leptons.

Recently Fermilab Lattice and MILC Collaborations [28] performed the calculation of $f_+(q^2)$

and $f_0(q^2)$ form factors in $2 + 1$ lattice QCD using the Fermilab's action [27]. The results are presented in the Fig. 1. in [28]. They calculate the following two observables:

$$R(D) = 0.316(12)(7)$$
$$P_L(D) = 0.325(4)(3).$$
(9)

Also, authors of the Ref. [29] find the similair result ($R(D) = 0.31 \pm 0.02$) by combining the experimental and theoretical input.

2.1.1 $B \to D^* \ell \nu$

The matrix elements of the $V - A$ current between the pseudo-scalar $\bar{B}$ and vector D^* mesons depend on four independent form factors, $V(q^2)$, $A_0(q^2)$, $A_1(q^2)$ and $A_2(q^2)$

$$\langle D^*(p', \epsilon_\alpha) | \bar{c}\gamma_\mu b | B(p) \rangle = \frac{2iV(q^2)}{m_B + m_{D^*}} \epsilon_{\mu\nu\alpha\beta} \epsilon^{*\nu} p^\alpha p'^\beta ,$$
(10a)

$$\langle D^*(p', \epsilon_\alpha) | \bar{c}\gamma_\mu \gamma_5 b | B(p) \rangle = 2m_{D^*} A_0(q^2) \frac{\epsilon^* \cdot q}{q^2} q_\mu + (m_B + m_{D^*}) A_1(q^2) \left(\epsilon_\mu^* - \frac{\epsilon^* \cdot q}{q^2} q_\mu \right)$$
$$- A_2(q^2) \frac{\epsilon^* \cdot q}{m_B + m_{D^*}} \left((p + p')_\mu - \frac{m_B^2 - m_{D^*}^2}{q^2} q_\mu \right) .$$
(10b)

The calculation of the matrix element of $V - A$ current in $B \to D^*$ transition turns out to be untrivial problem in Lattice QCD and results are unavailable at this moment. However, we may learn something about these form factors by using the HQET, which is the topic of the next section. We note that the form factor $A_0(q^2)$ does not enter the decay rates of the decays that involve the leptons of negligible mass (electron, muon). It is important to learn more about this form factor from the non-perturbative QCD, as it may hide the resolution for the current disagreement with the experiment.

3   Heavy quark effective theory and B decays

In this section we present the short introduction to Heavy quark symmetry and corresponding effective theory. More detailed and complete expositions of the subject can be found in numerous reviews. Clear exposition is given by [34], where also the higher order corrections are explained.

The degrees of freedom (fields) of Quantum Chromodynamics (QCD) at short distance are quarks and gluons. Lagrangians that describe the phenomena change through Renormalization Group (RG) transformations. This is the leading idea of Wilsonian effective field theory. The important feature of the QCD is asymptotic freedom[2]. At short distances, or equivalently in processes characterized by high momentum transfer, the effective gauge coupling becomes weak and the perturbative methods of calculation are well applicable. In deep infra-red, instead of gluons and quarks it is often more useful to define the theory in terms of another effective degrees of freedom. Such Lagrangians are based on some approximate symmetries of QCD. In principle, it is possible to match them to fundamental QCD Lagrangian, but because QCD is genuine strongly coupled theory at large distances, this is rarely possible in practice.   At

---

[2]This property is in four dimensions unique to the non-Abelian theories, QCD being an example.

the energy scales smaller than approximately $\Lambda_{QCD} = 0.2\,GeV$, new complex structures arise which are intractable to analytical calculation tools. Such a phenomenon is confinement of gluons and quarks. The hadronic properties are therefore described within QCD using the numerical calculations on space-time lattices.

On the other hand, the progress has been made by discovering the approximate symmetries of the hadronic systems; the earliest example being the isospin symmetry. This is approximate symmetry that arises due to the difference in mass of up and down quarks, $m_u - m_d$ much smaller than the characteristic QCD scale. Another example is chiral symmetry $SU(2)_L \times SU(2)_R$, the approximate symmetry of QCD that originates from the observation that masses of both u and d quarks are much smaller than the QCD scale. The treatment simplifies by going to the effective theory where $m_{u,d}$ are set to zero. Chiral symmetry is spontaneously broken in reality, but the resulting effective theory (Chiral Perturbation Theory) allows systematic calculations of corrections of order $m_{u,d}/\Lambda_{QCD}$.

In this chapter we will explain the basic physical picture of HQET, which we construct when we recognize the new spin-flavour symmetry of QCD of the systems containing one heavy quark (c or b). We will be interested in the hadron that contains a heavy quark whose mass $m_Q \gg \Lambda_{QCD}$ and light degrees of freedom which we denote light cloud (complicated cloud of light quarks and soft gluons[3]). In such hadron, and here we will consider mesons, mass becomes rather irrelevant for the non-perturbative dynamics of the light cloud. Exchange of the momentum between light cloud and heavy quark are of the order of Λ_{QCD} and the changes in four-velocity[4] of heavy quark are of order Λ_{QCD}/m_Q, so quark can be modelled as static source of colour with conserved velocity. The creation of heavy quark-antiquark pairs is absent. This also means that light cloud does not probe the relativistic degrees of freedom of heavy quark, so its spin and colour magnetism decouple.

It is then instructive to construct the effective theory in which m_Q can be taken to infinity while keeping the velocity of heavy quark fixed. Flavour of heavy quark can be changed by the interaction with some external current (i.e. through W boson field) but as long as the new flavour is also heavier than the QCD scale, light cloud stays the same. This observations still does not allow us to calculate the properties of the light cloud, but is useful in finding the connections between the properties of different mesons containing heavy quarks. Also, the systematic method of obtaining the corrections of order $1/M_Q$ will be provided. The situation is reminiscent of the well known observation in atomic physics in which chemical properties of the atoms are independent on the isotope of the nucleus. The only parameters that matters is electric charge of nucleus, while its spin and mass decouple, up to some required precision.

3.1   HQET Lagrangian

The HQET is constructed to give simple description of processes in which heavy quark interacts with the light quark by the exchange of soft gluons. The high energy scale (cutoff) of this theory is of order m_Q. Momentum of heavy quark is

$$p_Q^\mu = p_M^\mu - q^\mu = m_Q v^\mu + k^\mu \tag{11}$$

where p_M is momentum of meson, q^μ is momentum of the light cloud, and we define the residual momentum as $k^\mu = (m_M - m_Q)v^\mu - q^\mu$, much smaller than the m_Q. Velocity is normalized

---

[3]Light cloud is also called "brown muck" in some literature.
[4]In the rest of the text the four-velocity is simply denoted as velocity.

to $v^2 = 1$ in our metric convention. The velocity of the heavy quark is $v_Q^\mu = \frac{p_Q^\mu}{m_Q} = v^\mu + \frac{k^\mu}{m_Q}$ and we notice that in the limit $m_Q \to \infty$ meson travels at the same four-velocity as heavy quark. This means that the interaction with the light cloud leaves the velocity of heavy quark conserved.

Let us approach to construction of HQET by writing the heavy quark field in the following form:

$$Q(x) = e^{-m_Q v \cdot x}[Q_v(x) + \mathcal{Q}_v(x)], \tag{12}$$

where new fields are defined as

$$\begin{aligned} Q_v(x) &= e^{m_Q v \cdot x}\frac{1 + \slashed{v}}{2}Q(x), \\ \mathcal{Q}_v &= e^{m_Q v \cdot x}\frac{1 - \slashed{v}}{2}Q(x). \end{aligned} \tag{13}$$

Notice that fields $Q_v(x)$ and $\mathcal{Q}_v(x)$ are constrained by:

$$\slashed{v}Q_v(x) = Q_v(x), \ \ \slashed{v}\mathcal{Q}_v(x) = -\mathcal{Q}_v(x). \tag{14}$$

Field $Q_v(x)$ produces the effects at leading order, whereas the field $\mathcal{Q}_v$ produces the $1/m_Q$ effects. We work in Dirac basis of gamma matrices, in which $Q(x)_v$ is upper component of quark Dirac spinor, as it can be seen from first equation in (13), because the matrix $(1 + \slashed{v})/2$ becomes $(1 + \gamma_0)/2$, in the rest frame of heavy quark.

Field $Q(x)$ annihilates heavy quark with velocity v, but does not create antiquark. This field is called "large component". Since in the HQET the creation of heavy quark-antiquark pairs is absent, quark and antiquark live in totally different regions in momentum space, infinitely far away in the limit $m_Q \to \infty$. For simplicity, we will now deal with one quark field only, although everything can be done with antiquark also; the only changes are $v \to -v$ and $Q_v \to \mathcal{Q}_v$. In that case the effects of the quark component are absent [31].

Let us insert the expansion (12) into the relevant kinetic part of QCD Lagrangian to get:

$$\begin{aligned} \mathcal{L} &= \bar{Q}(i\slashed{D} - m_Q)Q(x) \\ &= \bar{Q}_v iv \cdot DQ_v - \bar{\mathcal{Q}}_v(iv \cdot D + 2m_Q)\mathcal{Q}_v + \bar{\mathcal{Q}}_v i\slashed{D}_\perp Q_v + \bar{Q}_v i\slashed{D}_\perp \bar{\mathcal{Q}}_v, \end{aligned} \tag{15}$$

where $D_\perp^\mu = D^\mu - v^\mu v \cdot D$. For illustration we give explicit derivation of the first term in above formula:

$$\begin{aligned} &\bar{Q}_v e^{m_Q v \cdot x}(i\slashed{D} - m_Q)e^{m_Q v \cdot x}Q_v \\ &= \bar{Q}_v[m_Q(\slashed{v} - 1) + i\slashed{D}]Q_v \\ &= \bar{Q}_v iQ_v \slashed{D}Q_v \\ &= \bar{Q}_v \frac{1 + i\slashed{v}}{2}i\slashed{D}\frac{1 + i\slashed{v}}{2}Q_v \\ &= \bar{Q}_v iv \cdot DQ_v. \end{aligned} \tag{16}$$

where third and fourth row are obtained by use of constraints (14). A remark is in order at this point. The QCD Lagrangian (15) is the effective Lagrangian whose parameters are defined at the scale of order of heavy quark mass, while the effects of short distance gluons are integrated

out. It is the fact that after integrating out short distance field modes a la Wilson, besides the running of dimensionless couplings, the tower of higher dimensional operators appears. We neglect these operators in the Lagrangian(15), but their effects can be introduced through radiative α_S corrections, which are perturbative due to the asymptotic freedom.

From the Lagrangian (15) we see that field $Q_v(x)$ is massless, while the field component $\mathcal{Q}_v$ has mass $2m_Q$. These massive degrees of freedom we integrate out. We could proceed by writing the generating functional for QCD with the Lagrangian (16), and then explicitly solve the path integral for field $\mathcal{Q}_v$, which would lead to the generating functional determined by the action functional containing the HQET Lagrangian. This method of derivation has been achieved in Ref. [39].

Instead of performing this procedure, we will use the observation that the integrating out the dynamical degree of freedom is equivalent up to overall normalization constant to solving the equation of motion for the variable and then substituting back to the Lagrangian, under the condition that the integral is of Gaussian type. It turns out that the renormalization constant is functional determinant that can be absorbed into the normalization of generating functional in gauge invariant manner, (see Ref. [39]).

We first insert the expansion (12) of the quark field into the QCD equation of motion that follows from the Lagrangian (15) and get the:

$$i\slashed{D}\mathcal{Q}_v + (i\slashed{D} - 2m_Q)Q_v = 0 \tag{17}$$

Multiplying the above equation by $P_- = \frac{1-\slashed{v}}{2}$ and solving for $\mathcal{Q}_v$ one gets:

$$\mathcal{Q}_v = \frac{1}{iv \cdot D + 2m_Q - i\epsilon} i\slashed{D}_\perp Q_v. \tag{18}$$

One can see that small component is really suppressed by powers of order $1/m_Q$, and after the insertion of this relation to the starting Lagrangian (15), one obtains the Lagrangian of HQET:

$$\mathcal{L}_{eff.} = \bar{Q}_v iv \cdot DQ_v + \bar{Q}_v i\slashed{D}_\perp \frac{1}{iv \cdot D + 2m_Q - i\epsilon} i\slashed{D}_\perp Q_v. \tag{19}$$

We can now expand the non-local second term from the above Lagrangian in powers of $1/m_Q$. We use the following identity

$$\bar{Q}_v \slashed{D}_\perp \slashed{D}_\perp = \bar{Q}_v D^2 Q_v - \bar{Q}_v (D \cdot v)^2 Q_v + \frac{g}{2}\bar{Q}_v \sigma^{\mu\nu} F_{\mu\nu} Q_v. \tag{20}$$

The resulting expansion up to first order in $1/m_Q$ is then the following one

$$\mathcal{L}_{HQET} = \bar{Q}_v\, i\, vDQ_v + \frac{1}{2m_Q}\bar{Q}_v D^\mu(\eta_{\mu\nu} - v_\mu v_\nu)D^\nu Q_v + \frac{g}{4m_Q}\bar{Q}_v \sigma^{\mu\nu} F_{\mu\nu} Q_v. \tag{21}$$

In the heavy quark rest frame ($\vec{v} = 0$) $1/m_Q$ terms correspond to non-relativistic kinetic energy term and QCD version of Pauli's term, respectively. In the infinite mass limit, only the first term in the Lagrangian is present and the HQ symmetries are evident. In the presence of two heavy quarks (b and c) the Lagrangian contains the sum of two corresponding terms. Since there is no dependence in m_Q, the $SU(2)$ flavour symmetry emerges. Coupling of the gluons to spin of the heavy quark is also contained in higher order term - we get the spin symmetry. One can conclude that the heavy quark symmetry group is then $SU(4)$. The new symmetry implies some immediate application in spectroscopy of heavy mesons, see e.g. [36].

3.2 Weak matrix elements and HQ

Let us now introduce the basic physical picture that allows the derivation of the relations between different matrix elements of electroweak currents.

In HQ limit the state of the meson can be factorized as a product of states corresponding to the state of heavy meson and light cloud

$$|M, j_Q, j_l\rangle \simeq |Q, j_Q\rangle |light\ cloud, j_l\rangle. \tag{22}$$

Imagine that we want to calculate the matrix element of any covariant weak current between two (not necessarily the same) states of pseudoscalar heavy mesons $\langle P', j_Q, j_l'|\Gamma|P, j_Q, j_l\rangle$, in the kinematical point in which there is no change in velocity, $v = v'$. Using the factorization we get

$$\begin{aligned}\langle P', j_Q, j_l'|\Gamma|P, j_Q, j_l\rangle &\simeq \langle Q, j_Q\,|\Gamma|Q', j_Q'\rangle\langle light\ cloud', j_l'\,|\ light\ cloud, j_l\rangle \\ &= \langle Q, j_Q\,|\Gamma|Q', j_Q'\rangle\delta_{j_l, j_l'}.\end{aligned} \tag{23}$$

While there is no velocity change, the state of the light cloud is left unchanged and the overlap (scalar product) of light cloud states is equal to 1. Also, if the flavour of the final heavy quark state is changed, the overlap of light clouds is still the same. In this way it is possible to connect matrix elements of the weak currents between different heavy mesons. In more general situation the overlap is not trivial but can be parametrized by the function of the product of velocities $w = v \cdot v'$.

The HQ symmetry alone will not let us discover anything about this function and some non-perturbative method of calculation, like QCD sum rules will be needed, but nevertheless relation (23) contains great deal of information [31].

3.3 Isgur-Wise function

In this section we use the basic idea from previous section and study the matrix elements of weak hadronic vector and axial currents between the meson states B and $D^{(*)}$. Following ref. [34], usual relativistic normalization of meson states is given by:

$$\langle M(p')|M(p)\rangle = 2E(2\pi)^3\delta^3(\vec{p} - \vec{p'}). \tag{24}$$

Since HQ symmetry relates heavy quarks at equal velocities, and the dependence of the mass of heavy quark is absent, it is more suitable to use the following mass independent normalization:

$$\langle M(v')|M(v)\rangle = \frac{2E}{m_M}(2\pi)^3\delta^3(\vec{p} - \vec{p'}), \tag{25}$$

with trivial relation to the conventional definition.

In HQ limit $|M(v)\rangle$ is only characterized by configuration of its light degrees of freedom.

Let us consider the elastic scattering of pseudoscalar meson $P(v) \to P(v')$ by an external vector current. Action of the current is to replace $v \to v'$ and the corresponding change in the momentum of the light cloud is:

$$q^2 \simeq \Lambda_{QCD}^2(v' - v)^2 \simeq \Lambda_{QCD}^2(v \cdot v' - 1). \tag{26}$$

Lorentz covariance imposes the parametrization of the current matrix element by the functions $h_\pm$ in the following way:

$$\langle P(v')|\bar{Q}_{v'}\gamma^\mu Q(v)|P(v)\rangle = h_+(w)\,(v+v')^\mu + h_-(w)(v-v')^\mu, \tag{27}$$

where $w = v \cdot v'$ is conveniently chosen Lorentz invariant variable. By contracting the both sides of above definition with $(v-v')_\mu$ and using the constraints (14), one finds that $h_-(w) = 0$. Let us now switch the notation and give function h_+ special name, $h_+(w) \equiv \xi(w)$. Due to the HQ flavour symmetry, the dynamics of light cloud does not differentiate between two different heavy quarks, so the following relation is also true:

$$\langle P'(v')|\bar{Q}_{v'}\gamma^\mu Q(v)|P(v)\rangle = \xi(w)\,(v+v')^\mu, \tag{28}$$

where P' is a different psudoscalar meson. The universal function $\xi(w)$ is called Isgur-Wise function, [38], and in HQ limit it describes any matrix element of the type $\langle M', j'_Q, j'_l|\Gamma|M, j_Q, j_l\rangle$, where Γ is arbitrary Dirac's covariant current.

For equal velocities, $j^\mu = \bar{Q}'_v\gamma^\mu Q_v$ is conserved current of heavy quark symmetry.[5] The corresponding conserved charges are the generators of this flavour symmetry:

$$N_{Q'Q} = \int d^3x j^0(x). \tag{29}$$

The diagonal elements are number operators and off-diagonal terms change one heavy quark to another $N_{Q'Q}|P(v)\rangle = |P'(v)\rangle$. It then follows that:

$$\langle P'(v)|N_{Q'Q}|P(v)\rangle = \langle P(v)|P(v)\rangle = 2v^0(2\pi)^3\delta^3(0), \tag{30}$$

and comparing to the relation (28) one concludes:

$$\xi(1) = 1, \tag{31}$$

which can be understood in terms of the heuristic physical picture we gave in the previous section. Isgur-Wise function can be visualized as the overlap of the light clouds boosted relative to each other by $v \cdot v'$.

The recoil energy of the meson P' in its rest frame is given by:

$$E = m_{P'}(v \cdot v' - 1) \tag{32}$$

so the kinematical point $v \cdot v' = 1$ is called zero recoil point. Now let us apply the above results to the usual parametrization of $B \to D$ form factors in the relativistic normalization of meson states (24):

$$\langle D(p')|\bar{c}\gamma^\mu b|B(p)\rangle = f_+(q^2)\Big[(p+p')^\mu - \frac{m_B^2 - m_D^2}{q^2}q^\mu\Big]$$
$$+ f_0(q^2)\frac{m_B^2 - m_D^2}{q^2}q^\mu, \tag{33}$$

---

[5]which can be checked from the leading term of the Lagrangian (21)

where the transferred momentum $q = p - p'$. Comparing (33) to (28) we get the following relations:

$$
\begin{aligned}
\xi(v \cdot v') &= \lim_{m \to \infty} R f_+(q^2) \\
&= \lim_{m \to \infty} R \Big[1 - \frac{q^2}{(m_B + m_D)^2} \Big]^{-1} f_0(q^2),
\end{aligned}
\tag{34}
$$

where the constant R is given as $R = \frac{m_B^2 + m_D^2 - q^2}{2 m_B m_D}$ and

$$
v \cdot v' = \frac{m_B^2 + m_D^2 - q^2}{2 m_B m_D}.
\tag{35}
$$

The limit $m \to \infty$ is taken in such a way that $v \cdot v'$ is kept fixed. The relations (34) are valid as long as the momentum of the light cloud is not large enough to probe the scale m_Q. This condition is fairly satisfied in the case of $B \to D$ transition, for which

$$
\Lambda_{QCD} \ll m_{b,c},
\tag{36}
$$

due to smallness of the factor

$$
(v \cdot v' - 1)_{max} = \frac{(m_B^2 - m_D^2)^2}{2 m_B m_D} = 0.6.
\tag{37}
$$

The new spin symmetry leads to relation between pseudoscalar and vector meson matrix elements, as well. The vector meson with longitudinal polarization ϵ_3 is related to pseudoscalar meson in the effective theory through the action of the spin operator:

$$
|V(v, \epsilon_3)\rangle = 2 S_Q^3 |P(v)\rangle.
\tag{38}
$$

It then follows that

$$
\langle V'(v', \epsilon_3) | \bar{Q}'_{v'} \Gamma Q_v | P(v) \rangle = \langle P'(v') | \bar{Q}'_{v'} (2 S^3 \Gamma) Q_v | P(v) \rangle.
\tag{39}
$$

We can evaluate the above expression in the rest frame of the final meson:

$$
\begin{aligned}
v'^\mu &= (1, 0, 0, 0), \\
\epsilon_3^\mu &= (0, 0, 0, 1), \\
S^3 &= \frac{1}{2} \gamma_5 \gamma^0 \gamma^3.
\end{aligned}
\tag{40}
$$

We then obtain the following commutation relations, for vector current:

$$
\begin{aligned}
2[S_{Q'}^3, V^0 - A^0] &= A^3 - V^3, \\
2[S_{Q'}^3, V^3 - A^3] &= A^0 - V^0, \\
2[S_{Q'}^3, V^1 - A^1] &= i(A^2 - V^2), \\
2[S_{Q'}^3, V^2 - A^2] &= -i(A^1 - V^1).
\end{aligned}
\tag{41}
$$

Combining (39) and (41) one relates the matrix elements of weak vector minus axial current between the psudoscalars meson to the Isgur-Wise function:

$$\langle V'(v',\epsilon)|\bar{Q}_v\gamma^\mu(1-\gamma_5)Q_v|P(v)\rangle = i\epsilon^{\mu\nu\alpha\beta}\epsilon_\nu^* v_\alpha v_\beta\, \xi(v\cdot v')- $$
$$[\epsilon^{*\mu}(v\cdot v'+1) - v^\mu\epsilon^*\cdot v]\,\xi(v\cdot v'). \tag{42}$$

where the completely antisymmetric Levi-Civita symbol is normalized as $\epsilon^{0123} = -1$. In more conventional parametrization vector minus axial matrix element is given by:

$$\langle D(p',\epsilon)|\bar{c}\gamma^\mu(1-\gamma_5)b|B(p)\rangle = \frac{2i\epsilon^{\mu\nu\alpha\beta}}{m_B+m_{D*}}\epsilon_\nu^* p'_\alpha p_\beta V(q^2)$$
$$- \left[(m_B+m_{D*})\epsilon^{*\mu}A_1(q^2) - \frac{\epsilon^*\cdot q}{m_B+m_D^*}(p'+p)^\mu A_2(q^2)\right] \tag{43}$$
$$- 2m_{D*}\frac{\epsilon^*\cdot q}{q^2}q^\mu A_0(q^2).$$

The function $A_3(q^2)$ is given as linear combination of form factors $A_1(q^2)$ and $A_2(q^2)$, subject to a constraint $A_3(0) = A_0(q^2)$ to cancel unphysical pole at $q^2 = 0$:

$$A_3(q^2) = \frac{m_B+m_D}{2m_{D*}}A_1(q^2) - \frac{m_B-m_{D*}}{2m_{D*}}A_2(q^2) \tag{44}$$

Comparing (42) to (43) one finds the following relations [40]:

$$\xi(v\cdot v') = \lim_{m\to\infty}R^*V(q^2) = \lim_{m\to\infty}R^*A_0(q^2) = \lim_{m\to\infty}R^*A_2(q^2)$$
$$\lim_{m\to\infty}R^*\left[1-\frac{q^2}{(m_B+m_{D*})^2}\right]^{-1}A_1(q^2), \tag{45}$$

where $R^* = 0.9$ is the D^* version of constant R in the case of D meson.

Caprini, Lellouch and Neubert obtained dispersive constraints on the form factors in $B \to (D^*)$ transitions fully exploiting the HQS including the $1/m$ corrections, [41]. The full expressions for form factors can be found in Appendix of Ref. [43], where the form factor $A_0(q^2)$ is also estimated. The recent results on the extraction of Isgur-Wise function from experimental results, as well as several other useful results are found in [58].

4 New physics and helicity amplitudes

Let us introduce the following effective Hamiltonian

$$\mathcal{H}_{\text{eff}} = \frac{4G_F V_{cb}}{\sqrt{2}}J_{bc,\mu}\sum_{\ell=e,\mu,\tau}\left(\bar{\ell}\gamma^\mu P_L\nu_\ell\right) + \text{h.c.}\,, \tag{46}$$

where $P_{L,R} \equiv (1\mp\gamma_5)/2$, while J_{bc}^μ is $b\to c$ charged current that includes the $V-A$ current and additional beyond SM current given by the derivative of (pseudo)scalar density, and contributes to the helicity suppressed amplitude and becomes important in the process with the tau lepton is in final state:

$$J_{bc}^\mu = \bar{c}\gamma^\mu P_L b + g_{SL}i\partial^\mu(\bar{c}P_L b) + g_{SR}i\partial^\mu(\bar{c}P_R b)\,. \tag{47}$$

The leptonic current has the structure as in the SM, however, using the equation of motion it can be shown that the above Hamiltonian can be realized in Two Higgs Doublet Models (2HDM) of the type II [12], where the dimensionful coupling $g_{SR} \sim -m_b \frac{\tan^2 \beta}{m_{H^+}^2}$.

It is convenient to introduce the helicity amplitudes formalism for a simpler calculations of decay distributions. Let the momenta of the initial B meson, final M (D or D^*) meson, the final final charged lepton and (anti)neutrino be p, p', k_1, k_2, respectively. The angle θ_l is defined as the angle between three momenta[6] of D^* and ℓ in the $\ell - \nu$ center of mass (CM) frame (see Fig. 2).

Let us introduce the lepton helicity amplitude, where m_l is the helicity of the lepton in $\ell \nu$ CM frame

$$L_{\lambda_l, m}(q^2, \cos \theta_\ell) = \tilde{\epsilon}_\mu(m)\langle l(k_1, m_l)\nu_\ell(k_2)|\bar{l}\gamma^\mu(1 - \gamma_5)\nu_\ell|0\rangle, \tag{48}$$

and hadronic helicity amplitude:

$$H^{m_M, m}(q^2, \cos \theta_\ell) = \tilde{\epsilon}_\mu^*(m)\langle M(p', \epsilon)|\bar{l}\gamma^\mu(1 - \gamma_5)\nu_\ell|\bar{B}(p)\rangle, \tag{49}$$

where $\tilde{\epsilon}(m)$ are polarization vectors of virtual W boson (in the case of SM) or, equivalently, of the lepton-neutrino pair. The m_M labels the polarization of the vector meson in the final state. The $\tilde{\epsilon}(m)$ satisfy the normalization and completeness relations

$$\tilde{\epsilon}^*(m)\tilde{\epsilon}(m') = g_{mm'}, \quad \sum_{mm'} \tilde{\epsilon}_\mu(m)\tilde{\epsilon}^*(m') = g_{\mu\nu}. \tag{50}$$

The polarization vectors of the meson M satisfy the analogous relations:

$$\epsilon_\alpha^*(m)\epsilon^\alpha(m') = -\delta_{mm'}, \quad \sum_{mm'} \tilde{\epsilon}_\alpha(m)\tilde{\epsilon}^*(m')\delta_{mm'} = -g_{\alpha\beta} + \frac{p_\alpha p'_\beta}{m_M^2}. \tag{51}$$

Then the SM amplitudes can be expressed as the following sum of products of helicity amplitudes, where m takes values $(t, 0, \pm)$

$$\mathcal{A}_{SM}^{\lambda_\tau, m_M} = \frac{G_F}{\sqrt{2}} \sum_m \eta_m H_{\lambda_M, m} L_{\lambda_\ell, m}. \tag{52}$$

The factor η_m takes the values $\eta_{\pm, 0} = 1$ and $\eta_s = -1$. In the same way we can calculate the hadronic helicity amplitudes for effective vector current (47) and observe that the additional terms in the current affect only H_{0t} helicity amplitude:

$$H_{0t} = H_{0t}^{SM}\left[1 + (g_{SR} - g_{SL})\frac{q^2}{m_b + m_c}\right]. \tag{53}$$

In Ref. [43] several observables were explored and the contributions from the Hamiltonian (46) is possible in all of them (for updated results see also [44]).

---

[6]for masses of the particles we reserve the explicit labels written in subscript
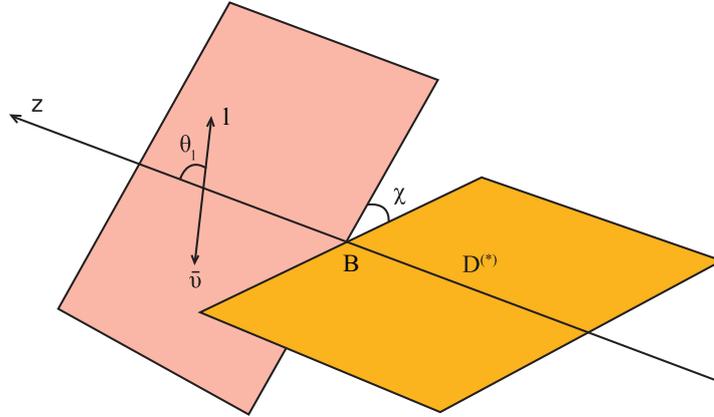
Figure 2: The relevant kinematical variables in the semileptonic B decay

In the following we shortly summarize the findings from the paper [43]. The helicity amplitudes H_{00} and H_{0t} contribute to amplitudes involving D_L^*'s, leading to a prediction for the longitudinal decay rate. One can also study the singly differential longitudinal rate ratio $R_L^*(q^2)$ defined analogously to $R^*(q^2)$ as described in [43]. A simple angular (opening angle) asymmetry is defined as the difference between partial rates where the angle θ between the D^* and τ three-momenta in the $\tau - \bar{\nu}_\tau$ rest-frame is bigger or smaller than $\pi/2$. In the decay modes with light leptons, this asymmetry (A_θ^ℓ) can be used to probe for the presence of right-handed $b \to c$ currents, since these contribute with opposite sign to $H_{\pm\pm}$ relative to the SM. In the tau modes, it is sensitive only to the real part of NP $g_{SR} - g_{SL}$ contributions and thus provides complementary information compared to the total rate (or R^*). On the other hand, the inclusive asymmetry A_θ integrated over q^2 is very small in the SM with $A_{\theta,\mathrm{SM}} = -6.0(8)\%$; for our NP benchmark point we obtain $A_{\theta,\mathrm{NP}} = 3.4\%$, but even values as low as -30% are still allowed. In [43] it was found that the tau spin asymmetry, defined as $A_\lambda(q^2) = [d\Gamma_\tau/dq^2(\lambda_\tau = -1/2) - d\Gamma_\tau/dq^2(\lambda_\tau = 1/2)]/[d\Gamma_\tau/dq^2]$, where $\lambda_\tau = \pm 1/2$ are tau helicities defined in $\tau\nu_\tau$ center of mass frame, can provide additional useful information.

5 Lepton flavour universality violation in B decays

During the last three years there has been a systematic disagreement between the experimental and SM predicted theoretical values for the branching ratio of $B \to \tau\nu$. The latest Belle collaboration result $\mathcal{B}(B^- \to \tau^-\bar{\nu}_\tau) = (0.72^{+0.27}_{-0.25} \pm 0.11) \times 10^{-4}$ [45] ameliorates somewhat the enduring tension with the measured value of $\sin 2\beta$ in the global CKM fit. However, the current world average experimental value still deviates from the SM prediction by 2.6σ significance if Gaussian errors are assumed [9].

The B meson coupling constant is the only hadronic parameter entering the theoretical branching ratio prediction. The errors of the most recent lattice QCD results are at the level of 5% [46] and already sub leading compared to the dominant parametric uncertainty due to $|V_{ub}|$. One can eliminate the V_{ub} dependence completely by introducing the LFU probing ratio $\mathcal{R}_{\tau/\ell}^\pi \equiv [\tau(B^0)/\tau(B^-)][\mathcal{B}(B^- \to \tau^-\bar{\nu}_\tau)/\mathcal{B}(\bar{B}^0 \to \pi^+\ell^-\bar{\nu}_\ell)] = 0.73 \pm 0.1$. This is to be compared to the SM prediction of $\mathcal{R}_{\tau/\ell}^{\pi,\mathrm{SM}} = 0.31(6)$ [42]. The measured value is more than a factor of 2

bigger - a discrepancy with 2.6σ significance if Gaussian errors are assumed.

The τ lepton in the final state of the (semi)leptonic B meson decays is particularly interesting due to the large τ mass which allows to probe parts of amplitudes in B meson (semi)leptonic decays which are not accessible if the final state contains only light leptons. Possible NP effects in the ratios $\mathcal{R}^{(*)}_{\tau/\ell}$ and $\mathcal{R}^{\pi}_{\tau/\ell}$ can be approached by using the effective Lagrangian approach [42], [43].

We interpret the above anomalies as a possible sign of lepton flavour universality violation (LFUV). The lepton flavour universality is one of the key predictions of the SM and is strongly constrained in the pion and kaon sectors, where it was found to be in excellent agreement with the SM. The signs of LFUV in B decays might be signs of NP which we parametrize through the following extension of the SM Lagrangian with a set of higher dimensional operators ($\mathcal{Q}_i$) that are generated at a NP scale Λ above the electroweak symmetry breaking scale $v = (\sqrt{2}/4G_F)^{1/2} \simeq 174$ GeV

$$\mathcal{L} = \mathcal{L}_{\text{SM}} + \sum_a \frac{z_a}{\Lambda^{d_a-4}}\mathcal{Q}_i + \text{h.c.} \tag{54}$$

The label d_a stands for the dimensions of the operators $\mathcal{Q}_a$, while z_a are the dimensionless Wilson coefficients (below we also use $c_a \equiv z_a(v/\Lambda)^{d_a-4}$). Two restrictions are enforced: (i) dangerous down-type flavour changing neutral currents (FCNCs) and (ii) LFU violations in the pion and kaon sectors are not to be generated at the tree level. The lowest dimensional operators that can modify $R^{(*)}_{\tau/\ell}$ and $\mathcal{R}^{\pi}_{\tau/\ell}$ are then

$$\mathcal{Q}_L = (\bar{q}_3\gamma_\mu\tau^a q_3)\mathcal{J}^\mu_{3,a}, \qquad\qquad \mathcal{Q}^i_R = (\bar{u}_{R,i}\gamma_\mu b_R)(H^\dagger\tau^a\tilde{H})\mathcal{J}^\mu_{3,a}, \tag{55a}$$

$$\mathcal{Q}_{LR} = i\partial_\mu(\bar{q}_3\tau^a H b_R)\sum_j\mathcal{J}^\mu_{j,a}, \qquad \mathcal{Q}^i_{RL} = i\partial_\mu(\bar{u}_{R,i}\tilde{H}^\dagger\tau^a q_3)\sum_j\mathcal{J}^\mu_{j,a}, \tag{55b}$$

where $\tau_a = \sigma_a/2$, $\mathcal{J}^\mu_{j,a} = (\bar{l}_j\gamma^\mu\tau_a l_j)$, $\tilde{H} \equiv i\sigma_2 H^*$ and i,j are generational indices.
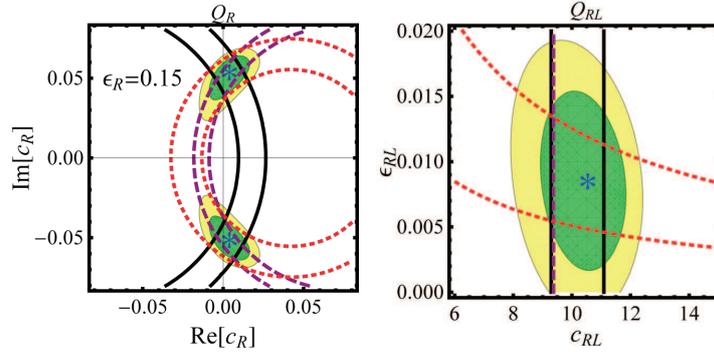
Figure 3: Preferred parameter regions for effective operators $\mathcal{Q}^i_R$ (left plot, as a funciton of complex c_R Wilson coefficient, and ϵ_R fixed to the best fit value), and for $\mathcal{Q}^i_{RL}$ (right plot, as a function of real c_{RL} Wilson coefficient and the mixing ratio ϵ_{RL}). The best fit points are marked with an asterisk.

We work in the down quark mass basis, where $q_i = (V^{ji*}_{CKM}u_{L,j}, d_{L,i})^T$, and charged lepton mass basis, $l_i = (V^{ji*}_{PMNS}\nu_{L,j}, e_{L,i})^T$. The requirement that there are no down-type tree-level FCNCs imposes flavour alignment in the down sector for the operators $\mathcal{Q}_L, \mathcal{Q}_{LR}$ and $\mathcal{Q}^i_{RL}$. An

additional possibility is to assume [43] the presence of new light invisible fermions, imitating the missing energy signature of SM neutrinos in the $b \to u_i\tau\nu$ decays. In the presence of general flavour violating NP, contributions to $b \to u$ transitions are not generally related to $b \to c$ transitions. In the case of $\mathcal{Q}_R^i$ for example, the SM expectations are rescaled by $|1 - c_R/2V_{cb}|^2$ in the case of $\mathcal{R}_{\tau/\ell}$ and by $|1 + \epsilon_R c_R/2V_{ub}|^2$ for $\mathcal{R}_{\tau/\ell}^\pi$. The parameters (c_i, ϵ_i) can be obtained by fitting the data using CKM inputs from the global fit as given in [42]. The results are presented in Fig. 3. Among existing NP models the two-Higgs doublet models (2HDMs) are obvious candidates to induce the $\mathcal{Q}_{RL}^i$ operators. Unfortunately, none of the 2HDMs with natural flavour conservation can simultaneously account for the three considered LFU ratios, while in ref. [42] a 2HDM with more general flavour structure has been considered explaining all the observed deviations. The results of the fits to 2HDM of Type III (this model has general flavour structure) are given in Ref. [61].

6 The leptoquark and $B \to D^{(*)}\tau\nu$

In this section we shortly describe effects of the leptoquark which residues in the SM representation $(3, 2, 7/6)$ on the $B \to D^{(*)}$ transition. This field can be embedded into **45** dimensional representation of $SU(5)$ which can help in providing the unification of the SM gauge couplings in non-supersymmetric framework. Also, this representation may correct the mass relations between the down-type quarks and charged leptons [47]. Out of four scalar leptoquarks that couple to leptons and quarks through renormalizable couplings, the two are viable: $(3, 2, 1/6)$ and $(3, 2, 7/6)$. Other possibilities, $(3, 1, -1/3)$ and $(3, 3, -1/3)$, can destabilize proton, [54]. Since the $(3, 2, 1/6)$ couples to right-handed neutrino, for minimality reasons we stick to the analysis of the impact of $\Delta \equiv (3, 2, 7/6)$ leptoquark [48], which couples to the SM fermions through the following interaction Lagrangian

$$\mathcal{L} = \bar{\ell}_R Y \Delta^\dagger Q + \bar{u}_R Z \tilde{\Delta}^\dagger L + h.c. \tag{56}$$

In the mass diagonal basis of the down-type quarks and charged leptons, the two isospin components of the scalar couple to quarks and leptons as following:

$$\begin{aligned}
\mathcal{L}^{(2/3)} &= (\bar{\ell}_R Y d_L)\, \Delta^{(2/3)*} + (\bar{u}_R[ZV_{PMNS}]\nu_L)\, \Delta^{(2/3)} + h.c, \\
\mathcal{L}^{(5/3)} &= (\bar{\ell}_R[YV_{CKM}^\dagger]u_L)\, \Delta^{(5/3)*} - (\bar{u}_R Z\ell_L)\, \Delta^{(5/3)} + h.c.
\end{aligned} \tag{57}$$

In the first two generations, the flavour violation is well fitted with the parameters CKM and PMNS, so in order to explain the BaBar's anomaly with the leptoquark contribution we may require the couplings of Δ to $\bar{b}\tau$ and not to $\bar{b}e$ and $\bar{b}\mu$ bilinear. Also, we require that only c quark and not u or t couple to neutrinos. This can be achieved by demanding the following Yukawa couplings *ansatz*:

$$Y = \begin{pmatrix} 0 & 0 & 0 \\ 0 & 0 & 0 \\ 0 & 0 & y_{33} \end{pmatrix}, \qquad ZV_{PMNS} = \begin{pmatrix} 0 & 0 & 0 \\ z_{21} & z_{22} & z_{23} \\ 0 & 0 & 0 \end{pmatrix}. \tag{58}$$

The $\Delta^{(5/3)}$ Yukawa couplings are related to these by the CKM and $PMNS$ rotations as follows:

$$YV_{CKM}^\dagger = y_{33} \begin{pmatrix} 0 & 0 & 0 \\ 0 & 0 & 0 \\ V_{ub}^* & V_{cb}^* & V_{tb}^* \end{pmatrix}, \qquad Z = \begin{pmatrix} 0 & 0 & 0 \\ \tilde{z}_{21} & \tilde{z}_{22} & \tilde{z}_{23} \\ 0 & 0 & 0 \end{pmatrix}. \tag{59}$$

After integrating out heavy Δ field and performing appropriate Fierz transformations, we derive the following Hamiltonian relevant for $b \to c\ell\nu$ transition

$$\mathcal{H} = \frac{4G_F}{\sqrt{2}} V_{cb} \Big[(\bar{\tau}_L \gamma^\mu \nu_L)(\bar{c}_L \gamma_\mu b_L) + g_S (\bar{\tau}_R \nu_L)(\bar{c}_R b_L) + g_T (\bar{\tau}_R \sigma^{\mu\nu} \nu_L)(\bar{c}_R \sigma_{\mu\nu} b_L) \Big], \tag{60}$$

including the SM contribution, where the dimensionless couplings $g_{S,T}$ are introduced through the definition: $g_S(m_\Delta) = 4g_T(m_\Delta) \equiv \frac{1}{4} \frac{y_{33} z_{23}}{2m_\Delta^2} \frac{\sqrt{2}}{G_F V_{cb}}$. This relation between Wilson's coefficients is valid at matching scale m_Δ which we set to the reference mass of $m_\Delta = 500$ GeV and changes due to the QCD anomalous dimensions of scalar and tensor operators. The scale dependence of the operators is cancelled in the leading logarithm approximation by the scale dependence of corresponding Wilson's coefficients:

$$
\begin{aligned}
g_S(m_b) &= \left(\frac{\alpha_S(m_b)}{\alpha_S(m_t)} \right)^{-\frac{\gamma_S}{2\beta_0^{(5)}}} \left(\frac{\alpha_S(m_t)}{\alpha_S(m_\Delta)} \right)^{-\frac{\gamma_S}{2\beta_0^{(6)}}} g_S(m_\Delta), \\
g_T(m_b) &= \left(\frac{\alpha_S(m_b)}{\alpha_S(m_t)} \right)^{-\frac{\gamma_T}{2\beta_0^{(5)}}} \left(\frac{\alpha_S(m_t)}{\alpha_S(m_\Delta)} \right)^{-\frac{\gamma_T}{2\beta_0^{(6)}}} g_S(m_\Delta).
\end{aligned}
\tag{61}
$$

Anomalous dimension coefficients are $\gamma_S = -8$, $\gamma_T = 8/3$ and coefficient $\beta_0^{(f)} = 11 - 2/3 n_f$, where n_f is a number of active quark flavours. The coefficients are then run to the beauty quark scale, $\mu = m_b = 4.2$ GeV, at which the matrix elements of hadronic currents are calculated. Difference between running of g_S and g_T modifies the original matching scale relation to

$$g_T(m_b) \simeq 0.14 \, g_S(m_b). \tag{62}$$
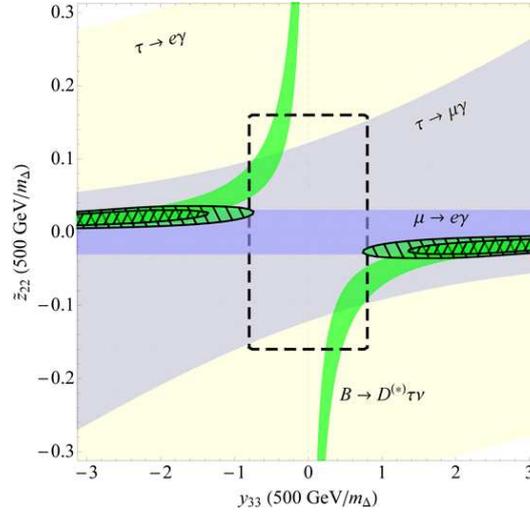
Figure 4: Constraints on the couplings to $b\tau$ (y_{33}) and to $c\mu$ ($\tilde{z}_{22}$) coming from the 1σ region of $\mathcal{R}_{\tau/\ell}^{(*)}$ (thin hyperbolic region), 90% CL upper bounds on $\tau \to \mu\gamma$ (dark band) and $\tau \to e\gamma$ (bright band). Muon magnetic moment upper bound is denoted by horizontal dashed lines. Vertical dashed lines are the perturbativity cuts in the y_{33} direction. Doubly (singly) hatched region is the 1σ (2σ) region

The presence of both (pseudo)scalar and tensor operators requires the calculation of matrix elements of the (pseudo)scalar and tensor matrix elements. The matrix element of the (pseudo)scalar operator can be readily calculated by using the identity (7).

Further, the matrix elements of tensor operator between the B and D states can be parametrized with the single function $T(q^2)$ [29]

$$\langle D(p_D)|\bar{c}\sigma^{\mu\nu}b|\bar{B}(p_B)\rangle = -i(p_B^\mu p_D^\nu - p_D^\mu p_B^\nu)\frac{2f_T(q^2)}{m_B + m_D} \,, \tag{63}$$

while the matrix element of tensor operator between B and vector D^* state has the form [58]

$$\begin{aligned}
\langle D^*(p_{D^*}, \epsilon)|\bar{c}\sigma_{\mu\nu}(1 - \gamma_5)b|\bar{B}(p_B)\rangle &= T_0(q^2)\frac{\epsilon^* \cdot q}{(m_B + m_{D^*})^2}\epsilon_{\mu\nu\alpha\beta}\, p_B^\alpha\, p_{D^*}^\beta + T_1(q^2)\epsilon_{\mu\nu\alpha\beta}p_B^\alpha\epsilon^{*\beta} \\
&+ i\Big[T_3(q^2)(\epsilon_\mu^* p_{B,\nu} - \epsilon_\nu^* p_{B,\mu}) + T_4(q^2)(\epsilon_\mu^* p_{D^*,\nu} - \epsilon_\nu^* p_{D^*,\mu}) \\
&+ T_5(q^2)\frac{\epsilon^* \cdot q}{(m_B + m_{D^*})^2}(p_{B,\mu}p_{D^*,\nu} - p_{B,\nu}p_{D^*,\mu})\Big]. \tag{64}
\end{aligned}$$

The scalar and tensor helicity amplitudes can be readily calculated by using:

$$\begin{aligned}
\mathcal{A}_S^{m_M, m_\ell} &= -g_S H_S^{m_M} L_l^{m_\tau} \\
\mathcal{A}_T^{m_M, m_\ell} &= -g_T \sum_{m,m'} \eta_m \eta_{m'} H_{m,m'}^{m_M} L_{m,m'}^{m_\ell}. \tag{65}
\end{aligned}$$

where the tensor helicity amplitudes are given in analog to (48) and (49), with the only difference that we now calculate contractions of the tensorial matrix elements with two polarization vectors of the $\ell - \nu$ pair, see e.g. [53].

The corresponding form factors are discussed in [29], [58], [48] and are out of scope of the present text.

It turns out that multitude of the processes constrain the above Yukawa couplings ansatz, particularly $l' \to l\gamma$ lepton flavour changing processes. More details on relevant calculations can be found in [48]. Here we insert only the final graph with all constraints, see Fig. 4. It turns out that the contribution of Δ can fit the BaBar's anomaly through the minimal predictive couplings ansatz, and also have interplay with the physics of GUT scale.

The Yukawa ansatz (58) can be consistently implemented in $SU(5)$ GUT model and the preferable ratios of the couplings $\tilde{z}_i$ can be evaluated. This shows remarkable potential of low energy precision flavour constraints for physics of very high energies.

7 Summary

We investigated possibilities to observe NP contributions in $B \to D^*\tau\nu_\tau$ and $B \to D^\tau\nu_\tau$. In addition to the ratio of $B \to D^*\tau\nu_\tau$ and $B \to D^\tau\nu_\tau$, the NP might modify a number of new variables. The study is performed within most general framework of the effective Lagrangian, as well as within few models of NP. The complete study of a particular leptoquark contribution in $B \to D^*\tau\nu_\tau$ and $B \to D^\tau\nu_\tau$ has been performed, accompanied by the constraints coming from from low energy phenomenology. The existing discrepancy can be well explained within a proposed model.

References

[1] J. Beringer et al. (Particle Data Group), Phys. Rev. D86, 010001 (2012).

[2] R.P.Feynman, M. Gell-Mann, Theory of Fermi interaction, Phys. Rev. **109** (1958) 193-198.

[3] E.C.G. Sudarshan and R. E. Marshak, Chirality invariance and the universal Fermi interaction, Phys. Rev. **109** (1958) 1860-1860.

[4] N.Cabibbo, Unitary Symmetry and Leptonic Decays, Phys. Rev. Lett.**10** (1963) 531-533.

[5] J.H.Christenson, J.W. Cronin, V.L. Fitch and R. Turlay, Evidence for the 2 pi Decay of the k(2)0 Meson, Phys. Rev. Lett.**13** (1964) 138-140.

[6] M. Kobayashi and T. Maskawa, CP Violation in the Renormalizable Theory of Weak Interaction Prog. Theor. Phys. 49 (1973) 652-657.

[7] Y. Nir, CP violation: A New era, hep-ph/0109090

[8] O. Gedalia and G. Perez, "TASI 2009 Lectures - Flavor Physics," arXiv:1005.3106 [hep-ph].

[9] J. Charles et al. [CKMfitter Group Collaboration], "CP violation and the CKM matrix: Assessing the impact of the asymmetric B factories," Eur. Phys. J. C **41** (2005) 1 [hep-ph/0406184], see also updates at http://ckmfitter.in2p3.fr

[10] M. Bona et al. [UTfit Collaboration], "The 2004 UTfit collaboration report on the status of the unitarity triangle in the standard model," JHEP **0507**, 028 (2005) [hep-ph/0501199], also see updates at http://www.utfit.org/UTfit/

[11] J. G. Korner and G. A. Schuler, Z. Phys. C **38** (1988) 511 [Erratum-ibid. C **41** (1989) 690].

[12] G. C. Branco, P. M. Ferreira, L. Lavoura, M. N. Rebelo, M. Sher and J. P. Silva, "Theory and phenomenology of two-Higgs-doublet models," Phys. Rept. **516** (2012) 1 [arXiv:1106.0034 [hep-ph]].

[13] J. F. Kamenik and F. Mescia, Phys. Rev. D **78** (2008) 014003 [arXiv:0802.3790 [hep-ph]].

[14] U. Nierste, S. Trine and S. Westhoff, Phys. Rev. D **78** (2008) 015006 [arXiv:0801.4938 [hep-ph]].

[15] R. S. Chivukula and H. Georgi, "Composite Technicolor Standard Model," Phys. Lett. B **188** (1987) 99.

[16] G. D'Ambrosio, G. F. Giudice, G. Isidori and A. Strumia, "Minimal flavor violation: An Effective field theory approach," Nucl. Phys. B **645** (2002) 155 [hep-ph/0207036].

[17] A. J. Buras, "Minimal flavor violation," Acta Phys. Polon. B **34** (2003) 5615 [hep-ph/0310208].

[18] I. I. Y. Bigi and A. I. Sanda, "CP violation," Camb. Monogr. Part. Phys. Nucl. Phys. Cosmol. **9** (2000) 1.

[19] G. C. Branco, L. Lavoura and J. P. Silva, "CP Violation," Int. Ser. Monogr. Phys. **103** (1999) 1.

[20] S. L. Glashow and S. Weinberg, "Natural Conservation Laws for Neutral Currents," Phys. Rev. D **15** (1977) 1958.

[21] E. A. Paschos, "Diagonal Neutral Currents," Phys. Rev. D **15** (1977) 1966.

[22] L. Wolfenstein, "Parametrization of the Kobayashi-Maskawa Matrix," Phys. Rev. Lett. **51** (1983) 1945.

[23] I. I. Y. Bigi, M. A. Shifman, N. G. Uraltsev and A. I. Vainshtein, "QCD predictions for lepton spectra in inclusive heavy flavor decays," Phys. Rev. Lett. **71** (1993) 496 [hep-ph/9304225].

[24] A. V. Manohar and M. B. Wise, "Inclusive semileptonic B and polarized Lambda(b) decays from QCD," Phys. Rev. D **49** (1994) 1310 [hep-ph/9308246].

[25] J. P. Lees et al. [BaBar Collaboration], "Evidence for an excess of $\bar{B} \to D^{(*)}\tau^-\bar{\nu}_\tau$ decays," Phys. Rev. Lett. **109** (2012) 101802 [arXiv:1205.5442 [hep-ex]].

[26] A. Matyja et al. [Belle Collaboration], Phys. Rev. Lett. **99**, 191807 (2007) [arXiv:0706.4429 [hep-ex]].

[27] A. X. El-Khadra, A. S. Kronfeld and P. B. Mackenzie, Phys. Rev. D **55** (1997) 3933 [hep-lat/9604004].

[28] J. A. Bailey, A. Bazavov, C. Bernard, C. M. Bouchard, C. DeTar, D. Du, A. X. El-Khadra and J. Foley et al., "Refining new-physics searches in $B-> D\tau\nu$ decay with lattice QCD," Phys. Rev. Lett. **109** (2012) 071802 [arXiv:1206.4992 [hep-ph]].

[29] D. Becirevic, N. Kosnik and A. Tayduganov, "$\bar{B} \to D\tau\bar{\nu}_\tau$ vs. $\bar{B} \to D\mu\bar{\nu}_\mu$," Phys. Lett. B **716** (2012) 208 [arXiv:1206.4977 [hep-ph]].

[30] M. Atoui, D. Becirevic, V. Morenas and F. Sanfilippo, arXiv:1310.5238 [hep-lat].

[31] H. Georgi, Heavy quark effective field theory, (Boulder TASI 91:0589-630).

[32] H. Georgi, "An Effective Field Theory for Heavy Quarks at Low-energies," Phys. Lett. B **240** (1990) 447.

[33] M. Neubert, "Theoretical update on the model independent determination of —V(cb)— using heavy quark symmetry," Phys. Lett. B **338** (1994) 84 [hep-ph/9408290].

[34] M. Neubert, "Heavy quark symmetry," Phys. Rept. **245** (1994) 259 [hep-ph/9306320].

[35] N. Isgur and M. B. Wise, "Spectroscopy with heavy quark symmetry," Phys. Rev. Lett. **66** (1991) 1130.

[36] N. Isgur and M. B. Wise, Phys. Rev. Lett. **66** (1991) 1130.

[37] D. Becirevic, V. Lubicz, F. Sanfilippo, S. Simula and C. Tarantino, JHEP **1202** (2012) 042 [arXiv:1201.4039 [hep-lat]].

[38] N. Isgur and M. B. Wise, "Weak Transition Form-factors Between Heavy Mesons," Phys. Lett. B **237** (1990) 527.

[39] T. Mannel, W. Roberts and Z. Ryzak, Nucl. Phys. B **368** (1992) 204.

[40] M. Neubert and V. Rieckert, Nucl. Phys. B **382** (1992) 97.

[41] I. Caprini, L. Lellouch and M. Neubert, Nucl. Phys. B **530** (1998) 153 [hep-ph/9712417].

[42] S. Fajfer, J. F. Kamenik, I. Nisandzic and J. Zupan, Phys. Rev. Lett. **109** (2012) 161801 [arXiv:1206.1872 [hep-ph]].

[43] S. Fajfer, J. F. Kamenik and I. Nisandzic, Phys. Rev. D **85** (2012) 094025 [arXiv:1203.2654 [hep-ph]].

[44] S. Fajfer and I. Nisandzic, arXiv:1301.1167 [hep-ph].

[45] I. Adachi *et al.* [Belle Collaboration], Phys. Rev. Lett. **110** (2013) 131801 [arXiv:1208.4678 [hep-ex]].

[46] J. Laiho, E. Lunghi and R. Van de Water, PoS LATTICE **2011** (2011) 018 [arXiv:1204.0791 [hep-ph]].

[47] H. Georgi and C. Jarlskog, Phys. Lett. B **86** (1979) 297.

[48] I. Dorsner, S. Fajfer, N. Kosnik and I. Nisandzic, arXiv:1306.6493 [hep-ph].

[49] Y. Sakaki, M. Tanaka, A. Tayduganov and R. Watanabe, arXiv:1309.0301 [hep-ph].

[50] A. Crivellin, A. Kokulu and C. Greub, Phys. Rev. D **87** (2013) 094031 [arXiv:1303.5877 [hep-ph]].

[51] J. P. Lees *et al.* [BaBar Collaboration], arXiv:1303.0571 [hep-ex].

[52] M. Duraisamy and A. Datta, JHEP **1309** (2013) 059 [arXiv:1302.7031 [hep-ph]].

[53] M. Tanaka and R. Watanabe, Phys. Rev. D **87** (2013) 3, 034028 [arXiv:1212.1878 [hep-ph]].

[54] I. Dorsner, S. Fajfer and N. Kosnik, Phys. Rev. D **86** (2012) 015013 [arXiv:1204.0674 [hep-ph]].

[55] I. Dorsner, J. Drobnak, S. Fajfer, J. F. Kamenik and N. Kosnik, JHEP **1111** (2011) 002 [arXiv:1107.5393 [hep-ph]].

[56] I. Dorsner, S. Fajfer, J. F. Kamenik and N. Kosnik, Phys. Rev. D **81** (2010) 055009 [arXiv:0912.0972 [hep-ph]].

[57] I. Dorsner, S. Fajfer, J. F. Kamenik and N. Kosnik, Phys. Lett. B **682** (2009) 67 [arXiv:0906.5585 [hep-ph]].

[58] P. Biancofiore, P. Colangelo and F. De Fazio, Phys. Rev. D **87** (2013) 074010 [arXiv:1302.1042 [hep-ph]].

[59] A. Celis, M. Jung, X. -Q. Li and A. Pich, JHEP **1301** (2013) 054 [arXiv:1210.8443 [hep-ph]].

[60] N. G. Deshpande and A. Menon, JHEP **1301** (2013) 025 [arXiv:1208.4134 [hep-ph]].

[61] A. Crivellin, C. Greub and A. Kokulu, Phys. Rev. D **86** (2012) 054014 [arXiv:1206.2634 [hep-ph]].

Spectroscopy and Regge Trajectories of Heavy Quarkonia

D. Ebert[1], R.N. Faustov[2], V.O. Galkin[2]

[1]Institut für Physik, Humboldt–Universität zu Berlin, Newtonstr. 15, D-12489 Berlin, Germany
[2]Dorodnicyn Computing Centre, Russian Academy of Sciences, Vavilov Str. 40, 119333 Moscow, Russia

The mass spectra of charmonia and bottomonia are calculated in the framework of the relativistic quark model. The Regge trajectories of heavy quarkonia are constructed. All daughter trajectories are almost linear and parallel, while parent trajectories exhibit some nonlinearity. Such nonlinearity occurs only in the vicinity of ground states and few lowest excitations and is more pronounced for bottomonia, while it is only marginal for charmonia. The obtained results are compared with available experimental data, and a possible interpretation of the new charmonium-like states above open charm production threshold is discussed.

1 Introduction

In recent years a vast amount of experimental data on the heavy quarkonium spectroscopy has been accumulated [1]. The number of known states is constantly increasing. Thus, in the last eight years more than ten new charmonium-like states have been discovered [2]. The total number of charmonium states, listed in the Particle Data Group Listings [1], is 25 at present. Some of the new states (such as $\eta_c(2S)$, h_c, $\chi_{c2}(2P)$, etc.) are the long-awaited ones within the quark model, while some others, with masses higher than the threshold of the open charm production, have narrow widths and unexpected decay properties [2]. There are theoretical indications that some of these new states could be the first manifestation of the existence of exotic hadrons (tetraquarks, molecules, hybrids etc.), which are predicted in QCD [3]. In order to explore such options, a comprehensive understanding of the heavy quarkonium spectroscopy up to rather high orbital and radial excitations is required. The experimentally known bottomonium spectrum consists of 20 states [1]. Therefore, the investigation of the masses of the excited heavy quarkonia states presents an important and interesting problem. To achieve this goal one should treat the quark dynamics in mesons completely relativistically. Here we extend the approach previously used for the investigation of light meson spectroscopy [4] to heavy quarkonia. In order to improve our description, leading radiative corrections to the heavy quark potential [5] are also taken into account. Such corrections are suppressed by additional powers of α_s, which are rather small for heavy quarkonia, and are known only in the framework of the v^2/c^2 expansion. Therefore we treat them perturbatively. The calculation of the masses of highly orbitally and radially excited states up to the fifth excitation is carried out. On this basis, the Regge trajectories for charmonia and bottomonia can be constructed both in the total angular momentum J and radial quantum number n_r, and properties like linearity, parallelism and equidistance of these trajectories can be checked. There are reasons

to expect that the parent Regge trajectories can be nonlinear [6, 7] due to the compactness of their ground and lowest excited states, which puts them in the region where both the linear confining and Coulomb parts of the quark-antiquark potential play a comparable role.

2 Relativistic quark model

In the relativistic quark model based on the quasipotential approach a meson is described by the wave function of the bound quark-antiquark state, which satisfies the quasipotential equation of the Schrödinger type [8, 9]

$$
\left(\frac{b^2(M)}{2\mu_R} - \frac{\mathbf{p}^2}{2\mu_R} \right) \Psi_M(\mathbf{p}) = \int \frac{d^3q}{(2\pi)^3} V(\mathbf{p}, \mathbf{q}; M) \Psi_M(\mathbf{q}),
\tag{1}
$$

where

$$
\mu_R = \frac{M^4 - (m_1^2 - m_2^2)^2}{4M^3}, \qquad b^2(M) = \frac{[M^2 - (m_1 + m_2)^2][M^2 - (m_1 - m_2)^2]}{4M^2}.
\tag{2}
$$

Here M is the meson mass, $m_{1,2}$ are the quark masses, and $\mathbf{p}$ is their relative momentum.

The kernel $V(\mathbf{p}, \mathbf{q}; M)$ in Eq. (1) is the QCD-motivated quasipotential operator of the quark-antiquark interaction, which is constructed with the help of the off-mass-shell scattering amplitude, projected onto the positive energy states. It is assumed that the effective interaction is the sum of the usual one-gluon exchange term with the mixture of long-range vector and scalar linear confining potentials

$$
V(\mathbf{p}, \mathbf{q}; M) = \bar{u}_1(p)\bar{u}_2(-p) \left\{ \frac{4}{3}\alpha_s D_{\mu\nu}(\mathbf{k})\gamma_1^\mu\gamma_2^\nu + V_{\text{conf}}^V(\mathbf{k})\Gamma_1^\mu\Gamma_{2;\mu} + V_{\text{conf}}^S(\mathbf{k}) \right\} u_1(q)u_2(-q),
\tag{3}
$$

where the vector confining potential contains the Pauli interaction: $\Gamma_\mu(\mathbf{k}) = \gamma_\mu + \frac{i\kappa}{2m}\sigma_{\mu\nu}k^\nu$. Here α_s is the QCD coupling constant, $D_{\mu\nu}$ is the gluon propagator in the Coulomb gauge, γ_μ and $u(p)$ are the Dirac matrices and spinors and $\mathbf{k} = \mathbf{p} - \mathbf{q}$; κ is the Pauli interaction constant characterizing the anomalous chromomagnetic moment of quarks. Vector and scalar confining potentials in the nonrelativistic limit reduce to

$$
V_{\text{conf}}^V(r) = (1 - \varepsilon)(Ar + B), \qquad V_{\text{conf}}^S(r) = \varepsilon(Ar + B),
\tag{4}
$$

where ε is the mixing coefficient. Therefore, in this limit the Cornell-type potential is reproduced $V_{\text{NR}}(r) = -\frac{4}{3}\frac{\alpha_s}{r} + Ar + B$.

All the model parameters have the same values as in our previous papers [8, 4, 10]: the constituent quark masses $m_u = m_d = 0.33$ GeV, $m_s = 0.5$ GeV, $m_c = 1.55$ GeV, $m_b = 4.88$ GeV, and the parameters of the linear potential $A = 0.18$ GeV^2 and $B = -0.16$ GeV. The value of the mixing coefficient of vector and scalar confining potentials $\varepsilon = -1$ has been determined from the consideration of charmonium radiative decays [8] and matching heavy quark effective theory (HQET). Finally, the universal Pauli interaction constant $\kappa = -1$ has been fixed from the analysis of the fine splitting of heavy quarkonia ^3P_J- states [8]. In this case, the long-range chromomagnetic interaction of quarks, which is proportional to $(1 + \kappa)$, vanishes in accordance with the flux-tube model.

The investigations of the heavy quark dynamics in heavy mesons indicate that the charm quark is not heavy enough to be considered as nonrelativistic. Indeed, estimates of the averaged

velocity squared for the ground-state charmonium give the value $\langle v^2/c^2 \rangle \sim 0.25$. For excited charmonium states the $\langle v^2/c^2 \rangle$ values are even higher. Therefore, a reliable calculation of the charmonium spectroscopy requires a completely relativistic treatment of the charmed quark without an expansion in its velocity. The quasipotential (3) can in principal be used for arbitrary quark masses. The substitution of the Dirac spinors into (3) results in an extremely nonlocal potential in the configuration space. Clearly, it is very hard to deal with such potentials without any additional approximations. In order to simplify the relativistic $Q\bar{Q}$ potential, we make the following replacement in the Dirac spinors: $\epsilon_{1,2}(p) = \sqrt{m_{1,2}^2 + \mathbf{p}^2} \rightarrow E_{1,2} \equiv (M^2 - m_{2,1}^2 + m_{1,2}^2)/2M$ (see the discussion of this point in [4, 10]). This substitution makes the Fourier transformation of the potential (3) local. The resulting $Q\bar{Q}$ potential then reads

$$V(r) = V_{\mathrm{SI}}(r) + V_{\mathrm{SD}}(r), \qquad (5)$$

where the explicit expression for the spin-independent $V_{\mathrm{SI}}(r)$ and spin-dependent $V_{\mathrm{SD}}(r)$ parts can be found in Ref. [4].

3 Results and discussion

We solve the quasipotential equation with the quasipotential (5), which nonperturbatively accounts for the relativistic dynamics of both heavy quarks, numerically. Then we add the one-loop radiative corrections and the additional one-loop correction for bottomonium due to the finite mass [8] of the charmed quark by using perturbation theory. The calculated masses of charmonia and bottomonia are given in Tables 1,2, where $n = n_r + 1$, n_r is the radial quantum number, L, S and J are the quantum numbers of the orbital, total spin and total angular momenta, respectively. They are confronted with available experimental data from PDG [1], good agreement is found. It is important to note that the nonperturbative relativistic treatment gives a better agreement with data than our previous heavy quarkonium mass spectrum calculation [8], where only relativistic corrections up to v^2/c^2 order were taken into account. However, the differences between former and new predictions are rather small for most of the low-lying states and become noticeable only for higher excitations, where relativistic effects turn out to be particularly important.

In our analysis we calculated masses of both orbitally and radially excited heavy quarkonia up to rather high excitation numbers ($L = 5$ and $n_r = 5$). This makes it possible to construct the Regge trajectories in the (J, M^2) and (n_r, M^2) planes using the following definitions:
(a) the (J, M^2) Regge trajectory: $J = \alpha M^2 + \alpha_0$;
(b) the (n_r, M^2) Regge trajectory: $n_r = \beta M^2 + \beta_0$,
where α, β are the slopes and α_0, β_0 are the intercepts. These relations arise in most models of quark confinement, but with different values of the slopes.

In Figs. 1, 2 we plot the Regge trajectories in the (J, M^2) and (n_r, M^2) planes for charmonia and bottomonia. We see that the calculated charmonium masses fit nicely to the linear trajectories in both planes (maybe with the exception of the parent trajectories, where the J/ψ and η_c mesons seem to have slightly lower masses). These trajectories are almost parallel and equidistant. For the bottomonium the situation is more complicated. The daughter trajectories, which involve both radially and orbitally excited states, turn out to be almost linear. On the other hand, the parent trajectories, which start from ground states, are exhibiting a nonlinear behaviour in the lower mass region. Such nonlinearity is most pronounced in bottomonium.

State		Theory	Experiment		State		Theory	Experiment	
$n^{2S+1}L_J$	J^{PC}		meson	mass	$n^{2S+1}L_J$	J^{PC}		meson	mass
1^1S_0	0^{-+}	2981	$\eta_c(1S)$	2980.3(1.2)	2^3D_1	1^{--}	4150	$\psi(4160)$	4153(3)
1^3S_1	1^{--}	3096	$J/\psi(1S)$	3096.916(11)	2^3D_2	2^{--}	4190		
2^1S_0	0^{-+}	3635	$\eta_c(2S)$	3637(4)	2^3D_3	3^{--}	4220		
2^3S_1	1^{--}	3685	$\psi(2S)$	3686.09(4)	2^1D_2	2^{-+}	4196	$X(4160)?$	$4156(^{29}_{25})$
3^1S_0	0^{-+}	3989			3^3D_1	1^{--}	4507		
3^3S_1	1^{--}	4039	$\psi(4040)$	4039(1)	3^3D_2	2^{--}	4544		
4^1S_0	0^{-+}	4401			3^3D_3	3^{--}	4574		
4^3S_1	1^{--}	4427	$\psi(4415)$	4421(4)	3^1D_2	2^{-+}	4549		
5^1S_0	0^{-+}	4811			4^3D_1	1^{--}	4857		
5^3S_1	1^{--}	4837			4^3D_2	2^{--}	4896		
6^1S_0	0^{-+}	5155			4^3D_3	3^{--}	4920		
6^3S_1	1^{--}	5167			4^1D_2	2^{-+}	4898		
1^3P_0	0^{++}	3413	$\chi_{c0}(1P)$	3414.75(31)	1^3F_2	2^{++}	4041		
1^3P_1	1^{++}	3511	$\chi_{c1}(1P)$	3510.66(7)	1^3F_3	3^{++}	4068		
1^3P_2	2^{++}	3555	$\chi_{c2}(1P)$	3556.20(9)	1^3F_4	4^{++}	4093		
1^1P_1	1^{+-}	3525	$h_c(1P)$	3525.41(16)	1^1F_3	3^{+-}	4071		
2^3P_0	0^{++}	3870	$\chi_{c0}(2P)$	3918.4(1.9)	2^3F_2	2^{++}	4361		
2^3P_1	1^{++}	3906			2^3F_3	3^{++}	4400		
2^3P_2	2^{++}	3949	$\chi_{c2}(2P)$	3927.2(2.6)	2^3F_4	4^{++}	4434		
2^1P_1	1^{+-}	3926			2^1F_3	3^{+-}	4406		
3^3P_0	0^{++}	4301			1^3G_3	3^{--}	4321		
3^3P_1	1^{++}	4319			1^3G_4	4^{--}	4343		
3^3P_2	2^{++}	4354	$X(4350)?$	4351(5)	1^3G_5	5^{--}	4357		
3^1P_1	1^{+-}	4337			1^1G_4	4^{-+}	4345		
4^3P_0	0^{++}	4698			1^3H_4	4^{++}	4572		
4^3P_1	1^{++}	4728			1^3H_5	5^{++}	4592		
4^3P_2	2^{++}	4763			1^3H_6	6^{++}	4608		
4^1P_1	1^{+-}	4744			1^3H_5	5^{+-}	4594		
1^3D_1	1^{--}	3783	$\psi(3770)$	3772.92(35)					
1^3D_2	2^{--}	3795							
1^3D_3	3^{--}	3813	$X(3820)$	3823.5(2.5)					
1^1D_2	2^{-+}	3807							

Table 1: Charmonium mass spectrum (in MeV).

State		Theory	Experiment		State		Theory
$n^{2S+1}L_J$	J^{PC}		meson	mass	$n^{2S+1}L_J$	J^{PC}	
1^1S_0	0^{-+}	9398	$\eta_b(1S)$	9398.0(3.2)	2^3D_1	1^{--}	10435
1^3S_1	1^{--}	9460	$\Upsilon(1S)$	9460.30(26)	2^3D_2	2^{--}	10443
2^1S_0	0^{-+}	9990	$\eta_b(2S)$	9999(4)	2^3D_3	3^{--}	10449
2^3S_1	1^{--}	10023	$\Upsilon(2S)$	10023.26(31)	2^1D_2	2^{-+}	10445
3^1S_0	0^{-+}	10329			3^3D_1	1^{--}	10704
3^3S_1	1^{--}	10355	$\Upsilon(3S)$	10355.2(5)	3^3D_2	2^{--}	10711
4^1S_0	0^{-+}	10573			3^3D_3	3^{--}	10717
4^3S_1	1^{--}	10586	$\Upsilon(4S)$	10579.4(1.2)	3^1D_2	2^{-+}	10713
5^1S_0	0^{-+}	10851			4^3D_1	1^{--}	10949
5^3S_1	1^{--}	10869	$\Upsilon(10860)$	10876(11)	4^3D_2	2^{--}	10957
6^1S_0	0^{-+}	11061			4^3D_3	3^{--}	10963
6^3S_1	1^{--}	11088	$\Upsilon(11020)$	11019(8)	4^1D_2	2^{-+}	10959
1^3P_0	0^{++}	9859	$\chi_{b0}(1P)$	9859.44(52)	1^3F_2	2^{++}	10343
1^3P_1	1^{++}	9892	$\chi_{b1}(1P)$	9892.78(40)	1^3F_3	3^{++}	10346
1^3P_2	2^{++}	9912	$\chi_{b2}(1P)$	9912.21(40)	1^3F_4	4^{++}	10349
1^1P_1	1^{+-}	9900	$h_b(1P)$	9899.3(1.0)	1^1F_3	3^{+-}	10347
2^3P_0	0^{++}	10233	$\chi_{b0}(2P)$	10232.5(6)	2^3F_2	2^{++}	10610
2^3P_1	1^{++}	10255	$\chi_{b1}(2P)$	10255.46(55)	2^3F_3	3^{++}	10614
2^3P_2	2^{++}	10268	$\chi_{b2}(2P)$	10268.65(55)	2^3F_4	4^{++}	10617
2^1P_1	1^{+-}	10260	$h_b(2P)$	10259.8(1.2)	2^1F_3	3^{+-}	10615
3^3P_0	0^{++}	10521			1^3G_3	3^{--}	10511
3^3P_1	1^{++}	10541	$\chi_b(3P)$	10534(9)	1^3G_4	4^{--}	10512
3^3P_2	2^{++}	10550			1^3G_5	5^{--}	10514
3^1P_1	1^{+-}	10544			1^1G_4	4^{-+}	10513
4^3P_0	0^{++}	10781			1^3H_4	4^{++}	10670
4^3P_1	1^{++}	10802			1^3H_5	5^{++}	10671
4^3P_2	2^{++}	10812			1^3H_6	6^{++}	10672
4^1P_1	1^{+-}	10804			1^3H_5	5^{+-}	10671
1^3D_1	1^{--}	10154					
1^3D_2	2^{--}	10161	$\Upsilon(1D)$	10163.7(1.4)			
1^3D_3	3^{--}	10166					
1^1D_2	2^{-+}	10163					

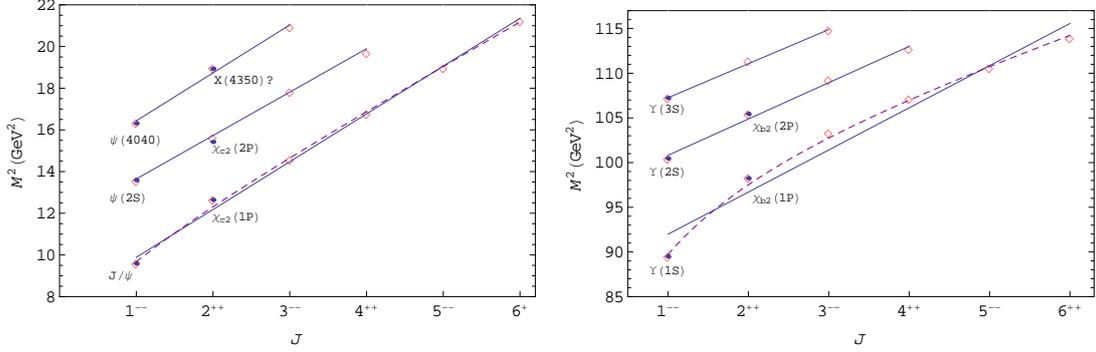Table 2: Bottomonium mass spectrum (in MeV).

Figure 1: Parent and daughter (J, M^2) Regge trajectories for charmonium (left) and bottomonium (right) states with natural $(P = (-1)^J)$ parity. Diamonds are predicted masses. Available experimental data are given by dots with particle names. The dashed line corresponds to a nonlinear fit for the parent trajectory.

The origin of this nonlinearity can be easily understood, if one compares the mean radii of these states.

The values of the mean square radii $\sqrt{\langle r^2 \rangle}$ of charmonia and bottomonia, calculated in our model, are given in Table 3. The static potential of the quark-antiquark interaction is plotted in Fig. 3 (solid line). In this figure we also separately plot the contributions from linear confinement (dashed line) and of the modulus of the Coulomb potential (dotted line).

State	$\sqrt{\langle r^2 \rangle}_\psi$	$\sqrt{\langle r^2 \rangle}_\Upsilon$	State	$\sqrt{\langle r^2 \rangle}_\psi$	$\sqrt{\langle r^2 \rangle}_\Upsilon$
$1S$	0.37	0.22	$2D$	0.99	0.76
$1P$	0.59	0.41	$1H$	1.08	0.85
$2S$	0.71	0.50	$3P$	1.09	0.84
$1D$	0.74	0.54	$2F$	1.09	0.85
$2P$	0.87	0.65	$4S$	1.16	0.90
$1F$	0.87	0.65	$3D$	1.18	0.94
$3S$	0.94	0.72	$4P$	1.26	1.01
$1G$	0.98	0.75	$5S$	1.32	1.07

Table 3: Mean square radii $\sqrt{\langle r^2 \rangle}$ for the spin-singlet states of charmonia and bottomonia (in fm).

As seen form Fig. 3, the Coulomb potential dominates for distances less than 0.15 fm, while the confining potential is dominant for distances larger than 0.5 fm. In the intermediate region both potentials play an equally important role. Therefore the light mesons and charmonia (with the exception of the η_c and J/ψ which are in the intermediate region) have characteristic sizes which belong to the region, where the confining potential dominates in the interquark potential. This leads to the emergence of the linear Regge trajectories. On the contrary, the ground and few first excited states of bottomonia have smaller sizes and fall into the region, where the Coulomb part of the potential gives an important contribution. As a result, the parent Regge trajectories of bottomonia are nonlinear, while the daughter trajectories (which fall into the region, where the confining potential is dominant) are still linear ones. In Ref. [6] an interpolating formula between the limiting cases of pure Coulomb and linear interactions was proposed. It can be written as follows:

(a) for the parent trajectory in the (J, M^2) plane: $M^2 = \left(J - \frac{\gamma_1}{(J+2)^2} + \gamma_0 \right) / \gamma$,
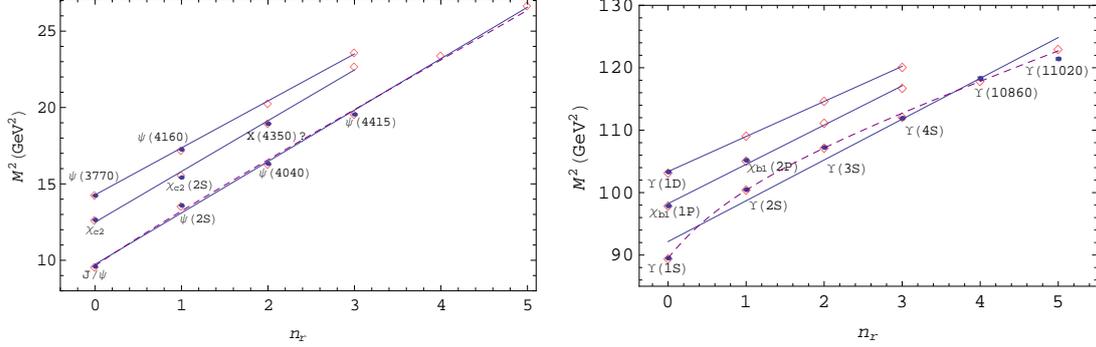
Figure 2: The (n_r, M^2) Regge trajectories for vector (S-wave), tensor and vector (D-wave) charmonium (left) and bottomonium (right) states (from bottom to top). Notations are the same as in Fig. 1.

(b) for the $J = 1$ trajectory in the (n_r, M^2) plane: $M^2 = \left(n_r - \frac{\tau_1}{(n_r+2)^2} + \tau_0\right)/\tau$,

where the parameters γ, τ, γ_0, τ_0 and γ_1, τ_1 determine the slopes, intercepts and nonlinearity of the Regge trajectories, respectively [9]. We find that the nonlinearity of the charmonium Regge trajectories is almost negligible, and its account does not significantly improve the quality of the fit compared to the linear one.

3.1   Comparison with experiment

We first discuss the recently found quarkonium states below the open flavour production threshold. The observation and measurement of the mass of the pseudoscalar ground state η_b [1] provides a significant information about the spin-spin interaction in heavy quarkonia. The averaged bottomonium hyperfine splitting measured in $\Upsilon(3S) \rightarrow \eta_b(1S)\gamma$, $\Upsilon(2S) \rightarrow \eta_b(1S)\gamma$ and $\Upsilon(2S) \rightarrow \eta_b(2S)\gamma$ decays is $\Delta M_{\text{hfs}}(1S) \equiv M_{\Upsilon(1S)} - M_{\eta_b(1S)} = 69.3 \pm 2.8$ MeV and $\Delta M_{\text{hfs}}(2S) \equiv M_{\Upsilon(2S)} - M_{\eta_b(2S)} = 48.7 \pm 2.3 \pm 2.1$ MeV [1, 11]. Very recently the Belle Collaboration [12] reported the first observation of the radiative transitions $h_b(1P) \rightarrow \eta_b(1S)\gamma$ and $h_b(2P) \rightarrow \eta_b(2S)\gamma$. The measured $\eta_b(1S)$ mass is $9401.0 \pm 1.9^{+1.4}_{-2.4}$ MeV, $\eta_b(2S)$ mass is $9999.0 \pm 3.5^{+2.8}_{-1.9}$ MeV and the hyperfine splittings $\Delta M_{\text{hfs}}(1S) = 59.3 \pm 1.9^{+2.4}_{-1.4}$ MeV and $\Delta M_{\text{hfs}}(2S) = 24.3^{+4.0}_{-4.5}$ MeV [12].

Figure 3: Static potential of the quark-antiquark interaction without the constant term (solid line). Dashed line shows the linear confining potential contribution, while dotted line corresponds to the modulus of the Coulomb potential.

Our predictions for these splittings, $\Delta M_{\text{hfs}}(1S) = 62$ MeV and $\Delta M_{\text{hfs}}(2S) = 33$ MeV, are in agreement with the experimental values. Note that our model correctly predicts the branching ratios of the corresponding radiative decays [8].

Another important experimental test of the structure of the spin splittings in heavy quarko-
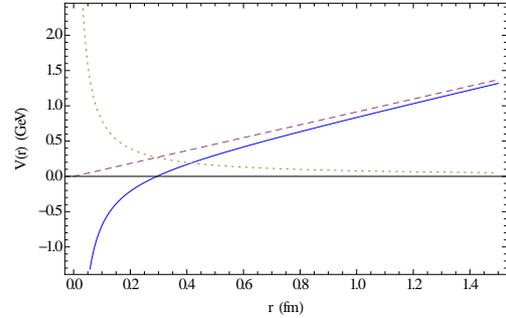
nia comes from the measurement of the masses of the spin-singlet P levels first in charmonium $h_c(1P)$ [1] and very recently in bottomonium $h_b(1P)$ and $h_b(2P)$ [13]. The measured masses of these states almost coincide with the spin-averaged centroid of the triplet states $\langle M(^3P_J)\rangle = [M(\chi_{Q0}) + 3M(\chi_{Q1}) + 5M(\chi_{Q2})]/9$. The hyperfine mass splittings $\Delta M_{\mathrm{hfs}}(nP) \equiv \langle M(n^3P_J)\rangle - M(n^1P_1)$ in bottomonium are found to be $\Delta M_{\mathrm{hfs}}(1P) = (1.62 \pm 1.52)$ MeV and $\Delta M_{\mathrm{hfs}}(2P) = (0.48^{+1.57}_{-1.22})$ MeV [13]. This observation indicates that the spin-spin contribution is negligible for P levels, and thus shows the vanishing of the long-range chromomagnetic interaction in heavy quarkonia. In our model this is the result of the choice of the value of the long-range chromomagnetic quark moment $\kappa = -1$. Note that our original predictions [8] for the spin-singlet masses are confirmed by these measurements.

The recently observed $\Upsilon(1^3D_2)$ state is the only D-wave state found below the threshold of open flavour production. Our prediction for its mass (see Table 2) is in good agreement with the measured value. It will be interesting to observe other $\Upsilon(1D)$ states in order to test further our understanding of spin-orbit and spin-spin interactions in heavy quarkonia. The mass of the newly observed $\chi_b(3P)$ state is also in accord with our prediction.

Next we discuss the observed states above the open flavour production threshold. The most well-established states are the vector 1^{--} states. For charmonium PDG [1] lists seven such states: $\psi(3770)$, $\psi(4040)$, $\psi(4160)$, $X(4260)$, $X(4360)$, $\psi(4415)$ and $X(4660)$, from which only the ψ states are included in the PDG Summary Tables [1]. These states are believed to be ordinary $c\bar{c}$ charmonium (with isospin $I = 0$). They are well described by our model (see Table 1): $\psi(4040)$ and $\psi(4415)$ are the 3^3S_1 and 4^3S_1 states, while $\psi(3770)$ and $\psi(4160)$ are the 1^3D_1 and 2^3D_1 states, respectively. These ψ states fit well to the corresponding Regge trajectories (see Fig. 2). On the other hand, the three new vector states X are considered as unexpected exotic states (their isospin is not determined experimentally). Indeed, we do not have any $c\bar{c}$ candidates for these states in Table 1. Contrary, in Ref. [14] we have found that these states can be described in our model as tetraquarks composed from a diquark and antidiquark ($[cq][\bar{c}\bar{q}]$, $q = u, d$). In particular, the $X(4260)$ and $X(4660)$ states can be interpreted as the 1^{--} states of such tetraquarks with a scalar diquark $[cq]_{S=0}$ and scalar antidiquark $[\bar{c}\bar{q}]_{S=0}$ in the relative $1P$ and $2P$ states and predicted masses 4244 MeV and 4666 MeV, respectively [14]. The $X(4360)$ can be viewed as the 1^{--} tetraquark with the axial vector diquark $[cq]_{S=1}$ and axial vector antidiquark $[\bar{c}\bar{q}]_{S=1}$ in the relative $1P$ state, which mass is predicted to be 4350 MeV [14].

The three vector bottomonium states, $\Upsilon(10580)$, $\Upsilon(10860)$ and $\Upsilon(11020)$, observed above open bottom threshold [1], are rather well described in our model as 4^3S_1, 5^3S_1 and 6^3S_1 states (see Table 2), the mass of $\Upsilon(11020)$ being somewhat higher than the experimental value. They fit to the corresponding Regge trajectory in Fig. 2.

The experimentally observed $2P$ charmonium states are $\chi_{c2}(2P)$ and $\chi_{c0}(2P)$ which masses are predicted slightly higher (by about 20 MeV and 45 MeV, respectively) in our model. From Table 1 we see that the exotic state $X(3872)$ cannot be described as the 1^{++} 2^3P_1 $c\bar{c}$ state or the 2^{-+} 1^1D_2 $c\bar{c}$ state. If this state belonged to either $2P$ or $1D$ multiplets, this could signal a large fine splitting in these multiplets, since the $X(3872)$ mass is 55 MeV below $\chi_{c2}(2P)$ and 100 MeV above $\psi(3770)$. As we see from Table 1, our model does not support such large fine splittings. In Ref. [14] we argued that $X(3872)$ can be considered as the 1^{++} ground state tetraquark, composed from the scalar and axial vector diquark and antidiquark $(([cq]_{S=0}[\bar{c}\bar{q}]_{S=1} + [cq]_{S=1}[\bar{c}\bar{q}]_{S=0})/\sqrt{2})$, which mass is predicted to be 3871 MeV. As we see from Table 1, the $X(4160)$ and $X(4350)$ can be attributed judging from the mass value and charge parity $C = +$ both to the pseudo tensor 2^{-+} spin-singlet 2^1D_2 and tensor 2^{++}

spin-triplet 3^3P_2 charmonium states, respectively. They fit well to the corresponding Regge trajectories in Figs. 1, 2.

The $X(4140)$ state, observed by CDF in $B^+ \rightarrow K^+\phi J/\psi$ decays [15], can correspond in our model to the scalar 0^{++} charmed-strange diquark-antidiquark $[cs]_{S=1}[\bar{c}\bar{s}]_{S=1}$ ground state with predicted mass 4110 MeV, or the axial vector 1^{++} one $([cs]_{S=0}[\bar{c}\bar{s}]_{S=1} + [cs]_{S=1}[\bar{c}\bar{s}]_{S=0})/\sqrt{2}$ with calculated mass 4113 MeV [14]. Two of the three charmonium-like charged $X^\pm$ states reported by Belle [16], which are explicitly exotic, can be interpreted in our model as tetraquark states. We do not have tetraquark candidate for the $X(4040)^+$ structure, while the $X(4250)^+$ can be considered as the charged partner of the 1^- $1P$ state $[cu]_{S=0}[\bar{c}\bar{d}]_{S=0}$ or as the 0^- $1P$ state of the $([cu]_{S=0}[\bar{c}\bar{d}]_{S=1} + [cu]_{S=1}[\bar{c}\bar{d}]_{S=0})/\sqrt{2}$ tetraquark with predicted masses 4244 MeV and 4267 MeV, respectively [14]. The $X(4430)^+$ could be the first radial $(2S)$ excitation of the 1^+ $X(3872)$ tetraquark or the 0^+ $2S$ $[cu]_{S=1}[\bar{c}\bar{d}]_{S=1}$ tetraquark, which have very close masses 4431 MeV and 4434 MeV [14].

As we see, a consistent picture of the excited quarkonium states emerges in our model. All well-established states and most of the states, which need additional experimental confirmation, can be interpreted as excited quarkonium or diquark-antidiquark tetraquark states.

4   Conclusions

The mass spectra of charmonia, bottomonia and B_c mesons were calculated in the framework of the relativistic quark model based on the quasipotential approach. Highly radially and orbitally excited quarkonium states were considered. On this basis, the Regge trajectories of heavy quarkonia were constructed both in the (J, M^2) and (n_r, M^2) planes. A different behaviour of these trajectories was observed for parent and daughter trajectories. All daughter trajectories turn out to be almost linear and parallel, while parent trajectories exhibit some nonlinearity. Such nonlinearity occurs only in the vicinity of ground states and few lowest excitations and is mostly pronounced for bottomonia. For charmonia this nonlinearity is only marginal, and its account does not significantly improve the fit. It was shown that the masses of the excited states of heavy quarkonia are determined by the average distances between quarks larger than 0.5 fm, where the linear confining part of the quark-antiquark interaction dominates. This leads to the emergence of almost linear Regge trajectories. On the other hand, a few lowest quarkonium states have average sizes smaller than 0.5 fm and fall in the region, where both the Coulomb and confining potentials play an important role. As a result, the parent Regge trajectories exhibit a certain nonlinearity in this region.

A detailed comparison of the calculated heavy quarkonium masses with available experimental data was carried out. It was found that all data for the states below open flavour production threshold are well reproduced in our model: the difference between predicted and measured masses does not exceed few MeV. For higher excited states, which are above this threshold, most of the well-established conventional states are also well described by our approach, the difference between theory and experiment being somewhat larger, but still within 20 MeV. In this case the multichannel consideration is desirable. It was shown that these states fit well to the corresponding Regge trajectories. Other states, which have unexpected properties and are therefore believed to have an exotic origin, were also discussed. As it was shown in our previous calculation [14], most of these states can be described as diquark-antidiquark tetraquarks. Therefore we have a self-consistent picture of the heavy quarkonium spectra. Future experimental studies of yet unobserved conventional quarkonium states and a clarifica-

tion of the nature and quantum numbers of the exotic quarkonium-like states will provide an additional test of our model.

References

[1] J. Beringer et al. [Particle Data Group], Phys. Rev. D **86**, 010001 (2012).

[2] N. Brambilla *et al.*, Eur. Phys. J. C **71**, 1534 (2011).

[3] E. Klempt and A. Zaitsev, Phys. Rept. **454**, 1 (2007).

[4] D. Ebert, R. N. Faustov and V. O. Galkin, Phys. Rev. D **79**, 114029 (2009).

[5] S. Gupta and S. F. Radford, Phys. Rev. D **24**, 2309 (1981); ibid. **25**, 3430 (1982); J. Pantaleone, S.-H. H. Tye and Y. J. Ng, Phys. Rev. D **33**, 777 (1986).

[6] M. N. Sergeenko, Z. Phys. C **64**, 315 (1994); S. S. Gershtein, A. K. Likhoded and A. V. Luchinsky, Phys. Rev. D **74**, 016002 (2006).

[7] A. M. Badalian, Phys. Atom. Nucl. **74**, 1375 (2011).

[8] D. Ebert, R.N. Faustov and V.O. Galkin, Phys. Rev. D **67**, 014027 (2003).

[9] D. Ebert, R.N. Faustov and V.O. Galkin, Eur. Phys. J. C **71**, 1825 (2011).

[10] D. Ebert, R. N. Faustov and V. O. Galkin, Eur. Phys. J. C **66**, 197 (2010).

[11] S. Dobbs, Z. Metreveli, K. K. Seth, A. Tomaradze and T. Xiao, Phys. Rev. Lett. **109**, 082001 (2012).

[12] I. Adachi *et al.* [Belle Collaboration], arXiv:1110.3934 [hep-ex]; R. Mizuk *et al.* [Belle Collaboration], arXiv:1205.6351 [hep-ex].

[13] J. P. Lees [The BABAR Collaboration], arXiv:1102.4565 [hep-ex]; I. Adachi *et al.* [Belle Collaboration], arXiv:1103.3419 [hep-ex].

[14] D. Ebert, R. N. Faustov and V. O. Galkin, Phys. Lett. B **634**, 214 (2006); Eur. Phys. J. C **58**, 399 (2008); Mod. Phys. Lett. A **24**, 567 (2009).

[15] T. Aaltonen *et al.* [CDF Collaboration], Phys. Rev. Lett. **102**, 242002 (2009).

[16] S. K. Choi *et al.* [Belle Collaboration], Phys. Rev. Lett. **100**, 142001 (2008); R. Mizuk *et al.* [Belle Collaboration], Phys. Rev. D **78**, 072004 (2008); Phys. Rev. D **80**, 031104 (2009).

Weak Decays of B_s Mesons

R.N. Faustov[1], V.O. Galkin[1]

[1]Dorodnicyn Computing Centre, Russian Academy of Sciences, Vavilov Str. 40, 119333 Moscow, Russia

The branching fractions of the semileptonic and rare B_s decays are calculated in the framework of the QCD-motivated relativistic quark model. The form factors of the weak B_s transitions are expressed through the overlap integrals of the initial and final meson wave functions in the whole accessible kinematical range. The momentum transfer dependence of the form factors is explicitly determined without additional model assumptions and extrapolations. The obtained results agree well with available experimental data.

1 Introduction

In recent years significant experimental progress has been achieved in studying properties of B_s mesons. The Belle Collaboration considerably increased the number of observed B_s mesons and their decays due to the data collected in e^+e^- collisions at the $\Upsilon(10860)$ resonance [1]. On the other hand, B_s mesons are copiously produced at Large Hadron Collider (LHC). First precise data on their properties are coming from the LHCb Collaboration. Several weak decay modes of the B_s meson were observed for the first time [2]. New data are expected in near future.

In this lecture we consider the weak B_s transition form factors and decay rates in the framework of the relativistic quark model based on the quasipotential approach in quantum chromoynamics (QCD) [4]. We previously applied this model for the calculation of the weak B transitions [5]. Recently Belle and BaBar Collaborations [3] published new more precise data on differential distributions in $B \to \pi l \nu_l$ and $B \to \rho l \nu_l$ decays. In Fig. 1 we compare predictions of our model with these data. From this figure we see that our predictions agree well with new data. The fit of our model predictions to the combined Belle and BaBar data yields the following values of the CKM matrix element V_{ub}

- $B \to \pi l \nu_l$ decays $\qquad\qquad\qquad |V_{ub}| = (4.07 \pm 0.07_{\text{exp}} \pm 0.21_{\text{theor}}) \times 10^{-3}$

- $B \to \rho l \nu_l$ decays $\qquad\qquad\qquad |V_{ub}| = (4.03 \pm 0.15_{\text{exp}} \pm 0.21_{\text{theor}}) \times 10^{-3}$

- combined data on $B \to \pi(\rho) l \nu_l$ $\quad |V_{ub}| = (4.06 \pm 0.06_{\text{exp}} \pm 0.21_{\text{theor}}) \times 10^{-3}$

These values are in good agreement with the averaged value extracted from the inclusive B decays [6] $\quad |V_{ub}| = (4.41 \pm 0.15^{+0.15}_{-0.19}) \times 10^{-3}$.

2 Relativistic quark model

All considerations in this lecture are done in the framework of the relativistic quark model. The model is based on the quasipotential approach in quantum field theory with the QCD motivated
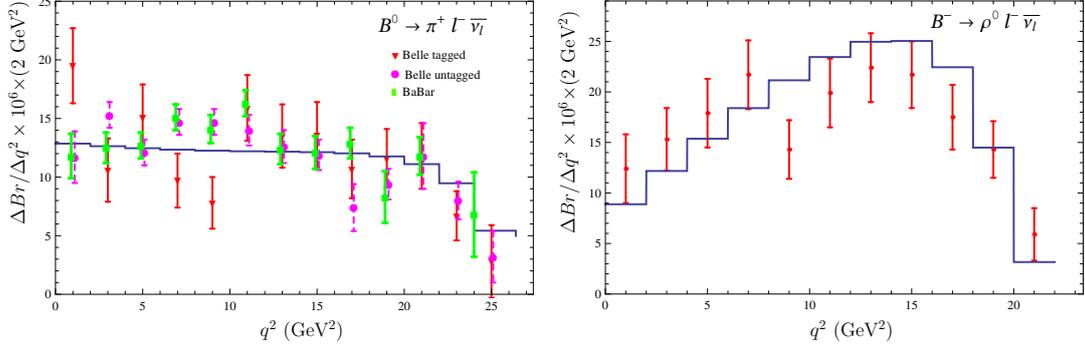
Figure 1: Comparison of predictions of our model with the recent experimental data (Belle 2011, 2013; BaBar 2012) for the $B^0 \to \pi^+ l^- \nu$ decay and Belle (2013) data for the $B \to \rho l \nu$ decay.

interaction. Hadrons are considered as the bound states of constituent quarks and are described by the single-time wave functions satisfying the three-dimensional Schrödinger-like equation, which is relativistically invariant [7]:

$$\left(\frac{b^2(M)}{2\mu_R} - \frac{\mathbf{p}^2}{2\mu_R} \right) \Psi_M(\mathbf{p}) = \int \frac{d^3q}{(2\pi)^3} V(\mathbf{p}, \mathbf{q}; M) \Psi_M(\mathbf{q}), \tag{1}$$

where

$$\mu_R = \frac{M^4 - (m_1^2 - m_2^2)^2}{4M^3}, \qquad b^2(M) = \frac{[M^2 - (m_1 + m_2)^2][M^2 - (m_1 - m_2)^2]}{4M^2}, \tag{2}$$

M is the meson mass, $m_{1,2}$ are the quark masses, and $\mathbf{p}$ is their relative momentum. The interaction quasipotential $V(\mathbf{p}, \mathbf{q}; M)$ consists of the perturbative one-gluon exchange part and the nonperturbative confining part [7]. The Lorentz structure of the latter part includes the scalar and vector linearly rising interactions. The long-range vector vertex contains the Pauli term (anomalous chromomagnetic quark moment) which enables vanishing of the spin-dependent chromomagnetic interaction in accord with the flux tube model.

For the consideration of the meson weak decays it is necessary to calculate the matrix element of the weak current between meson states. In the quasipotential approach, such a matrix element between a B_s meson with mass M_{B_s} and momentum p_{B_s} and a final F meson with mass M_F and momentum p_F is given by [7]

$$\langle F(p_F)|J_\mu^W|B_s(p_{B_s})\rangle = \int \frac{d^3p\, d^3q}{(2\pi)^6} \bar\Psi_{F\,\mathbf{p}_F}(\mathbf{p}) \Gamma_\mu(\mathbf{p}, \mathbf{q}) \Psi_{B_s\,\mathbf{p}_{B_s}}(\mathbf{q}), \tag{3}$$

where $\Gamma_\mu(\mathbf{p}, \mathbf{q})$ is the two-particle vertex function and $\Psi_{M\,\mathbf{p}_M}(\mathbf{p})$ are the meson ($M = B_s, F$) wave functions projected onto the positive energy states of quarks and boosted to the moving reference frame with momentum $\mathbf{p}_M$, and $\mathbf{p}, \mathbf{q}$ are relative quark momenta.

The explicit expression for the vertex function $\Gamma_\mu(\mathbf{p}, \mathbf{q})$ can be found in Ref. [4]. It contains contributions both from the leading order spectator diagram and from subleading order diagrams accounting for the contributions of the negative-energy intermediate states. The leading

order contribution contains the δ function which allows us to take one of the integrals in the matrix element (3). Calculation of the subleading order contribution is more complicated due to the dependence on the relative momentum in the energies of the initial heavy and final light quarks. For the energy of the heavy quarks we use heavy quark expansion. For the light quark such expansion is not applicable. However, if the final F meson is light (K, φ etc.) than it has a large (compared to its mass) recoil momentum ($|\boldsymbol{\Delta}_{\max}| = (M_{B_s}^2 - M_F^2)/(2M_{B_s}) \sim 2.6$ GeV) in almost the whole kinematical range except the small region near $q^2 = q_{\max}^2$ ($|\boldsymbol{\Delta}| = 0$). This also means that the recoil momentum of the final meson is large with respect to the mean relative quark momentum $|\mathbf{p}|$ in the meson (~ 0.5 GeV). Thus one can neglect $|\mathbf{p}|$ compared to $|\boldsymbol{\Delta}|$ in the light quark energies $\epsilon_q(p+\Delta) \equiv \sqrt{m_q^2 + (\mathbf{p} + \boldsymbol{\Delta})^2}$, replacing it with $\epsilon_q(\Delta) \equiv \sqrt{m_q^2 + \boldsymbol{\Delta}^2}$ in expressions for the subleading contribution. Such replacement removes the relative momentum dependence in the energies of quarks and thus permits the performance of one of the integrations in the subleading contribution using the quasipotential equation. Since the subleading contributions are suppressed the uncertainty introduced by such procedure is small. As a result, the weak decay matrix element is expressed through the usual overlap integral of initial and final meson wave functions and its momentum dependence can be determined in the whole accessible kinematical range without additional assumptions.

3 Semileptonic B_s decays to D_s mesons

The matrix elements of weak current J^W between meson ground states are usually parametrized by the following set of the invariant form factors

$$\langle D_s(p_{D_s})|\bar{c}\gamma^\mu b|B_s(p_{B_s})\rangle = f_+(q^2)\left[p_{B_s}^\mu + p_{D_s}^\mu - \frac{M_{B_s}^2 - M_{D_s}^2}{q^2}\ q^\mu\right] + f_0(q^2)\frac{M_{B_s}^2 - M_{D_s}^2}{q^2}\ q^\mu, \quad (4)$$

$$\langle D_s^*(p_{D_s^*})|\bar{c}\gamma^\mu b|B(p_{B_s})\rangle = \frac{2iV(q^2)}{M_{B_s} + M_{D_s^*}}\epsilon^{\mu\nu\rho\sigma}\epsilon_\nu^* p_{B_s\rho} p_{D_s^*\sigma}, \quad (5)$$

$$\langle D_s^*(p_{D_s^*})|\bar{c}\gamma^\mu\gamma_5 b|B_s(p_{B_s})\rangle = 2M_{D_s^*}A_0(q^2)\frac{\epsilon^*\cdot q}{q^2}\ q^\mu + (M_{B_s} + M_{D_s^*})A_1(q^2)\left(\epsilon^{*\mu} - \frac{\epsilon^*\cdot q}{q^2}\ q^\mu\right)$$
$$- A_2(q^2)\frac{\epsilon^*\cdot q}{M_{B_s} + M_{D_s^*}}\left[p_{B_s}^\mu + p_{D_s^*}^\mu - \frac{M_{B_s}^2 - M_{D_s^*}^2}{q^2}\ q^\mu\right]. \quad (6)$$

To calculate the weak decay matrix element we employ the heavy quark expansion, which permits us to take one of the integrals in the subleading contribution of the vertex function to the weak current matrix element. As a result we express all matrix elements through the usual overlap integrals of the meson wave functions. We find that the decay form factors can be approximated with sufficient accuracy by the following expressions:

$$\text{(a)} \qquad f_+(q^2), V(q^2), A_0(q^2) = F(q^2) = \frac{F(0)}{\left(1 - \frac{q^2}{M^2}\right)\left(1 - \sigma_1\frac{q^2}{M_{B_c^*}^2} + \sigma_2\frac{q^4}{M_{B_c^*}^4}\right)}, \qquad (7)$$

$$\text{(b)} \qquad f_0(q^2), A_1(q^2), A_2(q^2) = F(q^2) = \frac{F(0)}{\left(1 - \sigma_1\frac{q^2}{M_{B_c^*}^2} + \sigma_2\frac{q^4}{M_{B_c^*}^4}\right)}, \qquad (8)$$

where $M = M_{B_c^*} = 6.332$ GeV for the form factors $f_+(q^2), V(q^2)$ and $M = M_{B_c} = 6.272$ GeV for the form factor $A_0(q^2)$; the values $F(0)$ and $\sigma_{1,2}$ are given in Table 1. The values of $\sigma_{1,2}$ are determined with a few tenths of percent errors. The main uncertainties of the form factors originate from the account of $1/m_Q^2$ corrections at zero recoil only and from the higher order $1/m_Q^3$ contributions and can be roughly estimated in our approach to be about 2%.

	$B_s \to D_s$		$B_s \to D_s^*$			
	f_+	f_0	V	A_0	A_1	A_2
$F(0)$	0.74	0.74	0.95	0.67	0.70	0.75
$F(q_{\max}^2)$	1.15	0.88	1.50	1.06	0.84	1.04
σ_1	0.200	0.430	0.372	0.350	0.463	1.04
σ_2	-0.461	-0.464	-0.561	-0.600	-0.510	-0.070

Table 1: Form factors of weak $B_s \to D_s^{(*)}$ transitions.

In Table 2 we confront our predictions for the form factors of semileptonic decays $B_s \to D_s^{(*)}e\nu$ at maximum recoil point $q^2 = 0$ with results of other approaches [8, 9, 10, 11, 12]. Different quark models are used in Refs. [8, 10, 12], while the QCD and light cone sum rules are employed in Refs. [9, 11]. We find that these significantly different theoretical calculations lead to rather close values of the decay form factors. One of the main advantages of our model is its ability not only to obtain the decay form factors at the single kinematical point, but also to determine its q^2 dependence in the whole range without any additional assumptions or extrapolations.

	$f_+(0)$	$V(0)$	$A_0(0)$	$A_1(0)$	$A_2(0)$
our	0.74 ± 0.02	0.95 ± 0.02	0.67 ± 0.01	0.70 ± 0.01	0.75 ± 0.02
[8]	0.61	0.64		0.56	0.59
[9]	0.7 ± 0.1	0.63 ± 0.05	0.52 ± 0.06	0.62 ± 0.01	0.75 ± 0.07
[10]	$0.57^{+0.02}_{-0.03}$	$0.70^{+0.05}_{-0.04}$		$0.65^{+0.01}_{-0.01}$	$0.67^{+0.01}_{-0.01}$
[11]	$0.86^{+0.17}_{-0.15}$				
[12]		$0.74^{+0.05}_{-0.05}$	$0.63^{+0.04}_{-0.04}$	$0.61^{+0.04}_{-0.04}$	$0.59^{+0.04}_{-0.04}$

Table 2: Comparison of theoretical predictions for the form factors of semileptonic decays $B_s \to D_s^{(*)}e\nu$ at maximum recoil point $q^2 = 0$.

Using these weak decay form factors we calculate the total semileptonic decay rates. It is necessary to point out that the kinematical range accessible in these semileptonic decays is rather broad. Therefore the knowledge of the q^2 dependence of the form factors is very important for reducing theoretical uncertainties of the decay rates. Our results for the semileptonic $B_s \to D_s^{(*)}l\nu$ decay rates are given in Table 3 in comparison with previous calculations. The authors of Ref.[9] use the QCD sum rules, while the light cone sum rules approach is adopted in Ref. [11]. Different types of constituent quark models are employed in Refs. [12, 10, 13] and the three point QCD sum rules are used in Ref. [14]. We see that our predictions are consistent with results of quark model calculations in Refs. [12, 10]. They are approximately two times larger than the QCD sum rules and light cone sum rules results of Refs. [9, 11], but slightly lower than the values of Refs. [13, 14].

Using the same approach we calculate the form factors of B_s decays to radially and orbitally excited D_s mesons. The predictions for the branching fractions for B_s decays to radially excited D_s mesons are given in Table 4. We find that semileptonic B_s decays to the pseudoscalar

Decay	this paper	[9]	[10]	[11]	[12]	[13]	[14]
$B_s \to D_s e\nu$	2.1 ± 0.2	1.35 ± 0.21	1.4-1.7	$1.0^{+0.4}_{-0.3}$		2.73-3.00	2.8-3.8
$B_s \to D_s \tau\nu$	0.62 ± 0.05		0.47-0.55	$0.33^{+0.14}_{-0.11}$			
$B_s \to D_s^* e\nu$	5.3 ± 0.5	2.5 ± 0.1	5.1-5.8		5.2 ± 0.6	7.49-7.66	1.89-6.61
$B_s \to D_s^* \tau\nu$	1.3 ± 0.1		1.2-1.3		$1.3^{+0.2}_{-0.1}$		

Table 3: Comparison of theoretical predictions for the branching fractions of semileptonic decays $B_s \to D_s^{(*)} l\nu$ (in %).

$D_s(2S)$ and vector $D_s^*(2S)$ mesons have close values.

Our predictions for the branching fractions of the semileptonic B_s decays to orbitally excited D_s mesons are given in Table 5 in comparison with other calculations. We find that decays to D_{s1} and D_{s2}^* mesons are dominant. First we compare with our previous calculation [15] which was performed in the framework of the heavy quark expansion. We give results found in the infinitely heavy quark limit ($m_Q \to \infty$) and with the account of first order $1/m_Q$ corrections. It was argued [15]

Decay	Br
$B_s \to D_s(2S)e\nu$	0.27 ± 0.03
$B_s \to D_s(2S)\tau\nu$	0.011 ± 0.001
$B_s \to D_s^*(2S)e\nu$	0.38 ± 0.04
$B_s \to D_s^*(2S)\tau\nu$	0.015 ± 0.002

Table 4: Predictions for the branching fractions of semileptonic decays $B_s \to D_s^{(*)}(2S) l\nu$ (in %).

that $1/m_Q$ corrections are large and their inclusion significantly influences the decays rates. The large effect of subleading heavy quark corrections was found to be a consequence of the vanishing of the leading order contributions to the decay matrix elements, due to heavy quark spin-flavour symmetry, at the point of zero recoil of the final charmed meson, while the subleading order contributions do not vanish at this kinematical point. Here we calculated the decay rates without application of the heavy quark expansion. We find that nonperturbative results agree well with the ones obtained with the account of the leading order $1/m_Q$ corrections [15]. This means that the higher order in $1/m_Q$ corrections are small, as was expected. Then we compare our predictions with the results of calculations in other approaches. The authors of Refs. [16, 13] employ different types of constituent quark models for their calculations. Light cone and three point QCD sum rules are used in Refs. [11]. In general we find reasonable agreement between our predictions and results of Refs. [16, 11], but results of the quark model calculations [13] are slightly larger.

The first experimental measurement of the semileptonic decay $B_s \to D_{s1}\mu\nu$ was done by the D0 Collaboration [17]. The branching fraction was obtained by assuming that the D_{s1} production in semileptonic decay comes entirely from the B_s decay and using a prediction for $Br(D_{s1} \to D^* K_S^0) = 0.25$. Its value $Br(B_s \to D_{s1}X\mu\nu)_{\rm D0} = (1.03 \pm 0.20 \pm 0.17 \pm 0.14)\%$ is in good agreement with our prediction 0.84 ± 0.9 given in Table 5.

Recently the LHCb Collaboration [18] reported the first observation of the orbitally excited D_{s2}^* meson in the semileptonic B_s decays. The decay to the D_{s1} meson was also observed. The measured branching fractions relative to the total B_s semileptonic rate are $Br(B_s \to D_{s2}^*X\mu\nu)/Br(B_s \to X\mu\nu)_{\rm LHCb} = (3.3 \pm 1.0 \pm 0.4)\%$, $Br(B_s \to D_{s1}X\mu\nu)/Br(B_s \to X\mu\nu)_{\rm LHCb} = (5.4 \pm 1.2 \pm 0.5)\%$. The D_{s2}^*/D_{s1} event ratio is found to be $Br(B_s \to D_{s2}^*X\mu\nu)/Br(B_s \to D_{s1}X\mu\nu)_{\rm LHCb} = 0.61 \pm 0.14 \pm 0.05$. These values can be compared with our predictions if we assume that decays to D_{s1} and D_{s2}^* mesons give dominant contributions to the ratios. Summing up the semileptonic B_s decay branching fractions to ground state, first radial and orbital excitations of D_s mesons we get for the total B_s semileptonic rate $Br(B_s \to X\mu\nu) =$

Decay	this paper	$m \to \infty$ [15]	with $1/m_Q$ [15]	[16]	[13]	[11]
$B_s \to D_{s0}^* e\nu$	0.36 ± 0.04	0.10	0.37	0.443	0.49-0.571	$0.23^{+0.12}_{-0.10}$
$B_s \to D_{s0}^* \tau\nu$	0.019 ± 0.002					$0.057^{+0.028}_{-0.023}$
$B_s \to D_{s1}' e\nu$	0.19 ± 0.02	0.13	0.18	0.174-0.570	0.752-0.869	
$B_s \to D_{s1}' \tau\nu$	0.015 ± 0.002					
$B_s \to D_{s1} e\nu$	0.84 ± 0.09	0.36	1.06	0.477		
$B_s \to D_{s1} \tau\nu$	0.049 ± 0.005					
$B_s \to D_{s2}^* e\nu$	0.67 ± 0.07	0.56	0.75	0.376		
$B_s \to D_{s2}^* \tau\nu$	0.029 ± 0.003					

Table 5: Comparison of the predictions for the branching fractions of the semileptonic decays $B_s \to D_{sJ}^{(*)} l\nu$ (in %).

	$B_s \to K$			$B_s \to K^*$						
	f_+	f_0	f_T	V	A_0	A_1	A_2	T_1	T_2	T_3
$F(0)$	0.284	0.284	0.236	0.291	0.289	0.287	0.286	0.238	0.238	0.122
$F(q_{\max}^2)$	5.42	0.459	0.993	3.06	2.10	0.581	0.953	1.28	0.570	0.362
σ_1	-0.370	-0.072	-0.442	-0.516	-0.383	0	1.05	-1.20	0.241	0.521
σ_2	-1.41	-0.651	0.082	-2.10	-1.58	-1.06	0.074	-2.44	-0.857	-0.613

Table 6: Calculated form factors of weak $B_s \to K^{(*)}$ transitions.

$(10.2 \pm 1.0)\%$. Then using the calculated values from Table 5 we get $Br(B_s \to D_{s2}^* \mu\nu)/Br(B_s \to X\mu\nu)_{\text{theor}} = (6.5 \pm 1.2)\%$, $Br(B_s \to D_{s1}\mu\nu)/Br(B_s \to X\mu\nu)_{\text{theor}} = (8.2 \pm 1.6)\%$, and $Br(B_s \to D_{s2}^* \mu\nu)/Br(B_s \to D_{s1}\mu\nu)_{\text{theor}} = 0.79 \pm 0.14$. The predicted central values are larger than experimental ones, but the results agree with experiment within 2σ.

The following total semileptonic B_s branching ratios were found: (1) for decays to ground state $D_s^{(*)}$ mesons $Br(B_s \to D_s^{(*)} e\nu) = (7.4 \pm 0.7)\%$ and $Br(B_s \to D_s^{(*)} \tau\nu) = (1.92 \pm 0.15)\%$; (2) for decays to radially excited $D_s^{(*)}(2S)$ mesons $Br(B_s \to D_s^{(*)}(2S)e\nu) = (0.65 \pm 0.06)\%$ and $Br(B_s \to D_s^{(*)}(2S)\tau\nu) = (0.026 \pm 0.003)\%$; (3) for decays to orbitally excited $D_{sJ}^{(*)}$ mesons $Br(B_s \to D_{sJ}^{(*)} e\nu) = (2.1 \pm 0.2)\%$ and $Br(B_s \to D_{sJ}^{(*)} \tau\nu) = (0.11 \pm 0.01)\%$. We see that these branching fractions significantly decrease with excitation. Therefore, we can conclude that considered decays give the dominant contribution to the total semileptonic branching fraction $Br(B_s \to D_s e\nu + \text{anything})$. Summing up these contributions we get the value $(10.2 \pm 1.0)\%$, which agrees with the experimental value $Br(B_s \to D_s e\nu + \text{anything})_{\text{Exp.}} = (7.9 \pm 2.4)\%$ [6].

4   Charmless semileptonic B_s decays

Comparing the invariant form factor decomposition (4)–(6) with the results of the calculations of the weak current matrix element in our model we determine the form factors in the whole accessible kinematical range through the overlap integrals of the meson wave functions. The explicit expressions are given in Ref. [4]. For the numerical evaluations of the corresponding overlap integrals we use the quasipotential wave functions of B_s and $K^{(*)}$ mesons obtained in their mass spectra calculations [7]. The weak $B_s \to K^{(*)}$ transition form factors can be

approximated with good accuracy by Eqs. (7), (8). The obtained values $F(0)$ and $\sigma_{1,2}$ are given in Table 6.

Using these form factors we get predictions for the total decay rates. The kinematical range accessible in the heavy-to-light $B_s \to K^{(*)}$ transitions is very broad, making knowledge of the q^2 dependence of the form factors to be an important issue. Therefore, the explicit determination of the momentum dependence of the weak decay form fac-

Decay	this paper	[19]	[20]
$B_s \to K e \nu_e$	1.64 ± 0.17	$1.27^{+0.49}_{-0.30}$	1.47 ± 0.15
$B_s \to K \tau \nu_\tau$	0.96 ± 0.10	$0.778^{+0.268}_{-0.201}$	1.02 ± 0.11
$B_s \to K^* e \nu_e$	3.47 ± 0.35		2.91 ± 0.26
$B_s \to K^* \tau \nu_\tau$	1.67 ± 0.17		1.58 ± 0.13

Table 7: Comparison of theoretical predictions for the branching fractions of semileptonic decays $B_s \to K^{(*)} l \nu_l$ (in 10^{-4}).

tors in the whole q^2 range without any additional assumptions is an important advantage of our model. The calculated branching fractions of the semileptonic $B_s \to K^{(*)} l \nu_l$ decays are presented in Table 7 in comparison with other theoretical predictions [19, 20]. The perturbative QCD factorization approach is used in Ref. [19], while in Ref. [20] light cone sum rules are employed. From the comparison in Table 7 we see that all theoretical predictions for the B_s semileptonic branching fractions agree within uncertainties. This is not surprising since these significantly different approaches predict close values of the corresponding weak form factors.

We employ the same approach for the calculation of the form factors of the weak B_s decays to orbitally excited $K_J^{(*)}$ mesons. The total semileptonic $B_s \to K_J^{(*)} l \nu_l$ branching fractions are given in Table 8. We see that our model predicts close values (about 1×10^{-4}) for all semileptonic B_s branching fractions to the first orbitally excited $K_J^{(*)}$ mesons. Indeed, the difference between branching fractions is less than a factor of 2. This result is in contradiction to the dominance of specific modes (by more than a factor of 4) in the heavy-to-heavy semileptonic $B \to D_J^{(*)} l \nu_l$ and $B_s \to D_{sJ}^{(*)} l \nu_l$ decays, but it is consistent with predictions for the corresponding heavy-to-light semileptonic B decays to orbitally excited light mesons [21]. The above mentioned suppression of some heavy-to-heavy decay channels to orbitally excited heavy mesons was mostly pronounced in the heavy quark limit and then slightly reduced by the heavy quark mass corrections which are found to be large. Thus our result once again indicates that the s quark cannot be treated as a heavy one and should be considered to be light instead, as we always did in our calculations.

In Table 8 we compare our predictions for the semileptonic B_s branching fractions to orbitally excited $K_J^{(*)}$ mesons with previous calculations [22, 23, 24, 25, 11, 26]. The consideration in Ref. [22] is based on QCD sum rules. The light cone sum rules are used in Refs. [23, 25], while Refs. [24, 11, 26] employ the perturbative QCD approach. Reasonable agreement between our results and other predictions [22, 23, 26] is observed for the semileptonic B_s decays to the scalar and tensor K mesons. The values of Ref. [24] are almost a factor 3 higher. For the semileptonic B_s decays to axial vector K mesons predictions are significantly different even within rather large errors. Therefore experimental measurement of these decay branching fractions can help to discriminate between theoretical approaches.

We see that total branching fractions of semileptonic B_s decays to ground and first orbitally excited K mesons have close values of about 5×10^{-4}. Summing up these contributions, we get $(9.5 \pm 1.0) \times 10^{-4}$. This value is almost 2 orders of magnitude lower than our prediction for the corresponding sum of branching fractions of the semileptonic B_s to D_s mesons as it was expected from the ratio of CKM matrix elements $|V_{ub}|$ and $|V_{cb}|$. Therefore the total semileptonic B_s

Decay	this paper	[22]	[23]	[24]	[25]	[11]	[26]
$B_s \to K_0^* e \nu_e$	0.71 ± 0.14	$0.36^{+0.38}_{-0.24}$	$1.3^{+1.3}_{-0.4}$	$2.45^{+1.77}_{-1.05}$			
$B_s \to K_0^* \tau \nu_\tau$	0.21 ± 0.04		$0.52^{+0.57}_{-0.18}$	$1.09^{+0.82}_{-0.47}$			
$B_s \to K_1(1270) e \nu_e$	1.41 ± 0.28				$4.53^{+1.67}_{-2.05}$	$5.75^{+3.49}_{-2.89}$	
$B_s \to K_1(1270) \tau \nu_\tau$	0.30 ± 0.06					$2.62^{+1.58}_{-1.31}$	
$B_s \to K_1(1400) e \nu_e$	0.97 ± 0.20				$3.86^{+1.43}_{-1.75}$	$0.03^{+0.05}_{-0.02}$	
$B_s \to K_1(1400) \tau \nu_\tau$	0.25 ± 0.05					$0.01^{+0.02}_{-0.01}$	
$B_s \to K_2^* e \nu_e$	1.33 ± 0.27						$0.73^{+0.48}_{-0.33}$
$B_s \to K_2^* \tau \nu_\tau$	0.36 ± 0.07						$0.25^{+0.17}_{-0.12}$

Table 8: Comparison of theoretical predictions for the branching fractions of semileptonic decays $B_s \to K_J^{(*)} l \nu_l$ (in 10^{-4}).

	$B_s \to \eta_s$			$B_s \to \varphi$						
	f_+	f_0	f_T	V	A_0	A_1	A_2	T_1	T_2	T_3
$F(0)$	0.384	0.384	0.301	0.406	0.322	0.320	0.318	0.275	0.275	0.133
$F(q^2_{max})$	3.31	0.604	1.18	2.74	1.64	0.652	0.980	1.47	0.675	0.362
σ_1	-0.347	-0.120	-0.897	-0.861	-0.104	0.133	1.11	-0.491	0.396	0.639
σ_2	-1.55	-0.849	-1.34	-2.74	-1.19	-1.02	0.105	-1.90	-0.811	-0.531

Table 9: Calculated form factors of weak $B_s \to \eta_s$ and $B_s \to \varphi$ transitions.

decay branching fraction is dominated by the decays to D_s mesons and in our model is equal to $(10.3 \pm 1.0)\%$ in agreement with the experimental value $Br(B_s \to X e \nu_e)_{Exp.} = (9.5 \pm 2.7)\%$ [6].

5   Rare semileptonic B_s decays

Now we apply our model for the consideration of the rare B_s decays. Using described above method we explicitly determine the form factors in the whole accessible kinematical range through the overlap integrals of the meson wave functions. They again can be approximated with good accuracy by Eqs. (7), (8). The obtained values of $F(0)$ and $\sigma_{1,2}$ are given in Table 9. Using these form factors we consider the rare semileptonic decays. In the calculations the usual factorization of short-distance (described by Wilson coefficients) and long-distance (which matrix elements are proportional to hadronic form factors) contributions in the effective Hamiltonian for the $b \to s$ transitions is employed. The effective Wilson coefficient c_9^{eff} contains additional pertubative and long-distance contributions. The long-distance (nonperturbative) contributions are assumed to originate from the $c\bar{c}$ vector resonances (J/ψ, $\psi(2S)$, $\psi(3770)$, $\psi(4040)$, $\psi(4160)$ and $\psi(4415)$) and have a usual Breit-Wigner structure. In Fig. 2 we confront our predictions for differential branching fractions, dBr/dq^2, and the longitudinal polarization fraction, F_L, with experimental data from PDG (CDF) [6] and recent LHCb [27] data. By solid lines we show results for the nonresonant branching fractions, where long-distance contributions of the charmonium resonances to the coefficient c_9^{eff} are neglected. Plots given by the dashed lines contain such resonant contributions. For decays with the muon pair two largest peaks correspond to the contributions coming from the lowest vector charmonium states J/ψ and $\psi(2S)$, since they are narrow. The region of these resonance peaks is excluded in exper-
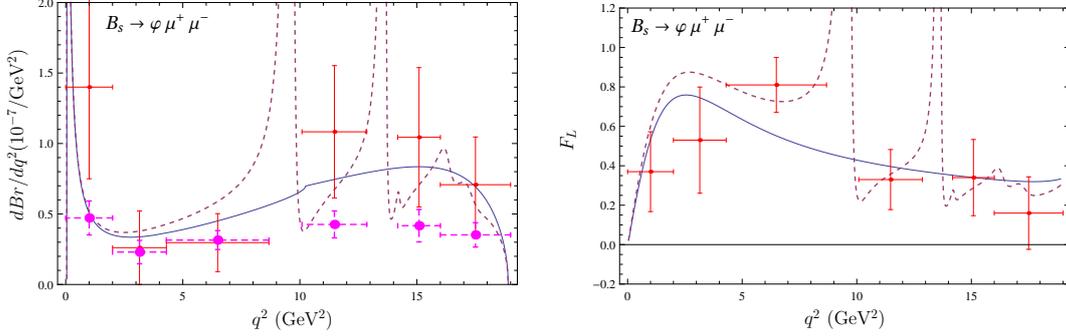
Figure 2: Comparison of theoretical predictions for the differential branching fractions $dBr(B_s \to \varphi\mu^+\mu^-)/dq^2$ and the φ longitudinal polarization F_L with available experimental data.

imental studies of these decays. Contributions in the low recoil region originating from the higher vector charmonium states, which are above the open charm threshold, are significantly less pronounced. The LHCb values for the differential branching fractions in most q^2 bins are lower than the CDF ones, but experimental error bars are rather large. Our predictions lie just in between these experimental measurements. For the φ longitudinal polarization fraction, F_L, only LHCb data are available which agree with our results within uncertainties. the differential branching fractions, forward-backward asymmetry and longitudinal polarization fraction.

In Table 10 we present our predictions for the nonresonant branching fractions of the rare semileptonic B_s decays and compare them with previous calculations [28, 29, 30, 31, 20] and available experimental data [6, 27]. In Ref. [28] the form factors were calculated on the basis of the light-cone QCD sum rules within the soft collinear effective theory. The authors of Ref. [29] employ the light front and constituent quark models for the evaluation of the rare decay branching fractions. Three-point QCD sum rules are used for the analysis of the rare semileptonic B_s decays into $\eta(\eta')$ and lepton pair in Ref. [30]. In Ref. [31] calculations are based on the light-front quark model, while light-cone sum rules in the framework of heavy quark effective field theory are applied in Ref. [20]. The analysis of the predictions given in Table 10 indicate that these significantly different approaches give close values of order 10^{-7} for the rare semileptonic $B_s \to \varphi(\eta^{(')})l^+l^-$ decay branching fractions and of order 10^{-8} for $B_s \to K^{(*)}l^+l^-$ decays. Experimental data are available for the branching fraction of the $B_s \to \varphi\mu^+\mu^-$ decay only. As we see from the table all theoretical predictions are well consistent with each other and experimental data for the $B_s \to \varphi\mu^+\mu^-$ decay from PDG [6]. Note that very recently the LHCb Collaboration [27] also reported measurement of this decay branching fraction with the value $7.07^{+0.97}_{-0.94} \times 10^{-7}$ which is somewhat lower than previous measurements. Our prediction is consistent with the latter value within 2σ.

6 Conclusions

The form factors parametrizing the transition matrix of the weak current between the B_s and heavy (D_s^*, $D_{sJ}^{(*)}$) or light ($K^{(*)}$, $K_J^{(*)}$, $\eta(\varphi)$) mesons were calculated on the basis of the relativistic quark model with the QCD-motivated quark-antiquark interaction potential. All

Decay	this paper	[28]	[29]	[30]	[31]	[20]	Exp.[6]
$B_s \to \eta \mu^+ \mu^-$	3.8 ± 0.4	3.4 ± 1.8	3.12	2.30 ± 0.97	2.4	1.2 ± 0.12	
$B_s \to \eta \tau^+ \tau^-$	0.90 ± 0.09	1.0 ± 0.55	0.67	0.373 ± 0.156	0.58	0.34 ± 0.04	
$B_s \to \eta \nu \bar{\nu}$	23.1 ± 2.3	29 ± 15	21.7	13.5 ± 5.6	17		
$B_s \to \eta' \mu^+ \mu^-$	3.2 ± 0.3	2.8 ± 1.5	3.42	2.24 ± 0.94	1.8		
$B_s \to \eta' \tau^+ \tau^-$	0.39 ± 0.04	0.47 ± 0.25	0.43	0.280 ± 0.118	0.26		
$B_s \to \eta' \nu \bar{\nu}$	19.7 ± 2.0	24 ± 13	23.8	13.3 ± 5.5	13		
$B_s \to \varphi \mu^+ \mu^-$	11.6 ± 1.2		16.4			11.8 ± 1.1	$12.3^{+4.0}_{-3.4}$
$B_s \to \varphi \tau^+ \tau^-$	1.5 ± 0.2		1.51			1.23 ± 0.11	
$B_s \to \varphi \nu \bar{\nu}$	79.6 ± 8.0		116.5				<54000
$B_s \to K \mu^+ \mu^-$	0.24 ± 0.03				0.14	0.199 ± 0.021	
$B_s \to K \tau^+ \tau^-$	0.059 ± 0.006				0.03	0.074 ± 0.007	
$B_s \to K \nu \bar{\nu}$	1.42 ± 0.14				1.01		
$B_s \to K^* \mu^+ \mu^-$	0.44 ± 0.05					0.38 ± 0.03	
$B_s \to K^* \tau^+ \tau^-$	0.075 ± 0.008					0.050 ± 0.004	
$B_s \to K^* \nu \bar{\nu}$	3.0 ± 0.3						

Table 10: Comparison of theoretical predictions for the nonresonant branching fractions of the rare semileptonic B_s decays and available experimental data (in 10^{-7}).

relativistic effects, including boosts of the meson wave functions and contributions of the intermediate negative-energy states, were consistently taken into account. The main advantage of the adopted approach consists in that it allows the determination of the momentum transfer dependence of the form factors in the whole accessible kinematical range. Therefore no additional assumptions and ad hoc extrapolations are needed for the description of the weak decay processes which have rather broad kinematical range. This significantly improves the reliability of the obtained results.

The calculated form factors were used for considering the semileptonic and rare B_s decays. The differential and total decay branching fractions as well as asymmetry and polarization parameters were evaluated. The obtained results were confronted with previous investigations based on significantly different theoretical approaches and available experimental data. Good agreement of our predictions with measured values is observed.

References

[1] R. Louvot *et al.* [Belle Collaboration], Phys. Rev. Lett. **102**, 021801 (2009).

[2] R. Aaij *et al.* [LHCb Collaboration], Phys. Lett. B **698**, 115 (2011); Phys. Lett. B **709**, 50 (2012).

[3] H. Ha *et al.* [BELLE Collaboration], Phys. Rev. D **83**, 071101 (2011); J. P. Lees *et al.* [BaBar Collaboration], Phys. Rev. D **86**, 092004 (2012); A. Sibidanov *et al.* [Belle Collaboration], Phys. Rev. D **88**, 032005 (2013).

[4] R. N. Faustov and V. O. Galkin, Phys. Rev. D **87**, 034033 (2013); Phys. Rev. D **87**, 094028 (2013); Eur. Phys. J. C **73**, 2593 (2013).

[5] D. Ebert, R. N. Faustov and V. O. Galkin, Phys. Rev. D **75**, 074008 (2007).

[6] J. Beringer *et al.* [Particle Data Group], Phys. Rev. D **86**, 010001 (2012).

[7] D. Ebert, R. N. Faustov and V. O. Galkin, Phys. Rev. D **67**, 014027 (2003); Phys. Rev. D **79**, 114029 (2009); Eur. Phys. J. C **71**, 1825 (2011).

[8] G. Kramer and W. F. Palmer, Phys. Rev. D **46**, 3197 (1992).

[9] P. Blasi, P. Colangelo, G. Nardulli and N. Paver, Phys. Rev. D **49**, 238 (1994).

[10] X. J. Chen, H. F. Fu, C. S. Kim and G. L. Wang, J. Phys. G **39**, 045002 (2012).

[11] R. -H. Li, C. -D. Lu and Y. -M. Wang, Phys. Rev. D **80**, 014005 (2009).

[12] G. Li, F. -l. Shao and W. Wang, Phys. Rev. D **82**, 094031 (2010).

[13] S. -M. Zhao, X. Liu and S. -J. Li, Eur. Phys. J. C **51**, 601 (2007).

[14] K. Azizi and M. Bayar, Phys. Rev. D **78**, 054011 (2008); K. Azizi, Nucl. Phys. B **801**, 70 (2008).

[15] D. Ebert, R. N. Faustov and V. O. Galkin, Phys. Rev. D **61**, 014016 (2000).

[16] J. Segovia *et al.* Phys. Rev. D **84**, 094029 (2011).

[17] V. M. Abazov *et al.* [D0 Collaboration], Phys. Rev. Lett. **102**, 051801 (2009).

[18] R. Aaij *et al.* [LHCb Collaboration], Phys. Lett. B **698**, 14 (2011); P. Urquijo, arXiv:1102.1160 [hep-ex].

[19] W. -F. Wang and Z. -J. Xiao, Phys. Rev. D **86**, 114025 (2012).

[20] Y. -L. Wu, M. Zhong and Y. -B. Zuo, Int. J. Mod. Phys. A **21**, 6125 (2006).

[21] D. Ebert, R. N. Faustov and V. O. Galkin, Phys. Rev. D **85**, 054006 (2012).

[22] M. -Z. Yang, Phys. Rev. D **73**, 034027 (2006) [Erratum-ibid. D **73**, 079901 (2006)].

[23] Y. -M. Wang, M. J. Aslam and C. -D. Lu, Phys. Rev. D **78**, 014006 (2008).

[24] R. -H. Li, C. -D. Lu, W. Wang and X. -X. Wang, Phys. Rev. D **79**, 014013 (2009).

[25] K. -C. Yang, Phys. Rev. D **78**, 034018 (2008).

[26] W. Wang, Phys. Rev. D **83**, 014008 (2011).

[27] R. Aaij *et al.* [LHCb Collaboration], JHEP **1307**, 084 (2013).

[28] M. V. Carlucci, P. Colangelo and F. De Fazio, Phys. Rev. D **80**, 055023 (2009).

[29] C. Q. Geng and C. C. Liu, J. Phys. G **29**, 1103 (2003).

[30] K. Azizi, R. Khosravi and F. Falahati, Phys. Rev. D **82**, 116001 (2010).

[31] H. -M. Choi, J. Phys. **37**, 085005 (2010).

On possible role of scalar glueball-quarkonia mixing in the f(0)(1370,1500,1710) resonances produced in charmonia decays

S.B. Gerasimov[1]

[1]Bogoliubov Laboratory of Theoretical Physics, Joint Institute for Nuclear Research, Dubna 141980, Russia

The next to lowest mass scalar multiplet is treated as the $q\bar{q}$, P-wave nonet, weakly mixed with the lower - mass, presumably $qq\bar{q}\bar{q}$ S-wave nonet and, in principle, with the $J^{PC} = 0^{++}$ -glueball. The modified Gell-Mann-Okubo-type mass-formulas are used to derive and discuss the quark-gluon configuration structure of the obtained meson states which are then used to obtain the relations between the decay ratios $Br(J/\psi \to \omega f_0)/Br(J/\psi \to \phi f_0)$, where $f_0(1720) \cong G$ is the glueball, the $f_0(1370)$ and $f_0(1506)$ are quarkonium states. Some other relations between the radiative and radiationless decays of the lowest mass charmonium states into scalar resonances are presented and discussed.

1. As is known, the precise understanding of mass and dynamics of the glueball decays is problematic up to now in spite of very large number of works devoted to the problems mentioned. We concentrate on the mass region $1.3 \div 1.7$ GeV occupied by the spin-zero 0^{++} mesons. In this group of mesons there are three isoscalar mesons with similar masses which, in the presence of the nearly lying isotriplet and isodoublet ones, suggest the overpopulated nonet where a possible glueball is hidden within structures of the three isoscalar states. Whether this idea is right or wrong one should deduce from data on the reactions creating them as well as from the relations between the branching ratios of their decays. With this in mind, we present the results of a simple approach enabling one to discuss an acute problem of the existence and properties of glueballs with quantum numbers $I^G J^{PC} = 0^+ 0^{++}$ (for the different approaches, see [1] and references mentioned therein).

2. We define the 3×3 mass-matrix $\hat{V}(i)$ as acting on the basis vectors N, S, G to transform them into one of three vectors of the physical meson states $f_0(i)$:

$$(f_0(i)) = \hat{V}(i) \cdot \begin{pmatrix} N \\ G \\ S \end{pmatrix} \tag{1}$$

where

$$N = \frac{1}{\sqrt{2}}(u\bar{u} + d\bar{d}), \qquad S = s\bar{s},$$

and G is the glueball.

We consider the mass-matrices $\hat{V}(i)$ taking into account explicitly the different appearance of the two types of gluon effects in mixing states of the differing flavor. In a certain sense, we

follow the way proposed in old works by Isgur [2] to connect the strong "non-ideality" of the $SU(3)$-singlet-octet mixing angle in the lowest pseudoscalar and scalar meson nonet with the overwhelmingly strong, as compared to the respective term in the vector or tensor meson nonet, annihilation term in the mass-matrix inducing the non-diagonal $q\bar{q} \leftrightarrow s\bar{s}, (q = u, d)$ transitions. We remind that the celebrated Gell-Mann–Okubo formula

$$3m_{f_8}^2 = 4m_{K_0^*}^2 - m_{a_0}^2$$

follows as the mass sum rule after exclusion of parameters introduced into the general mass term of the phenomenological meson lagrangian

$$\Delta L = M^2 \cdot Tr(V_8 V_8) - \mu^2 \cdot Tr(V_8 V_8 \lambda_8) \tag{2}$$

Okubo [3] proposed to replace $V_8 \rightarrow V_9$ in the GMO mass operator and drop the term proportional to $Tr(V_9)$. The well-known "ideal mixing" mass relations

$$m^2(\rho) = m^2(\omega), \quad 2m^2(K^*) - m^2(\rho) = m^2(\phi)$$

are fulfilled for the vector and reasonably well for tensor $q\bar{q}$ nonets but poor for the pseudoscalar one.

The standard hierarchy of meson masses following from the effective lagrangian with the $SU(3)$ breaking is

$$m^2(s\bar{s}) \geq m^2(q\bar{s}) \geq m^2(q\bar{q}).$$

The idea to relate the apparently specific situation for the pseudoscalar meson sector with additional strong annihilation mechanism transforming the given flavor quark field combinations into each other was put forward phenomenologically by Isgur [2] and is now interpreted as mediated by short-range fluctuations in the quark-gluon vacuum.

We follow these ideas in the further generalized form via introducing the "bare" scalar glueball mass and nondiagonal glueball-quarkonium transition-mass into the spin-zero meson mass-matrices.

Hence, in the $N' = \frac{1}{\sqrt{2}}(u\bar{u} + d\bar{d})', S' = (s\bar{s})'$ basis our symmetric real mass-matrix acquires the following form:

$$\hat{M}^2 = \begin{pmatrix} M_{N'}^2 + 2A_Q & \sqrt{2}A_G & \sqrt{2}A_Q \\ \sqrt{2}A_G & M_G^2 & A_G \\ \sqrt{2}A_Q & A_G & M_{S'}^2 + A_Q \end{pmatrix} \tag{3}$$

After reducing it to the diagonal form we should get the matrix of the eigenvalues $\hat{M}^2{}_{ph}$:

$$\hat{M}^2{}_{ph} = \begin{pmatrix} M_{f_0}^2(1) & 0 & 0 \\ 0 & M_{f_0}^2(2) & 0 \\ 0 & 0 & M_{f_0}^2(3) \end{pmatrix}$$

We start treating the mass relations with the higher-mass scalar 0^{++}-sector:

$$M_{a_0} = 1474 \pm 19, M_{K^*{}_0} = 1425 \pm 50$$

$$M_{f_0}(1) = 1370 \pm 50, M_{f_0}(2) = 1505 \pm 6,$$

$$M_{f_0}(3) = 1720 \pm 7$$

where all values are in MeV [4].

We define the "bare" mass values $M_{N'}$ and $M_{S'}$ devoid of the strong annihilation contributions via

$$M_{N'} = M_{a_0}, M_{S'}{}^2 = 2M_{K^*_0}{}^2 - M_{a_0}{}^2,$$

A short digression: the second relation is alike of the S-wave vector quarkonia, but we would like to note the opposite mass hierarchy sequence

$$M^2(s\bar{s})' \leq M^2(q\bar{s})' \leq M^2(q\bar{q})'$$

which can follow from the suggested [5] mixing of two scalar nonets composed of light (u,d,s)-quarks: the low-mass, presumably the two-quark-two-antiquark-nonet with the total orbital angular moment $L = 0$ and $(mass^2) \leq 1GeV^2$ and the higher-mass, quark-antiquark states with orbital moment $L = 1$.

Phenomenologically, we can indicate this just by changing the sign of the constant μ^2 in the general $SU(3)$ mass formula (2) and by formally introducing the "primed" quark amplitudes including the mentioned 4-quark admixtures and satisfying the inverted mass sequence.

The physical meaning of terms in the mixing-mass matrix is following. The term A_Q in the mass matrix represents the dynamical self-mass term determined by the short-ranged, quark-flavor changing processes, while M_G and A_G are the "bare" gluon mass and the non-diagonal self-mass term arising in the course of quarkonium-glueball transitions. These three unknown terms have to be found by solution of the system of three non-linear equations representing the equalities of three invariants of the diagonalization process: the trace, the determinant and the sum of main minors of the matrices before and after diagonalization. The diagonalized mass-matrix is assumed to contain only experimentally defined masses of scalar meson resonances. Successively excluding unknown variables A_Q and A_G in favor of M_G, we solve numerically the resulting equation by varying the remaining unknown M_G under constraint $A_G{}^2 \geq 0$. There is trivial "decoupling-solution" $A_G = 0$ and $M_G \simeq M_{f_0(3)}$ and none for the "postulated" $A_G{}^2 > 0$ representing, by convention, the nonzero mixing of the glueball G with the remaining quarkonia. Therefore, we have to accept for the physical glueball mass our solution practically coinciding with the mass of $M_{f_0}(3)$ and to derive conclusion about the decoupling of the gluon from two near-by f_0-quarkonium:

$$M_G(ph) \simeq 1730 \ MeV \iff M_{f_0}(3) = 1720 \pm 7 \ MeV \tag{4}$$

The state vectors of $f_0(1506)$ and $f_0(1370)$ are obtained then by the diagonalization of the rest 2×2 matrix:

$$f_0(1506) = 0.868 \cdot N' \pm 0.496 \cdot S' \tag{5}$$
$$f_0(1370) = \mp 0.496 \cdot N' + 0.868 \cdot S'. \tag{6}$$

The choice of signs (upper→ (u),or lower→ (l)) remains to be done on the physics ground.

3. The sensitive check of our results can be obtained from the radiative and hadronic decays of the lowest mass charmonium states. In the radiative transitions, it is natural to accept the dominance of diagrams of the annihilation of bound $c\bar{c}$-quarks to photon and the pair of intermediate gluon followed by the hadronization process, for instance, $J/\psi \to \gamma gg \to \gamma + hadrons$. We accept the following approximations. First, we drop the 4-quark admixtures to the $f_0(1370; 1500)$ quarkonium state vectors following a kind of the minimal "quark-counting"

approximation for the "hard" annihilation processes. In the processes with the two quarkoniums in the final state we keep only the singlet $SU(3)$ projection for the final total hadron state in the transitions $gluons \rightarrow hadrons(n_{q\bar{q}} \geq 2)$. Further, the final phase volume factors will be taken into account as the only explicitly taken into account momentum-dependent characteristics of the processes. Firstly we apply the simple $SU(3)$-symmetry approach to ratio of the branching ratio $J/\psi \rightarrow \gamma f_0(1370)$ vs $J/\psi \rightarrow \gamma f_0(1506)$ to fix the signs in (5)-(6). Rewriting (5)-(6) in terms of the $SU(3)$-basis vectors and leaving only coefficients referring to the transition $gg \rightarrow q\bar{q}|_{singlet}$ in the matrix elements, we obtain

$$\frac{\Gamma(J/\psi \rightarrow \gamma + f_0(1370))}{\Gamma(J/\psi \rightarrow \gamma + f_0(1506))} = \frac{|\vec{k}(f_0(1370))|}{|\vec{k}(f_0(1506))|} \cdot \begin{pmatrix} \frac{.904^2}{.426^2} \\ \\ \frac{.092^2}{.996^2} \end{pmatrix} = \begin{pmatrix} 4.74 \\ \\ .009 \end{pmatrix}$$

$$(5;6u)$$
$$(5;6l)$$

From this point onwards we accept the lower signs in (5)-(6) because the $Br(J/\psi \rightarrow \gamma f_0(1370))$ remains unknown and is presumably lower or much lower than measured radiative transitions to $f_0(1506)$ and $f_0(1720)$ resonances. The ratio of the 3-momenta stands for the ratio of the phase space factors accepted for the decays of the type $A \rightarrow B + C$ and giving a minimal kinematic dependence in terms of particle masses in the initial and final states. Under these assumptions, we turn to several processes with participation of the vector $\phi(1.02)$- and $\omega(.783)$-mesons that serving to be good flavor "filters" for the state vectors of scalars participating in a particular reaction. The matrix elements of the process $(J/\psi \rightarrow V + f_0(1720))$ includes a series of the virtual transitions, symbolically, $J/\psi \rightarrow 3g \rightarrow V + gg \rightarrow V + f_0(1720)$, that are proportional to the well-known SU(3)-singlet component of the ω- and ϕ- meson, and to the form-factors of the $3gV$-vertex. As gluons are assumed to be effectively-hard vector quanta we replace approximately the ratios of the full ω- and $\phi-$ form-factors by the respective ratios of their radial "functions-at-zero-distance", entering the ratios of the widths of $V \rightarrow e^-e^+$ - decays, according to the Van Royen - Weisskopf [6] relation. Thus

$$R_{\omega\phi}(f_0(1720)) = \frac{|\vec{k}_{\omega f_0(1720)}|}{|\vec{k}_{\phi f_0(1720)}|} \cdot (tan\theta_V)^{-2} \cdot \frac{V_\omega^2(0)}{V^2_\phi(0)} \simeq 1.1; (Exp: 1.33 \pm .34)[4] \qquad (7)$$

To get ratios $R_{\omega\phi}(f_0(1370))$ and $R_{\omega\phi}(f_0(1506))$ we need to consider the contributions of both $(1)_V \times (1)_f$- and $(8)_V \times (8)_f$ - terms in the ratios. We apply the $SU(3)$ isoscalar factor $-(1/\sqrt{8})$ corresponding to the singlet content of each $(8)_V \times (8)_{f_0}$ (see, $e.g$ [4]) and will treat both terms as acting either coherently or incoherently in all ratios. Comparing the results we found that the incoherent squaring option seem applies better for $R_{\omega\phi}(f_0(1370))$ where the BES2 Collaboration has observed the $J\psi \rightarrow f_0(1370)\phi \rightarrow 2\pi\phi$ -decay channel [7] and does not report the similar channel with ω-meson presumably due to its lower probability. Therefore

$$R_{\omega\phi}(f_0(1370)) = \frac{|\vec{k}_{\omega f_0(1370)}|}{|\vec{k}_{\phi f_0(1370)}|} \cdot \frac{[(1)_\omega \times (1)_{f_0(1370)}]^2 + [(8)_\omega \times (8)_{f_0(1370)}]^2 \cdot (1/\sqrt{8})^2}{[(1)_\phi \times (1)_{f_0(1370)}]^2 + [(8)_\phi \times (8)_{f_0(1370)}]^2 \cdot (1/\sqrt{8})^2} \simeq .76 \quad (8)$$

$$R_{\omega\phi}(f_0(1506)) = \frac{|\vec{k}_{\omega f_0(1506)}|}{|\vec{k}_{\phi f_0(1506)}|} \cdot \frac{[(1)_\omega \times (1)_{f_0(1506)}]^2 + [(8)_\omega \times (8)_{f_0(1506)}]^2 \cdot (1/\sqrt{8})^2}{[(1)_\phi \times (1)_{f_0(1506)}]^2 + [(8)_\phi \times (8)_{f_0(1506)}]^2 \cdot (1/\sqrt{8})^2} \simeq 2.04 \quad (9)$$

The approximate or even moderate-broken $SU(3)_{flav}$-symmetry seems, however, not applicable to pair-wise decays of more heavy scalar charmonium $\chi_{c0}(3.414)$ to $f_0(1370, 1506, 1720)$.

As was measured by BES Collaboration [8], the branching ratios upper-bounds for the transitions $\chi_{c0}(3.414) \to f_0(1370)f_0(1506); f_0(1720)f_0(1506)$ are much less than the branching ratio $\chi_{c0}(3.414) \to f_0(1370)f_0(1720)$ assuming the dominant contribution of the strange quarks in the intermediate processes $gg \to s\bar{s}$, due to larger values their momentum-scale dependent mass as compared to the masses of the non-strange quarks [9]. To estimate the relevance of this idea we apply the extremal case of taking into account the contribution of only strange quarks to ratio of the transitions $\chi_{c0}(1P; 3.414) \to f_0(1.720) + f_0(1370))$ and $\chi_{c0}(1P; 3.414) \to f_0(1.720) + f_0(1506))$. Returning to the quark-flavor basis (5)-(6) with the fixed lower signs, using the needed values of $Br(f_0 \to \pi\pi(K\bar{K}))$ from [4] to exclude them from the experimentally measured ratios, we obtain

$$R_{f_0(1.37), f_0(1.50)}(\chi_{c0}(3414)) = \frac{|\vec{k}_{f_0(1370), f_0(1720)}|}{|\vec{k}_{f_0(1506), f_0(1720)}|} \cdot \frac{[.868^2]}{[.496^2]} \simeq 3.9 \qquad (10)$$

while the lower limit of the experimental value is $13 \pm 4.6 + 6.8(-4.4)$ [8]. It is seen that even with the use of the extreme assumption about strange quark domination in the mechanism of the $\chi_{c0} \to f_0(1370; (1506)) + f_0(1720)$ decays the accord with experimental ratio is a marginal one.

To conclude, the further accumulation of more precise data on the decays of more massive scalar, tensor, etc., charmonium states into the meson resonances including the scalar glueball $G(0^{++}) \cong f_0(1720)$ decoupled off nearby quarkonium scalars , will provide more constrained and unequivocal way to study the dynamics of the gluon degrees of freedom in QCD.

The author is grateful to Organizers of the Heavy Quark School-2013 (JINR, Dubna) for invitation to take part in it.

References

[1] E. Gregory, A. Irving, S. Lucini, *et al.*, JHEP, **1210**, 170, (2012).

[2] N. Isgur, Phys. Rev., D 13, 122, (1976).

[3] S. Okubo, Phys. Lett., **5**, 165, 1963.

[4] J. Beringer, *et al.* (PDG), Phys. Rev. **D86** 010001 (1012).

[5] D. Black, A.H. Fariborz and J. Schechter, Phys. Rev. **D 61**, 074001, (2000).

[6] R. Van Royen and V.F. Weisskopf, Nuovo Cim., **A50**, 617, (1967).

[7] M. Ablikim, *et al.*, (BES Collaboration), Phys. Lett. **B607**, 243, (2005).

[8] M. Ablikim, *et al.*, (BES Collaboration), Phys. Rev., **D72**, 092002, (2005).

[9] M. Chanowitz, Phys. Rev. Lett., **95**, 172001, (2005).

Effective weak Lagrangians in the Standard Model and B decays

Andrey Grozin

Budker Institute of Nuclear Physics, Novosibirsk, Russia

Weak processes (e.g., B decays) with characteristic energies $\ll M_W$ can be described by an effective theory which does not contain W, Z and other heavy particles (Higgs, t). Its Lagrangian contains four-fermion interaction operators. Essentially it is the theory proposed by Fermi and improved by Feynman, Gell-Mann, Marshak, Sudarshan.

1 Introduction

We don't know *all* physics up to *infinitely high* energies (or down to *infinitely small* distances). *All* our theories are effective low-energy (or large-distance) theories (except *The Theory of Everything* if such a thing exists). There is a high energy scale M where an effective theory breaks down. Its Lagrangian describes light particles ($m_i \ll M$) and their interactions at low momenta ($p_i \ll M$). In other words, it describes physics at large distances $\gg 1/M$; physics at small distances $\lesssim 1/M$ produces local interactions of these light fields. The Lagrangian contains all possible operators (allowed by symmetries). Coefficients of operators of dimension $n + 4$ contain $1/M^n$. If M is much larger than energies we are interested in, we can retain only renormalizable terms (dimension 4), and, maybe, a power correction or two.

In order to describe weak processes with characteristic energies $\ll M_W$, such as b decays, we can use an effective theory without $W^\pm$, Z^0, Higgs, t. In these lectures we consider effective Lagrangians for some b decay processes. Coefficients of local interaction operators in this Lagrangian are obtained by matching at $\mu \sim M_W$. In order to calculate b decays one needs to know these coefficients at a much lower $\mu \sim m_b$. They are obtained by solving renormalization group equations. One needs to calculate the matrix of anomalous dimensions of the operators entering the effective Lagrangian.

Of course, the knowledge of the Lagrangian is not sufficient. In order to obtain full or differential decay rates into various channels, we need to calculate these decay rates in the framework of the effective theory. The largest energy scale in such calculations is m_b; all information about physics at the scale M_W is contained in the coefficients of interaction operators in the effective Lagrangian. For total decay rates into a channel with some flavor quantum numbers if is sufficient to calculate the spectral density of the correlator of the relevant interaction operators; this is a single-scale problem with the scale m_b (in some cases one has also to take $m_c \neq 0$ into account). For more detailed decay characteristics is is often useful to construct further effective theories for energy scales $\ll m_b$ (HQET, SCET; Fig. 1). One performs matching at $\mu \sim m_b$ to obtain coefficients in such effective Lagrangians, and then evolves them to lower μ using renormalization group. We shall not discuss these questions here.

Effective Lagrangians for B decays are discussed in great detail in the excellent lectures by
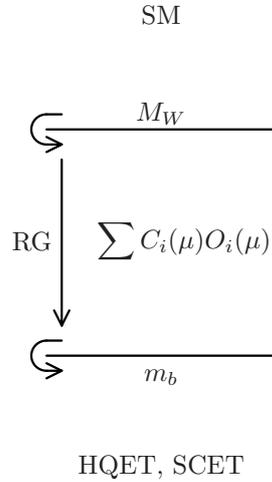
SM

Figure 1: Hierarchy of effective theories.

A. Buras [1]; the reader is encouraged to use them for learning any information missing here. References to the relevant papers can be found in [2]. Here I don't cite original papers, except a few ones which contain material directly used in these lectures.

The traditional Fermi constant G is not used in these lectures, because it is better to see the powers of $1/M_W$ and coupling constants explicitly. We mainly work at the leading $1/M_W^2$ order, see Sect. 2 for brief comments about $1/M_W^4$. Powers of couplings depend on the process: g_2^2 for ordinary weak decays, $g_2^2 e$ for $b \to s\gamma$, g_2^4 for $B^0 \leftrightarrow \bar{B}^0$ oscillations (Sect. 5).

The matrix γ_5 is not used. Left fermion fields are used; this is, of course, necessary, because left and right fields interact differently in the Standard Model. Some operators with left fields vanish at $d = 4$ (and thus become evanescent, Sect. 3.4); this is the only role played by the index L [3].

2 $b \to cl^-\bar{\nu}_l$

The amplitude of the semileptonic decay $b \to cl^-\bar{\nu}_l$ in the Standard Model (Fig. 2a) is

$$M = \frac{g_2^2}{2} V_{cb} \frac{1}{M_W^2 - q^2} (\bar{u}_{cL}\gamma^\alpha u_{bL})(\bar{u}_{lL}\gamma_\alpha v_{\nu L}) \tag{2.1}$$

where

$$g_2 = \frac{e}{\sin\theta_W}$$

is the $SU(2)$ gauge coupling constant. Expanding in $q^2/M_W^2 \ll 1$, we have at the leading order

$$M = \frac{g_2^2}{2M_W^2} V_{cb}(\bar{u}_{cL}\gamma^\alpha u_{bL})(\bar{u}_{lL}\gamma_\alpha v_{\nu L}). \tag{2.2}$$

This amplitude can be reproduced from the effective Lagrangian (Fig. 2b)

$$L = \frac{g_2^2}{2M_W^2} V_{cb} (\bar{c}_L \gamma^\alpha b_L) \, (\bar{l}_L \gamma_\alpha \nu_L) \,. \tag{2.3}$$
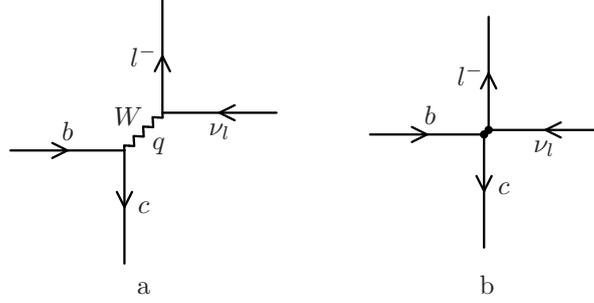

Figure 2: b semileptonic decay in the full theory (a) and in the effective theory (b).

Now we shall discuss one-loop QCD renormalization of the operator

$$O_0 = (\bar{c}_{0L} \gamma^\alpha b_{0L}) \, (\bar{l}_L \gamma_\alpha \nu_L) \tag{2.4}$$

(we are not going to consider electroweak loop corrections; therefore, the lepton fields don't renormalize). This bare operator is related to the renormalized one as

$$O_0 = Z(\alpha_s(\mu)) O(\mu) \,, \qquad O(\mu) = Z^{-1}(\alpha_s(\mu)) O_0 \tag{2.5}$$

in the $\overline{\text{MS}}$ scheme. In the matrix element of the bare operator

$$<O_0> = Z<O>$$

α_s/ε term comes only from Z. This matrix element is

$$<O_0> = Z_q \left[\quad + \quad \right] \,, \tag{2.6}$$

where Z_q is the $\overline{\text{MS}}$ quark field renormalization constant. We need only the $1/\varepsilon$ term in the α_s correction.

The UV divergence of the vertex (Fig. 3) does not depend on external momenta, therefore we may set them to 0:

$$\begin{aligned}
\Lambda_1 &= -iC_F g_0^2 \int \frac{d^d k}{(2\pi)^d} \frac{1}{(k^2)^3} \left(g_{\mu\nu} - \xi \frac{k_\mu k_\nu}{k^2} \right) \gamma^\mu \not{k} \gamma^\alpha \not{k} \gamma^\nu \otimes \gamma_\alpha \\
&= -iC_F g_0^2 \int \frac{d^d k}{(2\pi)^d} \frac{1}{(k^2)^2} \left[\frac{1}{d} \gamma^\mu \gamma^\lambda \gamma^\alpha \gamma_\lambda \gamma_\mu - \xi \gamma^\alpha \right] \otimes \gamma_\alpha \\
&= -iC_F g_0^2 \int \frac{d^d k}{(2\pi)^d} \frac{1}{(k^2)^2} \left[\frac{(d-2)^2}{d} - \xi \right] \gamma^\alpha \otimes \gamma_\alpha
\end{aligned} \tag{2.7}$$
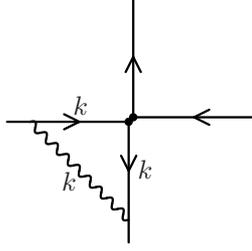
Figure 3: The one-loop correction to the vertex function of O_0.

where $A \otimes B$ means $(\bar{u}_{cL} A u_{bL}) (\bar{u}_{lL} B v_{\nu L})$, and the gluon propagator is

$$D_{\mu\nu}(k) = \frac{1}{k^2} \left[g_{\mu\nu} - \xi \frac{k_\mu k_\nu}{k^2} \right] .$$

Of course, we need some IR regularization here, e.g. a non-zero mass in the denominator:

$$\int \frac{d^d k}{(k^2)^2} \Rightarrow \int \frac{d^d k}{(k^2 - m^2)^2} \Rightarrow \frac{i}{(4\pi)^2} \frac{1}{\varepsilon} \tag{2.8}$$

(this is a simplest example of infrared rearrangement). Substituting the well-known one-loop Z_q and keeping only $1/\varepsilon$ in the α_s correction, we obtain

$$<O_0> = \left[1 - C_F \frac{\alpha_s}{4\pi\varepsilon} (1 - \xi) \right] \left[1 + C_F \frac{\alpha_s}{4\pi\varepsilon} (1 - \xi) \right] = 1 . \tag{2.9}$$

Hence $Z(\alpha_s) = 1$ — the vector current does not renormalize. This is true to all orders in α_s as follows from the Ward identity. Note that we haven't used γ_5 in this calculation: it is hidden in the index L of the external fermion wave functions; this implicitly means the anticommuting γ_5. Hence the axial current with the anticommuting γ_5 does not renormalize too; this is obvious — we can always anticommute γ_5 out of the calculation.

It is not difficult to construct an effective Lagrangian which reproduces results of the full theory expanded up to $1/M_W^4$. The $b \to c l^- \bar{\nu}_l$ decay matrix element (2.1 with this accuracy is

$$M = \frac{g_2^2}{2M_W^2} V_{cb} \left(1 + \frac{q^2}{M_W^2} \right) (\bar{u}_{cL} \gamma^\alpha u_{bL}) (\bar{u}_{lL} \gamma_\alpha v_{\nu L}) ; \tag{2.10}$$

it follows from the effective Lagrangian

$$L = \frac{g_2^2}{2M_W^2} V_{cb} (\bar{c}_L \gamma^\alpha b_L) \left(1 - \frac{\partial^2}{M_W^2} \right) (\bar{l}_L \gamma_\alpha \nu_L) . \tag{2.11}$$

When calculating any process with the $1/M_W^4$ accuracy, we can include in a diagram either a single $1/M_W^4$ vertex from the effective Lagrangian, or up to two $1/M_W^2$ vertices. We need to investigate renormalization of the dimension-8 operators which appear in the $1/M_W^4$ term in the Lagrangian; there is a finite number of such operators. We also need to renormalize bilocal products of pairs of dimension-6 operators which appear in the $1/M_W^2$ term in the Lagrangian. In addition to renormalization of each operator, local dimension-8 counterterms are needed. In general, at any order in $1/M_W^2$ a finite number of renormalization constant is needed, and the theory retains its predictive power.

3 $b \to cd\bar{u}$

3.1 Effective Lagrangian

In this Section we shall discuss the non-leptonic decay where all four flavors are different at the leading order in electroweak interaction. Its full-theory matrix element at the $1/M_W^2$ level is reproduced by the effective Lagrangian

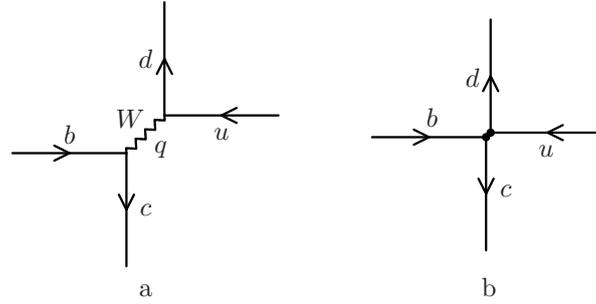$$L = \frac{g_2^2}{2M_W^2} V_{cb} V_{ud}^* (\bar{c}_L \gamma^\alpha b_L)(\bar{d}_L \gamma_\alpha u_L). \tag{3.1}$$

Figure 4: $b \to cd\bar{u}$ decay in the full theory (a) and in the effective theory (b).

We need to include a full set of operators closed under renormalization to the Lagrangian. It consists of two operators

$$O_1 = (\bar{c}_{Li} \gamma^\alpha b_L^i)(\bar{d}_{Lj} \gamma_\alpha u_L^j), \qquad O_2 = (\bar{c}_{Li} \gamma^\alpha b_L^j)(\bar{d}_{Lj} \gamma_\alpha u_L^i). \tag{3.2}$$

In $d = 4$ we can use Fierz rearrangement[1]

$$(\bar{\psi}_{1L} \gamma^\alpha \psi_{2L})(\bar{\psi}_{3L} \gamma_\alpha \psi_{4L}) = (\bar{\psi}_{3L} \gamma^\alpha \psi_{2L})(\bar{\psi}_{1L} \gamma_\alpha \psi_{4L}) \tag{3.3}$$

to re-write these operators as

$$O_1 = (\bar{d}_{Lj} \gamma^\alpha b_L^i)(\bar{c}_{Li} \gamma_\alpha u_L^j), \qquad O_2 = (\bar{d}_{Lj} \gamma^\alpha b_L^j)(\bar{c}_{Li} \gamma_\alpha u_L^i). \tag{3.4}$$

Fierz rearrangement is especially simple (3.3) in the case when all four wave functions are left: there is exactly one structure possible in the right-hand side ($1 \otimes 1$, $\gamma_5 \otimes \gamma_5$, $\sigma^{\alpha\beta} \otimes \sigma_{\alpha\beta}$ vanish; $\gamma^\alpha \gamma_5 \otimes \gamma_\alpha \gamma_5$ reduces to $\gamma^\alpha \otimes \gamma_\alpha$).

Sometimes the operator

$$O_2' = (\bar{c}_L t^a \gamma^\alpha b_L)(\bar{d}_L t^a \gamma_\alpha u_L) = T_F \left(O_2 - \frac{O_1}{N_c} \right) \tag{3.5}$$

---

[1] We know persons who became bosons. Markus Fierz has become a verb: physicists say "this can be proved by fierzing" or "let's fierz this product".

is used instead of O_2. This relation follows from Cvitanović algorithm for $SU(N_c)$

$$(t^a)^i{}_j (t^a)^k{}_l = T_F \left[\delta^i_l \delta^k_j - \frac{1}{N_c} \delta^i_j \delta^k_l \right],$$

$$\qquad (3.6)$$

(this is the color Fierz rearrangement).

The column vector of the bare operators O_0 is related to that of the renormalized operators $O(\mu)$ as

$$O_0 = Z(\alpha_s(\mu)) O(\mu), \qquad O(\mu) = Z^{-1}(\alpha_s(\mu)) O_0, \qquad (3.7)$$

where Z is the matrix of renormalization constants. Differentiating this formula, we obtain the renormalization group equation

$$\frac{dO(\mu)}{d\log\mu} + \gamma(\alpha_s(\mu)) O(\mu) = 0, \qquad (3.8)$$

where the anomalous dimension matrix is

$$\gamma = Z^{-1} \frac{dZ}{d\log\mu} = -\frac{dZ^{-1}}{d\log\mu} Z. \qquad (3.9)$$

The effective Lagrangian can be written via either bare or renormalized operators:

$$L = \frac{g_2^2}{2M_W^2} V_{cb} V_{ud}^* c_0^T O_0 = \frac{g_2^2}{2M_W^2} V_{cb} V_{ud}^* c^T(\mu) O(\mu), \qquad (3.10)$$

where $c(\mu) = Z^T(\alpha_s(\mu)) c_0$ is the column vector of Wilson coefficients. It satisfies the RG equation

$$\frac{dc(\mu)}{d\log\mu} = \gamma^T(\alpha_s(\mu)) c(\mu). \qquad (3.11)$$

Dividing (3.11) by the RG equation for $\alpha_s(\mu)$ we obtain

$$\frac{dc}{d\log\alpha_s} = -\frac{\gamma^T(\alpha_s)}{2\beta(\alpha_s)} c, \qquad (3.12)$$

where

$$\beta(\alpha_s) = \beta_0 \frac{\alpha_s}{4\pi} + \cdots, \qquad \gamma^T(\alpha_s) = \gamma_0^T \frac{\alpha_s}{4\pi} + \cdots$$

At the leading (one-loop) order the solution is the matrix exponent

$$c(\mu) = \left(\frac{\alpha_s(\mu)}{\alpha_s(M_W)} \right)^{-\frac{\gamma_0^T}{2\beta_0}} c(M_W). \qquad (3.13)$$

If eigenvectors v_i of γ_0^T ($\gamma_0^T v_i = \lambda_i v_i$) form a full basis[2], then

$$c(\mu) = \sum A_i \left(\frac{\alpha_s(\mu)}{\alpha_s(M)} \right)^{-\frac{\lambda_i}{2\beta_0}} v_i, \qquad (3.14)$$

---

[2] In some rare exceptional cases the Jordan form of γ_0^T may contain blocks of sizes > 1; then the form of the solution is slightly different.

where $c(M_W) = \sum A_i v_i$.

The Wilson coefficients $c_i(\mu_0)$ at some scale μ_0 are determined by matching — equating some S-matrix elements in the full theory (expanded in p_i/M_W) and in the effective theory. It is most convenient to use $\mu_0 \sim M_W$; then $c_i(\mu_0)$ are given by perturbative series in $\alpha_s(\mu_0)$ containing no large logarithms. They contain all the information about physics at the scale M_W which is important for low-energy processes. The Wilson coefficients $c_i(\mu)$ at low normalization scales μ are obtained by solving the RG equations. The effective theory knows nothing about M_W; the only information about it is contained in $c_i(\mu)$. When the effective Lagrangian is applied to some physical process with small momenta $p_i \ll M_W$, it is most convenient to use μ of the order of the characteristic momenta: then the results will contain no large logarithms. This solution of the RG equation sums large logarithmic terms in perturbation series.

3.2   One-loop anomalous dimensions

The matrix element of the bare operator O_1^0

$$(3.15)$$

has two color structures

$$T_1 = \delta_b^c \delta_u^d, \qquad T_2 = \delta_b^d \delta_u^c$$

(the quark color indices coincide with the quark names). The matrix element of O_2^0 can be obtained by simple substitutions of the color structures.

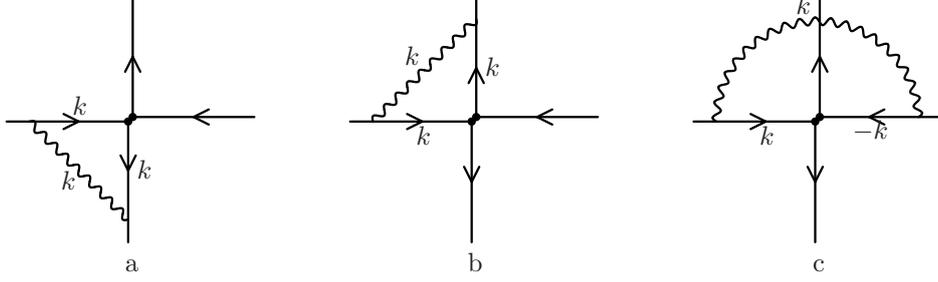The contribution of Fig. 5a differs from (2.7) only by adding the color factor T_1:

$$\Lambda_1 = C_F T_1 \frac{\alpha_s}{4\pi\varepsilon}(1-\xi)\gamma^\alpha \otimes \gamma_\alpha. \tag{3.16}$$

Fig. 5b has the color structure $T_F(T_2 - T_1/N_c)$ (3.6). We only need the $1/\varepsilon$ UV divergence, and hence we may do the γ-matrix algebra at $d = 4$. Fierz rearrangement makes this calculation identical to the previous one:

$$\Lambda_2 = T_F\left(T_2 - \frac{T_1}{N_c}\right)\frac{\alpha_s}{4\pi\varepsilon}(1-\xi)\gamma^\alpha \otimes \gamma_\alpha. \tag{3.17}$$

We can also do this calculation explicitly:

$$\Lambda_2 = T_F\left(T_2 - \frac{T_1}{N_c}\right)\frac{\alpha_s}{4\pi\varepsilon}\left[\frac{1}{d}\gamma^\alpha\gamma^\lambda\gamma^\mu \otimes \gamma_\mu\gamma_\lambda\gamma_\alpha - \xi\gamma^\alpha \otimes \gamma_\alpha\right], \tag{3.18}$$

Figure 5: One-loop O_1^0 vertex diagrams.

where $\gamma^\mu \otimes \gamma_\mu$ comes from the gluon propagator, and $\gamma^\lambda \otimes \gamma_\lambda$ from $\not{k} \otimes \not{k}$ after averaging over k directions. The γ-matrix structure appearing here can be calculated at $d = 4$ using Fierz rearrangement:

$$\gamma^\alpha \gamma^\lambda \gamma^\mu \otimes \gamma_\mu \gamma_\lambda \gamma_\alpha = \gamma_\mu \gamma_\lambda \gamma^\alpha \gamma^\lambda \gamma^\mu \otimes \gamma_\alpha = 4\gamma^\alpha \otimes \gamma_\alpha \,, \tag{3.19}$$

and we again obtain (3.17).

Fig. 5c also has the color structure $T_F(T_2 - T_1/N_c)$. It differs from Fig. 5b by the fact that one k is directed against the quark line (thus producing $-$), and by the opposite order of γ-matrices on the second quark line:

$$\Lambda_3 = -T_F \left(T_2 - \frac{T_1}{N_c} \right) \frac{\alpha_s}{4\pi\varepsilon} \left[\frac{1}{d} \gamma^\alpha \gamma^\lambda \gamma^\mu \otimes \gamma_\alpha \gamma_\lambda \gamma_\mu - \xi \gamma^\alpha \otimes \gamma_\alpha \right] \,,$$

cf. (3.18). We can reduce this structure to the previous one by anticommuting γ-matrices on the second line:

$$\gamma_\alpha \gamma_\lambda \gamma_\mu = -\gamma_\mu \gamma_\lambda \gamma_\alpha + 2 \left(g_{\alpha\lambda} \gamma_\mu - g_{\alpha\mu} \gamma_\lambda + g_{\lambda\mu} \gamma_\alpha \right) \,,$$

and hence

$$\gamma^\alpha \gamma^\lambda \gamma^\mu \otimes \gamma_\alpha \gamma_\lambda \gamma_\mu = -\gamma^\alpha \gamma^\lambda \gamma^\mu \otimes \gamma_\mu \gamma_\lambda \gamma_\alpha + 2(3d - 2)\gamma^\alpha \otimes \gamma_\alpha \,. \tag{3.20}$$

Finally,

$$\Lambda_3 = -T_F \left(T_2 - \frac{T_1}{N_c} \right) \frac{\alpha_s}{4\pi\varepsilon} (4 - \xi)\gamma^\alpha \otimes \gamma_\alpha \,. \tag{3.21}$$

Adding mirror-symmetric diagrams and inserting the external leg renormalization Z_q^2, we obtain the matrix element of the bare operator O_1^0:

$$\begin{aligned}
<O_1^0> = {}& \left[1 - 2C_F \frac{\alpha_s}{4\pi\varepsilon}(1 - \xi) \right] \left[T_1 \right. \\
& + 2C_F T_1 \frac{\alpha_s}{4\pi\varepsilon}(1 - \xi) \\
& + 2T_F \left(T_2 - \frac{T_1}{N_c} \right) \frac{\alpha_s}{4\pi\varepsilon}(1 - \xi) \\
& \left. - 2T_F \left(T_2 - \frac{T_1}{N_c} \right) \frac{\alpha_s}{4\pi\varepsilon}(4 - \xi) \right] \gamma^\alpha \otimes \gamma_\alpha \\
= {}& <O_1> - 6T_F \frac{\alpha_s}{4\pi\varepsilon} \left(<O_2> - \frac{<O_1>}{N_c} \right) \,.
\end{aligned} \tag{3.22}$$

It is gauge invariant, as expected. In the case of the operator O_2^0, Fig. 5b has the color structure $C_F T_2$, and Fig. 5a, c — $T_F(T_1 - T_2/N_c)$ (3.6):

$$
\begin{aligned}
<O_2^0> = & \left[1 - 2C_F \frac{\alpha_s}{4\pi\varepsilon}(1-\xi)\right] \Bigg[T_2 \\
& + 2T_F\left(T_1 - \frac{T_2}{N_c}\right)\frac{\alpha_s}{4\pi\varepsilon}(1-\xi) \\
& + 2C_F T_2 \frac{\alpha_s}{4\pi\varepsilon}(1-\xi) \\
& - 2T_F\left(T_1 - \frac{T_2}{N_c}\right)\frac{\alpha_s}{4\pi\varepsilon}(4-\xi)\Bigg]\gamma^\alpha \otimes \gamma_\alpha \\
= & <O_2> - 6T_F\frac{\alpha_s}{4\pi\varepsilon}\left(<O_1> - \frac{<O_2>}{N_c}\right).
\end{aligned}
\tag{3.23}
$$

We arrive at the renormalization constant matrix

$$
Z = 1 + 6T_F\frac{\alpha_s}{4\pi\varepsilon}\begin{pmatrix} \frac{1}{N_c} & -1 \\ -1 & \frac{1}{N_c} \end{pmatrix}
\tag{3.24}
$$

at one loop. In general, if

$$
Z = 1 + \frac{\alpha_s}{4\pi\varepsilon}z_1,
$$

then

$$
\frac{dZ}{d\log\mu} = -2\varepsilon\frac{\alpha_s}{4\pi\varepsilon}z_1 = \gamma_0\frac{\alpha_s}{4\pi},
$$

and

$$
\gamma_0 = -2z_1.
\tag{3.25}
$$

Therefore, in our case

$$
\gamma_0 = -12T_F\begin{pmatrix} \frac{1}{N_c} & -1 \\ -1 & \frac{1}{N_c} \end{pmatrix}.
\tag{3.26}
$$

It is easy to solve the eigenvalue problem $\gamma_0^T v_\pm = \lambda_\pm v_\pm$:

$$
v_\pm = \begin{pmatrix} 1 \\ \pm 1 \end{pmatrix}, \qquad \lambda_\pm = -12T_F\left(\frac{1}{N_c} \mp 1\right).
\tag{3.27}
$$

Substituting the initial condition at $\mu = M_W$

$$
c(M_W) = \begin{pmatrix} 1 \\ 0 \end{pmatrix} = \frac{1}{2}\left[\begin{pmatrix} 1 \\ 1 \end{pmatrix} + \begin{pmatrix} 1 \\ -1 \end{pmatrix}\right],
\tag{3.28}
$$

we obtain the running Wilson coefficients (3.14)

$$
c(\mu) = \frac{1}{2}\left[\begin{pmatrix} 1 \\ 1 \end{pmatrix}\left(\frac{\alpha_s(\mu)}{\alpha_s(M_W)}\right)^{-\frac{\lambda_+}{2\beta_0}} + \begin{pmatrix} 1 \\ -1 \end{pmatrix}\left(\frac{\alpha_s(\mu)}{\alpha_s(M_W)}\right)^{-\frac{\lambda_-}{2\beta_0}}\right].
\tag{3.29}
$$

Alternatively, one can introduce the operators

$$
O_\pm = O_1 \pm O_2,
\tag{3.30}
$$

so that

$$L = c_+ O_+ + c_- O_- \,, \qquad c_\pm = \frac{c_1 \pm c_2}{2} \,.$$

With the one-loop accuracy, these operators renormalize independently:

$$O_\pm^0 = Z_\pm(\alpha_s(\mu)) O_\pm(\mu) \,.$$

Substituting the initial conditions

$$c_+(M_W) = c_-(M_W) = \frac{1}{2} \,,$$

we obtain the one-loop running

$$c_\pm(\mu) = \frac{1}{2} \left(\frac{\alpha_s(\mu)}{\alpha_s(M_W)} \right)^{-\frac{\lambda_\pm}{2\beta_0}} \,. \tag{3.31}$$

However, the operators $O_\pm$ do mix starting from two loops, and therefore don't produce a great simplification.

3.3 One-loop matching

As already discussed, Wilson coefficients $c(\mu_0)$ ($\mu_0 \sim M_W$) are obtained by matching on-shell matrix elements in the full theory and the effective one. Matching can be done at any on-shell momenta and quark masses; it is most convenient to use the kinematic point where all $m_i = 0$ and $p_i = 0$. The full-theory matrix elements should be expanded in $(m_i, p_i)/M_W$ to some order for obtaining the coefficients in the effective Lagrangian up to the corresponding order in $1/M_W$. In particular, just setting all $m_i = 0$, $p_i = 0$ produces the leading term in this expansion, $1/M_W^2$.

With the one-loop accuracy the full-theory matrix element is

$$\tag{3.32}$$

where Z_q^{os} is the quark filed renormalization constant in the on-shell scheme ($Z_q = 1$ if all $m_i = 0$: loop corrections contain no scale). The one-loop diagrams in the first line of this equation vanish: they contain massless vacuum triangles with zero external momenta.

The effective-theory matrix element is given by the tree diagram Fig. 4b with the coupling constants c_i^0. All loop corrections vanish because they are scale-free. Note that the full-theory renormalized on shell matrix element is UV finite but contains IR divergences. The effective-theory one contains both UV and IR divergences which cancel each other producing vanishing loop corrections. IR divergences in the effective theory coincide with those in the full theory, because the effective theory is designed to reproduce the small-momenta behavior of the full one. Thus IR divergences cancel in the matching equation, and c_i^0 contain UV $1/\varepsilon$ terms. They are removed by renormalization when calculating $c_i(M_W)$.
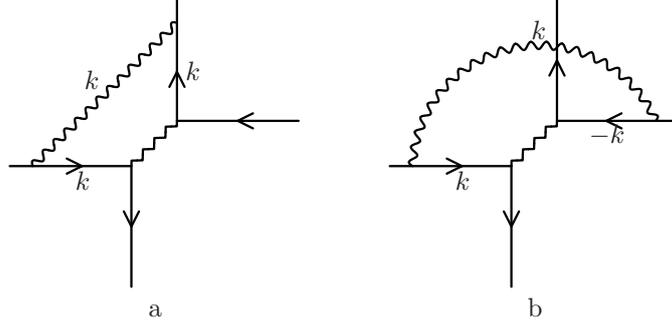

Figure 6: One-loop full-theory diagrams.

The diagram Fig. 6a is

$$-iT_F \left(T_2 - \frac{T_1}{N_c} \right) g_0^2 \int \frac{d^d k}{(2\pi)^d} \frac{\gamma^\alpha \slashed{k} \gamma^\mu \otimes \gamma^\nu \slashed{k} \gamma_\alpha}{(M_W^2 - k^2)(k^2)^3} \left(g_{\mu\nu} - \xi \frac{k_\mu k_\nu}{k^2} \right) ;$$

after averaging over k directions it becomes

$$T_F \left(T_2 - \frac{T_1}{N_c} \right) \frac{g_0^2 M_W^{-2-2\varepsilon}}{(4\pi)^{d/2}} I \left[\frac{1}{d} \gamma^\alpha \gamma^\lambda \gamma^\mu \otimes \gamma_\mu \gamma_\lambda \gamma_\alpha - \xi \gamma^\alpha \otimes \gamma_\alpha \right] ,$$

where the integral I is

$$\frac{1}{i\pi^{d/2}} \int \frac{d^d k}{(M_W^2 - k^2)(-k^2)^2} = I M_W^{d-6}$$

(the power of M_W is given by dimension counting). Similarly, the diagram Fig. 6b is

$$-T_F \left(T_2 - \frac{T_1}{N_c} \right) \frac{g_0^2 M_W^{-2-2\varepsilon}}{(4\pi)^{d/2}} I \left[\frac{1}{d} \gamma^\alpha \gamma^\lambda \gamma^\mu \otimes \gamma_\alpha \gamma_\lambda \gamma_\mu - \xi \gamma^\alpha \otimes \gamma_\alpha \right] .$$

It is easy to calculate I using partial fractions:

$$I = \frac{1}{i\pi^{d/2}} \int d^d k \left[\frac{1}{1 - k^2} + \frac{1}{(-k^2)^2} - \frac{1}{-k^2} \right] = \Gamma \left(1 - \frac{d}{2} \right)$$

(we set $M_W = 1$; integrals of powers of $-k^2$ vanish). Adding mirror-symmetric diagrams, we obtain the full-theory matrix element

$$\frac{1}{M_W^2} \left[T_1 \gamma^\alpha \otimes \gamma_\alpha + T_F \left(T_2 - \frac{T_1}{N_c} \right) \frac{g_0^2 M_W^{-2\varepsilon}}{(4\pi)^{d/2}} \frac{2}{d} \Gamma \left(1 - \frac{d}{2} \right) \gamma^\alpha \gamma^\lambda \gamma^\mu \otimes (\gamma_\mu \gamma_\lambda \gamma_\alpha - \gamma_\alpha \gamma_\lambda \gamma_\mu) \right] ;$$

using (3.20) we arrive at

$$
\frac{1}{M_W^2}\left\{ T_1\gamma^\alpha\otimes\gamma_\alpha - 12 T_F\left(T_2 - \frac{T_1}{N_c}\right)\frac{g_0^2 M_W^{-2\varepsilon}}{(4\pi)^{d/2}}\frac{1}{d}\Gamma\left(1-\frac{d}{2}\right) \right.
$$
$$
\left. \times\left[(d-2)\gamma^\alpha\otimes\gamma_\alpha - \frac{1}{3}\left(\gamma^\alpha\gamma^\beta\gamma^\gamma\otimes\gamma_\gamma\gamma_\beta\gamma_\alpha - 4\gamma^\alpha\otimes\gamma_\alpha\right)\right] \right\}. \tag{3.33}
$$

In addition to

$$
\frac{1}{M_W^2}\left(c_1^0 T_1 + c_2^0 T_2\right)\gamma^\alpha\otimes\gamma_\alpha
$$

(Fig. 4b), this result contains contributions of two bare evanescent operators $E_{1,2}^0$. We shall see in Sect. 3.4 that they are not zero; however, they are equal to the renormalized $O_{1,2}(\mu)$ times factors containing α_s, and may be neglected with the present accuracy. We obtain the bare Wilson coefficients

$$
c_1^0 = 1 - 6\frac{T_F}{N_c}\frac{g_0^2 M_W^{-2\varepsilon}}{(4\pi)^{d/2}}\Gamma(\varepsilon)\left(1+\frac{\varepsilon}{2}\right),
$$
$$
c_2^0 = 6 T_F\frac{g_0^2 M_W^{-2\varepsilon}}{(4\pi)^{d/2}}\Gamma(\varepsilon)\left(1+\frac{\varepsilon}{2}\right). \tag{3.34}
$$

Using the renormalization constant matrix (3.24) we see that $1/\varepsilon$ UV divergences cancel in the renormalized Wilson coefficients:

$$
c_1(\mu) = 1 - 12\frac{T_F}{N_c}\frac{\alpha_s(\mu)}{4\pi}\left(\log\frac{\mu}{M_W}+\frac{1}{4}\right),
$$
$$
c_2(\mu) = 12 T_F\frac{\alpha_s(\mu)}{4\pi}\left(\log\frac{\mu}{M_W}+\frac{1}{4}\right). \tag{3.35}
$$

It is most convenient to perform matching at $\mu = M_Z$; $c_i(M_Z)$ are given by series in $\alpha_s(M_Z)$ containing no logarithms:

$$
c_1(M_W) = 1 - 3\frac{T_F}{N_c}\frac{\alpha_s(M_W)}{4\pi},
$$
$$
c_2(M_W) = 3 T_F\frac{\alpha_s(M_W)}{4\pi}. \tag{3.36}
$$

They can be used as initial conditions for RG equations to find $c_i(\mu)$ for $\mu \ll M_W$.

3.4 Evanescent operators

In dimensional regularization we have to consider, in addition to the physical operators

$$
O_1^0 = (\bar{c}_{L0i}\gamma^\alpha b_{L0}^i)(\bar{d}_{L0j}\gamma_\alpha u_{L0}^j),
$$
$$
O_2^0 = (\bar{c}_{L0i}\gamma^\alpha b_{L0}^j)(\bar{d}_{L0j}\gamma_\alpha u_{L0}^i), \tag{3.37}
$$

also evanescent operators

$$
E_1^0 = (\bar{c}_{L0i}\gamma^\alpha\gamma^\beta\gamma^\gamma b_{L0}^i)(\bar{d}_{L0j}\gamma_\gamma\gamma_\beta\gamma_\alpha u_{L0}^j) - 4 O_1^0,
$$
$$
E_2^0 = (\bar{c}_{L0i}\gamma^\alpha\gamma^\beta\gamma^\gamma b_{L0}^j)(\bar{d}_{L0j}\gamma_\gamma\gamma_\beta\gamma_\alpha u_{L0}^i) - 4 O_2^0. \tag{3.38}
$$

At $d = 4$, Fierz rearrangement

$$(\bar{c}_{L0i}\gamma^\alpha\gamma^\beta\gamma^\gamma b_{L0}^i)\,(\bar{d}_{L0j}\gamma_\gamma\gamma_\beta\gamma_\alpha u_{L0}^j) = (\bar{d}_{L0j}\gamma_\gamma\gamma_\beta\gamma^\alpha\gamma^\beta\gamma^\gamma b_{L0}^i)\,(\bar{c}_{L0i}\gamma_\alpha u_{L0}^j)$$
$$= 4(\bar{d}_{L0j}\gamma^\alpha b_{L0}^i)\,(\bar{c}_{L0i}\gamma_\alpha u_{L0}^j) = 4(\bar{c}_{L0i}\gamma^\alpha b_{L0}^i)\,(\bar{d}_{L0j}\gamma_\alpha u_{L0}^j)$$

states that they vanish. However, these bare operators exist at $d \neq 4$. If we use the standard $\overline{\text{MS}}$ renormalization prescription, we'll see that the renormalized operators $E_{1,2}(\mu)$ also don't vanish. This is not what we want. Therefore we have to modify the $\overline{\text{MS}}$ prescription to ensure vanishing of renormalized evanescent operators [4].

Recall (Sect. 3.2) that the renormalized matrix element of the bare operator $(\bar{c}_{L0i}\Gamma b_{L0}^i)\,(\bar{d}_{L0j}\bar{\Gamma} u_{L0}^j)$ up to one loop,

is

$$\left(1 - 2C_F\frac{\alpha_s}{4\pi\varepsilon}\right)T_1\Gamma\otimes\bar{\Gamma} + 2C_F T_1\frac{\alpha_s}{4\pi\varepsilon}\frac{1}{d}\gamma^\mu\gamma^\lambda\Gamma\gamma_\lambda\gamma_\mu\otimes\bar{\Gamma}$$
$$+ 2T_F\left(T_2 - \frac{T_1}{N_c}\right)\frac{\alpha_s}{4\pi\varepsilon}\frac{1}{d}\Gamma\gamma^\lambda\gamma^\mu\otimes\gamma_\mu\gamma_\lambda\bar{\Gamma} - 2T_F\left(T_2 - \frac{T_1}{N_c}\right)\frac{\alpha_s}{4\pi\varepsilon}\frac{1}{d}\Gamma\gamma^\lambda\gamma^\mu\otimes\bar{\Gamma}\gamma_\lambda\gamma_\mu\,. \tag{3.39}$$

For the operator $(\bar{c}_{L0i}\Gamma b_{L0}^j)\,(\bar{d}_{L0j}\bar{\Gamma} u_{L0}^i)$ we have to adjust the color structures:

$$\left(1 - 2C_F\frac{\alpha_s}{4\pi\varepsilon}\right)T_2\Gamma\otimes\bar{\Gamma} + 2C_F T_2\frac{\alpha_s}{4\pi\varepsilon}\frac{1}{d}\Gamma\gamma^\lambda\gamma^\mu\otimes\gamma_\mu\gamma_\lambda\bar{\Gamma}$$
$$+ 2T_F\left(T_1 - \frac{T_2}{N_c}\right)\frac{\alpha_s}{4\pi\varepsilon}\frac{1}{d}\gamma^\mu\gamma^\lambda\Gamma\gamma_\lambda\gamma_\mu\otimes\bar{\Gamma} - 2T_F\left(T_1 - \frac{T_2}{N_c}\right)\frac{\alpha_s}{4\pi\varepsilon}\frac{1}{d}\Gamma\gamma^\lambda\gamma^\mu\otimes\bar{\Gamma}\gamma_\lambda\gamma_\mu\,. \tag{3.40}$$

We obtain the matrix elements

$$<O_1^0> = T_1\hat{O} + T_F\left(T_2 - \frac{T_1}{N_c}\right)\frac{\alpha_s}{4\pi\varepsilon}\left(-6\hat{O} + \hat{E}\right),$$
$$<O_2^0> = T_2\hat{O} + C_F T_2\frac{\alpha_s}{4\pi\varepsilon}\frac{1}{2}\hat{E} + T_F\left(T_1 - \frac{T_2}{N_c}\right)\frac{\alpha_s}{4\pi\varepsilon}\left(-6\hat{O} + \frac{1}{2}\hat{E}\right),$$
$$<E_1^0> = T_1\hat{E} - C_F T_1\frac{\alpha_s}{4\pi\varepsilon}48\varepsilon\hat{O} + T_F\left(T_2 - \frac{T_1}{N_c}\right)\frac{\alpha_s}{4\pi\varepsilon}\left(-48\varepsilon\hat{O} - 14\hat{E} + \hat{F}\right),$$
$$<E_2^0> = T_2\hat{E} + T_F\left(T_1 - \frac{T_2}{N_c}\right)\frac{\alpha_s}{4\pi\varepsilon}\left(96\varepsilon\hat{O} - 10\hat{E} + \frac{1}{2}\hat{F}\right), \tag{3.41}$$

where

$$\hat{O} = \gamma^\alpha\otimes\gamma_\alpha\,,$$
$$\hat{E} = \gamma^\alpha\gamma^\beta\gamma^\gamma\otimes\gamma_\gamma\gamma_\beta\gamma_\alpha - 4\hat{O}$$
$$\hat{F} = \gamma^\alpha\gamma^\beta\gamma^\gamma\gamma^\delta\gamma^\varepsilon\otimes\gamma_\varepsilon\gamma_\delta\gamma_\gamma\gamma_\beta\gamma_\alpha - 16\hat{O}$$

are the γ-matrix structures of the physical operators O_i, the evanescent operators E_i, and the further evanescent operators

$$
\begin{aligned}
F_1^0 &= (\bar{c}_{L0i}\gamma^\alpha\gamma^\beta\gamma^\gamma\gamma^\delta\gamma^\varepsilon b_{L0}^i)\,(\bar{d}_{L0j}\gamma_\varepsilon\gamma_\delta\gamma_\gamma\gamma_\beta\gamma_\alpha u_{L0}^j) - 16 O_1^0\,, \\
F_2^0 &= (\bar{c}_{L0i}\gamma^\alpha\gamma^\beta\gamma^\gamma\gamma^\delta\gamma^\varepsilon b_{L0}^j)\,(\bar{d}_{L0j}\gamma_\varepsilon\gamma_\delta\gamma_\gamma\gamma_\beta\gamma_\alpha u_{L0}^i) - 16 O_2^0\,.
\end{aligned}
\tag{3.42}
$$

which we need to introduce for calculating one-loop corrections to E_i.

We want renormalized evanescent operators to vanish:

$$
\begin{pmatrix} O_0 \\ E_0 \end{pmatrix} = Z(\alpha_s(\mu)) \begin{pmatrix} O(\mu) \\ 0 \end{pmatrix}, \qquad E(\mu) = 0\,.
\tag{3.43}
$$

This vanishing should not be spoiled by the RG evolution. Therefore, the anomalous dimension matrix should have the structure

$$
\gamma(\alpha_s) = \begin{pmatrix} \gamma_{OO} & \gamma_{OE} \\ 0 & \gamma_{EE} \end{pmatrix},
\tag{3.44}
$$

$$
\frac{d}{d\log\mu} \begin{pmatrix} O(\mu) \\ 0 \end{pmatrix} + \begin{pmatrix} \gamma_{OO} & \gamma_{OE} \\ 0 & \gamma_{EE} \end{pmatrix} \begin{pmatrix} O(\mu) \\ 0 \end{pmatrix},
\tag{3.45}
$$

The evolution of the physical operators is not affected by evanescent ones:

$$
\frac{dO(\mu)}{d\log\mu} + \gamma_{OO}(\alpha_s(\mu))O(\mu) = 0\,.
\tag{3.46}
$$

The RG evolution of the Wilson coefficients of the physical (c_O) and evanescent (c_E) operators is given by

$$
\frac{d}{d\log\mu} \begin{pmatrix} c_O(\mu) \\ c_E(\mu) \end{pmatrix} = \begin{pmatrix} \gamma_{OO}^T & 0 \\ \gamma_{OE}^T & \gamma_{EE}^T \end{pmatrix} \begin{pmatrix} c_O(\mu) \\ c_E(\mu) \end{pmatrix},
$$

or

$$
\begin{aligned}
\frac{d\,c_O(\mu)}{d\log\mu} &= \gamma_{OO}^T c_O(\mu)\,, \\
\frac{d\,c_E(\mu)}{d\log\mu} &= \gamma_{OE}^T c_O(\mu) + \gamma_{EE}^T c_E(\mu)\,.
\end{aligned}
\tag{3.47}
$$

The evolution of $c_O(\mu)$ does not involve $c_E(\mu)$; $c_E(\mu) \neq 0$, but they are irrelevant because they are multiplied by $E(\mu) = 0$.

Now let's have a close look at the one-loop matrix elements (3.41). We see that the matrix elements of the bare evanescent operators E_i contain terms with the physical γ-matrix structure $\hat{O}$ finite at $\varepsilon \to 0$! When we start from an evanescent γ-matrix structure (such as $\hat{E}$), which is 0 at $d = 4$, multiply it by some additional γ-matrices from a one-loop diagram, and extract a physical γ-matrix structure (such as $\hat{O}$), the coefficient must be proportional to ε. However, when it is multiplied by $1/\varepsilon$ from the UV divergence of the loop integral, the result is a finite contribution. This UV divergence does not depend on external momenta and masses, hence this physical term in the matrix element is similarly universal. Therefore we can use the one-loop renormalization constant of the form

$$
Z = 1 + \begin{pmatrix} b & c \\ a\varepsilon & d \end{pmatrix} \frac{\alpha_s}{4\pi\varepsilon}\,,
\tag{3.48}
$$

so that

$$<E(\mu)> = 0, \qquad <E_0> = a<O(\mu)>\frac{\alpha_s}{4\pi}. \tag{3.49}$$

In other words, the renormalization constant is no longer minimal:

$$Z = 1 + \left(Z_{10} + \frac{Z_{11}}{\varepsilon} \right) \frac{\alpha_s}{4\pi},$$
$$Z_{10} = \begin{pmatrix} 0 & 0 \\ a & 0 \end{pmatrix}, \qquad Z_{11} = \begin{pmatrix} b & c \\ 0 & d \end{pmatrix}. \tag{3.50}$$

The anomalous dimension (3.9) is

$$\gamma = \gamma_0 \frac{\alpha_s}{4\pi}, \qquad \gamma_0 = -2Z_{11}; \tag{3.51}$$

it has the required structure (3.44). When calculating the one-loop anomalous dimension, it is safe to forget about evanescent operators (as we did in Sect. 3.2).

Now let's discuss renormalization at two loops. We need a non-minimal renormalization matrix

$$Z(\alpha_s) = 1 + \left(Z_{10} + \frac{Z_{11}}{\varepsilon} \right) \frac{\alpha_s}{4\pi} + \left(Z_{20} + \frac{Z_{21}}{\varepsilon} + \frac{Z_{22}}{\varepsilon^2} \right) \left(\frac{\alpha_s}{4\pi} \right)^2. \tag{3.52}$$

The anomalous dimension matrix must be finite at $\varepsilon \to 0$; from this requirement we obtain

$$Z_{22} = \frac{1}{2} Z_{11}(Z_{11} - \beta_0) = \frac{1}{2} \begin{pmatrix} b(b - \beta_0) & bc + cd - \beta_0 c \\ 0 & d(d - \beta_0) \end{pmatrix}. \tag{3.53}$$

As usual, $1/\varepsilon^2$ terms in the two-loop Z are not independent — they are given by products of one-loop terms. The lower left corner is 0: ε from γ-matrix algebra moves this term to Z_{21}, see below. Supposing that the self-consistency condition (3.53) is satisfied, the anomalous dimension matrix (3.9) is

$$\gamma(\alpha_s) = \gamma_0 \frac{\alpha_s}{4\pi} + \gamma_1 \left(\frac{\alpha_s}{4\pi} \right)^2, \quad \gamma_0 = -2Z_{11}, \quad \gamma_1 = -2(2Z_{21} - Z_{10}Z_{11} - Z_{11}Z_{10} + \beta_0 Z_{10}). \tag{3.54}$$

Let

$$Z_{21} = \begin{pmatrix} e & f \\ g & h \end{pmatrix}; \tag{3.55}$$

g is the $1/\varepsilon^2$ divergences of the two-loop integral (which does not depend on external momenta) times ε from γ-matrix algebra. The lower left corner of γ_1 must vanish; this gives the second self-consistency condition

$$g = \frac{1}{2}(ab + da - \beta_0 a). \tag{3.56}$$

This contribution of $1/\varepsilon^2$ two-loop divergences is also given by products of one-loop terms.

What we are really interested in is the upper left corner γ_{OO} which determines the evolution of physical operators and Wilson coefficients. With the two-loop accuracy

$$\gamma_{OO} = -2b\frac{\alpha_s}{4\pi} - 2(2e + ca) \left(\frac{\alpha_s}{4\pi} \right)^2. \tag{3.57}$$

To calculate it correctly, we need not only e — the $1/\varepsilon$ part of two-loop diagrams with the insertion of a physical operator, but also a and c — one-loop terms related to evanescent operators. Forgetting about them would produce a wrong result.

3.5 Two-loop anomalous dimensions

Some typical diagrams for the calculation of the two-loop anomalous dimension matrix are shown in Fig. 7. We need only UV $1/\varepsilon$ divergences; the most efficient way to calculate them is to set all external momenta to 0, and to insert a small mass m into all denominators as an IR regulator [5, 3]. This is similar to what we did at one loop.
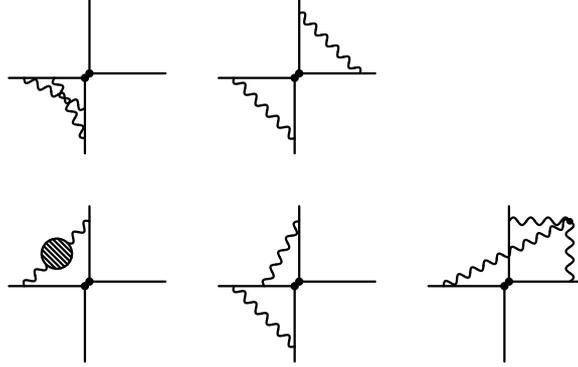

Figure 7: Some two-loop diagrams for the vertex functions of $O_{1,2}$.

Then all diagrams reduce to the Euclidean scalar integrals (Fig. 8)

$$\frac{1}{\pi^d} \int \frac{d^d k_1 \, d^d k_2}{(k_1^2 + m^2)^{n_1}(k_2^2 + m^2)^{n_2}((k_1 - k_2)^2 + m^2)^{n_3}} = I_{n_1 n_2 n_3} m^{2(d - n_1 - n_2 - n_3)} \,. \qquad (3.58)$$

If one of the indices is ≤ 0, it reduces to a trivial product of one-loop integrals. When all the indices are > 0, we can use integration by parts [6]:

$$\left[d - 3n_1 + 3n_1 \mathbf{1}^+ + n_2 \mathbf{2}^+ (\mathbf{3}^- - \mathbf{1}^-) + n_3 \mathbf{3}^+ (\mathbf{2}^- - \mathbf{1}^-) \right] I = 0 \,. \qquad (3.59)$$

This relation, together with symmetric ones, reduces any $I_{n_1 n_2 n_3}$ to trivial cases and a single non-trivial master integral I_{111}.
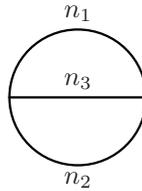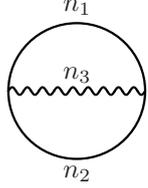

Figure 8: The two-loop massive vacuum integral.

It can be found using Mellin–Barnes representation

$$\bullet\!\!\!-\!\!\!\overset{n}{\underset{}{}}\!\!\!-\!\!\!\bullet = \frac{1}{\Gamma(n)} \frac{1}{2\pi i} \int_{-i\infty}^{+i\infty} dz \, \Gamma(-z) \Gamma(n + z) m^{2z} \, \bullet\!\!\!\leadsto\!\!\!\overset{n+z}{\underset{}{}}\!\!\!\bullet \,. \qquad (3.60)$$

Substituting

$$
\includegraphics{diagram} = \frac{\Gamma\left(\frac{d}{2} - n_3\right)\Gamma\left(n_1 + n_3 - \frac{d}{2}\right)\Gamma\left(n_2 + n_3 - \frac{d}{2}\right)\Gamma(n_1 + n_2 + n_3 - d)}{\Gamma\left(\frac{d}{2}\right)\Gamma(n_1)\Gamma(n_2)\Gamma(n_1 + n_2 + 2n_3 - d)}, \qquad (3.61)
$$

we obtain [6]

$$
I_{n_1 n_2 n_3} = \frac{1}{\Gamma\left(\frac{d}{2}\right)\Gamma(n_1)\Gamma(n_2)\Gamma(n_3)} \frac{1}{2\pi i} \int_{-i\infty}^{+i\infty} dz\, \Gamma(-z)\Gamma\left(\frac{d}{2} - n_3 - z\right)
$$
$$
\frac{\Gamma(n_3 + z)\Gamma\left(n_1 + n_3 - \frac{d}{2} + z\right)\Gamma\left(n_2 + n_3 - \frac{d}{2} + z\right)\Gamma(n_1 + n_2 + n_3 - d + z)}{\Gamma(n_1 + n_2 + 2n_3 - d + 2z)}.
\qquad (3.62)
$$

We can close the integration contour to the right. there are two series of right poles, $z = n$ and $z = n + \frac{d}{2} - n_3$, producing two hypergeometric series. In particular, the master integral is [6]

$$
I_{111} = \frac{\Gamma^2(\varepsilon)}{1 - \varepsilon}\left[\,{}_2F_1\left(\begin{array}{c} 1, \varepsilon \\ \frac{3}{2} \end{array}\bigg|\, \frac{1}{4}\right) + \frac{1}{1 - 2\varepsilon}\,{}_2F_1\left(\begin{array}{c} 1, -1 + 2\varepsilon \\ \frac{1}{2} + \varepsilon \end{array}\bigg|\, \frac{1}{4}\right)\right]. \qquad (3.63)
$$

This exact result can be expanded in ε.

Note that γ_5 is not used in the calculation [3]: it is hidden in the index L of the external fermion wave functions. These wave functions determine which γ-matrix structures vanish at $d = 4$, and hence which operators are evanescent.

4 $b \to s$

In this section we shall consider processes in which the number of b quarks reduce by 1, the number of s quarks increases by 1, and the other flavor numbers don't change. We shall consider the lowest order in electroweak interactions, but taking into account QCD corrections. The process $b \to s\gamma$ requires an additional factor e. We shall not discuss it here. Several additional operators appear in the effective Lagrangian at the next order in electroweak interaction, but it is not difficult to extend the methods discussed here to $b \to s\gamma$.

At first sight one might think that the diagram in Fig. 9 can produce the operator

$$
g\, \bar{s}_L G^a_{\mu\nu} t^a \sigma^{\mu\nu} b
$$

of dimension 5. But here b must be b_R, otherwise the operator vanishes at $d = 4$; and this is impossible at $m_b = 0$. Therefore in fact the operator

$$
O_g = g m_b \bar{s}_L G^a_{\mu\nu} t^a \sigma^{\mu\nu} b_R \qquad (4.1)
$$

of dimension 6 is produced. It is called the gluon dipole operator; it is a mixture of magnetic and electric dipole interactions.
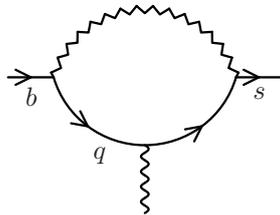
Figure 9: The bsg vertex.

The coefficient of this operator in the effective Lagrangian is

$$\frac{g_2^2}{M_W^2} \sum_{q=u,c,t} V_{qb} V_{qs}^* E(x_q) \, , \tag{4.2}$$

where

$$x_q = \frac{m_q^2}{M_W^2} \, , \tag{4.3}$$

and the function $E(x_q)$ can be easily calculated from the vacuum integral of Fig. 9 which depends on two masses, M_W and m_q. But

$$\sum_{q=u,c,t} V_{qb} V_{qs}^* = 0 \tag{4.4}$$

due to unitarity of the matrix V. Therefore we can rewrite (4.2) as

$$\frac{g_2^2}{M_W^2} \sum_{q=u,c,t} V_{qb} V_{qs}^* \left[E(x_q) - E(0) \right] \, .$$

The only x_q substantially different from 0 is x_t; therefore, the coefficient of the dipole operator (4.1) in the effective Lagrangian is

$$\frac{g_2^2}{M_W^2} V_{tb} V_{ts}^* \left[E(x_t) - E(0) \right] \, . \tag{4.5}$$

In order to obtain a non-vanishing contribution from the on-shell diagram in Fig. 9 we expanded in in m_b up to the linear term. Alternatively, we can expand it in the gluon momentum q up to the linear term, and obtain a non-vanishing operator

$$g \, \bar{s}_L D^\nu G_{\mu\nu}^a t^a \gamma^\mu b_L \, . \tag{4.6}$$

Due to the QCD equation of motion,

$$D^\nu G_{\mu\nu}^a = g \sum_q \bar{q} t^a \gamma_\mu q \, . \tag{4.7}$$

Therefore we can rewrite the operator (4.6) as

$$O_p = g^2 \left(\bar{s}_L t^a \gamma^\alpha b_L \right) \sum_q \left(\bar{q} t^a \gamma_\alpha q \right) \, , \tag{4.8}$$

up to an EOM-vanishing operator. On-shell matrix elements of EOM-vanishing operators vanish; we can safely omit them from the effective Lagrangian, which is constructed to reproduce the correct S-matrix. The operator O_p is called penguin[3]. Its coefficient in the Lagrangian is given by a formula similar to (4.5).

Of course, there is also the operator O_{c1} (Fig. 10a); we need a set of operators closed under renormalization, and hence have to include also O_{c2}:

$$O_{c1} = (\bar{c}_{Li}\gamma^\alpha b_L^i)(\bar{s}_{Lj}\gamma_\alpha c_L^j), \qquad O_{c2} = (\bar{c}_{Li}\gamma^\alpha b_L^j)(\bar{s}_{Lj}\gamma_\alpha c_L^i). \tag{4.9}$$

The similar operators

$$O_{u1} = (\bar{u}_{Li}\gamma^\alpha b_L^i)(\bar{s}_{Lj}\gamma_\alpha u_L^j), \qquad O_{u2} = (\bar{u}_{Li}\gamma^\alpha b_L^j)(\bar{s}_{Lj}\gamma_\alpha u_L^i) \tag{4.10}$$
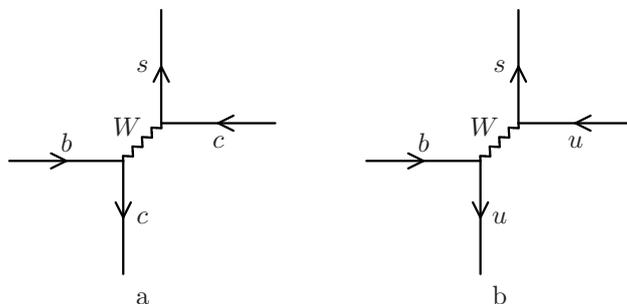
have CKM-suppressed coefficients.

Figure 10: $b \to c\bar{c}s$ (a) and $b \to u\bar{u}s$ (b).

Similarly, we should take into account not just one penguin operator O_p (4.8), but both color structures:

$$O_{p1} = (\bar{s}_{Li}\gamma^\alpha b_L^i)\sum_q(\bar{q}_j\gamma_\alpha q^j), \qquad O_{p2} = (\bar{s}_{Li}\gamma^\alpha b_L^j)\sum_q(\bar{q}_j\gamma_\alpha q^i) \tag{4.11}$$

($O_p = T_F g^2(O_{p2} - O_{p1}/N_c)$). Unlike the operators $O_{1,2}$ (3.2) (or $O_{c1,2}$ (4.9)), the penguin operators contain full quark fields q in Σ_q, not just their L components. Therefore the operators

$$O_{p3} = (\bar{s}_{Li}\gamma^\alpha\gamma^\beta\gamma^\gamma b_L^i)\sum_q(\bar{q}_j\gamma_\gamma\gamma_\beta\gamma_\alpha q^j), \qquad O_{p4} = (\bar{s}_{Li}\gamma^\alpha\gamma^\beta\gamma^\gamma b_L^j)\sum_q(\bar{q}_j\gamma_\gamma\gamma_\beta\gamma_\alpha q^i) \tag{4.12}$$

with 3 γ-matrices don't reduce to (4.11) plus evanescent operators, and should be included in our full set of operators. On the other hand, the operators with 5 γ matrices do reduce to (4.11), (4.12) plus evanescent ones.

Thus we arrive at the effective Lagrangian for $b \to s$ processes:

$$L = \frac{g_2^2}{2M_W^2}\left[V_{cs}^*V_{cb}(c_{c1}O_{c1} + c_{c2}O_{c2}) + V_{us}^*V_{ub}(c_{u1}O_{u1} + c_{u2}O_{u2})\right.$$
$$\left. + V_{ts}^*V_{tb}\left(c_g O_g + \sum_{i=1}^4 c_{pi}O_{pi}\right)\right]. \tag{4.13}$$

---

[3]In 1977 John Ellis made a bet with Melissa Franklin at a bar: if he loses a game of darts, he has to use the word "penguin" in his next paper. He lost, and has drawn the diagram in Fig. 9 in a penguin-like shape.

The Wilson coefficients at $\mu = M_W$ are obtained by matching: c_{c1}, c_{u1}, c_g are $1 + \mathcal{O}(\alpha_s)$; c_{c2}, c_{u2}, c_{pi} are $\mathcal{O}(\alpha_s)$. In order to find them at a low $\mu \sim m_b$, we need to solve the RG equations (3.11), and hence we need the anomalous dimension matrix of these operators.

Processes like $b \to s\gamma$ involve an extra electromagnetic interaction, and require some additional operators. There is the photon dipole operator O_γ similar to the gluon one O_g (4.1, and photon penguin operators similar to (4.11), (4.12).

5 $B^0 \leftrightarrow \bar{B}^0$

Finally, we shall briefly discuss a process which at the order g_2^4: $B^0 \leftrightarrow \bar{B}^0$ oscillations (Fig. 11). They are described by the effective Lagrangian

$$L = \frac{g_2^4}{512\pi^2 M_W^2} cO \,, \qquad O = (\bar{d}_L \gamma^\alpha b_L)(\bar{d}_L \gamma^\alpha b_L) \,. \tag{5.1}$$

The Wilson coefficient is given by

$$c = \sum_{q,q'=u,c,t} V_{qb}^* V_{qd} V_{q'b}^* V_{q'd} S(x_q, x_{q'}) \,, \tag{5.2}$$

where $S(x_q, x_{q'}) = S(x_{q'}, x_q)$ is given by the one-loop vacuum integrals (Fig. 11) with three masses: M_W, m_q, $m_{q'}$ (x_q is defined by (4.3)). Due to (4.4),

$$c = \sum_{q,q'=u,c,t} V_{qb}^* V_{qd} V_{q'b}^* V_{q'd} \left[S(x_q, x_{q'}) - S(x_q, 0) \right] = V_{tb}^* V_{td} \sum_{q=u,c,t} V_{qb}^* V_{qd} \left[S(x_q, x_t) - S(x_q, 0) \right] \,,$$

because only x_t substantially differs from 0. Finally,

$$\begin{aligned} c &= V_{tb}^* V_{td} \sum_{q=u,c,t} V_{qb}^* V_{qd} \left[S(x_q, x_t) - S(x_q, 0) - S(0, x_t) + S(0,0) \right] \\ &= (V_{tb}^* V_{td})^2 \left[S(x_t, x_t) - 2S(x_t, 0) + S(0,0) \right] \,. \end{aligned} \tag{5.3}$$
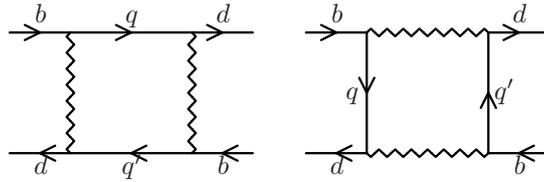

Figure 11: Diagrams of $b\bar{d} \leftrightarrow d\bar{b}$ transitions.

We don't need to calculate the one-loop anomalous dimension of the operator O (5.1) because it has been already done in Sect. 3.2:

$$\gamma_0 = \lambda_+ = 12 T_F \left(1 - \frac{1}{N_c} \right) \,, \tag{5.4}$$

see (3.27) (the operator similar to O_- is zero).

6 Conclusion

References

[1] A. J. Buras, hep-ph/9806471.

[2] A. J. Buras, arXiv:1102.5650.

[3] K. G. Chetyrkin, M. Misiak, M. Münz, Nucl. Phys. **B 520** (1998) 279 [hep-ph/9711280].

[4] M. J. Dugan, B. Grinstein, Phys. Lett. B **256** (1991) 239.

[5] K. G. Chetyrkin, M. Misiak, M. Münz, Nucl. Phys. **B 518** (1998) 473 [hep-ph/9711266].

[6] A. I. Davydychev, J. B. Tausk, Nucl. Phys. **B 397** (1993) 123.

Heavy quark physics in the covariant quark model

Mikhail A. Ivanov

BLTP JINR, 141980 Dubna, Russia

I give a short introduction to the covariant quark model and its applications to heavy quark physics. The special emphasis will be devoted to the semileptonic, rare and radiative decays of the Λ_b-baryon.

1 Introduction

This lecture is supposed to be a mini–review of the recent results obtained by the Dubna-Mainz-Tübingen Collaboration, see Refs. [1, 2, 3]. The research is aiming to study the semileptonic, rare and radiative decays of the Λ_b-baryon by using the covariant quark model previously developed by us.

The decay $\Lambda_b \to \Lambda \, \ell^+ \ell^-$ ($\ell = e, \mu, \tau$) is a rare $b - s$ favor-changing neutral current process that in the Standard Model proceeds through electroweak loop (penguin and $W-$box) diagrams. This decay can be considered to be a welcome complement to the well–analyzed rare meson decays $B \to K^{(*)} \, \ell^+ \ell^-$, $B_s \to \phi \, \ell^+ \ell^-$ etc. to study the short– and long–distance dynamics of rare decays induced by the transition $b \to s \, \ell^+ \ell^-$. However, the study of baryon decays is of more interest because the Λ_b baryon has spin one half compare with zero spin of the $B-$meson. Therefore, the matrix element of the baryon decay possesses more rich helicity structure.

For the first time, the CDF Collaboration has reported on the measurement of the $\Lambda_b \to \Lambda + \mu^+ \mu^-$ total branching ratio: $\mathcal{B}(\Lambda_b \to \Lambda + \mu^+ \mu^-) = (1.73 \pm 0.42 \pm 0.55) \cdot 10^{-6}$ [4]. Recently, the LHCb Collaboration [5] has measured the differential branching fraction of this decay as a function of the square of the dimuon invariant mass. Integrating the differential branching fraction gives a branching fraction of $\mathcal{B}(\Lambda_b \to \Lambda + \mu^+ \mu^-) = (0.96 \pm 0.16 \pm 0.13 \pm 0.21) \cdot 10^{-6}$. Here, the uncertainties are statistical, systematic and due to the normalisation mode, $\Lambda_b \to \Lambda J/\psi$, respectively. The physics of heavy baryon decays appears to have entered a new era with these experimental results.

There have been a number of theoretical papers on the rare $\Lambda_b \to \Lambda$ baryon decays involving the one-photon mode $\Lambda_b \to \Lambda \gamma$ and the dilepton modes $\Lambda_b \to \Lambda \, \ell^+ \ell^-$ ($\ell = e, \mu, \tau$). They use the same set of (penguin) operators or their non–Standard Model extensions to describe the short distance dynamics but differ in their use of theoretical models to calculate the nonperturbative transition matrix element $\langle \Lambda | \, O_i \, | \Lambda_b \rangle$.

We use the covariant constituent quark model (for short: covariant quark model) as dynamical input to calculate the nonperturbative transition matrix elements. In the covariant quark model the current–induced transitions between baryons are calculated from two–loop Feynman diagrams with free quark propagators in which the divergent high energy behavior of the loop integrations is tempered by Gaussian vertex functions. Quark confinement has incorporated in an effective way, first, by introducing the scale integration in the space of α-parameters, and, second, by cutting this scale integration on the upper limit which corresponds to an infrared

cutoff. In this manner one removes all possible thresholds presented in the initial quark diagram. The cutoff parameter is taken to be the same for all physical processes. We adjust other model parameters by fitting the calculated quantities of the basic physical processes to available experimental data. One has to emphasize that the covariant quark model is a truly frame–independent field–theoretic quark model in contrast to other constituent quark models which are basically quantum mechanical with built–in relativistic elements. One of the advantages of the covariant quark model is that it allows one to calculate the transition form factors in the full accessible range of q^2–values.

We review the basic notions of our dynamical approach — *the covariant quark model for baryons.* In particular, we derive the phenomenological Lagrangians describing the interaction of baryons with their constituent quarks. Then we introduce the corresponding interpolating 3–quark currents with the quantum numbers of the respective baryon and discuss the idea and implementation of quark confinement. Finally, we apply our approach to the rare one-photon decay $\Lambda_b \to \Lambda\gamma$ and the dilepton decay $\Lambda_b \to \Lambda(\to p\pi^-) + j_{\text{eff}}(\to \ell^+\ell^-)$. We present a detailed discussion of the helicity formalism that allows one to write down the joint angular distribution of the cascade decay $\Lambda_b \to \Lambda(\to p\pi^-) + j_{\text{eff}}(\to \ell^+\ell^-)$.

2   The covariant quark model for baryons

In the following we consider $\Lambda = (Q[ud])$-type baryons needed in the present application. They consist of a heavy quark and two light quarks in a $^1S_0$ spin 0 configuration. The coupling of a Λ-type baryon to its constituent quarks is described by the Lagrangian

$$\mathcal{L}^\Lambda_{\text{int}}(x) = g_\Lambda \, \bar\Lambda(x) \cdot J_\Lambda(x) + g_\Lambda \, \bar J_\Lambda(x) \cdot \Lambda(x) \,,$$

$$J_\Lambda(x) = \int dx_1 \int dx_2 \int dx_3 \, F_\Lambda(x; x_1, x_2, x_3) \, J^{(\Lambda)}_{3q}(x_1, x_2, x_3) \,,$$

$$J^{(\Lambda)}_{3q}(x_1, x_2, x_3) = \epsilon^{a_1 a_2 a_3} \, Q^{a_1}(x_1) \, u^{T\,a_2}(x_2) \, C \, \gamma^5 \, d^{a_3}(x_3) \,,$$

$$\bar J_\Lambda(x) = J^\dagger_\Lambda(x)\gamma^0 \,,$$

where $Q = s, c, b$. Here the matrix $C = \gamma^0\gamma^2$ is the usual charge conjugation matrix and the a_i $(i = 1, 2, 3)$ are color indices.

The vertex function F_Λ characterizes the finite size of the Λ-type baryon. We assume that the vertex function is real. To satisfy translational invariance the function F_N has to fulfill the identity

$$F_\Lambda(x + a; x_1 + a, x_2 + a, x_3 + a) = F_\Lambda(x; x_1, x_2, x_3)$$

for any given four-vector a. In the following we use a particular form for the vertex function

$$F_\Lambda(x; x_1, x_2, x_3) = \delta^{(4)}(x - \sum_{i=1}^3 w_i x_i) \, \Phi_\Lambda\left(\sum_{i<j}(x_i - x_j)^2\right) \tag{1}$$

where Φ_Λ is the correlation function of the three constituent quarks with the coordinates x_1, x_2, x_3 and masses m_1, m_2, m_3, respectively. The variable w_i is defined by $w_i = m_i/(m_1 + m_2 + m_3)$ such that $\sum_{i=1}^3 w_i = 1$.

We shall make use of the Jacobi coordinates $\rho_{1,2}$ and the CM coordinate x which are defined by

$$
\begin{aligned}
x_1 &= x + \tfrac{1}{\sqrt{2}}\,w_3\,\rho_1 - \tfrac{1}{\sqrt{6}}\,(2w_2 + w_3)\,\rho_2 \,, \\
x_2 &= x + \tfrac{1}{\sqrt{2}}\,w_3\,\rho_1 + \tfrac{1}{\sqrt{6}}\,(2w_1 + w_3)\,\rho_2 \,, \\
x_3 &= x - \tfrac{1}{\sqrt{2}}\,(w_1 + w_2)\,\rho_1 + \tfrac{1}{\sqrt{6}}\,(w_1 - w_2)\,\rho_2 \,.
\end{aligned}
$$

The CM coordinate is given by $x = \sum_{i=1}^{3} w_i x_i$. In terms of the Jacobi coordinates one obtains

$$
\sum_{i<j}(x_i - x_j)^2 = \rho_1^2 + \rho_2^2 \,.
$$

Note that the choice of Jacobi coordinates is not unique. By using the particular choice of Jacobi coordinates given by Eq. (2) one obtains the following representation for the correlation function Φ_Λ in Eq. (1)

$$
\begin{aligned}
\Phi_\Lambda\left(\sum_{i<j}(x_i - x_j)^2\right) &= \int \frac{d^4 p_1}{(2\pi)^4}\int\frac{d^4 p_2}{(2\pi)^4}\, e^{-ip_1(x_1 - x_3) - ip_2(x_2 - x_3)}\,\bar{\Phi}_\Lambda(-P_1^2 - P_2^2)\,, \quad (2)\\
\bar{\Phi}_\Lambda(-P_1^2 - P_2^2) &= \tfrac{1}{9}\int d^4\rho_1 \int d^4\rho_2\, e^{iP_1\rho_1 + iP_2\rho_2}\,\Phi_\Lambda(\rho_1^2 + \rho_2^2)\,,\\
P_1 &= \tfrac{1}{\sqrt{2}}(p_1 + p_2)\,, \qquad P_2 = -\tfrac{1}{\sqrt{6}}(p_1 - p_2)\,.
\end{aligned}
$$

This representation is valid for any choice of the set of Jacobi coordinates. The particular choice (2) is a preferred choice since it leads to the specific form of the argument $-P_1^2 - P_2^2 = -\frac{2}{3}(p_1^2 + p_2^2 + p_1 p_2)$. Since this expression is invariant under the transformations: $p_1 \leftrightarrow p_2$, $p_2 \to -p_2 - p_1$ and $p_1 \to -p_1 - p_2$, the r.h.s. in Eq. (2) is invariant under permutations of all x_i as it should be.

In the next step we have to specify the function $\bar{\Phi}_\Lambda(-P_1^2 - P_2^2) \equiv \bar{\Phi}_\Lambda(-P^2)$ which characterizes the finite size of the baryons. We will choose a simple Gaussian form for the function $\bar{\Phi}_\Lambda$:

$$
\bar{\Phi}_\Lambda(-P^2) = \exp(P^2/\Lambda_\Lambda^2)\,, \tag{3}
$$

where Λ_Λ is a size parameter parametrized the distribution of quarks inside a Λ-type baryon. We use different values of the Λ_Λ parameter for different types of the Λ-type baryon: Λ_{Λ_s}, Λ_{Λ_c} and Λ_{Λ_b} for the Λ, Λ_c and Λ_b baryons, respectively.

Since P^2 turns into $-P_E^2$ in Euclidean space the form (3) has the appropriate falloff behavior in the Euclidean region. We emphasize that any choice for Φ_Λ is appropriate as long as it falls off sufficiently fast in the ultraviolet region of Euclidean space to render the corresponding Feynman diagrams ultraviolet finite. The choice of a Gaussian form for Φ_Λ has obvious calculational advantages.

The coupling constants g_Λ are determined by the compositeness condition suggested by Weinberg [6] and Salam [7] (for review, see Ref. [8]) and extensively used in our approach (for details, see Ref. [9]). The compositeness condition in the case of baryons implies that the renormalization constant of the baryon wave function is set equal to zero:

$$
Z_\Lambda = 1 - \Sigma'_\Lambda(m_\Lambda) = 0
$$

where Σ'_Λ is the on-shell derivative of the Λ-type baryon mass function Σ_Λ, i.e. $\Sigma'_\Lambda = \partial \Sigma_\Lambda / \partial \not{p}$, at $\not{p} = m_\Lambda$. The compositeness condition is the central equation of our covariant quark model. The physical meaning, the implications and corollaries of the compositeness condition have been discussed in some detail in our previous papers (see e.g. [10]).

2.1 Infrared confinement

We have shown in [10] how the confinement of quarks can be effectively incorporated in the covariant quark model. In a first step, we introduced an additional scale integration in the space of Schwinger's α–parameters with an integration range from zero to infinity. In a second step the scale integration was cut off at the upper limit which corresponds to the introduction of an infrared (IR) cutoff. In this manner all possible thresholds present in the initial quark diagram were removed. The cutoff parameter was taken to be the same for all physical processes. Other model parameters such as the constituent quark masses and size parameters were determined from a fit to experimental data.

Let us describe the basic features of how IR confinement is implemented in our model. All physical matrix elements are described by Feynman diagrams written in terms of a convolution of free quark propagators and the vertex functions. In computation of Feynman diagrams we use, in the momentum space, the Schwinger representation of the quark propagator

$$S(k) = \frac{m + \not{k}}{m^2 - k^2} = (m + \not{k}) \int\limits_0^\infty d\alpha \, e^{-\alpha\left(m^2 - k^2\right)} .$$

The general form of a resulting Feynman diagrams is

$$\Pi(p_1, \ldots, p_m) = \int\limits_0^\infty d^n\alpha \int \left[d^4 k\right]^\ell \Phi \times \exp\left\{-\sum_{i=1}^n \alpha_i \left[m_i^2 - (K_i + P_i)^2\right]\right\}, \qquad (4)$$

where K_i represents a linear combination of loop momenta, P_i stands for a linear combination of external momenta and Φ refers to the numerator product of propagators and vertex functions. The integrand in Eq. (4) has a Gaussian form with the exponential factor

$$kak + 2kr + R = k_i a_{ij} k_j + 2k_i r_i + R, \qquad (i, j = 1, \ldots, \ell),$$

where k_i is a 4-vector of the "i"-loop integration, a is a $\ell \times \ell$ matrix depending on the parameters α_i and size parameters Λ, r_i is a 4- vector composed from the external momenta p_i and R is a quadratic form of the external momenta. Tensor loop integrals are calculated with the help of the differential representation

$$k_i^\mu e^{2kr} = \frac{1}{2}\frac{\partial}{\partial r_{i\,\mu}} e^{2kr} ,$$

which in general may be written in the form

$$\int \left[d^4 k\right]^\ell P(k)\, e^{kak+2kr+R} = \int \left[d^4 k\right]^\ell P\left(\frac{1}{2}\frac{\partial}{\partial r}\right) e^{kak+2kr+R} = P\left(\frac{1}{2}\frac{\partial}{\partial r}\right) \int \left[d^4 k\right]^\ell e^{kak+2kr+R},$$

where the polynomial operator means $P(k) = k_1^{\mu_1} \ldots k_m^{\mu_m}$. After doing the loop integration the differential operators $\partial/\partial r_{i\,\mu}$ will give cause to outer momenta tensors. It may be done in

effective way by using the identity

$$\int\limits_0^\infty d^n\alpha\, P\left(\frac{1}{2}\frac{\partial}{\partial r}\right) e^{-\frac{r^2}{a}} = \int\limits_0^\infty d^n\alpha\, e^{-\frac{r^2}{a}} P\left(\frac{1}{2}\frac{\partial}{\partial r} - \frac{r}{a}\right).$$

The calculation of the polynomial $P\left(\frac{1}{2}\frac{\partial}{\partial r} - \frac{r}{a}\right)$ can be automized by using the commutator $\left[\frac{\partial}{\partial r_i^\mu}, r_j^\nu\right] = \delta_{ij}\, g^{\mu\nu}$. We have written a FORM [11] program that achieves the necessary commutations of the differential operators in a very efficient way.

The last point which remains to be discussed is the infrared cut-off we impose on the integration over the Schwinger parameters. This integration is multidimensional with the limits from 0 to $+\infty$. In order to arrive to a single cut-off parameter we firstly transform the integral over an infinite space into an integral over a simplex convoluted with only one-dimensional improper integral. For that purpose we use the δ-function form of the identity

$$1 = \int\limits_0^\infty dt\, \delta\left(t - \sum_{i=1}^n \alpha_i\right), \qquad (\forall \alpha_i \geq 0)$$

from which follows

$$\Pi = \int\limits_0^\infty dt\, t^{n-1} \int\limits_0^1 d^n\alpha\, \delta\left(1 - \sum_{i=1}^n \alpha_i\right) \times W\left(t\alpha_1, \ldots, t\alpha_1\right),$$

where W represents the integrand of Schwinger parameters. The cut-off λ is then introduced in a natural way

$$\int\limits_0^\infty dt\, t^{n-1} \ldots \rightarrow \int\limits_0^{1/\lambda^2} dt\, t^{n-1} \ldots .$$

Such a cut-off makes the integral to be an analytic function without any singularities. In this way all potential thresholds in the quark loop diagrams are removed together with corresponding branch points [10]. Within covariant quark model the cut-off parameter is universal for all processes and its value, as obtained from a fit to data, is

$$\lambda_{\text{cut-off}} = 0.181\,\text{GeV}.$$

The numerical evaluations have been done by a numerical program written in the FORTRAN code.

3 The rare baryon decays $\Lambda_b \to \Lambda + \ell^+\ell^-$ and $\Lambda_b \to \Lambda + \gamma$

The effective Hamiltonian [12] leads to the quark decay amplitudes $b \to s l^+ l^-$ and $b \to s\gamma$:

$$\begin{aligned}
M(b \to s\ell^+\ell^-) &= \frac{G_F}{\sqrt{2}}\frac{\alpha\lambda_t}{2\pi}\left\{C_9^{\text{eff}}\left(\bar{s}O^\mu b\right)\left(\bar{\ell}\gamma_\mu\ell\right) + C_{10}\left(\bar{s}O^\mu b\right)\left(\bar{\ell}\gamma_\mu\gamma_5\ell\right)\right.\\
&\quad \left. - \frac{2}{q^2}C_7^{\text{eff}}\left[m_b\left(\bar{s}\,i\sigma^{\mu q}\left(1+\gamma^5\right)b\right) + m_s\left(\bar{s}\,i\sigma^{\mu q}\left(1-\gamma^5\right)b\right)\right]\left(\bar{\ell}\gamma_\mu\ell\right)\right\}
\end{aligned}$$

and

$$M(b \to s\gamma) \;=\; -\frac{G_F}{\sqrt{2}}\frac{e\lambda_t}{4\pi^2}\,C_7^{\text{eff}}\,\big[m_b\,\big(\bar{s}\,i\sigma^{\mu q}\,(1+\gamma^5)\,b\big) + m_s\,\big(\bar{s}\,i\sigma^{\mu q}\,(1-\gamma^5)\,b\big)\big]\,\epsilon_\mu\,,$$

where $\sigma^{\mu q} = \frac{i}{2}(\gamma^\mu\gamma^\nu - \gamma^\nu\gamma^\mu)q_\nu$, $O^\mu = \gamma^\mu(1-\gamma^5)$ and $\lambda_t \equiv V_{ts}^\dagger V_{tb}$.

The Wilson coefficient C_9^{eff} effectively takes into account, first, the contributions from the four-quark operators $Q_i(i = 1, \cdots, 6)$ and, second, the nonperturbative effects (long–distance contributions) coming from the $c\bar{c}$-resonance contributions what are, as usual, parametrized by a Breit-Wigner ansatz [13].

The Feynman diagrams contributing to the exclusive transitions $\Lambda_b \to \Lambda\bar{\ell}\ell$ and $\Lambda_b \to \Lambda\gamma$ are shown in Fig. 1.

The corresponding matrix elements of the exclusive transitions $\Lambda_b \to \Lambda\bar{\ell}\ell$ and $\Lambda_b \to \Lambda\gamma$ are defined by

Figure 1: Diagrams contributing to the flavor-changing transition $\Lambda_{Q[ud]} \to \Lambda_{Q'[ud]} + X$, where $X = \ell^-\bar{\nu}_\ell, \ell^+\ell^-$ or γ.

$$
\begin{aligned}
M(\Lambda_b \to \Lambda\bar{\ell}\ell) \;=\; \frac{G_F}{\sqrt{2}}\frac{\alpha\lambda_t}{2\pi}\Bigg\{ &C_9^{\text{eff}}\,\langle\Lambda\,|\,\bar{s}\,O^\mu\,b\,|\,\Lambda_b\rangle\,\bar{\ell}\gamma_\mu\ell \\
&+ C_{10}\,\langle\Lambda\,|\,\bar{s}\,O^\mu\,b\,|\,\Lambda_b\rangle\,\bar{\ell}\gamma_\mu\gamma_5\ell \\
&- \frac{2m_b}{q^2}\,C_7^{\text{eff}}\,\langle\Lambda\,|\,\bar{s}\,i\sigma^{\mu q}\,(1+\gamma^5)\,b\,|\,\Lambda_b\rangle\,\bar{\ell}\gamma_\mu\ell\Bigg\}
\end{aligned}
\tag{5}
$$

and

$$M(\Lambda_b \to \Lambda\gamma) = -\frac{G_F}{\sqrt{2}}\frac{e\lambda_t}{4\pi^2}\,m_b\,C_7^{\text{eff}}\,\langle\Lambda\,|\,\bar{s}\,i\sigma^{\mu q}\,(1+\gamma^5)\,b\,|\,\Lambda_b\rangle\,\epsilon_\mu\,. \tag{6}$$

The hadronic matrix elements in Eqs. (5) and (6) are expanded in terms of dimensionless form factors f_i^J ($i = 1, 2, 3$ and $J = V, A, TV, TA$), viz.

$$
\begin{aligned}
\langle B_2\,|\,\bar{s}\,\gamma^\mu\,b\,|B_1\rangle \;&=\; \bar{u}_2(p_2)\Big[f_1^V(q^2)\gamma^\mu - f_2^V(q^2)i\sigma^{\mu q}/M_1 + f_3^V(q^2)q^\mu/M_1\Big]u_1(p_1)\,, \\
\langle B_2\,|\,\bar{s}\,\gamma^\mu\gamma^5\,b\,|B_1\rangle \;&=\; \bar{u}_2(p_2)\Big[f_1^A(q^2)\gamma^\mu - f_2^A(q^2)i\sigma^{\mu q}/M_1 + f_3^A(q^2)q^\mu/M_1\Big]\gamma^5 u_1(p_1)\,, \\
\langle B_2\,|\,\bar{s}\,i\sigma^{\mu q}/M_1\,b\,|B_1\rangle \;&=\; \bar{u}_2(p_2)\Big[f_1^{TV}(q^2)(\gamma^\mu q^2 - q^\mu\,\slashed{q})/M_1^2 - f_2^{TV}(q^2)i\sigma^{\mu q}/M_1\Big]u_1(p_1)\,, \\
\langle B_2\,|\,\bar{s}\,i\sigma^{\mu q}\gamma^5/M_1\,b\,|B_1\rangle \;&=\; \bar{u}_2(p_2)\Big[f_1^{TA}(q^2)(\gamma^\mu q^2 - q^\mu\,\slashed{q})/M_1^2 - f_2^{TA}(q^2)i\sigma^{\mu q}/M_1\Big]\gamma^5 u_1(p_1)\,.
\end{aligned}
$$

Here, p_1, M_1 and p_2, M_2 are momenta and masses of the ingoing and outgoing baryons, respectively. The transfer momentum is equal to $q = p_1 - p_2$. One can see that, in comparison with the Cabibbo-allowed $b \to c$ and $c \to s$ transitions, one has four more form factors $f_{1,2}^{TV,TA}$.

The $\Lambda_b \to \Lambda\gamma$ decay rate is calculated according to

$$\Gamma(\Lambda_b \to \Lambda\gamma) = \frac{\alpha}{2}\left(\frac{G_F m_b\,|\lambda_t|\,C_7^{\text{eff}}}{4\pi^2\sqrt{2}}\right)^2 \frac{(M_1^2 - M_2^2)^3}{M_1^3}\left[\left(f_2^{TV}(0)\right)^2 + \left(f_2^{TA}(0)\right)^2\right].$$
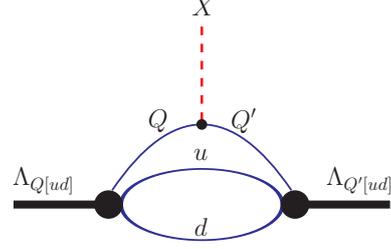
The angular decay distribution for the cascade decay $\Lambda_b \to \Lambda(\to p\pi^-)\gamma$ can be written as

$$\frac{1}{\Gamma_{\text{tot}}} \frac{d\Gamma(\Lambda_b \to \Lambda(\to p\pi^-)\gamma)}{d\cos\theta_B} = \text{Br}(\Lambda \to p\pi^-) \frac{1}{2} \text{Br}(\Lambda_b \to \Lambda\gamma)(1 - \alpha_B \cos\theta_B),$$

where α_B is the asymmetry parameter in the decay $\Lambda \to p + \pi^-$ for which we take the experimental value $\alpha_B = 0.642 \pm 0.013$ [14].

As in the case of the rare meson decays $B \to K^{(*)}\ell^+\ell^-$ ($\ell = e, \mu, \tau$) treated in [15] one can exploit the cascade nature of the decay $\Lambda_b \to \Lambda(\to p\pi^-) + j_{\text{eff}}(\to \ell^+\ell^-)$ to write down a joint angular decay distribution involving the polar angles θ, θ_B and the azimuthal angles χ defined by the decay products in their respective (center of mass) CM systems as shown in Fig. 2.

We write out the three-fold angular decay distribution in a manner where we collect together terms with the threshold behavior in a factor $v = \sqrt{1 - 4m_\ell^2/q^2} : v^0, v^1$ and v^2. Including the q^2 dependence one obtains a four-fold joint angular decay distribution for the decay of an unpolarized Λ_b. One has

Figure 2: Definition of angles θ, θ_B and χ in the cascade decay $\Lambda_b \to \Lambda(\to p\pi^-) + J_{\text{eff}}(\to \ell^+\ell^-)$.

$$W(\theta, \theta_B, \chi) \propto \frac{32\,q^2}{9} \left(A\,v^2 + B\,v + C\,\frac{2m_\ell^2}{q^2} \right),$$

where the coefficients A, B and C are given by

$$
\begin{aligned}
A &= \frac{9}{64}(1 + \cos^2\theta)\left(U^{11} + U^{22}\right) + \frac{9}{32}\sin^2\theta\left(L^{11} + L^{22}\right) \\
&+ \frac{9}{32}\alpha_B \cos\theta_B \left[\sin^2\theta\left(L_P^{11} + L_P^{22}\right) + \frac{1}{2}(1 + \cos^2\theta)\left(P^{11} + P^{22}\right) \right] \\
&+ \frac{9}{16\sqrt{2}}\alpha_B \sin 2\theta \sin\theta_B \left[\cos\chi\left(I1_P^{11} + I1_P^{22}\right) - \sin\chi\left(I2_P^{11} + I2_P^{22}\right) \right],
\end{aligned}
$$

$$
\begin{aligned}
B &= -\frac{9}{16}\cos\theta \left[P^{12} + \alpha_B \cos\theta_B\, U^{12} \right] \\
&- \frac{9}{4\sqrt{2}}\alpha_B \sin\theta \sin\theta_B \left[\cos\chi\, I3_P^{12} - \sin\chi\, I4_P^{12} \right],
\end{aligned}
$$

$$
C = \frac{9}{16}\left(U^{11} + L^{11} + S^{22}\right) + \frac{9}{16}\alpha_B \cos\theta_B \left(P^{11} + L_P^{11} + S_P^{22}\right).
$$

We have adopted the notations

$$X^{mm'} \equiv \frac{d\Gamma_X^{mm'}}{dq^2} = \frac{1}{2}\frac{G_F^2}{(2\pi)^3}\left(\frac{\alpha|\lambda_t|}{2\pi}\right)^2 \frac{|\mathbf{p_2}|\,q^2\,v}{12\,M_1^2} H_X^{mm'},$$
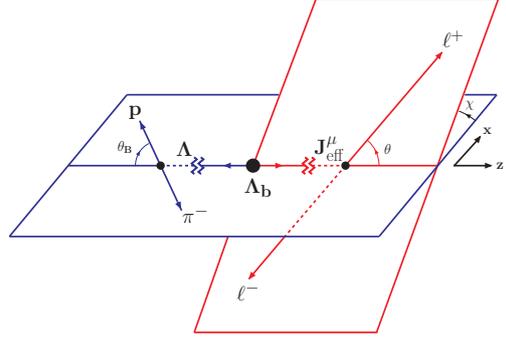
where the bilinear expressions $H_X^{mm'}$ $(X = U, L, S, P, L_P, S_P, I1_P, I2_P, I3_P, I4_P)$ are defined in Ref. [2]. Here, $|\mathbf{p_2}| = \lambda^{1/2}(M_1^2, M_2^2, q^2)/2M_1$ is the momentum of the Λ-hyperon in the Λ_b-rest frame. Note that we have included the statistical factor $1/(2S_{\Lambda_b} + 1) = 1/2$ in the definition of the rate functions.

Putting in the correct normalization factors one obtains the differential rate $d\Gamma/dq^2$ which reads

$$\frac{d\Gamma(\Lambda_b \to \Lambda\,\ell^+\ell^-)}{dq^2} = \frac{v^2}{2} \cdot \left(U^{11+22} + L^{11+22}\right) + \frac{2m_\ell^2}{q^2} \cdot \frac{3}{2} \cdot \left(U^{11} + L^{11} + S^{22}\right),$$

Here, and in the following, we do an importance sampling of our rate expressions by sorting the contributions according to powers of the threshold factor v. When one wants to compare our results to the corresponding results for the mesonic case written down in Ref. [15] one has to rearrange the contributions in Ref. [15] accordingly. And, one has to take into account the factor of 3 difference in the definition of the scalar structure function.

The total rate, finally, is obtained by q^2–integration in the range

$$4m_\ell^2 \ \leq \ q^2 \ \leq \ (M_1 - M_2)^2\,.$$

For the lower q^2 limit one has $4m_\ell^2 = (1.04 \times 10^{-6}, 0.045, 12.6284)$ GeV^2 for $\ell = (e, \mu, \tau)$. The upper limit of the q^2–integration is given by $(M_{\Lambda_b} - M_\Lambda)^2 = 20.29$ GeV^2. For $\ell = (e, \mu)$ one is practically probing the whole q^2 region while for $\ell = \tau$ the q^2–range is restricted to the low recoil half of phase-space starting at $\sqrt{q^2} = 3.55$ GeV just below the position of the $\Psi(2S)$ vector meson resonance.

4   Numerical results

With the choice of dimensional parameters $\Lambda_{\Lambda_s} = 0.490$ GeV, $\Lambda_{\Lambda_c} = 0.864$ GeV and $\Lambda_{\Lambda_b} = 0.569$ GeV we get a reasonable agreement with current data on exclusive Cabibbo-allowed decays of Λ_c and Λ_b as one can see from the Table 1.

For the magnetic moments we get the following results:

$$\mu_{\Lambda_s} = -0.73\,, \quad \mu_{\Lambda_c} = 0.39\,, \quad \mu_{\Lambda_b} = -0.06\,,$$

which compares well with data for the μ_{Λ_s} and theoretical estimates for the μ_{Λ_c} and μ_{Λ_b} (see the detailed discussion in Ref. [16]).

Mode	Our results	Data [14]
$\Lambda_c \to \Lambda e^+\nu_e$	2.0	2.1 ± 0.6
$\Lambda_c \to \Lambda\mu^+\nu_\mu$	2.0	2.0 ± 0.7
$\Lambda_b \to \Lambda_c e^-\bar{\nu}_e$	6.6	$6.5^{+3.2}_{-2.5}$
$\Lambda_b \to \Lambda_c \mu^-\bar{\nu}_\mu$	6.6	
$\Lambda_b \to \Lambda_c \tau^-\bar{\nu}_\tau$	1.8	

Table 1: Branching ratios of semileptonic decays of heavy baryons (in %).

In particular, our present results for the magnetic moments of heavy Λ-hyperons are very close to our predictions done before in the model without taking account of the mechanism of quark confinement: $\mu_{\Lambda_c} = 0.42$ and $\mu_{\Lambda_b} = -0.06$ [16].

We present our results for the branching ratios of the rare dileptonic decay $\Lambda_b \to \Lambda\ell^+\ell^-$ in Table 2. The results without long-distance effects are shown in brackets. Our predictions for the radiative decay $\Lambda_b \to \Lambda\gamma$ are also displayed.

In our calculations we do not include the regions around the two charmonium resonances $R_{c\bar{c}} = J/\psi, \Psi(2S)$. We exclude the regions $M_{J/\Psi} - 0.20$ GeV to $M_{J/\Psi} + 0.04$ GeV and $M_{\Psi(2S)} -$

0.10 GeV to $M_{\Psi(2S)}+0.02$ GeV. As stressed in Ref. [17] these regions are experimentally vetoed, because the rates of nonleptonic decays $\Lambda_b \to \Lambda + R_{c\bar{c}}$, followed by the dileptonic decays of the charmonium, are much larger than rates of the $b \to s$-induced rare decays $\Lambda_b \to \Lambda\ell^+\ell^-$. Vetoing the regions near the charmonium resonances leads to physically acceptable results — the predictions with and without the inclusion of long–distance effects are comparable with each other. Otherwise (without such a vetoing) the results with long–distance effects are dramatically enhanced as shown in different theoretical calculations.

Mode	Our results	Data
$\Lambda_b \to \Lambda e^+ e^-$	1.0 (1.0)	
$\Lambda_b \to \Lambda \mu^+ \mu^-$	1.0 (1.0)	$0.96 \pm 0.16 \pm 0.13 \pm 0.21$ [5]
		$1.73 \pm 0.42 \pm 0.55$ [4]
$\Lambda_b \to \Lambda \tau^+ \tau^-$	0.2 (0.3)	
$\Lambda_b \to \Lambda\gamma$	4.0	$< 1.3\,10^3$

Table 2: Branching ratios of rare decays $\Lambda_b \to \Lambda\ell^+\ell^-$ with (without) long–distance contributions and radiative decay $\Lambda_b \to \Lambda\gamma$ (in units of 10^{-6}).

5 Summary and conclusions

We have given a short review of the covariant quark model with infrared confinement and applied this approach to describe the semileptonic, rare and radiative decays of heavy Λ_b-baryon.

We have described from a unified point of view exclusive Cabibbo-allowed semileptonic decays $\Lambda_b \to \Lambda_c\ell^-\bar{\nu}_\ell$, $\Lambda_c \to \Lambda\ell^+\nu_\ell$ and rare decays $\Lambda_b \to \Lambda\ell^+\ell^-$, $\Lambda_b \to \Lambda\gamma$ with the use of only three model parameters: the size parameters Λ_{Λ_s}, Λ_{Λ_c} and Λ_{Λ_b} defining the distribution of quarks in the Λ, Λ_c and Λ_b baryons.

We have used the helicity formalism to express a number of observables in the rare baryon decay $\Lambda_b \to \Lambda(\to p\pi^-)\,\ell^+\ell^-$ in terms of a basic set of hadronic helicity structure functions. In the helicity method one provides complete information on the spin density matrix of each particle in the cascade decay chain which can be conveniently read out by considering angular decay distributions in the rest frame of that particular particle. The advantage of the helicity method is that it is straightforward to define any of the observables of the problem and to express them in terms of bilinear forms of the hadronic helicity matrix elements.

The helicity formulas can be used as input in a MC event generator patterned after the existing event generator for $\Xi^0(\uparrow) \to \Sigma^+(\to p\pi^0)\ell^-\bar{\nu}_\ell$ $\ell = (e, \mu)$ which is described and put to use in [18] and which has been used by the NA48 Collaboration to analyze its data on the above decay [19].

Acknowledgments

References

[1] T. Gutsche, M. A. Ivanov, J. G. Körner, V. E. Lyubovitskij and P. Santorelli, Phys. Rev. **D88** 114018 (2013).

[2] T. Gutsche, M. A. Ivanov, J. G. Körner, V. E. Lyubovitskij and P. Santorelli, Phys. Rev. **D87** 074031 (2013).

[3] T. Gutsche, M. A. Ivanov, J. G. Körner, V. E. Lyubovitskij and P. Santorelli, Phys. Rev. **D86** 074013 (2012).

[4] T. Aaltonen *et al.* [CDF Collaboration], Phys. Rev. Lett. **107** 201802 (2011).

[5] RAaij *et al.* [LHCb Collaboration], Phys. Lett. B **B725** 25 (2013).

[6] S. Weinberg, Phys. Rev. **130** 776 (1963).

[7] A. Salam, Nuovo Cim. **25** 224 (1962).

[8] K. Hayashi, M. Hirayama, T. Muta, N. Seto and T. Shirafuji, Fortsch. Phys. **15** 625 (1967).

[9] G. V. Efimov and M. A. Ivanov, *The Quark Confinement Model of Hadrons*, (IOP Publishing, Bristol & Philadelphia, 1993).

[10] T. Branz, A. Faessler, T. Gutsche, M. A. Ivanov, J. G. Körner and V. E. Lyubovitskij, Phys. Rev. **D81** 034010 (2010).

[11] J. A. M. Vermaseren, Nucl. Phys. Proc. Suppl. **183** 19 (2008).

[12] G. Buchalla, A. J. Buras and M. E. Lautenbacher, Rev. Mod. Phys. **68** 1125 (1996).

[13] A. Ali, T. Mannel and T. Morozumi, Phys. Lett. **B273** 505 (1991).

[14] J. Beringer *et al.* [Particle Data Group Collaboration], Phys. Rev. **D86** 010001 (2012).

[15] A. Faessler, T. Gutsche, M. A. Ivanov, J. G. Körner, V. E. Lyubovitskij, Eur. Phys. J. direct **C4** 18 (2002).

[16] A. Faessler, T. .Gutsche, M. A. Ivanov, J. G. Körner, V. E. Lyubovitskij, D. Nicmorus and K. Pumsa-ard, Phys. Rev. D **D73** 094013 (2006).

[17] L. Mott and W. Roberts, Int. J. Mod. Phys. **A27** 1250016 (2012).

[18] A. Kadeer, J. G. Körner, U. Moosbrugger, Eur. Phys. J. **C59** 27 (2009).

[19] J. R. Batley *et al.* [NA48/1 Collaboration], Phys. Lett. **B720** 105 (2013).

Applications of QCD Sum Rules
to Heavy Quark Physics

Alexander Khodjamirian

Theoretische Physik 1, Naturwissenschaftlich-Technische Fakultät,
Universität Siegen, D-57068 Siegen, Germany

In these lectures, I present several important applications of QCD sum rules to the decay processes involving heavy-flavour hadrons. The first lecture is introductory. As a study case, the sum rules for decay constants of the heavy-light mesons are considered. They are relevant for the leptonic decays of B-mesons. In the second lecture I describe the method of QCD light-cone sum rules used to calculate the heavy-to-light form factors at large hadronic recoil, such as the $B \to \pi \ell \nu_\ell$ form factors. In the third lecture, the nonlocal hadronic amplitudes in the flavour-changing neutral current decays $B \to K^{(*)} \ell\ell$ are discussed. Light-cone sum rules provide important nonfactorizable contributions to these effects.

Introduction

The method of sum rules in quantum chromodynamics (QCD) developed in [1] relates hadronic parameters, such as decay constants or transition form factors, with the correlation functions of quark currents. Let me outline the three key elements of this method.

- **Correlation function of local quark currents** is defined. The simplest, two-point correlation function is formed by two quark-antiquark current operators sandwiched between the QCD vacuum states. This is a function of the 4-momentum transfer between the currents. In the region of large spacelike momentum transfers, the correlation function represents a short-distance fluctuation of quark-antiquark fields. The propagation of quarks and antiquarks at short distances is asymptotically free, the gluon exchanges being suppressed by a small QCD coupling. In addition, the interactions with "soft" (low momentum) quark-antiquark and gluon fields populating the QCD vacuum have to be taken into account.

- **Operator-product expansion (OPE)** of the correlation function is worked out. This expansion provides an analytical expression for the correlation function at spacelike momentum transfers, with a systematic separation of short- and long-distance effects. The former are described by Feynman diagrams with quark and gluon propagators and vertices, whereas the latter are encoded by universal parameters related to the nonperturbative QCD dynamics. In the case of two-point sum rules, these parameters are the averaged local densities of the QCD vacuum fields, the condensates. The contributions of vacuum effects in OPE are suppressed by inverse powers of the large momentum and/or heavy-quark mass scale, allowing one to truncate the expansion at some maximal power.

- **Hadronic dispersion relation** for the correlation function is employed. The basic unitarity condition allows one to express the imaginary part (spectral density) of the correlation function in terms of the sum and/or integral over all intermediate hadronic states with the quantum numbers of the quark currents. On the other hand, employing the analyticity of the correlation function in the momentum transfer variable, one relates the OPE result at spacelike momentum transfers to the integral over hadronic spectral density. In this way a link between QCD and hadrons is established, and the resulting relation between the OPE expression and hadronic sum is naturally called a "QCD sum rule".

After this general description of the method, let me quote a shorter but more emotional definition of QCD sum rules: "Snapshots of hadrons or the story of how the vacuum medium determines the properties of the classical mesons which are produced, live and die in the QCD vacuum", given as a title to the review [2] written by one of the founders of this method.

Due to a vast amount of applications of QCD sum rules accumulated during many years, these lectures represent only a brief guide to the field, exemplifying applications to a few important processes involving heavy flavoured hadrons. More detailed reviews are listed in [3, 4, 5, 6].

1. Lecture: Calculating the B-meson decay constant

In this introductory lecture, I consider, as a study case, the QCD sum rule derivation for an important hadronic parameter – the B-meson decay constant.
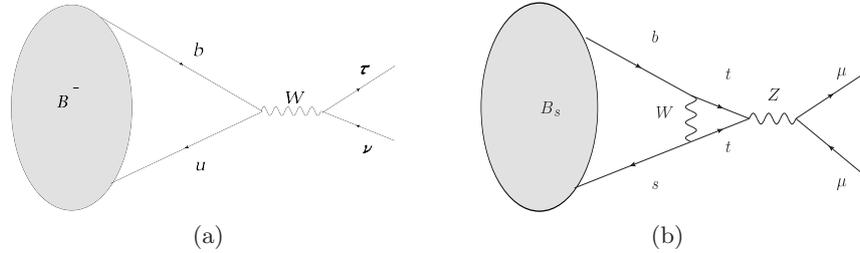
1.1 B-meson leptonic decays

Figure 1: Diagram of the weak leptonic decay $B^- \to \tau \bar{\nu}_\tau$ (a) and one of the diagrams of the FCNC leptonic decay $B_s \to \mu^+ \mu^-$ (b). The initial B meson is denoted by a blob.

The decay diagrams are shown in Fig. 1. The first leptonic decay is a weak transition $B^- \to \ell \bar{\nu}_\ell$ via virtual W boson exchange. For $\ell = \tau$ its branching fraction was measured at B factories [7]. The second decay, $\bar{B}_s \to \ell^+ \ell^-$, is a rare flavour-changing neutral current (FCNC) transition generated by the loop diagrams with heavy particles (t, Z, W). Its recent observation at LHC [8] was a great experimental achievement. Although short-distance electroweak interactions are quite different, these decays have one common feature: the initial B-meson annihilates and the final state contains no hadrons i.e. it is a vacuum (lowest energy) state of QCD. The decay

amplitude of the weak decay in Standard Model (SM):

$$A(B^- \to \tau^- \bar{\nu}_\tau)_{SM} = \frac{G_F}{\sqrt{2}} V_{ub} \, \bar{\tau}\gamma^\mu(1-\gamma_5)\nu_\tau \langle 0|\bar{u}\gamma_\mu\gamma_5 b|B^-\rangle \,, \tag{1}$$

contains the simplest possible hadronic matrix element

$$\langle 0|\bar{u}\gamma^\mu\gamma_5 b|B(p_B)\rangle = i p_B^\mu f_B, \tag{2}$$

in which the local operator of $b \to u$ weak transition current is sandwiched between B and the vacuum state. The above formula in terms of a constant parameter f_B reflects the fact that p_B^μ is the only 4-momentum involved in this hadronic matrix element and $p_B^2 = m_B^2$. The quantity f_B is the B-meson decay constant we are interested in. In order to use the experimental measurement of the decay branching fraction:

$$BR(B^- \to \tau^- \bar{\nu}_\tau) = \frac{G_F^2 |V_{ub}|^2}{8\pi} m_\tau^2 m_B \left(1 - \frac{m_\tau^2}{m_B^2}\right)^2 f_B^2 \tau_{B^-} \,, \tag{3}$$

where τ_{B^-} is the lifetime of B^-, one needs to know f_B from the theory. This will allow one to to extract the fundamental CKM parameter $|V_{ub}|$ or to check if there is an admixture of new physics, e.g., of a charged Higgs boson exchange, in this decay.

The rare leptonic decay, $B_s \to \mu^+\mu^-$, is even more sensitive to new physics contributions, due to the presence of heavy particle loops . But the corresponding hadronic matrix element

$$\langle 0|\bar{s}\gamma^\mu\gamma_5 b|B_s(p_B)\rangle = i p_B^\mu f_{B_s} \tag{4}$$

is very similar to Eq. (2), and the squared decay constant $f_{B_s}^2$ enters the decay width. The CKM suppressed $B_d \to \mu^+\mu^-$ decay contains the decay constant of B_d. Due to isospin symmetry between u and d quarks, $f_{B_d} \simeq f_{B_u} \equiv f_B$ with a good accuracy. On the other hand, f_{B_s} and f_B noticeably differ, because the $SU(3)_{flavor}$ symmetry is violated by the quark mass difference $m_s - m_{u,d}$. Hence, an accurate calculation of f_{B_s} has to take into account the finite s-quark mass.

We conclude that a QCD calculation of f_B is indispensable for disentangling the fundamental flavour-changing transitions from the measurements of leptonic B decays.

1.2 B-meson decay constant in QCD

The task is to calculate the hadronic matrix element (2) which is shown in Fig. 2, separated from the electroweak part of the leptonic decay amplitude. The wavy lines and loops in this figure indicate gluons and quark-antiquark pairs interacting with the valence b and $\bar{u}$ quarks inside B^- meson. But these lines and loops are only illustrative: it is not possible to directly attribute QCD Feynman graphs to a hadronic amplitude.

The quantum field theory of quarks, gluons and their interactions is encoded in the QCD Lagrangian:

Figure 2: B meson transition to vacuum

$$L_{QCD}(x) = -\frac{1}{4} G_{\mu\nu}^a G^{a\,\mu\nu}(x) + \sum_{q=u,d,s,c,b,t} \bar{q}^{\,i}(x)(iD_\mu\gamma^\mu - m_q)q^{\,i}(x) \tag{5}$$
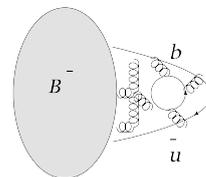
where $D_\mu = \partial_\mu - ig_s \frac{\lambda^a}{2} A_\mu^a$ is the covariant derivative, $G_{\mu\nu}^a = \partial_\mu A_\nu^a - \partial_\nu A_\mu^a + g_s f^{abc} A_\mu^a A_\nu^a$ is the gluon-field strength tensor and g_s is the quark-gluon coupling, so that $\alpha_s = g_s^2/(4\pi)$, with summation over the colour indices $i = 1,2,3$ and $a = 1,...8$. From Eq. (5) one derives the basic elements of the QCD Feynman graphs: quark and gluon propagators and quark-gluon, 3-gluon and 4-gluon vertices. In QCD, a crucial role is played by quark-gluon loop diagrams generating an effective scale dependent coupling $\alpha_s(\mu)$. As we know, it logarithmic decreases at large scales μ (*asymptotic freedom*) as illustrated in Fig. 3. The perturbation theory in terms of Feynman diagrams of quark-gluon interactions is well defined only at large energy/momentum transfers. Inversely, at small momenta (long distances) as is shown in the same Fig. 3 the coupling grows. At momentum transfers smaller than a few hundred MeV the perturbation theory for quarks and gluons in QCD is senseless. An intrinsic scale $\Lambda_{QCD} \sim 200 - 300$ MeV emerges, the quarks, antiquarks and gluons interact strongly. Moreover, they are only observable in a form of coulourless bound states - the hadrons, one of them is the B meson.

Another important feature of QCD is that the vacuum state in this theory is not an "empty space". It contains fluctuating quark-antiquark and gluon fields with characteristic wave lengths of $O(1/\Lambda_{QCD})$. Averaged densities of these fields known as vacuum condensate densities play an important role in our story. In fact, the most important role will be played by the quark condensate with a density parametrized as the vacuum average of the Lorentz- and colour-invariant local operator $\langle 0|\bar{q}^i q^i|0\rangle \equiv \langle \bar{q}q \rangle \neq 0$,

Figure 3: Dependence of the effective coupling in QCD on the energy/momentum scale Q.

$(q = u, d, s)$ with dimension $d = 3$. Let me remind you that $\langle \bar{q}q \rangle \neq 0$ reflects the spontaneous breaking of chiral symmetry in QCD. One acquires a set of vacuum condensate densities with dimensions $d = 3, 4, 5, ..$ formed by all possible colourless Lorentz-invariant operators built from quark and gluon fields. E.g., the $d = 4$ operator formed from two gluon-field strengths yields the gluon condensate density $\langle 0|(\alpha_s/\pi)G_{\mu\nu}^a G^{a\,\mu\nu}|0\rangle \equiv \langle GG \rangle \neq 0$. Importantly, there is no $d = 2$ condensate in QCD. A review on vacuum condensates can be found in [9].

Returning to the process of B-meson annihilation, from the point of view of QCD it is important that the energy scale of quark-gluon interactions binding b and $\bar{u}$ inside B is characterized by the mass difference between the meson ($m_B \simeq 5.3$ GeV) and heavy b-quark:

$$\bar{\Lambda} \sim m_B - m_b \sim 500 - 700 \text{ MeV}. \tag{6}$$

To quantify the above estimate we literally take $m_b = 4.6 - 4.8$ GeV, the so called "pole" quark mass. Important is that quarks and gluons inside the B meson have energies $\leq \bar{\Lambda}$ and hence interact strongly. At such scales no perturbative expansion in $\alpha_s(\bar{\Lambda})$ is possible and QCD Feynman graphs cannot be used. Moreover, in addition to "valence" quarks, the partonic
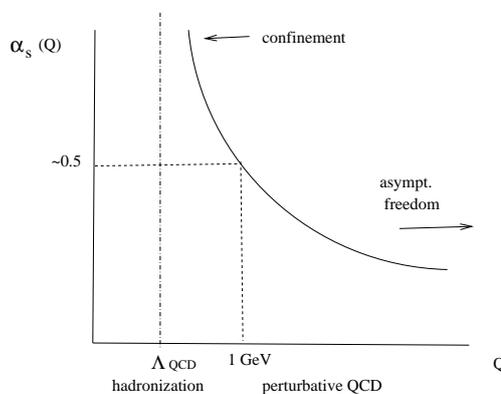
components with soft gluons and $\bar{q}q$ -pairs inside B-meson

$$|B^-\rangle = |b\bar{u}\rangle \oplus |b\bar{u}G\rangle \oplus |b\bar{u}\bar{q}q\rangle \oplus \dots \tag{7}$$

are becoming important in forming the complete "wave function" of the hadronic state $|B\rangle$. We also have to keep in mind that the QCD vacuum state $\langle 0|$ is populated by nonperturbative fluctuating quark-antiquark and gluon fields. We conclude that for the hadronic matrix element $\langle 0|\bar{u}\gamma_5 b|B\rangle \sim f_B$ there is no solution in QCD within perturbation theory.

One possibility to calculate this matrix element is to use a numerical simulation of QCD on the lattice. An impressive progress in this direction has been achieved in recent years. We will stay within continuum QCD and follow the method of QCD sum rules.

1.3 Correlation function of heavy-light quark currents

According to the original idea [1], (see also one of the first papers on this subject [10]) we start from defining a suitable correlation function: an object calculable in QCD and simultaneously related to the hadronic parameter f_B:

$$\Pi_{\mu\nu}(q) = \int d^4x \ e^{iqx} \langle 0|T\{\bar{u}(x)\gamma_\mu\gamma_5 b(x)\bar{u}(0)\gamma_\mu\gamma_5 b(0)\}|0\rangle . \tag{8}$$

This is an amplitude of an emission and absorbtion of the $b\bar{u}$ quark pair in the vacuum by the external current $\bar{u}\gamma_\mu\gamma_5 b$ and its conjugate $\bar{b}\gamma_\mu\gamma_5 u$ with a 4-momentum q. The $b \to u$ current is the same as in the hadronic matrix element (2) of the leptonic decay. To simplify the further derivation, it is convenient to deal with a Lorentz-invariant amplitude, multiplying the above correlation function by the 4-momenta: $q^\mu q^\nu \Pi_{\mu\nu}(q) \equiv \Pi_5(q^2)$. This is equivalent to taking divergences of the axial current operators under the x integral: $\partial^\mu(\bar{u}\gamma_\mu\gamma_5 b) = (m_b + m_u)\bar{u}i\gamma_5 b \equiv j_5$ and replacing the axial currents by the pseudoscalar ones, hence we may redefine the correlation function to a slightly different form

$$\Pi_5(q^2) = \int d^4x \ e^{iqx} \langle 0|T\{j_5(x)j_5^\dagger(0)\}|0\rangle , \tag{9}$$

so that $\Pi_5(q^2)$ depends only on the invariant 4-momentum square. We accordingly modify the definition of the decay constant

$$p_B^\mu \langle 0|\bar{u}\gamma_\mu\gamma_5 b|B(p_B)\rangle = \langle 0|j_5|B(p_B)\rangle = m_B^2 f_B \tag{10}$$

Let us consider the correlation function (9) in the region $q^2 \ll m_b^2$. In the rest frame, $\vec{q} = 0$, $q^2 = q_0^2$ and the energy deficit to produce a real B meson state from the current is $\Delta q_0 = m_B - q_0 \sim m_b$, up to small corrections. Thus, the propagation of the $b\bar{u}$ pair emitted by the current $j_5(x)$ and absorbed by the current $j_5^+(0)$ lasts a time interval $\Delta x_0 \sim 1/\Delta q_0 \sim 1/m_b$, much shorter than a time/distance interval $\Delta x_0 \sim \Delta x_i \sim 1/\Lambda_{QCD}$ typical for the nonperturbative, strong interaction regime of QCD. Hence the quark-antiquark pair propagation described by the correlation function at $q^2 \ll m_b^2$ remains highly virtual and therefore calculable in perturbative QCD.

In the leading order of perturbation theory, the function $\Pi_5(q^2)$ is determined by a simple quark-loop diagram shown in Fig. 4 (upper left). Gluon radiative corrections to this diagram, one of them shown in Fig. 4 (upper right) are suppressed by small coupling $\alpha_s(\mu \sim m_b)$. The
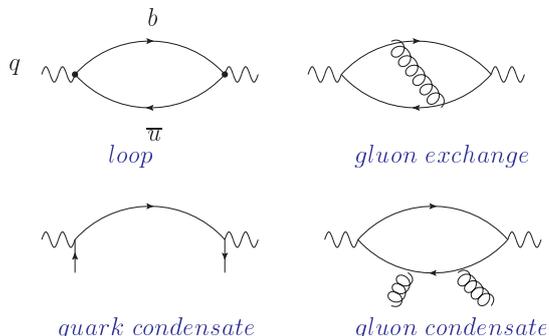
Figure 4: Diagrams corresponding to the correlation function (9): simple quark-antiquark loop diagram (upper left), one of the perturbative gluon-exchanges (upper right), quark condensate (lower left) and one of the gluon condensate diagrams (lower right).

simple loop diagram and radiative gluon corrections expressed via two- and three-loop diagrams (the latter were calculated in [11]) form the perturbative part of the correlation function $\Pi(q^2)$.

Additional diagrams shown in Fig 4 take into account the interactions with QCD vacuum fields. A detailed calculation of the quark condensate diagram shown in Fig. 4 (lower left) can be found e.g. in the review [4]. The gluon condensate diagrams (one of them in Fig 4 (lower right)) are more complicated because they represent a combination of the loop and vacuum insertions. Useful methods to calculate these diagrams are introduced in the review [12]. Technically, one uses Feynman rules of QCD and considers the vacuum quark-antiquark pairs and gluons as external static fields. There are also contributions combining the quark-antiquark and gluon vacuum lines. All condensate diagrams forming the nonperturbative part of $\Pi_5(q^2)$ and calculated at $q^2 \ll m_b^2$ contain a short-distance part, formed by the propagating quarks and antiquarks, and a long-distance part approximated by locally averaged condensate densities. This is how a short-distance quark-antiquark fluctuation "sees" the QCD vacuum or makes the "snapshots of QCD vacuum" in terms of [2].

The result for the correlation $\Pi_5(q^2)$ is an analytical expression in terms of quark masses m_b, m_u, quark-gluon coupling α_s and universal QCD condensate densities. Interpreting the calculational procedure as a systematic OPE is another important theoretical aspect. An introduction to the OPE adapted for the correlation functions in the presence of vacuum condensates can be found e.g., in [2, 5]. Formally, one expands the product of the two current operators in a series of local operators

$$T\{j_5(x)j_5^\dagger(0)\} = \sum_{d=0,3,4,..} C_d(x^2, m_b, m_u, \alpha_s) O_d(0) \tag{11}$$

with growing dimensions built from quark, antiquark fields and gluon field strength

Taking vacuum average of the above formula and integrating it over x we recover the correlation function

$$\Pi_5(q^2) = \int d^4x \, e^{iqx} \langle 0|T\{j_5(x)j_5^\dagger(0)\}|0\rangle = \sum_{d=0,3,4,..} \overline{C}_d(q^2, m_b, m_u, \alpha_s) \langle 0|O_d|0\rangle \,, \tag{12}$$

where $\overline{C}_d(q^2, ...) = \int d^4x e^{iqx} C_d(x^2, ...)$. Evidently, only the operators with vacuum quantum

numbers (Lorentz-scalar, C-, P-, T-invariant, colourless) contribute to the r.h.s :

$$O_0 = 1, \quad O_3 = \bar{q}q, \quad O_4 = G^a_{\mu\nu}G^{a\mu\nu}, \quad O_5 = \bar{q}\sigma_{\mu\nu}\frac{\lambda^a}{2}G^a_{\mu\nu}q, \quad O_6 = (\bar{q}\Gamma_r q)((\bar{q}\Gamma_r q), ... \quad , \quad (13)$$

where $q = u, d, s$, and Γ_r are certain combinations of Dirac matrices. The unit operator with $\langle 0|O_0|0 \rangle = 1$ and no fields is added for the sake of uniformity. Its coefficient represents the perturbative part of the correlation function, $\Pi_5^{(pert)}(q^2) = \overline{C}_0(q^2)$. This part of the correlation function is obtained from the loop diagram and gluon radiative corrections and is conveniently represented in the form of a dispersion integral:

$$\Pi_5^{(pert)}(q^2) - \Pi_5^{(pert)}(0) - q^2\frac{d}{dq^2}\Pi_5^{(pert)}(0) = (q^2)^2 \int\limits_{m_b^2}^{\infty} ds\, \frac{\rho_5^{(pert)}(s)}{s^2(s - q^2)} \quad (14)$$

with the spectral density

$$\rho_5^{(pert)}(s) = \frac{1}{\pi}\mathrm{Im}\Pi_5^{(pert)}(s) = \frac{3m_b^2}{8\pi^2}s\left(1 - \frac{m_b^2}{s}\right)^2 + O(\alpha_s) + O(\alpha_s^2). \quad (15)$$

The two subtractions are needed for the convergence of the integral. Note that for simplicity we neglected the light-quark mass in Eq. (15). The $O(\alpha_s)$ and $O(\alpha_s)^2$ corrections in this equation are considerably more complicated and can be found in [11, 14] (see also e.g., [13]).

The dominant nonperturbative contribution to the OPE (12) stems from the quark condensate:

$$\Pi_5^{\langle \bar{q}q \rangle}(q^2) = \overline{C}_3(q^2)\langle \bar{q}q \rangle, \quad \text{where} \quad \overline{C}_3(q^2) = \frac{-m_b^3}{m_b^2 - q^2} + O(\alpha_s). \quad (16)$$

The leading order result for the Wilson coefficient $\overline{C}_3(q^2)$ is obtained from the diagram shown in Fig. 4 (lower left) and a more complicated expression for the $O(\alpha_s)$ gluon radiative correction can be found in [13]. In the above expression, the separation of short and long distances is visible: the short-distance part is given by a simple b-quark propagator with 4-momentum q whereas the quark condensate density represents the long-distance effect. The complete expression for the correlation function in a compact form is:

$$\Pi_5^{(OPE)}(q^2) = \Pi_5^{(pert)}(q^2) + \Pi_5^{\langle \bar{q}q \rangle}(q^2) + \Pi_5^{\langle d456 \rangle}(q^2). \quad (17)$$

where all $d = 4, 5, 6$ effects are collected in one term for brevity. The terms with $d > 6$ are usually neglected, provided one keeps the $d = 4, 5, 6$ contribution sufficiently small, due to a proper choice of the variable q^2.

1.4 Correlation function in terms of hadrons

Having at hand the expression (17) for the correlation function $\Pi_5(q^2)$ valid at $q^2 \ll m_b^2$, let us now investigate its relation to hadrons. To visualize the discussion, I consider a hypothetical neutrino-electron elastic scattering via a virtual W boson. One of the possible intermediate states in this process is the $b\bar{u}$ pair emitted from and annihilated into W (in the longitudinal state, to have $J^P = 0^-$) as depicted in Fig. 5. The $b\bar{u}$ fluctuation coincides with the correlation function we are considering. The c.m. energy of this process is equal to the momentum
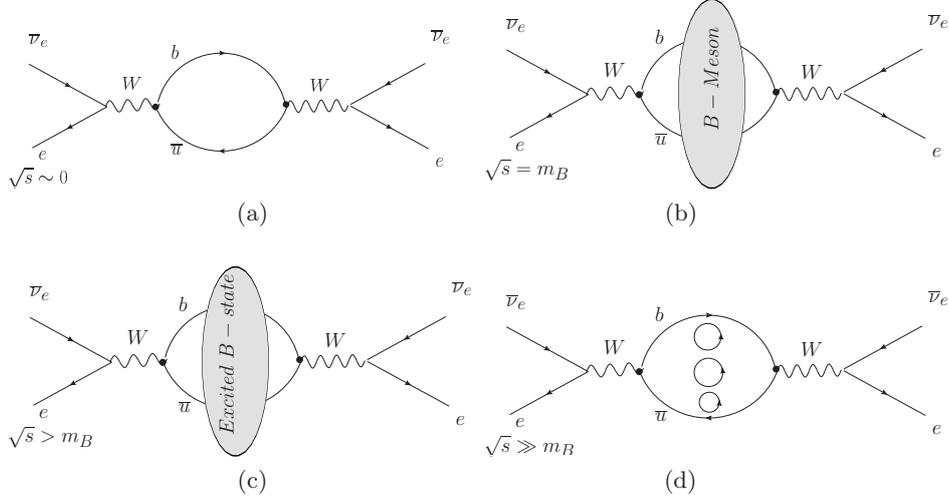
Figure 5: Correlation function as a part of the $\bar{\nu}_e e$ scattering amplitude at different energies $\sqrt{s} = \sqrt{q^2}$.

transfer flowing in the correlation function: $\sqrt{s} = \sqrt{q^2}$. In the region $q^2 \ll m_b^2$ the intermediate $b\bar{u}$ state (Fig.5(a)) represents a highly virtual heavy-light quark-antiquark pair. We are able to calculate this fluctuation in terms of OPE as already explained. On the other hand, increasing the energy one reaches the domain where real on-shell hadronic states propagate in the intermediate state. At $\sqrt{s} = m_B$, the B-meson (Fig.5(b)) contributes. This is the lowest possible intermediate hadronic state in this channel, it will show up as a sharp resonance in our hypothetical scattering process. Increasing the energy, one encounters heavier resonances, the radially excited B mesons, with growing total width (Fig.5(c)). These resonances are overlapped with multiparticle hadronic states with a net B flavor (Fig.5(d)), starting with the two-particle hadronic state $B^*\pi$ with the lowest threshold $s = q^2 = (m_{B^*} + m_\pi)^2$. Note that a $B\pi$ state is not allowed by spin-parity conservation. The multihadron state contributions build up the hadronic continuum mixed with excited states. At very large energies, resonances are smeared and multihadron states dominate. We come to conclusion that the correlation function $\Pi_5(q^2)$ in the region $q^2 > m_B^2$ describes a complicated overlap of interfering resonant and multiparticle hadronic states with B meson quantum numbers.

This qualitative picture of emerging intermediate hadronic states reflects the formal spectral representation of $\Pi_5(q^2)$ following from the basic unitarity relation. The imaginary part of the correlation function is equal to the sum of contributions of all possible hadronic states allowed by quantum numbers:

$$\frac{1}{\pi}\text{Im}\Pi_5(q^2) = \langle 0|j_5|B\rangle\langle B|j_5^\dagger|0\rangle\delta(m_B^2 - q^2) + \rho_5^h(s)\theta(s - (m_{B^*} + m_\pi)^2)\,, \qquad (18)$$

where we isolated the ground-state B meson contribution and introduce a shorthand notation for the spectral density of excited (resonance and multiparticle) states, schematically:

$$\rho_5^h(s) = \sum_{B_{exc}} \langle 0|j_5|B_{exc}\rangle\langle B_{exc}|j_5^\dagger|0\rangle \qquad (19)$$

where the sum includes the integration over phase space and sum over polarizations. A detailed derivation of the hadronic representation for two-point correlation function can be found e.g., in [5].

The next important step is to employ the analyticity of the function $\Pi(q^2)$ which, according to the unitarity relation (18) has singularities – poles (cuts) related to resonances (multiparticle thresholds) – on the real axis of the complex q^2 plane. The Cauchy theorem leads to the dispersion relation between $\Pi_5(q^2)$ and its imaginary part integrated over positive $s \geq m_B^2$:

$$\Pi_5(q^2) = \frac{1}{\pi} \int_{m_B^2}^{\infty} ds \frac{\mathrm{Im}\Pi_5(s)}{s - q^2 - i\epsilon} , \qquad (20)$$

where the subtraction terms are hereafter neglected for simplicity. Importantly, this relation is valid at any q^2. We will apply it at $q^2 \ll m_b^2$ where the correlation function represents a short-lived $b\bar{u}$ -fluctuation calculable in terms of OPE, so that l.h.s. in the above dispersion relation can be approximated by $\Pi_5^{(OPE)}(q^2)$ given by Eq. (17). Hence, we obtain a remarkable opportunity to relate the correlation function calculated in QCD to a sum/integral containing hadronic parameters, including the B-meson mass and decay constant.

1.5   Deriving the sum rule for f_B^2

Substituting Eq. (18) in the dispersion relation (20) and expressing the hadronic matrix element via f_B, we obtain at $q^2 \ll m_b^2$:

$$\Pi_5(q^2) = \frac{f_B^2 m_B^4}{m_B^2 - q^2} + \int_{s_h}^{\infty} ds \frac{\rho^h(s)}{s - q^2} \simeq \Pi_5^{(OPE)}(q^2) . \qquad (21)$$

where $s_h = (m_{B^*} + m_\pi)^2$ is the lowest threshold of the excited B states.

Let us now employ another important feature of the correlation function. In the deep spacelike region $q^2 \to -\infty$ the power suppressed condensate terms in Eq. (17) vanish and the correlation function coincides with the perturbative part of OPE:

$$\Pi_5(q^2 \to -\infty) = \Pi_5^{(OPE)}(q^2 \to -\infty) = \Pi_5^{(pert)}(q^2 \to -\infty) \qquad (22)$$

dominated by the simple loop diagram.

It is convenient to express the perturbative part of the OPE in a form of dispersion relation. In this case the imaginary part starts at the $b\bar{u}$-quark pair threshold and is equal to the spectral density of the loop diagrams presented in Eq. (15):

$$\Pi^{(pert)}(q^2) = \frac{1}{\pi} \int_{m_b^2}^{\infty} ds \frac{\mathrm{Im}\Pi_5^{(pert)}(s)}{s - q^2} , \qquad (23)$$

where we again neglect the subtractions and put $m_u \to 0$.

To fulfill the asymptotic condition (22), the spectral functions entering the hadronic and OPE (perturbative) dispersion relations should be equal at sufficiently large s:

$$\rho^h(s) \simeq \frac{1}{\pi} \mathrm{Im}\Pi_5^{(pert)}(s), \qquad (24)$$

This approximation is called local quark-hadron duality. It suffices to use a weaker condition, approximately equating the integrals of the hadronic and perturbative spectral densities over the large s region:

$$\int\limits_{s_h}^{\infty} ds \frac{\rho^h(s)}{s-q^2} \simeq \frac{1}{\pi} \int\limits_{s_0}^{\infty} ds \frac{\text{Im}\Pi_5^{(pert)}(s)}{s-q^2}, \qquad (25)$$

where an effective threshold s_0 is introduced. Returning to the hadronic dispersion relation (21), we use Eq. (25) to replace the integral over excited B states and the OPE (17) in r.h.s., with the perturbative part replaced by its dispersion representation. The resulting relation:

$$\frac{f_B^2 m_B^4}{m_B^2-q^2} + \frac{1}{\pi} \int\limits_{s_0}^{\infty} ds \frac{\text{Im}\Pi_5^{(pert)}(s)}{s-q^2} = \frac{1}{\pi} \int\limits_{m_b^2}^{\infty} ds \frac{\text{Im}\Pi_5^{(pert)}(s)}{s-q^2} + \Pi_5^{\langle \bar{q}q \rangle}(q^2) + \Pi_5^{\langle d456 \rangle}(q^2), \qquad (26)$$

allows one to subtract the approximately equal integrals from both sides yielding an analytical relation for the decay constant:

$$\frac{f_B^2 m_B^4}{m_B^2-q^2} = \frac{1}{\pi} \int\limits_{m_b^2}^{s_0} ds \frac{\text{Im}\Pi_5^{(pert)}(s)}{s-q^2} + \Pi_5^{\langle \bar{q}q \rangle}(q^2) + \Pi_5^{\langle d456 \rangle}(q^2). \qquad (27)$$

A substantial improvement of this relation is further achieved with the help of the Borel transformation defined as:

$$\Pi_5(M^2) \equiv \mathcal{B}_{M^2} \Pi_5(q^2) = \lim_{\substack{-q^2, n \to \infty \\ -q^2/n = M^2}} \frac{(-q^2)^{(n+1)}}{n!} \left(\frac{d}{dq^2}\right)^n \Pi_5(q^2), \qquad (28)$$

so that $\mathcal{B}_{M^2}(\frac{1}{m^2-q^2}) = \exp(-m^2/M^2)$.

The resulting QCD sum rule for f_B^2 obtained from Eq. (27) after this transformation reads:

$$f_B^2 m_B^4 e^{-m_B^2/M^2} = \int\limits_{m_b^2}^{s_0} ds\, e^{-s/M^2} \text{Im}\Pi_5^{(pert)}(s, m_b, m_u, \alpha_s) + \Pi_5^{\langle \bar{q}q \rangle}(M^2) + \Pi_5^{\langle d456 \rangle}(M^2). \qquad (29)$$

Note that the Borel transformation suppresses the higher-state contributions to the hadronic sum above s_0 so that the above sum rule is less sensitive to the accuracy of the quark-hadron duality approximation (25). Everything is ready to calculate the decay constant of B meson numerically.

1.6 Input parameters and results

In the sum rule (29) one has to choose an optimal interval of the Borel parameter. The lower boundary for M^2 is controlled by the OPE convergence, e.g., we demand that the $d = 4, 5, 6$ terms are sufficiently small with respect to the quark condensate term. The upper boundary for M^2 is adopted from the condition that the contribution of excited states subtracted from the sum rules remains subdominant. Furthermore, a standard way to fix the effective parameter s_0 is to fit the sum rule to the measured mass of B-meson by differentiating both parts of Eq. (29)

in $-(1/M^2)$ and dividing the result by the initial sum rule, so that f_B^2 cancels, and one obtains a relation for m_B^2.

One of the advantages of the sum rule method is its flexibility: replacing quark flavours in the correlation function, e.g., $b \to c$ or $\bar{u} \to \bar{s}$ provides the access to the decay constants of D or B_s mesons.. Nonzero strange quark mass and a difference in condensate densities, $\langle \bar{s}s \rangle \neq \langle \bar{u}u \rangle$,

Decay constant	Lattice QCD [ref.]	QCD sum rules [13]
f_B[MeV]	196.9 ± 9.1 [20] 186 ± 4 [21]	207^{+17}_{-9}
f_{B_s}[MeV]	242.0 ± 10.0 [20] 224 ± 5 [21]	242^{+17}_{-12}
f_{B_s}/f_B	1.229 ± 0.026 [20] 1.205 ± 0.007 [21]	$1.17^{+0.04}_{-0.03}$
f_D[MeV]	218.9 ± 11.3 [20] 213 ± 4 [22]	201^{+12}_{-13}
f_{D_s}[MeV]	260.1 ± 10.8 [20] 248.0 ± 2.5 [22]	238^{+13}_{-23}
f_{D_s}/f_D	1.188 ± 0.025 [20] 1.164 ± 0.018 [22]	$1.15^{+0.04}_{-0.05}$

Table 1: Decay constants of heavy-light mesons calculated with different methods.

generate the $SU(3)_{flavour}$ symmetry violation.

The universal input parameters needed for the numerical analysis of the sum rules include the quark masses, quark-gluon coupling and the vacuum condensate densities. Since the calculation is done at short distances the natural choice for quark masses is the $\overline{MS}$ scheme. The sum rule is quite sensitive to the b-quark mass, hence to have a reliable estimate of f_B one needs an independent and accurate determination of m_b. This task was fulfilled by considering quarkonium sum rules, where the correlation function of two $\bar{Q}\gamma_\mu Q$ currents ($Q = b, c$) is calculated in QCD. The accuracy of this calculation [15] has reached $O(\alpha_s^3)$ in the perturbative part. The hadronic representation of this correlation function is largely fixed from experiment [16] and consists of $J^{PC} = 1^{--}$ heavy quarkonia levels, their decay constants measured in $e^+e^- \to \Upsilon, \Upsilon(2S), ...$ or $e^+e^- \to J/\psi, \psi(2S), ...$ processes. Hence, the quarkonium sum rules can be used to extract the heavy quark masses. The most recent results of these determinations, expressed in $\overline{MS}$ scheme are: $\bar{m}_b(\bar{m}_b) = (4.18 \pm 0.03)\,\text{GeV}$ [15], $\bar{m}_c(\bar{m}_c) = (1.275 \pm 0.025)\,\text{GeV}$[15, 17]. In the same way, employing QCD sum rules for strange meson pseudoscalar and scalar channels [18] one obtains $m_s(\mu = 2\,\text{GeV}) = (98 \pm 16)\,\text{MeV}$. Combined with ChPT relations [19] one finds the quark condensate density $\langle \bar{q}q \rangle(2\,\text{GeV}) = -(277^{+12}_{-10}\,\text{MeV})^3$. Condensate densities with $d > 3$ entering the subleading power corrections in OPE are discussed in the review [9]. The sample of recent determinations of the B and D decay constants in Table 1 is taken from [13] where one can also find a detailed discussion of numerical procedure and formulae for OPE, as well as references to other important papers on the subject of this lecture.

2. Lecture: $B \to \pi$ form factors and light-cone sum rules

In this lecture more complicated hadronic matrix elements – the form factors of heavy-to-light transitions are considered. The best studied among them are the $B \to \pi$ transition form factors relevant for $B \to \pi \ell \nu_\ell$ semileptonic decay. I will explain how the QCD sum rule method was modified to calculate these and other hadronic form factors.
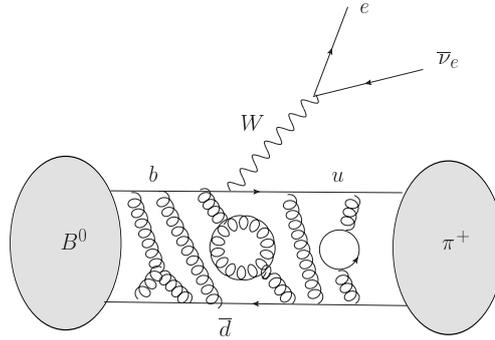
2.1 $B \to \pi \ell \nu_\ell$ decay and form factors

Figure 6: Schematic view of $B \to \pi \ell \nu_\ell$ decay

The exclusive semileptonic decay $B \to \pi \ell \nu_\ell$ shown in Fig. 6 proceeds via weak $b \to u$ transition with a squared momentum transfer q^2 to the leptonic pair varying within the interval $0 < q^2 < (m_B - m_\pi)^2 \sim 26 \text{ GeV}^2$ (here we neglect the lepton mass).

The form factors $f_{B\pi}^+(q^2)$ and $f_{B\pi}^0(q^2)$ are invariant functions of q^2 parameterizing the hadronic matrix element of this decay:

$$\langle \pi^+(p)|\bar{u}\gamma_\mu b|B(p+q)\rangle = f_{B\pi}^+(q^2)\Big[2p_\mu + \Big(1 - \frac{m_B^2 - m_\pi^2}{q^2}\Big)q_\mu\Big] + f_{B\pi}^0(q^2)\frac{m_B^2 - m_\pi^2}{q^2}q_\mu, \quad (30)$$

where $p + q$ and p are the four-momenta of B and π, respectively. Similar to the B decay constant, the $B \to \pi$ form factors have to be calculated in QCD. This is a challenging problem because not only the initial B meson but also the final pion is involved in the hadronic matrix element. In what follows we consider the region of small q^2, in which case the pion has a large recoil in the B meson rest system, with the momentum $p_\pi \equiv |\vec{p}| \sim m_B/2$ at $q^2 = 0$.

Analyzing the $B \to \pi$ form factors from the point of view of QCD, one expects a certain perturbative contribution corresponding to an energetic virtual gluon exchange between the quarks participating in the weak transition and the spectator quark. This "hard scattering" mechanism boosts the spectator quark in B meson and provides a natural configuration for the final pion with symmetric collinear quark and antiquark. On the other hand one has to take into account also the "end-point" mechanism where the pion is formed from an asymmetric quark-antiquark pair. This part of the form factor is dominated by soft nonperturbative gluons. The proportion of the hard scattering and soft end-point contributions to the hadronic form factors is a nontrivial problem. It can only be addressed within a calculational method that allows one to take into account both contributions.

An accurate determination of the $B \to \pi$ form factors is important for quark flavour physics because the semileptonic decay $B \to \pi \ell \nu_\ell$ is an excellent source of the CKM parameter $|V_{ub}|$. In fact, one practically needs only the vector form factor $f_{B\pi}^+$ for this purpose, because in the partial width the contribution of the form factor $f_{B\pi}^0$ is suppressed by the lepton mass:

$$\frac{1}{\tau_B} \frac{dBR(\bar{B}^0 \to \pi^+ l^- \nu)}{dq^2} = \frac{G_F^2 |V_{ub}|^2}{24\pi^3} p_\pi^3 |f_{B\pi}^+(q^2)|^2 + O(m_l^2). \tag{31}$$

Importantly, in lattice QCD the $B \to \pi$ form factors are currently accessible at comparatively large $q^2 \geq 15$ GeV^2. In this region the phase space in the decay width (31) is suppressed by small p_π. The calculation of the form factors at small q^2 (large recoil of the pion) discussed below, complements the lattice QCD results in a kinematically dominant region.

2.2 Vacuum-to-pion correlation function

The method of light-cone sum rules (LCSR) developed in [23, 24] is used to calculate the $B \to \pi$ form factors at large hadronic recoil. In this approach, the correlation function itself is an amplitude of the vacuum-to-hadron transition [1]:

$$F_\lambda(q,p) = i \int d^4x \, e^{iqx} \langle \pi(p) \mid T\{\bar{u}(x)\gamma_\lambda b(x), j_5(0)\} \mid 0 \rangle$$
$$= F(q^2, (p+q)^2)p_\mu + \tilde{F}(q^2, (p+q)^2)q_\mu, \tag{32}$$

containing the product of the weak $b \to u$ and $j_5 = m_b \bar{b} i \gamma_5 u$ currents. The latter was also used in the two-point correlation function for f_B. In what follows, only the invariant amplitude F is essential, depending on the two independent kinematical variables: q^2, the squared momentum transfer in the weak $b \to u$ transition, and $(p+q)^2$, the square of the 4-momentum flowing into the current j_5. The correlation function (32) allows for a systematic QCD calculation in the specific region: $q^2, (p+q)^2 \ll m_b^2$ where the b quark is a highly-virtual object. In this region of external momenta the x integral in the correlation function is dominated by small $x^2 \sim 1/m_b^2$, near the light-cone $x^2 \sim 0$. The leading order diagram for the correlation function is shown in Fig. 7(a). It consists of the free b-quark propagator convoluted with the matrix element of light quark and antiquark operators sandwiched between the vacuum and on-shell pion state. The perturbative gluon corrections to the leading order diagram are shown in Fig. 8. The diagram in Fig. 7(b) takes into account the emission of a soft (low-virtuality) gluon emitted from the b quark. The corresponding vacuum-to-pion matrix element involves light quark-antiquark and gluon fields.

A schematic expression for the correlation function (32) decomposed near the light-cone can be written as:

$$F(q,p) = i \int d^4x \, e^{iqx} \left\{ \left[S^0(x^2, m_b^2) + \alpha_s S^1(x^2, m_b^2) \right] \langle \pi(p) \mid \bar{u}(x)\Gamma d(0) \mid 0 \rangle \right.$$
$$\left. + \int_0^1 dv \, \tilde{S}(x^2, m_b^2, v) \langle \pi(p) \mid \bar{u}(x)G(vx)\tilde{\Gamma}d(0)\} \mid 0 \rangle \right\} + \dots \tag{33}$$

---

[1] Vacuum-to-vacuum correlation functions with the quark currents interpolating both B meson and pion and with the OPE in terms of condensates are not applicable for heavy-to-light form factors; see a detailed discussion in the review [6].
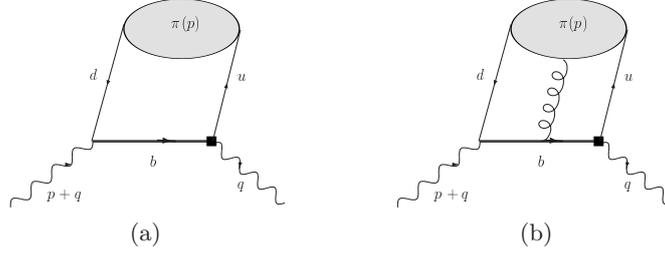
Figure 7: Diagrams corresponding to the correlation function (32): leading order (a) and soft gluon emission forming the 3-particle B meson DA (b).

where S_0 , S_1 and $\tilde{S}$ are the perturbative parts of the amplitudes, involving b-quark propagators. They are convoluted with the vacuum-pion matrix elements, taken near $x^2 = 0$, where $\Gamma, \tilde{\Gamma}$ are generic Dirac-matrix structures and the Lorentz-indices are omitted for simplicity.

The vacuum-to-pion matrix elements in Eq. (33) are nonperturbative but universal objects. They absorb all long-distance effects in the correlation function. The expansion in Eq.(33) goes over α_s and powers of x^2, which in the momentum space translates into an expansion in $\alpha_s(\mu)$ and the powers of $1/\mu$. Here $\mu \sim \sqrt{\chi m_b}$, with χ being an intermediate scale, $\Lambda_{QCD} \ll \chi < m_b$. In particular, in (33) the quark-antiquark gluon part has a power suppression with respect to the leading order part. Hence, the expansion (33) can safely be truncated. I skip a more formal and systematic description of this expansion based on the twist t (dimension minus Lorentz-spin) of the light quark-antiquark operators entering the vacuum-to-pion matrix elements (see, e.g., [5] for an introductory explanation).

The main nonperturbative object determining the leading-order answer for the light-cone expanded correlation function (33) is the vacuum-to-pion matrix element

$$\langle\pi(q)|\bar{u}(x)[x,0]\gamma_\mu\gamma_5 d(0)|0\rangle_{x^2=0} = -iq_\mu f_\pi \int_0^1 du\, e^{iuqx}\varphi_\pi(u) + O(x^2) \ , \qquad (34)$$

where $[x,0] = exp[ig_s \int_0^1 dt x_\mu A^{a\mu}(tx)\lambda^a/2]$ is the factor added to secure gauge invariance. The
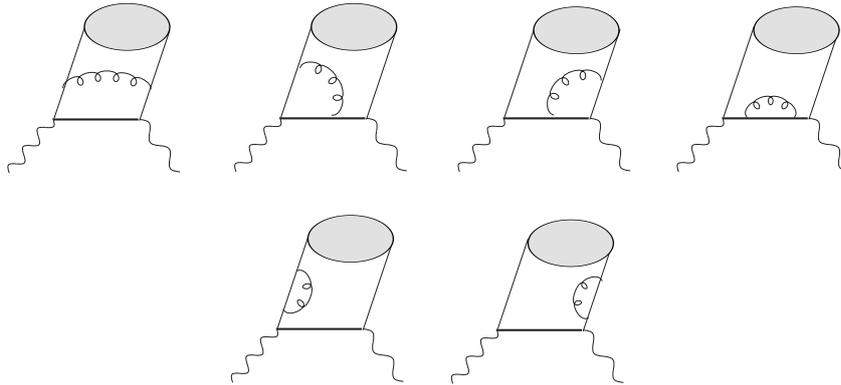

Figure 8: Gluon radiative corrections to the correlation function (32).

above matrix element is normalized to the pion decay constant, that is evident if one puts $x \to 0$ and takes into account that the function $\varphi_\pi(u)$ is normalized to unit. This and similar functions parameterizing vacuum-to-pion matrix elements play central role in the LCSR approach and replace the vacuum condensates. They are called light-cone distribution amplitudes (DA's) of the pion. Physically DA's correspond to various Fock components of the fast pion and the variable u denotes the share of the pion momentum carried by the quark or antiquark.

Inserting in Eq. (33) the vacuum-to pion matrix elements expressed in terms of DA's and integrating over x, one obtains the OPE result for the invariant amplitude defined in (32) in the following generic form:

$$F^{(OPE)}(q^2, (p+q)^2) = \sum_{t=2,3,4,..} \int du \, T^{(t)}(q^2, (p+q)^2, m_b^2, \alpha_s, u, \mu) \, \varphi_\pi^{(t)}(u, \mu) \,, \qquad (35)$$

where the summation goes over the growing twist, and the twist-2 part contains the DA defined in Eq. (34). The perturbative hard-scattering amplitudes $T^{(t)}$ stemming from the b-quark propagators and perturbative loops are process-dependent whereas the pion DA's are universal. One can analyse DA's using the light-cone OPE for other processes, not even involving heavy quarks, like e.g., the pion electromagnetic form factor at spacelike momentum transfers or the photon-pion transition form factor (see e.g. [5]). Within the currently achieved accuracy, the light-cone OPE (35) includes the twist 2,3,4 quark-antiquark and quark-antiquark-gluon DA's [25], and the hard -scattering amplitudes for twist 2,3 parts are calculated up to NLO, in $O(\alpha_s)$ [26, 27, 28, 29]. Recently, the $O(\alpha_s^2)$ correction to the twist-2 part was also calculated [30].

2.3 What do we know about the light-cone DA's

Before applying them in LCSR's, the pion DA's were already introduced in the context of the hard-scattering mechanism for the pion e.m. form factor at large momentum transfer [31, 32]. A convenient expansion in Gegenbauer polynomials was defined

$$\varphi_\pi(u, \mu) = 6u(1-u) \left[1 + \sum_{n=2,4,..} a_n^\pi(\mu) C_n^{3/2}(2u-1) \right] \,, \qquad (36)$$

with logarithmic evolution of its coefficients (Gegenbauer moments):

$$a_{2n}^\pi(\mu) \sim [\ln(\mu/\Lambda_{QCD})]^{-\gamma_{2n}} \,, \qquad (37)$$

vanishing at asymptotically large scale $\mu \to \infty$. The input values of Gegenbauer moments at low scale, $a_{2,4,6,...}^\pi(\mu_0 \sim 1 \text{ GeV})$ are determined from different sources: matching experimentally measured pion form factors to LCSR's , calculating a_2 from two-point QCD sum rules and in lattice QCD. Recent determinations lie within the intervals: $a_2^\pi = 0.25 \pm 0.15$, $a_2^\pi + a_4^\pi = 0.1 \pm 0.1$, if one neglects the higher coefficients. The remaining parameters of twist 3,4 DA's are determined mainly from dedicated two-point sum rules [33].

2.4 LCSR for $B \to \pi$ form factors

After obtaining the OPE expression for the amplitude $F((p+q)^2, q^2)$, the derivation of LCSR follows the same strategy as in the case of two-point sum rule. The hadronic dispersion relation for $F((p+q)^2, q^2)$ in the variable $(p+q)^2$ (at fixed small q^2) is used. The dispersion relation

contains a pole term with intermediate B meson and a hadronic sum over excited and multi-hadron states with B quantum numbers. Matching the OPE with this dispersion relation, we obtain

$$F^{(OPE)}((p+q)^2, q^2) = \frac{m_B^2 f_B f_{B\pi}^+(q^2)}{m_B^2 - (p+q)^2} + \int\limits_{s_0}^{\infty} ds \frac{\mathrm{Im} F^{(OPE)}(s, q^2)}{s - (p+q)^2}, \qquad (38)$$

where the residue of the B meson pole term contains the product of matrix elements $\langle \pi \mid \bar{u} \gamma_\lambda b \mid B \rangle$ and $\langle B \mid j_5 \mid 0 \rangle$ yielding the product of the form factor $f_{B\pi}^+(q^2)$ and the decay constant f_B. For the latter, the result obtained from the two-point sum rule discussed in the previous lecture can be used. Furthermore, on r.h.s. of (38) we also use the quark-hadron duality approximation, replacing the integral over excited states by the integral over the spectral density of the OPE result with an effective threshold s_0. Subtracting the integrals from s_0 to ∞ from both sides of the above relation and performing the Borel transformation we finally obtain the desired LCSR for the form factor:

$$f_B f_{B\pi}^+(q^2) = \int\limits_{m_b^2}^{s_0} ds\, \mathrm{Im} F^{(OPE)}(s, q^2) e^{(m_B^2 - s)/M^2}. \qquad (39)$$

The inputs include the b quark mass $\overline{m}_b$, α_s, and the set of pion DA's $\varphi_\pi^{(t)}(u)$, t=2,3,4. The resulting numerical interval for the form factor is formed by the uncertainties due to variation of the input and of M^2 within the interval where one can trust OPE and where simultaneously the contribution of excited states remains subdominant. A very detailed numerical analysis of this sum rule can be found in [29]. The effective threshold can be controlled by the m_B^2 calculation from LCSR. The LCSR for the scalar $B \to \pi$ form factor $f_{B\pi}^0$ is obtained employing the second invariant amplitude in the correlation function (32).

Let me emphasize that the method discussed here employs a finite b-quark mass. At the same time LCSRs allow for a systematic transition to the infinite heavy-quark mass . This limit described in detail, e.g., in the review [4], reproduces the heavy-mass scaling of the form factor at large hadronic recoil

$$f_{B\pi}^+(q^2 = 0) \sim 1/m_b^{3/2}, \qquad (40)$$

first predicted in [24]. Another important feature of LCSRs is that they contain both soft end-point and hard-scattering contributions to the form factor. The hard-scattering part is contained in the $O(\alpha_s)$ contributions to LCSR, described by the diagrams with perturbative gluon exchanges. The soft end-point mechanism originates from the part of OPE that do not contain gluon exchanges, and is dominated by the leading order diagram. It is therefore not surprising that the hard scattering part is suppressed, supporting the dominance of the end-point mechanism for the form factor. Note however that sum rules are not directly calculating the form factor but rather its "dual counterpart" in the OPE.

In Fig. 9 the recent predictions [34] of LCSR for both $B \to \pi$ form factors are shown in comparison with the lattice QCD results [20, 21]. The sum rules are used at $q^2 < q_{max}^2 \simeq$ 12 GeV^2 and the results are then extrapolated to larger momentum transfers with a certain analytical parametrization of the form factors [35] as explained in detail in [34]. Finally, the LCSR results were used to evaluate an integral over the weighted form factor squared, which,
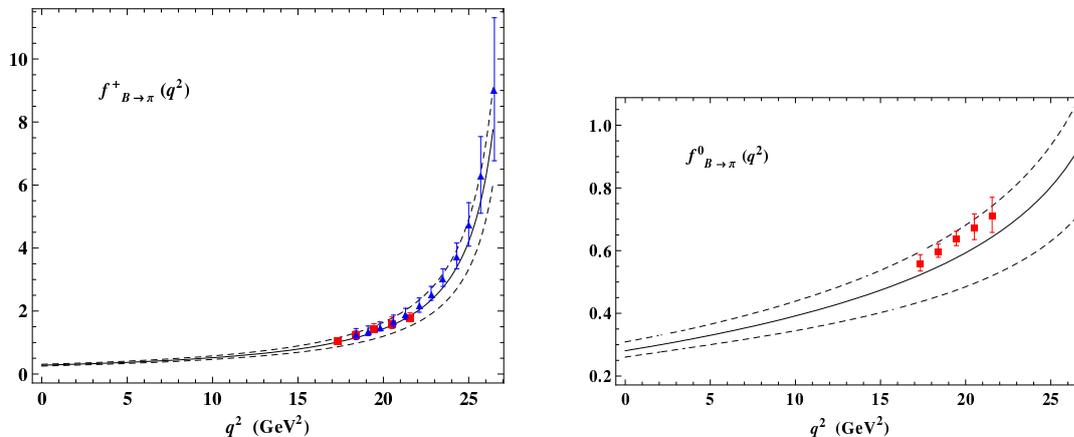
Figure 9: LCSR results for $B \to \pi$ form factors, extrapolated to $q^2 > 12$ GeV^2 in comparison with the lattice QCD predictions

as follows from (31), is related to the integral over the partial width:

$$\frac{G_F^2}{24\pi^3} \int\limits_0^{q_{max}^2} dq^2 p_\pi^3 |f_{B\pi}^+(q^2)|^2 = \frac{1}{|V_{ub}|^2 \tau_{B^0}} \int\limits_0^{q_{max}^2} dq^2 \frac{d\mathcal{B}(B \to \pi \ell \nu_\ell)}{dq^2} , \qquad (41)$$

This relation together with the measurements of the integrated partial width of $B \to \pi \ell \nu_\ell$ was used to extract $|V_{ub}|$ in [38].

Simple replacements $b \to c$ and the adjustment of light quark flavours in the underlying correlation function (32) allows to obtain the LCSR's for $D \to \pi, K$ form factors [36] employing the same OPE diagrams. In this case, only a narrow region above $q^2 = 0$ is accessible with LCSR's. The $SU(3)_{flavour}$ symmetry violation is encoded in the Gegenbauer moments of the kaon a_n^K, in particular, the odd moments with $n = 1, 3, ...$ have to be added in the expansion (36). The results for the form factors were used in [36] to extract V_{cs} and V_{cd} from the data on $D \to \pi(K)e\nu_e$ decays.

2.5 Alternative sum rules with B -meson DA's

The positions of the B-meson interpolating current and pion in the correlation function (32) can be exchanged introducing a new, vacuum-to-B correlation function, in which the B meson is represented by an on-shell state and the pion is replaced by an interpolating quark current, as shown in Fig. 10. Here q is the momentum transfer in the weak $b \to u$ transition current and p is the external momentum of the light-meson interpolating current, whereas $p_B = p + q$ with $p_B^2 = m_B^2$ is the B-meson momentum.

This approach was initiated in [37] (see also [39]). Its main advantage is an easy extension to other light hadrons, also the non-stable ones. It is relatively easy to obtain LCSRs for the B-meson transition form factors to light vector, scalar or axial mesons, by simply varying the quantum numbers of the intepolating current and adjusting the quark-hadron duality ansatz.

The description in terms of the light-cone OPE is done in the framework of heavy-quark effective theory (HQET). The 4-momentum of b-quark and B meson are represented as a sum of the static component and residual momentum: e.g, $p_B = p + q = m_b v + k$ where v is the velocity 4-vector. After the transition to HQET the vacuum-to-B correlation function is independent of the scale m_b. In this effective theory the following definition [41, 40] of the vacuum-to-B meson matrix element is used

Figure 10: Correlation function with B-meson DA's

$$\langle 0|\bar{q}_{2\alpha}(x)[x,0]h_{v\beta}(0)|\bar{B}_v\rangle$$
$$= -\frac{if_B m_B}{4} \int\limits_0^\infty d\omega e^{-i\omega v \cdot x} \left[(1+\slashed{v}) \left\{ \phi_+^B(\omega) - \frac{\phi_+^B(\omega) - \phi_-^B(\omega)}{2v \cdot x} \slashed{x} \right\} \gamma_5 \right]_{\beta\alpha}, \qquad (42)$$

where $h_{v\beta}$ is the effective field, α, β are Dirac indices. The functions $\phi_\pm^B(\omega)$ are the B-meson two-particle DA's and ω is the light-quark momentum fraction which formally (in the infinite heavy quark limit) varies up to $\omega = \infty$, however, in all realistic models is limited by $\omega \sim \bar{\Lambda}$ where $\bar{\Lambda}$ is the mass difference introduced in Eq. (6). More details on B-meson DA's can be found in the review [42]. These DA's were used earlier in the context of factorization approach to the heavy-light form factors in HQET [40]. In addition, the diagram with soft gluon emitted from u quark in the correlation function was taken into account, generating the three-particle DA's . Their detailed discussion can be found in the second paper in [37]

The rest of LCSR derivation follows the same way as in the case of pion DA's. The OPE in terms of B-meson DA's is matched to the dispersion relation in the variable p^2 which is the invariant momentum squared of the light-meson interpolating current. The accuracy of resulting LCSR's for $B \to \pi, K, \rho, K^*$ form factors obtained in [37] is still lower than for the conventional sum rules. One reason is that the key nonperturbative input parameter, the inverse moment: $\frac{1}{\lambda_B(\mu)} = \int_0^\infty d\omega \frac{\phi_+^B(\omega,\mu)}{\omega}$ is not yet accurately determined. Two-point QCD sum rules in HQET predict $\lambda_B(1\,\text{GeV}) = 460 \pm 110$ MeV [43]. This parameter is accessible in the photoleptonic' $B \to \gamma \ell \nu_\ell$ decay (for a recent analysis see [44] and [45]). Another reason is that the radiative gluon corrections to the correlation function in Fig. 10 are still missing. Therefore, the LCSR's with B-meson DA's have a room for improvement. Finally, let me quote another important application of these sum rules [46] to $B \to D^{(*)}$ form factors. The sum rules were obtained for the same correlation function as in Fig. 10 replacing the light quark in the correlation function by a c quark - another manifestation of the flexibility and universality of the method.

2.6 Heavy baryon form factors and $\Lambda_b \to p\,\ell\nu_\ell$

The LCSR method for B-meson form factors was also extended to the heavy baryon form factors. In particular, let me briefly outline the recent calculation [47] of the $\Lambda_b \to p$ form factors employing the following vacuum-to-nucleon correlation function:

$$\Pi_{\mu(5)}(P,q) = i \int d^4z \; e^{iq \cdot z} \langle 0|T\left\{\eta_{\Lambda_b}(0), \bar{b}(z)\gamma_\mu(\gamma_5)u(z)\right\}|N(P)\rangle . \qquad (43)$$
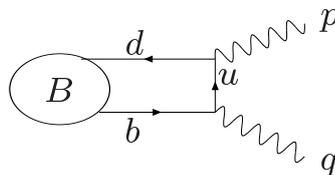
Here the three-quark heavy-light current operator η_{Λ_b} with quantum numbers of Λ_b has a nonvanishing matrix element $\langle \Lambda_b \mid \eta_{\Lambda_b} \mid 0 \rangle \neq 0$. It is traditionally called the Λ_b "decay constant", although literally an annihilation of Λ_b would violate the baryon number conservation and is absent in SM. Nevertheless, in QCD nothing prevents from introducing the auxiliary operator η_{Λ_b} as an external source of b-quark baryonic states. As opposed to the meson case, one has a multiple choice for constructing the three-quark currents. In [47] two different operators were used:

$$\eta_{\Lambda_b}^{(\mathcal{P})} = (u\, C\, \gamma_5\, d)\, b, \quad \eta_{\Lambda_b}^{(\mathcal{A})} = (u\, C\, \gamma_5 \gamma_\lambda\, d)\, \gamma^\lambda\, b, \qquad (44)$$

Figure 11: Diagrammatic representation of the correlation function with nucleon DA's used to derive LCSR's for heavy-to-light baryon form factors

and the difference between the results for the form factors was considered as a part of the "systematic" uncertainty.

The diagram for the correlation function in LO is shown in Fig. 11, with the on-shell nucleon, carrying the 4-momentum P ($P^2 = m_N^2$) and with the horizontal line denoting the virtual b-quark. The approximation of the free b-quark propagation is valid in the kinematical region $q^2 \ll m_b^2$, $(P - q)^2 \ll m_b^2$, where the integral over z in Eq. (43) is dominated by small intervals near the light-cone, $z^2 \sim 0$.

Contracting the virtual b-quark fields in Eq. (43), we recover new nonperturbative objects: the nucleon DA's. Their definitions and properties were worked out in [48], where also the LCSR's for nucleon electromagnetic form factors were obtained. The latter sum rules are described by the same diagram of Fig. 11 with a light u, d quark in the horizontal line. The definition of DA's is schematically given by the following decomposition of the vacuum-to-nucleon matrix element:

$$\langle 0|\epsilon^{ijk} u_\alpha^i(0) u_\beta^j(z) d_\gamma^k(0)|N(P)\rangle = \sum_t \mathcal{S}_{\alpha\beta\gamma}^{(t)} \times \int dx_1 dx_2 dx_3 \delta(1 - \sum_{i=1}^3 x_i) e^{-ix_2 P\cdot z} F_t(x_i), \quad (45)$$

where the expansion goes over twist $t = 3, 4, 5, 6$ of light-quark operators and contains 27 DA's $F_t(x_i)$ depending on the shares $x_{1,2,3}$ of the nucleon momentum.

The hadronic dispersion relation for the correlation function (43) aimed at isolating the ground-state Λ_b-pole contribution also has its peculiarities. The baryonic quark currents not only interpolate ground states but also their counterparts with the opposite P parity. In our case, the Λ_b^* baryon with $J^P = 1/2^-$ located at $m_{\Lambda_b^*} \simeq m_{\Lambda_b} + (200 \div 300)$ MeV, should also be counted as a ground state in the hadronic spectrum. Therefore we have to include this state in the resulting dispersion relation separately from the excited states:

$$\Pi_{\mu(5)}(P, q) = \frac{\langle 0|\eta_{\Lambda_b}|\Lambda_b\rangle\langle \Lambda_b|\bar{b}\gamma_\mu(\gamma_5)u|N\rangle}{m_{\Lambda_b}^2 - (P - q)^2} + \frac{\langle 0|\eta_{\Lambda_b}|\Lambda_b^*\rangle\langle \Lambda_b^*|\bar{b}\gamma_\mu(\gamma_5)u|N\rangle}{m_{\Lambda_b^*}^2 - (P - q)^2} + \int\limits_{s_0^h}^{\infty} \frac{ds\, \rho_{\mu(5)}(s, q^2)}{s - (P - q)^2}. \quad (46)$$

In [47] a simple procedure was introduced to eliminate the Λ^* baryon term in the dispersion relation by forming linear combinations of kinematical structures in the correlation function. The Λ_b term contains the product of decay constant and the transition form factors. There are altogether six form factors of $\Lambda_b \to p$ transition, actually their definition is very similar to
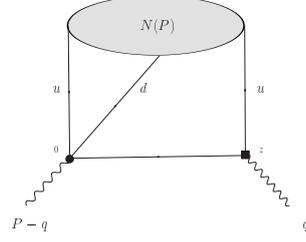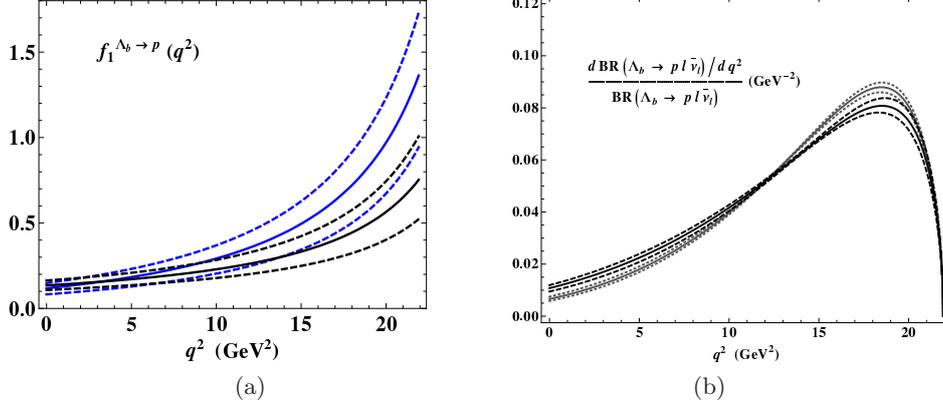
Figure 12: (a)- one of the $\Lambda_p \to N$ form factors predicted from LCSR [47], the spread between solid lines (solid and dashed lines) indicates the difference due to the choice of Λ_b currents (the uncertainties due to the input variation); (b) - normalized differential width of $\Lambda_b \to p\ell\nu_\ell$.

familiar one in the nucleon β decay. The three form factors for the vector part of the weak transition current are defined as:

$$\langle \Lambda_b(P-q)|\bar{b}\gamma_\mu u|N(P)\rangle = \bar{u}_{\Lambda_b}(P-q)\left\{ f_1(q^2)\gamma_\mu + i\frac{f_2(q^2)}{m_{\Lambda_b}}\sigma_{\mu\nu}q^\nu + \frac{f_3(q^2)}{m_{\Lambda_b}}q_\mu \right\}u_N(P), \quad (47)$$

For the axial vector current one has to replace in the above: $\gamma_\mu \to \gamma_\mu\gamma_5$ and $f_i(q^2) \to g_i(q^2)$.

The resulting sum rule for each form factor is obtained in a standard way. The result of the diagram calculation in terms of nucleon DA's is matched to the dispersion relation and the quark-hadron duality approximation in the Λ_b channel is employed. The decay constant of Λ_b is independently estimated from the QCD sum rules for the two-point vacuum correlation functions of the η_{Λ_b} current and its conjugate.

The kinematical region of the $\Lambda_b \to p\ell\nu_\ell$ semileptonic decay, $0 \le q^2 \le (m_{\Lambda_b} - m_N)^2$, is only partly covered by the LCSR calculation. The OPE is not reliable at large q^2, typically at $q^2 > 12-14$ GeV^2 because the virtual three-quark bud-state approaches the hadronic threshold in the q^2 channel. The numerical results obtained in [47] include the form factors at $q^2 \le 11$ GeV^2 calculated with the universal inputs including the b-quark mass and a few parameters determining the nucleon DA's. To improve LCSRs one also has to calculate the radiative gluon corrections to the correlation function which is however technically very challenging.

In Fig. 12 (left) one of the vector form factors is plotted, where the analytical parametrization [35] fitted to the LCSR prediction at low q^2 is used to extrapolate this form factor to the whole region of momentun transfer. One observes a reasonable agreement between the sum rules with different η_{Λ_b}-currents. The $\Lambda_b \to p\ell\nu_\ell$ decay width measurements combined with the calculated form factors provide an alternative source of $|V_{ub}|$ determination.

3. Lecture: Hadronic effects in $B \to K^{(*)} \ell^+ \ell^-$

In this lecture I will discuss a more complex problem of calculating the hadronic input for exclusive flavour-changing neutral current (FCNC) decays. As we shall see, the LCSRs provide not only the form factors but also nonlocal hadronic matrix elements specific for these decays.

3.1 FCNC transitions and nonlocal hadronix matrix elements

The $b \to s\,\ell^+\ell^-$ FCNC transitions observed in the form of exclusive decays such as $B \to K^{(*)}\ell\ell$ are intensively studied at LHC and B factories. The main interest in these decays is their sensitivity to the contributions of new heavy particles. In SM the $b \to s\ell^+\ell^-$ transitions are described by an effective Hamiltonian

$$H_{eff} = -\frac{4G_F}{\sqrt{2}} V_{tb} V_{ts}^* \sum_{i=1}^{10} C_i(\mu) O_i \Big|_{\mu \sim m_b}, \tag{48}$$

where the loop diagrams with heavy SM particle (t, Z, W) are absorbed in the Wilson coefficients C_i. The lighter fields, including b quark field, form effective local operators O_i. The $B \to K^{(*)} \ell^+ \ell^-$ decay amplitude

$$A(B \to K^{(*)} \ell^+ \ell^-) = \frac{G_F}{\sqrt{2}} V_{tb} V_{ts}^* \sum_{i=1}^{10} C_i(\mu) \langle K^{(*)}\ell^+\ell^- \mid O_i \mid B \rangle \Big|_{\mu \sim m_b} \tag{49}$$

is written formally as a sum of matrix elements of effective operators between the initial and final states, weighted by their Wilson coefficients. The dependence on the scale μ indicates the separation of gluon radiative corrections with momenta larger and smaller than μ between the Wilson coefficients and hadronic matrix elements, respectively.

In the above, the dominant contributions to the amplitude (49) are given by the operators

$$O_{9(10)} = \frac{\alpha_{em}}{4\pi}[\bar{s}_L \gamma_\mu b_L]\ell\gamma^\mu(\gamma_5)\ell, \quad O_{7\gamma} = -\frac{em_b}{8\pi^2}[\bar{s}\sigma_{\mu\nu}(1+\gamma_5)b]F^{\mu\nu} \tag{50}$$

with large coefficients $C_9(m_b) \simeq 4.4$, $C_{10}(m_b) \simeq -4.7$ and $C_7(m_b) \simeq -0.3$. The corresponding diagrams are shown in Fig. 13. The new physics effects can substantially modify the coefficients
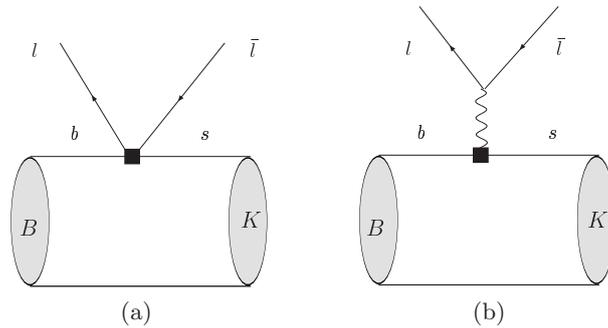

(a)   (b)

Figure 13: Hadronic matrix elements of FCNC operators $O_{9,10}$ (a) and O_7 (b) in the $B \to K\ell^+\ell^-$ decays.

$C_{9,10,7,...}$, and/or add new operators with different spin-parity combinations. In the contributions of $O_{9,10,7}$, the leptons are factorized out from the matrix elements in (49) and the only hadronic input one needs are the $B \to K^{(*)}$ form factors. The latter can be calculated with LCSR methods considered in the previous lecture.

However, at this stage the problem of determining the hadronic input in $B \to K^{(*)}\ell^+\ell^-$ is not yet solved. Note that the effective Hamiltonian (48) also contains effective operators without leptons or photon: the gluon-penguin $O_{8g} = -\frac{m_b}{8\pi^2}\bar{s}\sigma_{\mu\nu}(1+\gamma_5)bG^{\mu\nu}$, 4-quark penguin operators O_{3-6} with small Wilson coefficients and, most importantly, the current-current operators $O_1^{(c)} = [\bar{s}_L\gamma_\rho c_L][\bar{c}_L\gamma^\rho b_L]$ and $O_2^{(c)} = [\bar{c}_L\gamma_\rho c_L][\bar{s}_L\gamma^\rho b_L]$ of the "ordinary" weak interaction, with large coefficients $C_1(m_b) \simeq 1.1$ and $C_2(m_b) \simeq -0.25$, respectively [2]. These operators also contribute to the $b \to s\ell^+\ell^-$ transition. In a combination with weak interaction, the lepton pair in the final state is electromagnetically emitted from one of the quark lines. The main problem is that the average distances between the photon emission and the weak interaction points are not necessarily short, hence these additional contributions to the decay amplitude are essentially nonlocal, and cannot be simply reduced to the form factors.

The following decomposition of the decay amplitude in terms of hadronic matrix elements:

$$A(B \to K^{(*)}\ell^+\ell^-) = \frac{G_F}{\sqrt{2}}V_{tb}V_{ts}^*\frac{\alpha_{em}}{2\pi}\left[(\bar{\ell}\gamma^\rho\gamma_5\ell)C_{10}\langle K^{(*)}|\bar{s}\gamma_\rho(1-\gamma_5)b|B\rangle\right.$$

$$+(\bar{\ell}\gamma^\rho\ell)\Big(C_9\langle K^{(*)}|\bar{s}\gamma_\rho b|B\rangle + C_7\frac{2m_b}{q^2}q^\nu\langle K^{(*)}|\bar{s}i\sigma_{\nu\rho}(1+\gamma_5)b|B\rangle$$

$$\left.+\frac{8\pi^2}{q^2}\sum_{i=1,2,...,6,8}C_i\,\mathcal{H}_i^\rho\Big)\right] \tag{51}$$

includes "direct" FCNC contrbutions proportional to $C_{9,10,7}$ multiplied by the $B \to K^{(*)}$ form factors and the nonlocal hadronic matrix elements

$$\mathcal{H}_i^\rho(q,p) = \langle K^{(*)}(p)|i\int d^4x\,e^{iqx}\,T\{j_{em}^\rho(x),O_i(0)\}|B(p+q)\rangle \tag{52}$$

where $j_{em}^\rho = \sum_{q=u,d,s,c,b}Q_q\bar{q}\gamma^\rho q$ is the quark electromagnetic current. The factor $1/q^2$ multiplying the nonlocal part of the amplitude is due to the photon propagator connecting the quarks with the lepton e.m. current.

Hereafter, for simplicity we consider the decay $B \to K\ell^+\ell^-$ with the kaon final state. The QCD LCSRs similar to the ones used to calculate $B \to \pi$ form factors (see the previous lecture), provide also $B \to K$ form factors. One has to replace the pion DA's by kaon DA's in the correlation function. Apart from the vector form factor f_{BK}^+, the tensor form factor f_{BK}^T enters due to the O_7 operator. The LCSR results for all $B \to K$ form factors at $q^2 \leq 12 - 15$ GeV^2 were updated in [49] and the numerical results can be found there. One obtains values up to 30% larger than for the corresponding $B \to \pi$ form factors, revealing a noticeable violation of $SU(3)_{flavour}$ symmetry. Our analysis of the $B \to K\ell^+\ell^-$ amplitude will be constrained by the large hadronic recoil region ($q^2 < 6 - 8$GeV^2) which is fully covered by LCSR form factors. Note that the alternative LCSR's with B DA's also provide the $B \to K$ form factors [37], albeit with larger uncertainties.

---

[2]The same operators with u quarks are strongly suppressed by the CKM factor and therefore usually neglected in $b \to s$ transitions

The $B \to K\ell^+\ell^-$ amplitude, after inserting the form factors, reads:

$$A(B \to K\ell^+\ell^-) = \frac{G_F}{\sqrt{2}} \frac{\alpha_{em}}{\pi} V_{tb} V_{ts}^* \left[\bar{\ell}\gamma_\mu \ell \, p^\mu \Big(C_9 f_{BK}^+(q^2) \right.$$

$$\left. + \frac{2(m_b + m_s)}{m_B + m_K} C_7^{eff} f_{BK}^T(q^2) + \sum_{i=1,2,\dots,6,8} C_i \, \mathcal{H}_i^{(BK)}(q^2) \Big) + \bar{\ell}\gamma_\mu \gamma_5 \ell \, p^\mu C_{10} f_{BK}^+(q^2) \right], \qquad (53)$$

where $\mathcal{H}_i^{(BK)}(q^2)$ are the invariant amplitudes in the Lorentz-decomposition of (52).

3.2 Anatomy of the nonlocal hadronic matrix elements

The nonlocal contributions to the decay amplitude (53) can be cast in a form of corrections to the short-distance Wilson coefficient:

$$C_9 \to C_9 + \Delta C_9^{(BK)}(q^2), \quad \text{where} \quad \Delta C_9^{(BK)}(q^2) = \sum_{i=1,2,\dots,6,8} C_i \, \frac{\mathcal{H}_i^{(BK)}(q^2)}{f_{BK}^+(q^2)} . \qquad (54)$$

These corrections are q^2- and process-dependent and have to be estimated one by one for separate operators. The main question we address here is: are the nonlocal matrix elements $\mathcal{H}_i^{(BK)}(q^2)$ calculable in QCD?

First of all one has to sort out various contributions diagrammatically. The most important diagram in LO (without additional gluons) is in Fig. 14: a virtual photon emission via intermediate quark loop originating from the current-current operators $O_{1,2}$ or from quark-penguin operators O_{3-6}. In Fig. 15 the same mechanism is accompanied by gluon exchanges including also the gluon penguin contribution. The remaining mechanism of the weak annihilation with virtual photon emission has a small impact.

Calculation of these effects in $B \to K^{(*)}\ell^+\ell^-$ was done in the framework of HQET and QCD factorization approach [51] valid at $E_{K^{(*)}} \sim m_b/2$ and $m_b \to \infty$.

The results are obtained in the region of large hadronic recoil (small and intermediate q^2). The nonlocal amplitudes are expressed in terms of $B \to K$ form factors or factorized as a convolution of B- and light-meson DA's with hard-scattering kernels. There are however two problems to clarify. First, at timelike $q^2 \sim$ a few GeV^2, the virtual photon is emitted via intermediate on-shell vector mesons with the masses $m_V = \sqrt{q^2}$ ($V = \rho, \omega, \phi, J/\psi, ...$) rather than off quarks, hence the accuracy of the perturbative treatment has to be assessed.

The second related problem is the role of soft virtual gluons in the nonlocal amplitudes. The diagrams shown schematically in Fig. 16 are "fully nonfactorizable", i.e., with no possibility to separate a hard scattering amplitude from the long-distance one . The whole hadronic matix element has to be considered as a nonperturbative object.
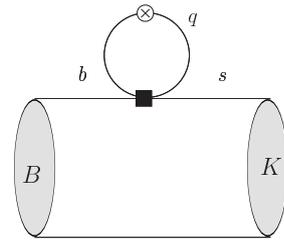

Figure 14: The quark-loop diagram of the nonlocal contribution to $B \to K\ell^+\ell^-$. The cross denotes the virtual photon emission point.
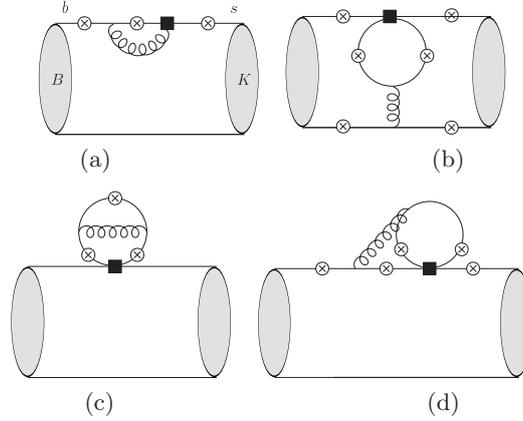
Figure 15: Factorizable diagrams with hard gluon exchanges

3.3 Charm-loop effect and light-cone OPE

Let me briefly outline the approach to nonlocal hadronic matrix elements applied in [49] where the two problems formulated above were addressed, concentrating on the most important (due to large Wilson coefficients) part of the nonlocal amplitude generated by the operators $O_{1,2}$. This is a combination of the $(\bar{s}c)(\bar{c}b)$ weak interaction and the $(\bar{c}c)(\bar{\ell}\ell)$ e.m.interaction, which effectively leads to $b \to s\ell^+\ell^-$ transition due to the fact that the charmed quark pair appears in the intermediate state only.

The leading order diagram shown in Fig. 17(a) contains the simple c-quark loop similar to the heavy-light loop in the two-point correlation function considered in the first lecture. Also here the physics depends on the region of the q^2 variable. At $q^2 \to m_{J/\psi}^2,...$ the charm loop turns into an on-shell hadronic J/ψ state, and the semileptonic decay we are considering becomes a combination of nonleptonic weak transition $B \to J/\psi K$, followed by the e.m. decay $J/\psi \to \ell^+\ell^-$. At larger q^2, the $\psi(2S)$ and other charmonia with $J^P = 1^-$, as well as the open-charm intermediate states contribute, with increasing masses up to the kinematical threshold $\sqrt{q^2} = m_B - m_K$. To avoid a "direct" charmonium background, the q^2 intervals around J/ψ and $\psi(2S)$ are subtracted from the measured lepton-pair mass distributions in $B \to K^{(*)}\ell^+\ell^-$. This subtraction does not however exclude the contribution of intermediate virtual $\bar{c}c$ state below
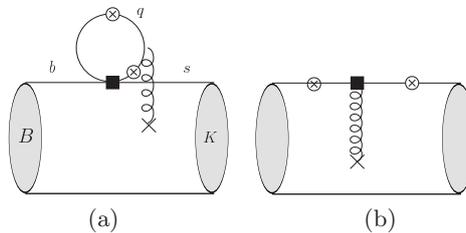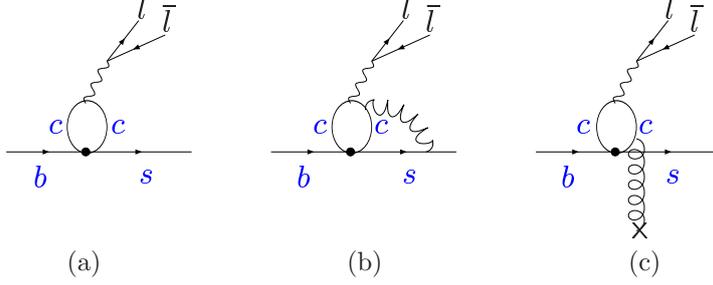

Figure 16: Soft-gluon nonfactorizable diagrams

Figure 17: $\bar{c}c$-quark loop effect at quark level

the charmonium levels. Can one use the "loop plus corrections" ansatz for this contribution and at which q^2?

To investigate this question, let us isolate the charm-loop effect in the decay amplitude:

$$A(B \to K^{(*)}\ell^+\ell^-)^{(O_{1,2})} = -(4\pi\alpha_{em}Q_c)\frac{4G_F}{\sqrt{2}}V_{tb}V_{ts}^*\frac{\bar{\ell}\gamma^\mu\ell}{q^2}\mathcal{H}_\mu^{(B\to K^{(*)})} \, , \qquad (55)$$

where the hadronic matrix element:

$$\mathcal{H}_\mu^{(B\to K)}(p,q) = i\int d^4x e^{iq\cdot x}\langle K(p)|T\Big\{\bar{c}(x)\gamma_\mu c(x)\,,\Big[C_1 O_1(0) + C_2 O_2(0)\Big]\Big\}|B(p+q)\rangle \, , \qquad (56)$$

contains the T-product of two $\bar{c}c$ operators

$$\mathcal{C}_\mu^a(q) = \int d^4x e^{iq\cdot x}T\Big\{\bar{c}(x)\gamma_\mu c(x),\bar{c}_L(0)\Gamma^a c_L(0)\Big\} \, . \qquad (57)$$

As shown in [49], only at momentum transfers, much lower than the charm-anticharm threshold, $q^2 \ll 4m_c^2$ one is allowed to use the operator-product expansion (OPE), and, importantly the expansion is near the light-cone. The dominant region in this T-product is $\langle x^2\rangle \sim 1/(2m_c - \sqrt{q^2})^2$. In this region the T- product of $\bar{c}c$-operators can be expanded near $x^2 \sim 0$, schematically,

$$T\{\bar{c}(x)\gamma_\mu c(x),\bar{c}_L(0)\gamma_\rho c_L(0)\} = C_0^{\mu\rho}(x^2,m_c^2) + \text{two-gluon term} + ... \qquad (58)$$

$$T\{\bar{c}(x)\gamma_\mu c(x),\bar{c}_L(0)\gamma_\rho\frac{\lambda^a}{2}c_L(0)\} = \int_0^1 du C_1^{\mu\rho\alpha\beta}(x^2,m_c^2,u)G_{\alpha\beta}^a(ux) + ... \qquad (59)$$

The leading-order term of this expansion $C_0^{\mu\rho}(x^2,m_c^2)$ is reduced to the simple $\bar{c}c$ loop. Substituting this term back in the decay amplitude (56), after the x-integration one obtains

$$\mathcal{O}_\mu(q) = (q_\mu q_\rho - q^2 g_{\mu\rho})\frac{9}{32\pi^2}\,g(m_c^2,q^2)\bar{s}_L\gamma^\rho b_L \, , \qquad (60)$$

the simple loop function denoted as $g(m_c^2,q^2)$ times the $b \to s$ transition current (see Fig. 17a). After taking the hadronic matrix element we recover the *factorizable* part of the amplitude:

$$\Big[\mathcal{H}_\mu^{(B\to K)}(p,q)\Big]_{fact} = \left(\frac{C_1}{3} + C_2\right)\langle K(p)|\mathcal{O}_\mu(q)|B(p+q)\rangle \, , \qquad (61)$$

factorized in the loop function and $B \to K$ form factor (Fig. 14(a)). Note that at this level of OPE there is no difference between light-cone ($x^2 \sim 0$) and local ($x \sim 0$) expansion. I skip perturbative gluon corrections to this operator, one of them shown in Fig. 17(b). They are factorizable too after taking the hadronic matrix elements. For them one can use the results of [51], with the only difference that now we consistently avoid the region $q^2 \sim 4m_c^2$. The genuine nonfactorizable effect is related to the one-gluon term (59) in the light-cone OPE. It is obtained using the c-quark propagator in the external gluon field and yields a new *nonlocal* operator depicted in Fig. 17(c):

$$\widetilde{\mathcal{O}}_\mu(q) = \int d\omega \, I_{\mu\rho\alpha\beta}(q, m_c, \omega) \bar{s}_L \gamma^\rho \delta[\omega - \frac{(in_+\mathcal{D})}{2}]\widetilde{G}_{\alpha\beta}b_L \ , (62)$$

where the coefficient $I_{\mu\rho\alpha\beta}(q, m_c, \omega)$ represents a loop function with gluon insertion and n_+ is the light-like vector defined in B rest frame, so that $q \sim (m_b/2)n_+$. More details can be found in [49]. The gluon emission term yields a new *nonfactorizable* hadronic matrix element:

Figure 18: Correlation function used to calculate the nonfactorizable hadronic matrix element (63).

$$\left[\mathcal{H}_\mu^{(B \to K)}(p,q)\right]_{nonfact} = 2C_1 \langle K(p)|\widetilde{\mathcal{O}}_\mu(q)|B(p+q)\rangle. \ (63)$$

which is not reduced to simple $B \to K$ form factors and corresponds to the diagram in Fig. 16a.

To calculate the soft-gluon hadronic matrix element (63), the method of LCSRs with B meson DA's outlined in the previous lecture was used in [49], introducing a correlation function:

$$\mathcal{F}_{\nu\mu}^{(B \to K)}(p,q) = i \int d^4y e^{ip\cdot y}\langle 0|T\{j_\nu^K(y)\widetilde{\mathcal{O}}_\mu(q)\}|B(p+q)\rangle. \ (64)$$

The diagram of the correlation function is shown in Fig. 18 and the OPE contains the 3-particle DAs of B meson.

Summarizing, the charm-loop effect in $B \to K\ell^+\ell^-$ is the sum of two hadronic matrix elements calculated in QCD, but this calculation is only valid at $q^2 \ll 4m_c^2$. In [49] the perturbative corrections were not yet included. Still, to have some idea on the importance of the charm loop effect let me quote the value $\Delta C_9^{(\bar{c}c)}(0) = 0.17_{-0.18}^{+0.09}$ obtained for the charm-loop correction to the effective coefficient C_9.

3.4 Hadronic input for $B \to K\ell^+\ell^-$ decay

Following the method suggested in [49], in [50] a complete "bookkeeping" of nonlocal contributions to $B \to K\ell^+\ell^-$ decay amplitude was done. The soft-gluon effects originating from quark loops with various flavours were calculated from LCSRs, including also the soft-gluon contribution due to the gluon-penguin operator shown in Fig. 16b. In addition also the perturbative gluon exchanges (Fig. 15) were taken into account employing the results of [51]. Note that the latter contributions generate an imaginary part in $\Delta C_9^{(BK)}(q^2)$ as explained in details in [50]. Furthermore, after including the photon emission from the light quarks, the q^2 region accessible to OPE was shifted towards large negative values of q^2, to stay sufficiently far from all hadronic thresholds.
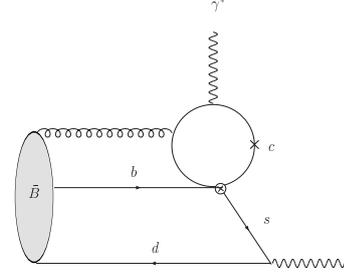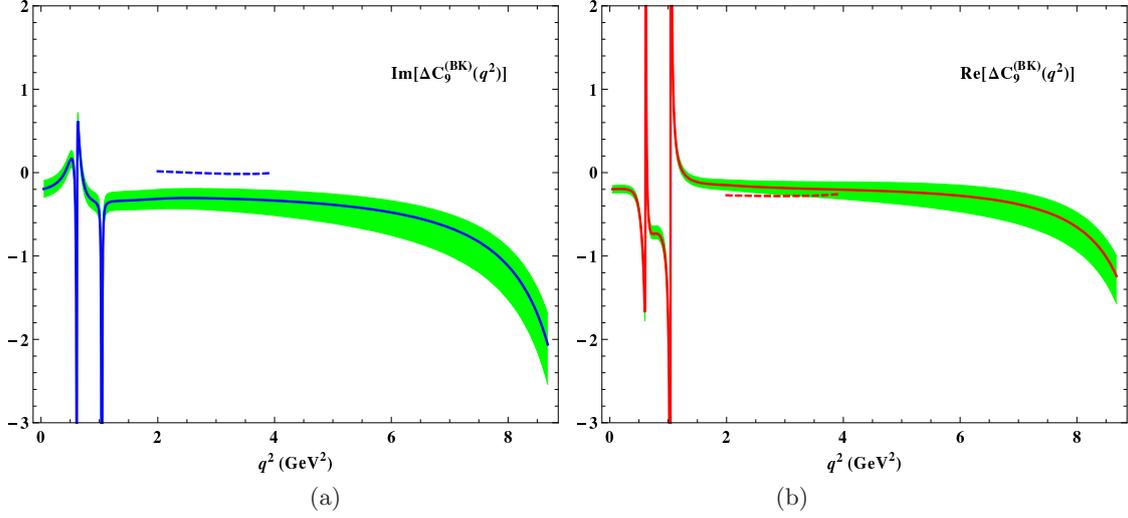
Figure 19: [50] The contribution of nonlocal hadronic effects in a form of correction $\Delta C_9(q^2)$ to the Wilson coefficient C_9 in the physical region of $B \to K\ell^+\ell^-$ decay obtained from the hadronic dispersion relation, fitted to the QCD calculation at $q^2 < 0$. The shaded areas indicate the uncertainty of the predictions. The dashed lines are the predictions of QCD factorization [51].

This calculation was then used for a phenomenological analysis of the $B \to K\ell^+\ell^-$ decay. To access the timelike q^2 region where OPE is not applicable a hadronic dispersion relation in the variable q^2 was employed [49, 50] for the nonlocal hadronic amplitude. To illustrate the idea, let us return to the previous subsection where only the charm-loop effect was taken into account. In this case the dispersion relation contains only hadronic states with $\bar{c}c$ flavour content: [49]:

$$\mathcal{H}^{(B \to K)}(q^2) = \mathcal{H}^{(B \to K)}(0) + q^2 \Big[\sum_{\psi = J/\psi, \psi(2S)} \frac{f_\psi A_{B\psi K}}{m_\psi^2(m_\psi^2 - q^2 - im_\psi \Gamma_\psi^{tot})} + \int_{4m_D^2}^\infty ds \frac{\rho(s)}{s(s - q^2 - i\epsilon)} \Big]. \tag{65}$$

The QCD calculation at small q^2 is used to fit the parameters of this relation and then it is used in the timelike region. In addition, the absolute values of the residues $|f_\psi A_{B\psi K}|$ are fixed from experimental data on nonleptonic decays $B \to J/\psi K$, $B \to \psi(2S)K$ and leptonic decays of charmonium [16].

For a full phenomenological analysis of nonlocal amplitude $\mathcal{H}^{(B \to K)}(q^2)$ in the semileptonic region below charmonium resonances a more complete dispersion relation was used in[50], adding vector mesons with light flavours to the r.h.s. of Eq. (65). The main outcome of this analysis is displayed in Fig. 19 where the resulting correction to C_9 due to all nonlocal effects is plotted, obtained from the dispersion relation fitted to the OPE results at negative q^2. Adding these correction to the short-distance coefficients and employing the $B \to K$ form factors from LCSRs the partial width of $B \to K\ell^+\ell^-$ was predicted in [50]. It is displayed in Fig. 20. The influence of nonlocal effects on the decay observables is very moderate and the form factor
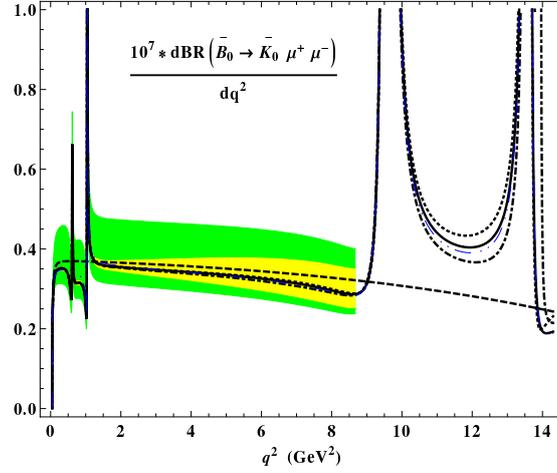
Figure 20: [50] Differential partial branching fraction of $B \to K\ell^+\ell^-$. The darker (brighter) shaded area indicates the uncertainties including(excluding) the one from the $B \to K$ form factors. The long-dashed line corresponds to the width calculated without nonlocal hadronic effects.

uncertainty still dominates. For $B \to K^*\ell^+\ell^-$ decay the full analysis still has to be done. Hints that the nonlocal hadronic effects in this process are more pronounced than in the kaon mode come from the results for the charm-loop contribution done in [49].

Let me emphasize that in future studies of FCNC semileptonic decays of B mesons based on more accurate data the effects studied in this lecture are indispensable, without them the predictions for SM observables are incomplete. The methods based on OPE, LCSRs and dispersion relations combined with QCD factorization for perturbative contributions provide a useful tool to tackle this problem.

Acknowledgments

References

[1] M. A. Shifman, A. I. Vainshtein and V. I. Zakharov, Nucl. Phys. B **147** (1979) 385, 448.

[2] M. A. Shifman, Prog. Theor. Phys. Suppl. **131**, 1 (1998) [hep-ph/9802214].

[3] V. A. Novikov, L. B. Okun, M. A. Shifman, A. I. Vainshtein, M. B. Voloshin and V. I. Zakharov, Phys. Rept. **41**, 1 (1978);
L. J. Reinders, H. Rubinstein and S. Yazaki, Phys. Rept. **127**, 1 (1985);
S. Narison, World Sci. Lect. Notes Phys. **26**, 1 (1989).

[4] A. Khodjamirian and R. Rückl, Adv. Ser. Direct. High Energy Phys. **15**, 345 (1998) [hep-ph/9801443].

[5] P. Colangelo and A. Khodjamirian, In Shifman, M. (ed.): At the frontier of particle physics, vol. 3 1495-1576 [hep-ph/0010175].

[6] V. M. Braun, In Rostock 1997, Progress in heavy quark physics, 105-118 [hep-ph/9801222].

[7] I. Adachi *et al.* [Belle Collaboration], Phys. Rev. Lett. **110**, 131801 (2013).

[8] R.Aaij *et al.* [LHCb Collaboration], Phys. Rev. Lett. **110** (2013) 021801. CMS and LHCb Collaborations [CMS and LHCb Collaboration], CMS-PAS-BPH-13-007.

[9] B. L. Ioffe, Phys. Atom. Nucl. **66**, 30 (2003) [Yad. Fiz. **66**, 32 (2003)] [hep-ph/0207191].

[10] T. M. Aliev and V. L. Eletsky, Sov. J. Nucl. Phys. **38** (1983) 936 [Yad. Fiz. **38** (1983) 1537].

[11] K. G. Chetyrkin and M. Steinhauser, Eur. Phys. J. C **21**, 319 (2001).

[12] V. A. Novikov, M. A. Shifman, A. I. Vainshtein and V. I. Zakharov, Fortsch. Phys. **32**, 585 (1984).

[13] P. Gelhausen, A. Khodjamirian, A. A. Pivovarov and D. Rosenthal, Phys. Rev. D **88**, 014015 (2013).

[14] M. Jamin and B. O. Lange, Phys. Rev. D **65**, 056005 (2002).

[15] K. Chetyrkin, J. H. Kuhn, A. Maier, P. Maierhofer, P. Marquard, M. Steinhauser and C. Sturm, Theor. Math. Phys. **170**, 217 (2012) [arXiv:1010.6157 [hep-ph]].

[16] J. Beringer *et al.* [Particle Data Group Collaboration], Phys. Rev. D **86**, 010001 (2012), *see also www.pdg.gov.*

[17] B. Dehnadi, A. H. Hoang, V. Mateu and S. M. Zebarjad, JHEP **1309**, 103 (2013).

[18] K. G. Chetyrkin and A. Khodjamirian, Eur. Phys. J. C **46** (2006) 721;
M. Jamin, J. A. Oller and A. Pich, Phys. Rev. D **74** (2006) 074009.

[19] H. Leutwyler, Phys. Lett. B **378**, 313 (1996).

[20] A. Bazavov *et al.* [Fermilab Lattice and MILC Collaborations], Phys. Rev. D **85**, 114506 (2012).

[21] R. J. Dowdall, C. T. H. Davies, R. R. Horgan, C. J. Monahan and J. Shigemitsu, arXiv:1302.2644 [hep-lat].

[22] C. T. H. Davies, C. McNeile, E. Follana, G. P. Lepage, H. Na and J. Shigemitsu, Phys. Rev. D **82** (2010) 114504.

[23] I. I. Balitsky, V. M. Braun and A. V. Kolesnichenko, Sov. J. Nucl. Phys. **44** 1028 (1986) [Yad. Fiz. **44** 1582 (1986)]; Nucl. Phys. B **312**, 509 (1989).

[24] V. L. Chernyak and I. R. Zhitnitsky, Nucl. Phys. B **345**, 137 (1990).

[25] V. M. Belyaev, A. Khodjamirian and R. Rückl, Z. Phys. C **60**, 349 (1993); V. M. Belyaev, V. M. Braun, A. Khodjamirian and R. Rückl, Phys. Rev. D **51**, 6177 (1995).

[26] A. Khodjamirian, R. Ruckl, S. Weinzierl and O. I. Yakovlev, Phys. Lett. B **410**, 275 (1997);

[27] E. Bagan, P. Ball and V. M. Braun, Phys. Lett. B **417**, 154 (1998).

[28] P. Ball and R. Zwicky, Phys. Rev. D **71**, 014015 (2005).

[29] G. Duplancic, A. Khodjamirian, T. Mannel, B. Melic and N. Offen, JHEP **0804**, 014 (2008).

[30] A. Bharucha, JHEP **1205**, 092 (2012).

[31] V. L. Chernyak and A. R. Zhitnitsky, JETP Lett. **25**, 510 (1977);
A. V. Efremov and A. V. Radyushkin, Phys. Lett. B **94**, 245 (1980).

[32] G. P. Lepage and S. J. Brodsky, Phys. Lett. B **87**, 359 (1979).

[33] P. Ball, V. M. Braun and A. Lenz, JHEP **0605**, 004 (2006).

[34] A. Khodjamirian, T. Mannel, N. Offen and Y. -M. Wang, Phys. Rev. D **83** (2011) 094031.

[35] C. Bourrely, I. Caprini and L. Lellouch, Phys. Rev. D **79**, 013008 (2009) [Erratum-ibid. D **82**, 099902 (2010)] .

[36] A. Khodjamirian, C. Klein, T. Mannel and N. Offen, Phys. Rev. D **80** (2009) 114005.

[37] A. Khodjamirian, T. Mannel and N. Offen, Phys. Lett. B **620**, 52 (2005);

[38] A. Khodjamirian, T. Mannel and N. Offen, Phys. Rev. D **75**, 054013 (2007).

[39] F. De Fazio, T. Feldmann and T. Hurth, Nucl. Phys. B **733**, 1 (2006) [Erratum-ibid. B **800**, 405 (2008)] .

[40] M. Beneke and T. Feldmann, Nucl. Phys. B **592**, 3 (2001).

[41] A. G. Grozin and M. Neubert, Phys. Rev. D **55**, 272 (1997).

[42] A. G. Grozin, Int. J. Mod. Phys. A **20**, 7451 (2005) [hep-ph/0506226].

[43] V. M. Braun, D. Y. .Ivanov and G. P. Korchemsky, Phys. Rev. D **69**, 034014 (2004) .

[44] M. Beneke and J. Rohrwild, Eur. Phys. J. C **71**, 1818 (2011) .

[45] V. M. Braun and A. Khodjamirian, Phys. Lett. B **718**, 1014 (2013) .

[46] S. Faller, A. Khodjamirian, C. .Klein and T. .Mannel, Eur. Phys. J. C **60**, 603 (2009) .

[47] A. Khodjamirian, C. Klein, T. Mannel and Y. -M. Wang, JHEP **1109**, 106 (2011).

[48] V. Braun, R. J. Fries, N. Mahnke and E. Stein, Nucl. Phys. B **589** (2000) 381 [Erratum-ibid. B **607** (2001) 433]; V. M. Braun, A. Lenz, N. Mahnke and E. Stein, Phys. Rev. D **65**, 074011 (2002); A. Lenz, M. Gockeler, T. Kaltenbrunner and N. Warkentin, Phys. Rev. D **79**, 093007 (2009).

[49] A. Khodjamirian, T. Mannel, A. A. Pivovarov and Y. -M. Wang, JHEP **1009**, 089 (2010).

[50] A. Khodjamirian, T. Mannel and Y. M. Wang, JHEP **1302**, 010 (2013).

[51] M. Beneke, T. Feldmann and D. Seidel, Nucl. Phys. B **612**, 25 (2001).

Top Quark Production

Nikolaos Kidonakis

Kennesaw State University, Physics #1202, 1000 Chastain Rd., Kennesaw, GA 30144, USA

I discuss top quark production in hadronic collisions. I present the soft-gluon resummation formalism and its derivation from factorization and renormalization-group evolution, and two-loop calculations of soft anomalous dimensions in the eikonal approximation. I discuss the contributions of next-to-next-to-leading order (NNLO) soft-gluon corrections to the total cross sections and top-quark transverse momentum and rapidity distributions for top-antitop pair production, and for single-top production in the t and s channels and in association with a W boson or a charged Higgs boson.

1 Introduction

The top quark is the heaviest elementary particle known to date. It was discovered in proton-antiproton collisions at the Fermilab Tevatron in 1995 in top-antitop pair production events by the CDF and D0 Collaborations [1, 2]. The uniqueness of the top quark is not only due to its heavy mass, which makes it important for Higgs physics, but also due to the fact that it is the only quark that decays before it can hadronize. Top-antitop pair and single-top production have by now been fully established at both the Tevatron and the LHC and are in good agreement with theoretical expectations, as we will see later in detail.

In these lectures I discuss top quark production in hadron colliders, paying particular attention to higher-order corrections from soft-gluon resummation. I begin with a discussion of higher-order soft-gluon corrections, factorization, renormalization-group evolution (RGE), resummation, and next-to-next-to-leading order (NNLO) expansions.

I continue with one- and two-loop eikonal diagrams, calculations of the massive cusp anomalous dimension, and presentation of the the two-loop soft anomalous dimension matrices for top-pair production.

I then provide results for $t\bar{t}$ production, including the total $t\bar{t}$ cross sections at the LHC and the Tevatron, the top-quark transverse momentum, p_T, distributions, and the top-quark rapidity distributions. Finally, I discuss single-top production, in particular t-channel and s-channel production, and tW^- and tH^- production, and present total cross sections and top-quark p_T distributions.

2 Higher-order soft-gluon corrections

QCD corrections are significant for hard-scattering cross-sections, and in particular for top-pair and single-top production. The complete next-to-leading order (NLO) corrections were calculated for $t\bar{t}$ production in [3, 4] and for single-top production in [5].

Soft-gluon corrections, i.e. perturbative corrections from the emission of soft (low-energy) gluons, originate from incomplete cancellations of infrared divergences between virtual diagrams

and real diagrams with soft gluons.

The soft-gluon terms are of the form $\left[\frac{\ln^k(s_4/m_t^2)}{s_4}\right]_+$ where $k \leq 2n-1$ for the nth-order perturbative corrections, and s_4 is the kinematical distance from partonic threshold. The leading logarithms (LL) are those with the highest power, $2n-1$; the next-to-leading logarithms (NLL) have a power of one less; the next-to-next-to-leading logarithms (NNLL) have a power of two less, etc. The importance of soft-gluon corrections is because they are dominant near threshold. It is possible to resum (i.e. exponentiate) these corrections to all orders in perturbative QCD. This resummation follows from factorization of the cross section and RGE of its factors. The resummation of the leading logarithms requires universal terms describing the emission of collinear and soft gluons that only depend on the identity of the incoming and outgoing partons, i.e. the details of the hard process are irrelevant. However, at NLL accuracy [6] and beyond it is necessary to involve the process-dependent color exchange in the hard-scattering process and to perform the corresponding loop calculations in the eikonal approximation.

In addition to these soft-gluon logarithmic terms there also arise terms of purely collinear origin, of the form $\frac{1}{m_t^2} \ln^k(s_4/m_t^2)$, but we will not dicuss these kind of terms in this paper.

Complete results are now available at NNLL accuracy, which requires the calculation of two-loop soft anomalous dimensions. For a review of resummation for top quark production see Ref. [7]. Approximate next-to-next-to-leading order (NNLO) double-differential cross sections and even next-to-next-to-next-to-leading order (NNNLO) corrections have been derived from the expansion of the resummed results [8].

2.1 Factorization, RGE, and Resummation

We consider hadronic processes of the form

$$h_1(p_{h_1}) + h_2(p_{h_2}) \rightarrow t(p) + X$$

where h_1, h_2, are colliding hadrons (protons at the LHC; protons and antiprotons at the Tevatron) and t denotes the observed top quark with X all additional final-state particles. The underlying partonic processes are of the form

$$f_1(p_1) + f_2(p_2) \rightarrow t(p) + X$$

where f_1 and f_2 represent partons (quarks or gluons). We define $s = (p_1 + p_2)^2$, $t = (p_1 - p)^2$, $u = (p_2 - p)^2$. Also $s_4 = s + t + u - \sum m^2$, where the sum is over the squared masses of all particles in the process. Thus, s_4 measures distance from partonic threshold, where there is no energy for additional radiation, but the top quark may have arbitrary momentum and is not restricted to be produced at rest (thus partonic threshold is more general than absolute, or production, threshold where the top quark is produced at rest). At partonic threshold $s_4 = 0$.

The factorization for the (in general differential) cross section is expressed by the formula

$$d\sigma_{h_1 h_2 \rightarrow tX} = \sum_{f_1, f_2} \int dx_1 \, dx_2 \, \phi_{f_1/h_1}(x_1, \mu_F) \, \phi_{f_2/h_2}(x_2, \mu_F) \, \hat{\sigma}_{f_1 f_2 \rightarrow tX}(s_4, s, t, u, \mu_F, \mu_R)$$

where ϕ are parton distribution functions with x_1 and x_2 the momentum fractions of partons f_1 and f_2 in hadrons h_1 and h_2 respectively, μ_F is the factorization scale and μ_R is the renormalization scale. We factorize the initial-state collinear divergences into the parton distribution functions, ϕ. Soft-gluon corrections appear in the partonic hard-scattering cross section,

$\hat{\sigma}_{f_1 f_2 \to tX}$, as plus distributions of logarithmic terms, defined through their integral with parton distribution functions

$$\int_0^{s_{4\,max}} ds_4\, \phi(s_4) \left[\frac{\ln^k(s_4/m_t^2)}{s_4} \right]_+ \equiv \int_0^{s_{4\,max}} ds_4 \frac{\ln^k(s_4/m_t^2)}{s_4} [\phi(s_4) - \phi(0)]$$

$$+ \frac{1}{k+1} \ln^{k+1}\left(\frac{s_{4\,max}}{m_t^2} \right) \phi(0).$$

Resummation follows from the factorization properties of the cross section, performed in moment space. We define moments of the partonic cross section by $\hat{\sigma}(N) = \int (ds_4/s)\, e^{-Ns_4/s} \hat{\sigma}(s_4)$. The logarithms of s_4 give rise to logarithms of N in moment space, and we will show that the logarithms of N appearing in $\hat{\sigma}(N)$ exponentiate.

We then write a factorized expression for the infrared-regularized (with $\epsilon = 4 - n$) parton-parton scattering cross section, $\sigma_{f_1 f_2 \to tX}(N, \epsilon)$, in moment space

$$\sigma_{f_1 f_2 \to tX}(N, \epsilon) = \phi_{f_1/f_1}(N, \mu_F, \epsilon)\, \phi_{f_2/f_2}(N, \mu_F, \epsilon)\, \hat{\sigma}_{f_1 f_2 \to tX}(N, \mu_F, \mu_R)$$

which factorizes similarly to the hadronic cross section, with $\phi(N) = \int_0^1 dx\, x^{N-1} \phi(x)$.

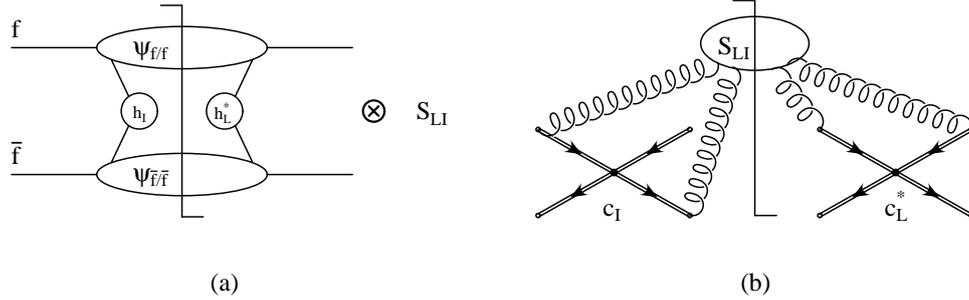(a)   (b)

Figure 1: Factorization of the partonic cross section for $t\bar{t}$ production: (a) The functions involved in the partonic process; (b) the soft-gluon function S.

The partonic function $\hat{\sigma}_{f_1 f_2 \to tX}$ still has sensitivity to soft-gluon dynamics via its N dependence. We then refactorize the cross section [6] in terms of modified parton distributions ψ, defined in the partonic center-of-mass frame at fixed energy, as

$$\sigma_{f_1 f_2 \to tX}(N, \epsilon) = \psi_{f_1/f_1}(N, \mu_F, \epsilon)\, \psi_{f_2/f_2}(N, \mu_F, \epsilon)$$

$$\times H_{IL}^{f_1 f_2 \to tX}(\alpha_s(\mu_R))\, S_{LI}^{f_1 f_2 \to tX}\left(\frac{m_t}{N\mu_F}, \alpha_s(\mu_R) \right) \prod_j J_j(N, \mu_F, \epsilon).$$

This factorization is shown for the case of top-antitop pair production in Fig. 1(a).

The $H_{IL}^{f_1 f_2 \to tX}$ are N-independent hard-scattering terms which involve contributions from the amplitude of the process and the complex conjugate of the amplitude, in the form $H_{IL} = h_L^* h_I$. Also, $S_{LI}^{f_1 f_2 \to tX}$ is the soft gluon function for non-collinear soft-gluon emission; it represents the coupling of soft gluons to the partons in the scattering with color tensors c_I, c_L (see Fig. 1(b)). Both H_{IL} and S_{LI} are process dependent and they are matrices in the space

of color exchanges in the partonic scattering. J are jet functions describing universal soft and collinear emission from any outgoing massless partons.

Comparing the two previous equations, we find

$$
\begin{aligned}
\hat{\sigma}_{f_1 f_2 \to tX}(N, \mu_F, \mu_R) \;=\; & \frac{\psi_{f_1/f_1}(N, \mu_F, \epsilon)\, \psi_{f_2/f_2}(N, \mu_F, \epsilon)}{\phi_{f_1/f_1}(N, \mu_F, \epsilon)\, \phi_{f_2/f_2}(N, \mu_F, \epsilon)} \\
& \times H_{IL}^{f_1 f_2 \to tX}(\alpha_s(\mu_R))\, S_{LI}^{f_1 f_2 \to tX}\left(\frac{m_t}{N\mu_F}, \alpha_s(\mu_R)\right) \prod_j J_j(N, \mu_F, \epsilon)\,.
\end{aligned}
$$

All the factors in the above equation are gauge and factorization scale dependent. The requirement that the product of these factors be independent of the gauge and the factorization scale results in the exponentiation of logarithms of N in the ratios $\psi_{f_1/f_1}/\phi_{f_1/f_1}$ and $\psi_{f_2/f_2}/\phi_{f_2/f_2}$, in the soft-gluon matrix S_{LI}, and in the functions J_j.

The soft matrix S_{LI} requires renormalization as a composite operator; its N-dependence can then be resummed via RGE [6]. The product $H_{IL}S_{LI}$ however needs no overall renormalization, because the UV divergences of H_{IL} balance those of S_{LI}. We have

$$
\begin{aligned}
H_{IL}^b \;&=\; \left(\prod_{i=1,2} Z_i^{-1}\right) (Z_S^{-1})_{IA}\, H_{AB}\left[\left(Z_S^\dagger\right)^{-1}\right]_{BL} \\
S_{LI}^b \;&=\; (Z_S^\dagger)_{LC} S_{CD} Z_{S,DI}
\end{aligned}
$$

where H^b and S^b are the unrenormalized quantities, Z_i are the renormalization constants of the incoming partonic fields, and Z_S is a matrix of renormalization constants, which describe the renormalization of the soft function, including the wave functions for outgoing heavy-quark eikonal lines.

Thus S_{LI} satisfies the renormalization group equation

$$
\left(\mu\frac{\partial}{\partial\mu} + \beta(g_s)\frac{\partial}{\partial g_s}\right) S_{LI} = -(\Gamma_S^\dagger)_{LC} S_{CI} - S_{LD}(\Gamma_S)_{DI}
$$

where $g_s^2 = 4\pi\alpha_s$ and β is the QCD beta function

$$
\beta(\alpha_s) \equiv \frac{1}{2\alpha_s}\frac{d\alpha_s}{d\ln\mu} = \mu\, d\ln g_s/d\mu = -\beta_0\alpha_s/(4\pi) - \beta_1\alpha_s^2/(4\pi)^2 + \cdots,
$$

with $\beta_0 = (11C_A - 2n_f)/3$ and $\beta_1 = 34C_A^2/3 - 2n_f(C_F + 5C_A/3)$. Here $C_F = (N_c^2 - 1)/(2N_c)$ and $C_A = N_c$, with $N_c = 3$ the number of colors, and n_f is the number of light quark flavors ($n_f = 5$ for top production).

Γ_S is the soft anomalous dimension matrix that controls the evolution of the soft function S. In dimensional regularization Z_S has $1/\epsilon$ poles, and Γ_S is given at one loop in terms of the residue of Z_S by

$$
\Gamma_S^{(1-loop)}(g_s) = -\frac{g_s}{2}\frac{\partial}{\partial g_s}\mathrm{Res}_{\epsilon\to 0} Z_S(g_s, \epsilon)\,.
$$

The soft anomalous dimension Γ_S is a matrix in color space and a function of the kinematical invariants s, t, u. The process-dependent matrices Γ_S have been calculated at one loop for all

$2 \to 2$ partonic processes. For the $q\bar{q} \to t\bar{t}$ process, Γ_S is a 2×2 matrix [6]. For the $gg \to t\bar{t}$ process, Γ_S is a 3×3 matrix [6]. Explicit expressions at one and two loops will be provided in Section 4.

The resummed cross section in moment space, denoted as $\hat{\sigma}^{res}_{f_1 f_2 \to tX}(N)$ below, follows from the RGE of all the functions in the factorized cross section, and can be written in the form:

$$
\hat{\sigma}^{res}_{f_1 f_2 \to tX}(N) = \exp\left[\sum_{i=1,2} E_i(N_i)\right] \exp\left[\sum_j E'_j(N')\right] \exp\left[\sum_{i=1,2} 2\int_{\mu_F}^{\sqrt{s}} \frac{d\mu}{\mu}\, \gamma_{i/i}\left(\tilde{N}_i, \alpha_s(\mu)\right)\right]
$$

$$
\times \operatorname{tr}\left\{ H^{f_1 f_2 \to tX}\left(\alpha_s(\sqrt{s})\right) \exp\left[\int_{\sqrt{s}}^{\sqrt{s}/\tilde{N}'} \frac{d\mu}{\mu}\, \Gamma_S^{\dagger\, f_1 f_2 \to tX}\left(\alpha_s(\mu)\right)\right]\right.
$$

$$
\left. \times S^{f_1 f_2 \to tX}\left(\alpha_s\left(\frac{\sqrt{s}}{\tilde{N}'}\right)\right) \exp\left[\int_{\sqrt{s}}^{\sqrt{s}/\tilde{N}'} \frac{d\mu}{\mu}\, \Gamma_S^{f_1 f_2 \to tX}\left(\alpha_s(\mu)\right)\right]\right\}
$$

where the trace is taken of the product of the color-space matrices H, S, and exponents of Γ_S and its Hermitian conjugate, $\Gamma_S^\dagger$.

The collinear and soft radiation from incoming partons is resummed via the first exponential with

$$
E_i(N_i) = \int_0^1 dz \frac{z^{N_i-1}-1}{1-z} \left\{ \int_1^{(1-z)^2} \frac{d\lambda}{\lambda} A_i\left(\alpha_s(\lambda s)\right) + D_i\left[\alpha_s((1-z)^2 s)\right]\right\}
$$

(for purely collinear corrections, replace $\frac{z^{N-1}-1}{1-z}$ by $-z^{N-1}$ in the above expression). Here $N_1 = N(m_t^2 - u)/m_t^2$ and $N_2 = N(m_t^2 - t)/m_t^2$. The term A_i has the perturbative expansion $A_i = \frac{\alpha_s}{\pi} A_i^{(1)} + \left(\frac{\alpha_s}{\pi}\right)^2 A_i^{(2)} + \cdots$ where $A_i^{(1)} = C_i$ [9] with $C_i = C_F$ for a quark or antiquark and $C_i = C_A$ for a gluon, while $A_i^{(2)} = C_i K/2$ [10] with $K = C_A\left(67/18 - \zeta_2\right) - 5n_f/9$ [11]. Here and below we use $\zeta_2 = \pi^2/6$, $\zeta_3 = 1.2020569\cdots$, and $\zeta_4 = \pi^4/90$. Also $D_i = (\alpha_s/\pi)D_i^{(1)} + (\alpha_s/\pi)^2 D_i^{(2)} + \cdots$ with $D_i^{(1)} = 0$ in Feynman gauge ($D_i^{(1)} = -C_i$ in axial gauge). In Feynman gauge the two-loop result is [12]

$$
D_i^{(2)} = C_i C_A \left(-\frac{101}{54} + \frac{11}{6}\zeta_2 + \frac{7}{4}\zeta_3\right) + C_i n_f \left(\frac{7}{27} - \frac{\zeta_2}{3}\right).
$$

The collinear and soft radiation from outgoing massless quarks and gluons is resummed via the second exponential

$$
E'_j(N') = \int_0^1 dz \frac{z^{N'-1}-1}{1-z} \left\{ \int_{(1-z)^2}^{1-z} \frac{d\lambda}{\lambda} A_j\left(\alpha_s(\lambda s)\right) + B_j\left[\alpha_s((1-z)s)\right]\right.
$$

$$
\left. + D_j\left[\alpha_s((1-z)^2 s)\right]\right\}
$$

where $N' = N s/m_t^2$. Note that this exponent is not needed in $t\bar{t}$ production but it is used in single-top production. The term B_j has the perturbative expansion $B_j = (\alpha_s/\pi)B_j^{(1)} + (\alpha_s/\pi)^2 B_j^{(2)} + \cdots$ with $B_q^{(1)} = -3C_F/4$ for a quark or antiquark, and $B_g^{(1)} = -\beta_0/4$ for a gluon [9, 10]. Also (c.f. [12, 13])

$$
B_q^{(2)} = C_F^2 \left(-\frac{3}{32} + \frac{3}{4}\zeta_2 - \frac{3}{2}\zeta_3\right) + C_F C_A \left(-\frac{57}{32} - \frac{11}{12}\zeta_2 + \frac{3}{4}\zeta_3\right) + n_f C_F \left(\frac{5}{16} + \frac{\zeta_2}{6}\right),
$$

$$B_g^{(2)} = C_A^2 \left(-\frac{1025}{432} - \frac{3}{4}\zeta_3 \right) + \frac{79}{108}C_A\, n_f + C_F \frac{n_f}{8} - \frac{5}{108}n_f^2 \, .$$

The factorization scale dependence in the third exponential is controlled by the moment-space anomalous dimension of the $\overline{\text{MS}}$ density $\phi_{i/i}$, which is $\gamma_{i/i} = -A_i \ln \tilde{N}_i + \gamma_i$ [14, 15], where $\tilde{N}_i = N_i e^{\gamma_E}$ with γ_E the Euler constant. The parton anomalous dimensions γ_i have the perturbative expansion

$$\gamma_i = (\alpha_s/\pi)\gamma_i^{(1)} + (\alpha_s/\pi)^2\gamma_i^{(2)} + \cdots$$

with $\gamma_q^{(1)} = 3C_F/4$, $\gamma_g^{(1)} = \beta_0/4$,

$$\gamma_q^{(2)} = C_F^2 \left(\frac{3}{32} - \frac{3}{4}\zeta_2 + \frac{3}{2}\zeta_3 \right) + C_F C_A \left(\frac{17}{96} + \frac{11}{12}\zeta_2 - \frac{3}{4}\zeta_3 \right) + n_f C_F \left(-\frac{1}{48} - \frac{\zeta_2}{6} \right)$$

and

$$\gamma_g^{(2)} = C_A^2 \left(\frac{2}{3} + \frac{3}{4}\zeta_3 \right) - n_f \left(\frac{C_F}{8} + \frac{C_A}{6} \right) \, .$$

The relation between α_s at two different scales, μ and μ_R, is

$$\alpha_s(\mu) = \alpha_s(\mu_R) \left[1 - \frac{\beta_0}{4\pi}\alpha_s(\mu_R) \ln \left(\frac{\mu^2}{\mu_R^2} \right) + \frac{\beta_0^2}{16\pi^2}\alpha_s^2(\mu_R) \ln^2 \left(\frac{\mu^2}{\mu_R^2} \right) - \frac{\beta_1}{16\pi^2}\alpha_s^2(\mu_R) \ln \left(\frac{\mu^2}{\mu_R^2} \right) \right.$$
$$\left. + \cdots \right] \, .$$

We write the perturbative expansions for the hard-scattering function H and the soft-gluon function S as

$$H = \alpha_s^{d_{\alpha_s}} H^{(0)} + \frac{\alpha_s^{d_{\alpha_s}+1}}{\pi} H^{(1)} + \frac{\alpha_s^{d_{\alpha_s}+2}}{\pi^2} H^{(2)} + \cdots$$

and

$$S = S^{(0)} + \frac{\alpha_s}{\pi}S^{(1)} + \frac{\alpha_s^2}{\pi^2}S^{(2)} + \cdots$$

respectively, where d_{α_s} denotes the power of α_s in the Born cross section. At lowest order, the trace of the product of the hard matrices H and soft matrices S gives the Born cross section for each partonic process, $\sigma^B = \alpha_s^{d_{\alpha_s}} \text{tr}[H^{(0)} S^{(0)}]$.

Noncollinear soft gluon emission is controlled by the soft anomalous dimension Γ_S, which has the perturbative expansion

$$\Gamma_S = \frac{\alpha_s}{\pi}\Gamma_S^{(1)} + \frac{\alpha_s^2}{\pi^2}\Gamma_S^{(2)} + \cdots$$

We determine Γ_S from the coefficients of ultraviolet poles in dimensionally regularized eikonal diagrams. The determination of $\Gamma_S^{(1)}$ is needed for NLL resummation and it requires one-loop calculations in the eikonal approximation; $\Gamma_S^{(2)}$ is needed for NNLL resummation and requires two-loop calculations.

Complete two-loop results are now known for the soft anomalous dimensions for many processes, and in these lectures I will review results for:
- the soft (cusp) anomalous dimension for $e^+e^- \to t\bar{t}$
- $t\bar{t}$ hadroproduction
- t-channel single top production
- s-channel single top production
- $bg \to tW^-$ and $bg \to tH^-$

2.2 NLO and NNLO expansions

The resummed cross section suffers from infrared divergences that need a prescription to be dealt with. However, the numerical results depend on the prescription, and differences between prescriptions are typically larger than corrections beyond NNLO. Thus, an alternative and preferred procedure is to expand the resummed cross section to a fixed order in the perturbative expansion, thus avoiding arbitrary prescription dependences. Thus the resummed cross section is used as a generator of higher-order soft-gluon corrections, and here we present expansions to NNLO (for NNNLO see the second paper in [8]).

In the moment-space resummed cross section we are resumming $\ln^k N$; we then expand to fixed order and invert back to momentum space to get the usual $\ln^k(s_4/m_t^2)/s_4$ terms.

We will use the following notation for the logarithmic plus distributions,

$$\mathcal{D}_k(s_4) \equiv \left[\frac{\ln^k(s_4/m_t^2)}{s_4} \right]_+ .$$

The NLO soft-gluon corrections from the expansion of the resummed cross section can be written as

$$\hat{\sigma}^{(1)} = \sigma^B \frac{\alpha_s(\mu_R)}{\pi} \{c_3 \mathcal{D}_1(s_4) + c_2 \mathcal{D}_0(s_4) + c_1 \delta(s_4)\} + \frac{\alpha_s^{d_{\alpha_s}+1}(\mu_R)}{\pi} [A^c \mathcal{D}_0(s_4) + T_1^c \delta(s_4)]$$

where we have separated contributions into a part proportional to the Born term, i.e. the leading-order (LO) term, σ^B, and a part that is not (in general) proportional to it. The leading logarithmic coefficient is

$$c_3 = \sum_i 2 A_i^{(1)} - \sum_j A_j^{(1)} ,$$

and is always multiplied by σ^B. The next-to-leading logarithmic terms are in general not all proportional to σ^B and are separated into two parts. The first part has coefficient c_2 which is defined by $c_2 = c_2^\mu + T_2$, with $c_2^\mu = -\sum_i A_i^{(1)} \ln(\mu_F^2/m_t^2)$ denoting the terms involving logarithms of the scale, and

$$T_2 = \sum_i \left[-2 A_i^{(1)} \ln\left(\frac{-t_i}{m_t^2} \right) + D_i^{(1)} - A_i^{(1)} \ln\left(\frac{m_t^2}{s} \right) \right] + \sum_j \left[B_j^{(1)} + D_j^{(1)} - A_j^{(1)} \ln\left(\frac{m_t^2}{s} \right) \right] .$$

The part not in general proportional to σ^B is defined by

$$A^c = \text{tr} \left(H^{(0)} \Gamma_S^{(1)\,\dagger} S^{(0)} + H^{(0)} S^{(0)} \Gamma_S^{(1)} \right) .$$

The terms proportional to $\delta(s_4)$ include virtual corrections which cannot be determined from resummation as well as some terms that involve logarithms of the scales μ_F and μ_R and which can be calculated from the expansion of the resummed cross section. We write $c_1 = c_1^\mu + T_1$ with c_1^μ denoting the terms involving logarithms of the scale

$$c_1^\mu = \sum_i \left[A_i^{(1)} \ln\left(\frac{-t_i}{m_t^2}\right) - \gamma_i^{(1)} \right] \ln\left(\frac{\mu_F^2}{m_t^2}\right) + d_{\alpha_s} \frac{\beta_0}{4} \ln\left(\frac{\mu_R^2}{m_t^2}\right).$$

However T_1 as well as T_1^c can only be found from a complete NLO calculation.

The NNLO soft-gluon corrections from the expansion of the resummed cross section are then

$$
\begin{aligned}
\hat{\sigma}^{(2)} = {} & \sigma^B \frac{\alpha_s^2(\mu_R)}{\pi^2} \left\{ \frac{1}{2} c_3^2 \mathcal{D}_3(s_4) + \left[\frac{3}{2} c_3 c_2 - \frac{\beta_0}{4} c_3 + \sum_j \frac{\beta_0}{8} A_j^{(1)} \right] \mathcal{D}_2(s_4) \right. \\
& + \left[c_3 c_1 + c_2^2 - \zeta_2 c_3^2 - \frac{\beta_0}{2} T_2 + \frac{\beta_0}{4} c_3 \ln\left(\frac{\mu_R^2}{m_t^2}\right) + \sum_i 2 A_i^{(2)} - \sum_j A_j^{(2)} + \sum_j \frac{\beta_0}{4} B_j^{(1)} \right] \mathcal{D}_1(s_4) \\
& + \left[c_2 c_1 - \zeta_2 c_3 c_2 + \zeta_3 c_3^2 + \frac{\beta_0}{4} c_2 \ln\left(\frac{\mu_R^2}{s}\right) - \sum_i \frac{\beta_0}{2} A_i^{(1)} \ln^2\left(\frac{-t_i}{m_t^2}\right) \right. \\
& + \sum_i \left[\left(-2 A_i^{(2)} + \frac{\beta_0}{2} D_i^{(1)} \right) \ln\left(\frac{-t_i}{m_t^2}\right) + D_i^{(2)} + \frac{\beta_0}{8} A_i^{(1)} \ln^2\left(\frac{\mu_F^2}{s}\right) - A_i^{(2)} \ln\left(\frac{\mu_F^2}{s}\right) \right] \\
& + \sum_j \left[B_j^{(2)} + D_j^{(2)} - \left(A_j^{(2)} + \frac{\beta_0}{4} (B_j^{(1)} + 2 D_j^{(1)}) \right) \ln\left(\frac{m_t^2}{s}\right) \right. \\
& \left. \left. \left. + \frac{3\beta_0}{8} A_j^{(1)} \ln^2\left(\frac{m_t^2}{s}\right) \right] \right] \mathcal{D}_0(s_4) \right\} \\
& + \frac{\alpha_s^{d_{\alpha_s}+2}(\mu_R)}{\pi^2} \left\{ \frac{3}{2} c_3 A^c \mathcal{D}_2(s_4) + \left[\left(2 c_2 - \frac{\beta_0}{2} \right) A^c + c_3 T_1^c + F^c \right] \mathcal{D}_1(s_4) \right. \\
& \left. + \left[\left(c_1 - \zeta_2 c_3 + \frac{\beta_0}{4} \ln\left(\frac{\mu_R^2}{s}\right) \right) A^c + c_2 T_1^c + F^c \ln\left(\frac{m_t^2}{s}\right) + G^c \right] \mathcal{D}_0(s_4) \right\}
\end{aligned}
$$

where

$$F^c = \mathrm{tr} \left[H^{(0)} \left(\Gamma_S^{(1)\,\dagger} \right)^2 S^{(0)} + H^{(0)} S^{(0)} \left(\Gamma_S^{(1)} \right)^2 + 2 H^{(0)} \Gamma_S^{(1)\,\dagger} S^{(0)} \Gamma_S^{(1)} \right]$$

$$
\begin{aligned}
G^c = {} & \mathrm{tr} \left[H^{(1)} \Gamma_S^{(1)\,\dagger} S^{(0)} + H^{(1)} S^{(0)} \Gamma_S^{(1)} + H^{(0)} \Gamma_S^{(1)\,\dagger} S^{(1)} + H^{(0)} S^{(1)} \Gamma_S^{(1)} \right. \\
& \left. + H^{(0)} \Gamma_S^{(2)\,\dagger} S^{(0)} + H^{(0)} S^{(0)} \Gamma_S^{(2)} \right]
\end{aligned}
$$

and c_3, c_2, c_1, etc are from the NLO expansion. The two-loop universal quantities $A^{(2)}$, $B^{(2)}$, $D^{(2)}$ were given previously. The two-loop process-dependent $\Gamma_S^{(2)}$ have been recently calculated for several processes, including top quark production in various channels.

In addition to the plus distributions, the factorization and renormalization scale dependent terms proportional to $\delta(s_4)$ at NNLO have also been calculated [8].
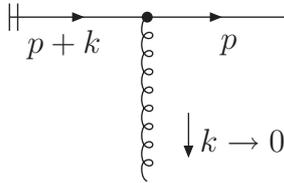
Figure 2: Elementary eikonal diagram for soft-gluon emission from an outgoing quark.
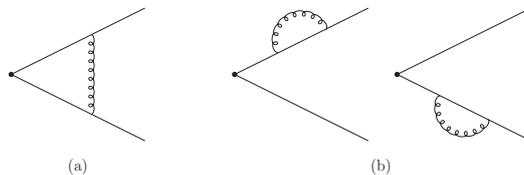

Figure 3: One-loop eikonal diagrams for the cusp anomalous dimension.

3 Two-loop calculations for the massive cusp anomalous dimension

The Feynman rules for diagrams with soft gluon emission, see Fig. 2, simplify as

$$\bar{u}(p)\,(-ig_s T_F^c)\,\gamma^\mu \frac{i(\slashed{p} + \slashed{k} + m)}{(p+k)^2 - m^2 + i\epsilon} \to \bar{u}(p)\,g_s T_F^c\,\gamma^\mu \frac{\slashed{p} + m}{2p\cdot k + i\epsilon} \;\; = \;\; \bar{u}(p)\,g_s T_F^c\,\frac{v^\mu}{v\cdot k + i\epsilon}$$

with $\bar{u}$ a Dirac spinor, T_F^c the generators of SU(3), and $p \propto v$, for example we may take $p^\mu = \sqrt{\frac{s}{2}}v^\mu$, though other choices are possible. This is the eikonal approximation.

We perform the calculations here in momentum space and Feynman gauge. The first soft anomalous dimension that we consider is the massive cusp anomalous dimension, which is also the soft anomalous dimension for the process $e^+e^- \to t\bar{t}$ [16, 17].

3.1 One-loop cusp anomalous dimension

The one-loop eikonal diagrams for the cusp anomalous dimension are shown in Fig. 3. The eikonal lines represent the top and the antitop quarks. The one-loop vertex correction is graph (a) and the one-loop top and antitop self-energy diagrams are the two graphs (b).

The one-loop soft anomalous dimension, $\Gamma_S^{(1)}$, can be read off the coefficient of the ultraviolet (UV) pole of the one-loop diagrams. The calculation gives [16, 17]

$$\Gamma_S^{(1)} = C_F \left[-\frac{(1+\beta^2)}{2\beta} \ln\left(\frac{1-\beta}{1+\beta}\right) - 1 \right]$$

with $\beta = \sqrt{1 - \frac{4m_t^2}{s}}$.

As an example of the calculation we provide some details for the vertex correction graph, i.e. diagram (a) of Fig. 3. This one-loop vertex correction is shown in more detail, and with momenta assignments, in Fig. 4. The integral corresponding to this diagram is

$$I_{1a} = g_s^2 \int \frac{d^n k}{(2\pi)^n} \frac{(-i)g^{\mu\nu}}{k^2} \frac{v_i^\mu}{v_i \cdot k} \frac{(-v_j^\nu)}{(-v_j \cdot k)}$$

which has three factors. The first factor is the gluon propagator and the last two are the eikonal rules for the two lines. Using Feynman parameterization, this can be rewritten as

$$I_{1a} = -2ig_s^2 \frac{v_i \cdot v_j}{(2\pi)^n} \int_0^1 dx \int_0^{1-x} dy \int \frac{d^n k}{[xk^2 + yv_i \cdot k + (1-x-y)v_j \cdot k]^3}$$

which, after the integration over k, gives

$$
\begin{aligned}
I_{1a} &= g_s^2 \, v_i \cdot v_j \, 2^{6-2n} \, \pi^{-n/2} \, \Gamma\left(3 - \frac{n}{2}\right) \int_0^1 dx \, x^{3-n} \\
&\quad \times \int_0^{1-x} dy \left[-y^2 v_i^2 - (1-x-y)^2 v_j^2 - 2y \, v_i \cdot v_j (1-x-y)\right]^{n/2-3} .
\end{aligned}
$$

After several manipulations, and with $n = 4 - \epsilon$, we find

$$
\begin{aligned}
I_{1a} &= \frac{\alpha_s}{\pi} (-1)^{-1-\epsilon/2} \, 2^{5\epsilon/2} \, \pi^{\epsilon/2} \, \Gamma\left(1 + \frac{\epsilon}{2}\right) (1 + \beta^2) \int_0^1 dx \, x^{-1+\epsilon} (1-x)^{-1-\epsilon} \\
&\quad \times \left\{ \int_0^1 dz \left[4z\beta^2(1-z) + 1 - \beta^2\right]^{-1} - \frac{\epsilon}{2} \int_0^1 dz \frac{\ln\left[4z\beta^2(1-z) + 1 - \beta^2\right]}{4z\beta^2(1-z) + 1 - \beta^2} + \mathcal{O}\left(\epsilon^2\right) \right\} .
\end{aligned}
$$

The integral over x contains both ultraviolet (UV) and infrared (IR) singularities. We isolate the UV singularities via

$$\int_0^1 dx \, x^{-1+\epsilon} (1-x)^{-1-\epsilon} = \frac{1}{\epsilon} + \text{IR} .$$

Then the UV pole of the integral is

$$I_{1a}^{UV} = \frac{\alpha_s}{\pi} \frac{(1 + \beta^2)}{2\beta} \frac{1}{\epsilon} \ln\left(\frac{1-\beta}{1+\beta}\right) .$$

Together with the contributions of the top self-energy diagrams, and including color factors, this gives the one-loop result for the cusp anomalous dimension that we presented above.
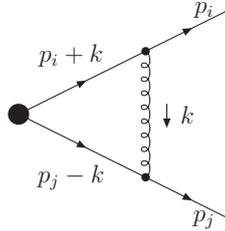

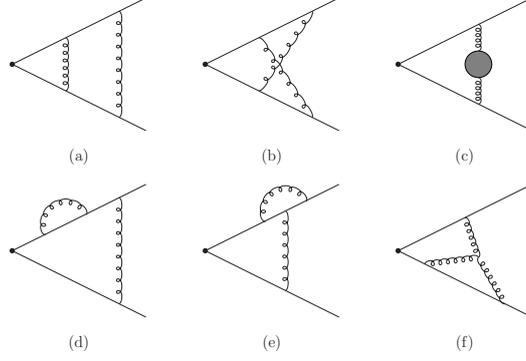Figure 4: One-loop vertex-correction diagram.

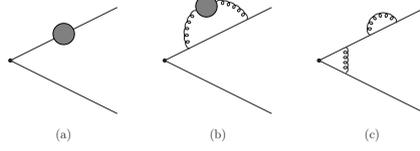Figure 5: Two-loop vertex-correction diagrams for the cusp anomalous dimension.

Figure 6: Two-loop top-quark self-energy graphs.

3.2 Two-loop cusp anomalous dimension

The two-loop vertex-correction graphs for the massive cusp anomalous dimension are shown in Fig. 5. Additional two-loop top-quark self-energy graphs that also need to be included are shown in Fig. 6. The grey blobs indicate quark, gluon, and ghost loops.

As an example of the calculation, consider the two-loop crossed diagram in Fig. 5(b) with details of momenta assignments in Fig. 7. The corresponding integral is

$$I_{2b} = g_s^4 \int \frac{d^n k_1}{(2\pi)^n} \frac{d^n k_2}{(2\pi)^n} \frac{(-i)g^{\mu\nu}}{k_1^2} \frac{(-i)g^{\rho\sigma}}{k_2^2} \frac{v_i^\mu}{v_i \cdot k_1} \frac{v_i^\rho}{v_i \cdot (k_1 + k_2)} \frac{(-v_j^\nu)}{(-v_j \cdot (k_1 + k_2))} \frac{(-v_j^\sigma)}{(-v_j \cdot k_2)} .$$

We perform the k_2 integral first, using Feynman parameterization similarly to the one-loop example, and find

$$
\begin{aligned}
I_{2b} &= -i \frac{\alpha_s^2}{\pi^2} 2^{-4+\epsilon} \pi^{-2+3\epsilon/2} \Gamma\left(1 - \frac{\epsilon}{2}\right) \Gamma(1+\epsilon)(1+\beta^2)^2 \int_0^1 dz \\
&\times \int_0^1 \frac{dy (1-y)^{-\epsilon}}{\left[2\beta^2(1-y)^2 z^2 - 2\beta^2(1-y)z - \frac{(1-\beta^2)}{2}\right]^{1-\epsilon/2}} \int \frac{d^n k_1}{k_1^2 \, v_i \cdot k_1 \, [((v_i - v_j)z + v_j) \cdot k_1]^{1+\epsilon}} .
\end{aligned}
$$

We then proceed with the k_1 integral, and isolate the UV and IR poles. After many steps we
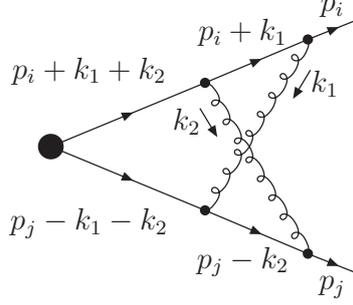
Figure 7: Two-loop crossed diagram.

find

$$I_{2b}^{UV} = \frac{\alpha_s^2}{\pi^2} \frac{(1+\beta^2)^2}{8\beta^2} \frac{1}{\epsilon} \left\{ -\frac{1}{3} \ln^3 \left(\frac{1-\beta}{1+\beta} \right) - \ln \left(\frac{1-\beta}{1+\beta} \right) \left[\mathrm{Li}_2 \left(\frac{(1-\beta)^2}{(1+\beta)^2} \right) + \zeta_2 \right] \right.$$
$$\left. + \mathrm{Li}_3 \left(\frac{(1-\beta)^2}{(1+\beta)^2} \right) - \zeta_3 \right\}.$$

We similarly calculate all other two-loop graphs, and we include the counterterms for all graphs and multiply with the corresponding color factors. We determine the two-loop cusp anomalous dimension from the UV poles of the sum of the graphs [16, 17]:

$$\begin{aligned}
\Gamma_S^{(2)} &= \frac{K}{2} \Gamma_S^{(1)} + C_F C_A M_\beta \\
&= \frac{K}{2} \Gamma_S^{(1)} + C_F C_A \left\{ \frac{1}{2} + \frac{\zeta_2}{2} + \frac{1}{2} \ln^2 \left(\frac{1-\beta}{1+\beta} \right) \right. \\
&\quad - \frac{(1+\beta^2)^2}{8\beta^2} \left[\zeta_3 + \zeta_2 \ln \left(\frac{1-\beta}{1+\beta} \right) + \frac{1}{3} \ln^3 \left(\frac{1-\beta}{1+\beta} \right) + \ln \left(\frac{1-\beta}{1+\beta} \right) \mathrm{Li}_2 \left(\frac{(1-\beta)^2}{(1+\beta)^2} \right) \right. \\
&\quad \left. - \mathrm{Li}_3 \left(\frac{(1-\beta)^2}{(1+\beta)^2} \right) \right] \\
&\quad - \frac{(1+\beta^2)}{4\beta} \left[\zeta_2 - \zeta_2 \ln \left(\frac{1-\beta}{1+\beta} \right) + \ln^2 \left(\frac{1-\beta}{1+\beta} \right) - \frac{1}{3} \ln^3 \left(\frac{1-\beta}{1+\beta} \right) \right. \\
&\quad \left. \left. + 2 \ln \left(\frac{1-\beta}{1+\beta} \right) \ln \left(\frac{(1+\beta)^2}{4\beta} \right) - \mathrm{Li}_2 \left(\frac{(1-\beta)^2}{(1+\beta)^2} \right) \right] \right\}
\end{aligned}$$

where, as before, $K = C_A(67/18 - \zeta_2) - 5n_f/9$, and where for shorthand notation and for later use we have introduced M_β to denote all the terms in curly brackets in the above equation. As can be seen from the above expression, the color structure of $\Gamma_S^{(2)}$ involves only the factors $C_F C_A$ and $C_F n_f$.

In terms of the cusp angle [18] $\gamma = \cosh^{-1}(v_i \cdot v_j / \sqrt{v_i^2 v_j^2}) = \ln[(1+\beta)/(1-\beta)]$ we can rewrite the one-loop expression as

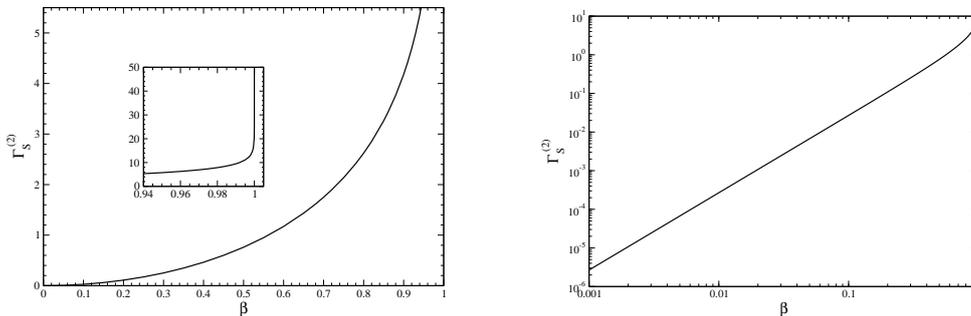$$\Gamma_S^{(1)} = C_F(\gamma \coth \gamma - 1)$$

Figure 8: The two-loop cusp anomalous dimension, $\Gamma_S^{(2)}$, as a function of β in a linear (left) and logarithmic (right) plot.

and the two-loop expression [16, 17] as

$$
\begin{aligned}
\Gamma_S^{(2)} \;=\;& \frac{K}{2}\,\Gamma_S^{(1)} + C_F C_A \left\{ \frac{1}{2} + \frac{\zeta_2}{2} + \frac{\gamma^2}{2} \right. \\
& - \frac{1}{2}\coth^2\gamma \left[\zeta_3 - \zeta_2\gamma - \frac{\gamma^3}{3} - \gamma\,\mathrm{Li}_2\left(e^{-2\gamma}\right) - \mathrm{Li}_3\left(e^{-2\gamma}\right) \right] \\
& \left. - \frac{1}{2}\coth\gamma \left[\zeta_2 + \zeta_2\gamma + \gamma^2 + \frac{\gamma^3}{3} + 2\,\gamma\,\ln\left(1 - e^{-2\gamma}\right) - \mathrm{Li}_2\left(e^{-2\gamma}\right) \right] \right\}.
\end{aligned}
$$

The cusp anomalous dimension is an essential component of other calculations for QCD processes, where the color structure gets more complicated with more than two colored partons in the process.

Linear and logarithmic plots of $\Gamma_S^{(2)}$ are shown in Fig. 8. $\Gamma_S^{(2)}$ vanishes at $\beta = 0$, the threshold limit, and diverges at $\beta = 1$, the massless limit.

We next determine analytically the small and large β behavior of $\Gamma_S^{(2)}$. For the small β behavior we expand around $\beta = 0$ and find

$$
\Gamma_{S\,\mathrm{exp}}^{(2)} \;=\; -\frac{2}{27}\beta^2 \left[C_F C_A(18\zeta_2 - 47) + 5C_F n_f \right] + \mathcal{O}(\beta^4)\,.
$$

We note that $\Gamma_S^{(2)}$ is an even function of β. For the large β behavior, as $\beta \to 1$, we find $\Gamma_S^{(2)} \to \frac{K}{2}\Gamma_S^{(1)}$.

We next construct an approximation valid for all β [16]:

$$
\begin{aligned}
\Gamma_{S\,\mathrm{approx}}^{(2)} \;=\;& \Gamma_{S\,\mathrm{exp}}^{(2)} + \frac{K}{2}\Gamma_S^{(1)} - \frac{K}{2}\Gamma_{S\,\mathrm{exp}}^{(1)} \\
\;=\;& \frac{K}{2}\Gamma_S^{(1)} + C_F C_A \left(1 - \frac{2}{3}\zeta_2\right)\beta^2 + \mathcal{O}\left(\beta^4\right)\,.
\end{aligned}
$$

The expansions and approximations to $\Gamma_S^{(2)}$ are shown in Fig. 9. $\Gamma_{S\,\mathrm{approx}}^{(2)}$ is a remarkably good approximation to the complete $\Gamma_S^{(2)}$.
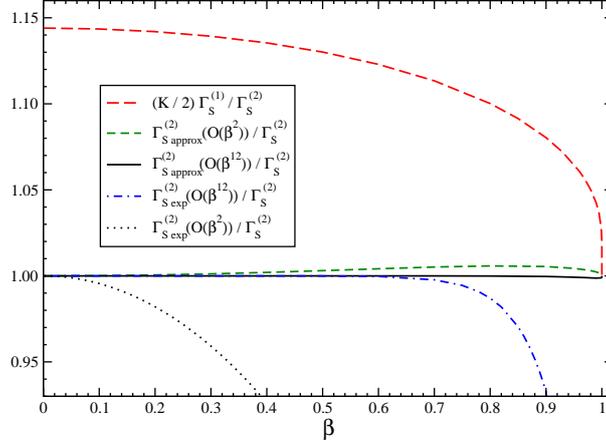
Figure 9: Expansions and approximations for $\Gamma_S^{(2)}$.
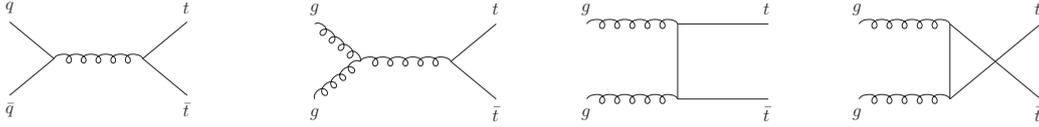
Figure 10: Lowest-order diagrams for the $q\bar{q} \to t\bar{t}$ channel (left diagram) and the $gg \to t\bar{t}$ channel (right three diagrams).

4   Soft anomalous dimension matrices for $t\bar{t}$ production

The top-antitop pair production partonic processes at LO are

$$q(p_1) + \bar{q}(p_2) \to t(p_3) + \bar{t}(p_4)$$

and

$$g(p_1) + g(p_2) \to t(p_3) + \bar{t}(p_4)$$

The LO diagrams for these processes are shown in Fig. 10. We define $s = (p_1 + p_2)^2$, $t_1 = (p_1 - p_3)^2 - m_t^2$, $u_1 = (p_2 - p_3)^2 - m_t^2$, and $\beta = \sqrt{1 - 4m_t^2/s}$. Note that β is the top-quark speed in the LO kinematics. At the Tevatron and the LHC the $t\bar{t}$ cross section receives most contributions in the region around $0.3 < \beta < 0.8$ which peak roughly around $\beta \sim 0.6$.

We next present the results at one and two loops for the soft anomalous matrices for these partonic processes. The soft anomalous dimension matrix for $q(p_1) + \bar{q}(p_2) \to t(p_3) + \bar{t}(p_4)$ in a color tensor basis consisting of singlet and octet exchange in the s channel,

$$c_1 = \delta_{12}\delta_{34}, \qquad c_2 = T_{F\ 21}^c T_{F\ 34}^c,$$

has elements

$$\Gamma_S^{q\bar{q} \to t\bar{t}} = \begin{bmatrix} \Gamma_{q\bar{q}\,11} & \Gamma_{q\bar{q}\,12} \\ \Gamma_{q\bar{q}\,21} & \Gamma_{q\bar{q}\,22} \end{bmatrix}.$$

At one loop we find [6, 19]

$$
\begin{aligned}
\Gamma^{(1)}_{q\bar{q}\,11} &= -C_F \left[L_\beta + 1 \right] \\
\Gamma^{(1)}_{q\bar{q}\,12} &= \frac{C_F}{C_A} \ln \left(\frac{t_1}{u_1} \right) \\
\Gamma^{(1)}_{q\bar{q}\,21} &= 2 \ln \left(\frac{t_1}{u_1} \right) \\
\Gamma^{(1)}_{q\bar{q}\,22} &= C_F \left[4 \ln \left(\frac{t_1}{u_1} \right) - L_\beta - 1 \right] + \frac{C_A}{2} \left[-3 \ln \left(\frac{t_1}{u_1} \right) + \ln \left(\frac{t_1 u_1}{sm_t^2} \right) + L_\beta \right]
\end{aligned}
$$

where $L_\beta = \frac{1+\beta^2}{2\beta} \ln \left(\frac{1-\beta}{1+\beta} \right)$. We note that the first element of this matrix is identical to the one-loop massive cusp anomalous dimension.

Then the elements of the soft anomalous dimension matrix for the process $q\bar{q} \to t\bar{t}$ at two loops are [19]

$$
\begin{aligned}
\Gamma^{(2)}_{q\bar{q}\,11} &= \frac{K}{2} \Gamma^{(1)}_{q\bar{q}\,11} + C_F C_A \, M_\beta \\
\Gamma^{(2)}_{q\bar{q}\,12} &= \frac{K}{2} \Gamma^{(1)}_{q\bar{q}\,12} - \frac{C_F}{2} N_\beta \ln \left(\frac{t_1}{u_1} \right) \\
\Gamma^{(2)}_{q\bar{q}\,21} &= \frac{K}{2} \Gamma^{(1)}_{q\bar{q}\,21} + C_A N_\beta \ln \left(\frac{t_1}{u_1} \right) \\
\Gamma^{(2)}_{q\bar{q}\,22} &= \frac{K}{2} \Gamma^{(1)}_{q\bar{q}\,22} + C_A \left(C_F - \frac{C_A}{2} \right) M_\beta
\end{aligned}
$$

We note that the first element of this matrix is identical to the two-loop massive cusp anomalous dimension, and M_β was defined in the previous section. Here N_β is a subset of the terms of M_β,

$$
\begin{aligned}
N_\beta &= -\frac{(1+\beta^2)}{4\beta} \left[\ln^2 \left(\frac{1-\beta}{1+\beta} \right) + 2 \ln \left(\frac{1-\beta}{1+\beta} \right) \ln \left(\frac{(1+\beta)^2}{4\beta} \right) - \text{Li}_2 \left(\frac{(1-\beta)^2}{(1+\beta)^2} \right) \right] \\
&\quad + \frac{1}{2} \ln^2 \left(\frac{1-\beta}{1+\beta} \right) .
\end{aligned}
$$

The soft anomalous dimension matrix for $g(p_1) + g(p_2) \to t(p_3) + \bar{t}(p_4)$ in a color tensor basis

$$
c_1 = \delta^{12} \delta_{34}, \quad c_2 = d^{12c} T^c_{34}, \quad c_3 = i f^{12c} T^c_{34}
$$

where d and f are the totally symmetric and antisymmetric $SU(3)$ invariant tensors, is

$$
\Gamma^{gg \to t\bar{t}}_S = \begin{bmatrix} \Gamma_{gg\,11} & 0 & \Gamma_{gg\,13} \\ 0 & \Gamma_{gg\,22} & \Gamma_{gg\,23} \\ \Gamma_{gg\,31} & \Gamma_{gg\,32} & \Gamma_{gg\,22} \end{bmatrix} .
$$

At one loop we have [6, 19]

$$
\begin{aligned}
\Gamma^{(1)}_{gg\,11} &= -C_F[L_\beta + 1] \\
\Gamma^{(1)}_{gg\,13} &= \ln\left(\frac{t_1}{u_1}\right) \\
\Gamma^{(1)}_{gg\,31} &= 2\ln\left(\frac{t_1}{u_1}\right) \\
\Gamma^{(1)}_{gg\,22} &= -C_F[L_\beta + 1] + \frac{C_A}{2}\left[\ln\left(\frac{t_1 u_1}{m^2 s}\right) + L_\beta\right] \\
\Gamma^{(1)}_{gg\,23} &= \frac{C_A}{2}\ln\left(\frac{t_1}{u_1}\right) \\
\Gamma^{(1)}_{gg\,32} &= \frac{N_c^2 - 4}{2N_c}\ln\left(\frac{t_1}{u_1}\right)
\end{aligned}
$$

At two loops we find [19]

$$
\begin{aligned}
\Gamma^{(2)}_{gg\,11} &= \frac{K}{2}\Gamma^{(1)}_{gg\,11} + C_F C_A\, M_\beta \\
\Gamma^{(2)}_{gg\,13} &= \frac{K}{2}\Gamma^{(1)}_{gg\,13} - \frac{C_A}{2}N_\beta \ln\left(\frac{t_1}{u_1}\right) \\
\Gamma^{(2)}_{gg\,31} &= \frac{K}{2}\Gamma^{(1)}_{gg\,31} + C_A N_\beta \ln\left(\frac{t_1}{u_1}\right) \\
\Gamma^{(2)}_{gg\,22} &= \frac{K}{2}\Gamma^{(1)}_{gg\,22} + C_A\left(C_F - \frac{C_A}{2}\right)M_\beta \\
\Gamma^{(2)}_{gg\,23} &= \frac{K}{2}\Gamma^{(1)}_{gg\,23} \\
\Gamma^{(2)}_{gg\,32} &= \frac{K}{2}\Gamma^{(1)}_{gg\,32}
\end{aligned}
$$

5 Double-differential kinematics

We consider a generic hadronic process with momenta $p_{h_1} + p_{h_2} \to p_3 + p_4$ with underlying partonic process $p_1 + p_2 \to p_3 + p_4$. We write general kinematics formulas that can be used for both top-antitop pair and single-top production.

5.1 Kinematics with S, T, U

The hadronic variables are $S = (p_{h1} + p_{h2})^2$, $T = (p_{h1} - p_3)^2$, $U = (p_{h2} - p_3)^2$. The partonic variables are $s = (p_1 + p_2)^2$, $t = (p_1 - p_3)^2$, $u = (p_2 - p_3)^2$; we also define $s_4 = s + t + u - m_3^2 - m_4^2$ which describes the excess energy for additional radiation in the process, and thus measures kinematical distance from partonic threshold. Note that $p_1 = x_1 p_{h1}$, $p_2 = x_2 p_{h2}$, $s = x_1 x_2 S$, $t - m_3^2 = x_1(T - m_3^2)$, $u - m_3^2 = x_2(U - m_3^2)$, with x_1 and x_2 the momentum fractions of the colliding partons in the corresponding hadrons. The total hadronic cross section is found by integrating over the double-differential partonic cross section convoluted with the parton

distribution functions ϕ:

$$\sigma_{p_{h1}p_{h2}\rightarrow p_3 p_4}(S) = \int_{T_{min}}^{T_{max}} dT \int_{U_{min}}^{U_{max}} dU \int_{x_{2min}}^{1} dx_2 \int_{0}^{s_{4max}} ds_4$$

$$\times \frac{x_1 x_2}{x_2 S + T - m_3^2} \, \phi(x_1) \, \phi(x_2) \, \frac{d^2 \hat{\sigma}_{p_1 p_2 \rightarrow p_3 p_4}}{dt \, du}$$

where

$$x_1 = \frac{s_4 - m_3^2 + m_4^2 - x_2(U - m_3^2)}{x_2 S + T - m_3^2}$$

$$T_{max \atop min} = -\frac{1}{2}(S - m_3^2 - m_4^2) \pm \frac{1}{2}\sqrt{(S - m_3^2 - m_4^2)^2 - 4m_3^2 m_4^2}$$

$$U_{max} = m_3^2 + \frac{S \, m_3^2}{T - m_3^2}$$

$U_{min} = -S - T + m_3^2 + m_4^2$, $x_{2min} = (m_4^2 - T)/(S + U - m_3^2)$ and $s_{4max} = x_2(S + U - m_3^2) + T - m_4^2$.

5.2 Kinematics with p_T and rapidity

We next provide an alternative cross-section calculation in terms of the transverse momentum, p_T, and the rapidity, Y, of the outgoing particle with momentum p_3. We further define $T_1 = T - m_3^2$, $U_1 = U - m_3^2$, $t_1 = t - m_3^2$, and $u_1 = u - m_3^2$. Also, $U_1 = -\sqrt{S} m_T e^Y$ and $T_1 = -\sqrt{S} m_T e^{-Y}$ with $m_T = \sqrt{m_3^2 + p_T^2}$. We then calculate the total hadronic cross section via

$$\sigma_{p_{h1}p_{h2}\rightarrow p_3 p_4}(S) = \int_{0}^{p_{T\,max}^2} dp_T^2 \int_{Y^-}^{Y^+} dY \int_{x_1^-}^{1} dx_1 \int_{0}^{s_{4max}} ds_4$$

$$\times \frac{x_1 x_2 \, S}{x_1 S + U_1} \, \phi(x_1) \, \phi(x_2) \, \frac{d^2 \hat{\sigma}_{p_1 p_2 \rightarrow p_3 p_4}}{dt_1 \, du_1}$$

where

$$x_2 = \frac{s_4 - m_3^2 + m_4^2 - x_1 T_1}{x_1 S + U_1},$$

$$p_{T\,max}^2 = \frac{(S - m_3^2 - m_4^2)^2 - 4m_3^2 m_4^2}{4S}$$

$$Y^{\pm} = \pm \frac{1}{2} \ln \frac{1 + \sqrt{1 - \frac{4m_T^2}{S[1 + (m_3^2 - m_4^2)/S]^2}}}{1 - \sqrt{1 - \frac{4m_T^2}{S[1 + (m_3^2 - m_4^2)/S]^2}}}$$

$$x_1^- = \frac{-(U_1 + m_3^2 - m_4^2)}{S + T_1}$$

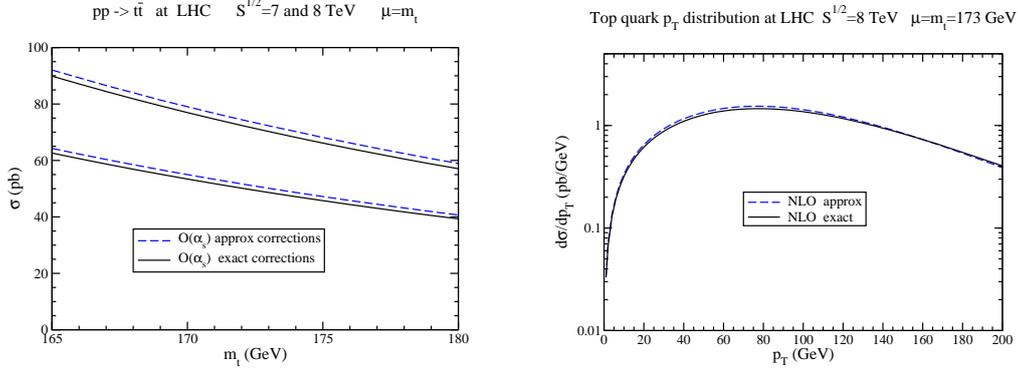$$s_{4max} = x_1(S + T_1) + U_1 + m_3^2 - m_4^2.$$

Figure 11: (Left) NLO exact and approximate corrections to the top-pair cross section at 7 TeV (lower lines) and 8 TeV (upper lines) LHC energy; (Right) NLO exact and approximate top-quark transverse momentum distributions at 8 TeV.
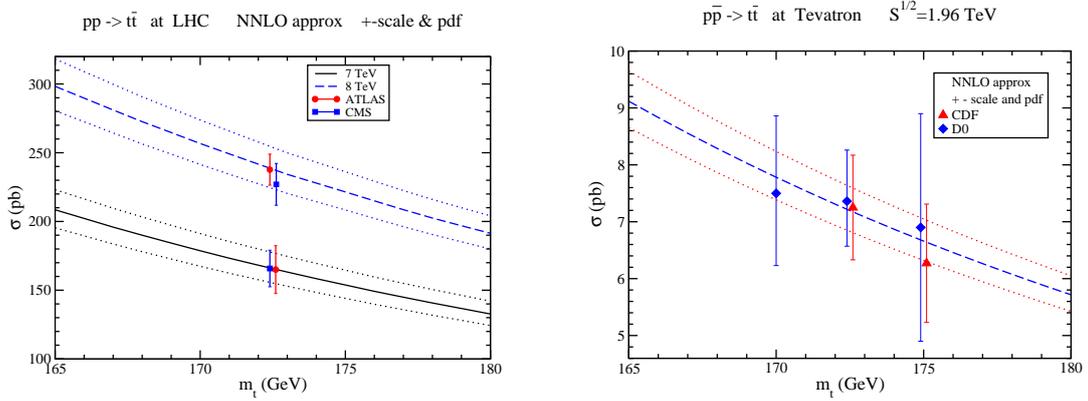
Figure 12: The top-pair total cross section at LHC (left) and Tevatron (right) energies.

6   Total cross section for $t\bar{t}$ production

We begin our presentation of numerical results with the total cross section for top-antitop pair production. We use the MSTW2008 NNLO [20] parton distribution functions (pdf) for all the numerical results. We first show that the threshold approximation works very well both for total cross sections and differential distributions.

We denote the NLO soft-gluon corrections from the expansion of the NNLL resummed cross section as NLO approximate corrections. Similarly the NNLO soft-gluon corrections are denoted as NNLO approximate corrections. Furthermore, the sum of the exact NLO cross section and the NNLO approximate corrections is denoted as the NNLO approximate cross section (and this applies to both total and differential cross sections).

Figure 11 shows that the NLO exact and approximate corrections to the total cross section as well as the top-quark p_T distribution are nearly identical. We have an excellent approximation: there is less than 1% difference between NLO approximate and exact cross sections. For the

Figure 13: Theoretical results for the $t\bar{t}$ cross section at 7 and 8 TeV LHC energies.

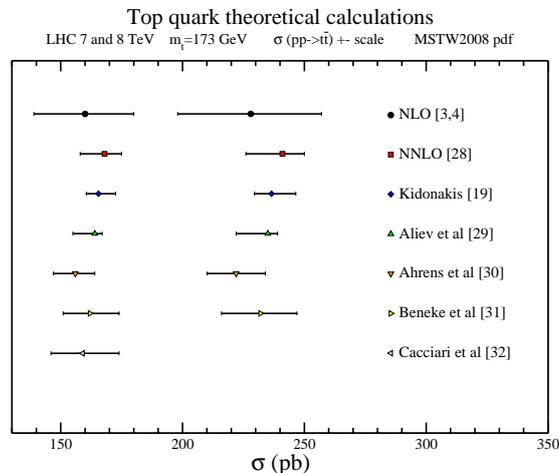best prediction we add the NNLO approximate corrections to the exact NLO cross section. We find that that the scale dependence is greatly reduced when the NNLO approximate corrections are included.

In Fig. 12 we display theoretical predictions at approximate NNLO for the total cross section as a function of top-quark mass at the LHC (left plot) and the Tevatron (right plot) and compare them with data from the LHC at 7 TeV [21, 22] and 8 TeV [23, 24] and from the Tevatron at 1.96 TeV [25, 26]. We find very good agreement between the theoretical predictions and the data. The approximate NNLO prediction [19] for $m_t = 173$ GeV is $7.08^{+0.20+0.36}_{-0.24-0.27}$ pb at the Tevatron at 1.96 TeV; $163^{+7}_{-5} \pm 9$ pb at the LHC at 7 TeV; $234^{+10}_{-7} \pm 12$ pb at 8 TeV LHC; and 920^{+50+33}_{-39-35} pb at 14 TeV LHC. The central result is with $\mu_F = \mu_R = m_t$, the first uncertainty is from independent variation of μ_F and μ_R over the range $m_t/2$ to $2m_t$, and the second uncertainty is from the MSTW2008 NNLO pdf at 90% CL. Of course the numerical results depend on the choice of pdf, α_s, and choices of top quark mass and scales.

There are many differences between various resummation/NNLO approximate approaches in the literature and these have been detailed previously in [7, 27]. The differences include whether the resummation is for the total-only cross section versus for the double-differential cross section, whether it uses moment-space perturbative QCD (pQCD) versus Soft-Collinear Effective Theory (SCET), etc.

Resummations that only use the total cross section refer to production (or absolute) threshold and resum logarithms of $\beta = \sqrt{1 - 4m_t^2/s}$. The soft limit here is the production threshold limit $\beta \to 0$ (where the top quark velocities are zero), which is a special case of the more general partonic threshold. The partonic threshold is where there is just enough energy to produce the top quarks but they can have arbitrary p_T and are not restrained to be at rest. This more general double-differential approach to resummation can be expressed in single-particle-inclusive kinematics for the differential cross section $d\sigma/dp_T dy$ where the logarithms involve $s_4 = s + t_1 + u_1$ and the soft limit is $s_4 \to 0$.

The double-differential approach, in addition to using a more general definition of threshold, also allows the calculation of transverse momentum and rapidity distributions. For differential
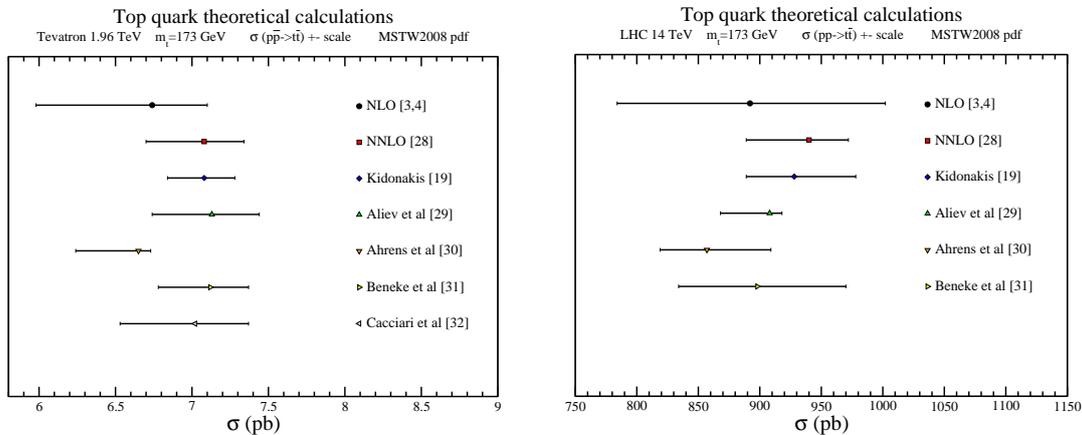
Figure 14: Theoretical results for the $t\bar{t}$ cross section at the Tevatron (left) and at 14 TeV LHC energy (right).

calculations, further differences between approaches arise from how the relation $s + t_1 + u_1 = 0$ is used in the plus-distribution coefficients, how subleading terms are treated, if/how damping factors are implemented to reduce the influence of contributions far from threshold, etc.

A comparison of various NNLO approximate approaches is shown in Fig. 13, all with the same choice of parameters, at 7 and 8 TeV LHC energies. In addition, exact NLO [3, 4] and NNLO [28] results for the total cross sections are also shown on the plot.

Ref. [19] uses our pQCD resummation formalism for the double-differential cross section. Ref. [29] uses pQCD resummation for the total-only cross section. Ref. [30] uses the SCET resummation formalism for the double-differential cross section. Ref. [31] uses the SCET resummation formalism for the total-only cross section. Lastly, Ref. [32] uses pQCD resummation for the total-only cross section.

Figure 14 shows the corresponding comparison for the Tevatron (left) and for 14 TeV LHC energy (right). One notes the varying degree of success of the various approaches in approximating the exact NNLO result.

The result in Ref. [19] from our formalism is very close to the exact NNLO [28] result: both the central values and the scale uncertainty are nearly the same and this holds true for all collider energies and top quark masses. This was expected from the comparison of exact and approximate corrections at NLO for both total and differential cross sections, and also from the comparison of approximate NNLO results in different kinematics in 2003 [33] (see also the discussions in [19] and [27]). There is less than 1% difference between approximate and exact cross sections at both NLO and NNLO.

The stability of the theoretical prediction over the past decade and the reliability of the NNLO approximate result and near-identical value to exact NNLO is very important for several reasons:

• it provides confidence for applications to other processes (notably single-top production, W production, and other processes);

   • it has been used extensively as a background for many analyses (Higgs searches, etc);

   • it means that we have reliable and near-exact NNLO p_T and rapidity distributions, which

Top quark p_T at Tevatron $S^{1/2}$=1.96 TeV m_t=173 GeV

Top quark p_T at Tevatron $S^{1/2}$=1.96 TeV m_t=170 GeV
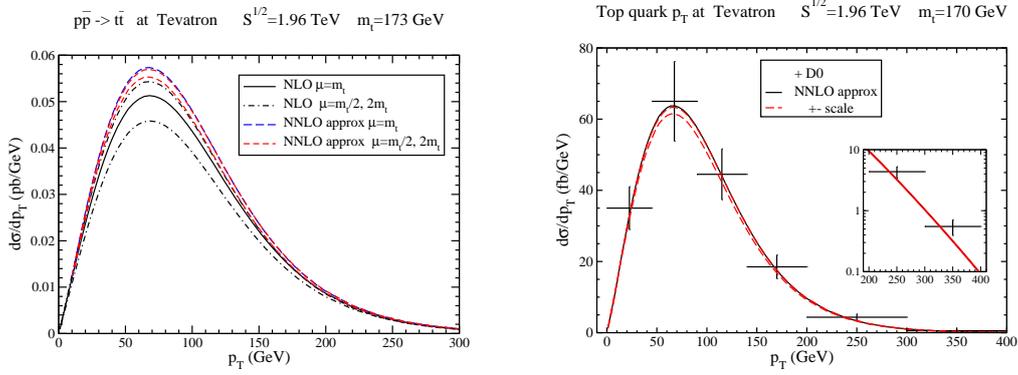
Figure 15: The top quark p_T distribution at the Tevatron.

Top quark p_T distribution at LHC NNLO approx m_t=173 GeV

Normalized top p_T distribution at LHC $S^{1/2}$=7 TeV m_t=173 GeV
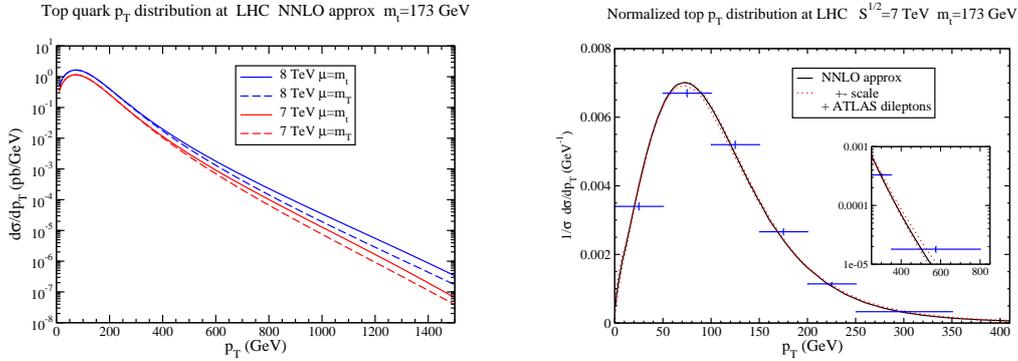
Figure 16: (Left) The top quark p_T distribution at the LHC at 7 and 8 TeV energies. (Right) The normalized top quark p_T distribution at 7 TeV LHC energy compared with ATLAS data in the dileptons channel.

is important since at present there do not exist any exact NNLO results for differential distributions;

  • it suggests that NNNLO soft-gluon corrections may be good approximations to exact results at that order if/when they ever become available.

7 Top-quark p_T and rapidity distributions in $t\bar{t}$ production

We continue with top quark differential distributions in $t\bar{t}$ production. We present theoretical results for the top-quark transverse momentum and rapidity distributions at Tevatron and LHC energies.

7.1 Top-quark p_T distribution

Figure 15 displays the theoretical top quark p_T distribution at the Tevatron. A reduction in scale dependence relative to NLO is observed when the NNLO soft-gluon corrections are

Figure 17: The normalized top quark p_T distribution at 7 TeV LHC energy compared with CMS data in the ℓ+jets channel (left) and the dileptons channel (right).
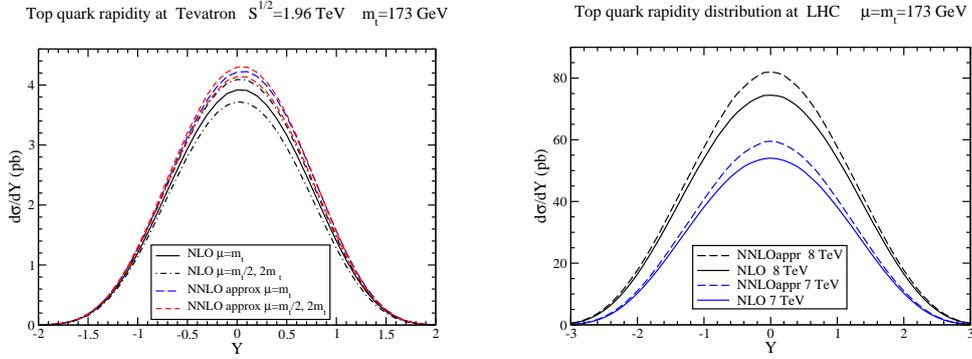
Figure 18: The top quark rapidity distribution at the Tevatron (left) and the LHC (right).

included. Excellent agreement of the NNLO approximate results with D0 data [34] can be seen over all the p_T range from the plot on the right. The theoretical results are also in good agreement with newer D0 data [35].

The top quark p_T distribution at LHC energies is shown on the left plot of Fig. 16 with two different choices of scale: m_t and $m_T = \sqrt{p_T^2 + m_t^2}$. The right plot shows a comparison of the theoretical approximate NNLO normalized p_T distribution, $(1/\sigma)d\sigma/dp_T$, to recent ATLAS data [36] at 7 TeV energy up to p_T of 800 GeV.

Figure 17 shows the same theoretical normalized top quark p_T distribution at the LHC compared to CMS data [37] at 7 TeV energy in the ℓ+jets channel (left plot) and the dileptons channel (right plot). There is excellent agreement with CMS data, and the NNLO approximate result describes the data better than event generators (see the discussion in [37]); a similar conclusion is drawn in the comparison with CMS data at 8 TeV energy [38].

7.2   Top-quark rapidity distribution

The top-quark rapidity distribution has been calculated [39] for Tevatron energy (left plot in Fig. 18) and is in good agreement with recent data from D0 [35].
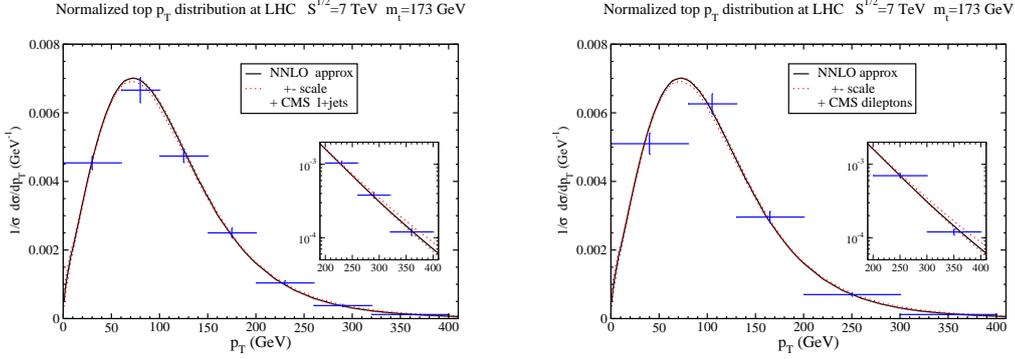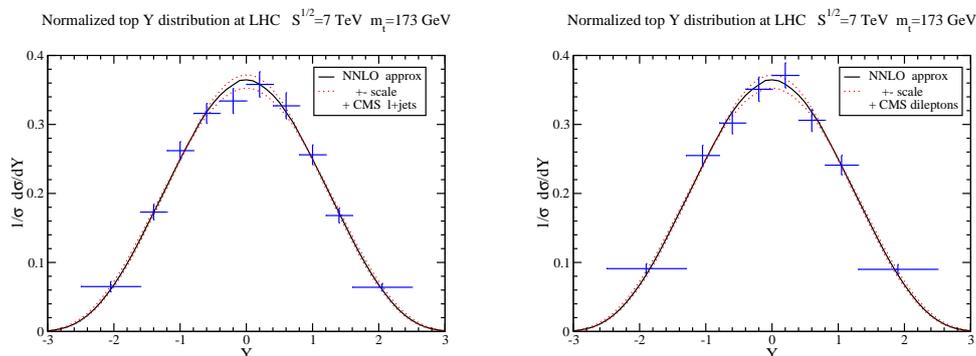
Figure 19: The normalized top quark rapidity distribution at 7 TeV LHC energy compared with CMS data in the ℓ+jets channel (left) and the dileptons channel (right).
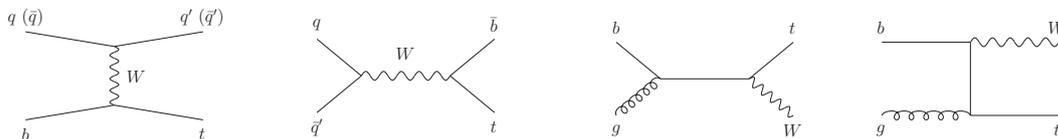

Figure 20: LO diagrams for single-top production in the t-channel (left diagram), s-channel (second from left), and in tW production (right two diagrams).

The top-quark forward-backward asymmetry is defined by

$$A_{\text{FB}} = \frac{\sigma(Y > 0) - \sigma(Y < 0)}{\sigma(Y > 0) + \sigma(Y < 0)}.$$

The asymmetry is significant at the Tevatron. The theoretical result [39] for Tevatron energy is $A_{\text{FB}} = 0.052^{+0.000}_{-0.006}$ which is significantly smaller than observed values.

The theoretical top quark rapidity distribution at LHC energies [39] is shown in the right plot of Fig. 18 at NLO and approximate NNLO.

The normalized top quark rapidity distribution at the LHC at 7 TeV energy is shown in Fig. 19. Excellent agreement is found with CMS data at 7 TeV [37] and also at 8 TeV [38].

8   Single-top production

Single-top-quark production was first observed at the Tevatron in 2009 [40, 41]. The single-top partonic processes at LO are shown in Fig. 20.

The t-channel processes are of the form $qb \to q't$ and $\bar{q}b \to \bar{q}'t$ and are numerically dominant at Tevatron and LHC energies. The s-channel processes are of the form $q\bar{q}' \to \bar{b}t$ and are small at both the Tevatron and the LHC. The associated tW production proceeds via $bg \to tW^-$ and is negligible at the Tevatron but significant (second largest) at the LHC. A related process to tW production is the associated production of a charged Higgs boson with a top quark, $bg \to tH^-$.
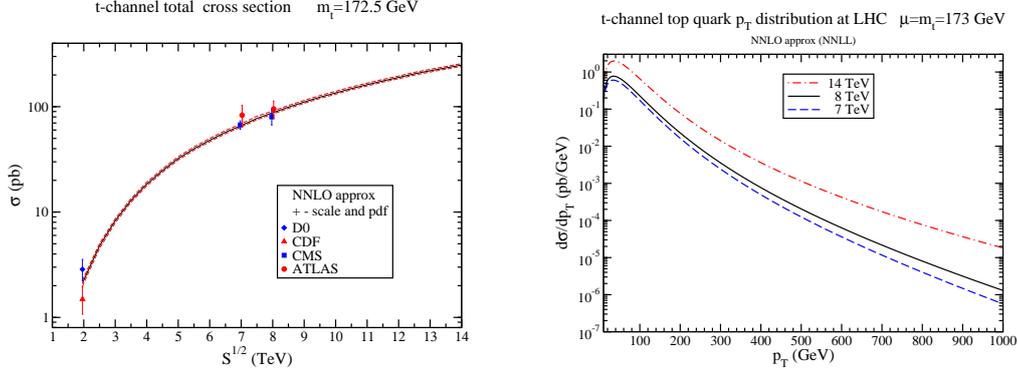
Figure 21: The t-channel total cross section (left); the top-quark p_T distribution in t-channel production (right).

LHC	t	$\bar{t}$	Total (pb)
7 TeV	$43.0^{+1.6}_{-0.2} \pm 0.8$	$22.9 \pm 0.5^{+0.7}_{-0.9}$	$65.9^{+2.1+1.5}_{-0.7-1.7}$
8 TeV	$56.4^{+2.1}_{-0.3} \pm 1.1$	$30.7 \pm 0.7^{+0.9}_{-1.1}$	$87.2^{+2.8+2.0}_{-1.0-2.2}$
14 TeV	$154^{+4}_{-1} \pm 3$	94^{+2+2}_{-1-3}	248^{+6+5}_{-2-6}

Table 1: NNLO approximate t-channel single-top and single-antitop cross sections with $m_t = 173$ GeV. The first uncertainty is from scale variation between $m_t/2$ and $2m_t$ and the second uncertainty is from the MSTW2008 NNLO pdf [20] at 90% CL.

8.1 t-channel production

We begin with single top quark production in the t-channel. This is the dominant single-top production channel at both Tevatron and LHC energies. The complete NLO corrections were calculated in [5].

The soft anomalous dimension matrix for t-channel single top production at one and two loops has been calculated [42, 43]. The first element of this 2×2 matrix is given at one-loop by [42, 43]

$$\Gamma^{(1)}_{S\,t-11} = C_F \left[\ln \left(\frac{-t}{s} \right) + \ln \left(\frac{m_t^2 - t}{m_t \sqrt{s}} \right) - \frac{1}{2} \right]$$

and at two loops by [43]

$$\Gamma^{(2)}_{S\,t-11} = \frac{K}{2} \Gamma^{(1)}_{S\,t-11} + C_F C_A \frac{(1 - \zeta_3)}{4} .$$

The left plot of Fig. 21 shows the total t-channel cross section as a function of collider energy. Excellent agreement is found with D0 [44], CDF [45], CMS [46, 47], and ATLAS [48, 49] results.

Table 1 lists the t-channel single-top and single-antitop cross sections, and their sum, at 7, 8, and 14 TeV LHC energies, for a top quark mass $m_t = 173$ GeV. The central results are with $\mu_F = \mu_R = m_t$ and the first uncertainty is due to scale variation over the interval $m_t/2$ to $2m_t$, while the second uncertainty denotes the pdf errors using MSTW2008 NNLO pdf at 90% CL.
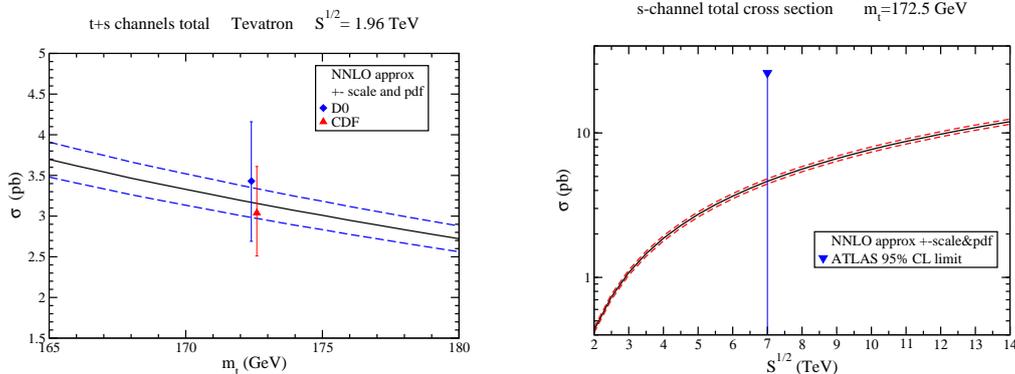
Figure 22: (Left) t and s channel combined cross sections compared with Tevatron data. (Right) s-channel cross section at LHC energies.

LHC	t	$\bar{t}$	Total (pb)
7 TeV	$3.14 \pm 0.06^{+0.12}_{-0.10}$	$1.42 \pm 0.01^{+0.06}_{-0.07}$	$4.56 \pm 0.07^{+0.18}_{-0.17}$
8 TeV	$3.79 \pm 0.07 \pm 0.13$	$1.76 \pm 0.01 \pm 0.08$	$5.55 \pm 0.08 \pm 0.21$
14 TeV	$7.87 \pm 0.14^{+0.31}_{-0.28}$	$3.99 \pm 0.05^{+0.14}_{-0.21}$	$11.86 \pm 0.19^{+0.45}_{-0.49}$

Table 2: NNLO approximate s-channel single-top and single-antitop cross sections with $m_t = 173$ GeV. The first uncertainty is from scale variation between $m_t/2$ and $2m_t$ and the second uncertainty is from the MSTW2008 NNLO pdf [20] at 90% CL.

The theoretical ratio $\sigma(t)/\sigma(\bar{t}) = 1.88^{+0.11}_{-0.09}$ at 7 TeV compares well with the ATLAS result of $1.81^{+0.23}_{-0.22}$ [50].

In addition to the total cross section, the top-quark p_T distribution in t-channel production is of interest and has been calculated at NLO in [5, 51, 52, 53, 54]. More recently, approximate NNLO results based on NNLL resummation appeared in [55] (for another approach based on SCET, see [56]). The right plot of Fig. 21 shows the theoretical results for t-channel top-quark p_T distributions at LHC energies [55].

8.2 s-channel production

We continue with single top quark production in the s-channel. The NLO corrections were calculated in [5].

The soft anomalous dimension matrix for this process has been calculated at one and two loops [42, 57]. The first element of this 2×2 matrix for s-channel single top production at one loop is [42, 57]

$$\Gamma^{(1)}_{S\,s-11} = C_F \left[\ln \left(\frac{s - m_t^2}{m_t \sqrt{s}} \right) - \frac{1}{2} \right]$$

and at two loops it is [57]

$$\Gamma^{(2)}_{S\,s-11} = \frac{K}{2} \Gamma^{(1)}_{S\,s-11} + C_F C_A \frac{(1 - \zeta_3)}{4} \,.$$

Tevatron	Total (pb) at 1.96 TeV
t-channel	$2.08^{+0.00}_{-0.04} \pm 0.12$
s-channel	$1.05^{+0.00}_{-0.01} \pm 0.06$
$t + s$ sum	$3.13^{+0.00}_{-0.05} \pm 0.18$

Table 3: NNLO approximate t and s channel total cross sections at the Tevatron with $m_t = 173$ GeV.
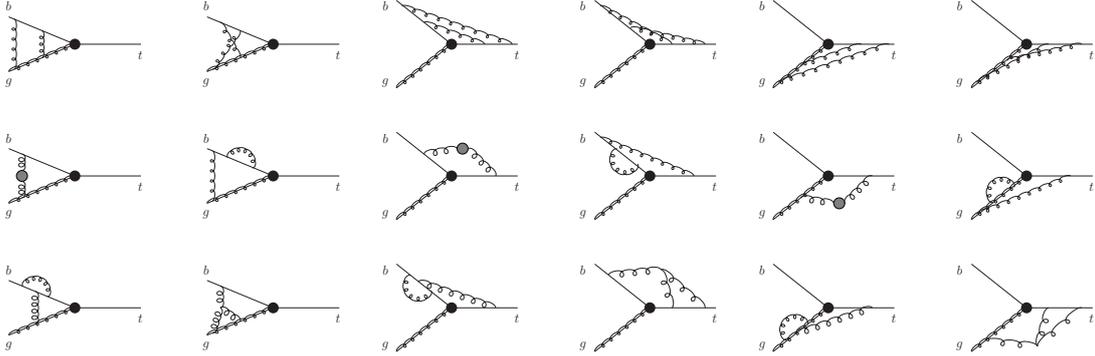
Figure 23: Two-loop eikonal diagrams for tW production.

Table 2 shows the single top and antitop s-channel cross sections at the LHC for $m_t = 173$ GeV. The NNLO approximate corrections provide an enhancement over NLO (with the same pdf) of $\sim 10\%$.

In the left plot of Fig. 22 the sum of the t and s-channel cross sections at the Tevatron are displayed and compared with D0 [44] and CDF [45] data; the agreement is very good. The right plot of Fig. 22 shows the s-channel cross section as a function of LHC energy together with the current limit from ATLAS [58].

Table 3 shows the single top and antitop t-channel and s-channel NNLO approximate cross sections at the Tevatron for $m_t = 173$ GeV.

8.3 tW^- production

We continue with the associated production of a top quark with a W^-. The NLO corrections for this process were calculated in [59]. The two-loop eikonal diagrams that contribute to the soft anomalous dimension are shown in Fig. 23 (additional top-quark self-energy graphs also contribute).

The soft anomalous dimension for $bg \to tW^-$ is given at one loop by [42, 60]

$$\Gamma^{(1)}_{S\,tW^-} = C_F \left[\ln \left(\frac{m_t^2 - t}{m_t \sqrt{s}} \right) - \frac{1}{2} \right] + \frac{C_A}{2} \ln \left(\frac{m_t^2 - u}{m_t^2 - t} \right)$$

and at two loops by [60]

$$\Gamma^{(2)}_{S\,tW^-} = \frac{K}{2} \Gamma^{(1)}_{S\,tW^-} + C_F C_A \frac{(1 - \zeta_3)}{4} \,.$$

164
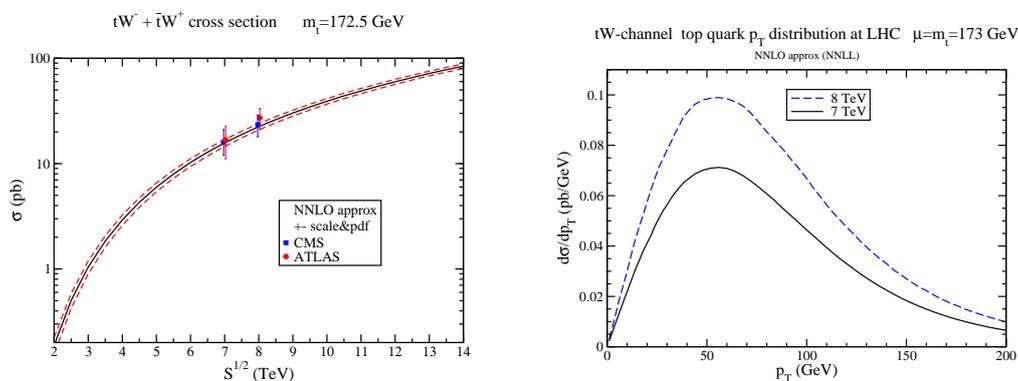
Figure 24: Total cross section for tW production (left); top-quark p_T distribution in tW^- production (right).

LHC	tW^- (pb)
7 TeV	$7.8 \pm 0.2^{+0.5}_{-0.6}$
8 TeV	$11.1 \pm 0.3 \pm 0.7$
14 TeV	$41.8 \pm 1.0^{+1.5}_{-2.4}$

Table 4: NNLO approximate tW^- production cross sections with $m_t = 173$ GeV.

The left plot in Fig. 24 shows the total tW cross section as a function of LHC energy together with LHC data at 7 TeV [61, 62] and 8 TeV [63, 64] energy. The agreement of data with theory is very good. The right plot displays the top-quark p_T distribution in tW^- production at LHC energies.

Table 4 shows the cross sections for tW^- production at LHC energies for a top quark mass $m_t = 173$ GeV. The NNLO approximate corrections increase the NLO cross section by $\sim 8\%$. The cross section for $\bar{t}W^+$ production is identical to that for tW^-.

8.4   Associated production of a top quark with a charged Higgs

Finally, we consider the production of a top quark in association with a charged Higgs boson [60]. Charged Higgs bosons appear in the Minimal Supersymmetric Standard Model (MSSM) and other two-Higgs doublet models. The soft anomalous dimension for this process is the same as for tW production.

Figure 25 shows the cross section for tH^- production in the MSSM at LHC energies as a function of charged Higgs mass. The NNLO approximate corrections increase the NLO cross section by ~ 15 to $\sim 20\%$, depending on the charged Higgs mass.

9   Summary

In these lectures I have presented higher-order calculations for top-quark production in hadronic collisions. I have discussed the resummation of soft-gluon corrections for top quark production via different partonic channels. NNLL resummation is achieved via two-loop eikonal calculations

bg-> tH⁻ at LHC   NNLO approx (NNLL)   tanβ=30 μ=m_H⁻
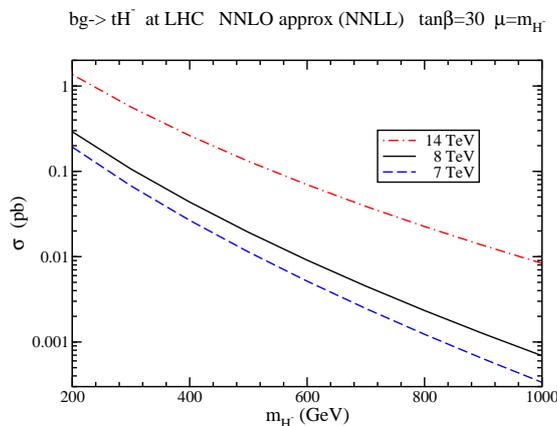
Figure 25: Total cross sections for charged Higgs production in association with a top quark.

of soft anomalous dimension matrices. NNLO approximate results for the $t\bar{t}$ production cross section and the top quark p_T and rapidity distributions are in excellent agreement with data from the LHC and the Tevatron. Single top cross sections and p_T distributions have been presented in all partonic channels and are also in excellent agreement with collider data. The NNLO approximate corrections are very significant and they reduce the theoretical errors.

Acknowledgements

References

[1] CDF Collaboration, Phys. Rev. Lett. **74**, 2626 (1995) [hep-ex/9503002].

[2] D0 Collaboration, Phys. Rev. Lett. **74**, 2632 (1995) [hep-ex/9503003].

[3] P. Nason, S. Dawson, and R.K. Ellis, Nucl. Phys. B **303**, 607 (1988).

[4] W. Beenakker, H. Kuijf, W.L. van Neerven, and J. Smith, Phys. Rev. D **40**, 54 (1989); W. Beenakker, W.L. van Neerven, R. Meng, G.A. Schuler, and J. Smith, Nucl. Phys. B **351**, 507 (1991).

[5] B.W. Harris, E. Laenen, L. Phaf, Z. Sullivan, and S. Weinzierl, Phys. Rev. D **66**, 054024 (2002) [hep-ph/0207055].

[6] N. Kidonakis and G. Sterman, Phys. Lett. B **387**, 867 (1996); Nucl. Phys. B **505**, 321 (1997) [hep-ph/9705234].

[7] N. Kidonakis and B.D. Pecjak, Eur. Phys. J. C **72**, 2084 (2012) [arXiv:1108.6063 [hep-ph]].

[8] N. Kidonakis, Mod. Phys. Lett. A **19**, 405 (2004) [hep-ph/0401147]; Phys. Rev. D **73**, 034001 (2006) [hep-ph/0509079].

[9] G. Sterman, Nucl. Phys. B **281**, 310 (1987).

[10] S. Catani and L. Trentadue, Nucl. Phys. B **327**, 323 (1989).

[11] J. Kodaira and L. Trentadue, Phys. Lett. **112B**, 66 (1982).

[12] H. Contopanagos, E. Laenen, and G. Sterman, Nucl. Phys. B **484**, 303 (1997) [hep-ph/9604313].

[13] S. Moch, J.A.M. Vermaseren, and A. Vogt, Nucl. Phys. B **646**, 181 (2002) [hep-ph/0209100]; Nucl. Phys. B **726**, 317 (2005) [hep-ph/0506288].

[14] A. Gonzalez-Arroyo, C. Lopez, and F.J. Yndurain, Nucl. Phys. B **153**, 161 (1979).

[15] G. Curci, W. Furmanski, and R. Petronzio, Nucl. Phys. B **175**, 27 (1980).

[16] N. Kidonakis, Phys. Rev. Lett. **102**, 232003 (2009) [arXiv:0903.2561 [hep-ph]].

[17] N. Kidonakis, arXiv:0910.0473 [hep-ph], in DPF 2009, eConf C090726.

[18] S.V. Ivanov, G.P. Korchemsky, and A.V. Radyushkin, Yad. Fiz. **44**, 230 (1986) [Sov. J. Nucl. Phys. **44**, 145 (1986)]; G.P. Korchemsky and A.V. Radyushkin, Phys. Lett. B **171**, 459 (1986); Nucl. Phys. B **283**, 342 (1987); Phys. Lett. B **279**, 359 (1992) [hep-ph/9203222].

[19] N. Kidonakis, Phys. Rev. D **82**, 114030 (2010) [arXiv:1009.4935 [hep-ph]].

[20] A.D. Martin, W.J. Stirling, R.S. Thorne, and G. Watt, Eur. Phys. J. C **63**, 189 (2009) [arXiv:0901.0002 [hep-ph]].

[21] ATLAS Collaboration, ATLAS-CONF-2012-131.

[22] CMS Collaboration, CMS-PAS-TOP-11-024.

[23] ATLAS Collaboration, ATLAS-CONF-2013-097.

[24] CMS Collaboration, CMS-PAS-TOP-12-007.

[25] CDF Collaboration, Phys. Rev. D **82**, 052002 (2010) [arXiv:1002.2919 [hep-ex]]; Conf. Note 10163.

[26] D0 Collaboration, Phys. Lett. B **679**, 177 (2009) [arXiv:0901.2137 [hep-ex]]; Phys. Rev. D **82**, 032002 (2010) [arXiv:0911.4286 [hep-ex]]; Phys. Lett. **B** 704, 403 (2011) [arXiv:1105.5384 [hep-ex]].

[27] N. Kidonakis, arXiv:1210.7813 [hep-ph] (to appear in Particles and Nuclei); in Snowmass 2013 Proceedings, SNOW13-00008 [arXiv:1304.7775 [hep-ph]]; PoS (EPS-HEP 2013) 432 [arXiv:1309.1442 [hep-ph]].

[28] M. Czakon, P. Fiedler, and A. Mitov, Phys. Rev. Lett. **110**, 252004 (2013) [arXiv:1303.6254 [hep-ph]].

[29] M. Aliev, H. Lacker, U. Langenfeld, S. Moch, P. Uwer, and M. Wiedemann, Comput. Phys. Commun. **182**, 1034 (2011) [arXiv:1007.1327 [hep-ph]].

[30] V. Ahrens, A. Ferroglia, M. Neubert, B.D. Pecjak, and L.L. Yang, Phys. Lett. B **703**, 135 (2011) [arXiv:1105.5824 [hep-ph]].

[31] M. Beneke, P. Falgari, S. Klein, and C. Schwinn, Nucl. Phys. B **855**, 695 (2012) [arXiv:1109.1536 [hep-ph]].

[32] M. Cacciari, M. Czakon, M. Mangano, A. Mitov, and P. Nason, Phys. Lett. B **710**, 612 (2012) [arXiv:1111.5869 [hep-ph]].

[33] N. Kidonakis and R. Vogt, Phys. Rev. D **68**, 114014 (2003) [hep-ph/0308222].

[34] D0 Collaboration, Phys. Lett. B **693**, 515 (2010) [arXiv:1001.1900 [hep-ex]].

[35] D0 Collaboration, D0 Note 6379-CONF.

[36] ATLAS Collaboration, ATLAS-CONF-2013-099.

[37] CMS Collaboration, Eur. Phys. J. C **73**, 2339 (2013) [arXiv:1211.2220 [hep-ex]].

[38] CMS Collaboration, CMS-PAS-TOP-12-028.

[39] N. Kidonakis, Phys. Rev. D **84**, 011504 (2011) [arXiv:1105.5167 [hep-ph]].

[40] D0 Collaboration, Phys. Rev. Lett. **103**, 092001 (2009) [arXiv:0903.0850 [hep-ex]].

[41] CDF Collaboration, Phys. Rev. Lett. **103**, 092002 (2009) [arXiv:0903.0885 [hep-ex]].

[42] N. Kidonakis, Phys. Rev. D **74**, 114012 (2006) [hep-ph/0609287].

[43] N. Kidonakis, Phys. Rev. D **83**, 091503 (2011) [arXiv:1103.2792 [hep-ph]].

[44] D0 Collaboration, Phys. Rev. D **84**, 112001 (2011) [arXiv:1108.3091 [hep-ex]].

[45] CDF Collaboration, CDF Note 10793.

[46] CMS Collaboration, JHEP 1212 (2012) 035 [arXiv:1209.4533 [hep-ex]].

[47] CMS Collaboration, CMS-PAS-TOP-12-011.

[48] ATLAS Collaboration, Phys. Lett. B **717**, 330 (2012) [arXiv:1205.3130 [hep-ex]].

[49] ATLAS Collaboration, ATLAS-CONF-2012-132.

[50] ATLAS Collaboration, ATLAS-CONF-2012-056.

[51] J.M. Campbell, R. Frederix, F. Maltoni, and F. Tramontano, Phys. Rev. Lett. **102**, 182003 (2009) [arXiv:0903.0005 [hep-ph]].

[52] R. Schwienhorst, C.-P. Yuan, C. Mueller, and Q.-H. Cao, Phys. Rev. D **83**, 034019 (2011) [arXiv:1012.5132 [hep-ph]].

[53] P. Falgari, F. Giannuzzi, P. Mellor, and A. Signer, Phys. Rev. D **83**, 094013 (2011) [arXiv:1102.5267 [hep-ph]].

[54] R. Frederix, E. Re, and P. Torrielli, JHEP 1209 (2012) 130 [arXiv:1207.5391 [hep-ph]].

[55] N. Kidonakis, Phys. Rev. D **88**, 031504 (2013) [arXiv:1306.3592 [hep-ph]].

[56] J. Wang, C.S. Li, and H.X. Zhu, Phys. Rev. D **87**, 034030 (2013) [arXiv:1210.7698 [hep-ph]].

[57] N. Kidonakis, Phys. Rev. D **81**, 054028 (2010) [arXiv:1001.5034 [hep-ph]].

[58] ATLAS Collaboration, ATLAS-CONF-2011-118.

[59] S. Zhu, Phys. Lett. B **524**, 283 (2002); (E) B **537**, 351 (2002).

[60] N. Kidonakis, Phys. Rev. D **82**, 054018 (2010) [arXiv:1005.4451 [hep-ph]].

[61] ATLAS Collaboration, Phys. Lett. B **716**, 142 (2012) [arXiv:1205.5764 [hep-ex]].

[62] CMS Collaboration, Phys. Rev. Lett. **110**, 022003 (2013) [arXiv:1209.3489 [hep-ex]].

[63] ATLAS Collaboration, ATLAS-CONF-2013-100.

[64] CMS Collaboration, CMS-PAS-TOP-12-040.

Helicity Amplitudes and
Angular Decay Distributions

J.G. Körner[1]

[1]PRISMA Cluster of Excellence, Institut für Physik, Johannes-Gutenberg-Universität,

Staudinger Weg 7, 55099 Mainz, Germany

I discuss how to obtain angular decay distributions for sequential cascade decays using helicity methods. The angular decay distributions follow from a reasonably simple master formula involving bilinear forms of helicity amplitudes and Wigner's d functions. I discuss in some detail the issue of gauge invariance for off-shell gauge bosons. As a technical exercise I calculate the linear relation between the helicity amplitudes and the invariant amplitudes of semileptonic and rare baryon decays. I discuss two explicit examples of angular decay distributions for (i) the decay $t \to b + W^+(\to \ell^+ \nu_\ell)$ (which leads to the notion of the helicity fractions of the W^+), and (ii) the sequential decay $\Lambda_b \to \Lambda(\to p\pi^-) + J/\psi(\to \ell^+\ell^-)$.

1 Introductory remarks

In these lectures I want to discuss some examples of sequential cascade decays and their corresponding angular decay distributions. The angular decay distributions follow from a reasonably simple master formula involving bilinear forms of helicity amplitudes and Wigner's d functions. Some sample cascade decay processes are

- Polarized top quark decay [1, 2] $t(\uparrow) \to b + W^+(\to \ell^+\nu_\ell)$

- Rare $\Lambda_b(\uparrow)$ decays [3] $\Lambda_b(\uparrow) \to \Lambda_s(\to p\pi^-) + j_{\text{eff}}(\to \ell^+\ell^-)$

- Higgs decay to gauge bosons [4] $H \to W^+(\to \ell^+\nu_\ell) + W^{-*}(\to \ell^-\bar\nu_\ell)$
$\qquad\qquad\qquad\qquad\qquad\quad H \to Z(\to \ell^+\ell^-) + Z^*(\to \ell^+\ell^-)$

- Rare B decays [5] $B \to D + j_{\text{eff}}(\to \ell^+\ell^-)$
$\qquad\qquad\qquad\quad B \to D^*(\to D\pi) + j_{\text{eff}}(\to \ell^+\ell^-)$

- Semileptonic Λ_b decays [6] $\Lambda_b \to \Lambda_c(\to \Lambda\pi^+) + W^{-*}(\to \ell^-\bar\nu_\ell)$

- Semileptonic B decays [7, 8, 9] $B \to D + W^*(\to \ell\nu)$
$\qquad\qquad\qquad\qquad\qquad\quad B \to D^*(\to D\pi) + W^*(\to \ell\nu)$

- Nonleptonic Λ_b decays [10] $\Lambda_b \to \Lambda(\to p\pi^-) + J/\psi(\to \ell^+\ell^-)$

- Semileptonic hyperon decays $(\ell^- = e^-, \mu^-)$ [11] $\Xi^0(\uparrow) \to \Sigma^+(\to p+\pi^0) + W^{-*}(\to \ell^-\bar\nu_\ell)$

In our treatment of these decay processes we have accounted for lepton mass effects whenever this is warranted for by the decay kinematics.

The generic form of most of the above cascade decays is $H_1 \to H_2(\to H_3 + H_4) + W, W^*$, $j_{\text{eff}}(\to \ell + \bar\ell)$ where the H_i can be mesons, baryons or quarks, and the W and W^* denote either on-shell or off-shell charged W's. For neutral current transitions, j_{eff} denotes an effective four-vector and/or four-axial vector current relevant for the desription of rare decays. The interest in deriving angular decay distributions via helicity methods is two-fold. First it facilitates the theoretical analysis of a decay distribution in terms of parity or CP violating contributions. Second it allows one to generate experimental decay distributions via a suitable Monte Carlo program (see e.g. Ref. [11]).

Take as an example the semileptonic hyperon decay $\Xi^0(\uparrow) \to \Sigma^+(\to p + \pi^0) + \ell^- + \bar\nu_\ell$ ($\ell^- = e^-, \mu^-$). The decay process is described by three polar angles θ, θ_B and θ_P (as e.g. in Fig. 2) and two azimuthal angles ϕ_B and ϕ_ℓ which describe the relative azimuthal orientation of the two planes that characterize the cascade decay process.

As we shall learn in this lecture, the angular decay distribution can be derived from the master formula [11]

$$
\begin{aligned}
W(\theta, \theta_P, \theta_B, \phi_B, \phi_\ell) \;\propto\; &\sum_{\lambda_\ell, \lambda_W, \lambda'_W, J, J', \lambda_2, \lambda'_2, \lambda_3} (-1)^{J+J'} |h^{V-A}_{\lambda_\ell \lambda_{\nu=\pm 1/2}}|^2 e^{i(\lambda_W - \lambda'_W)\phi_\ell} \\
&\times \rho_{\lambda_2 - \lambda_W, \lambda'_2 - \lambda'_W}(\theta_P) d^J_{\lambda_W, \lambda_\ell - \lambda_\nu}(\theta) d^{J'}_{\lambda'_W, \lambda_\ell - \lambda_\nu}(\theta) H_{\lambda_2 \lambda_W} H^*_{\lambda'_2 \lambda'_W} \\
&\times e^{i(\lambda_2 - \lambda'_2)\phi_B} d^{1/2}_{\lambda_2 \lambda_3}(\theta_B) d^{1/2}_{\lambda'_2 \lambda_3}(\theta_B) |h^B_{\lambda_3 0}|^2
\end{aligned}
\tag{1}
$$

where

$$
\begin{array}{rcl}
h^{V-A}_{\lambda_\ell \lambda_{\nu=\pm 1/2}} & : & \text{helicity amplitudes for the transition } W^* \to \ell + \nu_\ell : \\
& & \lambda_{\bar\nu} = 1/2 \text{ for } (\ell^- \bar\nu_\ell); \; \lambda_\nu = -1/2 \text{ for } (\ell^+ \nu_\ell) \\
\rho_{\lambda_1 \lambda'_1} & : & \text{density matrix for the polarized parent baryon } B_1 \\
H_{\lambda_2 \lambda_W} & : & \text{helicity amplitudes for the transition } B_1 \to B_2 + W^* \\
h^B_{\lambda_3 0} & : & \text{helicity amplitudes for the transition } B_2 \to B_3 + \pi \\
d^J_{mm'} & : & \text{Wigner's } d \text{ functions}
\end{array}
$$

The λ_ℓ, λ_W, ... are helicity labels of the baryons, leptons and the W^* that participate in the process. They take the values

$$
\begin{aligned}
\lambda_\ell, \lambda_1, \lambda_2, \lambda_3 &= \pm 1/2 \\
\lambda_W &= 1, 0, -1 \; (J=1); \quad t \; (J=0) \\
\lambda_{\bar\nu} &= +1/2; \; \lambda_\nu = -1/2
\end{aligned}
$$

We shall see in these lectures that the off-shell gauge boson W has a spin-1 and a spin-0 component. Thus we have to sum over $J = 0, 1$. The phase factor $(-1)^{J+J'} = \pm 1$ is associated with the Minkowski metric of our world. The angular decay distribution (1) covers both final lepton states $(\ell^- \bar\nu_\ell)$ and $(\ell^+ \nu_\ell)$ which are distinguished through the labelling $\lambda_\nu = \pm 1/2$ ($\lambda_{\bar\nu} = +1/2$, $\lambda_\nu = -1/2$). This covers the charge conjugated process or also the semileptonic decay $\Sigma^+ \to \Lambda + e^+ \nu_e$.

The master formula (1) is quite general. After appropiate angular integrations over θ_B and ϕ_B the master formula also applies to the three-fold angular decay distribution of polarized top decay $t(\uparrow) \to b + \ell^+ \nu_\ell$, etc., etc.. The summation over helicities can be quite elaborate if done by hand. However, the summation can be done by computer. A FORM package doing the summation automatically is available from M.A. Ivanov.

1.1 Polarization of the lepton

In the master formula (1) I have summed over the helicities of the lepton. To obtain the polarization of the lepton leave the lepton helicity unsummed, i.e.

$$\sum_{\lambda_\ell, \dots} \quad \to \quad \sum_{\dots}$$

For example, the longitudinal polarization of the charged lepton is then given by

$$P^z(\ell) = \frac{W_{\lambda_\ell = +1/2} - W_{\lambda_\ell = -1/2}}{W_{\lambda_\ell = +1/2} + W_{\lambda_\ell = -1/2}} \tag{2}$$

In the same vein the transverse polarization components $P^x(\ell)$ and $P^y(\ell)$ can be obtained from the nondiagonal elements of the W^* density matrix. Note that the longitudinal polarization of the lepton in Eq. (2) refers to the lepton-neutrino cm system, and *not* to the Ξ^0 rest system.

2 Gauge boson off-shell effects

2.1 Off-shell effects and scalar degrees of freedom

When the gauge boson is off its mass shell $q^2 \neq m^2_{W,Z}$ one has to take into account the scalar degree of freedom of the gauge boson. Take the unitary gauge and write out the numerator of the W gauge boson propagator as

$$H_{\mu\nu} L^{\mu\nu} = H_{\mu\nu} \, g^{\mu\mu'} g^{\nu\nu'} \, L_{\mu'\nu'} \quad \longrightarrow \quad H_{\mu\nu} \left(g^{\mu\mu'} - \frac{q^\mu q^{\mu'}}{m_W^2} \right) \left(g^{\nu\nu'} - \frac{q^\nu q^{\nu'}}{m_W^2} \right) L_{\mu'\nu'}.$$

The term $q^\mu q^{\mu'}/m_W^2$ is usually dropped in low energy applications such as μ-decay and also in the charm and bottom sector. Split the propagator numerator into a spin-1 and a spin-0 piece

$$\left(\underbrace{-g^{\mu\mu'} + \frac{q^\mu q^{\mu'}}{q^2}}_{\text{spin 1}} - \underbrace{\frac{q^\mu q^{\mu'}}{q^2}(1 - \frac{q^2}{m_W^2})}_{\text{spin 0}} \right) \left(\underbrace{-g^{\nu\nu'} + \frac{q^\nu q^{\nu'}}{q^2}}_{\text{spin 1}} - \underbrace{\frac{q^\nu q^{\nu'}}{q^2}(1 - \frac{q^2}{m_W^2})}_{\text{spin 0}} \right).$$

There are three contributions $i)$ spin $1 \otimes$ spin 1, $ii) - ($ spin $1 \otimes$ spin $0 +$ spin $0 \otimes$ spin $1)$ and $iii)$ spin $0 \otimes$ spin 0.

Note the minus sign in case ii) which results from the Minkowski metric. This extra minus sign can be readily incorporated into the master formulas for angular decay distributions by introducing the factor $(-1)^{J+J'}$ and summing over $J, J' = 0, 1$. The scalar contributions are $O(m_\ell^2)$ since $q^\mu L_{\mu\nu} \sim O(m_\ell)$. Note, however, that q^2 can be small since the range of off-shellness is

$$(m_{\ell\,1} + m_{\ell\,2})^2 \leq q^2 \leq (M_1 - M_2)^2$$

for the decay $H_1(M_1) \to H_2(M_2) + \ell_1(m_{\ell_1}) + \bar{\ell}_2(m_{\ell_2})$.

2.2 The issue of gauge invariance

Consider the gauge boson propagator in the general R_ξ gauge and rewrite it into a convenient form. For definiteness we consider the decay $t \to b + W^+$ where we shall also consider gauge boson off-shell effects which allows one to calculate finite width effects as will be done in Sec. 2.3.

$$D^{\mu\nu} = \frac{i}{q^2 - m_W^2}\left(-g^{\mu\nu} + \frac{q^\mu q^\nu(1 - \xi_W)}{q^2 - \xi_W m_W^2}\right) \tag{3}$$
$$= \frac{i}{q^2 - m_W^2}\left(-g^{\mu\nu} + \frac{q^\mu q^\nu}{m_W^2} - \frac{q^\mu q^\nu}{m_W^2} + \frac{q^\mu q^\nu(1 - \xi_W)}{q^2 - \xi_W m_W^2}\right)$$

resulting in

$$D^{\mu\nu} = \frac{i}{q^2 - m_W^2}\left(-g^{\mu\nu} + \frac{q^\mu q^\nu}{m_W^2}\right) - i\frac{q^\mu q^\nu}{m_W^2}\frac{1}{q^2 - \xi_W m_W^2}. \tag{4}$$

The first term in Eq. (4) is referred to as the unitary propagator. The second gauge-dependent term in Eq. (4) can be seen to exactly cancel the contribution of the charged Goldstone ϕ^+ exchange if fermion lines are attached to the gauge boson and the charged Goldstone boson contribution. One uses the Dirac equation to convert the q^μ and q^ν contributions in the second term of Eq. (4) to fermion masses. In our case one would have

$$q^\nu \bar{u}_f \gamma_\nu(1 - \gamma_5)v_{\bar{f}} = m_f \bar{u}_f(1 - \gamma_5)v_{\bar{f}} + m_{\bar{f}}\bar{u}_f(1 + \gamma_5)v_{\bar{f}},$$
$$q^\mu \bar{u}_b \gamma_\mu(1 - \gamma_5)u_t = m_t \bar{u}_b(1 + \gamma_5)u_t - m_b \bar{u}_b(1 - \gamma_5)u_t.$$

One can then see that the second term in Eq. (4) is exactly cancelled by the corresponding ϕ^+-exchange contribution (with the same fermion pair attached). This exercise shows that it does not make sense to talk of an external off-shell gauge boson in isolation. One must include the coupling to a final state fermion pair if one wants to obtain a gauge invariant result.

2.3 Off-shell effects in the decay $t \to b + W^+$

In the zero width approximation and using the unitary gauge the differential rate for $t \to b + W^+$ is given by

$$\frac{d\Gamma}{dq^2} \sim H_{\mu\nu}\left(g^{\mu\mu'} - \frac{q^\mu q^{\mu'}}{m_W^2}\right)\left(g^{\nu\nu'} - \frac{q^\nu q^{\nu'}}{m_W^2}\right)L_{\mu'\nu'}\,\delta(q^2 - m_W^2).$$

On shell one has $q^2 = m_W^2$, and it makes no difference whether one uses the Landau gauge ($\xi = 0$) with $(g^{\mu\nu} - q^\mu q^\nu/q^2)$ or the unitary gauge ($\xi = \infty$) with $(g^{\mu\nu} - q^\mu q^\nu/m_W^2)$. Since we want to account for off-shell effects the use of the unitary gauge is mandatory as explained in Sec. 2.2. Finite width effects can be accounted for by smearing the zero-width formula with the replacement

$$\delta(q^2 - m_W^2) \quad \longrightarrow \quad \frac{m_W \Gamma_W}{\pi}\frac{1}{(q^2 - m_W^2)^2 + m_W^2 \Gamma_W^2}.$$

One then integrates in the limits

$$m_\ell^2 \le q^2 \le (m_t - m_b)^2.$$

Numerically the finite width corrections amount to -1.55% in $\Gamma_{t \to b + W^+}$ [12, 13]. Curiously, the negative finite width corrections are almost completely cancelled by the positive first order electroweak corrections [13].

2.4 Scalar contributions in some sample decay processes

Scalar contributions are of $O(m_\ell^2)$. They are therefore important for decay processes where the lepton mass is comparable to the scale of the decay process. For semileptonic and rare processes the characteristic scale would be given by the mass difference $M_1 - M_2$. A more symmetric scale is used in the PDG tables, namely the largest momentum of any of the decay products in the rest frame of the decaying particle. Sample decay processes are

- Decays involving the τ

$$
\begin{aligned}
B \to D + \tau\nu_\tau \quad &: \quad \Gamma_S/\Gamma \approx 58\,\% \quad [8,\ 9] \\
B \to D^* + \tau\nu_\tau \quad &: \quad \Gamma_S/\Gamma \approx 7\,\% \quad [8,\ 9] \\
B \to \pi + \tau\nu_\tau \quad &: \quad \Gamma_S/\Gamma \approx (30 \div 50)\,\% \quad [14] \\
H \to W^+ W^{-*}(\to \tau^-\nu_\tau) \quad &: \quad \Gamma_S/\Gamma = 0.73\,\% \quad [4] \\
H \to ZZ^*(\to \tau^+\tau^-) \quad &: \quad \Gamma_S/\Gamma = 1.19\,\% \quad [4]
\end{aligned}
$$

The decays $B \to D^{(*)} + \tau\nu_\tau$ and $B \to \pi + \tau\nu_\tau$ have been widely discussed in the literature because the scalar contribution can be augmented by charged Higgs exchange [15, 16].

- Hadronic semi-inclusive decays $H \to ZZ^*(\to b\bar{b})$

$$
H \to ZZ^*(\to b\bar{b}) \quad : \quad \Gamma_S/\Gamma = 7.9\,\% \quad [17]
$$

Since the ratio $m_e/(m_n - m_p) = 0.395$ is not small it comes of no surprise that there is a sizeable scalar contribution to the neutron β decay $n \to p + e^- \bar{\nu}_e$. In fact one finds $\Gamma_S/\Gamma = 19\,\%$.

2.5 Scalar contribution to the FB asymmetry A_{FB} of the lepton pair

An interesting observation concerns the scalar contribution to the Forward-Backward (FB) asymmetry of the lepton pair in the cm frame of the lepton pair or, put differently, in the W^* rest frame where its momentum is $(\sqrt{q^2}, \vec{0})$. The notation $\vec{0}$ is rather symbolic and stands for the boost direction which brings the W^* to rest. The observation is that there are parity-conserving contributions to the FB asymmetry arising from scalar-vector interference effects.

Consider the FB asymmetry

$$
A_{FB} = \frac{\Gamma_F - \Gamma_B}{\Gamma_F + \Gamma_B} \tag{5}
$$
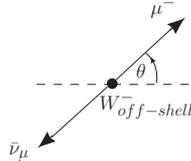
If $A_{FB} \neq 0$ one speaks of a parity-odd effect. Consider the J^P content of the currents coupling to the W^*: $V^\mu(1^-, 0^+)$ and $A^\mu(1^+, 0^-)$. There are two sources of parity-odd effects leading to $A_{FB} \neq 0$ given by

1. parity-violating interaction from $V(1^-)A(1^+)$, $V(0^+)A(0^-)$ interference

2. parity-conserving interaction from $V(0^+)V(1^-)$, $A(0^-)A(1^+)$ interference

Take, for example, the semileptonic decay $\Lambda_b \to \Lambda_c + \ell^- \bar{\nu}_\ell$. The numerator of Eq. (5) is given by (see Ref. [11])

$$\frac{d\Gamma_F}{dq^2} - \frac{d\Gamma_B}{dq^2} = \frac{G^2}{(2\pi)^3}|V_{us}|^2 \frac{(q^2 - m_\ell^2)^2 p}{8M_1^2 q^2} \left[-H_{\frac{1}{2}1}^V H_{\frac{1}{2}1}^A - 2\frac{m_\ell^2}{2q^2}(H_{\frac{1}{2}t}^V H_{\frac{1}{2}0}^V + H_{\frac{1}{2}t}^A H_{\frac{1}{2}0}^A) \right]. \quad (6)$$

The amplitudes $H_{\lambda_{\Lambda_c} \lambda_W}$ in Eq. (6) denote the helicity amplitudes in the transitions $\Lambda_b(\lambda_{\Lambda_b}) \to \Lambda_c(\lambda_{\Lambda_c}) + W^{-*}(\lambda_W)$. The first term in Eq. (6) arises from a truly parity-violating contribution while the remaining two contributions are parity-odd contributions arising from parity conserving interactions. The second contribution is negligible for the e^- and μ^- modes due to the helicity flip factor m_ℓ^2/q^2, but can be sizeable for the τ^- mode. In fact, for the τ mode $\Lambda_b \to \Lambda_c + \tau^- \bar{\nu}_\tau$ the FB asymmetry is dominated by the helicity flip contribution in Eq. (6) leading to a sign change in A_{FB} when going from the e^-, μ^- modes to the τ^- mode (see the corresponding quark-level calculation in Ref. [9]).

3   Helicity amplitudes and invariant amplitudes

The results of a dynamical calculation are usually obtained in terms of invariant amplitudes. The helicity amplitudes can be expressed as a linear superposition of the invariant amplitudes. In this section we show how to calculate the coefficient of this linear expansion for the process $B_1 \to B_2 + j_{\text{eff}}$. In order to calculate the coefficients of the linear expansion one has to choose a definite frame.

3.1   System 1: Parent baryon B_1 at rest

Consider the decay $B_1(M_1) \to B_2(M_2) + j_{\text{eff}}$ in the rest system of B_1. The effective current j_{eff} with momentum q^μ moves in the positive z direction while B_2 moves in the negative z direction.

$$p_1 = (M_1; 0, 0, 0) \qquad q^\mu = (q_0; 0, 0, |\vec{q}|) \qquad p_2^\mu = (E_2; 0, 0, -|\vec{q}|)$$

We do not explicitly annote the helicity of the parent baryon B_1 in the helicity amplitudes since, in system 1, λ_1 is fixed by the relation $\lambda_1 = -\lambda_2 + \lambda_j$.

Possible helicity configurations are

λ_1	λ_2	λ_j
1/2	-1/2	0 (t)
-1/2	1/2	0 (t)
1/2	1/2	1
-1/2	-1/2	-1

Convenient relations in system 1 are ($Q_\pm = (M_1 \pm M_2)^2 - q^2$)

$$2M_1(E_2 + M_2) = Q_+, \qquad 2M_1|\vec{q}| = \sqrt{Q_+ Q_-}. \tag{7}$$

The helicity spinors are given by

$$\bar{u}_2(\pm\tfrac{1}{2}, p_2) = \sqrt{E_2 + M_2}\left(\chi_\mp^\dagger, \frac{\mp|\vec{q}|}{E_2 + M_2}\chi_\mp^\dagger\right), \quad u_1(\pm\tfrac{1}{2}, p_1) = \sqrt{2M_1}\left(\begin{array}{c}\chi_\pm \\ 0\end{array}\right), \tag{8}$$

where $\chi_+ = \left(\begin{array}{c}1 \\ 0\end{array}\right)$ and $\chi_- = \left(\begin{array}{c}0 \\ 1\end{array}\right)$ are the usual Pauli two-spinors.

The helicity spinors satisfy the relations

$$\begin{aligned}
\tfrac{1}{2}(1 + \gamma_5 \slashed{s}_\pm)u(\pm\tfrac{1}{2}, p) &= u(\pm\tfrac{1}{2}, p), \tag{9} \\
\tfrac{1}{2}(1 + \gamma_5 \slashed{s}_\mp)u(\pm\tfrac{1}{2}, p) &= 0,
\end{aligned}$$

where $s_{\mu\,\pm} = \pm(|\vec{p}|/M; 0, 0, E/M)$ is the spin four-vector of the fermion with helicity $\pm 1/2$.

For the four polarization four-vectors of the effective current we have

$$\varepsilon^\mu(t) = \frac{1}{\sqrt{q^2}}\left(q_0; 0, 0, |\vec{q}|\right), \quad \varepsilon^\mu(\pm 1) = \frac{1}{\sqrt{2}}\left(0; \mp 1, -i, 0\right), \quad \varepsilon^\mu(0) = \frac{1}{\sqrt{q^2}}\left(|\vec{q}|; 0, 0, q_0\right). \tag{10}$$

They can be obtained by boosting the corresponding rest frame polarization vectors $\varepsilon^\mu(t; q = 0) = (1; 0, 0, 0)$ and $\varepsilon^\mu(0; q = 0) = (0; 0, 0, 1)$ by a boost with the boost matrix given by $M_{tt} = M_{00} = q_0/\sqrt{q^2}$ and $M_{t0} = M_{0t} = |\vec{q}|/\sqrt{q^2}$ (the transverse polarization vectors are boost invariant).

One defines helicity amplitudes through

$$H^{V,A}_{\lambda_2 \lambda_W} = M^{V,A}_\mu(\lambda_2)\epsilon^{*\mu}(\lambda_j). \tag{11}$$

The current matrix elements can be expanded in terms of a complete set of invariants

$$\begin{aligned}
M^V_\mu &= \langle B_2|J^V_\mu|B_1\rangle = \bar{u}_2(p_2)\left[F^V_1(q^2)\gamma_\mu - \frac{F^V_2(q^2)}{M_1}i\sigma_{\mu\nu}q^\nu + \frac{F^V_3(q^2)}{M_1}q_\mu\right]u_1(p_1), \tag{12} \\
M^A_\mu &= \langle B_2|J^A_\mu|B_1\rangle = \bar{u}_2(p_2)\left[F^A_1(q^2)\gamma_\mu - \frac{F^A_2(q^2)}{M_1}i\sigma_{\mu\nu}q^\nu + \frac{F^A_3(q^2)}{M_1}q_\mu\right]\gamma_5 u_1(p_1)
\end{aligned}$$

(we define $\sigma_{\mu\nu} = \frac{i}{2}(\gamma_\mu\gamma_\nu - \gamma_\nu\gamma_\mu)$). Using the definitions (11, 12), the helicity spinors (8) and polarization vectors (10), the helicity amplitudes can be calculated to be

$$\begin{aligned}
H^{V/A}_{-\frac{1}{2}t} &= \frac{\sqrt{Q_\pm}}{\sqrt{q^2}}\left((M_1 \mp M_2)F^{V/A}_1 \pm q^2/M_1 F^{V/A}_3\right), \tag{13} \\
H^{V/A}_{\frac{1}{2}1} &= \sqrt{2Q_\mp}\left(F^{V/A}_1 \pm (M_1 \pm M_2)/M_1 F^{V/A}_2\right), \\
H^{V/A}_{\frac{1}{2}0} &= \frac{\sqrt{Q_\mp}}{\sqrt{q^2}}\left((M_1 \pm M_2)F^{V/A}_1 \pm q^2/M_1 F^{V/A}_2\right).
\end{aligned}$$

From parity or from an explicit calculation one has

$$
\begin{aligned}
H^V_{-\lambda_2,-\lambda_j} &= H^V_{\lambda_2,\lambda_j}, \\
H^A_{-\lambda_2,-\lambda_j} &= -H^A_{\lambda_2,\lambda_j}.
\end{aligned}
$$

For a general linear combination $H_{\lambda_2,\lambda_j} = aH^V_{\lambda_2,\lambda_j} + bH^A_{\lambda_2,\lambda_j}$ it is advantageous to make use of the linear superpositions $H_{\lambda_2,\lambda_j} \pm H_{-\lambda_2,-\lambda_j}$ which have definite transformation properties under parity.

3.2 System 2: The effective current is at rest

The effective current j_{eff} is at rest, or put differently, in system 2 we work in the cm frame of the lepton pair in the decay $j_{\text{eff}} \to \ell\bar{\ell}$. Both B_1 and B_2 move in the negative z direction. One now has $\lambda_1 = \lambda_2 - \lambda_j$.

$$
p^\mu_1 = (E'_1; 0, 0, -|\vec{p}'|) \qquad q^\mu = (\sqrt{q^2}; 0, 0, 0) \qquad p^\mu_2 = (E'_2; 0, 0, -|\vec{p}'|)
$$

Convenient relations in system 2 are

$$
|\vec{p}'| = \frac{\sqrt{Q_+ Q_-}}{2\sqrt{q^2}}, \quad (E'_1 + M_1)(E'_2 + M_2) = \frac{Q_+}{4q^2}(M_1 - M_2 + \sqrt{q^2})^2. \tag{14}
$$

The relevant spinors can be obtained from the rest frame spinor in Eq. (8) by a boost according to $2M_1 u(p_1) = (\not{p}_1 + M_1)u(p_1 = 0)$ and $2M_1 \bar{u}(p_1) = \bar{u}(p_1 = 0)(\not{p}_1 + M_1)$. The spinors in system 2 are thus given by

$$
\bar{u}_2(\pm\tfrac{1}{2}, p_2) = \sqrt{E'_2 + M_2}\left(\chi^\dagger_\mp, \frac{\mp|\vec{p}'|}{E'_2 + M_2}\chi^\dagger_\mp\right), \quad u_1(\pm\tfrac{1}{2}, p_1) = \sqrt{E'_1 + M_1}\begin{pmatrix}\chi_\mp \\ \frac{\pm|\vec{p}'|}{E'_1 + M_1}\chi_\mp\end{pmatrix}
$$

For the four polarization four-vectors of the effective current we now have $\varepsilon^\mu(t) = (1; 0, 0, 0)$ and $\varepsilon^\mu(0) = (0; 0, 0, 1)$ while the transverse polarization vectors $\varepsilon^\mu(\pm 1) = \frac{1}{\sqrt{2}}(0; \mp 1, -i, 0)$ remain unchanged.

With a little bit of work one can show that

$$
H^{V,A}_{\lambda_2,\lambda_j}(\text{system 2})\ (F^{V,A}_i) = H^{V,A}_{\lambda_2,\lambda_j}(\text{system 1})\ (F^{V,A}_i),
$$

i.e. Eq. (13) holds for both systems 1 and 2. One has recovered a general property of the linear coefficients relating the helicity amplitudes to invariant amplitudes: the coefficients of this linear relation are boost invariant. In this sense the helicity amplitudes are boost invariant. I have gone through this exercise in some detail to convince the reader that e.g. the expression $\sum_{\lambda_2} |H_{\lambda_2,\lambda_j}|^2$ is nothing but the (unnormalized) density matrix of the off-shell gauge boson in its own rest frame regardless of the system in which the helicity amplitudes are evaluated (as long as the systems are connected by a boost). We mention that corresponding relations between helicity amplitudes and invariant amplitudes for the cases $(1/2^+; 3/2^+) \to (1/2^+; 3/2^+)$ have been given in Ref. [18].

3.3 Helicity amplitudes and (LS) amplitudes

Looking at Eq. (13) one notes that at threshold $q^2 = (M_1 - M_2)^2$ there are only two independent nonvanishing helicity amplitudes, namely $H^V_{1/2,t}$ and $H^A_{1/2,1} = \sqrt{2}H^A_{1/2,0}$. This is no accident and can be understood by performing an (LS) amplitude analysis in terms of the (LS) amplitudes $A^{V,A}_{LS}$. For the vector component with J^P content $(1^-; 0^+)$ one has the (LS) amplitudes $(A^V_{1,1/2}, A^V_{1,3/2}; A^V_{0,1/2})$, and for the axial component with J^P content $(1^+; 0^-)$ one has the (LS) amplitudes $(A^A_{0,1/2}, A^A_{2,3/2}; A^A_{1,1/2})$. At threshold only the two S-wave amplitudes survive, namely $A^V_{0,1/2}$ and $A^A_{0,1/2}$. In fact, there is a linear relation between the set of helicity and (LS) amplitudes which reads $(J = 0, 1)$

$$H_{\lambda_1\lambda_2}(J) = \sum_{LS} \left(\frac{2L+1}{2J+1}\right)^{1/2} \langle LS0\mu|J\lambda\rangle\langle s_1 s_2 - \lambda_2\lambda_1|S\mu\rangle A_{LS}, \qquad (15)$$

where $\lambda = \lambda_1 - \lambda_2$. Eq. (15) can be inverted, and upon setting $A^A_{2,3/2} = 0$ at threshold one recovers the above threshold relation $H^A_{1/2,1} = \sqrt{2}H^A_{1/2,0}$. We emphasize that the set of (LS) amplitudes is completely equivalent to the set of helicity amplitudes and the definition of both sets of amplitudes is based on fully relativistic concepts. Some examples of threshold and near threshold relations have recently been discussed in Refs. [19, 20, 21].

4 Rotation of density matrices

For concreteness we discus the decay of an on-shell W^+ into a fermion pair, i.e. $W^+ \to \bar{f}_3 f_4$ (as e.g. $W^+ \to \mu^+\nu_\mu$) described by the helicity amplitudes $h_{\lambda_3\lambda_4}$ ($\lambda_3, \lambda_4 = \pm 1/2$). First consider a frame where W^+ is at rest and where the antifermion $\bar{f}_3$ moves in the positive z' direction.

- Consider first the decay of an unpolarized W^+ into a fermion pair. The decay rate in the z' frame is given by

$$\Gamma \quad \sim \quad \sum_{\text{helicities}} |h_{\lambda_3\lambda_4}|^2.$$

- Consider next the decay of a polarized W^+ into a fermion pair. The polarization of the W^+ is given in terms of the spin density matrix ρ'_{mm} with $m = \lambda_3 - \lambda_4$. One then has

$$\Gamma \quad \sim \quad \sum_{\text{helicities}} \rho'_{mm} |h_{\lambda_3\lambda_4}|^2.$$
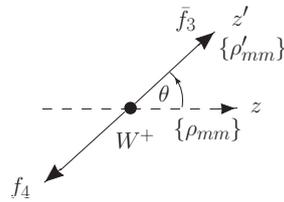
- Now assume that the W^+ was polarized in a production process characterized by a z axis as e.g. in the decay $t \to b + W^+$ discussed before. In this case the z axis is defined by the momentum direction of the W^+ in the top quark rest system. The spin density matrix of the W^+ is given in terms of the helicity amplitudes for the decay $t \to b + W^+$, i.e. by $\sum_{\lambda_2} H_{\lambda_2 \lambda_W}$. In the present case (no azimuthal correlations) one only needs the diagonal terms of the density matrix of the W^+. For the unnormalized density matrix elements of the W^+ one has

$$\rho_{m=\lambda_W,\, m=\lambda_W} = \sum_{\lambda_2} |H_{\lambda_2 \lambda_W}|^2.$$

Then "rotate" the density matrix. Rotation is from (x, y, z) to (x', y, z') by the angle θ around the y axis. The differential $\cos\theta$ rate reads

$$\frac{d\Gamma(\theta)}{d\cos\theta} \sim \sum_{\text{helicities}} |h_{\lambda_3 \lambda_4}|^2 \underbrace{d^1_{\lambda_W, \lambda_3 - \lambda_4}(\theta) \rho_{\lambda_W, \lambda_W} d^1_{\lambda_W, \lambda_3 - \lambda_4}(\theta)}_{\text{rotated density matrix } \rho'}$$

4.1 General polarized two-body decay

- Take the two particle decay $a \to b + c$ of a spin-J_a particle where the polarization of particle a in the frame (x, y, z) is given by $\rho_{\lambda_a \lambda'_a}$. Since we are also considering possible effects from azimuthal correlations one has to take into account the nondiagonal density matrix elements $\rho_{\lambda_a \lambda'_a}$ with $\lambda_a \neq \lambda'_a$.

- Consider a second frame (x', y', z') obtained from (x, y, z) by the rotation $R(\theta, \phi, 0)$ and whose z axis is defined by particle b. The polarization density matrix ρ' in the frame (x', y', z') is obtained by a "rotation" of the density matrix ρ from the frame (x, y, z) to the frame (x', y', z').

- The rate for $a \to b + c$ is then given by the sum of the decay probabilities $|h_{\lambda_b \lambda_c}|^2$ (with $\lambda_a = \lambda_b - \lambda_c$) weighted by the diagonal terms of the density matrix ρ' of particle a in the frame (x', y', z'). One has

$$\frac{d\Gamma_{a \to b+c}}{d\cos\theta\, d\phi} \sim \sum_{\lambda_a, \lambda'_a, \lambda_b, \lambda_c} |h_{\lambda_b \lambda_c}|^2 \underbrace{D^{J*}_{\lambda_a, \lambda_b - \lambda_c}(\theta, \phi)\, \rho_{\lambda_a, \lambda'_a}\, D^{J}_{\lambda'_a, \lambda_b - \lambda_c}(\theta, \phi)}_{\text{rotated density matrix } \rho'} \qquad (16)$$

where

$$D^{J}_{m, m'}(\theta, \phi) = e^{-im\phi} d^{J}_{m\, m'}(\theta).$$

- All master formulas discussed in this lecture can be obtained by a repeated application of the basic two-body formula.

5 T-odd contributions

Take again the cascade decay $\Xi^0 \to \Sigma^+(\to p\pi^0) + W^{-*}(\to \ell^- \nu_\ell)$ as an example. Using the master formula Eq. (1) one obtains, among others, contributions from the two helicity configurations [11]

$$(\lambda_\Sigma = 1/2, \lambda_W = 1; \lambda'_\Sigma = -1/2, \lambda'_W = 0) \quad \text{and} \quad (\lambda_\Sigma = -1/2, \lambda_W = 0; \lambda'_\Sigma = 1/2, \lambda'_W = 1).$$
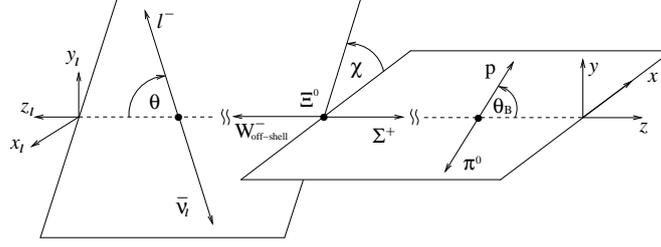
Figure 1: Definition of the polar angles θ and θ_B, and the azimuthal angle χ in the joint angular decay distribution of an unpolarized Ξ^0 in the cascade decay $\Xi^0 \to \Sigma^+ (\to p + \pi^0) + \ell^- + \bar{\nu}_l \ell$. The coordinate system (x_ℓ, y_ℓ, z_ℓ) is obtained from the coordinate system (x, y, z) by a 180° rotation around the y axis.

These will lead to the bilinear combinations

$$H_{\frac{1}{2}1} H^*_{-\frac{1}{2}0} e^{i(\pi-\chi)} + H_{-\frac{1}{2}0} H^*_{\frac{1}{2}1} e^{-i(\pi-\chi)}$$
$$= -2\cos\chi \operatorname{Re} H_{\frac{1}{2}1} H^*_{-\frac{1}{2}0} - 2\sin\chi \operatorname{Im} H_{\frac{1}{2}1} H^*_{-\frac{1}{2}0}.$$

Take the imaginary part contributions and put in the remaining θ- and θ_B-dependent trigonometric factors. One has two terms proportional to $\sin\chi$,

$$\sin\theta \sin\chi \sin\theta_B \operatorname{Im} H_{\frac{1}{2}1} H^*_{-\frac{1}{2}0} \qquad \text{and} \qquad \cos\theta \sin\theta \sin\chi \sin\theta_B \operatorname{Im} H_{\frac{1}{2}1} H^*_{-\frac{1}{2}0}. \qquad (17)$$

Rewrite the product of angular factors in terms of scalar and pseudoscalar products using the momentum representations in the (x, y, z) system. The normalized three-momenta are given by (see Fig. 1)

$$\hat{p}_{\ell^-} = (\sin\theta\cos\chi, \sin\theta\sin\chi, -\cos\theta), \qquad \hat{p}_W = (0, 0, -1),$$
$$\hat{p}_{\Sigma^+} = (0, 0, 1), \qquad \hat{p}_p = (\sin\theta_B, 0, \cos\theta_B),$$

where the three-momenta have unit length indicated by the hat notation.

The two angular factors (17) can be rewritten as

$$\sin\theta \sin\chi \sin\theta_B = \hat{p}_W \cdot (\hat{p}_{\ell^-} \times \hat{p}_p), \qquad (18)$$
$$\cos\theta \sin\theta \sin\chi \sin\theta_B = (\hat{p}_{\ell^-} \cdot \hat{p}_W) [\hat{p}_W \cdot (\hat{p}_{\ell^-} \times \hat{p}_p)] \qquad (19)$$

Under time reversal $(t \to -t)$ one has $(p \to -p)$. The above two invariants (18) and (19) involve an odd number of momenta, i.e. they change sign under time reversal. This has led to the notion of the so-called T-odd observables: Observables that multiply T-odd momentum invariants are called T-odd observables.

In the same vein we rewrite the angular factors multiplying $\cos\chi$. One finds

$$\sin\theta \cos\chi \sin\theta_B = \hat{p}_W \cdot \hat{p}_p + (\hat{p}_W \cdot \hat{p}_p)(\hat{p}_W \cdot \hat{p}_{\ell^-}),$$
$$\cos\theta \sin\theta \cos\chi \sin\theta_B = (\hat{p}_{\ell^-} \cdot \hat{p}_W)(\hat{p}_W \cdot \hat{p}_p + (\hat{p}_W \cdot \hat{p}_p)(\hat{p}_W \cdot \hat{p}_{\ell^-})).$$

There is an even number of momentum factors in the angular correlations involving $\cos\chi$, i.e. the momentum invariants correspond to T-even angular correlations.

The T-odd contributions can arise from two different sources. They can be contributed to by true CP-violating effects or by final state interaction effects (imaginary parts of loop contributions). One can distinguish between the two sources of T-odd effects by comparing with the corresponding antihyperon decays. Phases from CP-violating effects change sign whereas phases from final state interaction effects do not change sign when going from hyperon to antihyperon decays.

6 Two examples of polar angle decay distributions

6.1 The top quark decay $t \to b + W^+(\to \ell^+ + \nu_\ell)$

We are finally ready to derive the polar angle distribution $W(\theta) \sim L_{\mu\nu}H^{\mu\nu}$ in the decay $t \to b + W^+(\to \ell^+ + \nu_\ell)$ using helicity methods. We take the W^+ to be on-shell, i.e. the W^+ has three spin degrees of freedom with corresponding helicities $\lambda_W = \pm1, 0$. Heeding Eq. (16) one has

$$L_{\mu\nu}H^{\mu\nu} = \frac{1}{8} \sum_{\lambda_b,\lambda_W,\lambda_\ell} |H^{V-A}_{\lambda_b \lambda_W}|^2 \, d^1_{\lambda_W,\lambda_\ell+\frac{1}{2}}(\theta) \, d^1_{\lambda_W,\lambda_\ell+\frac{1}{2}}(\theta) \, |h^{V-A}_{\lambda_\ell,-\frac{1}{2}}|^2. \tag{20}$$

At the scale of the process one can put the lepton-side helicity flip amplitude to zero, i.e. $|h^{V-A}_{-\frac{1}{2},-\frac{1}{2}}|^2 = 0$. The helicity nonflip amplitude is given by $|h^{\frac{1}{2},-\frac{1}{2}}|^2 = 8m_W^2$. One obtains

$$L_{\mu\nu}H^{\mu\nu} = \frac{m_W^2}{4}\Big(|H^{V-A}_{\frac{1}{2}1}|^2(1+\cos\theta)^2 + 2(|H^{V-A}_{\frac{1}{2}0}|^2 + |H^{V-A}_{-\frac{1}{2}0}|^2)\sin^2\theta + |H^{V-A}_{-\frac{1}{2}1}|^2(1-\cos\theta)^2 \Big).$$

The corresponding three-fold angular decay distribution of polarized top decay $t(\uparrow) \to b + W^+(\to \ell^+ + \nu_\ell)$ [1, 2] can be derived with similar ease.

As emphasized in Sec. 3.2 the bilinear forms $\sum_{\lambda_b} |H^{V-A}_{\lambda_b \lambda_W}|^2$ ($\lambda_j = 1, 0, -1$) are the (unnormalized) density matrix elements of the on-shell W^+ in the W^+ rest frame. In their normalized form the density matrix elements $\sum_{\lambda_b} |\widehat{H}^{V-A}_{\lambda_b \lambda_j}|^2$ are usually referred to as the helicity fractions of the W^+ labelled by $\mathcal{H}_+$, $\mathcal{H}_0$ and $\mathcal{H}_-$. At the Born term level and for $m_b = 0$ one has ($y^2 = m_W^2/m_t^2$)

$$\mathcal{H}_+ : \mathcal{H}_0 : \mathcal{H}_- = 0 : \frac{1}{1+2y^2} : \frac{2y^2}{1+2y^2} = 0 : 0.70 : 0.30, \tag{21}$$

where we have used $m_t = 173.5\,\text{GeV}$. NLO and NNLO QCD corrections to the helicity fractions have been calculated in Refs. [1, 2] and in Ref. [22], respectively. Results on the NLO elctroweak corrections to the helicity fractions have been given in Ref. [13].

6.2 The decay $\Lambda_b(\uparrow) \to \Lambda + J/\psi(\to \ell^+\ell^-)$

There has been a longstanding interest to measure the polarization of hadronically produced hyperons, and charm and bottom baryons [24, 25]. Recently the LHCb Collaboration has measured the polarization of hadronically produced Λ_b's [26]. At the same time they measured ratios of squared helicity amplitudes in the decay $\Lambda_b(\uparrow) \to \Lambda + J/\psi$ through an analysis of polar correlations in the cascade decay process. Consider the three polar angles θ, θ_1 and θ_2 that characterize the cascade decay $\Lambda_b(\uparrow) \to \Lambda(\to p + \pi^-) + J/\psi(\to \ell^+\ell^-)$ (see Fig. 2)

By now we know how to write down the master formula for this three-fold polar angle distribution which could also be obtained by azimuthal integration of Eq. (1). Since I also want
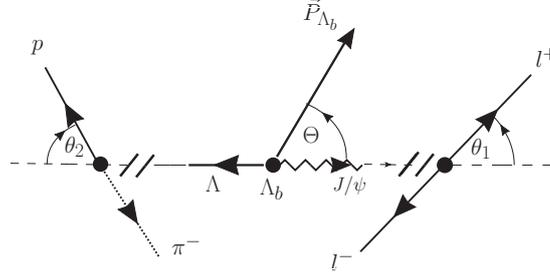
Figure 2: Definition of three polar angles in the decay $\Lambda_b(\uparrow) \to \Lambda(\to p + \pi^-) + J/\psi(\to \ell^+\ell^-)$

to discuss the decay $\Lambda_b(\uparrow) \to \Lambda(\to p + \pi^-) + \psi(2S)(\to \ell^+\ell^-)$ I use the generic notation V for the $J^{PC} = 1^{--}$ vector resonances J/ψ and $\psi(2S)$. In the $\psi(2S)$ mode one also has access to the decay $\psi(2S) \to \tau^+\tau^-$ which necessitates the incorporation of lepton mass effects in the decay distribution. One has

$$
W(\theta, \theta_1, \theta_2) \quad \propto \quad \frac{1}{2} \sum_{helicities} |h^V_{\lambda_1\lambda_2}|^2 \left[d^1_{\lambda_V, \lambda_1-\lambda_2}(\theta_2)\right]^2 \rho_{\lambda_b,\lambda_b}(\theta)
$$

$$
\times \; \delta_{\lambda_b, \lambda_V - \lambda_\Lambda} |H_{\lambda_\Lambda\lambda_V}|^2 \left[d^{1/2}_{\lambda_\Lambda\lambda_p}(\theta_1)\right]^2 |h^B_{\lambda_p,0}|^2,
$$

where λ_V is the helicity of the J/ψ or $\psi(2S)$. The lepton non-flip (n.f.) and flip (h.f.) helicity amplitudes for the parity conserving decays $V \to \ell^+\ell^-$ are given by

$$
\text{n.f.}: \qquad h^V_{-\frac{1}{2},-\frac{1}{2}} = h^V_{+\frac{1}{2},+\frac{1}{2}} = 2m_l, \qquad \text{h.f.}: \qquad h^V_{-\frac{1}{2},+\frac{1}{2}} = h^V_{+\frac{1}{2},-\frac{1}{2}} = \sqrt{2}m_V.
$$

We also know how to rotate the density matrix of the Λ_b from its production direction (perpendicular to the production plane)

$$
\rho_{\lambda_b\lambda'_b}(\theta_P) = \frac{1}{2} \begin{pmatrix} 1 + P_b \cos\theta_P & P_b \sin\theta_P \\ P_b \sin\theta_P & 1 - P_b \cos\theta_P \end{pmatrix}
$$

Since I am not considering azimuthal correlations in this application only the diagonal density matrix elements $\rho_{\lambda_b\lambda_b}$ are needed.

Next introduce the linear combinations of normalized helicity bispinors $|\widehat{H}_{\lambda_\Lambda\lambda_V}|^2$ (where $|\widehat{H}_{\lambda_\Lambda\lambda_V}|^2 = |H_{\lambda_\Lambda\lambda_V}|^2 / \sum_{\lambda_\Lambda,\lambda_V} |H_{\lambda_\Lambda\lambda_V}|^2$)

$$
\begin{aligned}
\alpha_b &= |\widehat{H}_{+\frac{1}{2}0}|^2 - |\widehat{H}_{-\frac{1}{2}0}|^2 + |\widehat{H}_{-\frac{1}{2}-1}|^2 - |\widehat{H}_{+\frac{1}{2}+1}|^2, \\
r_0 &= |\widehat{H}_{+\frac{1}{2}0}|^2 + |\widehat{H}_{-\frac{1}{2}0}|^2, \\
r_1 &= |\widehat{H}_{+\frac{1}{2}0}|^2 - |\widehat{H}_{-\frac{1}{2}0}|^2.
\end{aligned}
$$

We define $\varepsilon = m_\ell^2/m_V^2$ such that the velocity of the lepton is given by $v = (1 - 4\varepsilon)^{1/2}$.

The polar angle distribution can be written as

$$
\widetilde{W}(\theta, \theta_1, \theta_2) = \sum_{i=0}^{7} f_i(\alpha_b, r_0, r_1) \; g_i(P_b, \alpha_\Lambda) \; h_i(\cos\theta, \cos\theta_1, \cos\theta_2) \; \ell_i(\varepsilon). \tag{22}
$$

The functions f_i, g_i, h_i and ℓ_i are listed in the following table.

i	$f_i(\alpha_b, r_0, r_1)$	$g_i(P_b, \alpha_\Lambda)$	$h_i(\cos\theta, \cos\theta_1, \cos\theta_2)$	$\ell_i(\varepsilon)$
0	1	1	1	$v \cdot (1 + 2\varepsilon)$
1	α_b	P_b	$\cos\theta$	$v \cdot (1 + 2\varepsilon)$
2	$2r_1 - \alpha_b$	α_Λ	$\cos\theta_1$	$v \cdot (1 + 2\varepsilon)$
3	$2r_0 - 1$	$P_b\alpha_\Lambda$	$\cos\theta\cos\theta_1$	$v \cdot (1 + 2\varepsilon)$
4	$\frac{1}{2}(1 - 3r_0)$	1	$\frac{1}{2}(3\cos^2\theta_2 - 1)$	$v \cdot v^2$
5	$\frac{1}{2}(\alpha_b - 3r_1)$	P_b	$\frac{1}{2}(3\cos^2\theta_2 - 1)\cos\theta$	$v \cdot v^2$
6	$-\frac{1}{2}(\alpha_b + r_1)$	α_Λ	$\frac{1}{2}(3\cos^2\theta_2 - 1)\cos\theta_1$	$v \cdot v^2$
7	$-\frac{1}{2}(1 + r_0)$	$P_b\alpha_\Lambda$	$\frac{1}{2}(3\cos^2\theta_2 - 1)\cos\theta\cos\theta_1$	$v \cdot v^2$

The symbols in the table are

$$P_b \quad : \quad \text{polarization of } \Lambda_b$$
$$\alpha_b \quad : \quad \text{asymmetry parameter in the decay } \Lambda \to p + \pi^-$$

The overall factor v in the fifth column is the phase space factor for $V \to \ell^+\ell^-$. The factors $(1 + 2\epsilon)$ (S-wave dominance) and v^2 (($S - D$)-wave interference) were calculated by us for the first time. The LHCb Collaboration finds a very small polarization of the Λ_b [26]

$$P_b = 0.05 \pm 0.07 \pm 0.02.$$

Our results on helicity amplitudes for the transitions $\Lambda_b \to \Lambda$ [10] agree with the experimental results [26]. Our calculation is based on the confined covariant quark model developed by us (see e.g. Refs. [3, 10, 27, 28, 29]).

6.3 The confined covariant quark model in a nutshell

The confined covariant quark model provides a field theoretic frame work for the constituent quark model (see e.g. Refs. [3, 10, 27, 28, 29]). Its main features can be summarized as follows.

Particle transitions are calculated from Feynman diagrams involving quark loops. For example, the $\Lambda_b \to \Lambda$ transition is described by a two-loop diagram requiring a genuine two-loop calculation. The high energy behaviour of quark loops is tempered by nonlocal Gaussian-type vertex functions with a Gaussian-type fall-off behaviour. The particle-quark vertices have interpolating current structure. Use free local quark propagators $(m - \not{p})^{-1}$ in the Feynman diagrams. The normalization of the particle-quark vertices is provided by the compositeness condition which embodies the correct charge normalization of the respective hadron. The compositeness condition can be viewed as the field theoretic equivalent of the normalization of the wave function of a quantum mechanical state. A universal infrared cut-off provides for a effective confinement of quarks. There are no free quark poles in the Feynman diagrams.

HQET relations are recovered by using a static propagator for the heavy quark (k_1 is a loop momentum)

$$\frac{1}{m_b - \not{k}_1 - \not{p}_1} \quad \to \quad \frac{1 + \not{v}_1}{-2k_1v_1 - 2\bar\Lambda}.$$

7 Summary

The helicity method provides an easy and simple access to angular decay distributions in sequential cascade decays. Polarization and mass effects are readily incorporated. The corresponding techniques should belong to the basic tool kit of every experimentalist and theorist working in particle physics phenomenology.

Acknowledgements

References

[1] M. Fischer, S. Groote, J.G. Körner, M.C. Mauser and B. Lampe, Phys. Lett. **B451** (1999) 406

[2] M. Fischer, S. Groote, J.G. Körner and M.C. Mauser, Phys. Rev. **D65** (2002) 054036

[3] T. Gutsche, M.A. Ivanov, J.G. Körner, V.E. Lyubovitskij and P. Santorelli, Phys. Rev. **D87** (2013) 074031

[4] S. Berge, S. Groote and J.G. Körner, to be published

[5] A. Faessler, T. Gutsche, M.A. Ivanov, J.G. Körner and V.E. Lyubovitskij, Eur. Phys. J. direct **C4** (2002) 18

[6] J.G. Körner and M. Krämer, Phys. Lett. **B275** (1992) 495

[7] J.G. Körner and G.A. Schuler, Z. Phys. **C38** (1988) 511 [Erratum-ibid. C **41** (1989) 690]

[8] J.G. Körner and G.A. Schuler, Phys. Lett. **B231** (1989) 306

[9] J.G. Körner and G.A. Schuler, Z. Phys. **C46** (1990) 93

[10] T. Gutsche, M.A. Ivanov, J.G. Körner, V.E. Lyubovitskij and P. Santorelli, Phys. Rev. **D88** (2013) 114018

[11] A. Kadeer, J.G. Körner and U. Moosbrugger, Eur. Phys. J. **C59** (2009) 27

[12] M. Jeżabek and J.H. Kühn, Phys. Rev. **D48** (1993) 1910 [Erratum-ibid. D **49** (1994) 4970]

[13] H.S. Do, S. Groote, J.G. Körner and M.C. Mauser, Phys. Rev. **D67** (2003) 091501

[14] C.A. Dominguez, J.G. Körner and K. Schilcher, Phys. Lett. **B248** (1990) 399

[15] U. Nierste, S. Trine and S. Westhoff, Phys. Rev. **D78** (2008) 015006

[16] S. Fajfer, J.F. Kamenik and I. Nišandžić, Phys. Rev. **D85** (2012) 094025

[17] S. Groote, J.G. Körner and P. Tuvike, Phys. Part. Nucl. **45** (2014) 214

[18] A. Faessler, T. Gutsche, M.A. Ivanov, J.G. Körner and V.E. Lyubovitskij, Phys. Rev. **D80** (2009) 034025

[19] S. Groote, H. Liivat and I. Ots, Nucl. Phys. **B843** (2011) 213

[20] R. Zwicky, arXiv:1309.7802 [hep-ph]

[21] G. Hiller and R. Zwicky, arXiv:1312.1923 [hep-ph]

[22] A. Czarnecki, J.G. Körner and J.H. Piclum, Phys. Rev. **D81** (2010) 111503

[23] P. Bialas, J.G. Körner, M. Krämer and K. Zalewski, Z. Phys. **C57** (1993) 115

[24] R. Lednický, Sov. J. Nucl. Phys. **43** (1986) 817 [Yad. Fiz. **43** (1986) 1275]

[25] J. Hřivnáč, R. Lednický and M. Smižanská, J. Phys. **G21** (1995) 629

[26] R. Aaij *et al.* (LHCb Collaboration), Phys. Lett. **B724** (2013) 27

[27] T. Gutsche, M.A. Ivanov, J.G. Körner, V.E. Lyubovitskij and P. Santorelli, Phys. Rev. **D86** (2012) 074013

[28] M.A. Ivanov, J.G. Körner, S.G. Kovalenko, P.Santorelli and G.G. Saidullaeva, Phys. Rev. **D85** (2012) 034004

[29] S. Dubnicka, A. Z. Dubnickova, M. A. Ivanov, J. G. Körner and G.G. Saidullaeva, AIP Conf. Proc. **1343** (2011) 385

Small-x behavior of deep-inelastic structure functions $\mathbf{F}_2$ and $\mathbf{F}_2^{cc}$

Anatoly Kotikov

Bogolubov Laboratory of Theoretical Physics, JINR, 141980 Dubna, Russia

It is shown that in the leading twist approximation of the Wilson operator product expansion with "frozen" and analytic strong coupling constants, Bessel-inspired behavior of the structure functions F_2 and F_2^{cc} at small x values, obtained for a flat initial condition in the DGLAP evolution equations, leads to good agreement with the deep inelastic scattering experimental data from HERA.

1 Introduction

The experimental data from HERA on the deep-inelastic scattering (DIS) structure function (SF) F_2 [1, 2], its derivative $\partial \ln F_2 / \partial \ln(1/x)$ [3, 4] and the heavy quark parts F_2^{cc} and F_2^{bb} [5, 6, 7] enable us to enter into a very interesting kinematical range for testing the theoretical ideas on the behavior of quarks and gluons carrying a very low fraction of momentum of the proton, the so-called small-x region. In this limit one expects that the conventional treatment based on the Dokshitzer–Gribov–Lipatov–Altarelli–Parisi (DGLAP) equations [8] does not account for contributions to the cross section which are leading in $\alpha_s \ln(1/x)$ and, moreover, the parton distribution function (PDFs), in particular the gluon one, are becoming large and need to develop a high density formulation of QCD.

However, the reasonable agreement between HERA data and the next-to-leading-order (NLO) approximation of perturbative QCD has been observed for $Q^2 \geq 2$ GeV^2 (see reviews in [9] and references therein) and, thus, perturbative QCD could describe the evolution of F_2 and its derivatives up to very low Q^2 values, traditionally explained by soft processes.

The standard program to study the x behaviour of quarks and gluons is carried out comparing the experimental data with the numerical solution of the DGLAP equations [8] by fitting the QCD energy scale Λ and the parameters of the x-profile of partons at some initial Q_0^2 [10, 11]. However, to investigate exclusively the small-x region, there is the alternative of doing the simpler analysis by using some of the existing analytical solutions of DGLAP in the small-x limit [12]-[15]. It was pointed out in [12] that the HERA small-x data can be well interpreted in terms of the so-called doubled asymptotic scaling (DAS) phenomenon related to the asymptotic behaviour of the DGLAP evolution discovered many years ago [16].

The study of [12] was extended in [13]-[15] to include the finite parts of anomalous dimensions (ADs) of Wilson operators and Wilson coefficients[1]. This has led to predictions [14, 15] of the small-x asymptotic PDF form in the framework of the DGLAP dynamics, which were obtained starting at some Q_0^2 with the flat function

$$f_a(Q_0^2) \;=\; A_a \quad \text{(hereafter } a = q, g\text{)}, \tag{1}$$

---

[1]In the standard DAS approximation [16] only the AD singular parts were used.

where f_a are PDFs multiplied by x and A_a are unknown parameters to be determined from the data.

We refer to the approach of [13]-[15] as *generalized* DAS approximation. In this approach the flat initial conditions, Eq. (1), determine the basic role of the AD singular parts as in the standard DAS case, while the contribution from AD finite parts and from Wilson coefficients can be considered as corrections which are, however, important for better agreement with experimental data.

The use of the flat initial condition, given in Eq. (1), is supported by the actual experimental situation: low-Q^2 data [17, 18, 4] are well described for $Q^2 \leq 0.4$ GeV^2 by Regge theory with Pomeron intercept $\alpha_P(0) \equiv \lambda_P + 1 = 1.08$, closed to the adopted $(\alpha_P(0) = 1)$ one. The small rise of HERA data [1, 2, 18, 19] at low Q^2 can be explained, for example, by contributions of higher twist operators (see [15]).

The purpose of this paper is to demostrate a good agreement [20, 21, 22] between the predictions of the generalized DAS approach [14] and the HERA experimental data [1, 2] (see Figs. 1 and 2 below) and [5, 7] (see Fig. 4 below) for the structure functions F_2 and F_2^{cc}, respectively. We also compare the result of the slope $\partial \ln F_2 / \partial \ln(1/x)$ calculation with the H1 and ZEUS data [3, 4]. Looking at the H1 data [3] points shown in Fig. 3 one can conclude that $\lambda(Q^2)$ is independent on x within the experimental uncertainties for fixed Q^2 in the range $x < 0.01$. The rise of $\lambda(Q^2)$ linearly with $\ln Q^2$ could be tracted in strong nonperturbative way, i.e., $\lambda(Q^2) \sim 1/\alpha_s(Q^2)$. The analysis [23], however, demonstrated that this rise can be explained naturally in the framework of perturbative QCD.

The ZEUS and H1 Collaborations have also presented [4] the preliminary data for $\lambda(Q^2)$ at quite low values of Q^2. The ZEUS value for $\lambda(Q^2)$ is consistent with a constant ~ 0.1 at $Q^2 < 0.6$ GeV^2, as it is expected under the assumption of single soft Pomeron exchange within the framework of Regge phenomenology. It was important to extend the analysis of [23] to low Q^2 range with a help of well-known infrared modifications of the strong coupling constant. We used the "frozen" and analytic versions (see, [20]).

2   Generalized DAS approach

The flat initial condition (1) corresponds to the case when PDFs tend to some constant value at $x \to 0$ and at some initial value Q_0^2. The main ingredients of the results [14, 15], are:

- Both, the gluon and quark singlet densities [2] are presented in terms of two components (" $+$ " and " $-$ ") which are obtained from the analytic Q^2-dependent expressions of the corresponding (" $+$ " and " $-$ ") PDF moments.

- The twist-two part of the " $-$ " component is constant at small x at any values of Q^2, whereas the one of the " $+$ " component grows at $Q^2 \geq Q_0^2$ as

$$\sim e^\sigma, \quad \sigma = 2\sqrt{\left[\hat{d}_+ s - \left(\hat{D}_+ + \hat{d}_+ \frac{\beta_1}{\beta_0}\right) p\right] \ln\left(\frac{1}{x}\right)}, \quad \rho = \frac{\sigma}{2\ln(1/x)}, \qquad (2)$$

where σ and ρ are the generalized Ball–Forte variables,

$$s = \ln\left(\frac{a_s(Q_0^2)}{a_s(Q^2)}\right), \quad p = a_s(Q_0^2) - a_s(Q^2), \quad \hat{d}_+ = \frac{12}{\beta_0}, \quad \hat{D}_+ = \frac{412}{27\beta_0}. \qquad (3)$$

---

[2]The contribution of valence quarks is negligible at low x.

Hereafter we use the notation $a_s = \alpha_s/(4\pi)$. The first two coefficients of the QCD β-function in the $\overline{\text{MS}}$-scheme are $\beta_0 = 11 - (2/3)f$ and $\beta_1 = 102 - (114/9)f$ with f is being the number of active quark flavors.

Note here that the perturbative coupling constant $a_s(Q^2)$ is different at the leading-order (LO) and NLO approximations. Hereafter we consider for simplicity only the LO approximation[3], where the variables σ and ρ are given by Eq. (2) when $p = 0$.

2.1 Parton distributions and the structure function F_2

The SF F_2 and PDFs have the following form

$$F_2(x, Q^2) = e f_q(x, Q^2), \ \ f_a(x, Q^2) = f_a^+(x, Q^2) + f_a^-(x, Q^2), \ \ (a = q, g) \tag{4}$$

where $e = (\sum_1^f e_i^2)/f$ is the average charge square.

The small-x asymptotic results for PDFs $f_a^\pm$ are

$$f_g^+(x, Q^2) = \left(A_g + \frac{4}{9}A_q\right)I_0(\sigma)\, e^{-\overline{d}_+(1)s} + O(\rho), \ \ f_q^+(x, Q^2) = \frac{f}{9}\frac{\rho I_1(\sigma)}{I_0(\sigma)} + O(\rho),$$

$$f_g^-(x, Q^2) = -\frac{4}{9}A_q e^{-d_-(1)s} + O(x), \ \ f_q^-(x, Q^2) = A_q e^{-d_-(1)s} + O(x), \tag{5}$$

where I_ν ($\nu = 0, 1$) are the modified Bessel functions, $d_-(1) = 16f/(27\beta_0)$ and $\overline{d}_+(1) = 1 + 20f/(27\beta_0)$ is the regular part of AD $d_+(n)$ in the limit $n \to 1$. Here n is the variable in Mellin space.

2.2 Effective slopes

As it has been shown in [14], the behaviour of PDFs and F_2 given in the Bessel-like form by generalized DAS approach can mimic a power law shape over a limited region of x and Q^2

$$f_a(x, Q^2) \sim x^{-\lambda_a^{\text{eff}}(x, Q^2)} \ \ \text{and} \ \ F_2(x, Q^2) \sim x^{-\lambda_{F_2}^{\text{eff}}(x, Q^2)}.$$

The effective slopes $\lambda_a^{\text{eff}}(x, Q^2)$ and $\lambda_{F_2}^{\text{eff}}(x, Q^2)$ have the form:

$$\lambda_{F_2}^{\text{eff}}(x, Q^2) = \lambda_g^{\text{eff}}(x, Q^2) = \frac{f_g^+(x, Q^2)}{f_g(x, Q^2)}\, \rho\, \frac{\tilde{I}_1(\sigma)}{\tilde{I}_0(\sigma)} \approx \rho - \frac{1}{4\ln(1/x)},$$

$$\lambda_q^{\text{eff}}(x, Q^2) = \frac{f_q^+(x, Q^2)}{f_q(x, Q^2)}\, \rho\, \frac{\tilde{I}_2(\sigma)}{\tilde{I}_1(\sigma)} \approx \rho - \frac{3}{4\ln(1/x)}, \tag{6}$$

where the symbol $\approx$ marks the approximation obtained in the expansion of the modified Bessel functions, when the "$-$" component is negligible. These approximations are accurate only at very large σ values (i.e. at very large Q^2 and/or very small x).

---

[3]The NLO results may be found in [14, 15].

2.3 Structure functions F_2^{cc} and F_2^{bb}

In the framework of the photon-gluon fusion (PGF) process, the SFs F_2^{cc} and F_2^{bb} have the following form [24]

$$F_2^{ii}(x, Q^2) \approx M_{2,g}^i(1, Q^2, \mu^2) f_g(x, \mu^2), \quad (i = c, b) \tag{7}$$

where $M_{2,g}^i(1, Q^2, \mu^2)$ is the first Mellin moment of the so-called gluon coefficient function $C_{2,g}^i(x, Q^2, \mu^2)$. AT LO, it has the form [24]

$$M_{2,g}^i(1, c) = \frac{2}{3}[1 + 2(1 - c_i)J(c_i)] \tag{8}$$

with

$$J(c_i) = -\sqrt{b_i} \ln t_i, \qquad t_i = \frac{1 - \sqrt{b_i}}{1 + \sqrt{b_i}}, \qquad b_i = \frac{1}{1 + 4c_i}, \qquad c_i = \frac{m_i^2}{Q^2}. \tag{9}$$

3 Comparison with experimental data

Using the results of previous section we have analyzed HERA data for F_2 [1, 2] and F_2^{cc} [5, 7] and also the slope $\partial \ln F_2 / \partial \ln(1/x)$ [3, 4] at small x from the H1 and ZEUS Collaborations. In order to keep the analysis as simple as possible, we fix $f = 4$ and $\alpha_s(M_Z^2) = 0.1166$ (i.e., $\Lambda^{(4)} = 284$ MeV) in agreement with the recent ZEUS results in [1].

3.1 Structure function F_2

As it is possible to see in Figs. 1, 2 and 3, the twist-two approximation is reasonable at $Q^2 \geq 2 \div 4$ GeV^2. At smaller Q^2, some modification of the approximation should be considered.

In Refs. [20, 21], to improve the agreement at small Q^2 values, we modifed the QCD coupling constant. We have found a good agreement with experimental data at essentially lower Q^2 values: $Q^2 \geq 0.5$ GeV^2 (see Figs. 1 and 2).

We considered two modifications.

In one case, which is more phenomenological, we introduce freezing of the coupling constant by changing its argument $Q^2 \rightarrow Q^2 + M_\rho^2$, where M_ρ is the ρ-meson mass (see [20] and references therein). Thus, in the formulae of the Section 2 we should do the following replacement:

$$a_s(Q^2) \rightarrow a_{\mathrm{fr}}(Q^2) \equiv a_s(Q^2 + M_\rho^2) \tag{10}$$

The second possibility incorporates the Shirkov–Solovtsov idea [25] about analyticity of the coupling constant that leads to the additional its power dependence. Then, in the formulae of the previous section the coupling constant $a_s(Q^2)$ should be replaced as follows: ($k = 1$ and 2 at LO and NLO)

$$a_{\mathrm{an}}(Q^2) = a_s(Q^2) - \frac{1}{k\beta_0} \frac{\Lambda^2}{Q^2 - \Lambda^2} + \dots, \tag{11}$$

where the symbol $\dots$ stands for terms which are zero and negligible at $Q \geq 1$ GeV [25] at LO and NLO, respectively.
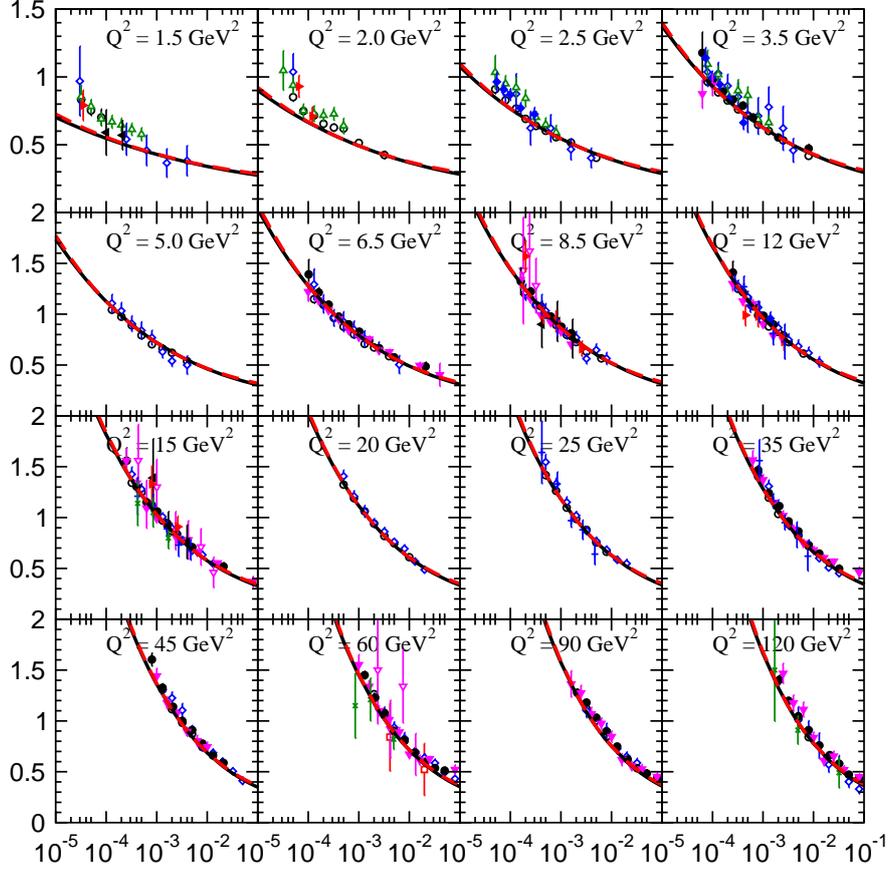
Figure 1: x dependence of $F_2(x, Q^2)$ in bins of Q^2. The experimental data from H1 (open points) and ZEUS (solid points) [1] are compared with the NLO fits for $Q^2 \geq 0.5$ GeV^2 implemented with the canonical (solid lines), frozen (dot-dashed lines), and analytic (dashed lines) versions of the strong-coupling constant.

3.2 Effective slopes

Figure 3 shows the experimental data for $\lambda_{F_2}^{\text{eff}}(x, Q^2)$ at $x \sim 10^{-3}$, which represents an average of the x-values of HERA experimental data. The top dashed line represents the aforementioned linear rise of $\lambda(Q^2)$ with $\ln(Q^2)$. The Figs. 1, 2 and 3 demonstrate that the theoretical description of the small-Q^2 ZEUS data for $\lambda_{F_2}^{\text{eff}}(x, Q^2)$ by NLO QCD is significantly improved by implementing the "frozen" and analytic coupling constants $\alpha_{\text{fr}}(Q^2)$ and $\alpha_{\text{an}}(Q^2)$, respectively, which in turn lead to very close results (see also [26]).

Indeed, the fits for $F_2(x, Q^2)$ in [15] yielded $Q_0^2 \approx 0.5$–0.8 GeV^2. So, initially we had $\lambda_{F_2}^{\text{eff}}(x, Q_0^2) = 0$, as suggested by Eq. (1). The replacements of Eqs. (10) and (11) modify the value of $\lambda_{F_2}^{\text{eff}}(x, Q_0^2)$. For the "frozen" and analytic coupling constants $\alpha_{\text{fr}}(Q^2)$ and $\alpha_{\text{an}}(Q^2)$, the value of $\lambda_{F_2}^{\text{eff}}(x, Q_0^2)$ is nonzero and the slopes are quite close to the experimental data at $Q^2 \approx 0.5$ GeV^2. Nevertheless, for $Q^2 \leq 0.5$ GeV^2, Fig. 3 shows that there is still some disagreement with the data, which needs additional investigation.
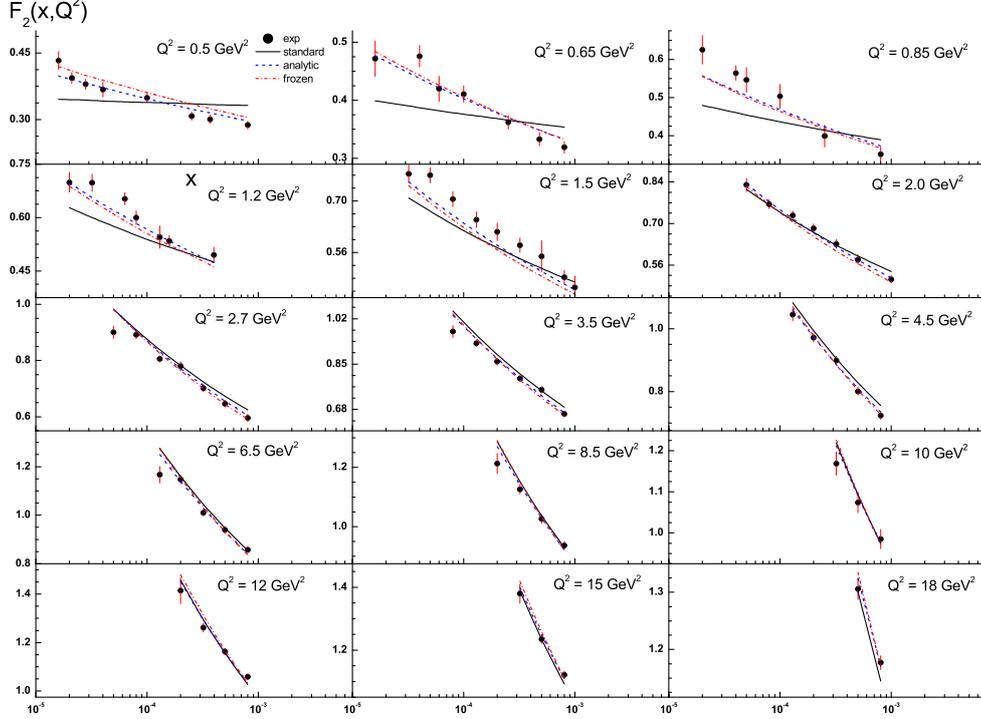
Figure 2: As in Fig.1 but for the combined H1&ZEUS exerimental data [2].

For comparison, we display in Fig. 3 also the results obtained by Kaidalov et al. [27] and by Donnachie and Landshoff [28] adopting phenomenological models based on Regge theory. While they yield an improved description of the experimental data for $Q^2 \leq 0.4$ GeV^2, the agreement generally worsens in the range 2 GeV$^2 \leq Q^2 \leq 8$ GeV^2.

The results of fits in [15, 20, 21] have an important property: they are very similar in LO and NLO approximations of perturbation theory. The similarity is related to the fact that the small-x asymptotics of the NLO corrections are usually large and negative (see, for example, α_s-corrections [29] to BFKL approach [30] [4]). Then, the LO form $\sim \alpha_s(Q^2)$ for some observable and the NLO one $\sim \alpha_s(Q^2)(1 - K\alpha_s(Q^2))$ with a large value of K, are similar because $\Lambda \gg \Lambda_{\mathrm{LO}}$ [5] and, thus, $\alpha_s(Q^2)$ at LO is considerably smaller then $\alpha_s(Q^2)$ at NLO for HERA Q^2 values.

In other words, performing some resummation procedure (such as Grunberg's effective-charge method [31]), one can see that the NLO form may be represented as $\sim \alpha_s(Q^2_{\mathrm{eff}})$, where $Q^2_{\mathrm{eff}} \gg Q^2$. Indeed, from different studies [32, 26], it is well known that at small-x values the effective argument of the coupling constant is higher then Q^2.

---

[4]It seems that it is a property of any processes in which gluons, but not quarks play a basic role.

[5]The equality of $\alpha_s(M_Z^2)$ at LO and NLO approximations, where M_Z is the Z-boson mass, relates Λ and Λ_{LO}: $\Lambda^{(4)} = 284$ MeV (as in ZEUS paper on [1]) corresponds to $\Lambda_{\mathrm{LO}} = 112$ MeV (see [15]).

Figure 3: As in Fig,1 but for the Q^2 dependence of $\lambda_{F_2}^{\mathrm{eff}}(x, Q^2)$ for an average small-x value of $x = 10^{-3}$. The linear rise of $\lambda_{F_2}^{\mathrm{eff}}(x, Q^2)$ with $\ln Q^2$ [3] 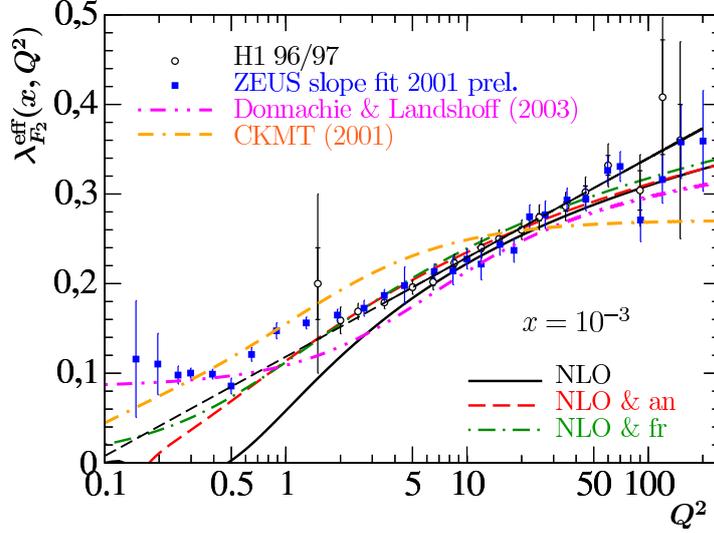is indicated by the straight dashed line. For comparison, also the results obtained in the phenomenological models by Kaidalov et al. [27] (dash-dash-dotted line) and by Donnachie and Landshoff [28] (dot-dot-dashed line) are shown.

3.3 Structure function F_2^{cc}

We are now in a position to explore the phenomenological implications of our results for SF F_2^{cc}. As for our input parameters, we choose $m_c = 1.25$ GeV in agreement with Particle Data Group [34]. In order to fix the unphysical mass scale μ, we put $\mu^2 = Q^2 + 4m_c^2$, which is the standart scale in heavy quark production.

The PDF parameters μ_0^2, A_q and A_g shown in (1), have been fixed in the fits of F_2 experimental data (see the subsection 3.1). Their values depend on conditions chosen in the fits: the order of perturbation theory and the number f of active quarks.

Below b-quark threshold, the scheme with $f = 4$ has been used [15, 20] in the fits of F_2 data. Note, that the F_2 structure function contains F_2^{cc} as a part. In the fits, the NLO gluon density and the LO and NLO quark ones contribute to F_2^c, as the part of to F_2. Then, now in PGF scattering the LO coefficient function (9) corresponds in $m \to 0$ limit to the standart NLO Wilson coefficient (together with the product of the LO anomalous dimension γ_{qg} and $\ln(m_c^2/Q^2)$. It is a general situation, i.e. the coefficient funstion of PGF scattering at some order of perturbation theory corresponds to the standart DIS Wilson coefficient with the one step higher order. The reason is following: the standart DIS analysis starts with handbag diagram of photon-quark scattering and photon-gluon interaction begins at one-loop level.

Thus, in our F_2^{cc} analysis in the LO approximation of PGF process we should take $f_a(x, Q^2)$ extracted from fits of F_2 data at $f = 4$ and NLO approximation. In practice, in [22] we have applied our $f = 4$ NLO twist-two fit [15] of H1 data for F_2 with Q^2 cut: $Q^2 > 1.5$ GeV^2, which produces $Q_0^2 = 0.523$ GeV^2, $A_g = 0.060$ and $A_q = 0.844$.

The results for F_2^{cc} are prsented in Fig.4. We can see a good agreement between our compact formulas (7) and (9) and the modern experimental data [5, 6, 7] for F_2^{cc}. To keep place on Fig.4,
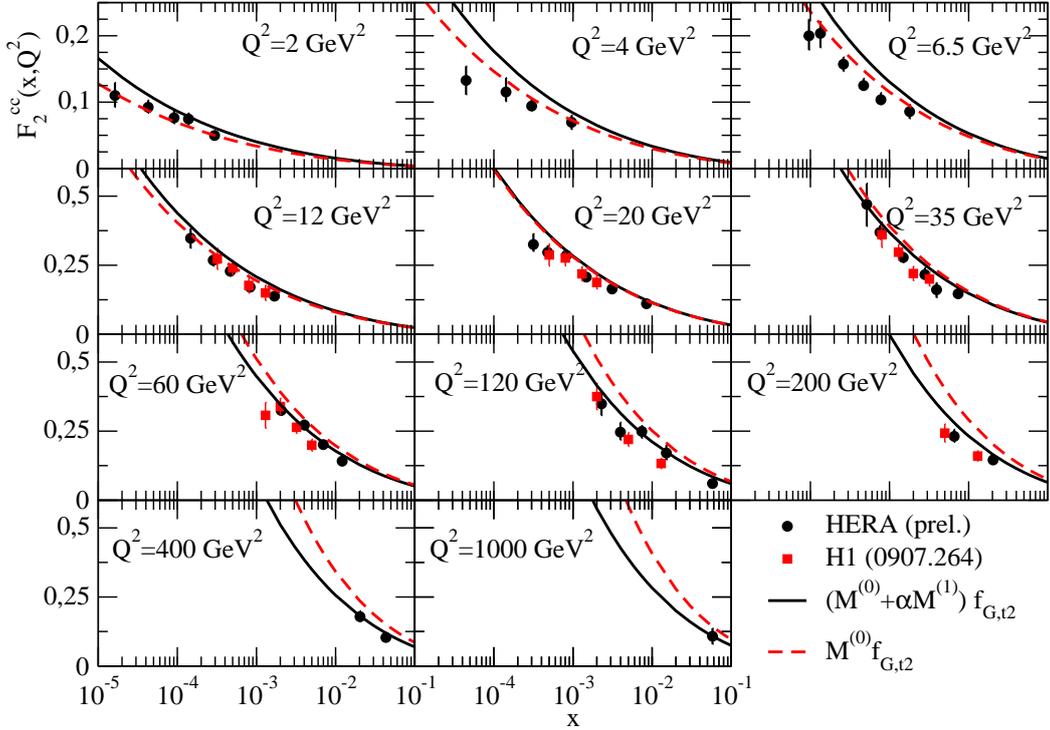
Figure 4: $F_2^{cc}(x, Q^2)$ evaluated as functions of x with the LO matrix elements (dashed lines) and with the NLO ones and with the factorization/renormalization scale $\mu^2 = Q^2 + 4m_c^2$ (solid lines). The black points and red squares correspond to the the combine H1ZEUS preliminary data [7] and H1 data [5], respectively.

we show only the H1 [5] data and the combine H1&ZEUS [7] one.

The good agreement between generalized double-asymptotic scaling DAS approach used here and F_2 and F_2^{cc} data demonstrates an equal importance of the both parton densities (gluon one and sea quark one) at low x. It is due to the fact that F_2 relates mostly to the sea quark distribution, while the F_2^{cc} relates mostly to the gluon one. Dropping sea quarks in analyse leads to the different gluon densities extracted from F_2 of from F_2^{cc} (see, for example, [33]).

4   Conclusions

We have shown the Q^2-dependence of the structure functions F_2 and F_2^{cc} and of the slope $\lambda_{F_2}^{\text{eff}} = \partial \ln F_2 / \partial \ln(1/x)$ at small-x values in the framework of perturbative QCD. Our twist-two results are in very good agreement with precise HERA data at $Q^2 \geq 2$ GeV^2, where perturbative theory can be applicable. The application of the "frozen" and analytic coupling constants $\alpha_{\text{fr}}(Q^2)$ and $\alpha_{\text{an}}(Q^2)$ improves the agreement at small Q^2 values, $Q^2 \geq 0.5$ GeV^2.

For the slope $\lambda_{F_2}^{\text{eff}}$ and for the structure function F_2^{cc}, our results agree with the corresponding experimental data [3, 4] and [5, 6, 7] well within errors without a free additional parameters. In the Q^2 range probed by the HERA data, our NLO predictions agree very well with the

LO ones. Since we worked in the fixed-flavour-number scheme, our results for F_2^{cc} are bound to break down for $Q^2 \gg 4m_c^2$, which manifests itself by appreciable QCD correction factors and scale dependences. As is well known, this problem is conveniently solved by adopting the variable-flavour-number scheme, which not considered here.

As a next step of investigations, we plan to add the BFKL corrections to our approach [14] (see appendix A in [35]) and to use our approach to analyse the cross sections of processes studied at LHC by analogy with our investigations [36] of the total cross section of ultrahigh-energy deep-inelastic neutrino-nucleon scattering.

References

[1] C. Adloff *et al.*, H1 Coll., Nucl.Phys. B497 (1997) 3; Eur.Phys.J. C21 (2001) 33; S. Chekanov *et al.*, ZEUS Coll., Eur.Phys.J. C21 (2001) 443.

[2] F.D. Aaron *et al.*, H1 and ZEUS Coll., JHEP 1001 (2010) 109.

[3] C. Adloff *et al.*, H1 Coll., Phys.Lett. B520 (2001) 183.

[4] T. Lastovicka, H1 Coll., Acta Phys.Polon. B33 (2002) 2835; B. Surrow, ZEUS Coll., hep-ph/0201025.

[5] F. D. Aaron *et al.*, H1 Coll., Phys. Lett. B686 (2010) 91; Eur. Phys. J. C65 (2010) 89.

[6] H. Abramowicz *et al.*, ZEUS coll., Eur. Phys. J. C69 (2010) 347; S. Chekanov *et al.*, ZEUS Coll., Eur. Phys. J. C65 (2010) 65.

[7] H. Abramowicz *et al.*, H1 and ZEUS Coll., Eur. Phys. J. C73 (2013) 2311.

[8] V.N. Gribov and L.N. Lipatov, Sov.J.Nucl.Phys. 15 (1972) 438, 675; L.N. Lipatov, Sov. J. Nucl. Phys. 20 (1975) 94; G. Altarelli and G. Parisi, Nucl.Phys. B126 (1977) 298; Yu.L. Dokshitzer, Sov. Phys. JETP 46 (1977) 641.

[9] A.M. Cooper-Sarkar *et al.*, Int.J.Mod.Phys. A13 (1998) 3385; A.V. Kotikov, Phys.Part.Nucl. 38 (2007) 1; [Erratum-ibid. 38 (2007) 828].

[10] W.K. Tung *et al.*, STEQ Coll., JHEP 0702 (2007) 053; A.D. Martin *et al.*, Phys.Lett. B652 (2007) 292; M. Gluck *et al.*, Phys.Rev. D77 (2008) 074002; S. Alekhin *et al.*, Phys.Rev. D81 (2010) 014032.

[11] A.V. Kotikov *et al.*, Z.Phys. C58 (1993) 465; G. Parente *et al.*, Phys.Lett. B333 (1994) 190; A.L. Kataev *et al.*, Phys.Lett. B388 (1996) 179; Phys.Lett. B417 (1998) 374; Nucl.Phys. B573 (2000) 405; A.V. Kotikov and V.G. Krivokhijine, Phys.At.Nucl. 68 (2005) 1873; B.G. Shaikhatdenov *et al.*, Phys.Rev. D81 (2010) 034008.

[12] R.D. Ball and S. Forte, Phys.Lett. B336 (1994) 77.

[13] L. Mankiewicz *et al.*, Phys.Lett. B393 (1997) 175.

[14] A. V. Kotikov and G. Parente, Nucl.Phys. B549 (1999) 242.

[15] A. Yu. Illarionov *et al.*, Phys.Part.Nucl. 39 (2008) 307.

[16] A. De Rújula *et al.*, Phys.Rev. D10 (1974) 1649.

[17] M. Arneodo *et al.*), NM Coll., Phys.Lett. B364 (1995) 107; Nucl.Phys. B483 (1997) 3; M.R. Adams *et al.*, E665 Coll., Phys.Rev. D54 (1996) 3006; A. Donnachie and P. V. Landshoff, Nucl.Phys. B244 (1984) 322; B267 (1986) 690; Z.Phys. C61 (1994) 139.

[18] J. Breitweg *et al.*, ZEUS Coll., Phys.Lett. B407 (1997) 432.

[19] J. Breitweg *et al.*, ZEUS Coll., Phys.Lett. B487 (2000) 53; Eur.Phys.J. C21 (2001) 443.

[20] G. Cvetic *et al.*, Phys.Lett. B679 (2009) 350.

[21] A. V. Kotikov and B. G. Shaikhatdenov, Phys. Part. Nucl. 44 (2013) 543.

[22] A. Y. .Illarionov and A. V. Kotikov, Phys. Atom. Nucl. 75 (2012) 1234.

[23] A.V. Kotikov and G. Parente, J. Exp. Theor. Phys. 97 (2003) 859.

[24] A. Y. Illarionov, B. A. Kniehl and A. V. Kotikov, Phys. Lett. B663 (2008) 66.

[25] D.V. Shirkov and I.L. Solovtsov, Phys.Rev.Lett 79 (1997) 1209.

[26] A.V. Kotikov *et al.*, J. Exp. Theor. Phys. 101 (2005) 811; Phys. Atom. Nucl. 75XS (2012) 507.

[27] A.B. Kaidalov *et al.*, Eur.Phys.J. C20 (2001) 301;

[28] A. Donnachie and P.V. Landshoff, Acta Phys.Polon. B34 (2003) 2989.

[29] V. S. Fadin and L. N. Lipatov, Phys.Lett. B429 (1998) 127; G. Camici and M. Ciafaloni, Phys.Lett. B430 (1998) 349; A.V. Kotikov and L.N. Lipatov, Nucl.Phys. B582 (2000) 19.

[30] L.N. Lipatov, Sov.J.Nucl.Phys. 23 (1976) 338; V.S. Fadin *et al.*, Phys.Lett. B60 (1975) 50; E.A. Kuraev *et al.*, Sov. Phys. JETP 44 (1976) 443; 45 (1977) 199; I.I. Balitsky and L.N. Lipatov, Sov.J.Nucl.Phys. 28 (1978) 822; JETP Lett. 30 (1979) 355.

[31] G. Grunberg, Phys.Rev. D29 (1984) 2315; Phys.Lett. B95 (1980) 70.

[32] Yu.L. Dokshitzer and D.V. Shirkov, Z.Phys. C67 (1995) 449; A.V. Kotikov, Phys.Lett. B338 (1994) 349; W.K. Wong, Phys.Rev. D54 (1996) 1094; S.J. Brodsky *et al.*, JETP. Lett. 70 (1999) 155; M. Ciafaloni *et al.*, Phys.Rev. D60 (1999) 114036; G. Altarelli *et al.*, Nucl.Phys. B621 (2002) 359; Bo Andersson *et al.*, Eur.Phys.J. C25 (2002) 77.

[33] H. Jung *et al.*, arXiv:0706.3793 [hep-ph]; arXiv:hep-ph/0611093.

[34] C. Amsler *et al.*, Particle Data Group, Phys. Lett. B667 (2008) 1.

[35] A. V. Kotikov, PoS Baldin -ISHEPP-XXI (2012) 033 [arXiv:1212.3733 [hep-ph]].

[36] R. Fiore *et al.*, Phys.Rev. D73 (2006) 053012; Phys.Rev. D71 (2005) 033002; Phys.Rev. D68 (2003) 093010; A. Y. Illarionov *et al.*, Phys.Rev.Lett. 106 (2011) 231802.

XYZ States - Results from Experiments

Sören Lange[1]

[1]Justus-Liebig-Universität Giessen, II. Physikalisches Institut
Heinrich-Buff-Ring 16, 35392 Giessen, Germany

1 Introduction

The static quark anti-quark potential in strong interaction is often expressed using the ansatz

$$
\begin{aligned}
V(r) \;=\; & -\frac{4}{3}\frac{\alpha_s}{r} + kr \\
& + \frac{32\pi\alpha_s}{9m_c^2}\delta(r)\vec{S_c}\vec{S_{\bar{c}}} \\
& + \frac{1}{m_c^2}\left(\frac{2\alpha_s}{r^3} - \frac{k}{2r}\right)\vec{L}\vec{S} \\
& + \frac{1}{m_c^2}\frac{4\alpha_s}{r^3}\left(\frac{3\vec{S_c}\vec{r}\cdot\vec{S_{\bar{c}}}\vec{r}}{r^2} - \vec{S_c}\vec{S_{\bar{c}}}\right) \quad .
\end{aligned}
\tag{1}
$$

For historic reasons, this potential is refered to as a Cornell-type potential [1] [2] [3]. The first term is a Coulomb-like term describing one-gluon exchange, which is very similar to the Coulomb term in QED potentials for e.g. positronium or the hydrogen atom, except that here the coupling constant is given by α_S instead of α_{em}. The second term is a linear term which phenomenologically describes QCD confinement, and which is completely absent in QED. The linear shape is e.g. supported by Lattice QCD calculations, and the parameter k is the string constant of QCD string between the quark and the anti-quark. The other terms represent spin-orbit, spin-spin and tensor potentials, leading to mass splittings in the spectrum.

Heavy quark combinations such as the charm anti-charm (called charmonium) and the beauty anti-beauty (called bottomonium) are in particular interesting, as they can be treated *(a)* as non-relativistic systems and *(b)* perturbatively due to $m_Q \gg \Lambda_{QCD}$, where $\Lambda_{QCD} \simeq 200$ MeV is the QCD scale.

Charmonium- and bottomonium spectroscopy has been a flourishing field recently, as many new states have been observed. Masses of expected states (such as the h_b, h_b', η_b, η_b', described below) have been measured accurately and enable precision tests of Eq. 1 to a level of $\Delta m/m \leq 10^{-4}$.

On the other hand, several non-expected states were found, which do not fit into the Cornell-type potential model prediction. While for many priorly observed charmonium and bottomonium states the difference between predicted and measured mass is impressively small in the order of $\Delta m \simeq$ 2-3 MeV, for some of the new states the closest predicted state is off by $\Delta m \geq 50$ MeV or more. Such states are often refered to as XYZ states. The Z states (as will

be described below) are in particular interesting, as they are charged states, and thus can not represent charmonium or bottomonium at all.

Many of the XYZ states were observed at the Belle [4] and BaBar [5] experiments in e^+e^- collisions at beam energies 10.5-11.0 GeV (i.e. in the Υ(nS) region). In this draft, at first charmonium-like states will be discussed, which are e.g. produced in B meson decays. Belle and BaBar are often called B meson factories, as the number of produced B mesons per time unit is very high. Often the size of a data sample is given as integrated lumnosity. With a typical instantenous luminosity of 1×10^{34} s^1 cm^2 and using 1 b("barn")=10^{24} cm^2, we get $\simeq1\times10^{-15}$ b^{-1} or $\simeq1$ fb^{-1} per 1 day. The center-of-mass energy of Belle and BaBar is $\sqrt{s}$=10.58 GeV, corresponding to the mass of the Υ(4S) resonance. The cross section is $\sigma(e^+e^-\rightarrow\Upsilon(4S))\simeq1$ nb, and thus we get about 1×10^6 produced B meson pairs per day.

Further below in this draft, examples for bottomonium-like states will be given, which are e.g. produced in radiative decays of Υ(nS) resonances. As an example of applications of the measurements, a few precision tests of the Cornell-type potential (Eq. 1) will be discussed. At the end, an outlook to a future experiment will be given, which will be able to measure the width of a state in the sub-MeV regime.

2 Charmonium(-like) states

2.1 The X(3872) state

The X(3872) state has been discovered in B meson decay in the decay X(3872) $\rightarrow J/\psi\pi^+\pi^-$ by Belle [6] and confirmed by other experiments [7] [8] [9] [10] [11]. Among the XYZ states, the X(3872) is the only one observed in several decay channels: X(3872)$\rightarrow J/\psi\pi^+\pi^-$, X(3872)$\rightarrow J/\psi\gamma$, X(3872)$\rightarrow J/\psi\pi^+\pi^-\pi^0$, X(3872)$\rightarrow D^0\overline{D}^0\pi^0$, and X(3872)$\rightarrow D^0\overline{D}^0\gamma$.
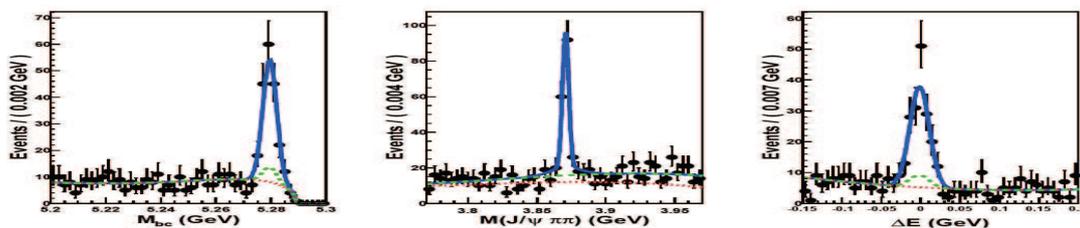
Figure 1: Beam constrained mass $M_{\mathrm{bc}}=\sqrt{(E_{beam}^{cms}/2)^2-(p_B^{cms})^2}$ (left) invariant mass $m(J/\psi\pi^+\pi^-)$ and the energy difference $\Delta E=E_B^{cms}-E_{beam}^{cms}$ for the decay $B^+\rightarrow K^+$X(3872)$(\rightarrow J/\psi\pi^+\pi^-)$. A 3-dimensional fit is performed. The blue line represents the fit result, which is used to extract the mass and the width of the X(3872).

The mass of the X(3872) can be determined with high precision. A recent mass measurement of the X(3872) at Belle was based upon the complete Belle data set of 711 fb^{-1} collected at the Υ(4S) resonance. Fig. 1 shows the beam constrained mass $M_{\mathrm{bc}}=\sqrt{(E_{beam}^{cms}/2)^2-(p_B^{cms})^2}$ (left, with the energy in the center-of-mass system E_{beam}^{cms} and the momentum of the B meson in the center-of-mass system p_B^{cms}), the invariant mass $m(J/\psi\pi^+\pi^-)$ (center) and the energy difference $\Delta E=E_B^{cms}-E_{beam}^{cms}$ (right, with the energy of the B meson in the center-of-mass

system E_B^{cms}). Data and fit (as a result of a 3-dimensional fit to the observables shown) for the decay $B^+ \rightarrow K^+ X(3872)(\rightarrow J/\psi \pi^+ \pi^-)$ are shown (blue line: signal, dashed green line: background). The fitted yield is 151±15 events. For details of the analysis procedure see [12]. The fitted mass is listed in Tab. 1 in comparison with mass measurements from other experiments.

The mass measurement reveals the surprising fact that the X(3872) is very close to the $D^{*0}\overline{D}^0$ threshold. Therefore it was discussed, if the X(3872) possibly represents an S-wave $D^{*0}\overline{D}^0$ molecular state [13]. In this case, the binding energy E_b would be given by the mass difference $m(X)-m(D^{*0})-m(D^0)$. Including the new Belle result, the new world average mass of the X(3872) is $m=3871.68\pm0.17$ MeV [14]. The present value for the sum of the masses is $m(D^0)+m(D^{*0})=3871.84\pm0.28$ MeV [14], Thus, a binding energy of $E_b=-0.16\pm0.33$ MeV can be calculated, which is enormously small. In addition, E_b is inverse proportional to the squared scattering length a [15]:

$$E_b = \frac{\hbar^2}{2\mu a^2} \tag{2}$$

using the reduced mass μ. The radius can in first order be approximated by $<r>=a/\sqrt{2}$. This would surprisingly mean a very large radius $<r>\geq10^{+\infty}_{-5}$ fm of the molecular state.

Experiment	Mass of X(3872)	
CDF2	3871.61±0.16±0.19 MeV	[8]
BaBar (B^+)	3871.4±0.6±0.1 MeV	[7]
BaBar (B^0)	3868.7±1.5±0.4 MeV	[7]
D0	3871.8±3.1±3.0 MeV	[9]
Belle	3871.84±0.27±0.19 MeV	[12]
LHCb	3871.95±0.48±0.12 MeV	[10]
New World Average	3871.68±0.17 MeV	[14]

Table 1: Mass measurements of the X(3872).

An important decay of the X(3872) is the radiative decay X(3872)$\rightarrow J/\psi\gamma$. The observation of this decay was reported by Belle with a data set of 256 fb^{-1}, a yield of 13.6±4.4 events and a statistical significance of 4.0σ [16]. The combined branching ratio was measured to $BR(B^\pm \rightarrow XK^\pm, X\rightarrow \gamma J/\psi)= (1.8\pm0.6\pm0.1)\times10^{-6}$), i.e. the branching fraction of X(3872)$\rightarrow J/\psi\gamma$ is a factor $\simeq6$ smaller than the one for X(3872)$\rightarrow J/\psi\pi^+\pi^-$, and thus this decay represents a rare decay. However, the decay is very important, as it represents a decay into two neutral particles, which are identical to their anti-particles. Therefore observation of the decay implies, that the charge conjugation of the X(3872) must be C=+1. BaBar was able to confirm the observation with a data set of 260 fb^{-1}, a yield of 19.4±5.7 events and a statistical significance of 3.4σ [17]. Charmonium states with C=+1 are interesting objects. While decay widths (which can be measured by branching fractions in the experiment) for C=−1 states scale with the squared modulus of the wave function ($\Gamma\sim|\Psi(r=0)|^2$), decay widths of C=+1 states scale with the squared modules of the *derivative* of the wave function ($\Gamma\sim|\partial\Psi/\partial r(r=0)|^2$).

An additional surprising property of the X(3872) is isospin violation. It was found, that in the decay X(3872)$\rightarrow J/\psi\pi^+\pi^-$ the invariant mass peaks at the mass of the ρ^0 meson. The

ρ^0 carries isospin I=0, but the initial state (if assumed to be a pure $c\bar{c}$ state) has I=0 (as it would not contain any u or d valence quarks). There are only two additional isospin violating transitions known in the charmonium system [14], namely $\psi'\to J/\psi\pi^0$ ($\mathcal{B}$=1.3±0.1·10^{-3}) and $\psi'\to h_c\pi^0$ ($\mathcal{B}$=8.4±1.6·10^{-4}). These branching fractions are very small. One of the mechanisms to induce isospin violation is the u/d quark mass difference in strong interaction. However, as the mass difference is small, the effect should be very small, consistent with the the measured branching fractions. Another possible mechanism to induce isospin violation is the u/d quark charge difference in electromagnetic interactions (EM). Isospin should only be conserved in strong interaction, but not in EM interaction. Thus one of the possible explanations might be, that the decay X(3872)$\to J/\psi\rho(\to\pi^+\pi^-)$ is proceeding via EM interaction, i.e. the ρ might not be created be two gluons, but by a virtual photon. However, then the decay should be suppressed by an additional factor $\alpha_{em}/\alpha_S\simeq$10. The observation for the X(3872) is different: the branching fraction of isospin violating transistion is (among the known decays) order of O(10%) and thus seems to be largely enhanced.

2.2 The Y(4260) family

	BaBar [18]	CLEO-c [19]	Belle [20]	Belle [21]	BaBar [22]	BaBar [23]
$\mathcal{L}$	211 fb^{-1}	13.3 fb^{-1}	553 fb^{-1}	548 fb^{-1}	454 fb^{-1}	454 fb^{-1}
N	125±23	$14.1^{+5.2}_{-4.2}$	165±24	324±21	344±39	–
Significance	$\simeq 8\sigma$	$\simeq 4.9\sigma$	$\geq 7\sigma$	$\geq 15\sigma$	–	–
m / MeV	$4259\pm 8^{+2}_{-6}$	$4283^{+17}_{-16}\pm 4$	$4295\pm 10^{+10}_{-3}$	$4247\pm 12^{+17}_{-32}$	$4252\pm 6^{+2}_{-3}$	$4244\pm 5\pm 4$
Γ / MeV	$88\pm 23^{+6}_{-4}$	70^{+40}_{-25}	$133\pm 26^{+13}_{-6}$	$108\pm 19\pm 10$	$105\pm 18^{+4}_{-6}$	$114^{+16}_{-15}\pm 7$

Table 2: Summary of the mass and width measurements of the Y(4260).

Another new charmonium-like state was observed by BaBar and confirmed by several experiments (see Tab. 2 for a list of the measured masses and widths) at a high mass of $m\simeq$4260 MeV, far above the $D\bar{D}$ threshold. The width is ≤100 MeV, which is quite narrow for such a high state. The observed decay is again a $\pi^+\pi^-$ transition to the J/ψ, similar to the above mentioned decay of the X(3872). However, the production mechanism is not B meson decay but instead ISR (initial state radiation), i.e. $e^+e^-\to\gamma_{ISR}$Y(4260), i.e. a photon is radiated by either the e^+ or the e^- in the initial state, lowering the $\sqrt{s}$ and producing the Y(4260) by a virtual photon. In fact, not only one state, but four states have been observed and are shown in Fig. 2, i.e. the Y(4008), the Y(4260), the Y(4250) and the Y(4660). In a search by Belle no additional state up to $m\leq$7 GeV was found. All the Y states must have the quantum numbers J^{PC}=1^{--}, due to the observation in an initial state radiation process. As an intriguing fact, there are known and assigned J^P=1^{--} charmonium states: J/ψ, $\psi(2S)$, $\psi(4040)$, $\psi(4160)$ and $\psi(4415)$. Thus, there is a clear over-population of 1^{--} states in the $m\geq$4 GeV region. Despite partial overlap, apparently there seems to be no mixing: *(a)* no mixing among them, i.e. the Y(4008) and the Y(4260) decay to $J/\psi\pi^+\pi^-$, and the Y(4350) and the Y(4660) decay to $\psi'\pi^+\pi^-$, and neither of one has been observed in the other channel, and *(b)* no mixing with ψ states with the Y states was observed so far. The pattern of the Y states appears non-trivial (see Fig. 3): two non-mixing doublets without parity flip and without charge flip. It remains completely unclear what the underlying symmetry is. In addition, there is no obvious pattern so far, how the masses of the ψ states and the masses of the Y states might be related.

Figure 2: Observations of the Y states. Invariant mass $m(J/\psi\pi^+\pi^-)$ at Belle [21] (top left) and at BaBar [22] (bottom left). Invariant mass $m(\psi'\pi^+\pi^-)$ at Belle [24] (top right) and at BaBar [25] (bottom right). Different curves indicate different fits with or without interference.

Due to their high masses, the Y states have been discussed as possible hybrid states [26]. In fact, the lowest lying $[cg\bar{c}]$ $J^P=1^{--}$ state was predicted by lattice QCD to have a mass $m\simeq4.3$ GeV [27]. The interpretation as a hybrid is supported by the fact, that the decay $Y(4260)\rightarrow e^+e^-$ has not been observed yet. However, it should be allowed, as $J^{PC}=1^{--}$ allows coupling to a virtual photon and subsequent $\gamma^*\rightarrow e^+e^-$. BaBar determined a very small partial decay width $\Gamma(Y(4260)\rightarrow J/\psi\pi^+\pi^-)\times\Gamma(e^+e^-)/\Gamma_{total} = (7.5\pm0.9\pm0.8)$ eV [22]. This should be compared to e.g. $\Gamma(\psi'\rightarrow J/\psi\pi^+\pi^-)\times\Gamma(e^+e^-)/\Gamma_{total} = (789\pm15)$ eV [14], which is a factor $\simeq10^2$ higher. A possible reason in the hybrid interpretation is, that the decay may be blocked by the valence gluon.

2.3 The X(4630) state

A state which is probably identical to the Y(4660) has also been observed at Belle [28] in the ISR production process with a data set of 670 fb^{-1}, but in the different decay channel, i.e. the signal was observed in $e^+e^-\rightarrow\gamma_{ISR}\Lambda_c^+\Lambda_c^-$. The state is usually refered to as X(4630). The Λ_c^+ is reconstructed in the final states $pK_s^0(\rightarrow\pi^+\pi^-)$ $pK^-\pi^+$ and $\Lambda(\rightarrow p\pi^-)\pi^+$. For the Λ_c^- only partial reconstruction is used: The recoil mass to $[\Lambda_c^+\gamma]$ is investigated while requiring an anti-proton (from the Λ_c^- decay) as a tag and then a cut around the Λ_c^- mass is applied. The
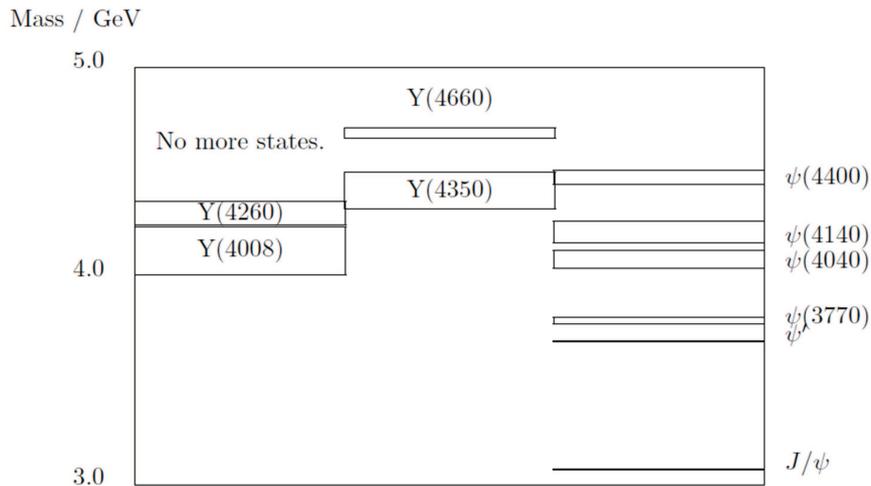
Figure 3: Level scheme for $J^{PC}=1^{--}$ states: states decaying into $J/\psi\pi^+\pi^-$ (left column), states decaying into $\psi'\pi^+\pi^-$ (center column), and known ψ states (radial quantum number $n=1,...,6$).

measured mass is $m=4634^{+8+5}_{-7-8}$ Mev and the measured width $\Gamma=92^{+40+10}_{-24-21}$ MeV. Fig. 4 shows the invariant mass $m(\Lambda_c^+\Lambda_c^-)$. A signal with a statistical significance of 8.2σ is observed. The observation of this state is remarkable because of two reasons:

- It is the highest charmonium state observed so far (together with the Y(4660) of almost same mass, but decaying into $J/\psi\pi^+\pi^-$), and

- the only new state so far observed to decay into baryons.

The potential model has an important boundary condition for the radial wave function, which is called the turning point R_{tp} and can be calculated as

$$R_{tp} = \frac{E-2m}{2\sigma} + \sqrt{\frac{4m^2-4mE+E^2}{4\sigma^2} + \frac{4\alpha_S}{3\sigma}} \qquad (3)$$

using $\sigma=\hbar ck$ with the string constant k. This is the radius, at which *(a)* the Wronski determinant must be zero and *(b)* the radial wave function changes into an asymtotic, exponential tail. For a box potential, the turning point would be identical to r_{box}, and the exponential tail of the wave function would be outside the box. Fig. 5 shows the turning point radius as a function of the mass. For the X(4630), if it is a charmonium state, the turning point is at $r_{turningpoint} > 2.1$ fm. However, a radius of $r \simeq 1.25$ fm marks the QCD string breaking regime. Thus, if the Y(4660) or the X(4630) are charmonium states, it is unclear, how such a large part of the wave function of a bound state can be in the string breaking regime. In any case, if it is a charmonium state, the radial quantum number must be $n \geq 4$.
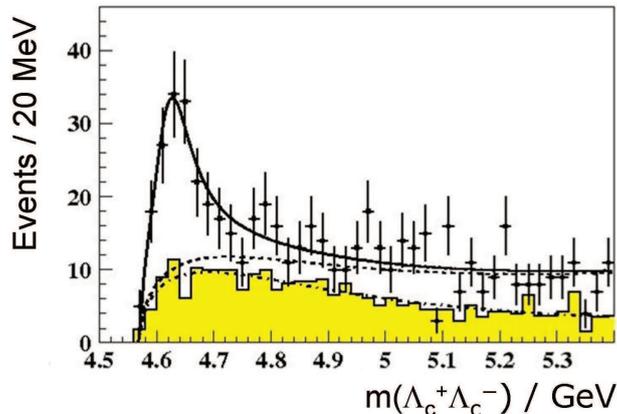
Figure 4: Invariant mass $m(\Lambda_c^+\Lambda_c^-)$ for the process $e^+e^-\to\gamma_{ISR}\Lambda_c^+\Lambda_c^-$ at Belle [28] showing the signal for the X(4630).

2.4   The $Z_c(3900)$ state

A new state, tentatively called the $Z_c^+(3900)$, was observed by BESIII [29] in the decay of the Y(4260)$\to Z_c^+(3900)\pi^\pm$ in a data set of 525 pb^{-1}. BESIII is operating with center-of-mass energies in the charmonium mass region, and producing the Y(4260) directly via $e^+e^-\to$Y(4260) at $\sqrt{s}$=4.26 GeV. Importantly the $Z_c^+(3900)$ is a charged state, and thus can not be a charmonium state. A charged combination could be formed by a state composed of four quarks. This may be tetraquark state (such as $[cu\bar{c}\bar{d}]$) or a molecular state (such as $D^\pm\overline{D}^{0*}$). The $Z_c^+(3900)$ was reconstructed in the decay to $J/\psi\pi^\mp$. Fig. 6 (left) shows the observed signal, which has a statistical significance of $>8\sigma$. From the two charged pions, the one is used, which gives the higher invariant mass for $J/\psi\pi^\pm$, in order to remove combinatorical background from the charged pion of the Y(4260) transition to the new state. The measured mass is m=3899.0$\pm$3.6$\pm$4.9 MeV and the measured width Γ=46$\pm$10$\pm$20 MeV. The observation of this new state is remarkable because this state seems to provide for the first time a connection between the Z states and the Y states, possibly pointing to the same interpretation of their nature. Only a few days later, the state was confirmed by Belle [30] in the same decay channel $J/\psi\pi^\mp$ and also in Y(4260) decays, while in the Belle case the Y(4260) was produced in the ISR process $\Upsilon(nS)\to\gamma_{ISR}$Y(4260). The measure mass of m=3894.5$\pm$6.6$\pm$4.5 MeV and width Γ=63$\pm$24$\pm$26 MeV are both consistent with the BESIII measurement. Fig. 6 (right) shows the observed signal, which has a statistical significance of $>8\sigma$ in a data set of 967 fb^{-1}. Again, as the $Z_c^+(4430)$, the state was observed as $Z_c^+(3900)$ and $Z_c^-(3900)$ with about the same yield [29], indicating a doublet. Concerning the quantum numbers, remarkably the isospin must be I=1, (as the isospin of the pion is I=1), if we assume I=0 for the Y(4260). If the heavy meson pair is assumed to be in the S-wave, the spin-parity of the state is uniquely determined as J^P=1$^+$. C-parity $(-1)^{L+S}$ is only defined for neutral particles, thus there can only be a G-parity assignment to the $Z_c^+(3900)$. The G-parity $(-1)^{L+S+I}$ with L=0, S=1 and I=1 thus gives G=+. As G-parity should be preserved in strong decays, this assignment, due to the G-parity G=$-$ for the pion, has the interesting implication that the Y(4260) would have G=$-$. This would be compatible with an
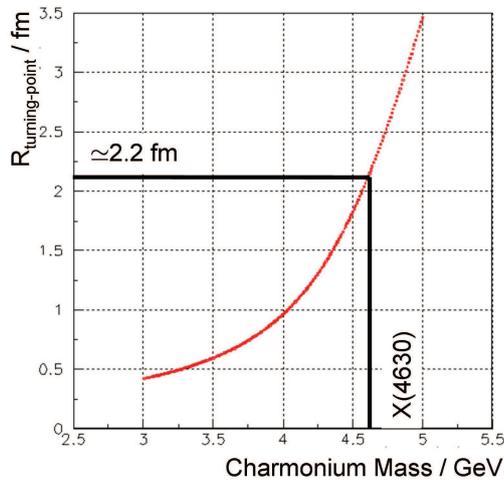
Figure 5: Radius of the turning point of a $c\bar{c}$ wave function in the Cornell potential vs. the charmonium mass.

I=0 isosinglet assignment for the Y(4260), which has the important implication, that there is no charged partner of the Y(4260) existing.

2.5 A D-wave state

Belle investigated the decay $B^+ \to K^+ \chi_{c1} \gamma$ with $\chi_{c1} \to J/\psi \gamma$ using a data set of 711 fb^{-1} [31]. A search for charmonium(-like) states decaying to $\chi_{c1}\gamma$ was performed. Fig. 7 shows the invariant mass $m(\chi_{c1}\gamma)$. In other words, the search was based upon a sequence of two radiative decays with both ΔL=1. The radiative transition also flips the parity due to the quantum numbers of the photon J^P=1^-, and therefore the requirement of the intermediate χ_{c1} with positive parity. A new state at a mass of 3823.1±1.8±0.7 MeV was observed with a 3.8σ significance. The product branching fraction was measured as $\mathcal{B}(B^+ \to K^+ X(3820)) \times \mathcal{B}(X(3820) \to \chi_{c1}\gamma)=$ $(9.7^{+2.8+1.1}_{2.5\ 1.0}) \times 10^4$, which is a factor $\simeq 10$ larger than e.g. the sum of all measured product branching fractions of the X(3872). The observed state might be one of the charmonium D-wave (L=2) states, as such states should primarily decay radiatively to χ_{cJ} states by L=2$\to L$=1 transitions and according branching fractions should be high $\geq$50% [32] [33]. There are four expected n=1 D-wave states: the η_{c2} ($^1D_2$) with J^{PC}=2^{-+} and $\psi_{1,2,3}$ ($^3D_{1,2,3}$) with J^{PC}=1,2,3^{--}. The prediction [3] for the ψ_1 ($^3D_1$) of 3.7699 GeV is much lower than the observed X(3820). The ψ_3 ($^3D_3$) can not decay radiatively by an E1 transition and should thus be suppressed. The η_{c2} ($^1D_2$) would require a spin-flip in the transition, and should be suppressed as well. The only candidate, which fulfills all the required properties, is the ψ_2 ($^3D_2$) state with J^{PC}=2^{--} and a predicted mass 3.838 MeV [3], which is close to the observed mass. In addition, the ψ_2 is predicted to be narrow $\Gamma \simeq$300-400 keV [32], consistent with a preliminary measured width Γ=4±6 MeV. As the observed state is above the open charm thresholds (3730 MeV for $D^0\overline{D}^0$ and 3739 MeV for D^+D^-, respectively), decays into final states with charm should be expected. However, for the ψ_2 the decay $2^{--} \to 0^{-+}0^{-+}$ with ΔL=2 (i.e. $(-1)^L$=$+1$) is forbidden
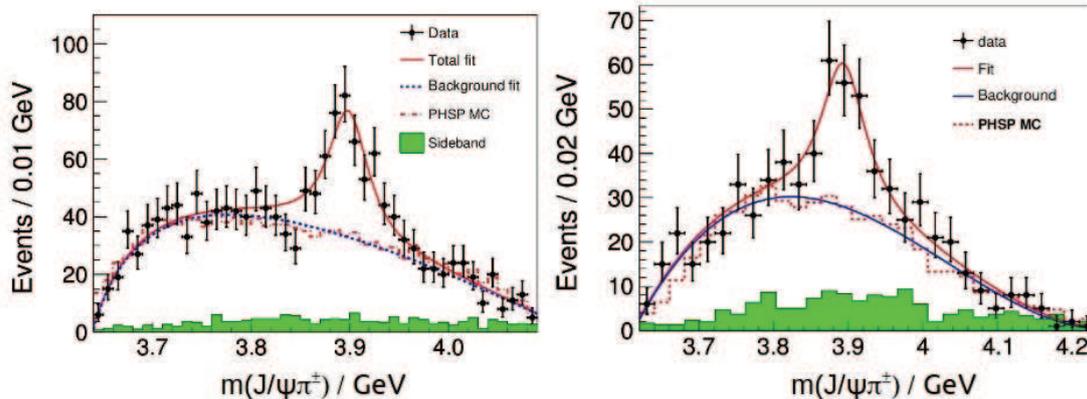
Figure 6: $J/\psi\pi^{\mp}$ invariant mass in Y(4260) decays, indicating the Z_c^+(3900) signal for BESIII (left) [29] and Belle (right) [30]. For details see text.

by parity conservation, and thus other decays (such as the observed one) should be enhanced. This mechanism could explain the high observed branching fraction into $J/\psi\gamma\gamma$. Note that the decays to $D\overline{D}^*$ or $D^*\overline{D}^*$ are forbidden by energy conservation. The observed product branching fraction is consistent with a calculation with color-octet amplitudes [34] predicting $\mathcal{B}(B\rightarrow K^3D_2)\times \mathcal{B}(^3D_2\rightarrow\chi_{c1}\gamma)= (3.7-7.5)\times10^{-4}$.

3 Bottomonium(-like) states

3.1 The h_b(1P) and the h_b(2P)

In a recent analysis by Belle, a particular technique was used, namely the study of *missing mass* to a $\pi^+\pi^-$ pairs in Υ(5S) decays [35]. Fig. 8 shows the background-subtracted missing mass for a Υ(5S) data set of 121.4 fb^{-1}. Among several known states such as the Υ(1S), Υ(2S), Υ(3S) and Υ(1D), there are addititional peaks arising from the transistions Υ(3S)$\rightarrow\Upsilon$(1S)$\pi^+\pi^-$ Υ(2S)$\rightarrow\Upsilon$(1S)$\pi^+\pi^-$, with the Υ(3S) and Υ(2S) being produced in the decay of the primary Υ(5S). In addition to the expected signals, first observations of the bottomonium singlet P-wave states h_b(1P) and h_b(2P) were made. Their measured masses are m=9898.3±1.1$^{+1.0}_{-1.1}$ MeV and m=10259.8±0.6$^{+1.4}_{-1.0}$ MeV, respectively. The red, dashed lines in Fig. 8 indicate regions of different paramtrisations of the background. For the h_b, this measurement is consistent with the first evidence (3.1σ stat. significance) by BaBar in Υ(3S) decays with a mass of 9902±4(stat.)±2(syst.) MeV [36]. The masses can be compared to predictions from potential model calculations [37] with 9901 MeV and 10261 MeV, respectively, i.e. the deviations are only 2.7 MeV and 1.2 MeV.

3.2 The η_b(1S) and the η_b(2S)

The $\eta_b(1S)$ is the bottomonium ground state 1^1S_0 with J^{PC}=0^{-+}. It was discovered by BaBar in the radiative decay $\Upsilon(3S)\rightarrow\gamma\eta_b$. The measured mass was 9388.9$^{+3.1}_{-2.3}$(stat)±2.7(syst) MeV,
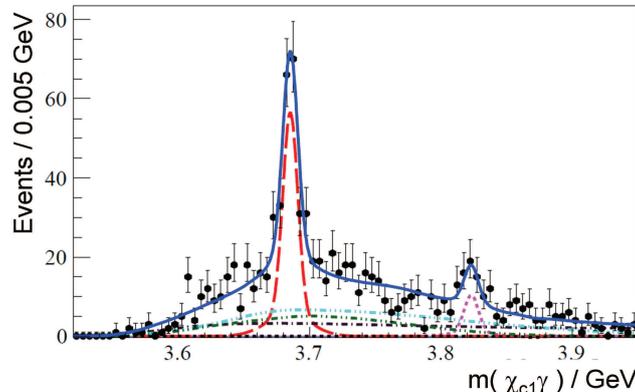
Figure 7: Invariant mass $m(\chi_{c1}\gamma)$ in B meson decays at Belle [31] showing the signal of the $^3D_2$ charmonium candidate X(3820). The dashed, dotted and dash-dotted line represent different backgrounds (combinatorial, peaking and non-peaking background from ψ' and X(3872) decays other than $\chi_{cJ}\gamma$, respectively, where the term peaking refers to peaking in m_{BC}).

The observation was confirmed by CLEO III using 6 million Upsilon(3S) decays with a measured mass m=9391.8±6.6±2.0 MeV. The observation of the h_b (see above) by Belle also enabled a search for the radiative decay $h_b(1P)\rightarrow\eta_b(1S)\gamma$, which was observed with a very high significance >13σ in a dataset of 133.4 fb^{-1} at the $\Upsilon(5S)$ and in the nearby continuum [38]. In addition, even the $\eta_b(2S)$ was observed in $h_b(2P)\rightarrow\eta_b(2S)\gamma$. Fig. 9 shows the $\pi^+\pi^-\gamma$ missing mass for the case of the $\eta_b(1S)$ (left) and $\eta_b(2S)$ (right), where the charged pion pair originates from the transition $\Upsilon(5S)\rightarrow h_b(1P,2P)\pi^+\pi^-$. The measured masses are $m(\eta_b(1S))$=9402.4±1.5±1.8 MeV and $m(\eta_b(2S))$=9999.0 ±3.5$^{+2.8}_{-1.9}$ MeV. Due to the high resolution, this measurement also enabled the measurement of the width of the η_b as Γ=10.8$^{+4.0+4.5}_{-3.7-2.0}$, which is consistent with the expectation from potential models to 5≤Γ≤20 MeV. The measurements of the $\eta_b(1S)$ and $\eta_b(2S)$ allow precision determination of the hyperfine mass splittings $\Upsilon(1S)$-$\eta_b(1S)$ and $\Upsilon(2S)$-$\eta_b(2S)$, using the masses of the $\Upsilon(1S)$ and $\Upsilon(2S)$ from [14]. The mass splittings are listed in Tab. 3. The splittings are in good agreement with the expectation from a potential model with relativistic corrections [37] or lattice QCD calculations with kinetic terms up to O(v^6) [39]. However, lattice QCD calculations to O(v^4) with charm sea quarks predict higher splittings which are $\simeq$10 MeV larger. Note that perturbative non-relativistic QCD calculations up to order $(m_b\alpha_S)^5$ predict significant smaller splittings e.g. 39±11$^{+9}_{-8}$ MeV [40].

4 Test of the tensor term in the potential

The measured masses of the h_b and h'_b can be used for a precision test of the hyperfine splitting in the Cornell-type potential (Eq. 1), i.e. a test of the relation
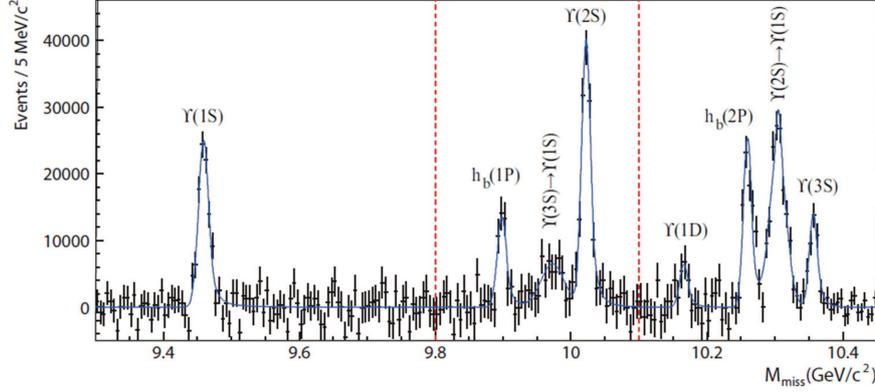
Figure 8: Observation of the h_b(1S) and h_b(2S) at Belle. For details see text.

	Belle [38]	Potential [37]	LQCD [41])	LQCD [39]
$\Upsilon(1S) - \eta_b$	57.9±2.3 MeV	60.0	70±9 MeV	60.3±5.5±5.0±2.1 MeV
$\Upsilon(2S) - \eta_b'$	$24.3^{+4.0}_{-4.5}$ MeV	30.0	35±3 MeV	23.5±4.1±2.1±0.8 MeV

Table 3: Bottomonium hyperfine splittings: measurement, calculated by potential model and calculated by Lattice QCD (LQCD).

$$m(h_b) \overset{?}{=} \frac{m(\chi_{b0}) + 3 \cdot m(\chi_{b1}) + 5 \cdot m(\chi_{b2})}{9} \tag{4}$$

using the world average masses of the $\chi_{b0,1,2}$ and $\chi'_{b0,1,2}$ from [14]. The hyperfine splitting $\Delta m_{HF} = <m(n^3P_J) - m(n^1P_1)$ was measured as $\Delta m_{HF} = (+1.6 \pm 1.5)$ MeV for $n=1$ and $\Delta m_{HF} = (+0.5^{+1.6}_{-1.2})$ MeV for $n=2$. This can be used as a test for the tensor term in the potential

$$V_{tensor} = \frac{1}{m^2} \frac{4\alpha_S}{r^3} \left(\frac{3\vec{S_1}\vec{r} \cdot \vec{S_2}\vec{r}}{r^2} - \vec{S_1}\vec{S_2} \right) \tag{5}$$

with the spins of the heavy quarks $\vec{S_1}$ and $\vec{S_2}$, the heavy quark mass m and the quark antiquark distance r, which is usually treated as a perturbation in the potential. It vanishes for $S=0$ (e.g. η_b, $\Upsilon(nS)$, h_b, ...) and $L=0$ (e.g. $^1D_2$ state, ...). In a simplified view, a non-zero Δm_{HF} would mean, that the wavefunction of the h_b at $r=0$ is non-vanishing. The sign of the potential term is positive, thus masses should be shifted up. Although the above mentioned measurements of Δm_{HF} are consistent with zero, however positive values seem to be preferred for the $b\bar{b}$ case, mildly suggesting to indicate an effect of the tensor term. This can be compared to measurements of $\Delta m_{HF} = 0.02 \pm 0.19 \pm 0.13$ MeV [42] and $\Delta m_{HF} = 0.10 \pm 0.13 \pm 0.18$ MeV [43] charmonium system, (i.e. the h_c).
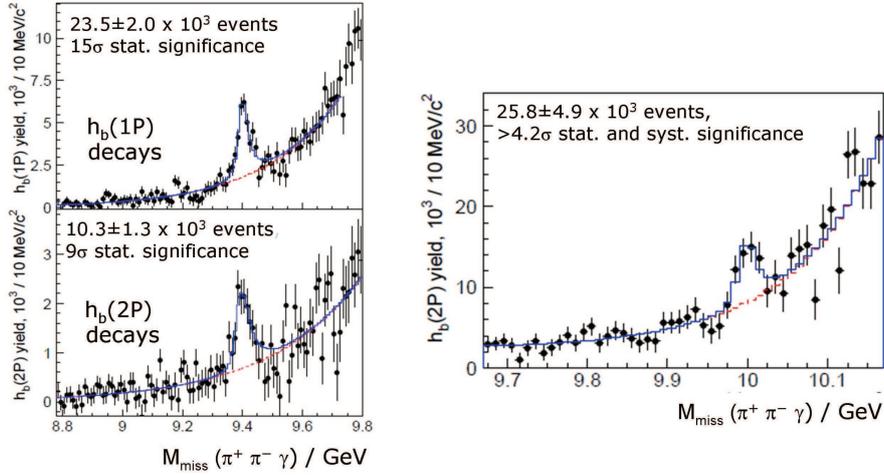
Figure 9: Observations of the $\eta_b(1P)$ (left) and $\eta_b(2P)$ (right) at Belle. For details see text.

4.1 Test of flavor independence of the potential

The new mass measurements in the bottomonium region enable for the first time a precision test of the flavour independance of the $c\bar{c}$ and $b\bar{b}$ systems. The important question is, if the level spacing is independant from the quark mass. According to [44], for a potential of the form $V(r){=}\lambda r^\nu$ the level spacing is $\Delta E \propto (2\mu/\hbar^2)^{-\nu/(2+\nu)}|\lambda|^{2/(2+\nu)}$. where μ is the (reduced) quark mass. For a pure Coulomb potential ($\nu{=}{-}1$), which should be dominating for the low lying states, this leads to $\Delta E \propto \mu$, This would imply that the level spacing would increase linearly with mass, i.e. $\Delta E(b\bar{b}) \simeq 3\Delta E(c\bar{c})$. For a pure linear potential it would be $\Delta E \propto \mu^{-1/3}$, thus the level spacing would decrease for higher quark masses, i.e. $\Delta E(b\bar{b}) \simeq 0.5\Delta E(c\bar{c})$. As can be seen in Fig. 10, for the mass splittings involving the h_b (S=0, L=1) the agreement between $c\bar{c}$ and $b\bar{b}$ is excellent, i.e. 10.2 vs. 10.1 MeV and 43.9 vs. 43.8 MeV. There are two possible explanations of this remarkable symmetry. *(1)* For a pure logarithmic potential V(r)=λln$r$ (i.e. the limit $\nu{\to}0$) the level spacing is $\Delta E \propto \lambda\mu^0$. This means, the flavour independance would be strictly fulfilled. *(2)* The other way to reach the flavour independance is, that the Coulomb potential with $\Delta E(b\bar{b}) \simeq 3\Delta E(c\bar{c})$ (see above) and the linear potential with $\Delta E(b\bar{b}) \simeq 0.5\Delta E(c\bar{c})$ (see above) cancel each other quantitatively in an exact way. It also implies that the size of the according λ pre-factors ($\lambda{=}{-}4/3\alpha_S$ for the Coulomb-like potential and $\lambda{=}k$ for the linear potential) just seem to have the exactly correct size assigned by nature in a fundamental way. For the ground states (S=0, L=0) the agreement of the mass splittings between $c\bar{c}$ and $b\bar{b}$ is not as good, i.e. 65.7 vs. 59.7 MeV, and may point to the fact, that there is an additional effect which lowers the η_c mass. This might be mixing of the η_c with the light quark states of the same quantum number 0^{-+} (i.e. η or η').

4.2 The $Y_b(10889)$ state

While investigating $\Upsilon(5S)$ decays, Belle discovered a highly anomalous behavior. For the $\Upsilon(5S)$, the beam energies of the KEK-B accelerator were changed in a way, to keep the center-of-mass boost the same as on the $\Upsilon(4S)$ resonance. Thus, all analysis techniques could be applied. In
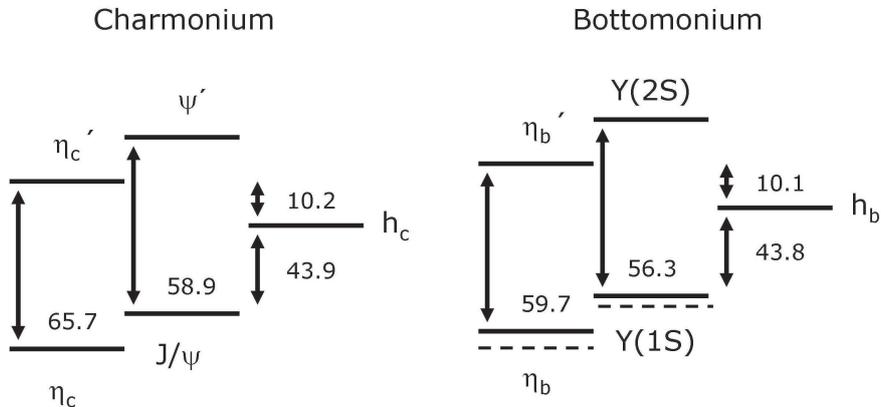
Figure 10: Mass splittings (in MeV) based upon the new measurements [38] of the h_b, η_b and η_b', using masses from [14] for the other states, for charmonium (left) and bottomonium (right). The dotted lines indicate levels for the theoretical case of exact flavour independence.

a data set of 21.7 fb^{-1}, the processes $e^+e^- \to \Upsilon(nS)\pi^+\pi^-$ with n=1,2,3 were investigated.

First of all, the cross section of decays to the Y(1S) was found to be anomalously large. While in a data set of 477 fb^{-1} on the $\Upsilon(4S)$, N=44±8 events of $\Upsilon(1S)\pi^+\pi^-$ were observed [45], in the data set of 21.7 fb^{-1} on the $\Upsilon(5S)$ N=325±20 events of $\Upsilon(1S)\pi^+\pi^-$ were observed [46]. This means, that in a data set corresponding to ≃1/20 the size of the data set and ≃1/10 of the production cross section, still a factor 7.4 more events are observed. This corresponds in total to a signal, which is more than a factor 10^3 higher than the expectation. In addition, not only the $\Upsilon(5S) \to \Upsilon(1S)\pi^+\pi^-$ but also the $\Upsilon(5S) \to \Upsilon(2S)\pi^+\pi^-$ was found to be larger than expected by more than a factor 5×10^2. Note that $\Upsilon(5S) \to \Upsilon(4S)\pi^+\pi^-$ is kinematically suppressed.

One of the possible explanation for the observed anomalously high yield was a new resonance nearby the $\Upsilon(5S)$, decaying into the same final state [47]. Therefore a beam energy scan was performed [48]. Typical step sizes in the variation of the $\sqrt{s}$ were 6-10 MeV. On each scan point more than 30 pb^{-1} were performed. For each energy point, the yield of $\Upsilon(1S,2S,3S)\pi^+\pi^-$ was determined by an unbinned maximum likelihood fit.

Fig. 11 (bottom) shows the fitted signal yield as a function of $\sqrt{s}$. These excitation curves are fitted with a Breit-Wigner shape with floating mean and width, but constraint to be identical parameters for all three curves. The normalizations for the three curves are floating independently. The fitted mean is at ≃20 MeV higher mass and the width is about a factor ≃2 narrower than the $\Upsilon(5S)$. This indicates that the observed resonance is not the $\Upsilon(5S)$, but instead a new state which was given the name Y_b(10889).

For comparison, Fig. 11 (top) shows the ratio R_b vs. $\sqrt{s}$, where R_b is defined as the ratio of the inclusive hadronic cross section $\sigma(e^+e^- \to$hadrons$)$ to $\sigma(e^+e^- \to \mu^+\mu^-)$. The final measurement for the new state yields a mass of m=10888.4$^{+2.7}_{2.6}$±1.2 MeV and a width of Γ=30.7$^{8.3}_{7.0}$±3.1 MeV. The final results for the widths, as measured in the resonance scan, are summarized in Tab. 4

As the Y_b(10889) does not coincide with a threshold, it cannot be interpreted as a molecule, neither as a threshold effect. there must be another explanation for its nature. The lowest

lying tetraquark state with $J^{PC}=1^{--}$ is predicted at a mass $m=10.890$ MeV [49], well consistent with the experimental observation. It would be a $[bq\bar{b}\bar{q}]$ tetraquark, where q denotes a light u or d quark, which are assumed to have the identical consituent mass of 305 MeV. In addition, the tetraquark model could explain the observed anomalous yield [49], . If the $Y_b(10889)$ is a pure $b\bar{b}$ state, there are no light quarks in the initial state. The $\pi^+\pi^-$ pair in the $\Upsilon(5S)\rightarrow\Upsilon(1S,2S,3S)\pi^+\pi^-$ transition must be created by two gluons and subsequent $g\rightarrow u\bar{u}$, $g\rightarrow d\bar{d}$, and rearrangement to $u\bar{d}$ and $d\bar{u}$. Thus, the transition would be Zweig forbidden. If the $Y_b(10889)$ is a $[bq][\bar{b}\bar{q}]$ tetraquark, then there is a $u\bar{u}$ or $d\bar{d}$ already present in the initial state, and only one additional pair must be formed from the QCD vacuum. Thus, the transition is Zweig allowed and the transition rate would be increased. An effect, which could explain the observed properties of the $Y_b(10889)$, however without assuming an exotic nature, is *rescattering*. In the rescattering model, the decay $\Upsilon(5S)\rightarrow\Upsilon(1S,2S,3S)\pi^+\pi^-$ would not proceed in a direct way, but by $\Upsilon(5S)\rightarrow B^{(*)}\overline{B}^{(*)}$ and subsequent $B^{(*)}\overline{B}^{(*)}\rightarrow\Upsilon(1S,2S,3S)\pi^+\pi^-$. On the one hand, the peak position could be shifted upwards by the rescattering by $+(7-20)$ MeV [50], compatible with the observed higher peak position of the $Y_b(10889)$ compared to the $\Upsilon(5S)$. On the other hand, the amplitude of the rescattering is proportional to $|\vec{p}_1|^3$, where $\vec{p}_1$ denotes the 3-momentum of the $B^{(*)}$ or $\overline{B}^{(*)}$, and would lead to an anhancement of the observed cross section by a factor $200-600$ [50]. This way this mechanism could also provide an explanation for the observed anomalous yield (see above). Quantitative predictions are however difficult, because unknown form factors [51] [50] must be assumed.

Process	Γ	$\Gamma_{e^+e^-}$	$\Gamma_{\Upsilon(1S)\pi^+\pi^-}$
$\Upsilon(2S)\rightarrow\Upsilon(1S)\pi^+\pi^-$	0.032 MeV	0.612 keV	0.0060 MeV
$\Upsilon(3S)\rightarrow\Upsilon(1S)\pi^+\pi^-$	0.020 MeV	0.443 keV	0.0009 MeV
$\Upsilon(4S)\rightarrow\Upsilon(1S)\pi^+\pi^-$	20.5 MeV	0.272 keV	0.0019 MeV
$\Upsilon(10860)\rightarrow\Upsilon(1S)\pi^+\pi^-$	110 MeV	0.31 keV	0.59 MeV

Table 4: Total widths, partial width for decay into e^+e^- and partial width for decay into $\Upsilon(1S)\pi^+\pi^-$ for the $\Upsilon(2S)$, $\Upsilon(3S)$ and $\Upsilon(5S)$. The $\Upsilon(5S)$ is denoted as $\Upsilon(10860)$, as it might be an admixture of several closeby states. As can be seen, $\Gamma_{\Upsilon(1S)\pi^+\pi^-}$ is anomolously large by a factor $>10^2$ for the $\Upsilon(10860)$.

5 A future Project: measurement of the width of the X(3872)

One of the important steps would be to measure not only the *masses* of newly observed states, but also the *widths*. As many states have natural widths in the sub-MeV regime, future experiments must be able to reach according precision. The $\overline{P}$ANDA experiment at FAIR (Facility for Antiproton and Ion research) at GSI Darmstadt, Germany, will be using a stored, cooled anti-proton beam. The measurement of the width of a state can be performed by a resonance scan technique. Both stochastic cooling and e^--cooling techniques will be used, providing a momentum resolution of the antiproton beam of down to $\Delta p/p\geq2\times10^{-5}$. The anti-protons will collide with protons in e.g. a frozen pellet target. With a maximum beam momentum of
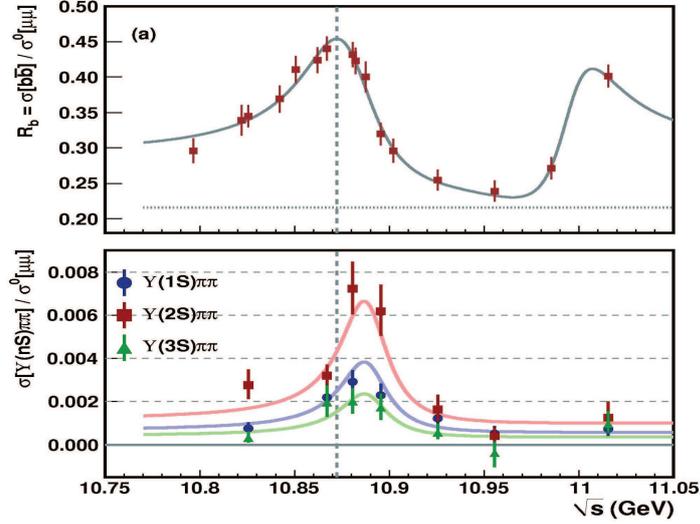
Figure 11: R_b as a function of $\sqrt{s}$ *(top)* and the energy-dependent cross sections for $e^+e^- \rightarrow \Upsilon(nS)\pi^+\pi^-$ $(n = 1, 2, 3)$ processes *(bottom)*. The results of the fits are shown as smooth curves. The vertical dashed line indicates the mass of the $\Upsilon(5S)$, as determined from the fit in the upper plot (i.e. the measured location of the maximum hadronic cross section).

$p \leq 15$ GeV/c, in this fixed target setup a maximum center-of-mass energy of $\sqrt{s} \leq 5.5$ GeV can be achieved, corresponding to a very high mass of an accessible charmonium(-like) state, which would kinematically not be accessible in B meson decays or in radiative decays of ψ resonances. For momentum reconstruction, a high magnetic solenoid field of $B=2$ T will be employed. One of the difficulties will be, that signal events (e.g. charmonium production, with subsequent decays into light mesons) and background events (hadronic production of light mesons) have very similar topologies. Thus, a hardware trigger using simple criteria, such as number of charged tracks or number of photons in the calorimeter, is not possible. Therefore $\overline{\mathsf{P}}$ANDA will perform complete online reconstruction of all events with a high interaction rate of $\leq 2 \times 10^7$/s. The planned luminosity of L=$2 \cdot 10^{32}$ cm^{-2} s^{-1} is high and would translate into a number of $2 \cdot 10^9$ J/ψ per year, if theoretically running on the J/ψ resonance only.

Cross sections in $p\bar{p}$ formation (as an example $\sigma(p\bar{p} \rightarrow X(3872))$) can be estimated from measured branching fractions (i.e. $\mathcal{B}(X(3872) \rightarrow p\bar{p})$) using the principle of detailed balance, which is shown in Eq. 6.

$$
\sigma[p\bar{p} \to X(3872)] = \sigma_{BW}[p\bar{p} \to X(3872) \to \text{all}](m_{X(3872)})
$$

$$
= \frac{(2J+1) \cdot 4\pi}{m_{X(3872)}^2 - 4m_p^2} \cdot \frac{\mathcal{B}(X(3872) \to p\bar{p}) \cdot \overbrace{\mathcal{B}(X(3872) \to f)}^{=1} \cdot \Gamma_{X(3872)}^2}{\underbrace{4(m_{X(3872)} - m_{X(3872)})^2}_{=0} + \Gamma_{X(3872)}^2}
$$

$$
\stackrel{(J=1)}{=} \frac{3 \cdot 4\pi}{m_{X(3872)}^2 - 4m_p^2} \cdot \mathcal{B}(X(3872) \to p\bar{p}) . \tag{6}
$$

R	J	m [MeV]	Γ [keV]	$\mathcal{B}(R{\to}p\bar{p})$	$\sigma(\bar{p}p{\to}R)$
J/ψ	1	3096.916 ± 0.011	92.9 ± 2.8	$(2.17\pm0.07)\times10^{-3}$	5.25 ± 0.17 μb
ψ'	1	3686.109^{+012}_{-014}	304 ± 9	$(2.76\pm0.12)\times10^{-4}$	402 ± 18 nb
η_c	0	2981.0 ± 1.1	$(29.7\pm1.0)\times10^3$	$(1.41\pm0.17)\times10^{-3}$	1.29 ± 0.16 μb
η_c'	0	3638.9 ± 1.3	$(10\pm4)\times10^3$	$(1.85\pm1.26)\times10^{-4}$	93 ± 63 nb
χ_{c0}	0	3414.75 ± 0.31	$(10.4\pm0.6)\times10^3$	$(2.23\pm0.13)\times10^{-4}$	134.1 ± 7.8 nb
h_c	1	3525.41 ± 0.16	$\leq1\times10^3$	$(8.95\pm5.21)\times10^{-4}$	1.47 ± 0.86 μb
X(3872)	1	3871.68 ± 0.17	$\leq1.2\times10^3$	$\leq5.31\times10^{-4}$	≤68.0 nb

Table 5: Total spin J, mass m, width Γ, branching fraction for the decay into $p\bar{p}$ and cross sections for production at $\overline{\text{P}}$ANDA, as derived by the principle of detailed balance for selected resonances R.

Tab. 5 summarizes cross sections for production at $\overline{\text{P}}$ANDA as derived by the principle of detailed balance for selected resonances R. For the J/ψ, the ψ', the η_c' and the χ_{c0} the branching fraction B($R{\to}p\bar{p}$) was taken from [14]. For the η_c', B($b{\to}K^+R{\to}K^+p\bar{p}$) was taken from [52] and B($B^+{\to}K^+R$) was taken from [14]. For the h_c and the X(3872) B($b{\to}K^+R{\to}K^+p\bar{p}$) was taken from [52] and the upper limit for B($B^+{\to}K^+R$) was taken from [14]. Typical cross sections for charmonium formation at $\overline{\text{P}}$ANDA are thus in the order of 10-100 nb. In the following, we assume $\sigma(p\bar{p}{\to}X(3872))$=50 nb.

Detailed Monte-Carlo simulation studies of a resonance scan for $p\bar{p}{\to}X(3872)$ at $\overline{\text{P}}$ANDA were performed. The advantage is, that in $p\bar{p}$ collisions the X(3872) with $J^{PC}=1^{++}$ can be formed directly, while in e^+e^- only $J^{PC}=1^{--}$ is possible. The Breit-Wigner cross section for the formation and subsequent decay of a $c\bar{c}$ resonance R of spin J, mass M_R and total width Γ_R formed in the reaction $\bar{p}p{\to}R$ is

$$
\sigma_{BW}(E_{cm}) = \frac{(2J+1)}{(2S+1)(2S+1)} \frac{4\pi(\hbar c)^2}{(E_{cm}^2 - 4(m_pc^2)^2)} \times \frac{\Gamma_R^2 BR(\bar{p}p \to R) \times BR(R \to f)}{(E_{cm} - M_Rc^2)^2 + \Gamma_R^2/4} \tag{7}
$$

where S is the spin of the (anti-)proton.

$$
\sigma(E_{cm}) = \int_0^\infty \sigma_{BW}(E')G(E' - E_{cm})dE' \tag{8}
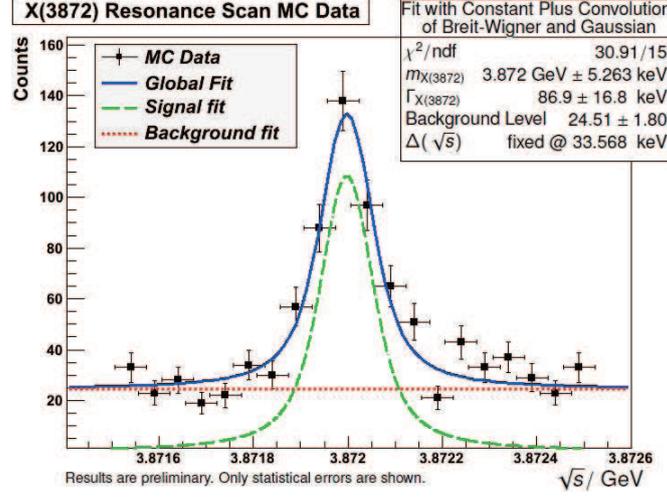$$

Figure 12: Final result for the simulated resonance scan of X(3872) at $\overline{\text{P}}$ANDA with 20 scan points. For details see [55].

is a convolution of a Breit-Wigner term for the resonance and the function G for the beam resolution. If G is given by a single Gaussian distribution, then the convolution is a Voigtian distribution. The area under the resonance peak is given by

$$A = \int_0^\infty \sigma(E_{cm})dE_{cm} = \frac{\pi}{2}\sigma_{peak}\Gamma_R \tag{9}$$

which importantly is independent of the form of $G(E)$. σ_{peak} is the cross section at $E_{cm}=M_Rc^2$ given by

$$\sigma_{peak} = \frac{(2J+1)}{(2S+1)(2S+1)}\frac{16\pi\hbar^2 BR(\bar{p}p \rightarrow R) \times BR(R \rightarrow f)}{(M_R - 4m_p^2)c^2} \tag{10}$$

By measuring A using a fit to the excitation function and inserting σ_{peak} into Eq. 9, the resonance width Γ_R can be determined. For a complete simulation of the resonance scan, 20 simulations for $p\bar{p} \rightarrow$ X(3872) $\rightarrow J/\psi\pi^+\pi^-$ with background were performed for 20 beam momenta in the resonance region. The beam momenta were chosen equidistant in center-of-mass energy. For each scan point, the yield of the X(3872) was fitted by a single Gaussian. Fig. 12 shows the fitted yield as a function of $\sqrt{s}$. The fit was performed using a Voigtian distribution. Direct background from $p\bar{p} \rightarrow J/\psi\pi^+\pi^-$ was taken into account as a zeroth order polynomial, although estimates [53] indicate that it is small with a cross section of 1.2 nb (i.e. a factor $\simeq 40$ smaller than the signal). The known momentum resolution in the HESR high resolution mode was fixed as the width of the Gaussian in the convoluted Voigtian. The width of the X(3872) was reconstructed as $\Gamma_{X(3872)}=86.9\pm16.8$ keV, which is consistent with the input width of 100 keV. This simulation is a proof for the concept, and the ability of $\overline{\text{P}}$ANDA to measure the width of a resonance in the sub-MeV regime. For additional details see [54] [55].

6 Summary

Recent results from e^+e^- collisions (and in particular the B meson factories) enable unique precision tests of the $q\bar{q}$ potential in the charmonium and bottomonium region. The static potential model fails for many newly observed states (called XYZ states), indicating non-$q\bar{q}$ phenomena such as possibly tetraquark states, charmed meson molecular states or hybrid states. Future experiments such as $\overline{\text{P}}$ANDA will provide precision tests not only of masses, but also widths in the sub-MeV regime.

Acknowledgments

References

[1] E. Eichten, K. Gottfried, T. Kinoshita, K. D. Lane, T.-M. Yan, Phys. Rev. D17(1978)3090.

[2] S. Godfrey, N. Isgur, Phys. Rev. D32(1985)189.

[3] T. Barnes, S. Godfrey, E. S. Swanson, arXiv:hep-ph/0505002, Phys. Rev. D72(2005)054026.

[4] Belle Collaboration, Nucl. Instr. Meth. A479(2002)117.

[5] BaBar Collaboration, Nucl. Instr. Meth. A479(2002)1.

[6] Belle Collaboration, arXiv:hep-ex/0309032, Phys. Rev. Lett. 91(2003)262001.

[7] BaBar Collaboration, Phys. Rev. D71(2005)071103, Phys. Rev. D77(2008)111101.

[8] CDF II Collaboration, Phys. Rev. Lett. 93(2004)072001;
CDF II Collaboration, Phys. Rev. Lett. 96(2006)102002;
CDF II Collaboration, Phys. Rev. Lett. 103(2009)152001.

[9] D0 Collaboration, Phys. Rev. Lett. 93(2004)162002.

[10] LHCb Collaboration, arXiv:1112.5310[hep-ex], Eur. Phys. J. C72(2012)1972.

[11] CMS Collaboration, CERN-CMS-DP-2011-005;
CMS Collaboration, arXiv:1302.3968[hep-ex].

[12] Belle Collaboration, arXiv:1107.0163[hep-ex], Phys. Rev. D84(2011)052004.

[13] N. A. Törnqvist, arXiv:hep-ph/0402237, Phys. Lett. B590(2004)209;
N. A. Törnqvist, Phys. Rev. Lett. 67(1991)556.

[14] J. Beringer et al. (Particle Data Group), Phys. Rev. D86(2012)010001.

[15] E. Braaten, M. Lu, arXiv:0709.2697[hep-ph], Phys. Rev. D76(2007)094028;
E. Braaten, M. Lu, arXiv:0710.5482[hep-ph], Phys. Rev. D77(2008)014029;
E. Braaten, M. Kusunoki, arXiv:hep-ph/0412268, Phys. Rev. D69(2004)074005.

[16] Belle Collaboration, arXiv:hep-ex/0505037.

[17] BaBar Collaboration, arXiv:hep-ex/0607050, Phys. Rev. D74(2006)071101.

[18] BaBar Collaboration, arXiv:hep-ex/0506081, Phys. Rev. Lett. 95(2005)142001.

[19] CLEO-c Collaboration, arXiv:hep-ex/0611021, Phys. Rev. D74(2006)091104.

[20] Belle Collaboration, arXiv:hep-ex/0612006.

[21] Belle Collaboration, arXiv:0707.2541[hep-ex], Phys. Rev. Lett. 99(2007)182004.

[22] BaBar Collaboration, arXiv:0808.1543[hep-ex].

[23] BaBar Collaboration, arXiv:1204.2158[hep-ex], Phys. Rev. D86(2012)051102.

[24] Belle Collaboration, arXiv:0707.3699, Phys. Rev. Lett. 99(2007)142002.

[25] BaBar Collaboration, arXiv:hep-ex/0610057, Phys. Rev. Lett. 98(2007)212001.

[26] F. E. Close, P. R. Page, arXiv:hep-ph/0507199, Phys. Lett. B628(2005)215.

[27] C. Bernard, J. E. Hetrick, T. A. DeGrand, M. Wingate, C. DeTar, C. McNeile, S. Gottlieb, U. M. Heller, K. Rummukainen, B. Sugar D. Toussaint, arXiv:hep-lat/9707008, Phys. Rev. D56(1997)7039; Z.-H. Mei, X.-Q. Luo, arXiv:hep-lat/0206012, Int. J. Mod. Phys. A18(2003)5713.

[28] Belle Collaboration, arXiv:0807.4458[hep-ex], Phys. Rev. Lett. 101(2008)172001.

[29] BESIII Collaboration, arXiv:1303.5949[hep-ex].

[30] Belle Collaboration, arXiv:1304.0121[hep-ex].

[31] Belle Collaboration, arXiv:1304.3975[hep-ex], Phys. Rev. Lett. 111(2013)032001.

[32] W. Kwong, J. L. Rosner, C. Quigg, Ann. Rev. Nucl. Part. Sci. 37(1987)325.

[33] E. J. Eichten, K. Lane, C. Quigg, arXiv:hep-ph/0401210, Phys. Rev. D69(2004)094019.

[34] P. Ko, J. Lee, H. S. Song, arXiv:hep-ph/9701235, Phys. Lett. B395(1997)107.

[35] Belle Collaboration, arXiv:1103.3419[hep-ex], Phys. Rev. Lett. 108(2011)032001.

[36] BaBar Collaboration, arXiv:1102.4565[hep-ex], Phys. Rev.D84(2011)091101(R).

[37] D. Ebert, R.N. Faustov, V.O. Galkin, arXiv:hep-ph/0210381, Phys. Rev. D67(2003)014027.

[38] Belle Collaboration, arXiv:1205.6351[hep-ex], Phys. Rev. Lett. 109(2012)232002.

[39] S. Meinel, arXiv:1007.3966[hep-lat], Phys. Rev. D82(2010)114502.

[40] A. A. Penin, arXiv:0905.4296[hep-ex].

[41] R. J. Dowdall, B. Colquhoun, J. O. Daldrop, C. T. H. Davies, I. D. Kendall, E. Follana, T. C. Hammant, R. R. Horgan, G. P. Lepage, C. J. Monahan, E. H. Müller, arXiv:1110.6887[hep-lat], Phys. Rev. D85(2012)054509.

[42] CLEO II Collaboration, arXiv:0805.4599[hep-ex], Phys.Rev.Lett.101(2008)182003.

[43] BESIII Collaboration, arXiv:1002.0501, Phys.Rev.Lett.104(2010)132002.

[44] C. Quigg, hep-ph/9707493.

[45] Belle Collaboration, arXiv:hep-ex/0611026, Phys. Rev. D75(2007)071103.

[46] Belle Collaboration, arXiv:0710.2577[hep-ex], Phys. Rev. Lett. 100(2008)112001.

[47] W.-S. Hou, arXiv:hep-ph/0606016, Phys. Rev. D74(2006)017504.

[48] Belle Collaboration, arXiv:0808.2445 [hep-ex], Phys. Rev. D82(2010)091106.

[49] A. Ali, C. Hambrock, I. Ahmed, M. J. Aslam, arXiv:0911.2787[hep-ph], Phys. Lett. B684(2010)28; A. Ali, C. Hambrock, M. J. Aslam, arXiv:0912.5016[hep-ph], Phys. Rev. Lett. 104(2010)162001, Erratum-ibid. 107(2011)049903; A. Ali, C. Hambrock, S. Mishima, arXiv:1011.485[hep-ph], Phys. Rev. Lett. 106(2011)092002.

[50] C. Meng, K.-T. Chao, arXiv:0805.0143[hep-ph], Phys. Rev. D78(2008)034022.

[51] Y. A. Simonov, 0804.4635[hep-ph], JETP Lett. 87(2008)121.

[52] LHCb collaboration, arXiv:1303.7133[hep-ex], submitted to Eur. Phys. Jour. C.

[53] G. Y. Chen, J. P. Ma, arXiv:0802.2982[hep-ph], Phys. Rev. D77(2008]097501.

[54] J. S. Lange, M. Galuska, Th. Geßler, W. Kühn, S. Künze, Y. Liang, D. Münchow, B. Spruck, M. Ullrich, M. Werner, arXiv:1010.2350[hep-ex].

[55] M. Galuska *Simulation of X(3872) Decays Using the PandaRoot Framework,* Master Thesis, Justus-Liebig-Universität Giessen, 2011.

Recent Belle results

Dmitri Liventsev[1]

[1]KEK, 1-1 Oho, Tsukuba-shi, Ibaraki-ken, 305-0801 Japan

We review the recent results from the Belle experiment: search for new physics in $B \to \tau\nu$ and related decays, study of charged bottomonium-like states Z_b and measurement of the parameters of the Cabibbo-Kobayashi-Maskawa matrix in $B^0 \to \pi^+\pi^-$ and $B^0 \to \rho^0\rho^0$ decays.

1 $B \to \tau\nu$ and related results

1.1 Introduction

The purely leptonic decay $B \to \tau\nu$ is of high interest since it provides a unique opportunity to test the Standard Model (SM) and search for new physics beyond the SM. In the absence of new physics, this measurement provides a direct experimental determination of the product of the B meson decay constant and the CKM matrix element $f_B|V_{ub}|$. Physics beyond the SM, however, could significantly suppress or enhance $\mathcal{B}(B \to \tau\nu)$ via exchange of a new charged particle, *e.g.* a charged Higgs boson from two-Higgs doublet models (2HDM) [1, 2]. Leptonic $B \to \ell\nu$, $\ell = e, \mu$ and semileptonic $B \to D^{(*)}\tau\nu$ decays are also sensitive to such exchange [3]. Here recent results obtained at the B-factories are reviewed. The comparison between the experimental results and the SM predictions is shown. The constraints on the Type II 2HDM are reported.

1.2 $B \to \tau\nu$

It is challenging to identify the $B \to \tau\nu$ decay experimentally, since it includes multiple neutrinos in the final state. At the e^+e^- B-factories a B meson pair is generated from the process $e^+e^- \to \Upsilon(4S) \to B\bar{B}$ and we can reconstruct one of the B mesons ("B_{tag}") to identify the decay of the other B meson ("B_{sig}"). Two independent types of the B meson decays may be used for reconstruction of B_{tag}: hadronic decays such as $B^- \to D^0\pi^-$ ("hadronic tag") and semileptonic decays such as $B^- \to D^0\ell^-\nu$, $\ell = e, \mu$ ("semileptonic tag"). The efficiency for reconstructing B_{tag} is higher for the semileptonic tag, while the purity is higher for the hadronic tag.

The first evidence for $B \to \tau\nu$ was reported by the Belle collaboration using hadronic tag and a data sample corresponding to 449×10^6 $B\bar{B}$ events [4]. This was followed by a measurement using semileptonic tag and a data sample corresponding to 657×10^6 $B\bar{B}$ events [5]. The branching ratio obtained by the semileptonic tag analysis is $\mathcal{B}(B \to \tau\nu) = [1.54^{+0.38}_{-0.37}(stat)^{+0.29}_{-0.31}(syst)] \times 10^{-4}$, with a significance of 3.6σ. The hadronic tag result has been updated using Belle final data sample corresponding to 772×10^6 $B\bar{B}$ events [6]. By employing a neural network-based method for the hadronic tag [7] and a two-dimensional fit for the signal extraction, along with a larger data sample, both statistical and systematic precision is significantly improved. The

branching ratio is obtained to be $\mathcal{B}(B \to \tau\nu) = [0.72^{+0.27}_{-0.25}(stat) \pm 0.11(syst)] \times 10^{-4}$, with significance of 3.0σ. Results of the fit are shown in Fig. 1. Combining the semileptonic tag and hadronic tag results and taking into account all the correlated systematic uncertainties, the branching ratio is found to be $\mathcal{B}(B \to \tau\nu) = (0.96 \pm 0.26) \times 10^{-4}$ with a significance of 4.0σ [6].
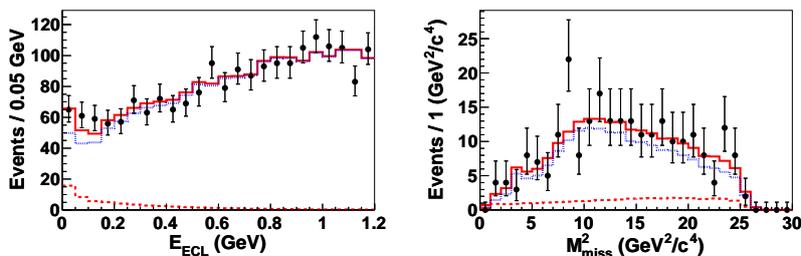

Figure 1: Signal extraction for $B \to \tau\nu$ in the latest Belle analysis [6]. Two-dimensional fit to residual energy E_{ECL} (left) and missing mass squared M_{miss} (right) is used. M_{miss} distribution is shown for a signal region of $E_{ECL} < 0.2\,\text{GeV}$. Solid circles with error bars represent data. Solid histograms show projections of the fits, dashed and dotted histograms show signal and background components, respectively.

The BaBar collaboration also reported the results of $B \to \tau\nu$ using hadronic and semileptonic tags. Using semileptonic tag and a data sample corresponding to 459×10^6 $B\bar{B}$ events, the branching ratio is obtained to be $\mathcal{B}(B \to \tau\nu) = [1.7 \pm 0.8(stat) \pm 0.2(syst)] \times 10^{-4}$ [8]. An evidence for $B \to \tau\nu$ is obtained with a significance of 3.8σ using hadronic tag and a data sample corresponding to 468×10^6 $B\bar{B}$ events [9]. The branching ratio is obtained to be $\mathcal{B}(B \to \tau\nu) = [1.83^{+0.53}_{-0.49}(stat) \pm 0.24(syst)] \times 10^{-4}$. Combining the two results, the branching ratio is found to be $\mathcal{B}(B \to \tau\nu) = (1.79 \pm 0.48) \times 10^{-4}$, where both statistical and systematic errors are combined in quadrature [9].

A world average for $B \to \tau\nu$ branching ratio is calculated to be $\mathcal{B}(B \to \tau\nu)_{WA} = (1.15 \pm 0.23) \times 10^{-4}$. For this calculation, the correlation in the systematic errors between the Belle and BaBar results was neglected since the statistical errors are dominant and the correlated parts in the systematic errors are relatively small. In the SM an estimate of $\mathcal{B}(B \to \tau\nu)_{SM} = (0.73^{+0.12}_{-0.07}) \times 10^{-4}$ is obtained by using f_B and $|V_{ub}|$ provided by a global fit to the CKM matrix elements [10]. The deviation is found to be 1.6σ.

In the Type II 2HDM [1], the branching ratio of $B \to \tau\nu$ is described by $\mathcal{B}(B \to \tau\nu) = \mathcal{B}(B \to \tau\nu)_{SM} \times r_H$, where $\mathcal{B}(B \to \tau\nu)_{SM}$ is the SM value of the branching ratio, r_H is a modification factor $r_H = (1 - \tan^2\beta\, m_{B^\pm}^2/m_{H^\pm}^2)^2$, $m_{B^\pm}$ is the charged B meson mass, $m_{H^\pm}$ is the charged Higgs mass and $\tan\beta$ is the ratio of the two Higgs bosons vacuum expectation values. Conservatively using $f_B = (191 \pm 9)\,\text{MeV}$ from the lattice calculation provided by the HPQCD collaboration [11] and $|V_{ub}| = (4.15 \pm 0.49) \times 10^{-3}$ from the $b \to u$ transitions provided by the PDG group [12], we evaluate excluded regions in the $\tan\beta - m_{H^\pm}$ plane as shown in Fig. 4 (left). Stringent constraint is obtained for relatively higher $\tan\beta$ region.

1.3 $B \to \ell\nu$

In Type 2 II 2HDM branching ratios of all leptonic B decays are modified by the same factor r_H and it is interesting to measure $B \to \ell\nu$ decays in addition to $B \to \tau\nu$ decay. The

highly suppressed $B \to \ell\nu$, $\ell = e, \mu$ final states are predicted to have SM branching fractions of $\mathcal{O}(10^{-11})$ and $\mathcal{O}(10^{-7})$ for $\ell = e$ and $\ell = \mu$, respectively. As these decays are two-body decays, the charged lepton momentum in the rest frame of the decaying B_{sig} is $p_\ell^B \simeq m_B/2$. This gives a unique signature which can be exploited in this analysis because the B_{sig} rest frame is known from the hadronic tagging. Most backgrounds are not expected to produce high momentum leptons that can reach the signal region, defined as $2.6\,\text{GeV}/c < p_\ell^B < 2.7\,\text{GeV}/c$. In the analysis using full Belle data sample of 772×10^6 $B\bar{B}$ events no events are observed in the signal region, as shown in Fig. 2, and 90% C.L. upper limits on the branching fractions are determined: $\mathcal{B}(B \to e\nu) < 3.5 \times 10^{-6}$ and $\mathcal{B}(B \to \mu\nu) < 2.5 \times 10^{-6}$ [13]. These are the most stringent limits on $B \to \ell\nu$ decays using a hadronic tag method. Previous results from Belle and BaBar using a loose tagging method (*i.e.* tracks and photons excluding the signal lepton have to be compatible with the recoiling B meson) are $\mathcal{B}(B \to e\nu) < 0.98 \times 10^{-6}$ [14] and $\mathcal{B}(B \to \mu\nu) < 1.0 \times 10^{-6}$ [15], respectively.

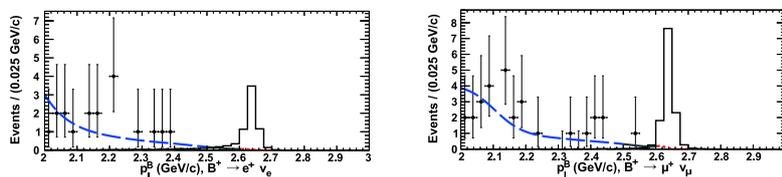Figure 2: Results of the fit to the p_ℓ^B spectrum for $B \to e\nu$ (left) and $B \to \mu\nu$ (right) decays. Data is shown as points with error bars. The solid histogram shows the expected signal shape with arbitrary normalization. The sum of PDFs is shown as a dashed line in the sideband region $(2.0\,\text{GeV} < p_\ell^B < 2.5\,\text{GeV})$, where the normalization was obtained. In the signal region $(2.6\,\text{GeV} < p_\ell^B < 2.7\,\text{GeV})$ the sum of PDFs is shown as a dotted line.

1.4 $B \to D^{(*)}\tau\nu$

The semileptonic $B \to D^{(*)}\tau\nu$ decays also include multiple neutrinos in the final states considering the following τ decays. The results shown up to now are based on the tags using hadronic B decays. The ratios $R(D^{(*)}) = \mathcal{B}(B \to D^{(*)}\tau\nu)/\mathcal{B}(B \to D^{(*)}\ell\nu)$, which are independent of the CKM element $|V_{cb}|$ and of the parameterization of the strong interaction to a large extent, are measured. With larger statistics, the q^2 distributions and the angular distributions of the τ and $D^{(*)}$ decays could also provide useful information for testing the SM and constraining new physics models.

The $B^0 \to D^{*+}\tau^-\nu_\tau$ decay was first observed by the Belle collaboration using the 535×10^6 $B\bar{B}$ data sample [16]. The Belle collaboration also obtained the results for the charged B meson decays to $D^{(*)}\tau\nu$ using the 657×10^6 $B\bar{B}$ data sample [17]. These measurements are done by inclusively reconstructing the B_{tag} candidates using all the remaining particles after selecting the B_{sig} decay products. The Belle collaboration also obtained a preliminary result by exclusively reconstructing the B_{tag} candidates and the B_{sig} decay products using the 657×10^6 $B\bar{B}$ data sample [18]. Figure 3 shows the distributions of the kinematic variables used for the signal extraction. The naive averages of $R(D^{(*)})$ for the above results are obtained to be $R(D) = 0.430 \pm 0.091$ and $R(D^*) = 0.405 \pm 0.047$ [19]. For the calculation, the correlations in the statistical errors between the different tagging analyses are neglected since the event overlap

is very limited. The correlations in the systematic errors between the different tagging analyses are assumed to be 60%.
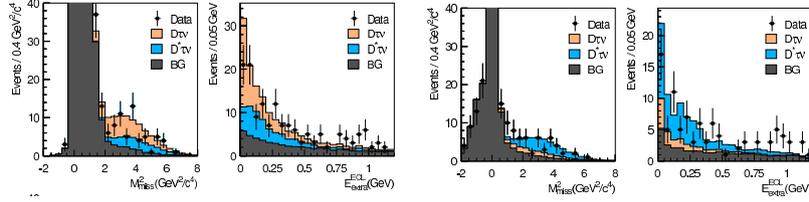

Figure 3: Signal extraction for $B \to D^{(*)}\tau\nu$ in Belle analysis [18] is shown for $B^+ \to \bar{D}^0\tau^+\nu$ (two left plots) and $B^+ \to \bar{D}^{*0}\tau^+\nu$ (two right plots). The missing mass squared M^2_{miss} and residual energy E^{ECL}_{extra} are used.

The BaBar collaboration showed the latest results for the $B \to D^{(*)}\tau\nu$ decays using hadronic tag and the full 471×10^6 $B\bar{B}$ data sample [20]. This analysis includes a signal efficiency increase by more than a factor of three compared to the previous analysis [21]. This improvement is provided by adding more B_{tag} decay chains and using a looser charged lepton selection. The background events are subtracted by employing the boosted decision tree multivariate method. Combining the results for the neutral and charged B decays to $D^{(*)}\tau\nu$, the $R(D^{(*)})$ ratios are obtained to be $R(D) = 0.440 \pm 0.058(stat) \pm 0.042(syst)$ and $R(D^*) = 0.332 \pm 0.024(stat) \pm 0.018(syst)$. A negative correlation of -0.27 between $R(D)$ and $R(D^*)$ is obtained including systematic uncertainties.

The results of $R(D^{(*)})$ are consistent between the Belle and BaBar experiments. The Belle results exceed the SM predictions $R(D)_{SM} = 0.297 \pm 0.017$ and $R(D^*)_{SM} = 0.252 \pm 0.003$ [22] by 1.4σ and 3.0σ, respectively [19]. The BaBar results exceed these SM predictions by 2.0σ and 2.7σ, respectively [20]. The combined disagreement of the discrepancy is at 4σ level [19].

In the Type II 2HDM, there is a substantial impact on the ratios $R(D^{(*)})$ due to the charged Higgs contribution [23]. The result for Belle, shown in Fig. 4 (right) has been obtained privately by ignoring the correlation between the experimental $R(D)$ and $R(D^{(*)})$ results and the dependency of the experimental $R(D^{(*)})$ results on $m_{H\pm}$ and $\tan\beta$. The BaBar result includes both of them [20]. Both results disfavor the Type II 2HDM by a level of more than 3σ for all $\tan\beta/m_{H\pm}$ region.

1.5 Summary

Exploiting the large number of events and the clean environment at the B-factories, the leptonic $B \to \tau\nu$ and the semileptonic $B \to D^{(*)}\tau\nu$ decays were measured with a good precision in spite of the existence of multiple neutrinos in the final states. Upper limits were set for the highly suppressed leptonic $B \to \ell\nu$, $\ell = e, \mu$ decays. Stringent constraints on the charged Higgs mass $m_{H\pm}$ and the vacuum-expectation-value ratio $\tan\beta$ were evaluated for the Type II 2HDM. Further investigation at the next-generation B-factories is important for testing the SM and for constraining new physics models.
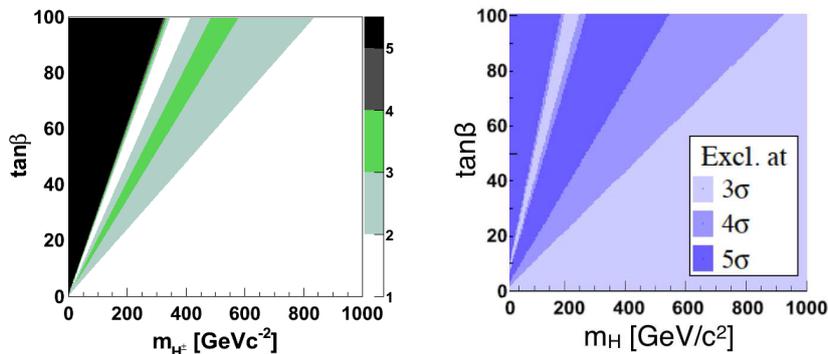
Figure 4: Constraint on $\tan\beta$ and $m_{H^\pm}$ in the Type II 2HDM obtained from Belle results, from measured $\mathcal{B}(B \to \tau\nu)$ (left) and $R(^{D(*)})$ values (right).

2   Bottomonium study

2.1   Observation of Z_b states in the $\Upsilon(nS)\pi^+\pi^-$ and $h_b(mP)\pi^+\pi^-$ channels

Recently Belle observed the $h_b(1P)$ and $h_b(2P)$ states in the transitions $\Upsilon(5S) \to h_b(mP)\pi^+\pi^-$ [24]. The rates of these transitions appeared to be unsuppressed relative to the $\Upsilon(5S) \to \Upsilon(nS)\pi^+\pi^-$ ($n = 1, 2, 3$). The $h_b(mP)$ production involves spin-flip of b-quark and is suppressed as $(\Lambda_{QCD}/m_b)^2$ in the multipole expansion; this unexpected result motivated further studies of the $h_b(mP)$ and $\Upsilon(nS)$ production mechanisms.

Belle studied the resonant structure of the $\Upsilon(5S) \to \Upsilon(nS)\pi^+\pi^-$ and $h_b(mP)\pi^+\pi^-$ decays ($n = 1, 2, 3$; $m = 1, 2$) [25]. The $\Upsilon(nS)$ [$h_b(mP)$] states are reconstructed in the $\mu^+\mu^-$ channel [inclusively using missing mass of the $\pi^+\pi^-$ pairs]. Invariant mass spectra of the $\Upsilon(nS)\pi^\pm$ and $h_b(mP)\pi^\pm$ combinations are shown in Fig. 5. Each distribution shows two peaks. For the channels $\Upsilon(nS)\pi^+\pi^-$ [$h_b(mP)\pi^+\pi^-$] the Dalitz plot analysis [fit to one-dimensional distributions] is performed. The non-resonant contributions in the $h_b(mP)\pi^+\pi^-$ channels are negligible, justifying the one-dimensional analysis. Preliminary results of the angular analysis indicate that both states have the same spin-parity $J^P = 1^+$ [26], therefore coherent sum of Breit-Wigner amplitudes is used to describe the signals. The Dalitz plot model for the $\Upsilon(5S) \to \Upsilon(nS)\pi^+\pi^-$ channels includes also the $\pi^+\pi^-$ resonances $f_0(980)$ and $f_2(1270)$, and non-resonant contribution, parameterized as $a + b\, M^2_{\pi^+\pi^-}$, where a and b are complex numbers floating in the fit. The masses and widths of the two peaks are found to be in good agreement among different channels.Averaged over the five decay channels parameters are $M_1 = (10607.4 \pm 2.0)\,\text{MeV}/c^2$, $\Gamma_1 = (18.4 \pm 2.4)\,\text{MeV}$, $M_2 = (10652.2 \pm 1.5)\,\text{MeV}/c^2$, $\Gamma_2 = (11.5 \pm 2.2)\,\text{MeV}$. The peaks are identified as signals of two new states, named $Z_b(10610)$ and $Z_b(10650)$.

Another result of the amplitude analyses is that the phase between the $Z_b(10610)$ and $Z_b(10650)$ amplitudes is zero for the $\Upsilon(nS)\pi^+\pi^-$ channels, and 180° for the $h_b(mP)$ channels.

The masses of the $Z_b(10610)$ and $Z_b(10650)$ states are close to the $B\bar{B}^*$ and $B^*\bar{B}^*$ thresholds, respectively. All the properties of the $Z_b(10610)$ and $Z_b(10650)$ find natural explanation once molecular structure for these states is assumed without even the need of dynamic model.
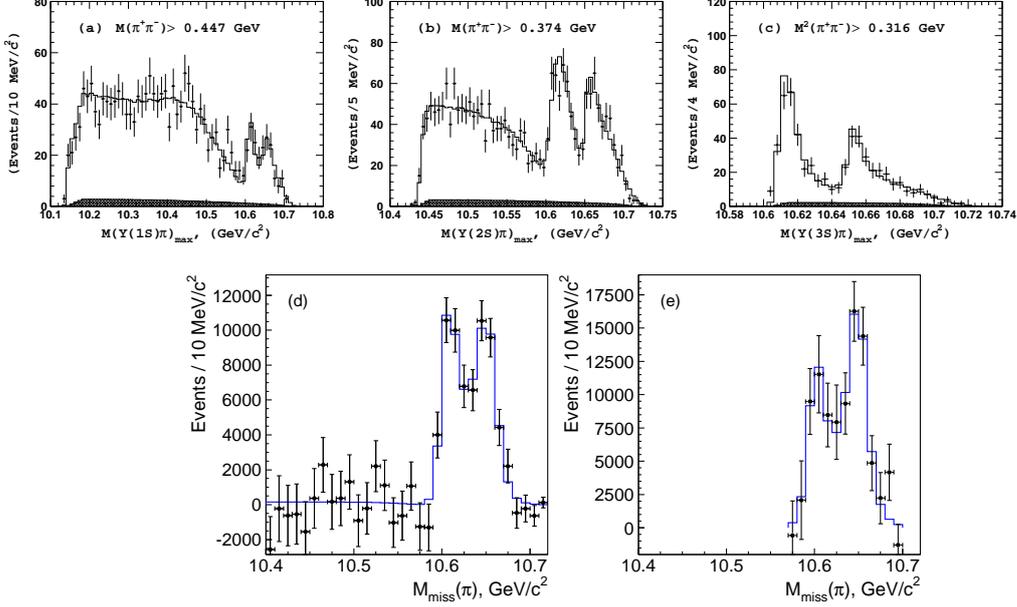
Figure 5: Invariant mass spectra of the (a) $\Upsilon(1S)\pi^{\pm}$, (b) $\Upsilon(2S)\pi^{\pm}$, (c) $\Upsilon(3S)\pi^{\pm}$, (d) $h_b(1P)\pi^{\pm}$ and (e) $h_b(2P)\pi^{\pm}$ combinations.

Considering the heavy-quark spin structure of the $B^{(*)}\bar{B}^*$ molecule with $I^G(J^P) = 1^+(1^+)$, one concludes that Z_b contain both ortho- and para-bottomonium components [27]. The weight of these components is equal, therefore the decay to the $h_b(mP)\pi^{\pm}$ is not suppressed relative to the $\Upsilon(nS)\pi^{\pm}$. The $Z_b(10610)$ and $Z_b(10650)$ differ by the sign between ortho- and para-bottomonium components, this explains why the $Z_b(10610)$ and $Z_b(10650)$ amplitudes appear with the sign plus for the $\Upsilon(nS)\pi^+\pi^-$ channels and with the sign minus for the $h_b(mP)\pi^+\pi^-$ channels. In the limit of infinitely heavy b quark the B and B^* mesons have equal mass, thus the $Z_b(10610)$ and $Z_b(10650)$ are also degenerate. Given minus sign between the Z_b amplitudes in the $h_b(mP)\pi^+\pi^-$ channel the contribution of this channel vanishes if the heavy quark symmetry is exact.

2.2 Observation of the $Z_b(10610) \to B\bar{B}^*$ and $Z_b(10650) \to B^*\bar{B}^*$ decays

Given proximity to the thresholds and finite widths, it is natural to expect that the rates of the "fall-apart" decays $Z_b(10610) \to B\bar{B}^*$ and $Z_b(10650) \to B^*\bar{B}^*$ are substantial in the molecular picture. To search for these transitions Belle studied the $\Upsilon(5S) \to [B^{(*)}\bar{B}^*]^{\pm}\pi^{\mp}$ decays [28]. One B meson is reconstructed fully using the $D^{(*)}\pi^+$ and $J/\psi K^{(*)}$ channels. The distribution of the missing mass of the $B\pi^{\pm}$ pairs shows clear signals of the $\Upsilon(5S) \to [B\bar{B}^*]^{\pm}\pi^{\mp}$ and $\Upsilon(5S) \to [B^*\bar{B}^*]^{\pm}\pi^{\mp}$ decays [see Fig. 6 (a)]; corresponding branching fractions of $(2.83 \pm 0.29 \pm 0.46)\,\%$ and $(1.41 \pm 0.19 \pm 0.24)\,\%$, respectively, are in agreement with previous Belle measurement [29]. No signal of the $\Upsilon(5S) \to [B\bar{B}]^{\pm}\pi^{\mp}$ decay is found, with upper limit on its fraction of $< 0.4\,\%$ at 90% confidence level.

The distributions in the $B\bar{B}^*$ and $B^*\bar{B}^*$ invariant mass for the $\Upsilon(5S) \to [B\bar{B}^*]^{\pm}\pi^{\mp}$ and
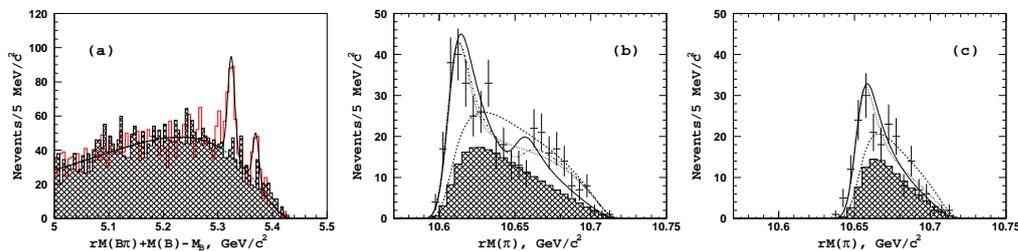
Figure 6: Missing mass of the pairs formed from the reconstructed B candidate and charged pion (a) and missing mass of the charged pions for the $B\pi$ combinations for (b) $\Upsilon(5S) \to B\bar{B}^*\pi$ and (c) $\Upsilon(5S) \to B^*\bar{B}^*\pi$ candidate events.

$\Upsilon(5S) \to [B^*\bar{B}^*]^{\pm}\pi^{\mp}$ signal regions, respectively, indicate clear excess of events over background, peaking at the thresholds [see Fig. 6 (b) and (c)]. These threshold peaks are interpreted as the signals of the $Z_b(10610) \to B\bar{B}^*$ and $Z_b(10650) \to B^*\bar{B}^*$ decays, with significances of 8σ and 6.8σ, respectively. Despite much larger phase-space, no significant signal of the $Z_b(10650) \to B\bar{B}^*$ decay is found.

Assuming that the Z_b decays are saturated by the channels so far observed, Belle calculated relative branching fractions of the $Z_b(10610)$ and $Z_b(10650)$ (see Table 1). The $B^{(*)}\bar{B}^*$ channel

Table 1: Branching fractions ($\mathcal{B}$) of $Z_b(10610)$ and $Z_b(10650)$ assuming that the observed so far channels saturate their decays.

Channel	$\mathcal{B}$ of $Z_b(10610)$, %	$\mathcal{B}$ of $Z_b(10650)$, %
$\Upsilon(1S)\pi^+$	0.32 ± 0.09	0.24 ± 0.07
$\Upsilon(2S)\pi^+$	4.38 ± 1.21	2.40 ± 0.63
$\Upsilon(3S)\pi^+$	2.15 ± 0.56	1.64 ± 0.40
$h_b(1P)\pi^+$	2.81 ± 1.10	7.43 ± 2.70
$h_b(2P)\pi^+$	2.15 ± 0.56	14.8 ± 6.22
$B^+\bar{B}^{*0} + \bar{B}^0 B^{*+}$	86.0 ± 3.6	$-$
$B^{*+}\bar{B}^{*0}$	$-$	73.4 ± 7.0

is dominant and accounts for about 80% of the Z_b decays. The $Z_b(10650) \to B\bar{B}^*$ channel is not included in the table because its significance is marginal. If considered, the $Z_b(10650) \to B\bar{B}^*$ branching fraction would be $(25.4 \pm 10.2)\%$. All other fractions would be reduced by a factor of 1.33.

2.3 Evidence for neutral isotriplet member $Z_b(10610)^0$

Both $Z_b(10610)$ and $Z_b(10650)$ are isotriplets with only charged components observed originally. Belle searched for their neutral components using the $\Upsilon(5S) \to \Upsilon(nS)\pi^0\pi^0$ $(n = 1, 2)$ decays [30]. These decays are observed for the first time and the measured branching fractions $\mathcal{B}[\Upsilon(5S) \to \Upsilon(1S)\pi^0\pi^0] = (2.25 \pm 0.11 \pm 0.22) \times 10^{-3}$ and $\mathcal{B}[\Upsilon(5S) \to \Upsilon(2S)\pi^0\pi^0] = (3.66 \pm 0.22 \pm 0.48) \times 10^{-3}$, are in agreement with isospin relations.

Belle performed the Dalitz plot analyses of the $\Upsilon(5S) \to \Upsilon(1S, 2S)\pi^0\pi^0$ transitions using the same model as for the charged pion channels (see Fig. 7). The $Z_b(10610)^0$ signal is found
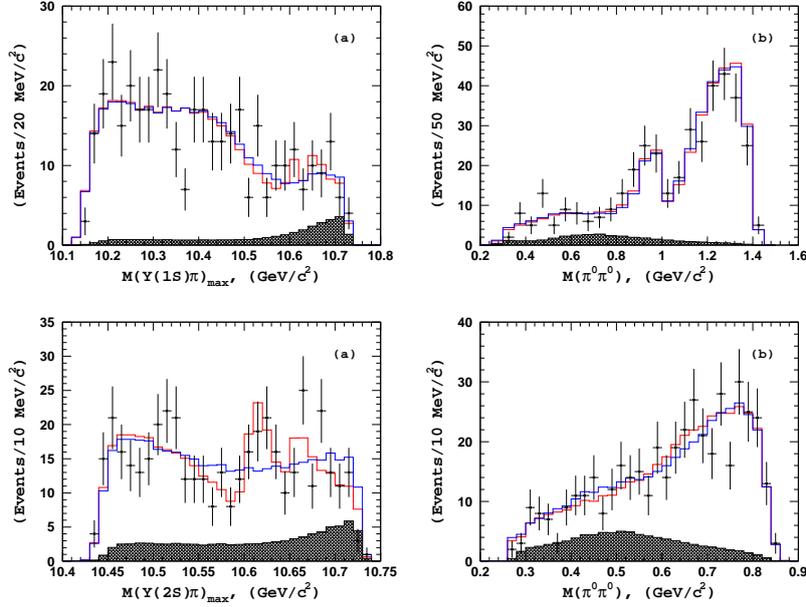

Figure 7: The projections of the Dalitz plot fit for the $\Upsilon(1S)\pi^0\pi^0 p$ (top row) and $\Upsilon(2S)\pi^0\pi^0$ (bottom row) channels on the $\Upsilon(nS)\pi^0$ (left column) and $\pi^0\pi^0$ invariant mass.

in the $\Upsilon(2S)\pi^0$ channel with the significance of $4.9\,\sigma$ including systematics. The $Z_b(10610)^0$ mass of $(10609^{+8}_{-6} \pm 6)\,\text{MeV}/c^2$ is consistent with the charged $Z_b(10610)^\pm$ mass. The signal of the $Z_b(10610)^0$ in the $\Upsilon(1S)\pi^0$ channel and the $Z_b(10650)^0$ signal are insignificant. The Belle data do not contradict the existence of the $Z_b(10610)^0 \to \Upsilon(1S)\pi^0$ and the $Z_b(10650)^0$, but the available statistics are insufficient to establish these signals.

2.4 Interpretations

As discussed at the end of Section 2.2, the assumption of molecular $B^{(*)}\bar{B}^*$ structure naturally explains all observed so far properties of the Z_b states. Their dynamical model, however, is an open question. Proposed interpretations include presence of the compact tetraquark [31], non-resonant rescattering [32], multiple rescatterings that result in the amplitude pole known as coupled channel resonance [33] and deutron-like molecule bound by meson exchanges [34]. All these mechanisms (except for the tetraquark) are intimately related and correspond rather to quantitative than to qualitative differences. Further experimental and theoretical studies are needed to clarify the nature of the Z_b states.

As discussed in Ref. [27], based on heavy quark symmetry one can expect more states with similar nature but with differing quantum numbers. Such states should be accessible in radiative and hadronic transitions in data samples with high statistics at and above the $\Upsilon(5S)$, that will be available at the SuperKEKB.

2.5 Summary

Despite observed only recently, the Z_b states provide a very rich phenomenological object with a lot of experimental information available. They could be very useful for understanding dynamics of the hadronic systems near and above the open flavor thresholds.

3 CKM measurements

Violation of the combined charge-parity symmetry (CP violation) in the SM arises from a single irreducible complex phase in the Cabibbo-Kobayashi-Maskawa (CKM) quark-mixing matrix [35, 36]. Decays that proceed dominantly through the $\bar{b} \rightarrow \bar{u}u\bar{d}$ transition are sensitive to the interior angle of the unitarity triangle $\phi_2\,(\alpha) \equiv \arg(-V_{td}V_{tb}^*)/(V_{ud}V_{ub}^*)$. A feature common to these measurements is that possible loop contributions, in addition to the leading order tree amplitude, can shift the measured angle to $\phi_2^{\mathrm{eff}} \equiv \phi_2 + \Delta\phi_2$. Fortunately, this inconvenience can be overcome with bounds on $\Delta\phi_2$ determined using either an isospin analysis [37] or $SU(3)$ flavor symmetry [38].

Recently Belle published two papers concerning study of $B^0 \rightarrow \pi^+\pi^-$ [39] and $B^0 \rightarrow \rho^0\rho^0$ [40] decays. Both analyses used the final Belle data sample containing 772×10^6 $B\bar{B}$ pairs collected at the $\Upsilon(4S)$ resonance.

In $B^0 \rightarrow \pi^+\pi^-$ decay analysis an improved measurement of the CP violation parameters was performed, which yielded $\mathcal{A}_{CP}(B^0 \rightarrow \pi^+\pi^-) = +0.33 \pm 0.06$ (stat) $\pm\, 0.03$ (syst) and $\mathcal{S}_{CP}(B^0 \rightarrow \pi^+\pi^-) = -0.64\pm0.08$ (stat)±0.03 (syst), confirming CP violation in these channels reported in previous measurements and other experiments. These results from the full Belle data sample after reprocessing with a new tracking algorithm and with an optimized analysis performed with a single simultaneous fit, supersede those of the previous Belle analysis [41]. They are now the world's most precise measurement of time-dependent CP violation parameters in $B^0 \rightarrow \pi^+\pi^-$, ruling out the range $23.8° < \phi_2 < 66.8°$, at the 1σ level.

Since the dominant tree process in $B^0 \rightarrow \rho^0\rho^0$ is color-suppressed, it is expected to be rarer than its isospin partners, making the isospin analysis less ambiguous. The vector state $\rho^0\rho^0$ is not a pure CP eigenstate, but rather a superposition of CP-even and -odd states, or three helicity amplitudes, with only the longitudinal one being a pure CP eigenstate. In general, the different helicity amplitudes can be separated through an angular analysis. This analysis is concerned with the branching fraction of $B^0 \rightarrow \rho^0\rho^0$ decays, the fraction of longitudinal polarization in these decays and decays into four charged pion final states as the ρ^0 decays dominantly into two charged pions.

Branching fraction was measured to be $\mathcal{B}(B^0 \rightarrow \rho^0\rho^0) = (1.02 \pm 0.30$ (stat) ± 0.22 (syst)$) \times 10^{-6}$ with a longitudinally polarization fraction $f_L = 0.21^{+0.18}_{-0.22}$ (stat)±0.11 (syst). The branching fraction's upper limit is $\mathcal{B}(B^0 \rightarrow \rho^0\rho^0) < 1.5 \times 10^{-6}$ at 90% confidence level. The longitudinal polarization fraction was used to determine the CKM matrix angle $\phi_2 = (91.0\pm7.2)°$ through an isospin analysis in the $B \rightarrow \rho\rho$ system. Furthermore for possible decays with the same final state the following branching fractions were obtained: $\mathcal{B}(B^0 \rightarrow f_0\rho^0) \times \mathcal{B}(f_0 \rightarrow \pi^+\pi^-) = (0.86\pm0.27$ (stat)±0.15 (syst)$)\times10^{-6}$, with a significance of 3.0 standard deviations, and upper limits at 90% confidence level on the (product) branching fractions, $\mathcal{B}(B^0 \rightarrow \pi^+\pi^-\pi^+\pi^-) < 11.7\times10^{-6}$, $\mathcal{B}(B^0 \rightarrow \rho^0\pi^+\pi^-) < 12.2\times10^{-6}$, $\mathcal{B}(B^0 \rightarrow f_0\pi^+\pi^-) \times \mathcal{B}(f_0 \rightarrow \pi^+\pi^-) < 3.1\times10^{-6}$ and $\mathcal{B}(B^0 \rightarrow f_0f_0) \times \mathcal{B}(f_0 \rightarrow \pi^+\pi^-)^2 < 0.2 \times 10^{-6}$. For $B^0 \rightarrow f_0\rho^0$ decay this is the first evidence with such a significance.

References

[1] W. S. Hou, Phys. Rev. D **48**, 2342 (1993).

[2] S. Baek and Y. G. Kim, Phys. Rev. D **60**, 077701 (1999).

[3] R. Garisto, Phys. Rev. D **51**, 1107 (1995); M. Tanaka, Z. Phys. C **67**, 321 (1995).

[4] K. Ikado *et al.* (Belle Collaboration), Phys. Rev. Lett. **97**, 251802 (2006).

[5] K. Hara *et al.* (Belle Collaboration), Phys. Rev. D **82**, 071101(R) (2010).

[6] K. Hara *et al.* (Belle Collaboration), Phys. Rev. Lett. **110**, 131801 (2013).

[7] M. Feindt *et al.*, Nucl. Instrum. Meth. A **654**, 432 (2011).

[8] B. Aubert *et al.* (BaBar Collaboration), Phys. Rev. D **81**, 051101(R) (2010).

[9] J. P. Lees *et al.* (BaBar Collaboration), Phys. Rev. D **88**, 031102 (2013).

[10] J. Charles *et al.* (CKMfitter Group), Eur. Phys. J. C **41**, 1 (2005).

[11] H. Na *et al.* (HPQCD Collaboration), Phys. Rev. D **86**, 034506 (2012).

[12] J. Beringer *et al.* (Particle Data Group), Phys. Rev. D **86**, 010001 (2012).

[13] Y. Yook, PoS ICHEP2012 369 (2012).

[14] N. Satoyama *et al.* (Belle Collaboration), Phys. Lett. B **647**, 67 (2007).

[15] B. Aubert *et al.* (BaBar Collaboration), Phys. Rev. D **79**, 091101 (2009).

[16] A. Matyja *et al.* (Belle Collaboratoin), Phys. Rev. Lett. **99**, 191807 (2007).

[17] A. Bozek *et al.* (Belle Collaboration), Phys. Rev. D **82**, 072005 (2010).

[18] I. Adachi *et al.* (Belle Collaboration), arXiv:0910.4301.

[19] A. Bozek, *Summary of $B \to D^{(*)}\tau\nu$ measurements*, 2nd KEK Flavor Factory Workshop, KEK, Tsukuba, Japan (2013).

[20] J. P. Lees *et al.* (BaBar Collaboration), Phys. Rev. Lett. **109**, 101802 (2012); arXiv:1303.0571.

[21] B. Aubert *et al.* (BaBar Collaboration), Phys. Rev. Lett. **100**, 021801 (2008).

[22] S. Fajfer, J. F. Kamenik and I. Nisandzic, Phys. Rev. D **85**, 094025 (2012).

[23] M. Tanaka and R. Watanabe, Phys. Rev. D **82**, 034027 (2010); M. Tanaka and R. Watanabe, Phys. Rev. D **87**, 034028 (2013).

[24] I. Adachi *et al.* (Belle Collaboration), Phys. Rev. Lett. **108**, 032001 (2012).

[25] A. Bondar *et al.* (Belle Collaboration), Phys. Rev. Lett. **108**, 122001 (2012).

[26] I. Adachi *et al.* (Belle Collaboration), arXiv:1105.4583 [hep-ex].

[27] A. E. Bondar, A. Garmash, A. I. Milstein, R. Mizuk and M. B. Voloshin, Phys. Rev. D **84**, 054010 (2011).

[28] I. Adachi *et al.* (Belle Collaboration), arXiv:1209.6450 [hep-ex].

[29] A. Drutskoy *et al.* (Belle Collaboration), Phys. Rev. D **81**, 112003 (2010).

[30] I. Adachi *et al.* (Belle Collaboration), arXiv:1207.4345 [hep-ex].

[31] A. Ali, C. Hambrock and W. Wang, Phys. Rev. D **85**, 054011 (2012).

[32] D. -Y. Chen and X. Liu, Phys. Rev. D **84**, 094003 (2011).

[33] I. V. Danilkin, V. D. Orlovsky and Y. .A. Simonov, Phys. Rev. D **85**, 034012 (2012).

[34] S. Ohkoda, Y. Yamaguchi, S. Yasui, K. Sudoh and A. Hosaka, Phys. Rev. D **86**, 014004 (2012).

[35] N. Cabibbo, Phys. Rev. Lett. **10**, 531 (1963).

[36] M. Kobayashi and T. Maskawa, Prog. Theor. Phys. **49**, 652 (1973).

[37] M. Gronau and D. London, Phys. Rev. Lett **65**, 3381 (1990).

[38] M. Gronau and J. Zupan, Phys. Rev. D **73**, 057502 (2006).

[39] J. Dalseno *et al.* (Belle Collaboration), Phys. Rev. D **88**, 092003 (2013).

[40] P. Vanhoefer *et al.* (Belle Collaboration), arXiv:1212.4015 [hep-ex].

[41] H. Ishino *et al.* (Belle Collaboration), Phys. Rev. Lett **98**, 211801 (2007).

Light and Heavy Hadrons in AdS/QCD

Valery E. Lyubovitskij[1],*, Thomas Gutsche[1], Ivan Schmidt[2], Alfredo Vega[3]

[1]Institut für Theoretische Physik, Universität Tübingen,
Kepler Center for Astro and Particle Physics,
Auf der Morgenstelle 14, D–72076 Tübingen, Germany
[2]Departamento de Física y Centro Científico Tecnológico de Valparaíso (CCTVal),
Universidad Técnica Federico Santa María, Casilla 110-V, Valparaíso, Chile
[3]Departamento de Física y Astronomía, Universidad de Valparaíso,
Avenida Gran Bretaña 1111, Valparaíso, Chile

We discuss light and heavy hadrons in a holographic soft-wall AdS/QCD model. This approach is based on an action which describes hadron structure with broken conformal and chiral invariance and incorporates confinement through the presence of a background dilaton field. According to the gauge/gravity duality the five-dimensional boson and fermion fields propagating in AdS space are dual to four-dimensional fields leaving on the surface of AdS sphere, which correspond to hadrons. In this picture hadronic wave functions — basics blocks of hadronic properties — are dual to the profiles of AdS fields in the fifth (holographic) dimension, which is identified with scale variable. As applications we consider properties of light and heavy hadrons from unified point of view: mass spectrum, form factors, decay rates and parton distributions.

Based on the gauge/gravity duality [1], a class of AdS/QCD approaches which model QCD by using methods of extra-dimensional field theories formulated in anti-de Sitter (AdS) space, was recently successfully developed for describing the phenomenology of hadronic properties (for a recent review see e.g. [2]). One of the popular formalisms of this kind is the "soft-wall" model [3]-[6] which uses a soft infrared (IR) cutoff in the fifth dimension. This procedure can be introduced in the following ways: i) as a background field (dilaton) in the overall exponential of the action ("dilaton" soft-wall model), ii) in the warping factor of the AdS metric ("metric" soft-wall model), iii) in the effective potential of the action. In Ref. [5] we showed that these three ways of proceeding are equivalent to each other via a redefinition of the bulk fields and by inclusion of extra effective potentials in the action. In our opinion, the "dilaton" form of the soft-wall model is more convenient in performing the calculations.

In this paper we consider such type of soft-wall AdS/QCD approach. We report the applications of our approach to the properties of light and heavy hadrons. In particular, we present results for hadronic mass spectra, coupling constants and form factors [4]-[6].

---

*On leave of absence from Department of Physics, Tomsk State University, 634050 Tomsk, Russia

VALERY E. LYUBOVITSKIJ, THOMAS GUTSCHE, IVAN SCHMIDT, ALFREDO VEGA

1 Approach

Here we briefly review our approach. First, we specify the five-dimensional AdS metric:

$$
\begin{aligned}
ds^2 = g_{MN}dx^M dx^N &= \eta_{ab}\, e^{2A(z)}\, dx^a dx^b = e^{2A(z)}\left(\eta_{\mu\nu}dx^\mu dx^\nu - dz^2\right), \\
\eta_{\mu\nu} &= \mathrm{diag}(1,-1,-1,-1,-1),
\end{aligned}
\tag{1}
$$

where M and $N = 0,1,\cdots,4$ are the space-time (base manifold) indices, $a = (\mu, z)$ and $b = (\nu, z)$ are the local Lorentz (tangent) indices, and g_{MN} and η_{ab} are curved and flat metric tensors, respectively, which are related by the vielbein $\epsilon_M^a(z) = e^{A(z)}\, \delta_M^a$ as $g_{MN} = \epsilon_M^a \epsilon_N^b \eta_{ab}$. Here z is the holographic coordinate, R is the AdS radius, and $g = |\det g_{MN}|$. In the following we restrict ourselves to a conformal-invariant metric with $A(z) = \log(R/z)$.

The relevant AdS/QCD actions for the boson and fermion field of spin J are [4]-[6]

$$
\begin{aligned}
S_B &= \int d^4x dz \, \sqrt{g}\, e^{-\varphi(z)} \Bigg[\mathcal{D}_M \Phi_{M_1\cdots M_J}(x,z) \mathcal{D}^M \Phi^{M_1\cdots M_J}(x,z) \\
&\quad - \left((\mu_J^B)^2 + U_J^B(z)\right) \Phi_{M_1\cdots M_J}(x,z)\Phi^{M_1\cdots M_J}(x,z) \Bigg],
\end{aligned}
\tag{2}
$$

$$
\begin{aligned}
S_F &= S_F^+ + S_F^-, \quad S_F^\pm = \int d^4x dz\, \sqrt{g}\, e^{-\varphi(z)} \sum_{i=+,-} \Bigg[\bar{\Psi}^\pm_{M_1\cdots M_J}(x,z) i\mathcal{D}_M^\pm \Psi^{\pm\, M_1\cdots M_J}(x,z) \\
&\quad \mp \bar{\Psi}^\pm_{M_1\cdots M_J}(x,z)\left((\mu_J^F)^2 + U_J^F(z)\right)\Psi^{\pm\, M_1\cdots M_J}(x,z)
\end{aligned}
\tag{3}
$$

where $\mathcal{D}_M$ and $\mathcal{D}_M^\pm$ are the covariant derivative (including external vector and axial fields) acting on boson $\Phi_{M_1\cdots M_J}$ and fermion $\Psi^\pm_{M_1\cdots M_J}$ fields, respectively. $\Psi^\pm_{M_1\cdots M_J}$ is the pair of bulk fermion fields, which are the holographic analogues of the left- and right-chirality fermion operators in the 4D theory. $\varphi(z) = \kappa^2 z^2$ is the dilaton field with κ being a free scale parameter. The quantities μ_J^B and μ_J^F are the bulk boson and fermion masses related to the conformal dimensions (Δ_J^B, Δ_J^F) of the spin-J AdS boson and fermion fields, respectively

$$
(\mu_J^B R)^2 = \Delta_J^B(\Delta_J^B - 4), \quad \mu_J^F R = \Delta_J^F - 2
\tag{4}
$$

As was shown in Refs. [7] and [5] the field dimensions Δ_J^B and Δ_J^F are related to twist-dimension $\tau_{B/F}$ of hadronic operators as

$$
\Delta_J^B = \tau_B = 2 + L, \quad \Delta_J^F = \tau_F + \frac{1}{2} = \frac{7}{2} + L.
\tag{5}
$$

where $L = \max|L_z|$ is the maximal value of the z component of the quark orbital angular momentum in hadron [7]: $U_J^B(z) = 4\varphi(z)(J-1)/R^2$ and $U_J^F(z) = \varphi(z)/R$ are the effective dilaton potentials. Note the choice of quadratic dilaton profile and potentials $U_J^B(z)$ and $U_J^F(z)$ is necessary in order to guarantee correct Regge behavior of hadronic mass spectra and asymptotic power scaling of hadronic factors at large momenta transfer in agreement with quark counting rules [4]-[6].

Notice that the fermion masses and the effective potentials corresponding to the fields Ψ^+ and Ψ^- have opposite signs according to the P-parity transformation. The absolute sign of the fermion mass is related to the chirality of the boundary operator. According to our conventions

the QCD operators $\mathcal{O}_R$ and $\mathcal{O}_L$ have positive and negative chirality, and therefore the mass terms of the bulk fields Ψ^+ and Ψ^- have absolute signs "plus" and "minus", respectively.

One of the main advantages of the soft-wall AdS/QCD model is that the most of the calculations can be done analytically. In a first step, we show how in this approach the hadron wave functions and spectrum are generated. We follow the procedure pursued in Refs. [4]-[6]. We drop the external vector and axial fields in covariant derivatives, turn to the tangent space with Lorentz signature, where the AdS fields are rescaled as

$$\Phi_{\mu_1\cdots\mu_J} = e^{\varphi(z)/2+A(z)J}\phi_{\mu_1\cdots\mu_J}\,, \quad \Psi^{\pm}_{\mu_1\cdots\mu_J} = e^{\varphi(z)/2+A(z)(J-1/2)}\psi^{\pm}_{\mu_1\cdots\mu_J}\,. \tag{6}$$

Next we split the fermion field into left- and right-chirality components

$$\psi^{\pm}_{\mu_1\cdots\mu_J}(x,z) = \psi^{\pm\,L}_{\mu_1\cdots\mu_J}(x,z) + \psi^{\pm\,R}_{\mu_1\cdots\mu_J}(x,z) \tag{7}$$

and perform Kaluza-Klein (KK) expansion for $\phi_{\mu_1\cdots\mu_J}(x,z)$ and $\psi^{\pm\,L/R}_{\mu_1\cdots\mu_J}(x,z)$

$$\begin{aligned}
\phi_{\mu_1\cdots\mu_J}(x,z) &= \sum_n \phi_{n\,\mu_1\cdots\mu_J}(x)\,F_{n\tau}(z)\,, \\
\psi^{\pm\,L/R}_{\mu_1\cdots\mu_J}(x,z) &= \frac{1}{\sqrt{2}}\sum_n \psi^{L/R}_{n\,\mu_1\cdots\mu_J}(x)\,G^{\pm\,L/R}_{n\tau}(z)\,,
\end{aligned} \tag{8}$$

where the tower of the KK fields $\phi_{n\,\mu_1\cdots\mu_J}(x)$ is dual to four-dimensional fields describing mesons with spin J, while KK fields $\psi^{L/R}_{n\,\mu_1\cdots\mu_J}(x)$ are dual left/right-chirality fermion fields describing baryons with spin J. The number n corresponds to the radial quantum number. The set of functions $F_{n\tau}(z)$ are the profiles of boson AdS fields in holographic direction, which are dual to the mesonic wave functions with twist τ and radial quantum number n. In case of baryon we have four sets of such profiles dual to baryonic wave functions, which satisfy to the following relation (due P- and C-invariance)

$$G^{\pm\,R}_{n\tau}(z) = \mp G^{\mp\,L}_{n\tau}(z)\,. \tag{9}$$

Then it is convenient to rescale the boson and fermion profiles as

$$F_{n\tau}(z) = e^{-3/2A(z)}f_{n\tau}(z)\,, \quad G^{\pm\,R/L}_{n\tau}(z) = e^{-2A(z)}g^{\pm\,R/L}_{n\tau}(z) \tag{10}$$

in order derive the Schrödinger-type equation of motions (EOMs) for the wave functions $f_{n\tau}$ and $g^{\pm\,L/R}_{n\tau}(z)$

$$\left[-\partial_z^2 + \frac{4L^2-1}{4z^2} + \kappa^4 z^2 + 2\kappa^2(J-1)\right]f_{n\tau}(z) = M^2_{B,n\tau J}\,f_{n\tau}(z) \tag{11}$$

and

$$\left[-\partial_z^2 + \kappa^4 z^2 + 2\kappa^2\left(m\mp\frac{1}{2}\right) + \frac{m(m\pm1)}{z^2}\right]g^{L/R}_{n\tau}(z) = M^2_{F,n\tau}\,g^{L/R}_{n\tau}(z)\,, \tag{12}$$

where $m = \tau - 3/2$; $M_{B,n\tau J}$ and $M_{F,n\tau}$ are the masses of bosons and fermions dual to corresponding hadrons (mesons and baryons) with specific values of quantum numbers.

Above EOMs have analytical solutions for both wave functions

$$
\begin{aligned}
f_{n\tau}(z) &= \sqrt{\frac{2\Gamma(n+1)}{\Gamma(n+\tau-1)}} \; \kappa^{\tau-1} \; z^{\tau-3/2} \; e^{-\kappa^2 z^2/2} \; L_n^{\tau-2}(\kappa^2 z^2), \\
g_{n\tau}^L(z) &= \sqrt{\frac{2\Gamma(n+1)}{\Gamma(n+\tau)}} \; \kappa^{\tau} \; z^{\tau-1/2} \; e^{-\kappa^2 z^2/2} \; L_n^{\tau-1}(\kappa^2 z^2), \\
g_{n\tau}^R(z) &= \sqrt{\frac{2\Gamma(n+1)}{\Gamma(n+\tau-1)}} \; \kappa^{\tau-1} \; z^{\tau-3/2} \; e^{-\kappa^2 z^2/2} \; L_n^{\tau-2}(\kappa^2 z^2)
\end{aligned}
\tag{13}
$$

and mass spectrum

$$
M_{B,n\tau J}^2 = 4\kappa^2\Big(n+\frac{\tau+J}{2}-1\Big), \qquad M_{F,n\tau}^2 = 4\kappa^2\Big(n+\tau-1\Big).
\tag{14}
$$

Therefore, our main idea is to find the solutions for the bulk profiles of the AdS field in the z–direction, and then calculate the physical properties of hadrons in terms of the bulk profiles of AdS fields dual to hadronic wave functions. In this way both mass spectrum and dynamical hadronic properties like form factors and parton distributions will be calculated from a unified point of view based on the solutions of the Schrödinger-type EOMs (13). One can see that the bulk profiles of AdS fields have the correct scaling behavior for small z, which leads to correct power behavior of calculated hadronic form factors at large Q^2. Another important property of the bulk profiles is that they vanish at large z (confinement). Up to now we discussed the solutions of EOMs for the bulk profiles on its mass shell $p^2 = M^2$. In case when we go beyond mass shell, we can calculate so-called bulk-to-boundary propagators describing the behavior of bulk profiles at arbitrary p^2, which are necessary for calculation of momentum dependence of matrix elements in our approach. In particular, the bulk-to-boundary propagator for the vector AdS field dual to electromagnetic field is given in analytical form in terms of the Gamma $\Gamma(n)$ and Tricomi $U(a,b,z)$ functions:

$$
V(Q,z) = \Gamma\Big(1+\frac{Q^2}{4\kappa^2}\Big) U\Big(\frac{Q^2}{4\kappa^2}, 0, \kappa^2 z^2\Big).
\tag{15}
$$

The bulk-to-boundary propagator $V(Q,z)$ obeys the normalization condition $V(0,z)=1$ consistent with gauge invariance and fulfils the following ultraviolet (UV) and infrared (IR) boundary conditions: $V(Q,0)=1$, $V(Q,\infty)=0$. The UV boundary condition corresponds to the local (structureless) coupling of the electromagnetic field to matter fields, while the IR boundary condition implies that the vector field vanishes at $z=\infty$. E.g. a generic expression for the meson form factor is given in the form integral over z variable of the product of $V(Q,z)$ and bulk profiles corresponding to the wave functions of initial (in) and final (fin) meson

$$
F_M(Q^2) = \int_0^\infty dz\, V(Q,z) f_{\text{in}}(z) f_{\text{fin}}(z).
\tag{16}
$$

Another advantage of our approach is a possibility to constraint the form of light-front wave functions (see detailed discussion in Refs. [4]-[6]) from matching of matrix elements of physical processes in AdS/QCD and Light-Front QCD. The idea of such matching was proposed in Ref. [7]. Next step is inclusion of effects of quark masses in agreement with constraints imposed by chiral symmetry and heavy quark effective theory.

2 Applications

2.1 Meson mass spectrum and leptonic decay constants

We consider applications of our approach to mass spectrum, decay constants, form factors and parton distributions. First we present the results for the mass spectrum and decay constants of mesons: light, heavy-light and heavy quarkonia (see Tables I-V).

Table I. Masses of light mesons.

Meson	n	L	S	Mass [MeV]			
π	0,1,2,3	0	0	140	1010	1421	1738
K	0	0,1,2,3	0	495	1116	1498	1801
η	0,1,2,3	0	0	566	11494	1523	1822
$f_0[\bar{n}n]$	0,1,2,3	1	1	721	1233	1587	1876
$f_0[\bar{s}s]$	0,1,2,3	1	1	985	1404	1723	1993
$\rho(770)$	0,1,2,3	0	1	721	1233	1587	1876
$\omega(782)$	0,1,2,3	0	1	721	1233	1587	1876
$\phi(1020)$	0,1,2,3	0	1	985	1404	1723	1993
$a_1(1260)$	0,1,2,3	1	1	1010	1421	1738	2005

Table II. Masses of heavy-light mesons.

Meson	J^P	n	L	S	Mass [MeV]			
$D(1870)$	0^-	0	0,1,2,3	0	1870	2000	2121	2235
$D^*(2010)$	1^-	0	0,1,2,3	1	2000	2121	2235	2345
$D_s(1969)$	0^-	0	0,1,2,3	0	1970	2093	2209	2320
$D_s^*(2107)$	1^-	0	0,1,2,3	1	2093	2209	2320	2425
$B(5279)$	0^-	0	0,1,2,3	0	5280	5327	5374	5420
$B^*(5325)$	1^-	0	0,1,2,3	1	5336	5374	5420	5466
$B_s(5366)$	0^-	0	0,1,2,3	0	5370	5416	5462	5508
$B_s^*(5413)$	1^-	0	0,1,2,3	1	5416	5462	5508	5553

Table III. Masses of heavy quarkonia.

Meson	J^P	n	L	S	Mass [MeV]			
$\eta_c(2980)$	0^-	0,1,2,3	0	0	2975	3477	3729	3938
$\psi(3097)$	1^-	0,1,2,3	0	1	3097	3583	3828	4032
$\chi_{c0}(3415)$	0^+	0,1,2,3	1	1	3369	3628	3843	4038
$\chi_{c1}(3510)$	1^+	0,1,2,3	1	1	3477	3729	3938	4129
$\chi_{c2}(3555)$	2^+	0,1,2,3	1	1	3583	3828	4032	4219
$\eta_b(9390)$	0^-	0,1,2,3	0	0	9337	9931	10224	10471
$\Upsilon(9460)$	1^-	0,1,2,3	0	1	9460	10048	10338	10581
$\chi_{b0}(9860)$	0^+	0,1,2,3	1	1	9813	10110	10359	10591
$\chi_{b1}(9893)$	1^+	0,1,2,3	1	1	9931	10224	10471	10700
$\chi_{b2}(9912)$	2^+	0,1,2,3	1	1	10048	10338	10581	10808
$B_c(6277)$	0^-	0,1,2,3	0	0	6277	6719	6892	7025

Table IV. Decay constants f_P (MeV) of pseudoscalar mesons.

Meson	Data	Our
π^-	$130.4 \pm 0.03 \pm 0.2$	153
K^-	$156.1 \pm 0.2 \pm 0.8$	153
D^+	206.7 ± 8.9	207
D_s^+	257.5 ± 6.1	224
B^-	193 ± 11	163
B_s^0	$253 \pm 8 \pm 7$	170
B_c	$489 \pm 5 \pm 3$	489

Table V. Decay constants f_V (MeV) of vector mesons.

Meson	Data	Our	Meson	Data	Our
ρ^+	210.5 ± 0.6	216	ρ^0	154.7 ± 0.7	153
D^*	$245 \pm 20^{+3}_{-2}$	207	ω	45.8 ± 0.8	51
D_s^*	$272 \pm 16^{+3}_{-20}$	224	ϕ	76 ± 1.2	72
B^*	$196 \pm 24^{+39}_{-2}$	170	J/ψ	277.6 ± 4	223
B_s^*	$229 \pm 20^{+41}_{-16}$	170	$\Upsilon(1s)$	238.5 ± 5.5	170

One should stress that our analytical results for the masses of light pseudoscalar mesons are consistent with chiral symmetry: $M_\pi^2, M_K^2, M_\eta^2 \to 0$ at $m_{u,d}, m_s \to 0$. The masses and leptonic decay constant of heavy-light mesons are consistent with constraints imposed by heavy quark mass limit. In particular, the heavy quark mass expansion of heavy-light mesons masses reads $M_{Qq} = m_Q + \bar{\Lambda} + \mathcal{O}(1/m_Q)$ and their leptonic decay constants scale as $f_{Qq} \sim 1/\sqrt{m_Q}$.

2.2 Electromagnetic structure of nucleon

Here from unified point of view we describe nucleon form factors and the electroproduction of the $N(1440)$ Roper resonance. The Roper resonance is identified as the first radially excited state of the nucleon. The obtained results for helicity amplitudes of the Roper electroproduction are in good agreement with the recent results of the CLAS Collaboration at JLab. In Table VI we present our results for the nucleon properties: mass, magnetic moments, electromagnetic and axial charge radii. In Figs. 1-2 we present selected results for the electromagnetic form factors of nucleon.

Table VI. Mass and electromagnetic properties of nucleons.

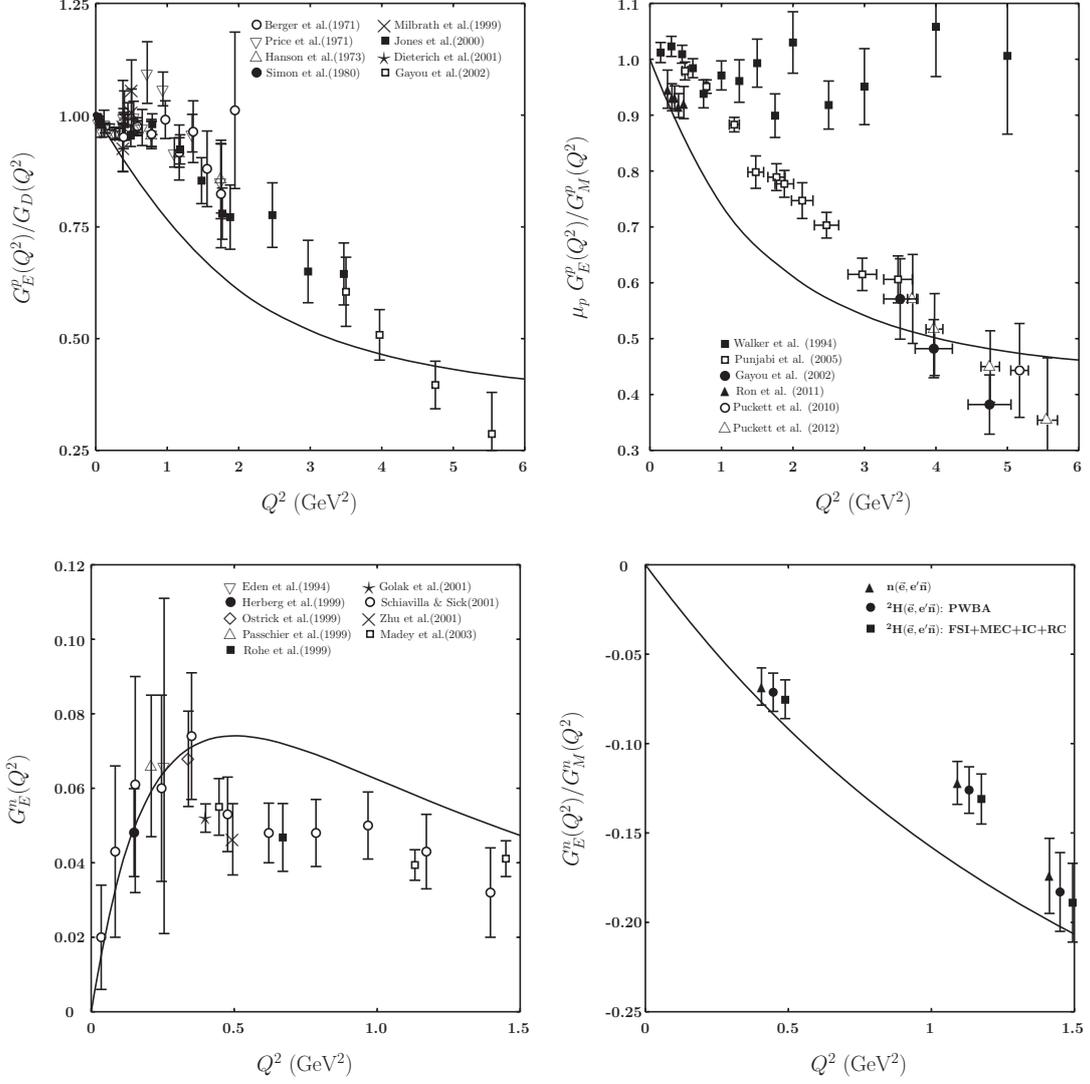| Quantity	Our results	Data [9]
m_p (GeV)	0.93827	0.93827
μ_p (in n.m.)	2.793	2.793
μ_n (in n.m.)	-1.913	-1.913
g_A	1.270	1.2701
r_E^p (fm)	0.840	0.8768 ± 0.0069
$\langle r_E^2 \rangle^n$ (fm^2)	-0.117	-0.1161 ± 0.0022
r_M^p (fm)	0.785	$0.777 \pm 0.013 \pm 0.010$
r_M^n (fm)	0.792	$0.862^{+0.009}_{-0.008}$
r_A (fm)	0.667	0.67 ± 0.01

Figure 1: The ratios $G_E^p(Q^2)/G_D(Q^2)$, $G_E^p(Q^2)/G_M^p(Q^2)$, $G_E^n(Q^2)/G_M^n(Q^2)$ and charge neutron form factor $G_E^n(Q^2)$.

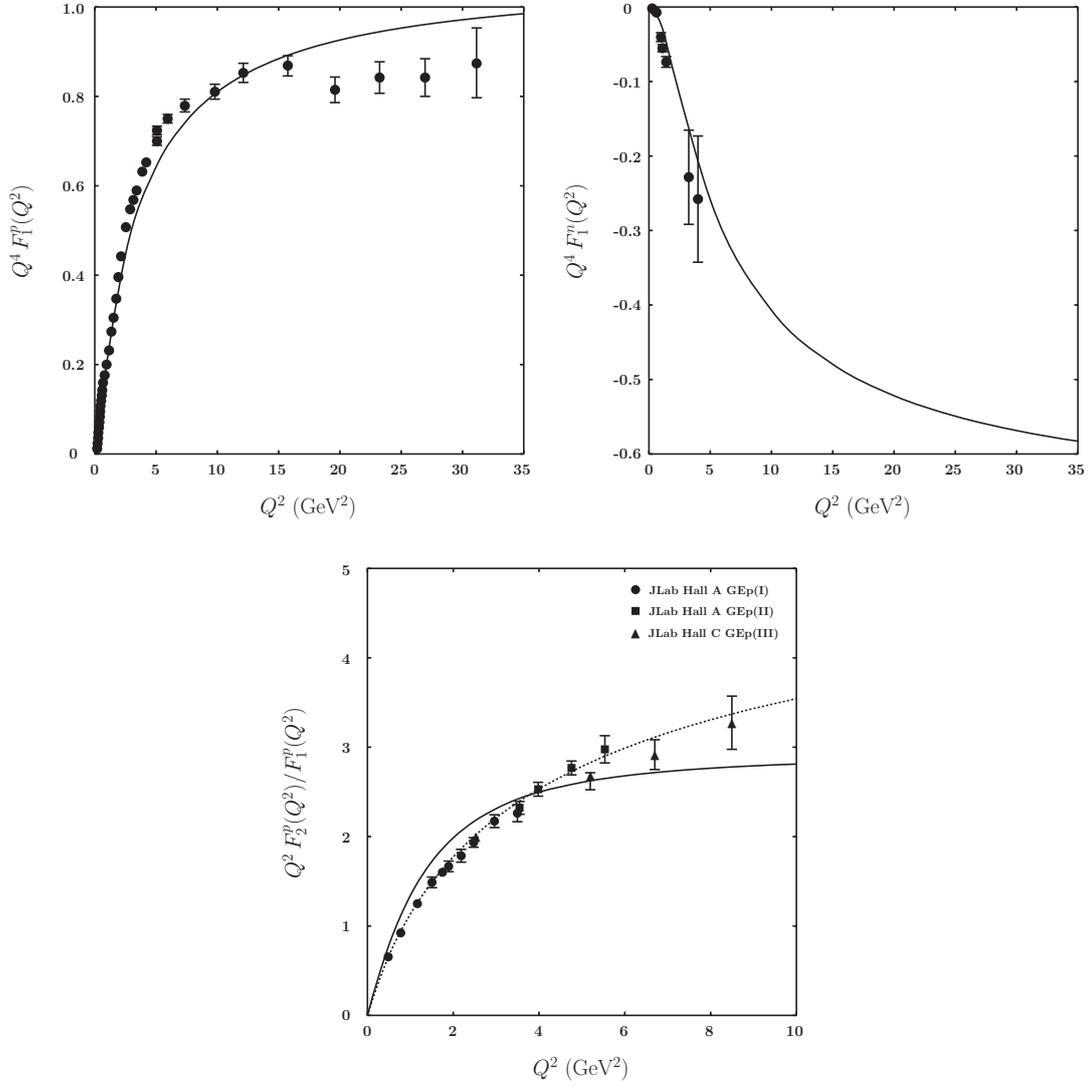VALERY E. LYUBOVITSKIJ, THOMAS GUTSCHE, IVAN SCHMIDT, ALFREDO VEGA

Figure 2: Proton and neutron Dirac form factor multiplied with Q^4, ratios $Q^2 F_2^p(Q^2)/F_1^p(Q^2)$ (the dashed line is the approximation of data suggested in Ref. [8]) and $G_A(Q^2)/G_A^D(Q^2)$.

Table VII. Helicity amplitudes $A_{1/2}^N(0)$ and $S_{1/2}^N(0)$, $N = p, n$.

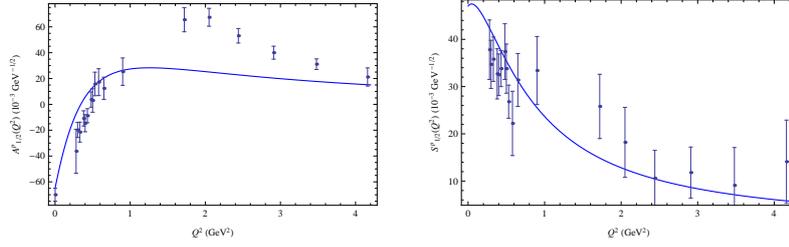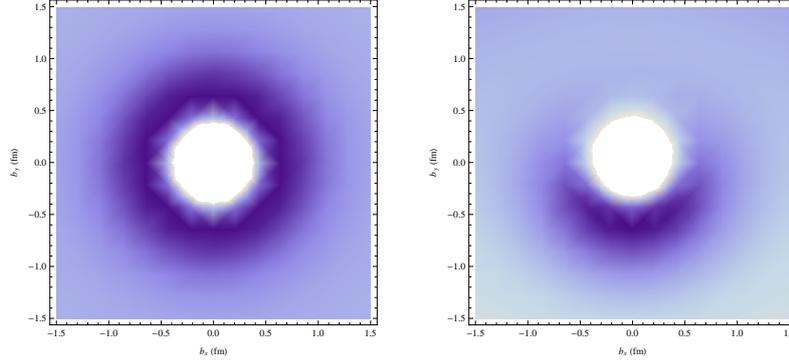| Quantity	Our results	Data [9]
$A_{1/2}^p(0)$ (GeV$^{-1/2}$)	-0.065 (-0.065)	-0.065 ± 0.004
$A_{1/2}^n(0)$ (GeV$^{-1/2}$)	0.040 (0.040)	0.040 ± 0.010
$S_{1/2}^p(0)$ (GeV$^{-1/2}$)	0.047 (0.048)	
$S_{1/2}^n(0)$ (GeV$^{-1/2}$)	-0.044 (-0.045)	

Figure 3: Helicity amplitudes $A_{1/2}^p(Q^2)$ and $S_{1/2}^p(Q^2)$ up to $Q^2 = 4$ GeV^2.

Figure 4: Transition charge densities for unpolarized and transversely polarized nucleon and Roper.

In Table VII we present our results for the helicity amplitudes $A_{1/2}^N(0)$ and $S_{1/2}^N(0)$, $N = p, n$ at $Q^2 = 0$. In Fig. 3 we present our predictions for the Q^2 dependence of helicity amplitudes. Results for the transition charge densities for unpolarized and transversely polarized nucleon and Roper in the transverse impact parameter plane $\mathbf{b}_\perp = (b_x, b_y)$ are shown in Fig. 4.

From Fig.3 it should be evident that our results for the helicity amplitudes in the proton case have qualitative agreement with the present data of the CLAS Collaboration [10]. Within the current approach it is difficult to reproduce the maximum of data for $A_{1/2}^p$ at about 2 GeV^2. Further data for the helicity amplitudes in the region from 1.6 to 4 GeV^2 could be accumulated at the upgraded facilities of JLab and certainly help to clarify the theoretical understanding.

Acknowledgements

References

[1] J. M. Maldacena, Adv. Theor. Math. Phys. **2**, 231 (1998) [Int. J. Theor. Phys. **38**, 1113 (1999)]; S. S. Gubser, I. R. Klebanov and A. M. Polyakov, Phys. Lett. B **428**, 105 (1998); E. Witten, Adv. Theor. Math. Phys. **2**, 253 (1998).

[2] Y. Kim and D. Yi, Adv. High Energy Phys. **2011**, 1 (2011).

[3] A. Karch, E. Katz, D. T. Son and M. A. Stephanov, "Linear Confinement and AdS/QCD," Phys. Rev. D **74**, 015005 (2006); S. J. Brodsky and G. F. de Teramond, "Hadronic spectra and light-front wavefunctions in holographic QCD," Phys. Rev. Lett. **96**, 201601 (2006); O. Andreev, "$1/q^2$ corrections and gauge / string duality," Phys. Rev. D **73**, 107901 (2006)

[4] T. Branz, T. Gutsche, V. E. Lyubovitskij, I. Schmidt and A. Vega, "Light and heavy mesons in a soft-wall holographic approach," Phys. Rev. D **82**, 074022 (2010); A. Vega, I. Schmidt, T. Branz, T. Gutsche and V. E. Lyubovitskij, "Meson wave function from holographic models," Phys. Rev. D **80**, 055014 (2009); T. Gutsche, V. E. Lyubovitskij, I. Schmidt and A. Vega, "Chiral Symmetry Breaking and Meson Wave Functions in Soft-Wall AdS/QCD," Phys. Rev. D **87**, 056001 (2013).

[5] T. Gutsche, V. E. Lyubovitskij, I. Schmidt and A. Vega, "Dilaton in a soft-wall holographic approach to mesons and baryons," Phys. Rev. D **85**, 076003 (2012).

[6] T. Gutsche, V. E. Lyubovitskij, I. Schmidt and A. Vega, "Nucleon structure including high Fock states in AdS/QCD," Phys. Rev. D **86**, 036007 (2012); A. Vega, I. Schmidt, T. Gutsche, V. E. Lyubovitskij, "Generalized parton distributions in AdS/QCD," Phys. Rev. D **83**, 036001 (2011); T. Gutsche, V. E. Lyubovitskij, I. Schmidt and A. Vega, "Nucleon resonances in AdS/QCD," Phys. Rev. D **87**, 016017 (2013).

[7] S. J. Brodsky, G. F. de Teramond, "Hadronic spectra and light-front wavefunctions in holographic QCD," Phys. Rev. Lett. **96**, 201601 (2006); S. J. Brodsky and G. F. de Teramond, "Light-Front Dynamics and AdS/QCD Correspondence: The Pion Form Factor in the Space- and Time-Like Regions," Phys. Rev. D **77**, 056007 (2008).

[8] S. J. Brodsky, "Perspectives on exclusive processes in QCD," arXiv:hep-ph/0208158 (2002).

[9] J. Beringer *et al.* (Particle Data Group), "Review of Particle Physics (RPP)," Phys. Rev. D **86**, 010001 (2012).

[10] V. I. Mokeev *et al.* (CLAS Collaboration), "Experimental Study of the $P_{11}(1440)$ and $D_{13}(1520)$ resonances from CLAS data on $ep \to e'\pi^+\pi^- p'$," Phys. Rev. C **86**, 035203 (2012).

Renormdynamics, Valence Quarks and Multiparticle Production

Nugzar Makhaldiani

JINR, Dubna, Russia

Concise introduction in QCD renormdynamics with prediction of the pion-nucleon and low energy QCD fine structure constants and valence quark mechanism of the multiparticle production given.

1 Renormdynamics

Quantum field theory (QFT) and Fractal calculus (FC) provide Universal language of fundamental physics (see e.g. [13]). In QFT existence of a given theory means, that we can control its behavior at some scales (short or large distances) by renormalization theory [3]. If the theory exists, than we want to solve it, which means to determine what happens on other (large or short) scales. This is the problem (and content) of Renormdynamics. The result of the Renormdynamics, the solution of its discrete or continual motion equations, is the effective QFT on a given scale (different from the initial one).

1.1 p-adic convergence of perturbation theory series

Perturbation theory series (PTS) have the following qualitative form

$$f(g) = f_0 + f_1 g + ... + f_n g^n + ..., \ f_n = n! P(n)$$
$$f(x) = \sum_{n \geq 0} P(n) n! x^n = P(\delta) \Gamma(1 + \delta) \frac{1}{1-x}, \ \delta = x \frac{d}{dx} \tag{1}$$

So, we reduce previous series to the standard geometric progression series. This series is convergent for $|x| < 1$ or for $|x|_p < 1$, $x = p^k a/b$, $k \geq 1$. With proper nomalization of the expansion parametre, the coefficients of the series are rational numbers and if experimental data indicates for some prime value for g, e.g. in QED

$$g = \frac{e^2}{4\pi} = \frac{1}{137.0...} \tag{2}$$

then we can take corresponding prime number and consider p-adic convergence of the series. In the case of QED, we have

$$f(g) = \sum f_n p^{-n}, \ f_n = n! P(n), \ p = 137, \ |f|_p \leq \sum |f_n|_p p^n \tag{3}$$

In the Yukawa theory of strong interactions (see e.g. [1]), we take $g = 13$,

$$f(g) = \sum f_n p^n, \ f_n = n!P(n), \ p = 13, |f|_p \leq \sum |f_n|_p p^{-n} < \frac{1}{1 - p^{-1}} \tag{4}$$

So, the series is convergent. If the limit is rational number, we consider it as an observable value of the corresponding physical quantity.

In $MSSM$ (see [10]) coupling constants unifies at $\alpha_u^{-1} = 26.3 \pm 1.9 \pm 1$. So,

$$23.4 < \alpha_u^{-1} < 29.2 \tag{5}$$

Question: how many primes are in this interval?

$$24, \ 25, \ 26, \ 27, \ 28, \ 29 \tag{6}$$

Only one!

Proposal: take the value $\alpha_u^{-1} = 29.0...$ which will be two orders of magnitude more precise prediction and find the consequences for the SM scale observables.

Let us make more explicit the formal representation of (1)

$$f(x) = \sum_{n \geq 0} P(n)n!x^n = P(\delta)\Gamma(1 + \delta)\frac{1}{1 - x},$$
$$= P(\delta)\int_0^\infty dt e^{-t} t^\delta \frac{1}{1 - x} = P(\delta)\int_0^\infty dt \frac{e^{-t}}{1 + (-x)t}, \ \delta = x\frac{d}{dx} \tag{7}$$

This integral is well defined for negative values of x. The Mathematica answer for the corresponding integral is

$$I(x) = \int_0^\infty dt \frac{e^{-t}}{1 + xt} = e^{1/x}\Gamma(0, 1/x)/x, \ Im(x) \neq 0, \ Re(x) \geq 0, \ I(0) = 1 \tag{8}$$

where $\Gamma(a, z)$ is the incomplete gamma function

$$\Gamma(a, z) = \int_z^\infty dt t^{a-1} e^{-t} \tag{9}$$

For $x = 0.001, \ I(x) = 0.999$

1.2 The Goldberger-Treiman relation and the pion-nucleon coupling constant

The Goldberger-Treiman relation (GTR) [5] plays an important role in theoretical hadronic and nuclear physics. GTR relates the Meson-Nucleon coupling constants to the axial-vector coupling constant in β-decay:

$$g_{\pi N} f_\pi = g_A m_N \tag{10}$$

where m_N is the nucleon mass, g_A is the axial-vector coupling constant in nucleon β-decay at vanishing momentum transfer, f_π is the π decay constant and $g_{\pi N}$ is the $\pi - N$ coupling constant.

Since the days when the Goldberger-Treiman relation was discovered, the value of g_A has increased considerably. Also, f_π decreased a little, on account of radiative corrections. The main source of uncertainty is $g_{\pi N}$.

If we take

$$\alpha_{\pi N} = \frac{g_{\pi N}^2}{4\pi} = 13 \Rightarrow g_{\pi N} = 12.78 \tag{11}$$

experimental value for f_π from pion decay and neutron mass

$$f_\pi = \frac{130}{\sqrt{2}} = 91.9 MeV, \ m_N = 940 MeV, \tag{12}$$

from (10), we find

$$g_A = \frac{f_\pi g_{\pi N}}{m_N} = \frac{91.9 \times \sqrt{52\pi}}{940} = 1.2496 \simeq 1.25 = \frac{5}{4} \tag{13}$$

In an old version of the unified theory [7], for the $\alpha_{\pi N}$ the following value were found

$$\alpha_{\pi N} = 4\pi(1 - \frac{m_\pi^2}{3m_p^2}) = 12.5 \tag{14}$$

Determination of $g_{\pi N}$ from $NN, N\bar{N}$ and πN data by the Nijmegen group [16] gave the following value

$$g_{\pi N} = 13.05 \pm .08, \ \Delta = 1 - \frac{g_A m_N}{g_{\pi N} f_\pi} = .014 \pm .009, \ 13.39 < \alpha_{\pi N} < 13.72 \tag{15}$$

This value is consistent with assumption $g_{\pi N} = 13 \Rightarrow \alpha_{\pi N} = 13.45$

Due to the smallness of the u and d quark masses, Δ is necessarily very small, and its determination requires a very precise knowledge of the $g_{\pi N}$ coupling (g_A and f_π are already known to enough precision, leaving most of the uncertainty in the determination of Δ to the uncertainty in $g_{\pi N}$).

2 Renormdynamics of QCD

QCD is the theory of the strong interactions with, as only inputs, one mass parameter for each quark species and the value of the QCD coupling constant at some energy or momentum scale in some renormalization scheme. This last free parameter of the theory can be fixed by Λ_{QCD}, the energy scale used as the typical boundary condition for the integration of the Renormdynamic (RD) equation for the strong coupling constant. This is the parameter which expresses the scale of strong interactions, the only parameter in the limit of massless quarks. While the evolution of the coupling with the momentum scale is determined by the quantum corrections induced by the renormalization of the bare coupling and can be computed in perturbation theory, the strength itself of the interaction, given at any scale by the value of the renormalized coupling at this scale, or equivalently by Λ_{QCD}, is one of the above mentioned parameters of the theory and has to be taken from experiment.

The RD equations play an important role in our understanding of Quantum Chromodynamics and the strong interactions. The beta function and the quarks mass anomalous dimension

are among the most prominent objects for QCD RD equations. The calculation of the one-loop β-function in QCD has lead to the discovery of asymptotic freedom in this model and to the establishment of QCD as the theory of strong interactions [8, 6, 15].

The MS-scheme [9] belongs to the class of massless schemes where the β-function does not depend on masses of the theory and the first two coefficients of the β-function are scheme-independent.

The Lagrangian of QCD with massive quarks in the covariant gauge is

$$L = -\frac{1}{4}F_{\mu\nu}^a F^{a\mu\nu} + \bar{q}_n(i\gamma D - m_n)q_n - \frac{1}{2\xi}(\partial A)^2 + \partial^\mu \bar{c}^a(\partial_\mu c^a + gf^{abc}A_\mu^b c^c)$$
$$F_{\mu\nu}^a = \partial_\mu A_\nu^a - \partial_\nu A_\mu^a + gf^{abc}A_\mu^b A_\nu^c, \ (D_\mu)_{kl} = \delta_{kl}\partial_\mu - igt_{kl}^a A_\mu^a, \tag{16}$$

$A_\mu^a, a = 1, ..., N_c^2 - 1$ are gluon; $q_n, n = 1, ..., n_f$ are quark; c^a are ghost fields; ξ is gauge parameter; t^a are generators of fundamental representation and f^{abc} are structure constants of the Lie algebra

$$[t^a, t^b] = if^{abc}t^c, \tag{17}$$

we consider an arbitrary compact semi-simple Lie group G. For QCD, $G = SU(N_c), N_c = 3$.

The RD equation for the coupling constant is

$$\dot{a} = \beta(a) = -\beta_2 a^2 - \beta_3 a^3 - \beta_4 a^4 - \beta_5 a^5 + O(a^6),$$
$$a = \frac{\alpha_s}{4\pi} = (\frac{g}{4\pi})^2, \ \int_{a_0}^a \frac{da}{\beta(a)} = t - t_0 = \ln\frac{\mu^2}{\mu_0^2}, \tag{18}$$

μ is the 't Hooft unit of mass, the renormalization point in the MS-scheme.

To calculate the β-function we need to calculate the renormalization constant Z of the coupling constant, $a_b = Za$, where a_b is the bare (unrenormalized) charge.

The expression of the β-function can be obtained in the following way

$$0 = d(a_b\mu^{2\varepsilon})/dt = \mu^{2\varepsilon}(\varepsilon Za + \frac{\partial(Za)}{\partial a}\frac{da}{dt})$$
$$\Rightarrow \frac{da}{dt} = \beta(a, \varepsilon) = \frac{-\varepsilon Za}{\frac{\partial(Za)}{\partial a}} = -\varepsilon a + \beta(a), \ \beta(a) = a\frac{d}{da}(aZ_1) \tag{19}$$

where

$$\beta(a, \varepsilon) = \frac{D-4}{2}a + \beta(a) \tag{20}$$

is $D-$dimensional $\beta-$function and Z_1 is the residue of the first pole in ε expansion

$$Z(a, \varepsilon) = 1 + Z_1\varepsilon^{-1} + ... + Z_n\varepsilon^{-n} + ... \tag{21}$$

Since Z does not depend explicitly on μ, the β-function is the same in all MS-like schemes, i.e. within the class of renormalization schemes which differ by the shift of the parameter μ.

For quark anomalous dimension, RD equation is

$$\dot{b} = \gamma(a) = -\gamma_1 a - \gamma_2 a^2 - \gamma_3 a^3 - \gamma_4 a^4 + O(a^5),$$
$$b(t) = b_0 + \int_{t_0}^t dt\gamma(a(t)) = b_0 + \int_{a_0}^a da\gamma(a)/\beta(a). \tag{22}$$

To calculate the quark mass anomalous dimension $\gamma(g)$ we need to calculate the renormalization constant Z_m of the quark mass $m_b = Z_m m$, m_b is the bare (unrenormalized) quark mass. Than we find the function $\gamma(g)$ in the following way

$$
\begin{aligned}
0 = \dot{m}_b &= \dot{Z}_m m + Z_m \dot{m} = Z_m m((\ln Z_m)^\cdot + (\ln m)^\cdot) \\
\Rightarrow \gamma(a) &= -\frac{d \ln Z_m}{dt} = \dot{b} = -\frac{d \ln Z_m}{da}\frac{da}{dt} = -\frac{d \ln Z_m}{da}(-\varepsilon a + \beta(a)) \\
&= a\frac{dZ_{m1}}{da}, \ b = -\ln Z_m = \ln \frac{m}{m_b},
\end{aligned}
\tag{23}
$$

where RD equation in $D-$dimension is

$$
\dot{a} = -\varepsilon a + \beta(a) = \beta_1 a + \beta_2 a^2 + \dots
\tag{24}
$$

and Z_{m1} is the coefficient of the first pole in the $\varepsilon-$expantion of the Z_m in MS-scheme

$$
Z_m(\varepsilon, g) = 1 + Z_{m1}(g)\varepsilon^{-1} + Z_{m2}(g)\varepsilon^{-2} + \dots
\tag{25}
$$

Since Z_m does not depend explicitly on μ and m, the γ_m-function is the same in all MS-like schemes.

2.1 Reparametrization and general method of solution of the RD equation

RD equation,

$$
\dot{a} = \beta_1 a + \beta_2 a^2 + \dots
\tag{26}
$$

can be reparametrized,

$$
a(t) = f(A(t)) = A + f_2 A^2 + \dots + f_n A^n + \dots = \sum_{n \geq 1} f_n A^n,
\tag{27}
$$

$$
\begin{aligned}
\dot{A} &= b_1 A + b_2 A^2 + \dots = \sum_{n \geq 1} b_n A^n, \\
\dot{a} &= \dot{A} f'(A) = (b_1 A + b_2 A^2 + \dots)(1 + 2f_2 A + \dots + nf_n A^{n-1} + \dots) \\
&= \beta_1(A + f_2 A^2 + \dots + f_n A^n + \dots) + \beta_2(A^2 + 2f_2 A^3 + \dots) + \dots \\
&+ \beta_n(A^n + nf_2 A^{n+1} + \dots) + \dots \\
&= \beta_1 A + (\beta_2 + \beta_1 f_2)A^2 + (\beta_3 + 2\beta_2 f_2 + \beta_1 f_3)A^3 + \\
&\dots + (\beta_n + (n-1)\beta_{n-1} f_2 + \dots + \beta_1 f_n)A^n + \dots \\
&= \sum_{n,n_1,n_2 \geq 1} A^n b_{n_1} n_2 f_{n_2} \delta_{n,n_1+n_2-1} \\
&= \sum_{n,m \geq 1; m_1,\dots,m_k \geq 0} A^n \beta_m f_1^{m_1} \dots f_k^{m_k} f(n, m, m_1, \dots, m_k), \\
f(n, m, m_1, \dots, m_k) &= \frac{m!}{m_1! \dots m_k!}\delta_{n,m_1+2m_2+\dots+km_k}\delta_{m,m_1+m_2+\dots+m_k},
\end{aligned}
\tag{28}
$$

$$
\begin{aligned}
b_1 &= \beta_1, \ b_2 = \beta_2 + f_2\beta_1 - 2f_2 b_1 = \beta_2 - f_2\beta_1, \\
b_3 &= \beta_3 + 2f_2\beta_2 + f_3\beta_1 - 2f_2 b_2 - 3f_3 b_1 = \beta_3 + 2(f_2^2 - f_3)\beta_1,
\end{aligned}
$$

$$b_4 = \beta_4 + 3f_2\beta_3 + f_2^2\beta_2 + 2f_3\beta_2 - 3f_4 b_1 - 3f_3 b_2 - 2f_2 b_3, ...$$
$$b_n = \beta_n + ... + \beta_1 f_n - 2f_2 b_{n-1} - ... - n f_n b_1, ...$$
(29)

so, by reparametrization, beyond the critical dimension ($\beta_1 \neq 0$) we can change any coefficient but β_1.

We can fix any higher coefficient with zero value, if we take

$$f_2 = \frac{\beta_2}{\beta_1}, \; f_3 = \frac{\beta_3}{2\beta_1} + f_2^2, \; ... , f_n = \frac{\beta_n + ...}{(n-1)\beta_1}, ...$$
(30)

In the critical dimension of space-time, $\beta_1 = 0$, and we can change by reparametrization any coefficient but β_2 and β_3.

From the relations (29), in the critical dimenshion ($\beta_1 = 0$), we find that, we can define the minimal form of the RD equation

$$\dot{A} = \beta_2 A^2 + \beta_3 A^3,$$
(31)

We can solve (31) as implicit function,

$$u^{\beta_3/\beta_2} e^{-u} = c e^{\beta_2 t}, \; u = \frac{1}{A} + \frac{\beta_3}{\beta_2}$$
(32)

then, as in the noncritical case, explicit solution will be given by reparametrization representation (27) [14].

If we know somehow the coefficients β_n, e.g. for first several exact and for others asymptotic values (see e.g. [11]) than we can construct reparametrization function (27) and find the dynamics of the running coupling constant. This is similar to the action-angular canonical transformation of the analytic mechanics (see e.g. [4]).

Statement: The reparametrization series for a is p-adically convergent, when β_n and A are rational numbers.

2.2 Reparametrization of the anomalous dimensions

Let us take the the anomalous dimension of some quantity

$$\gamma(a) = \gamma_1 a + \gamma_2 a^2 + \gamma_3 a^3 + ...$$
(33)

and make reparametrization

$$a = f(A) = A + f_2 A^2 + f_3 A^3 + ...$$
(34)

$$\gamma(a) = \gamma_1(A + f_2 A^2 + f_3 A^3 + ...) + \gamma_2(A^2 + 2f_2 A^3 + ...) + \gamma_3(A^3 + ...) + ...$$
$$= \Gamma_1 A + \Gamma_2 A^2 + \Gamma_3 A^3 + ...$$
$$\Gamma_1 = \gamma_1, \; \Gamma_2 = \gamma_2 + \gamma_1 f_2, \; \Gamma_3 = \gamma_3 + 2\gamma_2 f_2 + \gamma_1 f_3, ...$$
(35)

When $\gamma_1 \neq 0$, we can take $\Gamma_n = 0, \; n \geq 2$, if we define f_n as

$$f_2 = -\frac{\gamma_2}{\gamma_1}, \; f_3 = -\frac{\gamma_3 + 2\gamma_2 f_2}{\gamma_1} = -\frac{\gamma_3 - 2\gamma_2^2/\gamma_1}{\gamma_1}, ...$$
(36)

So, we get the exact value for the anomalous dimension

$$\gamma(A) = \gamma_1 A = \gamma_1 f^{-1}(a) = \gamma_1(a + \gamma_2/\gamma_1 a^2 + \gamma_3/\gamma_1 a^3 + ... :)$$
(37)

2.3   QCD, parton model, valence quarks and $\alpha_s = 2$

While it has been well established in the perturbative regime at high energies, QCD still lacks a comprehensive solution at low and intermediate energies, even 40 years after its invention. In order to deal with the wealth of non-perturbative phenomena, various approaches are followed with limited validity and applicability. This is especially also true for lattice QCD, various functional methods, or chiral perturbation theory, to name only a few. In neither one of these approaches the full dynamical content of QCD can yet be included. Basically, the difficulties are associated with a relativistically covariant treatment of confinement and the spontaneous breaking of chiral symmetry, the latter being a well-established property of QCD at low and intermediate energies. As a result, most hadron reactions, like resonance excitations, strong and electroweak decays etc., are nowadays only amenable to models of QCD. Most famous is the constituent-quark model (CQM), which essentially relies on a limited number of effective degrees of freedom with the aim of encoding the essential features of low- and intermediate-energy QCD.

The CQM has a long history, and it has made important contributions to the understanding of many hadron properties, think only of the fact that the systematization of hadrons in the standard particle-data base follows the valence-quark picture. Namely the Q dependence of the nucleon form factor corresponds to three-constituent picture of the nucleon and is well described by the simple equation [2], [12]

$$F(Q^2) \sim (Q^2)^{-2} \tag{38}$$

It was noted [17] that parton densities given by the following solution

$$
\begin{aligned}
M_2(Q^2) &= \frac{3}{25} + \frac{2}{3}\omega^{32/81} + \frac{16}{75}\omega^{50/81}, \\
\bar{M}_2(Q^2) &= M_2^s(Q^2) = \frac{3}{25} - \frac{1}{3}\omega^{32/81} + \frac{16}{75}\omega^{50/81}, \\
M_2^G(Q^2) &= \frac{16}{25}(1 - \omega^{50/81}), \\
\omega &= \frac{\alpha_s(Q^2)}{\alpha_s(m^2)}, \ Q^2 \in (5,20)GeV^2, \ b = 9, \ \alpha_s(Q^2) \simeq 0.2
\end{aligned}
\tag{39}
$$

of the Altarelli-Parisi equation

$$
\begin{aligned}
\dot{M} &= AM, \\
M^T &= (M_2, \bar{M}_2, M_2^s, M_2^G), \\
M_2 &= \int_0^1 dx x (u(x) + d(x)), \ \bar{M}_2 = \int_0^1 dx x (\bar{u}(x) + \bar{d}(x)), \\
M_2^s &= \int_0^1 dx x (s(x) + \bar{s}(x)), \ M_2^G = \int_0^1 dx x G(x), \\
A &= -a(Q^2) \begin{pmatrix} 32/9 & 0 & 0 & -2/3 \\ 0 & 32/9 & 0 & -2/3 \\ 0 & 0 & 32/9 & -2/3 \\ -32/9 & -32/9 & -32/9 & 2 \end{pmatrix}, \ a = (\frac{g}{4\pi})^2, \ \dot{M} = Q^2 \frac{dM}{dQ^2}
\end{aligned}
\tag{40}
$$

with the following "valence quark" initial condition at a scale m

$$M_2(m^2) = 1, \ \bar{M}_2(m^2) = M_2^s(m^2) = M_2^G(m^2) = 0, \tag{41}$$

and

$$\alpha_s(m^2) = 2, \tag{42}$$

gives the experimental values

$$M_2 = 0.44, \ \bar{M}_2 = M_2^s = 0.04, \ M_2^G = 0.48 \tag{43}$$

So, for valence quark model (VQCD), $\alpha_s(m^2) = 2$. We have seen, that for $\pi\rho N$ model $\alpha_{\pi\rho N} = 3$, and for πN model $\alpha_{\pi N} = 13$. It is nice that $\alpha_s^2 + \alpha_{\pi\rho N}^2 = \alpha_{\pi N}$. This relation can be seen, e.g., by considering pion propagator in the low energy πN model and in superposition of higher energy VQCD and $\pi\rho N$ models.

Note that $g = 5$ corresponds to the

$$\alpha_s = \frac{g^2}{4\pi} = 1.989 \simeq 2 \tag{44}$$

References

[1] N.N. Bogoliubov and D.V. Shirkov, *Introduction to the Theory of Quantized Fields*, New York 1959.

[2] S. Brodsky, G. Farrar, Phys. Rev. Lett. **31** 1153 (1973).

[3] J.C. Collins, *Renormalization*, Cambrige Univ. Press, London 1984.

[4] L.D. Faddeev and L.A. Takhtajan, *Hamiltonian methods in the theory of solitons*, Springer, Berlin 1987.

[5] M.L. Goldberger, S.B. Treiman, Phys. Rev. **110** 1178 (1958).

[6] D.J. Gross, F. Wilczek, Phys. Rev. Lett. **30** 1343 (1973).

[7] W. Heisenberg, *Introduction to the Unified field Theory of Elementary particles,* Interscience Publishers, London 1966.

[8] G. 't Hooft, report at the *Marseille Conference on Yang-Mills Fields*, 1972.

[9] G. 't Hooft, Nucl.Phys. **B 61** 455 (1973).

[10] D.I. Kazakov, *Supersymmetric Generalization of the Standard Model of Fundamental Interactions*, Textbook, JINR Dubna 2004.

[11] D.I. Kazakov, D.V. Shirkov, Fortschr. d. Phys. **28** 447 (1980).

[12] V. Matveev, R. Muradyan, A. Tavkhelidze, Lett. Nuovo Cimento **7** 719 (1973).

[13] N. Makhaldiani, *Fractal Calculus (H) and some Applications*, *Physics of Particles and Nuclei Letters*, **8** 325 (2011).

[14] N. V. Makhaldiani, *Renormdynamics, Multiparticle Production, Negative Binomial Distribution, and Riemann Zeta Function*, Physics of Atomic Nuclei, **76** 1169 (2013).

[15] H.D. Politzer, Phys. Rev. Lett. **30** 1346 (1973).

[16] M.C.M. Rentmeester, R.G.E. Timmermans, J.L. Friar, J.J. de Swart, Phys. Rev. Lett. **82** 4992 (1999).

[17] M.B. Voloshin, K.A. Ter-Martyrosian, *Gauge Theory of Elementary Particles*, Atomizdat, Moscow 1984.

Prompt photon and associated b,c-tagged jet production within the k_T-factorization approach

A.V. Lipatov[1], M.A. Malyshev[1,2], N.P. Zotov[1]

[1]Skobeltsyn Institute of Nuclear Physics, Lomonosov Moscow State University,
[2]Faculty of Physics, Lomonosov Moscow State University,
Leninskie Gory 1 (2), 119991 Moscow, Russia

We present the results of the numerical calculations of prompt photon and associated b- or c-quark tagged jet production at Tevatron in the framework of the k_T-factorization approach. Our predictions are compared with the DØ and CDF experimental data.

Prompt photon and associated jet production has been intensively investigated both theoretically and experimentally up to now since it is highly sensitive to parton distribution in the hadron (so it provides a test of hard subprocess dynamics) and contributes significantly to the background for the physics beyound the Standard Model processes.

Recently an attempt of the description of the newest ZEUS data on the prompt photon and associated non-tagged jet photoproduction at HERA has been made in the framework of the k_T-factorization approach [1]. The consideration was based on $2 \to 3$ matrix elements with the addition of box-diagrams contribution. However, the difficulties in the description of the data still remain. For instance, there is qualitative disagreement in jet rapidities distributions.

In this light it is interesting to look at the results, obtained with the tagged jets. Such investigation was made by the DØ and CDF collaborations for the prompt photon and associated heavy quark production at the Tevatron [2, 3, 4, 5, 6, 7, 8].

The k_T-factorization approach was used to describe the production of prompt photons associated with the charm or beauty quark in paper [9]. The consideration was based on the $\mathcal{O}(\alpha\alpha_s^2)$ amplitude for the gluon fusion subprocess $g^* g^* \to \gamma Q\bar{Q}$. Reasonably good agreement between the numerical predictions and the Tevatron data [5, 6] was obtained in the region of relatively low p_T^γ where the off-shell gluon fusion dominates. However, the quark-induced subprocesses become more important at moderate and large p^γ and therefore should be taken into account. In work [10] the analysis was extended by including into the consideration two additional $\mathcal{O}(\alpha\alpha_s^2)$ subprocesses: $q\bar{q} \to \gamma Q\bar{Q}$ and $qQ \to \gamma qQ$. The presented proceedings paper is based on this study.

According to the k_T-factorization theorem, the cross section of the prompt photon and associated heavy quark production is obtained by convoluting the off-shell partonic cross sections with the relevant unintegrated quark and/or gluon distributions in a proton:

$$\sigma = \sum_{a,b=q,\,g} \int \hat{\sigma}_{ab}^*(x_1, x_2, \mathbf{k}_{1T}^2, \mathbf{k}_{2T}^2)\, f_a(x_1, \mathbf{k}_{1T}^2, \mu^2) f_b(x_2, \mathbf{k}_{2T}^2, \mu^2)\, dx_1 dx_2\, d\mathbf{k}_{1T}^2 d\mathbf{k}_{2T}^2 \frac{d\phi_1}{2\pi} \frac{d\phi_2}{2\pi},$$

where $\hat{\sigma}_{ab}^*(x_1, x_2, \mathbf{k}_{1T}^2, \mathbf{k}_{2T}^2)$ is the relevant partonic cross section. The initial off-shell partons have fractions x_1 and x_2 of initial protons longitudinal momenta, non-zero transverse momenta $\mathbf{k}_{1T}$ and $\mathbf{k}_{2T}$ and azimuthal angles ϕ_1 and ϕ_2.
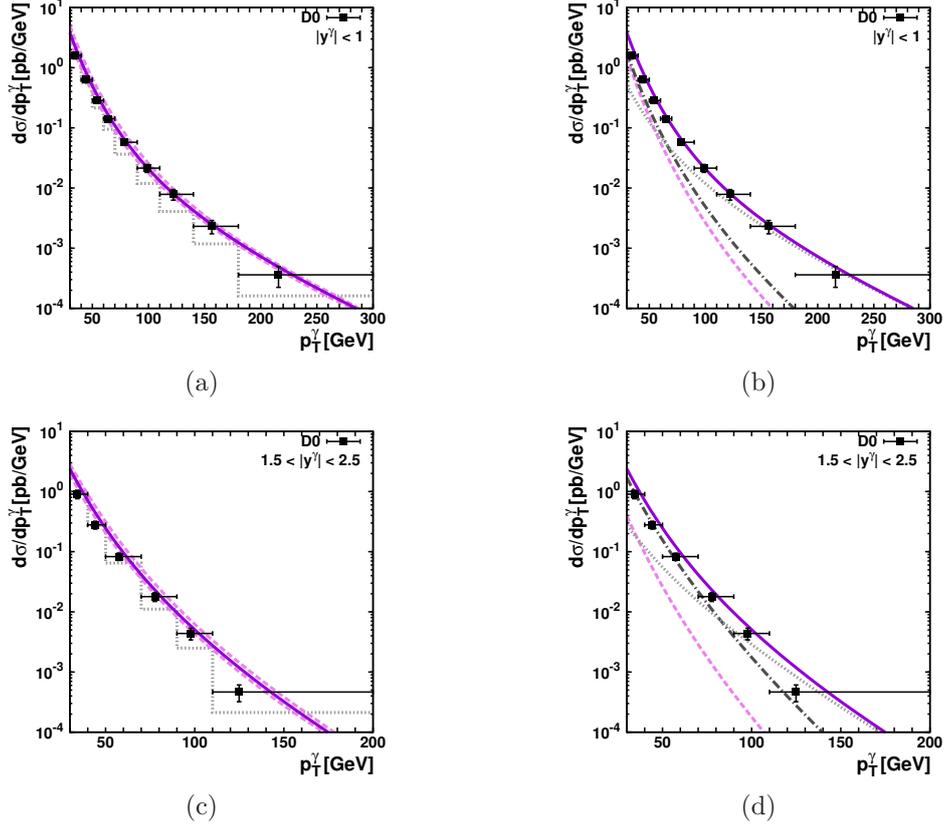
Figure 1: The associated $\gamma + b$-jet cross section as a function of photon transverse momentum p_T^γ in the kinematical region of $|y^{jet}| < 1.5$, $p_T^{jet} > 15$ GeV at $\sqrt{s} = 1960$ GeV. Left panels: the solid curve corresponds to the KMR predictions at the default scale $\mu = E_T$; the upper and lower dashed curves correspond to scale variations described in the text. The dotted histogram represents the NLO pQCD predictions [16] listed in [3]. Right panels: the different contributions to the $\gamma + b$-jet cross section. The dashed, dotted and dash-dotted curves correspond to the contributions from the $g^*g^* \to \gamma Q\bar{Q}$, $q^*\bar{q}^* \to \gamma Q\bar{Q}$ and $q^*Q \to \gamma qQ$ subprocesses, respectively. The solid curve represents their sum. The experimental data are from D∅ [3].
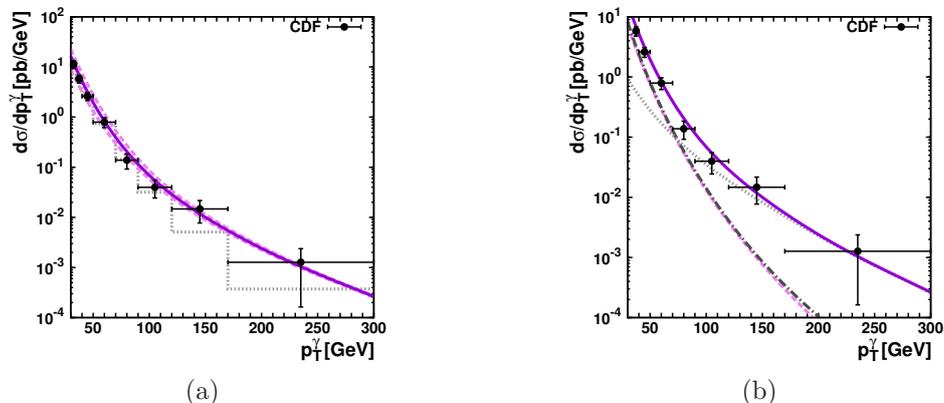
Figure 2: The associated $\gamma + c$-jet cross section as a function of photon transverse momentum p_T^γ in the kinematical region of $|y^\gamma| < 1.0$, $|y^{jet}| < 1.5$ and $p_T^{jet} > 20$ GeV at $\sqrt{s} = 1960$ GeV. The notations are the same as for Fig. 1. The experimental data are from CDF [8].

In this work we use the KMR uPDFs [11, 12]. The KMR approach is the formalism to construct the unintegrated parton distributions from the known conventional parton distributions[1].

The calcuation of the matrix elements generally follows the standard Feynman rules. The only difference comes from the modification of the polarization sum rules. In the k_T-factorization approach the gluon polarization density matrix takes so called BFKL form: $\sum \epsilon^\mu \epsilon^{*\nu} = k_T^\mu k_T^\nu / \mathbf{k}_T^2$. The spin density matrix for the off-shell quark with the momentum $k = xP + k_T$ in massless limit is [14] $\sum_s u^s(k)\bar{u}^s(k) = x\hat{P}$, where P is the momentum of the incoming proton (or antiproton). Since the expression was obtained in the massless approximation, we neglected the light quarks masses.

In our numerical calculations we took the renormalization and factorization scales $\mu_R^2 = \mu_F^2 = \xi^2 p_T^2$. In order to evaluate theoretical uncertainties, we varied ξ between $1/2$ and 2 about the default value $\xi = 1$. We used the LO formula for the strong coupling constant $\alpha_s(\mu^2)$ with $n_f = 4$ active quark flavours at $\Lambda_{QCD} = 200$ MeV, so that $\alpha_S(M_Z) = 0.1232$. We set the charm and beauty quark masses to $m_c = 1.5$ GeV and $m_b = 4.75$ GeV.

In order to reduce the huge background from the secondary photons produced by the decays of π^0 and η mesons the isolation criterion is introduced in the experimental analyses. The isolation not only reduces the background but also significantly reduces the so called fragmentation components, connected with collinear photon radiation (10%)[2]. The same isolation cuts were introduced into our calculations.

Some selected results of our calculation [10] for the production of the prompt photon with the associated heavy quark are shown in Figs. 1, 2. The results are compared with the data taken by the D∅ and CDF collaborations at $\sqrt{s} = 1960$ GeV [3, 8]. For comparison we also plot the NLO QCD predictions [16]. We find that the full set of experimental data is reasonably well described by the k_T-factorization approach: the shape and absolute normalization of measured cross sections are adequately reproduced (for more details see [10]).

---

[1]Numerically, as the input we used the MSTW2008 collinear parton distributions [13].
[2]For details see [15]
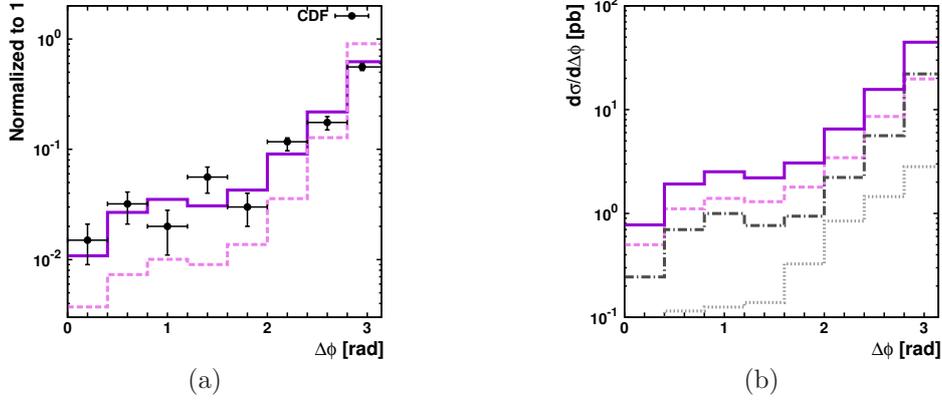
(a)   (b)

Figure 3: The associated $\gamma + \mu$ cross section as a function of the azimuthal angle difference between the photon and muon in the kinematical region of $|\eta^\gamma| < 0.9$, $|\eta^\mu| < 1.0$ and $p_T^\mu > 4$ GeV at $\sqrt{s} = 1800$ GeV. Panel (a): the solid and dashed lines correspond to the k_T-factorization and collinear QCD factorization calculations, respectively. The notations on the panel (b) are the same as for Fig. 1. The experimental data are from CDF [5].
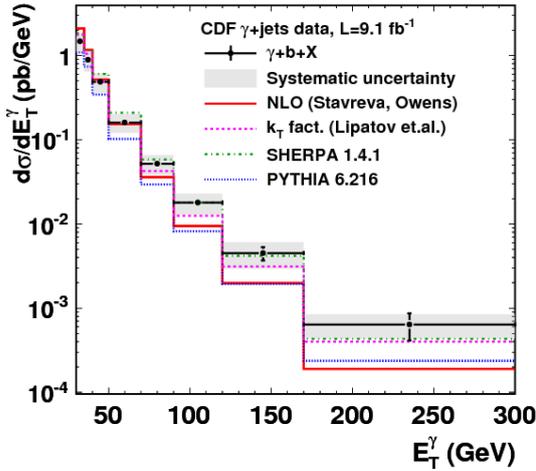

Figure 4: The associated $\gamma + b$-jet cross section as a function of photon transverse momentum p_T^γ in the kinematical region of $|y^\gamma| < 1.04$, $|y^{jet}| < 1.5$ and $p_T^{jet} > 20$ GeV at $\sqrt{s} = 1960$ GeV. The graph is taken from [8].

The results of the calculation for associated production of the prompt photon and the muon originated from the semileptonic decays of charm or beauty quarks are presented in Fig. 3. The experimental data are from CDF [5]. To produce muons from charmed and beauty quarks, we first convert them into D or B hadrons using the Peterson fragmentation function [17] and then simulate their semileptonic decay according to the standard electroweak theory. Additionally, the cascade decays $b \to c \to \mu$ have been taken into account. We set the fragmentation parameters $\epsilon_c = 0.06$ and $\epsilon_b = 0.006$ and corresponding branching fractions to $f(c \to \mu) = 0.0969$, $f(b \to \mu) = 0.1071$ and $f(b \to c \to \mu) = 0.0802$ [18]. We find that the k_T-factorization predictions describe the data very well. One can see that the CDF data clearly favor the k_T-factorization results.

Finally, on the Fig. 4 for an illustration we show the comparison of the $\gamma + b$ CDF data with different numerical calculations (including the k_T-factorization results), which was taken from the experimental paper [8]. In that paper the good description of the data by our simulation was specially pointed by the collaboration.

In summary, we have studied the process of the prompt photon production with the associated heavy (b, c) quark in the k_T-factorization QCD approach at Tevatron energies. A reasonably good description of D∅ and CDF data for the associated prompt photon and heavy quark production has been obtained. Also the associated prompt photon and μ-meson production has been studied. A theoretical uncertainties investigation has been made and a predictive power of the used approach has been shown. Compared to the associated prompt photon and non-tagged jet production at HERA [1], the obtained good agreement is notable. It shows, that the reliability of the predictions may be significantly improved if in the analyses the produced jets are tagged as in the case of the prompt photon and associated heavy quark production at Tevatron.

References

[1] A.V. Lipatov, M.A. Malyshev and N.P. Zotov, Phys. Rev. **D88** 074001 (2013).

[2] V.M. Abazov *et al.* (D∅ Collaboration), Phys. Rev. Lett. **102** 192002 (2009).

[3] V.M. Abazov *et al.* (D∅ Collaboration), Phys. Lett. **B714** 32 (2012).

[4] V.M. Abazov *et al.* (D∅ Collaboration), Phys. Lett. **B719** 354 (2013).

[5] F. Abe *et al.* (CDF Collaboration), Phys. Rev. **D60** 092003 (1999).

[6] T. Affolder *et al.* (CDF Collaboration), Phys. Rev. **D65** 012003 (2002).

[7] T. Aaltonen *et al.* (CDF Collaboration), Phys. Rev. **D81** 052006 (2010).

[8] T. Aaltonen *et al.* (CDF Collaboration), Phys. Rev. Lett. **111** 042003 (2013).

[9] S.P. Baranov, A.V. Lipatov and N.P. Zotov, Eur. Phys. J. **C56** 371 (2008).

[10] A.V. Lipatov, M.A. Malyshev and N.P. Zotov, JHEP **1205** 104 (2012).

[11] M.A. Kimber, A.D. Martin and M.G. Ryskin, Phys. Rev. **D63** 114027 (2001).

[12] G. Watt, A.D. Martin and M.G. Ryskin, Eur. Phys. J. **C31** 73 (2003).

[13] A.D. Martin, W.J. Stirling, R.S. Thorne and G. Watt, Eur. Phys. J. **C63** 189 (2009).

[14] S.P. Baranov, A.V. Lipatov and N.P. Zotov, Phys. Rev. **D81** 094034 (2010).

[15] A.V. Lipatov, M.A. Malyshev and N.P. Zotov, PoS Baldin-ISHEPP-XXI 032 (2012).

[16] T. Stavreva and J. Owens, Phys. Rev. **D79** 054017 (2009).

[17] C. Peterson, D. Schlatter, I. Schmitt and P.M. Zerwas, Phys. Rev. **D27** 105 (1983).

[18] K. Nakamura *et al.* (Particle Data Group Collaboration), J. Phys. **G37** 075021 (2010).

Heavy quarkonium production at the LHC in the framework of NRQCD and parton Reggeization approach

Maxim Nefedov[1], *Vladimir Saleev*[1]

[1] Samara State University, Academic Pavlov st. 1, 443111 Samara, Russia

Heavy quarkonium production in the framework of the nonrelativistic quantum chromodynamics and leading order of the parton Reggeization approach at the Tevatron and LHC Colliders is discussed. The new results, which are reviewed in this report, include the comparison with recent data on $\chi_{c1,2}$ production from ATLAS Collaboration and special discussion of heavy quarkonium polarization issues in the considered framework.

Introduction and basic formalism.

Production of heavy quarkonia at hadron colliders is the unique laboratory for the studies of the interplay between theory of perturbative hard subprocess and models of nonperturbative hadronization in the hadronic collision. The hope to understand the hadronization stage is associated with the nonrelativistic nature of the problem, which allows one to organize theoretical predictions in a form of double expansion in powers of strong coupling constant α_s and relative heavy quark velocity v.

In the nonrelativistic Quantum Chromodynamics (NRQCD) one can factorize the effects of short and long distances in the cross section of heavy quarkonium production as follows [1, 2]:

$$d\hat{\sigma}(I \to \mathcal{H}) = \sum_n d\hat{\sigma}(I \to Q\bar{Q}[n])\langle \mathcal{O}^{\mathcal{H}}[n]\rangle, \tag{1}$$

where the sum is over the possible intermediate states of heavy quark-antiquark $(Q\bar{Q})$ pair $[n] = {}^{2S+1}L_J^{(1,8)}$, with definite spin S, orbital momentum L, total angular momentum J and color-singlet (CS) [(1)] or color-octet (CO) [(8)] quantum numbers. Factor $d\hat{\sigma}$ is the partonic cross section of production of the state $Q\bar{Q}[n]$ from the partonic initial state I, and $\langle \mathcal{O}^{\mathcal{H}}[n]\rangle$ are the nonperturbative matrix elements (NMEs), describing the transition of the intermediate state $Q\bar{Q}[n]$ to the heavy quarkonia $\mathcal{H}$. In our calculations, the normalization of NMEs and cross section is chosen the same as in the Ref. [2].

According to the NRQCD velocity scaling rules [3], the following CS NMEs give the leading contribution to the production of quarkonia with the same spin-orbital quantum numbers: $\left\langle \mathcal{O}^{\mathcal{H}}\left[{}^3S_1^{(1)}\right]\right\rangle$, $\left\langle \mathcal{O}^{\mathcal{H}}\left[{}^3P_J^{(1)}\right]\right\rangle$. The CO NMEs – $\left\langle \mathcal{O}^{\mathcal{H}}\left[{}^1S_0^{(8)}\right]\right\rangle$, $\left\langle \mathcal{O}^{\mathcal{H}}\left[{}^3S_1^{(8)}\right]\right\rangle$, $\left\langle \mathcal{O}^{\mathcal{H}}\left[{}^3P_J^{(8)}\right]\right\rangle$, give the next to leading contributions in v. CS NMEs could be expressed through the quarkonia wave function, and then calculated in the potential quark model. CO NMEs describe the transition of CO $Q\bar{Q}$ pair into quarkonia by radiation of the soft gluons, and hence could not

be computed neither in perturbative QCD, nor in the potential quark models. The only option, available so far, is to fit this NMEs to reproduce experimental data.

The latter means, that the hard part of the cross-section should be calculated as precisely as possible, to get physically meaningful results. Nowadays the complete next-to-leading-order (NLO) results for inclusive heavy quarkonia production are available [4, 5]. However, fixed order calculations are applicable only in the region of $p_T \gg 2m_Q$. In the region of small p_T, the resummation of the large logarithms $log(m_Q/p_T)$ is needed to obtain reliable predictions. The existing calculations, based on the small-p_T resummation procedure, see e. g. [6], are restricted to the region $p_T \ll 2m_Q$, and require matching with the fixed order calculations at higher p_T. So, the approach, which takes into account both small and high p_T regions on the same grounds is needed to obtain the values of CO NMEs.

Such approach could be designed, using the k_T−factorization [7], which naturally regularizes the small-p_T divergences, present in the fixed-order calculations in the collinear PM.

The dominating contribution to the inclusive heavy quarkonium production at hadron colliders, comes from the gluon fusion subprocess. The cross section for this process in the framework of k_T−factorization is represented as a convolution of unintegrated parton (gluon) distribution functions (PDFs) in a proton $\Phi_g^p\left(x, t, \mu^2\right)$ with the partonic cross section. Unintegrated PDF depends on the longitudinal momentum fraction x, the virtuality of the parton $t = -q_T^2 = \mathbf{q}_T^2$, and the factorization scale μ.

Virtuality of the partons in the initial state of the hard subprocess, usually breaks the gauge invariance of the amplitude. However, it was shown [8], that in QCD at high energies, the so-called quasi-multi Regge kinematics dominates, when produced particles are arranged in clusters, strongly separated in rapidity. In this high-energy (Regge) limit, the gauge invariance condition holds for each of this clusters independently from the others, so the fields, carrying four-momentum between this clusters, are new gauge invariant degrees of freedom, accompanying the ordinary gluons and quarks in the effective field theory for the Regge limit of QCD [9]. They are Reggeized gluons and Reggeized quarks [9, 10].

In our calculations, we rely on the assumption, that particles produced in the hard subprocess are well separated in rapidity from ones, produced at the evolution stage. Therefore, partons incoming to the hard subprocess are Reggeized, and we use the Feynman rules of Ref. [10, 11] to compute the hard scattering matrix elements. Matrix elements for the relevant $2 \to 1$ and $2 \to 2$ subprocesses have been obtained in Refs. [12, 13, 14].

Although, unintegrated PDFs are not so constrained as usual collinear PDFs, there exists the method to obtain unintegrated PDFs from the collinear ones, which showed stable and consistent results in many phenomenological applications, it is the Kimber-Martin-Ryskin (KMR) method [15]. Together with the parton Reggeization approach (PRA), this method was recently applied to describe of dijet [16] and bottom-flavored jet [17] production, Drell-Yan lepton pair production [18], single jet and prompt photon production [19] at the Tevatron and LHC.

1   Charmonium and Bottomonium production.

Now we start the discussion of recent results in the phenomenology of heavy quarkonium production, obtained in the leading order of the NRQCD and PRA. In the Ref. [20], it was shown, that it is possible to describe the latest LHC experimental data on the prompt charmonium production at the $\sqrt{S} = 7$ TeV in a wide kinematical range ($2 < p_T < 20$ GeV and $|y| < 3.5$) with a good accuracy, using the CO NMEs extracted from Tevatron data at the $\sqrt{S} = 1.8$

TeV and 1.96 TeV [12, 20]. The fitted CO NMEs are also shown to be compatible with NLO collinear parton model (PM) results of Ref. [4].

Very recently, ATLAS collaboration has presented the measurement of the prompt and non-prompt χ_{c1} and χ_{c2} production in pp-collisions at $\sqrt{S} = 7$ TeV [22]. Comparison of the leading order (LO) PRA predictions with this new data is presented in the Fig. 1.
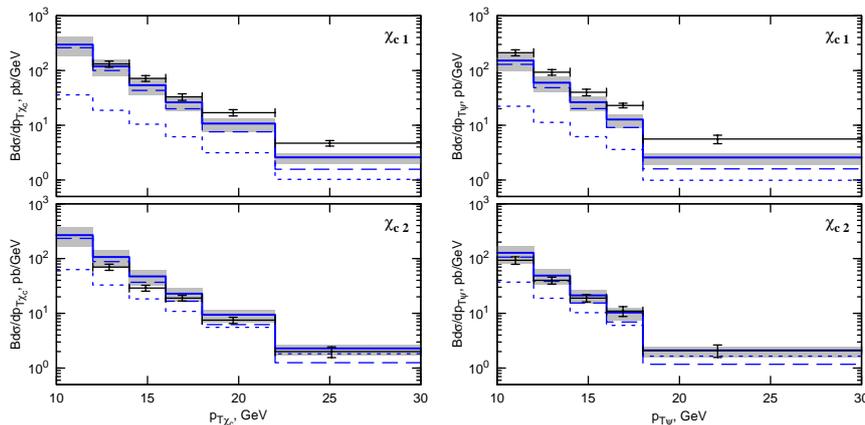

Figure 1: Transverse momentum spectra of prompt $\chi_{c1,2}$ production at $\sqrt{S} = 7$ TeV, measured through their radiative decay to J/ψ mesons. Experimental data by ATLAS collaboration [22]. In the left panel, the reconstructed spectrum over $p_{T\chi_c}$. In the right panel, the spectrum over $p_{TJ/\psi}$. Product of branching fractions $B = B(\chi_{c1,2} \to J/\psi\gamma)B(J/\psi \to \mu^+\mu^-)$ is included. Dashed line is the $^3P_J^{(1)}$ contribution, dotted line is the $^3S_1^{(8)}$ contribution, solid line is their sum.

To produce the predictions in the Fig. 1, we used the CO NMEs of Ref. [20], which where fitted to the Tevatron data at $\sqrt{S} = 1.8$ TeV. In our calculations, $m_c = M_{J/\psi}/2$, and momentum squared of produced $Q\bar{Q}$ pair is equal to $M_{J/\psi}^2$ for all states. The proper treatment of the mass difference between the $Q\bar{Q}$ pair and produced quarkonium, requires taking into account higher order relativistic corrections in v.

To estimate $d\sigma/dp_{T\chi_c}$, we rescaled the transverse momentum by the mass ratio $M_{J/\psi}/M_{\chi_{cJ}}$, which corresponds to the approximation of collinear radiation of the decay photon in the limit $M_{\chi_{cJ}} - M_{J/\psi} \ll M_{J/\psi}$, as it was used in Ref. [5].

The $\Upsilon(nS)$ production in the LO PRA and NRQCD was studied in the first time in Ref. [13], the detailed discussion of the recent LHC data is presented in the Ref. [21]. It is pointed out, that the inclusion of the region of small p_T, greatly constrains the fit, and suppresses possible negative values of CO NMEs. Also, negative values of NMEs could not be advocated in our formally LO calculation.

2 Heavy quarkonium polarization puzzle.

Study polarization of $S-$wave heavy quarkonia is very important for testing of the NRQCD factorization, since the soft gluon exchange at the hadronisation stage is belived to be not able to sufficiently change the polarization of the $Q\bar{Q}$ pair, produced in the hard scattering.

The polarisation variables are defined through the angular distribution of the products of the decay $\mathcal{H} \to \mu^+\mu^-$ in the rest frame of heavy quarkonium $\mathcal{H}$:

$$\frac{d\sigma}{d\Omega} \sim 1 + \lambda_\theta \cos^2(\theta) + \lambda_\varphi \sin^2(\theta)\cos(2\varphi) + \lambda_{\theta\varphi}\sin(2\theta)\cos(\varphi) \; , \qquad (2)$$

where θ and φ are polar and azimuthal angles of lepton (μ^+) momentum in the some coordinate system, chosen in the rest frame of $\mathcal{H}$, and λ_θ, λ_φ, $\lambda_{\theta\varphi}$ are polarization parameters. The issue of the choice of the coordinate system is important and widely discussed in the literature, see e. g. [23], here we use only the s-channel helicity frame.

In the Fig. 2 we present the comparison of the LO PRA predictions on polarization parameter λ_θ for $\psi(2S)$ and $\Upsilon(3S)$ states with the recent experimental data by CMS [24] and CDF [25] Collaborations. We choose these states, because in our model they are produced directly, and
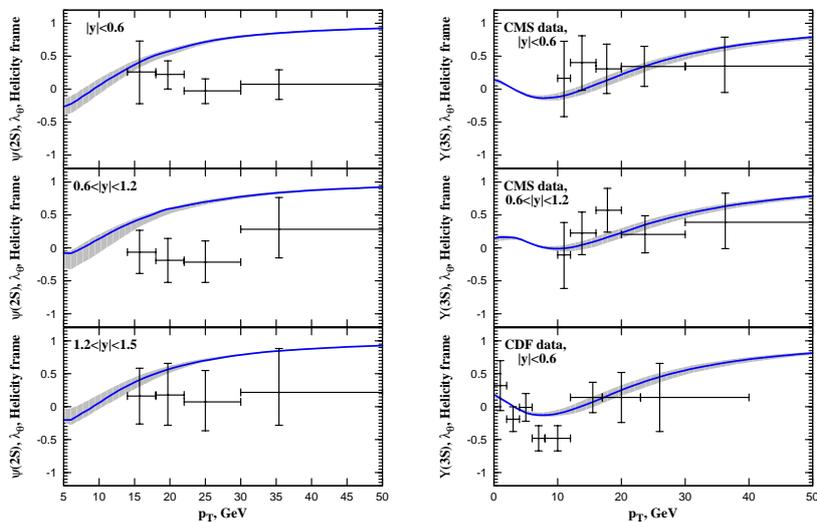

Figure 2: Left panel – the polarization parameter λ_θ as function of p_T for the $\psi(2S)$ production at $\sqrt{S} = 7$ TeV. Experimental data are from CMS Collaboration [24]. Right panel – the polarization parameter for the $\Upsilon(3S)$ production at $\sqrt{S} = 7$ TeV (CMS data [24]) and $\sqrt{S} = 1.8$ TeV (CDF data [25]).

give the most clear test of the production mechanism. From Fig. 2 we can conclude, that our prediction for $\Upsilon(3S)$ polarization is in a good agreement with experimental data. The situation here is very similar to the results of Ref. [5], obtained in the NLO of collinear PM. In contrast, the polarization of $\psi(2S)$ is not described. Because of the domination of the CO contributions at high $p_T \gg M_{J/\psi}$, theory predicts the strong transversal polarization of $\psi(2S)$, while experimental data are compatible with zero polarization. The same disagreement is observed in the NLO PM calculations [5]. Together with the observed inconsistency of the CO NMEs, obtained as a result of the global fit on cross section data, with the data on prompt J/ψ polarization [26], this result leads to the famous charmonium polarization puzzle. Attempts to resolve this puzzle require careful study of feeddown contributions and higher-order processes, such as $p + p \to J/\psi + c + \bar{c} + X$, which can sufficiently contribute at high p_T. In case

of bottomonium production, NRQCD agrees with experimental data as for p_T-spectra as for polarization parameters. It means that $b-$quark mass is sufficiently large to suppress relativistic corrections and nonperturbative effects during the hadronization.

Acknowledgments

References

[1] G. T. Bodwin, E. Braaten, and G. P. Lepage, Phys. Rev. **D51** 1125 (1995); **55** 5853(E) (1997).

[2] F. Maltoni, M. L. Mangano, and A. Petrelli, Nucl. Phys. **B519** 361 (1998).

[3] G. P. Lepage, *et. al.* Phys. Rev. **D46** 4052 (1992).

[4] M. Butenschoen and B. A. Kniehl, Phys. Rev. Lett. **106** 022003 (2011); Phys. Rev. **D84** 051501 (2011).

[5] B. Gong, J.-X. Wang, and H.-F. Zhang, Phys. Rev. bf D83 114021 (2011); K. Wang, Y.-Q. Ma, and K.-T.Chao, Phys. Rev. **D85** 114003 (2012); B. Gong, L.-P. Wan, J.-X. Wang, and H.-F. Zhang, arXiv: hep-ph/1305.0748 (2013).

[6] P. Sun, C.-P. Yuan, F. Yuan, Phys. Rev. **D88** 054008 (2013).

[7] L. Gribov, E. Levin, and M. Ryskin Phys.Rept. **100** 1150; S. Catani, M. Ciafaloni, and F. Hautmann Nucl. Phys. **B366** 135188 (1991).

[8] V. S. Fadin and L. N. Lipatov, Nucl. Phys. **B406** 259 (1993); **B477** 767 (1996).

[9] L. N. Lipatov, Nucl. Phys. **B452** 369 (1995).

[10] L. N. Lipatov and M. I. Vyazovsky, Nucl. Phys. **B597** 399 (2001).

[11] E. N. Antonov, L. N. Lipatov, E. A. Kuraev, and I. O. Cherednikov, Nucl. Phys. **B721** 111 (2005).

[12] B. A. Kniehl, D. V. Vasin, and V. A. Saleev, Phys. Rev. **D73**, 074022 (2006).

[13] B. A. Kniehl, V. A. Saleev, and D. V. Vasin, Phys. Rev. **D74** 014024 (2006).

[14] D. V. Vasin, V. A. Saleev, Phys. Part. Nucl. **38** 635-658 (2007).

[15] M. A. Kimber, A. D. Martin, and M. G. Ryskin, Eur. Phys. J. **C12** 655 (2000); Phys. Rev. **D63** 114027 (2001); G. Watt, A. D. Martin, and M. G. Ryskin, Eur. Phys. J. **C31** 73 (2003); Phys. Rev. **D70** 014012 (2004); **D70**, 079902(E) (2004).

[16] M. A. Nefedov, V. A. Saleev, A. V. Shipilova Phys. Rev. **D87** 094030 (2013).

[17] V. A. Saleev, A. V. Shipilova Phys. Rev. **D86** 034032 (2012).

[18] M. A. Nefedov, N. N. Nikolaev, V. A. Saleev Phys. Rev. **D87** 014022 (2013).

[19] B. A. Kniehl, V. A. Saleev, A. V. Shipilova and E. V. Yatsenko, Phys. Rev. **D84** 074017 (2011).

[20] V. A. Saleev, M. A. Nefedov and A. V. Shipilova, Phys. Rev. **D85** 074013 (2012).

[21] M. Nefedov, V. Saleev and A. Shipilova, Phys. Rev. **D88** 014003 (2013).

[22] G. Aad *et. al.* [ATLAS collaboration], ATLAS-CONF-2013-095 (2013).

[23] M. Beneke, M. Kramer and M. Vanttinen, Phys. Rev. **D57** 4258 (1998); P. Faccioli, C. Lourenco, J. Seixas and H. K. Wohri, Eur. Phys. J. **C69** 657 (2010).

[24] S. Chatrchyan *et al.* [CMS Collaboration], arXiv:hep-ex/1307.6070 (2013); S. Chatrchyan *et al.* [CMS Collaboration], Phys. Rev. Lett. **110** 081802 (2013).

[25] T. Aaltonen *et al.* [CDF Collaboration], Phys. Rev. Lett. **108** 151802 (2012).

[26] M. Butenschoen and B. A. Kniehl, Mod. Phys. Lett. **A28** 1350027 (2013).

Light-Cone Distribution Amplitudes of Bottom Baryons

Alexander Parkhomenko

P. G. Demidov Yaroslavl State University, Yaroslavl, Russia

A discussion of the three-quark light-cone distribution amplitudes (LCDAs) for the ground state heavy baryons with the spin-parities $J^P = 1/2^+$ and $J^P = 3/2^+$ in QCD in the heavy-quark limit is presented. Simple models for the bottom-baryon distribution amplitudes are analyzed with account of their scale dependence.

1   Introduction

The B-meson factories at SLAC and KEK, after approximately a decade of their operation, have made a great impact on a clarification of CP-violation origin in the quark sector of the Standard Model (SM). Study of heavy-light hadrons, in particular mesons and baryons containing the b-quark, at the LHC can serve as an additional test of the Kobayashi-Maskawa mechanism. Specific processes with bottom baryons, such as rare decays involving flavor-changing neutral currents (FCNC) transitions, are potential sources of new physics beyond the SM. In a difference to B-mesons, a non-zero spin of baryons allows also an experimental study of spin correlations. The spectrum of heavy bottom baryons have been enlarged substantially thanks to the effort done by the CDF and D0 Collaborations at the Tevatron collider and is presented in Table 1. During the LHC Run I, the majority of the bottom-baryon states has been confirmed and several new ones were observed. Unlike these progress, study of the FCNC motivated decays of bottom baryons remains to be statistically limited. A grater effort is expected during the next LHC run where heavy baryons will be copiously produced, and their weak decays may be measured precisely enough to provide important clues on physics beyond the Standard Model.

The theory of bottom baryon decays into light hadrons is more complicated compared to the B-meson decays and, hence, was receiving less attention. Calculations of heavy-baryon decays into light particles based on the heavy quark expansion, see e. g. [1], or using sum rules of the type proposed in [2, 3, 4] require the primary non-perturbative objects — the distribution amplitudes of heavy baryons. For a long period, the only existed models of heavy-baryon distribution amplitudes [5, 6] have been motivated by quark models and not consistent with QCD constraints. In the paper [7], the complete classification of three-quark light-cone distribution amplitudes (LCDAs) of the Λ_b-baryon in QCD in the heavy quark limit was given and the scale-dependence of the leading-twist LCDA is discussed. In addition, simple models of the LCDAs were suggested and their parameters were fixed based on estimates of the first few moments by the QCD sum rules method. The analysis of [7] has been extended on all the ground state b-baryons with the spin-parity both $J^P = 1/2^+$ and $J^P = 3/2^+$. The basic steps and main results of such an analysis are summarized in this lecture and all the details are presented in our papers [8, 9].

Baryon	$I(J^P)$	j^p	Experiment	HQET	Lattice QCD
Λ_b	$0(1/2^+)$	0^+	5619.4 ± 0.7	5637^{+68}_{-56}	$5641 \pm 21^{+15}_{-33}$
Σ_b^+	$1(1/2^+)$	1^+	5811.3 ± 1.9	5809^{+82}_{-76}	$5795 \pm 16^{+17}_{-26}$
Σ_b^-	$1(1/2^+)$	1^+	5815.5 ± 1.8	5809^{+82}_{-76}	$5795 \pm 16^{+17}_{-26}$
Σ_b^{*+}	$1(3/2^+)$	1^+	5832.1 ± 1.9	5835^{+82}_{-77}	$5842 \pm 26^{+20}_{-18}$
Σ_b^{*-}	$1(3/2^+)$	1^+	5835.1 ± 1.9	5835^{+82}_{-77}	$5842 \pm 26^{+20}_{-18}$
Ξ_b^-	$1/2(1/2^+)$	0^+	5791.1 ± 2.2	5780^{+73}_{-68}	$5781 \pm 17^{+17}_{-16}$
Ξ_b^0	$1/2(1/2^+)$	0^+	5788 ± 5	5903^{+81}_{-79}	$5903 \pm 12^{+18}_{-19}$
Ξ_b'	$1/2(1/2^+)$	1^+		5903^{+81}_{-79}	$5903 \pm 12^{+18}_{-19}$
$\Xi_b'^{*0}$	$1/2(3/2^+)$	1^+	5945.0 ± 2.8	5903^{+81}_{-79}	$5950 \pm 21^{+19}_{-21}$
Ω_b^-	$0(1/2^+)$	1^+	6071 ± 40	6036 ± 81	$6006 \pm 10^{+20}_{-19}$
Ω_b^*	$0(3/2^+)$	1^+		6063^{+83}_{-82}	$6044 \pm 18^{+20}_{-21}$

Table 1: Experimental measurements [10] and theoretical predictions based on HQET [11] and Lattice QCD [12] for masses of ground-state bottom baryons (in units of MeV). The mass of the $\Xi_b'^{*0}$-baryon was measured by the CMS Collaboration recently [13]. The LHCb Collaboration [14] have measured the masses of the Λ_b-, Ξ_b^--, and Ω_b^--baryons in agreement with the SM expectations.

2 Light-Cone Distribution Amplitudes

Light-cone distribution amplitudes (LCDAs) of heavy baryons are the transition matrix elements from the baryonic state to vacuum of non-local light-ray operators built off an effective heavy quark and two light quarks. The content of such operators supports a similarity in the construction of the heavy-baryon LCDAs to both the B-meson (within the HQET) [15, 16] and the nucleon (within QCD) [17, 18] LCDAs descriptions. An important simplifying feature of the operators containing one or more heavy quarks is an existence of the Heavy Quark Symmetry (HQS) which results into the decoupling of the heavy-quark spin from the system dynamics in the limit $m_Q \to \infty$, where m_Q is the heavy-quark mass. So, to understand the properties of heavy baryons in this limit, it is enough to switch off the heavy-quark spin and to introduce a total set of two-particle LCDAs corresponding to the light-quark system, called diquark, which quantum numbers completely determine a number of LCDAs and their asymptotic behavior.

In this simplified picture, there are the $SU(3)_F$ antitriplet of "scalar baryons" with the $J^P = 0^+$ spin-parity determined by the diquark spin-parity $j^p = 0^+$ and the $SU(3)_F$ sextet of "axial-vector baryons" with the $J^P = 1^+$ spin-parity which follows from the diquark spin-parity $j^p = 1^+$. It is reasonable to start with the description of the "scalar baryons" and then to generalize the procedure on the "axial-vector baryons". The changes originated by an account of the heavy-quark spin can be done after the total sets of the non-local operators and corresponding LCDAs are introduced in the decoupling limit. All these steps are discussed briefly in this section.

2.1 "Scalar Baryons"

The "scalar baryons" are combined into the $SU(3)_F$ antitriplet with $J^P = 0^+$ in which the light diquark states are also the scalar states with $j^p = 0^+$.

The set of the LCDAs is determined by the matrix elements between the baryonic state and vacuum of the four independent non-local light-ray operators [7, 8, 9]:

$$\epsilon^{abc}\langle 0| \left(q_1^a(t_1 n)C\gamma_5\slashed{n}q_2^b(t_2 n)\right) h_v^c(0)|H(v)\rangle = f_H^{(2)}\Psi_2(t_1, t_2) \tag{1}$$
$$\epsilon^{abc}\langle 0| \left(q_1^a(t_1 n)C\gamma_5 q_2^b(t_2 n)\right) h_v^c(0)|H(v)\rangle = f_H^{(1)}\Psi_3^s(t_1, t_2)$$
$$\epsilon^{abc}\langle 0| \left(q_1^a(t_1 n)C\gamma_5 i\sigma_{\bar{n}n}q_2^b(t_2 n)\right) h_v^c(0)|H(v)\rangle = 2f_H^{(1)}\Psi_3^\sigma(t_1, t_2)$$
$$\epsilon^{abc}\langle 0| \left(q_1^a(t_1 n)C\gamma_5\slashed{\bar{n}}q_2^b(t_2 n)\right) h_v^c(0)|H(v)\rangle = f_H^{(2)}\Psi_4(t_1, t_2)$$

where $q_i(x) = u(x), d(x), s(x)$ are the light-quark fields, $h_v(0)$ is the static heavy-quark field situated at the origin of the position-space frame, C is the charge conjugation matrix, n^μ and $\bar{n}^\mu$ are two light-like vectors normalized by the condition $(n\bar{n}) = 2$. In addition, the frame is adopted where the heavy-meson velocity is related to the light-like vectors as follows: $v^\mu = (n^\mu + \bar{n}^\mu)/2$. The light-quark fields on the light cone are assumed to be multiplied by the Wilson lines:

$$q(tn) = [0, tn]\, q(tn) = \mathrm{P}\exp\left\{-ig_{\mathrm{st}}t\int_0^1 d\alpha\, n^\mu A_\mu(\alpha tn)\right\} q(tn) = \sum_{N=0}^\infty \frac{t^N}{N!}\left(n^\mu D_\mu\right)^N q(0),$$

where the following definition of the covariant derivative $D_\mu = \partial_\mu - ig_{\mathrm{st}}A_\mu$ is accepted. The similar definition can be used for the gluonic field: $G_{\mu\nu}(tn) = [0, tn]\, G_{\mu\nu}(tn)$, where the Wilson line is determined in the adjoint representation of the color $SU(3)$-group.

The static heavy-quark field living on the light cone also includes the Wilson line but of the other type with the time-like link [19]:

$$h_v(0) = \mathrm{P}\exp\left\{ig_{\mathrm{st}}\int_{-\infty}^0 d\alpha\, v^\mu A_\mu(\alpha v)\right\}\phi(-\infty),$$

with which it is connected with the sterile field $\phi(-\infty)$.

The couplings $f_H^{(i)}$ introduced in Eqs. (1) to make the LCDAs dimensionless are defined by local operators [20, 21, 22, 23]:

$$\epsilon^{abc}\langle 0| \left(q_1^a(0)C\gamma_5 q_2^b(0)\right) h_v^c(0)|H(v)\rangle = f_H^{(1)}$$
$$\epsilon^{abc}\langle 0| \left(q_1^a(0)C\gamma_5\slashed{v}q_2^b(0)\right) h_v^c(0)|H(v)\rangle = f_H^{(2)}$$

The scale dependences of these couplings are governed by the anomalous dimensions $\gamma^{(i)}$ of local operators as follows:

$$\frac{d\ln f_H^{(i)}(\mu)}{d\ln\mu} \equiv -\gamma^{(i)} = -\sum_k \gamma_k^{(i)}\, a^k(\mu), \qquad a(\mu) \equiv \frac{\alpha_s^{\overline{\mathrm{MS}}}(\mu)}{4\pi},$$

where the strong coupling is determined in the $\overline{\mathrm{MS}}$-scheme. This equation can be solved order by order in the $a(\mu)$-power expansion and in the NLO order, one can use the following relations:

$$f_H^{(i)}(\mu) = f_H^{(i)}(\mu_0)\left(\frac{\alpha_s(\mu)}{\alpha_s(\mu_0)}\right)^{\gamma_1^{(i)}/\beta_0}\left[1 - \frac{\alpha_s(\mu_0) - \alpha_s(\mu)}{4\pi}\frac{\gamma_1^{(i)}}{\beta_0}\left(\frac{\gamma_2^{(i)}}{\gamma_1^{(i)}} - \frac{\beta_1}{\beta_0}\right)\right],$$
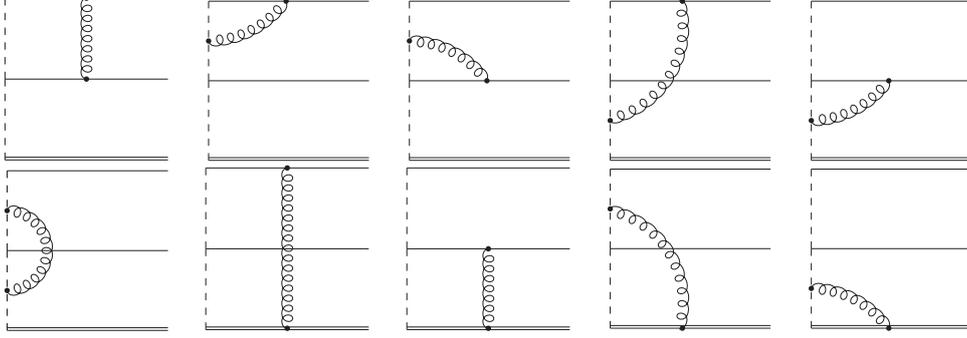
Figure 1: The complete set of the one-gluon-exchange diagrams necessary for the scale-dependence calculation of the heavy-baryon LCDAs. The normal and thick solid lines corresponds to the light and heavy quarks while dotted and wavy lines denote the Wilson lines and virtual gluons, respectively.

where $\beta_{0,1}$ are the first two coefficient in the perturbative expansion of the β-function. As the evolution to the required scale can be easily done now, one needs to know numerical values of the couplings $f_H^{(i)}(\mu)$ at some representative scale μ_0, say $\mu_0 = 1$ GeV. As this scale is rather low to use the perturbation theory, non-perturbative techniques are necessary to calculate these quantities. In particular, the QCD sum rules method in NLO for the Λ_b-baryon results the values [23]:

$$ f_{\Lambda_b}^{(1)}(\mu_0 = 1 \text{ GeV}) \simeq f_{\Lambda_b}^{(2)}(\mu_0 = 1 \text{ GeV}) \simeq 0.030 \pm 0.005 \text{ GeV}^3. $$

Non-relativistic constituent-quark picture of heavy baryons H suggests that $f_H^{(2)} \simeq f_H^{(1)}$ at low scales of order 1 GeV, and this expectation is supported by numerous QCD sum rule calculations [21, 20, 22, 23]. These couplings $f_H^{(i)}(\mu)$ cannot coincide at all scales because of different anomalous dimensions $\gamma^{(i)}$ of local operators.

Similar to the couplings $f_H^{(i)}(\mu)$, the LCDAs $\Psi_i(t_1, t_2)$ introduced in Eq. (1) are also scale-dependent functions. To find their scale evolution, it is convenient to make their Fourier transform to the momentum space:

$$ \Psi(t_1, t_2) = \int_0^\infty d\omega_1 \int_0^\infty d\omega_2 \, e^{-it_1\omega_1 - it_2\omega_2} \psi(\omega_1, \omega_2) = \int_0^\infty \omega \, d\omega \int_0^1 du \, e^{-i\omega(t_1 u + t_2 \bar{u})} \, \widetilde{\psi}(\omega, u) $$

where $\bar{u} = 1 - u$. In the first representation $\omega_1 = u\omega$ and $\omega_2 = (1 - u)\omega = \bar{u}\omega$ are the energies of the light quarks q_1 and q_2. The leading-order evolution equation for the $\psi_2(\omega_1, \omega_2; \mu)$ can be derived by identifying the ultra-violet singularities of the one-gluon-exchange diagrams presented in Fig. 1.

The evolution equation in the leading order is expressed in terms of two-particle kernels:

$$ \mu \frac{d}{d\mu} \psi_2(\omega_1, \omega_2; \mu) = -\frac{\alpha_s(\mu)}{2\pi} \frac{4}{3} \left\{ \int_0^\infty d\omega_1' \, \gamma^{\text{LN}}(\omega_1', \omega_1; \mu) \, \psi_2(\omega_1', \omega_2; \mu) \right. $$

$$ \left. + \int_0^\infty d\omega_2' \, \gamma^{\text{LN}}(\omega_2', \omega_2; \mu) \, \psi_2(\omega_1, \omega_2'; \mu) - \int_0^1 dv \, V(u, v) \, \psi_2(v\omega, \bar{v}\omega; \mu) + \frac{3}{2} \psi_2(\omega_1, \omega_2; \mu) \right\}, $$

where the kernel $\gamma^{\mathrm{LN}}(\omega', \omega; \mu)$ controls the evolution of the B-meson LCDA [24] and $V(u, v)$ is the Efremov-Radyushkin-Brodsky-Lepage (ER-BL) kernel [25, 26]. The term $3\psi_2(\omega_1, \omega_2; \mu)/2$ results from the one-loop $f_H^{(2)}$ renormalization subtraction. The evolution equation above can be solved either numerically or semi-analytically [7, 9]

2.2 "Axial-Vector Baryons"

The "axial-vector baryons" are components of the $SU(3)_F$ sextet with $J^P = 1^+$ in which the light diquark states are the axial-vector states with $j^p = 1^+$. In a difference to the "scalar baryons" case, one needs to consider the baryons with the longitudinal and transverse polarizations separately.

The set of the longitudinal LCDAs is determined by the matrix elements between the baryonic state with the appropriate polarization and vacuum of the four independent non-local light-ray operators [8, 9]:

$$
\begin{aligned}
\epsilon^{abc} \langle 0| \left(q_1^a(t_1) C \slashed{n} q_2^b(t_2) \right) h_v^c(0)|H(v, \varepsilon)\rangle &= (\bar{v}\varepsilon)\, f_H^{(2)}\, \Psi_2^{\|}(t_1, t_2) \\
\epsilon^{abc} \langle 0| \left(q_1^a(t_1) C\, q_2^b(t_2) \right) h_v^c(0)|H(v, \varepsilon)\rangle &= (\bar{v}\varepsilon)\, f_H^{(1)}\, \Psi_3^{\|s}(t_1, t_2) \\
\epsilon^{abc} \langle 0| \left(q_1^a(t_1) C\, i\sigma_{\bar{n}n} q_2^b(t_2) \right) h_v^c(0)|H(v, \varepsilon)\rangle &= 2\,(\bar{v}\varepsilon)\, f_H^{(1)}\, \Psi_3^{\|a}(t_1, t_2) \\
\epsilon^{abc} \langle 0| \left(q_1^a(t_1) C \slashed{\bar{n}} q_2^b(t_2) \right) h_v^c(0)|H(v, \varepsilon)\rangle &= -(\bar{v}\varepsilon)\, f_H^{(2)}\, \Psi_4^{\|}(t_1, t_2)
\end{aligned}
$$

where $\sigma_{\bar{n}n} = i\left(\slashed{\bar{n}}\slashed{n} - \slashed{n}\slashed{\bar{n}}\right)/2$, $\bar{v}^\mu = (\bar{n}^\mu - n^\mu)/2$ is the four-vector orthogonal to the four-velocity $(v\bar{v}) = 0$ and normalized by $(\bar{v}\bar{v}) = -1$. In the LCDA definitions above, the baryonic state is assumed to have a pure longitudinal polarization $\varepsilon_{\|}^\mu = \bar{v}^\mu$ and the prefactor on the r.h.s. is simply $(\bar{v}\varepsilon) = -1$.

The similar set of the transverse LCDAs is determined as follows [8, 9]:

$$
\begin{aligned}
\epsilon^{abc} \langle 0| \left(q_1^a(t_1) C\, \gamma_\perp^\mu \slashed{n} q_2^b(t_2) \right) h_v^c(0)|H(v, \varepsilon)\rangle &= f_H^{(2)}\, \Psi_2^{\perp}(t_1, t_2)\, \varepsilon_\perp^\mu \\
\epsilon^{abc} \langle 0| \left(q_1^a(t_1) C\, \gamma_\perp^\mu q_2^b(t_2) \right) h_v^c(0)|H(v, \varepsilon)\rangle &= f_H^{(1)}\, \Psi_3^{\perp s}(t_1, t_2)\, \varepsilon_\perp^\mu \\
\epsilon^{abc} \langle 0| \left(q_1^a(t_1) C\, \gamma_\perp^\mu i\sigma_{\bar{n}n} q_2^b(t_2) \right) h_v^c(0)|H(v, \varepsilon)\rangle &= 2 f_H^{(1)}\, \Psi_3^{\perp a}(t_1, t_2)\, \varepsilon_\perp^\mu \\
\epsilon^{abc} \langle 0| \left(q_1^a(t_1) C\, \gamma_\perp^\mu \slashed{\bar{n}} q_2^b(t_2) \right) h_v^c(0)|H(v, \varepsilon)\rangle &= f_H^{(2)}\, \Psi_4^{\perp}(t_1, t_2)\, \varepsilon_\perp^\mu
\end{aligned}
$$

where $\gamma_\perp^\mu = \gamma^\mu - \left(\slashed{\bar{n}}n^\mu + \slashed{n}\bar{n}^\mu\right)/2$ and $\varepsilon_\perp^\mu = \varepsilon^\mu - \varepsilon_{\|}^\mu$ is the transverse polarization of the baryon.

2.3 Real Baryons

As far as all the sets of the LCDAs are determined, it necessary to generalize their definitions to real baryons which simply means that the spin of the heavy quark should be included into the baryon wave function. In other words, the r.h.s. of matrix elements of all non-local operators must be multiplied on the Dirac spinor $U(v)$ of the heavy quark h_v, satisfying the conditions: $\slashed{v} U(v) = U(v)$ and $\overline{U}(v) U(v) = 1$. After these modifications, the "scalar baryons" transform to the baryons with the spin-parity $J^P = 1/2^+$ and the heavy-quark Dirac spinor $U(v)$ is nothing else but the heavy-baryon spinor $H(v)$, i.e. the spin of the heavy quark completely determines the spin structure of the heavy-baryon wave function. The case of "axial-vector baryons" is a little bit more complicated. It is well-known from quantum mechanics that the direct product
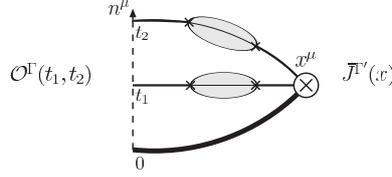
Figure 2: The two-point correlator of the local and light-ray operators in the QCD background.

of two angular momenta $j_1 = 1/2$ and $j_2 = 1$ is decomposed into two irreducible representation with the momenta $J_1 = 1/2$ and $J_2 = 3/2$. That is exactly the situation after the heavy-quark spin is switched on in the heavy baryon with the diquark in the axial-vector state $j^p = 1^+$:

$$\varepsilon_\mu\, U(v) = \left[\varepsilon_\mu\, U(v) - \frac{1}{3}\,(\gamma_\mu + v_\mu)\,\slashed{\varepsilon}\, U(v)\right] + \frac{1}{3}\,(\gamma_\mu + v_\mu)\,\slashed{\varepsilon}\, U(v) \equiv R_\mu^{3/2}(v) + \frac{1}{3}\,(\gamma_\mu + v_\mu)\, H(v).$$

As the result, there are two states with the spin-parities $J^P = 1/2^+$ and $J^P = 3/2^+$. The former one is described by the Dirac spinor $H(v)$ and for the $J^P = 3/2^+$ state the Rarita-Schwinger vector-spinor $R_\mu^{3/2}(v)$, which satisfies the relations $\slashed{v}\, R_\mu^{3/2}(v) = R_\mu^{3/2}(v)$, $v^\mu\, R_\mu^{3/2}(v) = 0$, and $\gamma^\mu\, R_\mu^{3/2}(v) = 0$, can be used.

3 QCD Sum Rules

In applications to a calculation of amplitudes with heavy baryons, one needs to know realistic models for LCDAs. Such models can be obtained by matching several few moments of LCDA models and the corresponding ones calculated by some non-perturbative methods, say by the QCD sum rules. The later method requires a calculation of a two-point correlator which involve the non-local light-ray operator and a suitable local current $J^{\Gamma'}(x)$, as it is shown in Fig. 2.

The general structure of the heavy-baryon local currents can be chosen as follows:

$$\bar{J}^{\Gamma'}(x) = \epsilon^{abc}\left(\bar{q}_2^a(x)\,[A + B\,\slashed{v}]\,\Gamma' C^T \bar{q}_1^b(x)\right)\bar{h}_v^c(x),$$

where A and B are two constants with the constraint $A + B = 1$ which accounts for an arbitrariness in the choice of local currents. The variation in $A \in [0, 1]$ is adopted as a systematic error of numerical estimations. Note that the central value $A = B = 1/2$ corresponds to the a constituent quark model picture [7]. The Dirac matrix Γ' is a suitable structure determined by the spin-parity of the baryon, in particular, $\Gamma' = \gamma_5$ for baryons from the $SU(3)_F$ antitriplet $(j^p = 0^+)$ and $\Gamma' = \gamma_\parallel, \gamma_\perp$ for the $SU(3)_F$-sextet baryons with $j^p = 1^+$.

In calculations of the correlation functions, one tacitly assumes that baryons are bound states of quarks which are not free particles inside but couple by virtue of the gluonic field. So, light quark propagators $\tilde{S}_q(x)$, being very sensitive to the influence of the background gluonic field, should be modified accordingly while for the heavy quark this effect is sub-dominant and to leading order in the heavy-quark mass m_Q expansion can be neglected. To take effects of the QCD background inside baryons into account, the method of non-local condensates [28, 29, 30] is used. In this approach the light-quark propagator can be decomposed into two parts: the perturbative $S_q(x)$ and non-perturbative $\mathcal{C}_q(x)$ ones,

$$\tilde{S}_q(x) \qquad\qquad S_q(x) \qquad\qquad \mathcal{C}_q(x)$$

and the later accumulates an information about the background inside the baryon in terms of non-local quark condensate $\langle \bar{q}(x)q(0)\rangle$:

$$S_q(x) = \frac{i\slashed{x}}{2\pi^2 x^4} - \frac{m}{4\pi^2 x^2} \qquad\qquad \mathcal{C}_q(x) = \frac{1}{12}\langle \bar{q}(x)q(0)\rangle$$

where color and spin indices are omitted. In both expressions the color structure is given by the identity. The factor $1/12$ in $\mathcal{C}_q(x)$ is chosen in a way that the expression is normalized by taking the trace of color and spin, i. e. $\mathrm{Tr}[\mathbb{1}_{\mathrm{spin}}] = 4$ and $\mathrm{Tr}[\mathbb{1}_{\mathrm{color}}] = 3$.

The general parametrization of the non-local condensates was suggested in Refs. [28, 29]:

$$\mathcal{C}_q(x) = \langle \bar{q}q\rangle \int_0^\infty d\nu\, e^{\nu x^2/4}\, f(\nu),$$

where $\langle \bar{q}q\rangle$ is local quark condensate and the shape of the distribution is determined by the function $f(\nu)$. Among the shape models suggested, the choice have been done in favor of the following one [31, 16]:

$$f(\nu) = \frac{\lambda^{a-2}}{\Gamma(a-2)}\, \nu^{1-a}\, e^{-\lambda/\nu}, \qquad a = 3 + \frac{4\lambda}{m_0^2}, \tag{2}$$

where $\lambda = \langle \bar{q}D^2 q\rangle$ is the correlation length and $m_0^2 = \langle \bar{q}g_s G^{\mu\nu}\sigma_{\mu\nu}q\rangle/\langle \bar{q}q\rangle$ is the ratio of the local mixed quark-gluon and quark condensates. If one assumes that virtualities of quarks inside the baryon are small and quarks are on the mass shell, the mixed quark-gluon condensate and the correlation length can be related (this is the usual procedure) but the smallness of such virtualities is not proven and, in general, the correlation length and the ration m_0^2 are independent.

To obtain the QCD sum rules, it is convenient to make the double Fourier transform of the correlation function:

$$\Pi_{\Gamma\Gamma'}(\omega_1, \omega_2; E) = i \int_{-\infty}^\infty \frac{dt_1\, dt_2}{(2\pi)^2}\, e^{i(\omega_1 t_1 + \omega_2 t_2)} \int d^4 x\, e^{-iE(vx)}\, \langle 0|\mathcal{O}^\Gamma(t_1, t_2)\, \bar{J}^{\Gamma'}(x)|0\rangle$$

In the momentum space, the correlation function reads diagrammatically as follows:

$$\Pi(\omega, u; E) = $$

As it is well-known from the QCD-SR analysis within the HQET, the heavy-quark condensate term is suppressed by $1/m_Q$ and absent in the Heavy-Quark Symmetry limit. So, the QCD Sum Rules can be read off after the phenomenological and perturbatively calculated considerations of the correlation function are equated based on the idea of the quark-hadron duality [27]:

$$|f_H|^2\, \psi^\Gamma(\omega, u)\, e^{-\bar{\Lambda}_H/\tau} = \mathbb{B}[\Pi](\omega, u; \tau, s_0),$$

where symbol $\mathbb{B}$ means the Borel-transform, $\bar{\Lambda}_H = m_H - m_Q$ is the effective baryon mass in the HQET, and s_0 is the momentum cutoff resulting from applying the quark-hadron duality. The explicit QCD-SRs for all the baryonic non-local operators can be found in Ref. [9] and we illustrate them here by the one written for the leading-twist (twist-2) transverse LCDA:

$$f_H^{(2)} \left[A f_H^{(1)} + B f_H^{(2)} \right] \tilde{\psi}_2^{SR}(\omega, u) \, \mathrm{e}^{-\bar{\Lambda}/\tau} =$$

$$\frac{3\tau^4}{2\pi^4} \left[B\hat{\omega}^2 \, u\bar{u} + A \hat{\omega} \left(\hat{m}_2 u + \hat{m}_1 \bar{u} \right) \right] E_1(2\hat{s}_\omega) \mathrm{e}^{-\hat{\omega}}$$

$$- \frac{\langle \bar{q}_1 q_1 \rangle \tau^3}{\pi^2} \left[A\hat{\omega}\bar{u} + B\hat{m}_2 \right] f(2\tau\omega u) \, E_{2-a}(2\hat{s}_\kappa) \, \mathrm{e}^{-\hat{\omega}}$$

$$- \frac{\langle \bar{q}_2 q_2 \rangle \tau^3}{\pi^2} \left[A\hat{\omega}u + B\hat{m}_1 \right] f(2\tau\omega\bar{u}) \, E_{2-a}(2\hat{s}_{\bar{\kappa}}) \, \mathrm{e}^{-\hat{\omega}}.$$

To simplify the presentation, the following auxiliary function was introduced:

$$E_a(x) = \frac{1}{\Gamma(a+1)} \int_0^x dt \, t^a \mathrm{e}^{-t} = 1 - \frac{\Gamma(a+1, x)}{\Gamma(a+1)}$$

where $\Gamma(a+1, x) = \int_x^\infty dt \, t^a \mathrm{e}^{-t}$ is the incomplete Γ-function. The other quantities are $\bar{\Lambda} = m_H - m_b$, $s_\omega = s_0 - \omega/2$, $\kappa = \lambda/(2u\omega\tau)$, $\bar{\kappa} = \lambda/(2\bar{u}\omega\tau)$, $\hat{\omega} = \omega/(2\tau)$, $\hat{s}_\omega = s_\omega/(2\tau)$, $\hat{m}_{1,2} = m_{1,2}/(2\tau)$, $\hat{s}_\kappa = \hat{s}_\omega - \kappa/2$, $\hat{s}_{\bar{\kappa}} = \hat{s}_\omega - \bar{\kappa}/2$. The normalizations of the symmetric LCDAs ($t = 2, 3s, 4$) can be fixed by the relation:

$$\int_0^{2s_0} \omega d\omega \int_0^1 du \, \tilde{\psi}_t^{\mathrm{SR}}(\omega, u) \equiv 1,$$

while the normalization of the antisymmetric LCDAs with $t = 3\sigma$ is different and can be fixed by the condition:

$$\int_0^{2s_0} \omega d\omega \int_0^1 du \, C_1^{1/2}(2u - 1) \, \tilde{\psi}_t^{\mathrm{SR}}(\omega, u) \equiv 1,$$

where $C_n^m(x)$ are the Gegenbauer polynomials [32].

These QCD sum rules are not directly applicable for getting the LCDA shapes but can be used to constrain certain moments which are calculated based on the following definition:

$$\langle f(\omega, u) \rangle_k \equiv \int_0^{2s_0} \omega d\omega \int_0^1 du \, f(\omega, u) \, \tilde{\psi}_t^{\mathrm{SR}}(\omega, u)$$

where $t = 2, 3s, 3\sigma, 4$.

4 Numerical analysis

Numerical values of first several moments of the bottom-baryon LCDAs estimated by the QCD-SRs can be found in Ref. [9]. These moments should be matched to the corresponding moments of the model functions for the LCDAs. The general presentation of the model functions for the b-baryon LCDAs is governed by their scale evolution and can be composed of the exponential part corresponding to the heavy-light interaction and the Gegenbauer polynomials to the light-light interaction. The order of the polynomials is determined by the twist of the diquark system.
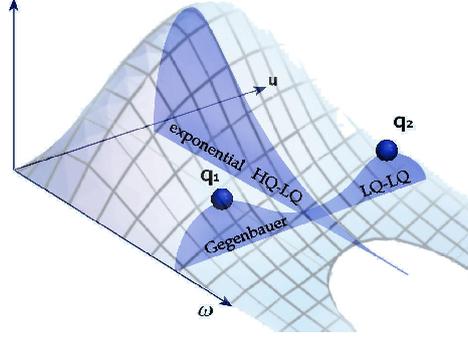
Figure 3: The general representation of the model functions for the heavy-baryon LCDAs with the ω-dependence specific for the B-meson LCDAs and the u-dependence in terms of an expansion in the Gegenbauer polynomials similar to the ones for the light mesons.

Motivated by the analysis done for the Λ_b-baryon [7], the following simple models for the LCDAs have proposed [8, 9]:

$$\tilde{\psi}_2(\omega, u) = \omega^2 u(1-u) \sum_{n=0}^{2} \frac{a_n^{(2)}}{\epsilon_n^{(2)^4}} C_n^{3/2}(2u-1) \, \mathrm{e}^{-\omega/\epsilon_n^{(2)}},$$

$$\tilde{\psi}_{3s}(\omega, u) = \frac{\omega}{2} \sum_{n=0}^{2} \frac{a_n^{(3)}}{\epsilon_n^{(3)^3}} C_n^{1/2}(2u-1) \, \mathrm{e}^{-\omega/\epsilon_n^{(3)}},$$

$$\tilde{\psi}_{3\sigma}(\omega, u) = \frac{\omega}{2} \sum_{n=0}^{3} \frac{b_n^{(3)}}{\eta_n^{(3)^3}} C_n^{1/2}(2u-1) \, \mathrm{e}^{-\omega/\eta_n^{(3)}},$$

$$\tilde{\psi}_4(\omega, u) = \sum_{n=0}^{2} \frac{a_n^{(4)}}{\epsilon_n^{(4)^2}} C_n^{1/2}(2u-1) \, \mathrm{e}^{-\omega/\epsilon_n^{(4)}}.$$

The qualitative behavior of the twist-2 LCDAs is presented in Fig. 3. The estimates of the parameters entering the theoretical models for the heavy-baryon LCDAs at the scale $\mu_0 = 1$ GeV can be found in Refs. [8, 9]. The dependence of the twist-2 LCDAs on the scaled energy u of the lightest quark and the diquark energy ω at the energy scales $\mu_0 = 1$ GeV are shown on the left and right plots in Fig. 4, respectively. The $SU(3)_F$-symmetry breaking in LCDAs based on taking into account the s-quark difference from the u- and d-quarks is clearly seen on these plots. The effect of the symmetry breaking is estimated to be approximately 15%.

5   Renormalization of higher twist operators

The renormalization of the heavy-light light-ray operators up to twist-three was performed in Ref. [33]. Here. both the $2 \to 2$ and $2 \to 3$ kernels were considered and the problem of the operator mixing under the renormalization has been discussed. To work out the evolution, the spinor formalism applied to QCD appears to be the most convenient. In addition, one-loop counterterms of the non-local operators were analyzed on an existence of the conformal
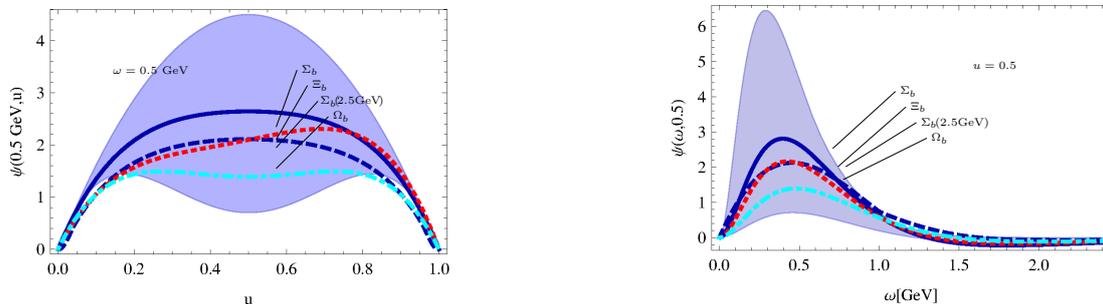
Figure 4: Twist-2 LCDAs of Σ (blue), Ξ (red) and Ω (cyan) baryons in dependence on the scaled energy u of the lightest quark (the left plot) and the diquark energy ω (the right plot) at the scale $\mu_0 = 1$ GeV estimated within the range for the most conservative error $A \in [0, 1]$.

symmetry and the main finding is that the ultra-violet renormalization of a cusp of two Wilson lines results the break down of this symmetry. As a technical output of this analysis, evolution equations for the twist-three operators were written explicitly.

The other step in working out solutions of the heavy-baryon evolution equations analytically was undertaken recently in Ref. [34]. In particular, the eigenfunctions of the Lange-Neubert evolution kernel were found and used for a systematic implementation of the renormalization-group effects for both the B-meson and Λ_b-baryon wave-function evolutions. Based on these foundations, the new strategy to construct the LCDA models in accordance with the Wandzura-Wilczek-like relations was presented. As a possible extension of the above analysis in application to baryons, the classification of the non-local baryonic operators constructed from four particles (three quarks and a gluon) is required to work out equations involving explicitly the there-particle LCDAs and the twist-four four-particle ones which should reduce to the Wandzura-Wilczek relations after four-particle LCDAs are neglected.

6 Conclusions

The total set of the non-local light-ray operators for the ground-state heavy baryons with $J^P = 1/2^+$ and $J^P = 3/2^+$ is constructed in QCD in the heavy-quark limit. Matrix elements of these operators sandwiched between the heavy-baryon state and vacuum determine the LCDAs of different twist through the diquark current. The first several moments of LCDAs are calculated within the method of QCD sum rules using the non-local light-quark condensates. Simple theoretical models for the LCDAs have been proposed and their parameters are fitted based on the QCD sum rules estimations. $SU(3)_F$ breaking effects result the correction of order 10%. The possibility to work out the LCDA evolution analytically is discussed.

Acknowledgements

lecture. I also thank Artem Dzyuba for comments about the recent LHCb results on the bottom-baryon spectroscopy.

References

[1] X. G. He, T. Li, X. Q. Li and Y. M. Wang, Phys. Rev. **D74**, 034026 (2006) [arXiv:hep-ph/0606025].

[2] A. Khodjamirian, T. Mannel and N. Offen, Phys. Rev. **D75**, 054013 (2007) [arXiv:hep-ph/0611193]

[3] F. De Fazio, T. Feldmann and T. Hurth, Nucl. Phys. **B733**, 1 (2006) [arXiv:hep-ph/0504088].

[4] F. De Fazio, T. Feldmann and T. Hurth, JHEP **0802**, 031 (2008) [arXiv:0711.3999].

[5] W. Loinaz and R. Akhoury, Phys. Rev. **D53**, 1416 (1996) [arXiv:hep-ph/9505378].

[6] F. Hussain, J. G. Korner, M. Kramer and G. Thompson, Z. Phys. **C51**, 321 (1991).

[7] P. Ball, V. M. Braun and E. Gardi, Phys. Lett. **B665**, 197 (2008) [arXiv:0804.2424].

[8] A. Ali, C. Hambrock and A. Ya. Parkhomenko, Theor. Math. Phys. **170**, 2 (2012) [Teor. Mat. Fiz. **170**, 5 (2012)].

[9] A. Ali, C. Hambrock, A. Ya. Parkhomenko and W. Wang, Eur. Phys. J. **C73**, 2302 (2013) [arXiv:1212.3280].

[10] J. Beringer *et al.* [Particle Data Group Collaboration], Phys. Rev. **D86**, 010001 (2012).

[11] X. Liu, H. X. Chen, Y. R. Liu, A. Hosaka and S. L. Zhu, Phys. Rev. **D77**, 014031 (2008) [arXiv:0710.0123].

[12] R. Lewis and R. M. Woloshyn, Phys. Rev. **D79**, 014502 (2009) [arXiv:0806.4783].

[13] S. Chatrchyan *et al.* [CMS Collaboration], Phys. Rev. Lett. **108**, 252002 (2012) [arXiv:1204.5955].

[14] R. Aaij *et al.* [LHCb Collaboration], Phys. Rev. Lett. **110**, 182001 (2013) [arXiv:1302.1072].

[15] A. G. Grozin and M. Neubert, Phys. Rev. **D55**, 272 (1997) [arXiv:hep-ph/9607366].

[16] V. M. Braun, D. Y. Ivanov and G. P. Korchemsky, Phys. Rev. **D69**, 034014 (2004) [arXiv:hep-ph/0309330].

[17] V. M. Braun, S. E. Derkachov, G. P. Korchemsky and A. N. Manashov, Nucl. Phys. **B553**, 355 (1999) [arXiv:hep-ph/9902375].

[18] V. Braun, R. J. Fries, N. Mahnke and E. Stein, Nucl. Phys. **B589**, 381 (2000) [Erratum-ibid. **B607**, 433 (2001)] [arXiv:hep-ph/0007279].

[19] G. P. Korchemsky and A. V. Radyushkin, Phys. Lett. **B279**, 359 (1992) [arXiv:hep-ph/9203222].

[20] A. G. Grozin and O. I. Yakovlev, Phys. Lett. **B285**, 254 (1992) [arXiv:hep-ph/9908364].

[21] E. Bagan, M. Chabab, H. G. Dosch and S. Narison, Phys. Lett. **B301** (1993) 243.

[22] S. Groote, J. G. Korner and O. I. Yakovlev, Phys. Rev. **D55** (1997) 3016 [arXiv:hep-ph/9609469].

[23] S. Groote, J. G. Korner and O. I. Yakovlev, Phys. Rev. **D56**, 3943 (1997) [arXiv:hep-ph/9705447].

[24] B. O. Lange and M. Neubert, Phys. Rev. Lett. **91** (2003) 102001 [arXiv:hep-ph/0303082].

[25] A. V. Efremov and A. V. Radyushkin, Theor. Math. Phys. **42**, 97 (1980) [Teor. Mat. Fiz. **42**, 147 (1980)]; Phys. Lett. **B94**, 245 (1980).

[26] G. P. Lepage and S. J. Brodsky, Phys. Lett. **B87**, 359 (1979); Phys. Rev. **D22** (1980) 2157.

[27] M. A. Shifman, A. I. Vainshtein and V. I. Zakharov, Nucl. Phys. **B147**, 385 (1979); Nucl. Phys. **B147**, 448 (1979).

[28] S. V. Mikhailov and A. V. Radyushkin, JETP Lett. **43**, 712 (1986) [Pisma Zh. Eksp. Teor. Fiz. **43**, 551 (1986)].

[29] S. V. Mikhailov and A. V. Radyushkin, Phys. Rev. **D45**, 1754 (1992).

[30] A. P. Bakulev and S. V. Mikhailov, Phys. Rev. **D65**, 114511 (2002) [arXiv:hep-ph/0203046].

[31] V. Braun, P. Gornicki and L. Mankiewicz, Phys. Rev. **D51**, 6036 (1995) [arXiv:hep-ph/9410318].

[32] A. Erdélyi, W. Magnus, F. Oberhettinger, and F. G. Tricomi, *Higher Transcendental Functions*. Vol. II. McGraw-Hill, New-York, 1954.

[33] M. Knodlseder and N. Offen, JHEP **1110**, 069 (2011) [arXiv:1105.4569].

[34] G. Bell, T. Feldmann, Y.-M. Wang and M. W. Y. Yip, JHEP **1311**, 191 (2013) [arXiv:1308.6114].

Rare Semileptonic $B^+ \to \pi^+ \ell^+ \ell^-$ Decay

Ahmed Ali[1], Alexander Parkhomenko[2], Aleksey Rusov[2]

[1]DESY, Notkestraße 85, 22607 Hamburg, Germany
[2]P. G Demidov Yaroslavl State University, Sovietskaya 14, 150000 Yaroslavl, Russia

We present a precise calculation of the dilepton invariant-mass spectrum and branching fraction for $B^+ \to \pi^+ \ell^+ \ell^-$ ($\ell^\pm = e^\pm, \mu^\pm$) in the Standard Model (SM) based on the effective Hamiltonian approach for the $b \to d \ell^+ \ell^-$ transitions. Theoretical estimates strongly depend on the form factors $f_+(q^2)$, $f_0(q^2)$ and $f_T(q^2)$. Of these, $f_+(q^2)$ is well measured in the semileptonic decays $B \to \pi \ell \nu_\ell$ and we use the B-factory data to parametrize it. Using an $SU(3)_F$-breaking Ansatz and Lattice-QCD data, we calculate the $B \to \pi$ form factors. The resulting total branching fraction $\mathcal{B}(B^+ \to \pi^+ \mu^+ \mu^-) = \left(1.88^{+0.32}_{-0.21}\right) \times 10^{-8}$ is in good agreement with the experimental value obtained by the LHCb collaboration.

1   Introduction

Recently, the LHCb collaboration has reported the first observation of the $B^+ \to \pi^+ \mu^+ \mu^-$ decay with 5.2σ significance, using 1.0 fb^{-1} integrated luminosity in proton-proton collisions at the Large Hadron Collider (LHC) at $\sqrt{s} = 7$ TeV [1]. The measured branching ratio $\mathcal{B}(B^+ \to \pi^+ \mu^+ \mu^-) = [2.3 \pm 0.6(\text{stat}) \pm 0.1(\text{syst})] \times 10^{-8}$ [1] is in good agreement with the SM expected rate [2], which, however, is based on model-dependent input for the $B \to \pi$ form factors. Hence, it is very desirable to calculate the form factors from first principles, such as the Lattice-QCD, which have their own range of validity restricted by the recoil energy. With improved lattice technology, one can use the lattice form factors to predict the decay rates in the $B \to \pi$ transitions in the low-recoil region, where the lattice results apply without any extrapolation, in a model-independent manner. We describe such a framework, which makes use of the methods based on the Heavy-Quark Symmetry (HQS) in the large-recoil region, data on the charged-current processes $B^0 \to \pi^- \ell^+ \nu_\ell$ and $B^+ \to \pi^0 \ell^+ \nu_\ell$, to determine one of the form factors, $f_+(q^2)$, and the available lattice results for the form factors in the low-recoil region. The details of the analysis are presented in our recent paper [3] and the main steps are summarized in this contribution.

2   Theory of $B^+ \to \pi^+ \ell^+ \ell^-$ Decay

The effective weak Hamiltonian encompassing the transitions $b \to d \ell^+ \ell^-$ ($\ell = e$, μ, or τ), in the Standard Model (SM) can be written as follows [4]:

$$\mathcal{H}_{\text{eff}}^{b \to d} = \frac{4 G_F}{\sqrt{2}} \left[V_{ud} V_{ub}^* \left(C_1 \, \mathcal{O}_1^{(u)} + C_2 \, \mathcal{O}_2^{(u)} \right) + V_{cd} V_{cb}^* \left(C_1 \, \mathcal{O}_1 + C_2 \, \mathcal{O}_2 \right) - V_{td} V_{tb}^* \sum_{i=3}^{10} C_i \, \mathcal{O}_i \right], \quad (1)$$

where G_F is the Fermi constant, $V_{q_1 q_2}$ are the CKM matrix elements which satisfy the unitary condition $V_{ud} V_{ub}^* + V_{cd} V_{cb}^* + V_{td} V_{tb}^* = 0$ (it can be used to eliminate one combination). In

contrast to the $b \to s$ transition, all three terms in the unitarity relation are of the same order in λ ($V_{ub}^* V_{ud} \sim V_{cb}^* V_{cd} \sim V_{tb}^* V_{td} \sim \lambda^3$), with $\lambda = \sin\theta_{12} \simeq 0.2232$ [5]. The local operators appearing in (1) are the dimension-six operators defined at an arbitrary scale μ as in [6]. The Wilson coefficients $C_i(\mu)$ ($i = 1, \ldots, 10$) depending on the renormalization scale μ are calculated at the matching scale $\mu_W \sim M_W$, the W-boson mass, as a perturbative expansion in the strong coupling constant $\alpha_s(\mu_W)$ [6] and can be evolved to a lower scale $\mu_b \sim m_b$ using the anomalous dimensions of the above operators to NNLL order [6].

The hadronic matrix elements of the operators $\mathcal{O}_i$ between the B- and π-meson states are expressed in terms of three independent form factors [7]:

$$\langle \pi(p_\pi) | \bar{b}\gamma^\mu d | B(p_B) \rangle = f_+(q^2) \left[p_B^\mu + p_\pi^\mu - \frac{m_B^2 - m_\pi^2}{q^2} q^\mu \right] + f_0(q^2) \frac{m_B^2 - m_\pi^2}{q^2} q^\mu, \qquad (2)$$

$$\langle \pi(p_\pi) | \bar{b}\sigma^{\mu\nu} q_\nu d | B(p_B) \rangle = \frac{i f_T(q^2)}{m_B + m_\pi} \left[q^2 \left(p_B^\mu + p_\pi^\mu \right) - \left(m_B^2 - m_\pi^2 \right) q^\mu \right], \qquad (3)$$

where p_B^μ and p_π^μ are the four-momenta of the B- and π-mesons, respectively, m_B and m_π are their masses, and $q^\mu = p_B^\mu - p_\pi^\mu$ is the momentum transferred to the lepton pair. The $B \to \pi$ transition form factors $f_+(q^2)$, $f_0(q^2)$ and $f_T(q^2)$ are scalar functions whose shapes are determined by using non-perturbative methods.

The differential branching fraction in the dilepton invariant mass q^2 can be expressed as follows:

$$\frac{d\mathcal{B}\left(B^+ \to \pi^+ \ell^+ \ell^-\right)}{dq^2} = \frac{G_F^2 \alpha_{\mathrm{em}}^2 \tau_B}{1024 \pi^5 m_B^3} \left| V_{tb} V_{td}^* \right|^2 \sqrt{\lambda(q^2)} \sqrt{1 - \frac{4m_\ell^2}{q^2}} F(q^2), \qquad (4)$$

where α_{em} is the fine-structure constant, m_ℓ is the lepton mass, τ_B is the B-meson lifetime, $\lambda(q^2) = \left(m_B^2 + m_\pi^2 - q^2\right)^2 - 4m_B^2 m_\pi^2$ is the kinematical function encountered in three-body decays (triangle function), and $F(q^2)$ is a dynamical function encoding the Wilson coefficients and the form factors:

$$
\begin{aligned}
F(q^2) &= \frac{2}{3} \lambda(q^2) \left(1 + \frac{2m_\ell^2}{q^2}\right) \left| C_9^{\mathrm{eff}}(q^2) f_+(q^2) + \frac{2m_b}{m_B + m_\pi} C_7^{\mathrm{eff}}(q^2) f_T(q^2) \right|^2 \\
&+ \frac{2}{3} \lambda(q^2) \left(1 - \frac{4m_\ell^2}{q^2}\right) \left| C_{10}^{\mathrm{eff}} f_+(q^2) \right|^2 + \frac{4m_\ell^2}{q^2} \left(m_B^2 - m_\pi^2\right)^2 \left| C_{10}^{\mathrm{eff}} f_0(q^2) \right|^2 .
\end{aligned}
\qquad (5)
$$

The dynamical function (5) contains the effective Wilson coefficients $C_7^{\mathrm{eff}}(q^2)$, $C_9^{\mathrm{eff}}(q^2)$ and C_{10}^{eff} which are specific combinations of the Wilson coefficients entering the effective Hamiltonian (1). To the NNLO approximation, the effective Wilson coefficients given in [6, 8, 9].

To perform a numerical analysis one needs to know the $B \to \pi$ transition form factors $f_+(q^2)$, $f_0(q^2)$ and $f_T(q^2)$ in the entire kinematic range: $4m_\ell^2 \leq q^2 \leq (m_B - m_\pi)^2$. Their model-independent determination is the main aim of this paper, which is described in detail in subsequent sections. Several parametrizations of the semileptonic form factors $f_+(q^2)$, $f_0(q^2)$ and $f_T(q^2)$ have been proposed in the literature. We especially outline the Boyd-Grinstein-Lebed (BGL) parametrization because namely this parametrization was used in our analysis. In the framework of BGL parametrization the shape for the form factors $f_i(q^2)$ with $i = +, 0, T$ is presented as follows [10]:

$$f_i(q^2) = \frac{1}{P(q^2)\phi_i(q^2, q_0^2)} \sum_{k=0}^{k_{\max}} a_k(q_0^2) \left[z(q^2, q_0^2)\right]^k, \quad z(q^2, q_0^2) = \frac{\sqrt{m_+^2 - q^2} - \sqrt{m_+^2 - q_0^2}}{\sqrt{m_+^2 - q^2} + \sqrt{m_+^2 - q_0^2}}, \qquad (6)$$
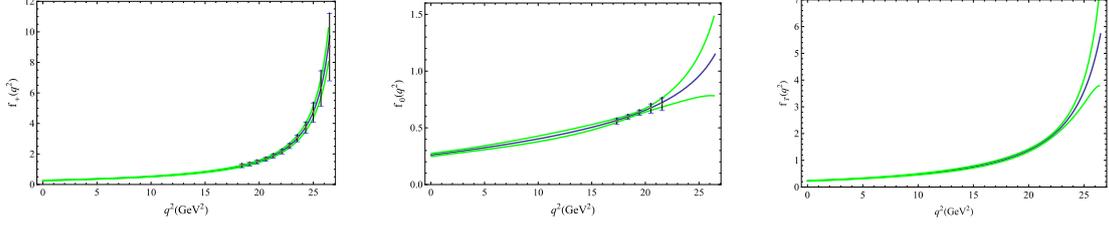
Figure 1: (Color online) The vector, scalar and tensor $B \to \pi$ transition form factors $f_P(q^2)$, $f_0(q^2)$ and $f_T(q^2)$, respectively, in the entire kinematical region using the BGL parametrization. The solid green lines show the uncertainty in the form factors. The vertical bars in the left and middle plots are the Lattice-QCD data [12]

with the pair-production threshold $m_+^2 = (m_B + m_\pi)^2$ and a free parameter q_0^2. In our analysis we make the choice $q_0^2 = 0.65 m_-^2$. The proposed shapes (6) for the form factors contains the so-called Blaschke factor $P(q^2)$ which accounts for the hadronic resonances in the sub-threshold region $q^2 < m_+^2$. For the semileptonic $B \to \pi \ell \nu_\ell$ decay, where ℓ is an electron or a muon, there is only B^*-meson with the mass $m_{B^*} = 5.325$ GeV satisfying the sub-threshold condition and producing the pole in the form factor at $q^2 = m_{B^*}^2$. In this case, the Blaschke factor is simply $P(q^2) = z(q^2, m_{B^*}^2)$ for $f_{+,T}(q^2)$ and $P(q^2) = 1$ for $f_0(q^2)$.

The coefficients a_k ($k = 0, 1, \ldots, k_{max}$) entering the Taylor series in Eq. (6) are the parameters, which are determined by fits of the data. The outer function $\phi_i(q^2, q_0^2)$ is an arbitrary analytic function, whose choice only affects particular values of the coefficients a_k and are given in [11]. Having relatively small values of $z(q^2, q_0^2)$ in the physical region of q^2, the shape of the form factor can be well approximated by the truncated series at $k_{max} = 2$ or 3.

3 Shapes of Form Factors

Measurements of the $B^0 \to \pi^- \ell^+ \nu_\ell$ and $B^+ \to \pi^0 \ell^+ \nu_\ell$ decays, where $\ell = e$, μ, allow to extract both the CKM matrix element V_{ub} and the shape of the $f_+(q^2)$ form factor. The differential branching fractions of the above processes can be written in the form [5]:

$$\frac{d\Gamma(B \to \pi \ell^+ \nu_\ell)}{dq^2} = C_P \frac{G_F^2 |V_{ub}|^2}{192 \pi^3 m_B^3} \lambda^{3/2}(q^2) f_+^2(q^2), \tag{7}$$

where C_P is the isospin factor with $C_P = 1$ for the π^+-meson and $C_P = 1/2$ for the π^0-meson, $q = p_\ell + p_\nu$ is the lepton-pair four-momentum bounded by $m_\ell^2 \leq q^2 \leq (m_B - m_\pi)^2$, and p_ℓ and p_ν are the four-momenta of the charged lepton and neutrino, respectively.

The partial branching fraction of $B^0 \to \pi^- \ell^+ \nu_\ell$ has been measured by the BaBar and Belle collaborations and of $B^0 \to \pi^- \ell^+ \nu_\ell$ by the Belle collaboration [13, 14, 15, 16]. Using these data we extracted the $f_+(q^2)$ form factor shape using the standard minimization procedure of the χ^2-distribution function [5]. The resulting form factor $f_+(q^2)$ from the combined analysis of the BaBar and Belle datasets is shown in the left plot in Fig. 1. In this analysis we have assumed that the experimental points are all uncorrelated.

The parameters of $f_0(q^2)$ can be obtained from the existing results of the $B \to \pi$ transition form factor calculated by the HPQCD collaboration [12]. In addition one can use the exact
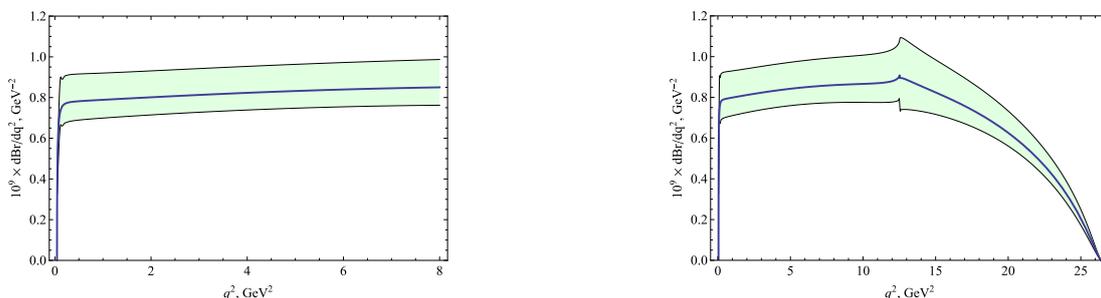
Figure 2: The dilepton invariant-mass distributions in the $B^+ \to \pi^+ \ell^+ \ell^-$ decay in the range $0 \le q^2 \le 8$ GeV^2 (left plot) and in the entire range $0 \le q^2 \le 26.4$ GeV^2 (right plot).

relation $f_+(0) = f_0(0)$, where $f_+(q^2)$ is extracted from the experimental data. The form-factor parametrization we use for $f_0(q^2)$ follows our default choice from the analysis of $f_+(q^2)$ — the BGL expansion in $z(q^2, q_0^2)$ truncated at $k_{\max} = 2$. The resulting $f_0(q^2)$ form factor shape is shown in Fig. 1 (middle plot), where we also present the Lattice-QCD data [12].

One should mention that there is only scant information about the $f_T^{B\pi}(q^2)$ form factor at present. So, one needs to find a reliable method to extract it from the existing model-independent data. We use an $SU(3)_F$-symmetry-breaking Ansatz involving the $B \to K$ and $B \to \pi$ form factors. We recall that all three $B \to K$ transition form factors $f_+^{BK}(q^2)$, $f_0^{BK}(q^2)$ and $f_T^{BK}(q^2)$ have been calculated recently by the HPQCD collaboration [17, 18] and the two $B \to \pi$ transition form factors $f_+^{B\pi}(q^2)$ and $f_0^{B\pi}(q^2)$ are also known [12]. With this knowledge, we first estimate the $SU(3)_F$-breaking corrections in the already known vector and scalar form factors and use these corrections for estimating the $B \to \pi$ tensor form factor $f_T^{B\pi}(q^2)$ from the corresponding $B \to K$ transition form factor $f_T^{BK}(q^2)$. The resulting $f_T^{B\pi}(q^2)$ form factor obtained is shown in the right plot in Fig. 1.

As all the form factors in the $B \to \pi$ transition are now known, we can make predictions for the dilepton invariant-mass spectrum and decay width in the semileptonic $B \to \pi \ell^+ \ell^-$ decays for $\ell^\pm = e^\pm, \mu^\pm$.

4 Predictions for $B^+ \to \pi^+ \ell^+ \ell^-$ Decay

The B^+-meson is a bound state of the heavy $\bar{b}$- and light u-quarks, hence one can apply the so-called Heavy-Quark Symmetry (HQS), which is valid in the large-recoil limit (at small values of q^2). Using the HQS allows one to simplify significantly the description of the $B^+ \to \pi^+ \ell^+ \ell^-$ decay at small q^2 ($q^2 \le 8$ GeV^2), namely, applying the HQS results in reducing the number of independent form factors of the $B \to \pi$ transition from three to one. The relations between the three form-factors $f_+(q^2)$, $f_0(q^2)$ and $f_T(q^2)$ in the HQS limit with taking into account symmetry-breaking corrections are worked out in Ref. [7]. With use of these relations the dimuon invariant mass spectrum was obtained and is presented in the left plot in Fig. 2.

In the low hadronic-recoil region (large-q^2) there is no heavy-quark symmetry relations among form factors $f_+(q^2)$, $f_0(q^2)$ and $f_T(q^2)$ any more and they should be considered as three independent quantities. All of them were extracted by us in the entire kinematic range and used for further calculations.

The invariant-mass spectrum in the entire range of q^2 ($4m_\ell^2 < q^2 < 26.4$ GeV^2) is presented in the right plot in Fig. 2. We get the following prediction for the total branching fraction [3]:

$$\mathcal{B}(B^+ \to \pi^+ \mu^+ \mu^-) = \left(1.88^{+0.32}_{-0.21}\right) \times 10^{-8},\tag{8}$$

where the resulting average uncertainty about 15% and is coming from the scale dependence μ_b of the Wilson coefficients, the CKM matrix element $|V_{td}|$ and form factors (FF).

5 Summary and Outlook

We have presented a theoretically improved calculation of the branching fraction for the $B^\pm \to \pi^\pm \mu^+ \mu^-$ decay, measured recently by the LHCb collaboration [1]. The combined accuracy on the branching ratio is estimated as $\pm 15\%$, and the resulting branching fraction $\mathcal{B}(B^\pm \to \pi^\pm \mu^+ \mu^-) = (1.88^{+0.32}_{-0.21}) \times 10^{-8}$ [3] is in agreement with the LHCb data [1].

Acknowledgements

References

[1] R. Aaij *et al.*, JHEP **1212** 125 (2012).

[2] J.-J. Wang *et al.*, Phys. Rev. **D77** 014017 (2008).

[3] A. Ali, A.Ya. Parkhomenko, and A.V. Rusov, DESY report DESY-13-153 (2013).

[4] G. Buchalla, A.J. Buras, and M.E. Lautenbacher, Rev. Mod. Phys. **68** 1125 (1996).

[5] J. Beringer *et al.*, Phys. Rev. **D86** 010001 (2012).

[6] C. Bobeth, M. Misiak, and J. Urban, Nucl. Phys. **B574** 291 (2000).

[7] M. Beneke and T. Feldmann, Nucl. Phys. **B592** 3 (2001).

[8] A. Ali *et al.*, Phys. Rev. **D66** 034002 (2002).

[9] H.M. Asatrian *et al.*, Phys. Rev. **D69** 074007 (2004).

[10] C.G. Boyd, B. Grinstein, and R.F. Lebed. Phys. Rev. Lett. **74** 4603 (1995).

[11] M.C. Arnesen *et al.*, Phys. Rev. Lett. **95** 071802 (2005).

[12] E. Dalgic *et al.*, Phys. Rev. **D73** 074502 (2006).

[13] P. del Amo Sanchez *et al.*, Phys. Rev. **D83** 052011 (2011).

[14] J.P. Lees *et al.*, Phys. Rev. **D86** 092004 (2012).

[15] H. Ha *et al.*, Phys. Rev. *D83* 071101 (2011).

[16] A. Sibidanov *et al.*, Phys. Rev. **D88** 032005 (2013).

[17] C. Bouchard *et al.*, Phys. Rev. **D88** 054509 (2013).

[18] C. Bouchard *et al.*, Phys. Rev. Lett. **111** 162002 (2013).

Bimodality Phenomenon in Finite and Infinite Systems Within an Exactly Solvable Statistical Model

V.V. Sagun[1], A.I. Ivanytskyi[1], K.A. Bugaev[1,2], D.R. Oliinychenko[1,2]

[1]Bogolyubov Institute for Theoretical Physics, National Academy of Sciences of Ukraine, Kiev, Ukraine
[2]Frankfurt Institute for Advanced Studies (FIAS), Goethe-University, Ruth-Moufang Str. 1, 60438 Frankfurt upon Main, Germany

We present a few explicit counterexamples to the widely spread belief about an exclusive role of the bimodal nuclear fragment size distributions as the first order phase transition signal. In thermodynamic limit the bimodality may appear at the supercritical temperatures due to the negative values of the surface tension coefficient. Such a result is found within a novel exactly solvable formulation of the simplified statistical multifragmentation model based on the virial expansion for a system of the nuclear fragments of all sizes. The developed statistical model corresponds to the compressible nuclear liquid with the tricritical endpoint located at one third of the normal nuclear density. Its exact solution for finite volumes demonstrates the bimodal fragment size distribution right inside the finite volume analog of a gaseous phase. These counterexamples clearly demonstrate the pitfalls of Hill approach to phase transitions in finite systems.

1   Introduction

Despite many efforts the phase transition (PT) thermodynamics of finite systems is far from being completed. Its consistent formulation remains a real theoretical challenge for the researchers working in statistical mechanics. On the other hand, nowadays it is of great practical importance since at intermediate and high energies the modern nuclear physics is dealing with the phase transformations of liquid-gas type occurring in finite or even small systems. The central issue of this field is related to a rigorous definition of finite volume analogs of phases.

The first attempt [1] to rigorously define the gaseous and liquid phases in finite systems was based on the properties of phases existing in infinite systems in which two phases coexist at phase equilibrium and generate two local maxima, i.e. a bimodality, of some order parameter. Each maximum is associated with a pure phase [1]. Since a few years ago such a concept of nuclear liquid-gas PT [2, 3] completely dominates in nuclear physics of intermediate energies. It considers the bimodal distributions as a robust signal of a PT in finite systems. However, this concept does not seem to be correct since in a finite system an analog of mixed phase is not just a simple mixture of two pure phases as it is explicitly shown within an exactly solvable statistical model [4, 5, 6]. The aim of this work is to demonstrate that in finite and infinite systems the bimodal distributions can appear without a PT and, hence, they cannot serve as robust signal of a PT in finite systems.

V. V. Sagun, A. I. Ivanytskyi, K. A. Bugaev, D. R. Oliinychenko

1.1 Constrained SMM with the compressible nuclear matter

The simplified statistical multifragmentation model (SMM) which has no Coulomb and no asymmetry energy was exactly solved in thermodynamic limit in [7], while its generalization constrained for finite systems, the CSMM, was solved in [4]. For a volume V the grand canonical partition of the CSMM can be identically written as [4, 5, 6]

$$\mathcal{Z}(V,T,\mu) = \sum_{\{\lambda_n\}} e^{\lambda_n V} \left[1 - \frac{\partial \mathcal{F}(V,\lambda_n)}{\partial \lambda_n} \right]^{-1}, \tag{1}$$

where the set of λ_n $(n = 0, 1, 2, 3, ..)$ are all the roots of the equation $\lambda_n = \mathcal{F}(V, \lambda_n)$.

The volume spectrum of our model $\mathcal{F}(V, \lambda)$ depends on the eigen volume $b = 1/\rho_0$ of a nucleon at the normal nuclear density $\rho_0 \simeq 0.17$ fm^3 taken at $T = 0$ and zero pressure, mass $m \simeq 940$ MeV, degeneracy factor $z_1 = 4$ of nucleons and it is defined as

$$\mathcal{F}(V,\lambda) = \left(\frac{mT}{2\pi}\right)^{\frac{3}{2}} z_1 \exp\left\{\frac{\mu - \lambda Tb}{T}\right\} + \sum_{k=2}^{K(V)} \phi_k(T) \exp\left\{\frac{(p_L(T,\mu) - \lambda T)bk}{T}\right\}. \tag{2}$$

Here $\phi_{k>1}(T) \equiv \left(\frac{mT}{2\pi}\right)^{\frac{3}{2}} k^{-\tau} \exp\left[-\frac{\sigma(T)\ k^\varsigma}{T}\right]$ is a reduced distribution function of the k-nucleon fragment, τ is the Fisher topological exponent and $\sigma(T)$ is the T-dependent surface tension coefficient. Usually, the constant, parameterizing the dimension of surface in terms of the volume is $\varsigma = \frac{2}{3}$. In the expression for $\mathcal{F}(V, \lambda)$ the maximal size of fragment is denoted as $K(V)$. In the usual SMM [8] and in its simplified version SMM the nuclear liquid pressure $p_L^{SMM} = \frac{\mu + W(T)}{b}$ corresponds to an incompressible matter. Since this is in contradiction with the experimental heavy ions collisions data [9], here we analyze the following equation of state with non-zero compressibility

$$p_L = \frac{W(T) + \mu + a_\nu(\mu - \mu_0)^\nu}{b} \tag{3}$$

which contains an additional term to the usual SMM liquid pressure. Here an integer power is $\nu = 2$ or $\nu = 4$, $W(T) = W_0 + \frac{T^2}{W_0}$ denotes the usual temperature dependent binding energy per nucleon with $W_0 = 16$ MeV [7], while the constants $\mu_0 = -W_0$, $a_2 \simeq 1.233 \cdot 10^{-2}$ MeV^{-1} and $a_4 \simeq 4.099 \cdot 10^{-7}$ MeV^{-3} are fixed in order to reproduce the properties of normal nuclear matter, i.e. at vanishing temperature $T = 0$ and normal nuclear density $\rho = \rho_0$ the liquid pressure must be zero. Under a new ansatz for p_L the nuclear liquid of CSMM becomes compressible [6, 10]. A careful analysis of the proposed parameterization [10] shows that it is fully consistent with the L. van Hove axioms of statistical mechanics [11].

In addition to a more general parameterization of the bulk free energy of nuclear fragments we also consider a more general parameterization of the surface tension coefficient

$$\sigma(T) = \sigma_0 \left|\frac{T_{cep} - T}{T_{cep}}\right|^\zeta \text{sign}(T_{cep} - T), \tag{4}$$

with $\zeta = const \geq 1$, $T_{cep} = 18$ MeV and $\sigma_0 = 18$ MeV the SMM. In contrast to the Fisher droplet model [12] and the usual SMM [8], the CSMM surface tension (4) is negative above the critical temperature T_{cep}. An extended discussion on the validity of such a parameterization can be found in Refs. [5, 6].

1.2 Infinite system

In the thermodynamic limit, i.e. for $V \to \infty$ and $K(V) \to \infty$, in the CSMM there is always a single solution λ_0 of the equation $\lambda_n = \mathcal{F}(V \to \infty, \lambda_n)$, but it can be of two kinds [4]: either the gaseous pole $\lambda_0(T, \mu) = p_g(T, \mu)/T$ for $\mathcal{F}(V \to \infty, \lambda_0 - 0) < \infty$ or the liquid essential singularity $\lambda_0(T, \mu) = p_L(T, \mu)/T$ for $\mathcal{F}(V \to \infty, \lambda_0 - 0) \to \infty$.

This model has a PT which occurs when the gaseous pole is changed by the liquid essential singularity or vice versa. The PT curve $\mu = \mu_c(T)$ is a solution of the equation $p_g(T, \mu) = p_L(T, \mu)$, which is just the Gibbs criterion of phase equilibrium. The properties of a PT are defined only by the liquid phase pressure $p_L(T, \mu)$ and by the temperature dependence of surface tension $\sigma(T)$. The phase diagram of the present model in thermodynamic limit in the plane of baryonic chemical potential μ and temperature T is shown in the left panel of Fig. 1.

1.3 Finite system

The treatment of the model for finite volumes is more complicated, since the roots λ_n of (1) have not only the real part R_n, but an imaginary part I_n as well ($\lambda_n = R_n + iI_n$). Therefore, equation for λ_n can be cast as a system of coupled transcendental equations for R_n and I_n

$$R_n = \sum_{k=1}^{K(V)} \phi_k(T) \, \exp\left[\frac{Re(\nu_n)\, k}{T}\right] \cos(I_n b k)\,, \qquad (5)$$

$$I_n = -\sum_{k=1}^{K(V)} \phi_k(T) \, \exp\left[\frac{Re(\nu_n)\, k}{T}\right] \sin(I_n b k)\,, \qquad (6)$$

where for convenience we introduced the following set of the effective chemical potentials ν_n

$$\nu_n \equiv \nu(\lambda_n) = p_l(T, \mu)b - (R_n + iI_n)b\,T\,, \qquad (7)$$

and the reduced distribution for nucleons $\phi_1(T) = \left(\frac{mT}{2\pi}\right)^{\frac{3}{2}} z_1 \exp((\mu - p_l(T, \mu)b)/T)$.

Consider the real root ($R_0 > 0, I_0 = 0$), first. The real root $\lambda_0 = R_0$ of the CSMM exists for any T and μ. From (1) and (5) for $R_n = R_0$ and $I_0 = 0$ one can see that TR_0 is a constrained grand canonical pressure of the mixture of ideal gases with the chemical potential ν_0. Hence, a single real solution $\lambda_0 = R_0$ with $I_0 = 0$ of the system (5, 6) corresponds to a gaseous phase (for more details see [7]). If for some thermodynamic parameters we have a real solution λ_0 and any finite number $n = 1, 2, 3, ...$ of the complex conjugate pairs of roots $\lambda_{n \geq 1}$, then such a system corresponds to a finite volume analog of mixed phase [7]. Note that, each pair of complex conjugate roots $\lambda_{n \geq 1}$ represents a metastable state with a complex value of chemical potential ν_n. Since $\nu_{n1} \neq \nu_{n2 \neq n1}$ these metastable states are not in a true chemical equilibrium with the gas and with each other. A finite system analog of a liquid phase corresponds to an infinite number of the complex roots of the system (5, 6), but in finite system it exists at infinite pressure only. Using these definitions, one can build up the finite system analog of the $T - \mu$ phase diagram (see the right panel of Fig.1).

Therefore, in contrast to assumptions of Refs. [2, 3], in finite systems the pure liquid phase cannot exist at finite pressures. Instead, in finite system and finite pressures we are dealing with the finite volume analogs of gaseous or mixed phases [4].
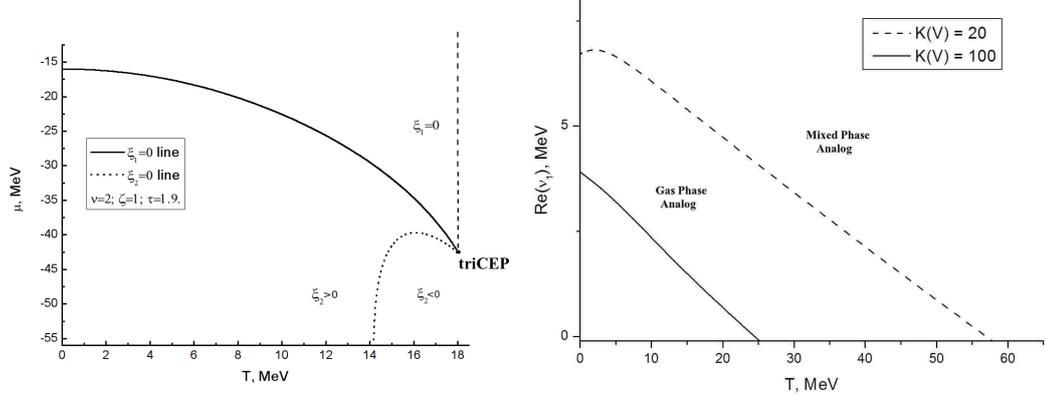
Figure 1: **Left panel:** Phase diagram in $T - \mu$ plane for the case $\nu = 2$, $\tau = 1.9$ with tricritical point at temperature $T_{cep} = 18$ MeV in thermodynamic limit. The solid line corresponds to the 1-st order PT, the dashed line shows the 2-nd order PT, while at the dotted line the surface tension coefficient vanishes. **Right panel:** the finite volume analog of the phase diagram in $T - Re(\nu_1)$ plane for given values of $K(V) = 20$ (dashed curve) and $K(V) = 100$ (solid curve). Below each of these phase boundaries there exists a gaseous phase only, but at and above each curve there are three or more solutions of the system (5, 6).

1.4 Bimodality phenomenon in finite and infinite systems

In this section we discuss another typical mistake of the approaches [2, 3] based on the bimodal properties of the first order PT in finite systems. The authors of [2, 3] implicitly assume that, like in the infinite systems, in finite systems there exist exactly two 'pure' phases and they exactly correspond to two peaks in the bimodal distribution of the order parameter. As two counterexamples to these assumptions we present the bimodal fragment distributions obtained for an infinite system at the supercritical temperature where the surface tension coefficient is negative (the left panel of Fig.2) and the one obtained inside the finite volume analog of a gaseous phase corresponding to positive values of the effective chemical potential ν_0 (the right panel of Fig.2). As one can see from Fig.2, in contrast to expectations of [2, 3], the bimodal fragment distributions occur without a PT.

2 Conclusions

A novel version of the CSMM is presented here. Its detailed analysis is performed in order to clarify an origin of the bimodality appearing both in finite and in infinite systems. An exact analytical solution of the present model allows us to perform a robust analysis of the fragment size distributions in the regions where there is and there is no PT. It is shown that the fragment size distribution can be bimodal-like inside of the finite volume analog of gaseous phase. Also we demonstrate that a bimodal fragment size distribution can be caused by negative values of the surface tension and, hence, it is not a robust signal of PT existence in finite systems.
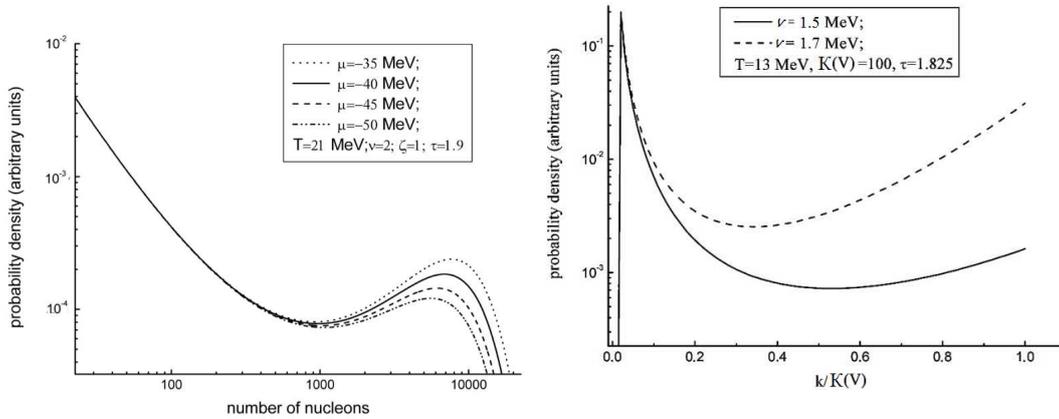
Figure 2: **Left panel:** Fragment size distributions of the model are shown for a fixed temperature $T = 21$ MeV and four values of the baryonic chemical potential μ for an infinite system. This region of phase diagram is characterised by the negative surface tension coefficient which prevents an existing of a PT. **Right panel:** Bimodal distributions existing inside the finite system analog of gaseous phase for a fixed temperature $T = 13$ MeV and different values of the effective chemical potential ν_0. Even in the region of fragments gas we observe a bimodal like shape of the fragment distribution. The maximal size of nuclear fragment is $K(V){=}k{=}100$ nucleons.

References

[1] T. L. Hill, "Thermodynamics of small systems", Dover, New York (1994).

[2] Ph. Chomaz and F. Gulminelli, Preprint GANIL-02-19 (2002).

[3] F. Gulminelli, Nucl. Phys. A **791**, 165 (2007).

[4] K. A. Bugaev, Acta. Phys. Polon. B **36**, 3083 (2005).

[5] K. A. Bugaev, A. I. Ivanytskyi, E. G. Nikonov, A. S. Sorin and G. M. Zinovjev, Can We Rigorously Define Phases in a Finite System?, Chapter 18 of the Proceedings of the XV-th Research Workshop *"Nucleation Theory and Applications"* (JINR, Dubna, Russia, April 1- 30, 2011): Edited by J. W. P. Schmetzer, G. Röpke and V. B. Priezzhev, – Dubna: JINR, 2011.– p. 32–3p. 287–300; arXiv:1106.5939 [nucl-th] (2011).

[6] K. A. Bugaev, A.I . Ivanytskyi, V. V. Sagun and D. R. Oliinychenko, Phys. Part. Nucl. Lett. **10**, 832 (2013).

[7] K. A. Bugaev, M. I. Gorenstein, I. N. Mishustin and W. Greiner, Phys. Rev. C **62**, 044320 (2000); Phys. Lett. B **498**, 144 (2001).

[8] J. P. Bondorf et al., Phys. Rep. 257, 131 (1995) and references therein.

[9] E. Khan, Phys. Rev. C **80**, 011307(R) (2009).

[10] V. V. Sagun, A. I. Ivanytskyi, K. A. Bugaev and I. N. Mishustin, arXiv:1306.2372 [nucl-th] (2013).

[11] L. Van Hove, Physica **15**, 951 (1949); Physica **16**, 137 (1950).

[12] M. E. Fisher, Physics **3**, 255 (1967).

CP Violation in D meson Decays

Pietro Santorelli

Dipartimento di Fisica, Università di Napoli Federico II, Complesso Universitario di Monte S. Angelo, Via Cintia, Edificio 6, 80126 Napoli, Italy
and
Istituto Nazionale di Fisica Nucleare, Sezione di Napoli

We discuss the direct CP violation in the singly Cabibbo suppressed two body decays of the neutral D mesons. Ascribing the large SU(3) violations to the final state interactions one gets large strong phase differences necessary for substantial direct CP violation. While the absolute value of the CP violating asymmetries depend on the uncertain strength of the penguin contribution, we predict an asymmetry for the decays into charged pions more than twice as large and having opposite sign with respect to that for charged kaons.

1 Introduction

The experimental results on CP violation in singly Cabibbo suppressed (SCS) decays of the D^0 and $\bar{D}^0$ mesons, larger of the common expectation beforehand, published in [1, 2] after the less conclusive results of the beauty factories [3, 4] have recently been contradicted by new analyses by the LHCb Collaboration that gave smaller results and moreover of different signs according to the method used [5, 6]. In the following, we report the analysis made in [7].
Defining the CP violating asymmetries for decay into the final state f as

$$a(f) = \frac{\Gamma(D^0 \to f) - \Gamma(\bar{D}^0 \to f)}{\Gamma(D^0 \to f) + \Gamma(\bar{D}^0 \to f)}$$

the difference of asymmetries, $a(f)$, in the decays into charged kaons and charged pions, $\Delta_{\mathrm{CP}} = a(K^+K^-) - a(\pi^+\pi^-)$, has been measured with the following results:

$$
\begin{aligned}
\Delta_{\mathrm{CP}} \quad = \quad & (-0.62 \pm 0.21 \pm 0.10)\% \text{ (CDF)}, && (1) \\
= \quad & (-0.82 \pm 0.21 \pm 0.11)\% \text{ (LHCb1)}, && (2) \\
= \quad & (-0.87 \pm 0.41 \pm 0.06)\% \text{ (Belle)}, && (3) \\
= \quad & (+0.24 \pm 0.62 \pm 0.26)\% \text{ (BaBaR)}, && (4) \\
= \quad & (-0.34 \pm 0.15 \pm 0.10)\% \text{ (LHCb2)}, && (5) \\
= \quad & (+0.49 \pm 0.30 \pm 0.14)\% \text{ (LHCb3)}. && (6)
\end{aligned}
$$

A naive weighted average [8] would give $\Delta_{\mathrm{CP}} = (-0.33 \pm 0.12)\%$, also compatible with a null result. Many authors think that it is a sign of new physics [9], while others think that such results are compatible with the standard model [10, 11]. In [7] we support the second hypothesis.

In [12] we presented a model to evaluate the decay branching ratios of D and D_{s} mesons. The model was based on factorization and include a way to take into account the rescattering

effects through nearby resonances and gives CP violation asymmetries at least one order of magnitude smaller than what was found in [1, 2]. The experimental data however did change in the meantime, so in [7] we have done a new analysis, limiting our consideration to the SCS decays.

In [12] we observed that the large flavor SU(3) violations in the data were mainly due to the rescattering effects (because of the difference in mass of the relevant resonances). Therefore we now assume SU(3) symmetry for the weak decay amplitudes prior to rescattering. Furthermore, we approximate the hamiltonian for D weak decays with its $\Delta U = 1$ part when estimating branching ratios, introducing the $\Delta U = 0$ terms only for the calculation of asymmetries. This is justified by the smallness of the relevant CKM elements, $|V_{\mathrm{ub}}V^*_{\mathrm{cb}}| << |V_{\mathrm{ud(s)}}V^*_{\mathrm{cd(s)}}|$.

2 Decay amplitudes and branching ratios

The weak effective hamiltonian for SCS charmed particles decays is:

$$
\begin{aligned}
\mathcal{H}_{\mathrm{w}} &= \frac{G_F}{\sqrt{2}} V_{ud} V^*_{cd} \left[C_1 Q_1^d + C_2 Q_2^d\right] + \frac{G_F}{\sqrt{2}} V_{us} V^*_{cs} \left[C_1 Q_1^s + C_2 Q_2^s\right] \\
&\quad - \frac{G_F}{\sqrt{2}} V_{ub} V^*_{cb} \sum_{i=3}^{6} C_i Q_i + h.c.
\end{aligned}
\tag{7}
$$

where the C_i are Wilson coefficients that multiply the four–fermion operators defined as [13]

$$
\begin{aligned}
Q_1^d &= \bar{u}^\alpha \gamma_\mu (1-\gamma_5) d_\beta \, \bar{d}^\beta \gamma^\mu (1-\gamma_5) \, c_\alpha \ , \\
Q_2^d &= \bar{u}^\alpha \gamma_\mu (1-\gamma_5) d_\alpha \, \bar{d}^\beta \gamma^\mu (1-\gamma_5) \, c_\beta \ , \\
Q_3 &= \bar{u}^\alpha \gamma_\mu (1-\gamma_5) \, c_\alpha \sum_q \bar{q}^\beta \gamma^\mu (1-\gamma_5) \, q_\beta, \\
Q_4 &= \bar{u}^\alpha \gamma_\mu (1-\gamma_5) \, c_\beta \sum_q \bar{q}^\beta \gamma^\mu (1-\gamma_5) \, q_\alpha, \\
Q_5 &= \bar{u}^\alpha \gamma_\mu (1-\gamma_5) \, c_\alpha \sum_q \bar{q}^\beta \gamma^\mu (1+\gamma_5) \, q_\beta. \\
Q_6 &= \bar{u}^\alpha \gamma_\mu (1-\gamma_5) \, c_\beta \sum_q \bar{q}^\beta \gamma^\mu (1+\gamma_5) \, q_\alpha.
\end{aligned}
\tag{8}
$$

The operators Q_1^s and Q_2^s are obtained by means of the substitution $d \to s$ in Q_1^d and Q_2^d.

Looking at the U spin transformation properties, the hamiltonian can be decomposed in two parts. The dominant part has $\Delta U = 1$ and it is

$$
\begin{aligned}
H_{\Delta U=1} &= \frac{G_F}{2\sqrt{2}} (V_{us} V^*_{cs} - V_{ud} V^*_{cd})[C_1(Q_1^s - Q_1^d) + C_2(Q_2^s - Q_2^d)] \\
&\simeq \frac{G_F}{\sqrt{2}} \sin\theta_C \cos\theta_C [C_1(Q_1^s - Q_1^d) + C_2(Q_2^s - Q_2^d)].
\end{aligned}
\tag{9}
$$

The remaining part, that using the unitarity of the CKM matrix can be written in the form

$$
H_{\Delta U=0} = -\frac{G_F}{\sqrt{2}} V_{ub} V^*_{cb} \left\{ \sum_{i=3}^{6} C_i Q_i + \frac{1}{2}[C_1(Q_1^s + Q_1^d) + C_2(Q_2^s + Q_2^d)] \right\},
\tag{10}
$$

may be neglected in the calculation of decay branching ratios (even if necessary for CP violation) given that $|V_{ub}V_{cb}^*| << \sin\theta_C \cos\theta_C$. In this approximation, the neutral charmed meson D^0 being a U-spin singlet, only two independent amplitudes are needed for D^0 SCS decays into two pseudoscalars belonging to SU(3) octets. In fact, there are two independent combinations of S-wave states having $U=1$:

$$\frac{1}{2}\left\{ |K^+K^->+|K^-K^+>-|\pi^+\pi^->-|\pi^-\pi^+> \right\} ; \tag{11}$$

$$\frac{\sqrt{3}}{2\sqrt{2}}\left\{ |\pi^0\pi^0>-|\eta_8\eta_8>-\frac{1}{\sqrt{3}}(|\pi^0\eta_8>+|\eta_8\pi^0>) \right\} ,$$

that may be combined in two states with given trasformation properties under SU(3):

$$|8,U=1>=\frac{\sqrt{3}}{2\sqrt{5}} \quad \left\{ \quad |K^+K^->+|K^-K^+>-|\pi^+\pi^->-|\pi^-\pi^+> \right. \tag{12}$$

$$\left. - \quad [|\pi^0\pi^0>-|\eta_8\eta_8>-\frac{1}{\sqrt{3}}(|\pi^0\eta_8>+|\eta_8\pi^0>)] \right\},$$

$$|27,U=1>=\frac{1}{\sqrt{10}} \quad \left\{ \quad |K^+K^->+|K^-K^+>-|\pi^+\pi^->-|\pi^-\pi^+> \right. \tag{13}$$

$$\left. + \quad \frac{3}{2}\left[|\pi^0\pi^0>-|\eta_8\eta_8>-\frac{1}{\sqrt{3}}(|\pi^0\eta_8>+|\eta_8\pi^0>)\right] \right\}.$$

Another independent amplitude would appear considering decays to states involving an SU(3) singlet. In order to keep the number of parameters to a minimum we disregard decays to states containing the singlet η_1 meson.

The eqs.(12,13) imply no decay to neutral kaons ($K^0\bar{K}^0$) and the decays to charged pions should be more frequent than to charged kaons because of the larger phase space, given the equal and opposite amplitudes. Both predictions are in disagreement with experiment.

The large SU(3) violations have been much discussed in the literature, a general first order analysis was done many years ago [14] and in recent works [9, 10] its relevance to CP violation has been stressed. In our model the necessary SU(3) breaking is determined by the final state interactions, described as the effect of resonances in the scattering of the final particles. Assuming no exotic resonances belonging to the 27 representation, the possible resonances have SU(3) and isospin quantum numbers $(8, I = 1)$, $(8, I = 0)$ and $(1, I = 0)$. Moreover, the two states with $I = 0$ can be mixed, yielding two resonances:

$$|f_0> \quad = \quad +\sin\phi \ |8,I=0>+\cos\phi \ |1,I=0>, \tag{14}$$

$$|f_0'> \quad = \quad -\cos\phi \ |8,I=0>+\sin\phi \ |1,I=0> . \tag{15}$$

The mixing angle ϕ and the strong phases δ_0, δ_0' and δ_1 are our model parameters, together with the two independent weak decay amplitudes. In principle, the strong phases should be related to the mass M_i and total width Γ_i of the corresponding resonance through the relation

$$\tan\delta_i = \frac{\Gamma_i}{2(M_i - M_{D^0})} ,$$

however the experimental data on these scalar resonances are sparse and do not allow a clean determination of the phases. One plausible hypothesis is that the phase $\delta_1 \sim \pi/2$, since the

isovector partner of the scalar resonance $K_0^*(1950)$ should have a mass close to the D^0 mass, as it follows deriving it from an equispacing formula [12]. Note also that we are putting to zero the small phase δ_{27}, so that the δ_i parameters actually correspond to the differences with respect to the phase in the non resonant channel.

The two independent and unknown weak amplitudes can be related to the commonly used diagrammatic amplitudes T and C (color connected and color suppressed respectively) [15] in the following way:

$$A_8(U=1) = \langle 8, U=1 | H_{\Delta U=1} | D^0 \rangle \quad \propto \quad T - \frac{2}{3} C \;, \tag{16}$$

$$A_{27}(U=1) = \langle 27, U=1 | H_{\Delta U=1} | D^0 \rangle \quad \propto \quad T + C. \tag{17}$$

It is important to stress that in our approach, differently from other authors, both the amplitudes T and C are real numbers, the strong phases being introduced as effects of rescattering. As an example, it is interesting to look at the decay amplitudes in charged pions and kaons including the effects of the final state interactions:

$$
\begin{aligned}
A(D^0 \rightarrow \pi^+\pi^-) &= \left(T - \frac{2}{3}C\right)\left\{-\frac{3}{10}\left(e^{\imath\delta_0} + e^{\imath\delta_0'}\right)\right. \\
&+ \left.\left(-\frac{3}{10}\cos(2\phi) + \frac{3}{4\sqrt{10}}\sin(2\phi)\right)\left(e^{\imath\delta_0'} - e^{\imath\delta_0}\right)\right\} \\
&- \left(T+C\right)\frac{2}{5}\;,
\end{aligned}
\tag{18}
$$

$$
\begin{aligned}
A(D^0 \rightarrow K^+K^-) &= \left(T - \frac{2}{3}C\right)\left\{\frac{3}{20}\left(e^{\imath\delta_0} + e^{\imath\delta_0'}\right)\right. \\
&+ \left.\left(\frac{3}{20}\cos(2\phi) + \frac{3}{4\sqrt{10}}\sin(2\phi)\right)\left(e^{\imath\delta_0'} - e^{\imath\delta_0}\right) + \frac{3}{10}e^{\imath\delta_1}\right\} \\
&+ \left(T+C\right)\frac{2}{5}\;.
\end{aligned}
\tag{19}
$$

The limit of exact flavor SU(3) would correspond to $\sin(\phi) = 1$, $\delta_0 = \delta_1$. In this limit the amplitudes do not depend on δ_0' (since in the approximation of keeping only the $\Delta U = 1$ hamiltonian the D^0 meson does not couple to the singlet state) they are of opposite sign and equal respectively to:

$$A[D^0 \rightarrow \pi^+\pi^-(K^+K^-)] \quad \rightarrow \quad \mp\left[\left(T - \frac{2}{3}C\right)\frac{3}{5}e^{\imath\delta_0} + \left(T+C\right)\frac{2}{5}\right]\;. \tag{20}$$

The expressions for the remaining amplitudes can be found in [7].

As it can be seen from the above equations, the SU(3) breaking corrections do not change the part of the amplitudes belonging to the 27 representation, but only the octet part, that also acquires a singlet component. Therefore, in our model the SU(3) breaking hamiltonian transforms as a triplet under SU(3), completely analogous to the simplifying hypothesis put forward in [14], first suggested in [16]. However, the number of parameters in our model is six, three of which describe the SU(3) symmetry breaking, while in [14] the symmetry breaking parameters are four.

We note that the experimental results for the decays of neutral and charged D mesons in a pion pair when analyzed in terms of amplitudes of given isospin A_2 and A_0, defined by

$\mathcal{A}(D^0 \to \pi^+\pi^-) = (\sqrt{2}\, A_0 - A_2)/\sqrt{6}$, give [11]:

$$
\begin{aligned}
|A_2| &= (3.08 \pm 0.08)\, 10^{-7}\ \text{GeV}\,, & (21) \\
|A_0| &= (7.6 \pm 0.1)\, 10^{-7}\ \text{GeV}\,, \\
\arg(A_2/A_0) &= \pm(93 \pm 3)^\circ\,.
\end{aligned}
$$

On the contrary, the presence of two independent amplitudes with isospin 1 in the $K\bar{K}$ channels does not allow a determination of the amplitudes from their decay branching ratios.

We found a good agreement with the experimental data for the rates with the following set of parameters (the upper or lower signs should be taken simultaneously):

$$
\begin{aligned}
C\,/\,T &= -0.529\,, & & & (22) \\
\sin(2\phi) = 0.701\,, & & \cos(2\phi) = 0.713\,, \\
\sin\delta_0 = \pm 0.529\,, & & \cos\delta_0 = -0.848\,, \\
\sin\delta_0' = \pm 0.794\,, & & \cos\delta_0' = 0.608\,, \\
\sin\delta_1 = \pm 0.992\,, & & \cos\delta_1 = 0.126\,.
\end{aligned}
$$

In fact, using these values we obtain the following results for the ratios of decay rates:

$$
\begin{aligned}
\frac{\Gamma(D^0 \to K_{\mathrm{S}}K_{\mathrm{S}})}{\Gamma(D^0 \to K^+K^-)} &= 0.0429\,, & (23) \\[2mm]
\frac{\Gamma(D^0 \to \pi^+\pi^-)}{\Gamma(D^0 \to K^+K^-)} &= 0.354\,, \\[2mm]
\frac{\Gamma(D^0 \to \pi^0\pi^0)}{\Gamma(D^0 \to K^+K^-)} &= 0.202\,,
\end{aligned}
$$

to be compared to the experimental values [17]: 0.043±0.010, 0.354±0.010, 0.202±0.013, respectively. Moreover, the ratio of the moduli of the two pion isospin amplitudes is $|A_2/A_0| = 0.40$ and its phase is $\mp 87.2^\circ$, in fair agreement with the experimental results reported in eq.(21). The result for the absolute values of the branching ratios, obtained using the experimental lifetime, agree within 20% with the values obtained using naive factorization (that may be derived in the $\pi^+\pi^-$ case from eq. (2.16) of [12]).

It may appear that describing four experimental data (the three ratios in eq.(23) and the analogous ratio for the two pion decay of a D^+, or equivalently the relative phase of the two pionic amplitudes with given isospin) with five parameters is trivial. However, four of these parameters are angles, and sines or cosines may only vary between -1 and 1, so that formulae like those given in the Appendix are not capable of describing any number. The result presented in eq.(22) has not been obtained with a least squares fit, and not every parameter has been taken as really free. In fact, we required $|\sin(\delta_1)| \simeq 1$ (as already said above) and $C\,/\,T \sim -0.5$, similar to the results of our old fits [12].

Finally, we note that identifying the η meson with η_8 the branching ratios to final states would come out

$$
\begin{aligned}
\frac{\Gamma(D^0 \to \pi^0\eta)}{\Gamma(D^0 \to K^+K^-)} &= 0.216 & (24) \\[2mm]
\frac{\Gamma(D^0 \to \eta\eta)}{\Gamma(D^0 \to K^+K^-)} &= 0.250,
\end{aligned}
$$

to be compared to the experimental values (0.172±0.018, 0.422±0.051) respectively. Also in this case, the final state rescattering is helpful in allowing a decay rate to $\eta\eta$ larger than to $\pi^0\pi^0$, albeit to an insufficient level, in spite of the phase space difference.

3 CP asymmetries

A nonzero direct CP asymmetry is present only when the decay amplitude is a sum of two amplitudes with different weak phases and having also two different strong phases. If the amplitude for D decay is

$$\mathcal{A} = A\ e^{\imath\delta_A} + B\ e^{\imath\delta_B}\ ,$$

the CP conjugate amplitude would be

$$\bar{\mathcal{A}} = A^*\ e^{\imath\delta_A} + B^*\ e^{\imath\delta_B}\ ,$$

and the CP asymmetry is:

$$a_{\mathrm{CP}} = \frac{|\mathcal{A}|^2 - |\bar{\mathcal{A}}|^2}{|\mathcal{A}|^2 + |\bar{\mathcal{A}}|^2} = \frac{2\ \Im(A^* B)\ \sin(\delta_A - \delta_B)}{|A|^2 + |B|^2 + 2\ \Re(A^* B)\ \cos(\delta_A - \delta_B)}. \tag{25}$$

In our case the amplitude B is provided by the matrix elements of the $\Delta U = 0$ hamiltonian, eq.(10), that contains both $Q_{1(2)}$ and "penguin" operators. In this case, there are three independent symmetric states of two pseudoscalar mesons:

$$\frac{1}{2}\Big\{|K^+ K^-> +|K^- K^+> +|\pi^+ \pi^-> +|\pi^- \pi^+>\Big\}\ ; \tag{26}$$

$$\frac{1}{4}\Big\{3\,|\pi^0 \pi^0> +|\eta_8 \eta_8> +\sqrt{3}\,(|\pi^0 \eta_8> +|\eta_8 \pi^0>)\Big\}\ ;$$

$$\frac{1}{\sqrt{3}}\Big\{\frac{1}{4}|\pi^0 \pi^0> +\frac{3}{4}\,|\eta_8 \eta_8> -\frac{\sqrt{3}}{4}\,(|\pi^0 \eta_8> +|\eta_8 \pi^0>) + |K^0 \bar{K^0}> +|\bar{K^0} K^0>\Big\}\ ,$$

that give rise to three amplitudes transforming as 27, 8 and 1 under SU(3) (for the $Q_{1(2)}$ part) and to two amplitudes transforming as 8 and 1 (for the penguin part). In the framework of quark diagrams (and neglecting annihilation) the third state in eq.(26) decouples, both for penguins and for the other terms. Moreover, the $\Delta I = 1/2$ property of the penguin selects one combination of the first two states. Taking into account that now also the singlet components of

the resonances couple to the D^0 meson state, after rescattering the relevant amplitudes become:

$$
\begin{aligned}
B(D^0 \to \pi^+\pi^-) \;=\;& \left(P + \frac{T'}{2}\right)\left\{\frac{1}{2}\left(e^{\imath\delta_0} + e^{\imath\delta_0'}\right)\right. & (27)\\
&+\; \left(-\frac{1}{6}\cos(2\phi) - \frac{7}{4\sqrt{10}}\sin(2\phi)\right)\left(e^{\imath\delta_0'} - e^{\imath\delta_0}\right)\Big\}\\
&+\; (T' + C')\left\{\frac{3}{20} - \frac{3}{40}\left(e^{\imath\delta_0} + e^{\imath\delta_0'}\right)\right.\\
&+\; \left.\left[\frac{1}{120}\cos(2\phi) + \frac{1}{4\sqrt{10}}\sin(2\phi)\right]\left(e^{\imath\delta_0'} - e^{\imath\delta_0}\right)\right\},\\
B(D^0 \to K^+K^-) \;=\;& \left(P + \frac{T'}{2}\right)\left\{\frac{1}{4}\left(e^{\imath\delta_0} + e^{\imath\delta_0'}\right)\right. & (28)\\
&+\; \left(-\frac{5}{12}\cos(2\phi) + \frac{1}{4\sqrt{10}}\sin(2\phi)\right)\left(e^{\imath\delta_0'} - e^{\imath\delta_0}\right) + \frac{1}{2}e^{\imath\delta_1}\Big\}\\
&+\; (T' + C')\left\{\frac{3}{20} - \frac{1}{40}\left(e^{\imath\delta_0} + e^{\imath\delta_0'}\right) + \frac{7}{120}\cos(2\phi)\left(e^{\imath\delta_0'} - e^{\imath\delta_0}\right) - \frac{1}{10}e^{\imath\delta_1}\right\}.
\end{aligned}
$$

The parameter P represents, in eqs.(27,28), the "penguin" diagram, while with T' and C' we indicate the color connected and color suppressed contributions (we are neglecting annihilations) and them are related to T and C by

$$
T' = -\,T\,\frac{V_{ub}\,V_{cb}^*}{\sin\theta_C\cos\theta_C} \quad\text{and}\quad C' = -\,C\,\frac{V_{ub}\,V_{cb}^*}{\sin\theta_C\cos\theta_C}\;. \tag{29}
$$

We note that if $T' + C' = 0$ the terms containing these amplitudes have the same structure of the penguin term, and that therefore could be reabsorbed in the uncertainty of the penguin contribution. In our phase convention the amplitudes T and C are real, while T', C' and P are complex, having the phase $\pi - \gamma = (111 \pm 4)°$ [17, 18].

The numerical value of the ratios $|T'/T|$ and $|C'/C|$ being $(6.6 \pm 0.9) \cdot 10^{-4}$, they would result in a CP asymmetry of this order. A large asymmetry may only be due to the penguin contribution. We recall that the penguin diagrams were introduced as a possible explanation of the "octet enhancement" by Shifman, Vainshtein and Zacharov [19] many years ago. A large matrix element for these operators could successfully describe both the kaon and the hyperon non–leptonic decays. There has not been a general consensus on this approach, and in particular a recent lattice calculation [20] seems to indicate a different origin for the $\Delta I = 1/2$ dominance in kaon decays.

Using the expressions in equations (19,28) and neglecting the contribution of the terms containing T' and C', the $\mathcal{A}(K^+K^-)$ can be approximated by the

$$
\mathcal{A}(K^+K^-) \simeq T\,f_T(\delta_i, \phi, C/T) \;+\; P\,f_P(\delta_i, \phi)\,,
$$

and equation (25) gives

$$
a_{CP}(K^+K^-) \simeq \frac{2\,T\,\Im(P)\,\Im(f_T\,f_P^*)}{T^2\,|f_T|^2 + \dots} \tag{30}
$$

where we neglected terms of order $|P|/T$ in the denominator, an approximation already made in the calculation of the decay rates.

Inserting in the relevant formulae the parameter values previously determined from the branching ratios and choosing the lower signs in eq.(22), the CP asymmetries for decays in charged mesons turn out to be

$$
\begin{aligned}
a_{CP}(K^+K^-) &= \frac{\Im(P)}{T} \cdot (+1.469) \,, \\
a_{CP}(\pi^+\pi^-) &= \frac{\Im(P)}{T} \cdot (-3.362) \,.
\end{aligned}
\tag{31}
$$

The sign would be opposite if one chooses instead the upper signs in eq.(22). Our choice is suggested by the fact that apparently the resonance $f_0(1710)$ - that has a lower mass - prefers to decay in a pair of kaons [17] and should therefore be identified with f_0'.

We also report the prediction for CP asymmetries for decays in final states with neutral mesons, although it will probably be difficult to test them by experiment:

$$
\begin{aligned}
a_{CP}(K^0\bar{K}^0) &= \frac{\Im(P)}{T} \cdot (-1.217) \,, \\
a_{CP}(\pi^0\pi^0) &= \frac{\Im(P)}{T} \cdot (-1.668) \,.
\end{aligned}
\tag{32}
$$

We note that our parameters predict an asymmetry in the decay to charged pions that is of opposite sign with respect to the asymmetry for decays to charged kaons, and more than twice as large. Assuming instead equal values for the phases δ_0, δ_0' and δ_1, the asymmetries would be equal and opposite, but of considerable less magnitude (even for a maximal strong phase). Therefore, the SU(3) breaking in rescattering favors, in a sense, a larger Δ_{CP}. Taking into account the CKM elements entering in the definition of T and P, one has

$$
\begin{aligned}
\frac{\Im(P)}{T} &= \frac{|V_{ub}\,V_{cb}|}{\sin\theta_C \cos\theta_C} \sin\gamma \frac{< K^+K^-|\; \sum_{i=3}^{6} C_i Q_i + \frac{1}{2}[C_1\{Q_1^s + Q_1^d\} + C_2\{Q_2^s + Q_2^d\}]\,|D^0 >}{< K^+K^-|\,C_1(Q_1^s - Q_1^d) + C_2(Q_2^s - Q_2^d)\,|D^0 >} \\
&= 6.3\,10^{-4}\kappa \,,
\end{aligned}
\tag{33}
$$

where the notation $< K^+K^-|\; \{Q_i\}\; |D^0 >$ indicates the matrix element evaluated with a penguin contraction of the operator. One obtains therefore:

$$
\Delta_{\mathrm{CP}} = 3.03\,10^{-3}\kappa \,.
\tag{34}
$$

A value of κ around three gives asymmetries at the percent level. Concerning the sign of Δ_{CP}, we note that if one uses factorization κ would be negative and Δ_{CP} would therefore be negative, in agreement with the majority of experimental results. We note however that if one uses factorization a considerably smaller value for κ would be expected, due to the smallness of the Wilson coefficients of QCD penguin operators.

Let us compare this result to what has been found in [11], where an analysis of the bounds imposed by unitarity on the final state interactions of the isospin zero amplitudes was pursued, both in a two–channel and in a three–channel situation. We note that the enhancement factor κ required is similar to what was found there in the three channel case, and that, in our SU(3) based scheme, the channels are in fact three (1, 8, 27).

4   Conclusion

We studied the singly Cabibbo suppressed decays of neutral D mesons by assuming that all the SU(3) violations are due to the final state interactions. Large values of the strong phases are necessary to predict consistent CP violation in the decay amplitudes. In our framework we were able to give an accurate description of decay branching ratios and of the isospin structure of the amplitudes for pionic decays.

The experimental situation regarding the CP violating asymmetries is at present rather confused, but we think anyhow of interest to have shown that large asymmetries can be obtained, considering the uncertainties of long distance contributions and with some stretching of the parameters, even without invoking New Physics.

A rather large value of the "penguin" matrix element would be needed to obtain asymmetries as large as in [1, 2, 3]. We recall that large "penguin" contributions were also suggested to reproduce rates and isospin structure of the decays of K mesons and hyperons [19], although it is not evident that the analogy can be pursued [16]. While the absolute value of the CP violating asymmetries cannot be safely predicted, we obtain an asymmetry for the decays into charged pions more than twice as large and having opposite sign with respect to that for charged kaons.

5   Acknowledgments

I would like to thank Franco Buccella, Maurizio Lusignoli and Alessandra Pugliese for collaboration. I thank Pietro Colangelo for discussions. Finally, It is a pleasure to thank the organizers of the Helmholtz International Summer School "Physics of Heavy Quarks and Hadrons" for the invitation and for providing a pleasant and stimulating atmosphere.

References

[1] CDF Collaboration, T. Aaltonen *et al.*, Phys. Rev. Lett. 109, 111801 (2012).

[2] LHCb Collaboration, R. Aaij *et al.*, Phys. Rev. Lett. 108, 111602 (2012).

[3] B. R. Ko, for the Belle Collaboration, at ICHEP 2012, arXiv:1212.1975.

[4] BABAR Collaboration, B. Aubert *et al.*, Phys. Rev. Lett. 100, 061803 (2008).

[5] LHCb Collaboration, R. Aaij *et al.*, LHCb-CONF-2013-003;
J. van Tilburg, on behalf of the LHCb Collaboration, CERN-LHC Seminar, 12/03/2013.

[6] LHCb Collaboration, R. Aaij *et al.*, arXiv:1303.2614 [hep-ex];
J. van Tilburg, on behalf of the LHCb Collaboration, CERN-LHC Seminar, 12/03/2013.

[7] F. Buccella, M. Lusignoli, A. Pugliese and P. Santorelli, Phys. Rev. D **88** (2013) 074011 [arXiv:1305.7343 [hep-ph]].

[8] J. van Tilburg, on behalf of the LHCb Collaboration, CERN-LHC Seminar, 12/03/2013.

[9] Y. Grossman, A. L. Kagan and Y. Nir, Phys. Rev. D **75** (2007) 036008 [hep-ph/0609178];
G. Isidori, J. F. Kamenik, Z. Ligeti and G. Perez, Phys. Lett. B **711** (2012) 46 [arXiv:1111.4987 [hep-ph]];
K. Wang and G. Zhu, Phys. Lett. B **709** (2012) 362 [arXiv:1111.5196 [hep-ph]];
G. Hiller, Y. Hochberg and Y. Nir, Phys. Rev. D **85** (2012) 116008 [arXiv:1204.1046 [hep-ph]];
G. F. Giudice, G. Isidori and P. Paradisi, JHEP **1204** (2012) 060 [arXiv:1201.6204 [hep-ph]];
W. Altmannshofer, R. Primulando, C. -T. Yu and F. Yu, JHEP **1204** (2012) 049 [arXiv:1202.2866 [hep-ph]];
C. -H. Chen, C. -Q. Geng and W. Wang, Phys. Rev. D **85** (2012) 077702 [arXiv:1202.3300 [hep-ph]];
O. Gedalia, J. F. Kamenik, Z. Ligeti and G. Perez, Phys. Lett. B **714** (2012) 55 [arXiv:1202.5038 [hep-ph]];

T. Mannel and N. Uraltsev, JHEP **1303** (2013) 064 [arXiv:1205.0233 [hep-ph]];

B. Keren-Zur, P. Lodone, M. Nardecchia, D. Pappadopulo, R. Rattazzi and L. Vecchi, Nucl. Phys. B **867** (2013) 429 [arXiv:1205.5803 [hep-ph]];

R. Barbieri, D. Buttazzo, F. Sala and D. M. Straub, JHEP **1210** (2012) 040 [arXiv:1206.1327 [hep-ph]];

A. D. Dolgov, S. I. Godunov, A. N. Rozanov and M. I. Vysotsky, JETP Lett. **96** (2012) 290 [arXiv:1206.6652 [hep-ph]];

C. Delaunay, J. F. Kamenik, G. Perez and L. Randall, JHEP **1301** (2013) 027 [arXiv:1207.0474 [hep-ph]].

[10] M. Golden and B. Grinstein, Phys. Lett. B **222** (1989) 501,

D. Pirtskhalava and P. Uttayarat, Phys. Lett. B **712** (2012) 81 [arXiv:1112.5451 [hep-ph]];

B. Bhattacharya, M. Gronau and J. L. Rosner, Phys. Rev. D **85** (2012) 054014 [arXiv:1201.2351 [hep-ph]];

T. Feldmann, S. Nandi and A. Soni, JHEP **1206** (2012) 007 [arXiv:1202.3795 [hep-ph]];

J. Brod, A. L. Kagan and J. Zupan, Phys. Rev. D **86** (2012) 014023 [arXiv:1111.5000 [hep-ph]];

J. Brod, Y. Grossman, A. L. Kagan and J. Zupan, JHEP **1210** (2012) 161 [arXiv:1203.6659 [hep-ph]];

H. -Y. Cheng and C. -W. Chiang, Phys. Rev. D **86** (2012) 014014 [arXiv:1205.0580 [hep-ph]];

G. Hiller, M. Jung and S. Schacht, Phys. Rev. D **87** (2013) 014024 [arXiv:1211.3734 [hep-ph]].

[11] E. Franco, S. Mishima and L. Silvestrini, JHEP **1205** (2012) 140 [arXiv:1203.3131 [hep-ph]].

[12] F. Buccella, M. Lusignoli, G. Miele, A. Pugliese and P. Santorelli, Phys. Rev. D **51** (1995) 3478 [hep-ph/9411286] ;

F. Buccella, M. Lusignoli and A. Pugliese, Phys. Lett. B **379** (1996) 249 [hep-ph/9601343].

[13] F. J. Gilman and M. B. Wise, Phys. Rev. D **20** (1979) 2392.

[14] M.J. Savage, Phys. Lett. B **257** (1991) 414;

I. Hinchliffe and T. A. Kaeding, Phys. Rev. D **54** (1996) 914 [hep-ph/9502275];

Y. Grossman and D. J. Robinson, JHEP **1304** (2013) 067 [arXiv:1211.3361 [hep-ph]].

[15] L.L. Chau, Physics Reports **95** (1983) 1;

M. Gronau, O.F. Hernandez, D. London, and J.L. Rosner, Phys. Rev. D **50** (1994) 4529.

[16] L. F. Abbott, P. Sikivie and M. B. Wise, Phys. Rev. D **21** (1980) 768.

[17] J. Beringer et al. (Particle Data Group), Phys. Rev. D **86** (2012) 010001.

[18] M. Bona et al. [UTfit Collab.], JHEP 0803, 049 (2008) [arXiv:0707.0636].

[19] M. A. Shifman, A. I. Vainshtein and V. I. Zakharov, Sov. Phys. JETP **45** (1977) 670 [Zh. Eksp. Teor. Fiz. **72** (1977) 1275].

[20] P. A. Boyle *et al.* [RBC and UKQCD Collaborations], Phys. Rev. Lett. **110** (2013) 15200, arXiv:1212.1474 [hep-lat].

The scalar mesons in multi-channel $\pi\pi$ scattering and decays of the ψ and Υ families

Yurii S. Surovtsev[1], Petr Bydžovský[2], Thomas Gutsche[3], Robert Kamiński[4], Valery E. Lyubovitskij[3]*, Miroslav Nagy[5]

[1]Bogoliubov Laboratory of Theoretical Physics, Joint Institute for Nuclear Research, Dubna 141980, Russia
[2]Nuclear Physics Institute, Czech Academy of Sciences, Řež near Prague 25068, Czech Republic
[3]Institut für Theoretische Physik, Universität Tübingen, Kepler Center for Astro and Particle Physics, Auf der Morgenstelle 14, D–72076 Tübingen, Germany
[4]Institute of Nuclear Physics, Polish Academy of Sciences, Cracow 31342, Poland
[5]Institute of Physics, Slovak Academy of Sciences, Bratislava 84511, Slovak Republic

The f_0 mesons are studied in a combined analysis of data on isoscalar S-wave processes $\pi\pi \to \pi\pi, K\overline{K}, \eta\eta$ and on decays $J/\psi \to \phi(\pi\pi, K\overline{K})$, $\psi(2S) \to J/\psi(\pi\pi)$ and $\Upsilon(2S) \to \Upsilon(1S)\pi\pi$ from the Argus, Crystal Ball, CLEO, CUSB, DM2, Mark II, Mark III, and BESIII Collaborations. The method of analysis, based on analyticity and unitarity and using an uniformization procedure, is set forth with some details. Some spectroscopic implications from results of the analysis are discussed.

1   Introduction

The problem of scalar mesons, particularly their nature, parameters, and status of some of them, is still not solved [1]. In the 3-channel analyses of $\pi\pi$ scattering, based on the uniformizing variable [2, 3], we obtained parameters of the $f_0(600)$ and $f_0(1500)$ which considerably differ from results of analyses utilizing other methods (mainly based on dispersion relation and Breit-Wigner approaches). Reasons for this difference were understood in Refs. [4, 5]. We showed that studying wide multi-channel resonances the Riemann-surface structure of the S-matrix of considered processes must be allowed for properly. For the scalar states this should be at least the 8-sheeted Riemann surface. This is related to a necessity to analyze jointly coupled processes $\pi\pi \to \pi\pi, K\overline{K}, \eta\eta$ because analyzing only $\pi\pi$ scattering it is impossible to obtain correct parameters for the scalar states. One can conclude: Even if a wide state does not decay into a channel which opens above its mass but it is strongly connected with this channel, one ought to consider this state taking into account the Riemann-surface sheets related to the threshold branch-point of this channel. I.e., the standard dispersion relation approach, in which amplitudes are considered on the 2-sheeted Riemann surface, does not suit for a correct determination of resonance parameters. These conclusions are important because our approach is based only on the demand for analyticity and unitarity of amplitude and using an uniformization procedure. The construction of the amplitude is essentially free from any dynamical (model) assumptions utilizing only the *mathematical* fact that a local behaviour of

---

*On leave of absence from the Department of Physics, Tomsk State University, 634050 Tomsk, Russia

analytic functions determined on the Riemann surface is governed by the nearest singularities on all corresponding sheets. Therefore, our approach permits us to omit theoretical prejudice in extracting the resonance parameters.

Analyzing only $\pi\pi \to \pi\pi, K\overline{K}, \eta\eta(\eta\eta')$ [3] we showed that data on the $\pi\pi$ scattering below 1 GeV admit two sets of parameters of the $f_0(600)$: in both cases $m_\sigma \approx m_\rho$ and the total widths about 600 and 950 MeV – solutions "A" and "B", respectively. For the states $f_0(1370)$, $f_0(1500)$ (as a superposition of a broad and narrow state) and $f_0(1710)$, we got four possible scenarios of representation by poles and zeros on the Riemann surface giving similar description of the above processes and, however, quite different parameters of some resonances. E.g., in A solution we got the following spread of the masses and total widths for the $f_0(600)$, $f_0(1370)$ and $f_0(1710)$, respectively: 605-735 and 567-686 MeV, 1326-1404 and 223-345 MeV, and 1751-1759 and 118-207 MeV. Adding the data on $J/\psi \to \phi(\pi\pi, K\overline{K})$ from the Mark III, DM2 and BESIII [6], we could diminished the number of possible scenarios [5]. Moreover, *the di-pion mass distribution of $J/\psi \to \phi\pi\pi$ of the BESIII data from the threshold to about 850 MeV prefers the solution with the wider $f_0(600)$ state – B-solution.* This is a problem because most of physicists [1] prefer the narrower $f_0(600)$. Therefore, we extend our analysis adding also data on $\psi(2S) \to J/\psi(\pi\pi)$ and $\Upsilon(2S) \to \Upsilon(1S)\pi\pi$ from the Argus, Crystal Ball, CLEO, CUSB, and Mark II collaborations [7, 8].

There are also problems related to interpretation of scalar mesons, e.g., as to an assignment of the scalar mesons to $q\bar{q}$ nonets. A number of properties of these states do not allow one simply to make up this. The main problem is a discordance of the approximately equal masses of the $f_0(980)$ and $a_0(980)$ and observed $s\bar{s}$ dominance in the wave function of the $f_0(980)$. If these states are in the same nonet, then the $f_0(980)$ must be heavier than $a_0(980)$ by 250-300 MeV because the difference of the s- and u-quark masses is 120-150 MeV. Due to this fact, various solutions are proposed. The most popular variant is the 4-quark interpretation of the $f_0(980)$ and $a_0(980)$ mesons, in favour of which as though additional arguments have been found based on interpretation of the data on $\phi \to \gamma\pi^0\pi^0, \gamma\pi^0\eta$ [9]. However, the 4-quark model, beautifully solving the old problem of the unusual properties of scalar mesons, sets new questions. Where are the 2-quark states, their radial excitations and the other members of 4-quark multiplets $9, 9^*, 36$ and 36^*, which are predicted to exist below 2.5 GeV [10]? We proposed our way to solve this problem.

Further we shall consider mainly the 3-channel case because this is a minimal number of channels needed for obtaining correct values of parameters of the scalar resonances.

2 Method of the uniformizing variable

Our model-independent method which essentially utilizes a uniformizing variable can be used only for the 2- and the 3-channel cases [2, 3]. The 3-channel S-matrix is determined on the 8-sheeted Riemann surface. The matrix elements S_{ij}, where $i, j = 1, 2, 3$ denote channels, have the right-hand cuts along the real axis of the s complex plane (s is the invariant total energy squared), starting with the channel thresholds s_i, and the left-hand cuts related to the crossed channels. The Riemann-surface sheets, denoted by the Roman numbers, are numbered according to the signs of analytic continuations of the square roots $\sqrt{s - s_i}$ as follows: signs $\left(\mathrm{Im}\sqrt{s - s_1}, \mathrm{Im}\sqrt{s - s_2}, \mathrm{Im}\sqrt{s - s_3} \right) = +++, -++, --+, +-+, +--, ---,$ $-+-, ++-$ correspond to sheets I, II, $\cdots$, VIII, respectively.

In the upper part of Fig. 1, the right-hand cuts of the 3-channel S-matrix are shown on the s-plane. The lower part shows how the Riemann sheets are sewed together. E.g., sheet I is sewed with sheet II, III, and VI between the thresholds $\pi\pi$ and $K\overline{K}$, $K\overline{K}$ and $\eta\eta$, and above the $\eta\eta$ threshold, respectively. Our approach is based on analyticity and unitarity and realizes an idea of the consistent account of the nearest (to the physical region) singularities on all sheets of the Riemann surface of the S-matrix, thus giving a chance to obtain a model-independent information on resonances from the data analysis. The main model-independent contribution of resonances is given by poles and corresponding zeros on the Riemann surface. A simple description of the background is a criterion of correctness of this statement.

If a resonance has the only decay mode (1-channel case), a general statement about the amplitude is that for energies in proximity of the resonance energy it describes the propagation of resonance as if it is a free par-

Figure 1: Sewing together the sheets of the Riemann surface.

ticle. This means that in the matrix element the resonance (in the limit of its narrow width) is represented by a pair of complex conjugate poles on sheet II and by a pair of conjugate zeros on sheet I at the same points of complex energy. This model-independent statement about the poles as the nearest singularities holds also when taking account of the finite width of a resonance and in the multi-channel case.

An arrangement of poles and zeros of a multi-channel resonance on the Riemann surface is obtained using the proved fact that on the physical sheet, the S-matrix elements can have only resonance zeros (beyond the real axis), at least, around the physical region. This allows to obtain formulas expressing analytic continuations of the S-matrix elements to all sheets in terms of those on the physical sheet [11]. To this end, let us consider the N-channel S-matrix (all are two-particle channels) determined on the 2^N-sheeted Riemann surface. The surface has the right-hand (unitary) cuts along the real axis of the s-variable complex plane (s_i, ∞) $(i = 1, 2, \cdots, N$ is a channel) through which the physical sheet is sewed together with other sheets. The branch points are at the zero channel momenta $k_\alpha = (s/4 - m_\alpha^2)^{1/2}$. For now we will neglect the left-hand cut on the Riemann surface related to the crossing-channel contributions, which, in principle, can be included in the background part of the amplitude.

It is convenient to label the sheets as follows (see, e.g., [12]): the physical sheet is denoted as L_0 and the other sheets as $L_{i_1 \cdots i_k}$ where $i_1 \cdots i_k$ is a system of subscripts of those channel-momenta k_{i_n} that change signs at analytical continuations from the physical onto the indicated sheet. Then the analytical continuation of S-matrix elements S_{ik} to the unphysical sheet $L_{i_1 \cdots i_k}$ is $S_{ik}^{(i_1 \cdots i_k)}$. We obtain the formula for $S_{ik}^{(i_1 \cdots i_k)}$ expressed in terms of $S_{ik}^{(0)}$ (the matrix elements S_{ik} on the physical sheet L_0), using the reality property of the analytic functions and the N-
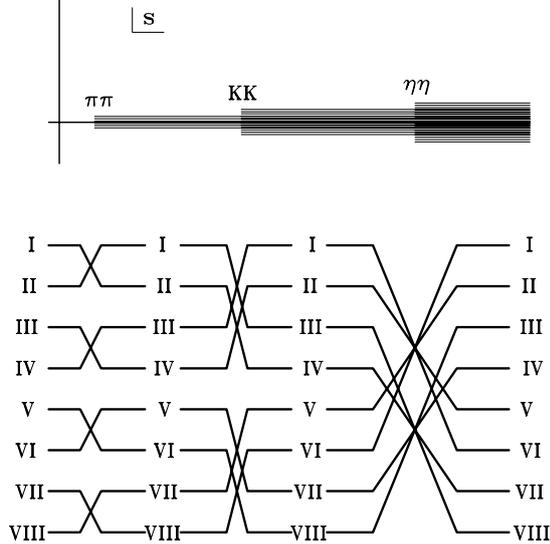
channel unitarity. The direct derivation of these formulas requires rather bulky algebra. It can be simplified if we use Hermiticity of the K-matrix.

First, let us introduce the notation: $\mathbf{S}^{[i_1\cdots i_k]}$ is a matrix with zero matrix elements except for the rows $i_1,\cdots,i_k$, that consist of elements $S_{i_n i_m}$. In the matrix $\mathbf{S}^{\{i_1\cdots i_k\}}$, on the contrary, the rows $i_1,\cdots,i_k$ are zeros. Therefore, $\mathbf{S}^{[i_1\cdots i_k]} + \mathbf{S}^{\{i_1\cdots i_k\}} = \mathbf{S}$. Further we introduce the diagonal matrices $\mathbf{\Delta}^{[i_1\cdots i_k]}$ and $\mathbf{\Delta}^{\{i_1\cdots i_k\}}$ with the diagonal elements

$$\Delta_{ii}^{[i_1\cdots i_k]} = \left\{ \begin{array}{ll} 1 & \text{if } i \in (i_1\cdots i_k), \\ 0 & \text{for remaining } i, \end{array} \right. \quad \text{and} \quad \Delta_{ii}^{\{i_1\cdots i_k\}} = \left\{ \begin{array}{ll} 0 & \text{if } i \in (i_1\cdots i_k). \\ 1 & \text{for remaining } i, \end{array} \right.$$

Further using relation of the S- and K-matrices

$$\mathbf{S} = \frac{I + i\rho^{1/2}\mathbf{K}\rho^{1/2}}{I - i\rho^{1/2}\mathbf{K}\rho^{1/2}} \quad \text{where } \rho_{ij} = 0 \ (i \neq j), \ \rho_{ii} = 2k_i/\sqrt{s} \tag{1}$$

and $\mathbf{SS}^+ = \mathbf{I}$, it is easy to obtain $\mathbf{K} = \mathbf{K}^+$, i.e., the K-matrix has no discontinuity when crossing the two-particle unitary cuts and has the same value in all sheets of the Riemann surface. Using the latter fact, we obtain the needed formula. The analytical continuations of the S-matrix to the sheet $L_{i_1\cdots i_k}$ will be represented as

$$\mathbf{S}^{(i_1\cdots i_k)} = \frac{\mathbf{S}^{(0)\{i_1\cdots i_k\}} - i\mathbf{\Delta}^{[i_1\cdots i_k]}}{\mathbf{\Delta}^{\{i_1\cdots i_k\}} - i\mathbf{S}^{(0)[i_1\cdots i_k]}}. \tag{2}$$

From eq. (2) the corresponding relations for the S-matrix elements can be derived by the formula for the matrix division. In Table 1 the result is shown for the 3-channel case. We have returned to more standard enumeration of sheets by Roman numerals I, II,...,VIII. In

Process	L_0 I	L_1 II	L_{12} III	L_2 IV	L_{23} V	L_{123} VI	L_{13} VII	L_3 VIII
$1 \rightarrow 1$	S_{11}	$1/S_{11}$	S_{22}/D_{33}	D_{33}/S_{22}	$\det S/D_{11}$	$D_{11}/\det S$	S_{33}/D_{22}	D_{22}/S_{33}
$1 \rightarrow 2$	S_{12}	iS_{12}/S_{11}	$-S_{12}/D_{33}$	iS_{12}/S_{22}	iD_{12}/D_{11}	$-D_{12}/\det S$	iD_{12}/D_{22}	D_{12}/S_{33}
$2 \rightarrow 2$	S_{22}	D_{33}/S_{11}	S_{11}/D_{33}	$1/S_{22}$	S_{33}/D_{11}	$D_{22}/\det S$	$\det S/D_{22}$	D_{11}/S_{33}
$1 \rightarrow 3$	S_{13}	iS_{13}/S_{11}	$-iD_{13}/D_{33}$	$-D_{13}/S_{22}$	$-iD_{13}/D_{11}$	$D_{13}/\det S$	$-S_{13}/D_{22}$	iS_{13}/S_{33}
$2 \rightarrow 3$	S_{23}	D_{23}/S_{11}	iD_{23}/D_{33}	iS_{23}/S_{22}	$-S_{23}/D_{11}$	$-D_{23}/\det S$	iD_{23}/D_{22}	iS_{23}/S_{33}
$3 \rightarrow 3$	S_{33}	D_{22}/S_{11}	$\det S/D_{33}$	D_{11}/S_{22}	S_{22}/D_{11}	$D_{33}/\det S$	S_{11}/D_{22}	$1/S_{33}$

Table 1: Analytic continuations of the 3-channel S-matrix elements to unphysical sheets.

Table 1, the superscript I is omitted to simplify the notation, $\det S$ is the determinant of the 3×3 S-matrix on sheet I, $D_{\alpha\beta}$ is the minor of the element $S_{\alpha\beta}$, that is, $D_{11} = S_{22}S_{33} - S_{23}^2$, $D_{22} = S_{11}S_{33} - S_{13}^2$, $D_{33} = S_{11}S_{22} - S_{12}^2$, $D_{12} = S_{12}S_{33} - S_{13}S_{23}$, $D_{23} = S_{11}S_{23} - S_{12}S_{13}$, etc.

These formulas show how singularities and resonance poles and zeros are transferred from the matrix element S_{11} to matrix elements of coupled processes. Starting from the resonance zeros on sheet I, one can obtain the arrangement of poles and zeros of resonance on the whole Riemann surface ("pole clusters"). In the 3-channel case, we obtain *7 types* of resonances corresponding to 7 possible situations when there are resonance zeros on sheet I only in S_{11} – (**a**); S_{22} – (**b**); S_{33} – (**c**); S_{11} and S_{22} – (**d**); S_{22} and S_{33} – (**e**); S_{11} and S_{33} – (**f**); S_{11}, S_{22} and S_{33} – (**g**). *A necessary and sufficient condition for existence of the multi-channel resonance is its representation by one of the types of pole clusters.* A main *model-independent*

YURII S. SUROVTSEV, PETR BYDŽOVSKÝ, THOMAS GUTSCHE, ROBERT KAMIŃSKI, ...

contribution of resonances is given by the pole clusters and possible remaining small (*model-dependent*) contributions of resonances can be included in the background. This is confirmed further by the obtained very simple description of the background.

The cluster type is related to the nature of state. *E.g.*, if we consider the $\pi\pi$, $K\overline{K}$ and $\eta\eta$ channels, then a resonance, coupled relatively more strongly to the $\pi\pi$ channel than to the $K\overline{K}$ and $\eta\eta$ ones is described by the cluster of type (**a**). In the opposite case, it is represented by the cluster of type (**e**) (say, the state with the dominant $s\bar{s}$ component). The glueball must be represented by the cluster of type (**g**) as a necessary condition for the ideal case.

One can formulate *a model-independent test as a necessary condition* to distinguish a bound state of colorless particles (*e.g.*, a $K\overline{K}$ molecule) and a $q\bar{q}$ bound state [11, 13]. In the 1-channel case, the existence of the particle bound-state means the presence of a pole on the real axis under the threshold on the physical sheet. In the 2-channel case, existence of the bound-state in channel 2 ($K\overline{K}$ molecule) that, however, can decay into channel 1 ($\pi\pi$ decay), would imply the presence of the pair of complex conjugate poles on sheet II under the second-channel threshold without the corresponding shifted pair of poles on sheet III.

In the 3-channel case, the bound state in channel 3 ($\eta\eta$) that, however, can decay into channels 1 ($\pi\pi$ decay) and 2 ($K\overline{K}$ decay), is represented by the pair of complex conjugate poles on sheet II and by the pair of shifted poles on sheet III under the $\eta\eta$ threshold without the corresponding poles on sheets VI and VII.

According to this test, earlier we rejected interpretation of the $f_0(980)$ as the $K\overline{K}$ molecule because this state is represented by the cluster of type (**a**) in the 2-channel analysis of $\pi\pi \to \pi\pi, K\overline{K}$ and, therefore, does not satisfy the necessary condition to be the $K\overline{K}$ molecule [11].

It is convenient to use the Le Couteur-Newton relations [14]. They express the S-matrix elements of all coupled processes in terms of the Jost matrix determinant $d(k_1, \cdots, k_N) \equiv d(s)$ that is a real analytic function with the only branch-points at $k_i = 0$:

$$S_{ii}(s) = \frac{d^{(i)}(s)}{d(s)}, \qquad \begin{vmatrix} S_{i_1 i_1}(s) & \cdots & S_{i_1 i_k}(s) \\ \vdots & \vdots & \vdots \\ S_{i_k i_1}(s) & \cdots & S_{i_k i_k}(s) \end{vmatrix} = \frac{d^{(i_1 \cdots i_k)}(s)}{d(s)}. \tag{3}$$

Rather simple derivation of these relations, using the ND^{-1} representation of amplitudes and Hermiticity of the K-matrix, can be found in Ref. [12]. The real analyticity implies $d(s^*) = d^*(s)$ for all s. The unitarity condition requires further restrictions on the d-function for physical s-values which will be discussed below in the example of 3-channel S-matrix.

In order to use really the representation of resonances by various pole clusters, it ought to transform our multi-valued S-matrix, determined on the 8-sheeted Riemann surface, to one-valued function. But that function can be uniformized only on torus with the help of a simple mapping. This is unsatisfactory for our purpose. Therefore, we neglect the influence of the lowest ($\pi\pi$) threshold branch-point (however, unitarity on the $\pi\pi$ cut is taken into account). This approximation means the consideration of the nearest to the physical region semi-sheets of the Riemann surface of the S-matrix. In fact, we construct a 4-sheeted model of the initial 8-sheeted Riemann surface that is in accordance with our approach of a consistent account of the nearest singularities on all the relevant sheets. In the corresponding uniformizing variable, we have neglected the $\pi\pi$-threshold branch-point and taken into account the $K\overline{K}$- and $\eta\eta$-threshold branch-points and the left-hand branch-point at $s = 0$:

$$w = \frac{\sqrt{(s - s_2)s_3} + \sqrt{(s - s_3)s_2}}{\sqrt{s(s_3 - s_2)}} \qquad (s_2 = 4m_K^2 \text{ and } s_3 = 4m_\eta^2). \tag{4}$$

In Fig. 2 we show the representation of resonances of types (**a**), (**b**), (**c**) and (**g**) used in this analysis on the uniformization w-plane for the 3-channel-$\pi\pi$-scattering S-matrix element. Representation of other type resonances can be found in Ref. [3].
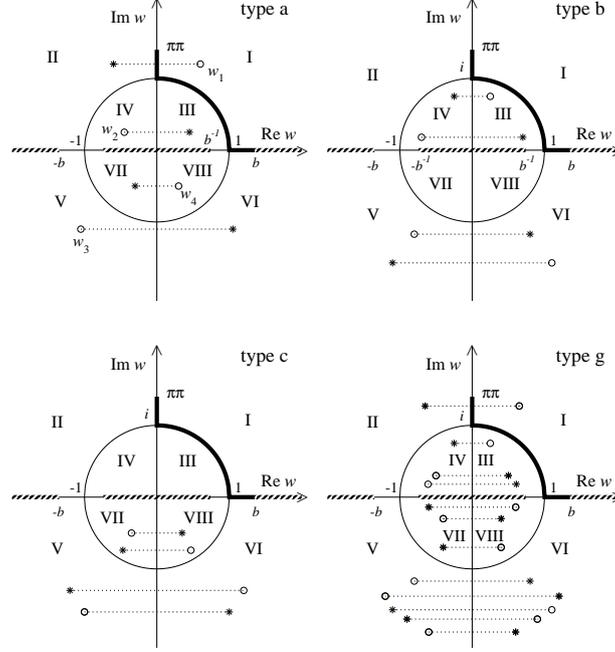

Figure 2: Uniformization w-plane. Representation of resonances of types (**a**), (**b**), (**c**) and (**g**) in S_{11} is shown.

On the w-plane, the Le Couteur–Newton relations are somewhat modified taking account of the used model of initial 8-sheeted Riemann surface:

$$S_{11} = \frac{d^*(-w^*)}{d(w)}, \qquad S_{22} = \frac{d(-w^{-1})}{d(w)}, \qquad S_{33} = \frac{d(w^{-1})}{d(w)}, \tag{5}$$

$$S_{11}S_{22} - S_{12}^2 = \frac{d^*(w^{*-1})}{d(w)}, \quad S_{11}S_{33} - S_{13}^2 = \frac{d^*(-w^{*-1})}{d(w)}, \quad S_{22}S_{33} - S_{23}^2 = \frac{d(-w)}{d(w)}. \tag{6}$$

The 3-channel unitarity requires the following relations to hold for physical w-values: $|d(-w^*)| \leq |d(w)|$, $|d(-w^{-1})| \leq |d(w)|$, $|d(w^{-1})| \leq |d(w)|$ and $|d(w^{*-1})| = |d(-w^{*-1})| = |d(-w)| = |d(w)|$.

The S-matrix elements in Le Couteur–Newton relations are taken as $S = S_B S_{res}$. The d-function is for the resonance part $d_{res}(w) = w^{-\frac{M}{2}} \prod_{r=1}^{M}(w + w_r^*)$ (M is a number of resonance zeros) and for the background part $d_B = \exp[-i \sum_{n=1}^{3}(\sqrt{s - s_n}/2m_n)(\alpha_n + i\beta_n)]$ where

$$\alpha_n = a_{n1} + a_{n\sigma} \frac{s - s_\sigma}{s_\sigma}\theta(s - s_\sigma) + a_{nv}\frac{s - s_v}{s_v}\theta(s - s_v),$$

$$\beta_n = b_{n1} + b_{n\sigma} \frac{s - s_\sigma}{s_\sigma}\theta(s - s_\sigma) + b_{nv}\frac{s - s_v}{s_v}\theta(s - s_v).$$

Here s_σ is the $\sigma\sigma$ threshold and s_v is the combined threshold of the $\eta\eta'$, $\rho\rho$ and $\omega\omega$ channels.

Di-meson mass distributions in decays $J/\psi \to \phi(\pi\pi, K\overline{K})$ and $V' \to V\pi\pi$ (e.g., $\psi(2S) \to J/\psi(\pi\pi)$ and $\Upsilon(2S) \to \Upsilon(1S)\pi\pi$) are calculated using formalism of Refs. [13]. There is assumed that pairs of pseudo-scalar mesons in final states have $I = J = 0$ and only they undergo strong interactions, whereas a final vector meson (ϕ, V) acts as a spectator. The decay amplitudes are related with the scattering amplitudes T_{ij} ($i, j = 1 - \pi\pi, 2 - K\overline{K}$) as follows:

$$
\begin{align}
F(J/\psi \to \phi\pi\pi) &= \sqrt{2/3}\,[c_1(s)T_{11} + c_2(s)T_{21}], \tag{7}\\
F(J/\psi \to \phi K\overline{K}) &= \sqrt{1/2}\,[c_1(s)T_{12} + c_2(s)T_{22}], \tag{8}\\
F(V' \to V\pi\pi\ (V = \psi, \Upsilon)) &= [(d_1, e_1)T_{11} + (d_2, e_2)T_{21}] \tag{9}
\end{align}
$$

where $c_1 = \gamma_{10} + \gamma_{11}s$, $c_2 = \alpha_2/(s - \beta_2) + \gamma_{20} + \gamma_{21}s$, and $(d_i, e_i) = (\delta_{i0}, \rho_{i0}) + (\delta_{i1}, \rho_{i1})s$ are functions of couplings of the J/ψ, $\psi(2S)$ and $\Upsilon(2S)$ to channel i; $\alpha_2, \beta_2, \gamma_{i0}, \gamma_{i1}, \delta_{i0}, \rho_{i0}, \delta_{i1}$ and ρ_{i1} are free parameters. The pole term in c_2 is an approximation of possible ϕK states, not forbidden by OZI rules when considering quark diagrams of these processes. Obviously this pole should be situated on the real s-axis below the $\pi\pi$ threshold.

The expressions $N|F|^2\sqrt{(s - s_i)\big(m_\psi^2 - (\sqrt{s} - m_\phi)^2\big)\big(m_\psi^2 - (\sqrt{s} + m_\phi)^2\big)}$ for $J/\psi \to \phi\pi\pi, \phi K\overline{K}$ (and the analogues ones for $V' \to V\pi\pi$) give the di-meson mass distributions. N (normalization to experiment) is 0.7512 for Mark III, 0.3705 for DM2, 5.699 for BESIII, 1.015 for Mark II, 0.98 for Crystal Ball(80), 4.3439 for Argus, 2.1776 for CLEO, 1.2011 for CUSB, and 0.0788 for Crystal Ball(85).

3   The combined 3-channel analysis of data

We performed the combined 3-channel analysis of data on isoscalar S-wave processes $\pi\pi \to \pi\pi, K\overline{K}, \eta\eta$ and on $J/\psi \to \phi(\pi\pi, K\overline{K})$, $\psi(2S) \to J/\psi(\pi\pi)$ and $\Upsilon(2S) \to \Upsilon(1S)\pi\pi$.

For the data on multi-channel $\pi\pi$ scattering we used the results of phase analyses which are given for phase shifts of the amplitudes $\delta_{\alpha\beta}$ and for the modules of the S-matrix elements $\eta_{\alpha\beta} = |S_{\alpha\beta}|$ ($\alpha, \beta = 1, 2, 3$): $S_{\alpha\alpha} = \eta_{\alpha\alpha} \exp\{2i\delta_{\alpha\alpha}\}$, $S_{\alpha\beta} = i\eta_{\alpha\beta} \exp\{i\phi_{\alpha\beta}\}$. If below the third threshold there is the 2-channel unitarity then the relations $\eta_{11} = \eta_{22}$, $\eta_{12} = (1 - \eta_{11}{}^2)^{1/2}$ and $\phi_{12} = \delta_{11} + \delta_{22}$ are fulfilled in this energy region.

References to used data for processes $\pi\pi \to \pi\pi, K\overline{K}, \eta\eta$ can be found in [3]. For decays $J/\psi \to \phi\pi\pi, \phi K\overline{K}$ we have taken data from Mark III, DM2 and BESIII [6]; for $\psi(2S) \to J/\psi(\pi^+\pi^-)$ from Mark II and for $\psi(2S) \to J/\psi(\pi^0\pi^0)$ from Crystal Ball Collaborations(80) [7]; for $\Upsilon(2S) \to \Upsilon(1S)(\pi^+\pi^-, \pi^0\pi^0)$ from Argus, CLEO, CUSB, and Crystal Ball Collaborations(85) [8]. In this analyses of the coupled scattering processes and decays, it is assumed that in the 1500-MeV region two states – the narrow $f_0(1500)$ and wide $f_0'(1500)$ – exist.

We have obtained the following scenarios: the $f_0(600)$ is described by the cluster of type (**a**); the $f_0(1370)$ and $f_0(1500)$, type (**c**) and $f_0'(1500)$, type (**g**); the $f_0(980)$ is represented only by the pole on sheet II and shifted pole on sheet III. However, the $f_0(1710)$ can be described by clusters either of type (**b**) or (**c**). For definiteness, we have taken type (**c**).

The resonances pole arrangement on the $\sqrt{s}$-plane can be found in [5]. The obtained background parameters are: $\underline{a_{11} = 0.0}$, $\underline{a_{1\sigma} = 0.0199}$, $\underline{a_{1v} = 0.0}$, $\underline{b_{11} = b_{1\sigma} = 0.0}$, $\underline{b_{1v} = 0.0338}$, $a_{21} = -2.4649$, $a_{2\sigma} = -2.3222$, $a_{2v} = -6.611$, $b_{21} = b_{2\sigma} = 0.0$, $b_{2v} = 7.073$, $b_{31} = 0.6421$, $b_{3\sigma} = 0.4851$, $b_{3v} = 0$; $s_\sigma = 1.6338$ GeV^2, $s_v = 2.0857$ GeV^2. The very simple description of the $\pi\pi$-scattering background (underlined values) confirms well our assumption $S = S_B S_{res}$ and

also that representation of multi-channel resonances by the pole clusters on the uniformization plane is good and quite sufficient. Moreover, this shows that *the consideration of the left-hand branch-point at $s = 0$ in the uniformizing variable solves partly a problem of some approaches (see, e.g., [15]) that the wide-resonance parameters are strongly controlled by the non-resonant background.*

Parameters of resonances and background are changed very insignificantly in comparison with our analysis in Ref. [5] performed without consideration of the $\psi(2S)$- and $\Upsilon(2S)$-decays confirming our previous results. Parameters of the coupling functions of the decay particles (J/ψ, $\psi(2S)$ and $\Upsilon(2S)$) to channel i, obtained in the analysis, are $\alpha_2, \beta_2 = 0.0843, 0.0385$, $\gamma_{10}, \gamma_{11}, \gamma_{20}, \gamma_{21} = 1.1826, 1.2798, -1.9393, -0.9808, \delta_{10}, \delta_{11}, \delta_{20}, \delta_{21} = -0.127, 16.621, 5.983, -57.653, \rho_{10}, \rho_{11}, \rho_{20}, \rho_{21} = 0.405, 47.0963, 1.3352, -21.4343$.

The data on the di-pion mass distribution in decay $J/\psi \to \phi\pi\pi$, obtained by the BESIII collaboration with rather small errors, rejects dramatically the A solution with the narrower $f_0(600)$: the corresponding curve lies considerably below the data from the threshold to about 850 MeV. Therefore in the following we will discuss mainly the B solution.

Satisfactory description of all analyzed processes is obtained with the total $\chi^2/\text{NDF} = 568.57/(481 - 65) \approx 1.37$; for the $\pi\pi$ scattering, $\chi^2/\text{NDF} \approx 1.15$; for $\pi\pi \to K\overline{K}$, $\chi^2/\text{NDF} \approx 1.65$; for $\pi\pi \to \eta\eta$, $\chi^2/\text{ndp} \approx 0.87$; for decays $J/\psi \to \phi(\pi\pi, K\overline{K})$, $\chi^2/\text{ndp} \approx 1.21$; for $\psi(2S) \to J/\psi(\pi\pi)$, $\chi^2/\text{ndp} \approx 2.43$; for $\Upsilon(2S) \to \Upsilon(1S)\pi\pi$, $\chi^2/\text{ndp} \approx 1.01$.

The combined description of the 3-channel $\pi\pi$ scattering, decays $J/\psi \to \phi(\pi\pi, K\overline{K})$ from the Mark III, DM2 and BESIII, and the data on $\psi(2S)$- and $\Upsilon(2S)$-decays is practically the same as that in Ref. [5] performed without considering decays of excited ψ- and Υ-mesons. Therefore, here we show results of fitting only to the experimental data on the $\psi(2S)$- and $\Upsilon(2S)$-decays (Figs. 3 and 4).

Generally, *wide multi-channel states are most adequately represented by pole clusters*, as the pole clusters give the main effect of resonances. The pole positions are rather stable characteristics for various models, whereas masses and widths are very model-dependent for wide resonances. However, mass values are needed in some cases, e.g., in mass relations for multiplets. We stress that such parameters of the wide multi-channel states, as *masses, total widths and coupling constants with channels, should be calculated using the poles on sheets II, IV and VIII*, because only on these sheets the analytic continuations have the forms: $\propto 1/S_{11}^{\text{I}}$, $\propto 1/S_{22}^{\text{I}}$ and $\propto 1/S_{33}^{\text{I}}$, respectively, i.e., the pole positions of resonances are at the same points of the complex-energy plane, as the resonance zeros on sheet I, and are not shifted due to the coupling of channels. E.g., if the resonance part of amplitude is taken as $T^{res} = \sqrt{s}\, \Gamma_{el}/(m_{res}^2 - s - i\sqrt{s}\,\Gamma_{tot})$, for the mass and total width, one obtains $m_{res} = \sqrt{\text{E}_r^2 + (\Gamma_r/2)^2}$ and $\Gamma_{tot} = \Gamma_r$ where the pole position $\sqrt{s_r} = \text{E}_r - i\Gamma_r/2$ must be taken on sheets II, IV, VIII, depending on the resonance classification.
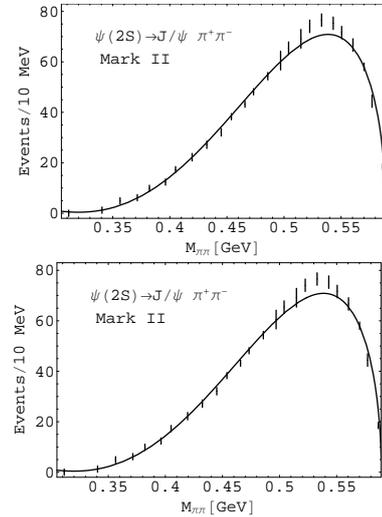

Figure 3: The $\psi(2S) \to J/\psi\pi\pi$ decays. Fitting to data [7].

Then masses and total widths are (in MeV): 693.9±10.0 and 931.2±11.8 for $f_0(600)$, 1008.1±3.1 and 64.0±3.0 for $f_0(980)$, 1399.0±24.7 and 357.0±74.4 for $f_0(1370)$, 1495.2±3.2 and 124.4±18.4 for $f_0(1500)$, 1539.5±5.4 and 571.6±25.8 for $f_0'(1500)$, 1733.8±43.2 and 117.6±32.8 for $f_0(1710)$.

4 Discussion and conclusions

In this combined analysis of data an additional confirmation of the $f_0(600)$ with mass about 700 MeV and width 930 MeV is obtained. This mass value accords with prediction ($m_\sigma \approx m_\rho$) on the basis of mended symmetry by Weinberg [16] and with an analysis using the large-N_c consistency conditions between the unitarization and resonance saturation suggesting $m_\rho - m_\sigma = O(N_c^{-1})$ [17]. Also, e.g., the prediction of a soft-wall AdS/QCD approach [18] for the mass of the lowest f_0 meson – 721 MeV – practically coincides with the value obtained in our work. Of course, such large width of this state is a problem. Maybe, we observe a superposition of two states – narrower σ-meson and wider state as it is the case in the 1500-MeV region.

Indication for $f_0(980)$ is obtained to be a non-$q\bar{q}$ state, e.g., the bound $\eta\eta$ state. The $f_0(1370)$ and $f_0(1710)$ have the dominant $s\bar{s}$ component that agrees with a number of experiments (see discussion in[3]). In the 1500-MeV region, there are two states: the $f_0(1500)$ ($m_{res} \approx 1495$ MeV, $\Gamma_{tot} \approx 124$ MeV) and the $f_0'(1500)$ ($m_{res} \approx 1539$ MeV, $\Gamma_{tot} \approx 574$ MeV). The $f_0'(1500)$ is interpreted as a glueball due to its biggest width among enclosing states [19].

We propose the following assignment of the scalar mesons to lower nonets, excluding the $f_0(980)$ as the non-$q\bar{q}$ state. The lowest nonet: the isovector $a_0(980)$, the isodoublet $K_0^*(900)$, and $f_0(600)$ and $f_0(1370)$ as mixtures of the 8th component of octet and the SU(3) singlet. The Gell-Mann–Okubo (GM-O) formula $3m_{f_8}^2 = 4m_{K_0^*}^2 - m_{a_0}^2$ gives $m_{f_8} = 870$ MeV. In relation for masses of nonet $m_\sigma + m_{f_0(1370)} = 2m_{K_0^*(900)}$ the left-hand side is by about 14% bigger than the right-hand one. For the next nonet we find: the isovector $a_0(1450)$, the isodoublet $K_0^*(1450)$, and two isoscalars $f_0(1500)$ and $f_0(1710)$. From the GM-O formula, $m_{f_8} \approx 1450$ MeV. In formula $m_{f_0(1500)} + m_{f_0(1710)} = 2m_{K_0^*(1450)}$ the left-hand side is by about 10% bigger than the right-hand one. This assignment removes a number of questions, stood earlier, and does not put any new.
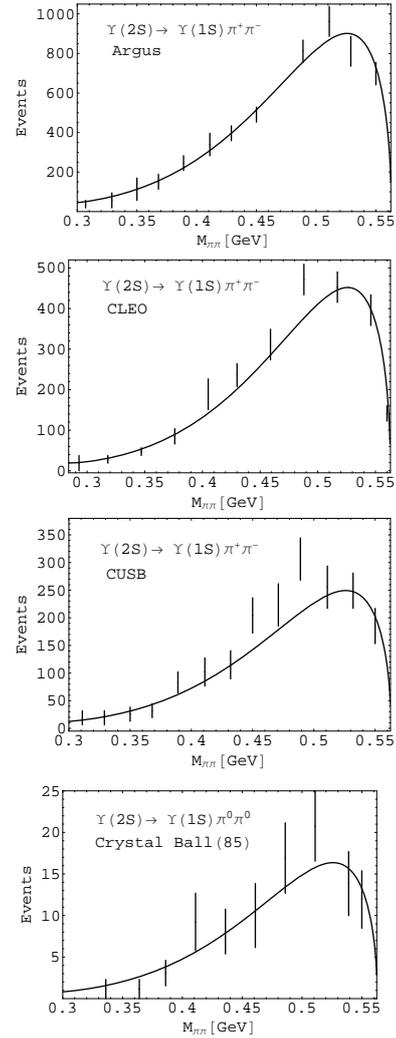

Figure 4: The $\Upsilon(2S) \rightarrow \Upsilon(1S)\pi\pi$ decays. Fitting to data [8].

References

[1] J. Beringer et al. (PDG), Phys. Rev. **D86** 010001 (2012).

[2] Yu.S. Surovtsev, P. Bydžovský, R. Kamiński, and M. Nagy, Phys. Rev. **D81** 016001 (2010).

[3] Yu.S. Surovtsev, P. Bydžovský and V.E. Lyubovitskij, Phys. Rev. **D85** 036002 (2012).

[4] Yu.S. Surovtsev, P. Bydžovský, R. Kamiński, V.E. Lyubovitskij, and M. Nagy, arXiv:1206.3438[hep-ph] (2012); Phys. Rev. **D86** 116002 (2012).

[5] Yu.S. Surovtsev, P. Bydžovský, R. Kamiński, V.E. Lyubovitskij, and M. Nagy, arXiv:1207.6937[hep-ph] (2012).

[6] W. Lockman (Mark III), Proceedings of the Hadron'89 Conference, ed. F. Binon et al. (Editions Frontières, Gif-sur-Yvette,1989) p.109; A. Falvard et al. (DM2), Phys. Rev. **D38** 2706 (1988); M. Ablikim et al. (BES III), Phys. Lett. **B607** 243 (2005).

[7] G. Gidal et al. (Mark II), Phys. Lett. **B107** 153 (1981); M. Oreglia et al. (Crystal Ball(80)), Phys. Rev. Lett. **45** 959 (1980).

[8] H. Albrecht et al. (Argus), Phys. Lett. **B134** 137 (1984); D. Gelphman et al. (Crystal Ball(85)), Phys. Rev. **D32** 2893 (1985); D. Besson et al. (CLEO), Phys. Rev. **D30** 1433 (1984); V. Fonseca et al. (CUSB), Nucl. Phys. **B242** 31 (1984).

[9] N.N. Achasov, Nucl. Phys. **A675** 279c (2000).

[10] R.L. Jaffe, Phys. Rev. **D15** 267, 281 (1977).

[11] D. Krupa, V.A. Meshcheryakov and Yu.S. Surovtsev, Nuovo Cim. **A109** 281 (1996).

[12] M. Kato, Ann. Phys. **31** 130 (1965).

[13] D. Morgan and M.R. Pennington, Phys. Rev. **D48** 1185, 5422 (1993).

[14] K.J. Le Couteur, Proc. R. London, Ser. A **256** 115 (1960); R.G. Newton, J. Math. Phys. **2** 188 (1961).

[15] N.N. Achasov and G.N. Shestakov, Phys. Rev. **D49** 5779 (1994).

[16] S. Weinberg, Phys. Rev. Lett. **65** 1177 (1990).

[17] J. Nieves and E.R. Arriola, Phys. Rev. **D80** 045023 (2009).

[18] T. Gutsche, V.E. Lyubovitskij, I. Schmidt, and A. Vega, Phys. Rev. **D87** 056001 (2013); arXiv:1212.5196 [hep-ph] (2012).

[19] V.V. Anisovich et al., Nucl. Phys. A (Proc Suppl.) **56** 270 (1997).

The Latest Results of the ATLAS Experiment on Heavy Quark Physics

Stano Tokar on behalf of the ATLAS Collaboration

Comenius University, FMPI, Mlynska dolina F1, 94248 Bratislava, Slovakia

The latest experimental results obtained by the ATLAS Collaboration using the data produced in pp collisions at $\sqrt{s} = 7$ and 8 TeV are shown. The data were collected by the ATLAS detector in 2011 (7 TeV) and 2012 (8 TeV) with the integrated luminosity of 4.9 fb^{-1} and 21 fb^{-1}, respectively. The main emphasis is on the top and bottom quark physics but the Higgs boson physics and searches of physics beyond the Standard Model are also reported. A lot of new results on the top quark and bottom quark physics are shown and new confirmation are given that the new boson seen at 125 GeV is compatible with the Standard Model Higgs boson at confidence level better than 7σ. No signs of physics beyond the Standard Model found.

1 Introduction

The Large Hadron Collider (LHC) experiments have started a new era of particle physics. The high collision energy available at LHC (7-14) GeV together with the high luminosity allow progress to be made in investigation of the main challenges of particle physics such as the status of the Higgs boson, precision tests of the Standard Model (SM), searches for new physics.

In the pre-LHC era there was a very good agreement between the experimental results and the SM predictions – see the pulls of Quantum Chromodynamics (QCD) and Electroweak (EW) observables in Ref. [1]. All the expected fundamental fermions in three generations and the expected gauge bosons have been experimentally confirmed. The only missing particle was the Higgs boson. Existence of the Higgs boson is critical for the SM as particles acquire mass by interacting with Higgs field which has non-zero vacuum expectation value. This mechanism, called usually Higgs mechanism, is responsible for electroweak symmetry breaking (EWSB). The discovery of a new boson with properties compatible with the SM Higgs boson announced by ATLAS and CMS in July 2012 has filled the last missing piece of the SM.

The SM, despite its success, is widely believed to be only an effective theory valid at the presently accessible energies. It has no appropriate answer to the global questions like the dark matter, baryon asymmetry and dark energy, it does not include the gravitational force, and it does not explain the pattern of fermion masses and the number of generations. The theory has no expplanation for the naturalness (or hierarchy) problem of the Higgs mass. Higgs mass corrections ($\triangle m_{\mathrm{H}}^2$) coming from the heaviest particles (mainly the top quark) are quadratically divergent: $\triangle m_{\mathrm{H}}^2 \sim \Lambda_{\mathrm{UV}}^2$, where Λ_{UV} is the ultraviolet cutoff for loop momentum integration. Among the suggestions to solve this problem the most attractive are approaches presented by Supersymmetry (SUSY) and extra dimensional (ED) models (see Sec. 4).

In the search for a manifestation of a BSM physics, a special role is played by processes with top quarks and b-quarks. Many BSM physics scenarios, if occur, could change significantly these

processes. BSM physics could significantly modify the forward - backward asymmetry in $t\bar{t}$ and $b\bar{b}$ production, the spin correlation in $t\bar{t}$ production, the size of the top quark decay width, the polarization of W bosons from the top quark decays, etc. Processes with b-quarks are important especially for a better understanding of CP violation phenomena and rare decays which, being suppressed in the SM, can be sensitive to BSM physics, e.g. the decay $B^0_{d(s)} \to \mu^+\mu^-$. The results of the ATLAS studies of processes with top quarks and b-quarks are main goal of this contribution.

2 The ATLAS Detector

The ATLAS detector [2] is a multipurpose particle physics apparatus operating at one of the beam interaction points of the LHC. It covers almost the entire solid angle around the collision point. ATLAS uses a right-handed coordinate system with its origin in the centre of the detector (the nominal interaction point) and the z-axis along the beam pipe. The x-axis points from the coordinate system origin to the centre of the LHC ring, and the y-axis points upward.

The innermost part of this detector is an inner tracking detector (ID) comprised of a silicon pixel detector, a silicon microstrip detector, and a transition radiation tracker. The ID covers the pseudo-rapidity[1] range $\mid \eta \mid< 2.5$ and is surrounded by a thin superconducting solenoid providing a 2 T magnetic field, and by liquid-argon electromagnetic sampling calorimeters with high granularity (LAr). An iron-scintillator tile calorimeter provides hadronic energy measurements in the central pseudorapidity range ($\mid \eta \mid< 1.7$). The end-cap and forward regions are instrumented with LAr calorimetry for both electromagnetic (EM) and hadronic energy measurements up to $\mid \eta \mid= 4.9$. The calorimeter system is surrounded by a muon spectrometer incorporating three superconducting toroid magnet assemblies, with bending power between 2.0 and 7.5 Tm and the pseudorapidity coverage is: $\mid \eta \mid< 2.7$.

3 Higgs boson search

The most significant results on the Higgs (H) boson search are obtained for the H boson decay to two photons ($H \to \gamma\gamma$) and its decay to four leptons ($H \to ZZ^* \to 4l$). In the analyses the proton-proton (pp) collision datasets corresponding to integrated luminosities of 4.8 fb^{-1} collected at $\sqrt{s} = 7$ TeV and 20.7 fb^{-1} collected at $\sqrt{s} = 8$ TeV have been used. Figure 1 shows the two-photon invariant mass, $m_{\gamma\gamma}$, for the combination of $\sqrt{s} = 7$ and 8 TeV data with the new boson clearly seen. The largest local significance of the effect for the data sample combination is 7.4σ at the H boson mass M_H =126.5 GeV

Figure 1: Two photon $m_{\gamma\gamma}$ spectrum.

[3]. Combining the H boson decay channels the $H \to \gamma\gamma$ and $H \to ZZ^{(*)} \to 4l$ channels the local significance exceeds 8σ and the combined mass is measured to be $M_H = 125.5 \pm 0.2(\text{stat}) \pm 0.6(\text{syst})$ GeV. For comparison the combined M_H measured by CMS experiment is $M_H = 125.7 \pm 0.3(\text{stat.}) \pm 0.3(\text{syst.})$ GeV. To confirm that the observed new boson is the H boson predicted by the SM, the global signal strength parameter, μ, as well as the strength parameters, μ_i, for the individual channels and a fixed mass M_H have been measured. The signal strength is defined as a ratio of the measured cross section for a given channel characterized by production and decay modes to that expected for the SM. Its value measured by ATLAS,
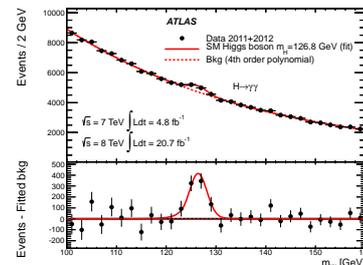
---

[1]The pseudorapidity is defined in terms of the polar angle θ as $\eta = -ln(tan(\theta/2))$

combining the individual channel strength parameters, is $\mu = 1.30 \pm 0.20$, a good compatibility with the SM ($\mu = 1$). An important test of the status of the new boson is the parity-spin determination. For the SM H boson this quantity is: $J^{\mathrm{P}} = 0^+$. The ATLAS and CMS experiments strongly favor $J^{\mathrm{P}} = 0^+$ for the new observed boson. The alternatives $J^{\mathrm{P}} = 0^-,\ 1^-,\ 1^+,\ 2^+$ are excluded at the 95 % confidence level (C.L.). Details of the H boson studies carried out by ATLAS and CMS can be found on their public results web pages [4, 5].

Though the experiments clearly favor the SM hypothesis, questions on the nature of H boson are still relevant. Is the H boson a fundamental boson or is it a composite boson with a new underlying dynamics? For a better understanding of these issues the planned increase in collision energy to 13-14 GeV and integrated luminosity to 300 fb^{-1} is vital.

4   Search of physics beyond the Standard model

The search for physics beyond the SM is a most important task of the ATLAS experiment. Searches are carried out in many directions, among the most promising are the searches within the SUSY and ED approaches.

Search for SUSY particles. The SUSY models [6, 7] are very attractive as they offer a recipe for the naturalness and have a candidate for solution of the dark matter problem. In the former case the large corrections to M_{H} from the top quark loops are compensated by the loop contributions from the SUSY top quark partner - top squark, provided that its mass is not far from the top quark mass. SUSY (R-parity conservation models) predicts pair production of SUSY particles and as a consequence of the lightest SUSY particle (LSP) being stable and serving as a candidate for the dark matter particle. In the minimal SUSY extension of the SM (MSSM) [8] such a particle is neutralino $\tilde{\chi}_1^0$.

The search for the top squark has been carried out by ATLAS in many final states. The superpartners of the left- and right-handed top quarks, $\tilde{t}_{\mathrm{L}}$ and $\tilde{t}_{\mathrm{R}}$, mix to form the two mass eigenstates $\tilde{t}_1$ and $\tilde{t}_2$, where $\tilde{t}_1$ is the lighter one. The pair produced top squarks, $\tilde{t}_1$, are assumed to decay to a top quark and a neutralino ($\tilde{t}_1 \rightarrow t + \tilde{\chi}_1^0$) or to a bottom quark and a chargino ($\tilde{t}_1 \rightarrow b + \tilde{\chi}_1^{\pm}$). An example of such a search, carried out by ATLAS at pp collision energy of 8 TeV on 20.7 fb^{-1} of data, is shown in Figure 2 where the mass limits on the top squark are presented. Assuming both the top squarks decay to a top quark and an LSP, the top

Figure 2: Limits on the top squark mass.

squark masses between 200 and 610 GeV are excluded at 95% C.L. for massless LSPs, and the masses below 500 GeV are excluded for the LSP masses up to 250 GeV. Assuming both the top squarks decay to a bottom quark and the lightest chargino, the top squark masses are excluded up to 410 GeV for massless LSPs and an assumed chargino mass of 150 GeV.

Search for non-SUSY new physics. The hierarchy problem can be solved within the theories with extra dimensions. In the ADD model [9] this problem is solved by lowering the fundamental scale of quantum gravity, M_{D}, to a few TeV instead of $M_{\mathrm{P}} = 10^{19}$ TeV. If M_{D} is of the order of 1 TeV, evaporating fast microscopic black holes (μBH) are predicted to be produced at LHC. The μBH are produced when the impact parameter of the two colliding partons is smaller than the Schwarchild radius of μBH ($R_{\mathrm{S}} = 2G_{\mathrm{N}}M_{\mathrm{BH}}/c^2$, G_{N} is gravitational

constant, $M_{\rm BH}$ is the μBH mass). An example of a search for μBH in ATLAS is the analysis carried out in a like-sign dimuon final state [10]. The search for μBH has been carried out using the data sample of 20.3 fb^{-1} at 8 TeV. No excess of events over the SM expectations has been observed. Assuming $M_{\rm D} = 1.5$ GeV a limit on the μBH mass is found to be 5 TeV.

An example of an ATLAS search for a new physics predicted by Technicolor [11], is the search for a resonant production of two high transverse momentum jets in association with a SM W or Z boson decaying leptonically. In this model a spin 1 particle called technirho ($\rho_{\rm T}$) decays into a lighter technimeson (technipion $\pi_{\rm T}$) and a SM W or Z boson, if the $\rho_{\rm T}$ mass is larger than the sum of the $\pi_{\rm T}$ and gauge boson masses. In the ATLAS search for resonant dijet production in $Wjj \rightarrow l\nu jj$ and $Zjj \rightarrow lljj$ ($l = e, \mu$) events [12], a data-set of 20.3 fb^{-1} at 8 TeV has been analysed, but no significant deviation from the SM background prediction is observed in the m_{jj} spectra. The upper limit (95% C.L.) for the technipion is 180 GeV for the Wjj channel and 170 GeV for the Zjj one under the assumption of $m_{\rho_{\rm T}} = 3/2 \times m_{\pi_{\rm T}} + 55$ GeV.

From the ATLAS and CMS searches at energies 7 and 8 TeV for the new physics phenomena, can be concluded that no hints of a physics beyond the SM are seen. Details can be found on the public results web-sides of the ATLAS and CMS experiments [4, 5].

5   Top quark physics studies

Top quark physics is one of the most important subjects presently studied at LHC. The top quark properties are still not known properly and the top quark is in many respects an extraordinary particle:

- The mass of top quark ($m_{\rm top}$) is very big - it is close to the EWSB scale. Its Yukawa coupling, $\lambda_{\rm t} = \sqrt{2}m_{\rm top}/\eta \approx 1$.
- The top quark is an excellent perturbative object for testing QCD as it is produced at small distances ($\sim 1/m_{\rm top}$) characterized by low value of coupling constant $\alpha_{\rm S} \approx 0.1$.
- It decays before hadronization: the production time ($1/m_{\rm top}$) < lifetime ($1/\Gamma_{\rm top}$) < hadronization time ($1/\Lambda_{\rm QCD}$). It permits study of spin characteristics of the top quark as it is not diluted by hadronization (test of the top production mechanisms) or measurement of W boson helicity (test of the EW V-A structure).
- the $t\bar{t}$ production cross section is sensitive to new physics, e.g. resonant production of $t\bar{t}$ pairs would be a hint of existence of a new boson (KK-gravitons, etc.) or the decay $t \rightarrow H^{+}b$ would indicate presence of a charged Higgs boson.

In addition, the top quark processes are a very important background for the Higgs processes. It can be concluded that the top quark physics can provide stringent tests of the SM as well as it is an excellent platform for searches for new physics.

The top quark decays rapidly (the decay width is $\Gamma(t \rightarrow Wb) = 1.42$ GeV [15]) without forming hadrons and almost exclusively through the mode $t \rightarrow Wb$, where the b-quark hadronizes producing shower of particles called b-jet and the W boson decays leptonically or hadronically. From the experimental point of view the $t\bar{t}$ events are classified according to the W bosons decays dividing them into three channels: the dilepton channel (D-L) – both W decay leptonically, the lepton+jets channel (L+J) – one W decays leptonically and the other one hadronically, and the all-hadronic channel (A-H) – both W decay hadronically.

Top quark pair production cross section. The top quark is produced via strong interactions mediated through gluon (production of $t\bar{t}$ pair) and in the electroweak ones (single top quark production). In the former case the main production mechanisms are : the quark annihilation ($q\bar{q} \rightarrow t\bar{t}$) and gluon fusion($gg \rightarrow t\bar{t}$). In the latter case the production is mediated

by W boson (e.g. $u\bar{d} \to W^+ \to t\bar{b}$). The top quark production cross section is calculated using the so-called factorization theorem:

$$\sigma = \sum_{i,j} \int dx_1 dx_2 F_i^{(1)}(x_1, \mu_F) F_j^{(2)}(x_2, \mu_F) \hat{\sigma}_{ij}(s; \mu_F, \mu_R), \qquad (1)$$

where $F_i^{(\lambda)}(x_1, \mu_F)$ is the probability density to observe a parton i with longitudinal momentum fraction x_λ in incoming hadron λ, when probed at a scale μ_F, μ_F is the factorization scale (a free parameter) - it determines the proton structure if probed (by virtual

Cross section	2 TeV	7 TeV	8 TeV	14 TeV
$t\bar{t}$ [nb]	7.2	172.0	245.8	953.6
single top [nb]	3.0	84.9	115.7	320.0

Table 1: Top quark production cross section for the energies: 2 TeV (Tevatron) and 7, 8 and 14 TeV (LHC), for the $t\bar{t}$ production and for the single top quark one (single top).
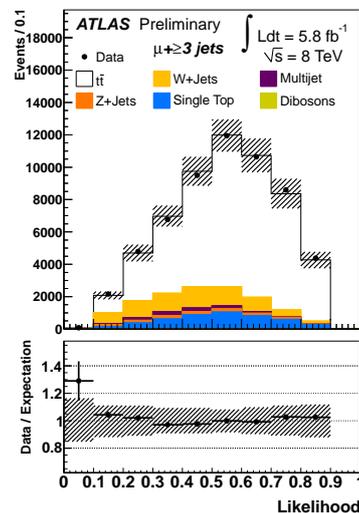
photon or gluon) with $q^2 = -\mu_F^2$, μ_R is the renormalization scale defining size of the strong coupling constant and $\hat{\sigma}_{ij}(s)$ is the partonic cross section.

Eq. 1 connects the experimentally measured cross section with the theoretical one and the proton structure functions. The theoretical $t\bar{t}$ partonic cross section is now calculated at the next-to-next-to-leading order (NNLO) with the next-to-next-to-leading logarithmic approximation (NNLL) [13]. The predicted $t\bar{t}$ production cross sections and the single top quark ones [14] are summarized in Table 1. The uncertainty of the theoretical calculations is 4% in the $t\bar{t}$ case and 3-4% in the single top one. The $t\bar{t}$ cross section analysis is carried out in all three above mentioned channels (the L+J, D-L and A-H channels). The most precise results are obtained for the L+J channel. The analysis is based on single lepton high transverse momentum (high p_T) trigger. The following reconstructed objects are required [16]: one high-p_T lepton, at least four high-p_T jets, one or two of them b-tagged, and high missing transverse energy E_T^{miss}. Electrons were required to have transverse energy $p_T > 40$ GeV and pseudorapidity in the range $|\eta| < 2.47$ excluding the region $1.37 < |\eta| < 1.52$. Muons were reconstructed using information from the muon spectrometer and the inner detector. They were required to have transverse momentum $p_T > 40$ GeV

Figure 3: Likelihood discriminant distributions in data in μ+jets channel used for the $t\bar{t}$ cross section determination. The hatched bands display the combined statistical and systematic uncertainty.

and pseudorapidity $|\eta| < 2.5$. The main background processes at this study are W boson + jets, Z boson + jets, diboson, single top quark and multi-jet production. The background processes are studied using MC dedicated samples and using a data driven technique [17].

The measured cross section, $\sigma_{t\bar{t}}$, is determined using the likelihood discriminant to separate signal events from the background ones and then a procedure is used based on the relation:

$$\sigma_{t\bar{t}} = \frac{N_{obs} - N_{bkg}}{A \cdot \epsilon \cdot \int L.dt}, \qquad (2)$$

where N_{obs} (N_{bkg}) is the number of the observed candidate (expected background) events, A is the acceptance, ϵ is the trigger efficiency and $\int Ldt$ is the integrated luminosity.

The analysis was carried out using the data sample of 5.8 fb^{-1} at the pp collision energy of 8 TeV. Figure 3 shows the likelihood discriminant distribution in data fitted to the sum of the signal and background templates for the μ+jets channel. The cross section is found to be

$$\sigma_{t\bar{t}} = 241 \pm 2(\text{stat.}) \pm 31(\text{syst.}) \pm 9(\text{lumi.}) \text{ pb}.$$

This result is in excellent agreement with the theoretical prediction [13]: $\sigma_{t\bar{t}}^{\text{theo}} = 245.8^{+6.2}_{-8.4}$ (stat.) $^{+6.2}_{-8.4}$ (pdf) pb as well as with the CMS results obtained in L+J (2.8 fb^{-1}) [18] and D-L (2.4 fb^{-1}) [19] channels: $\sigma_{t\bar{t}} = 228 \pm 9(\text{stat.}) \pm 29(\text{syst.}) \pm 10(\text{lumi.})$ pb and $\sigma_{t\bar{t}} = 227 \pm 3(\text{stat.}) \pm 11(\text{syst.}) \pm 10(\text{lumi.})$ pb, respectively.

The $t\bar{t}$ cross section measurements were carried out also at the collision energy of 7 TeV for different channels [20]. The measured $t\bar{t}$ cross sections at 7 and 8 TeV are summarized in Figure 4, where they are compared to the exact NNLO QCD calculation complemented with NNLL resummation [21]. The differential $t\bar{t}$ production cross section was also measured giving good agreement with the SM expectations, details are in Ref. [22].

Measurement of top quark mass. The top quark mass, m_{top}, is one of the SM parameters and is important also for the consistency tests of the SM (indirect determination of the Higgs boson mass). It is reconstructed from the invariant mass of the top quark decay products.

The top quark mass can be reconstructed in all $t\bar{t}$ topologies (L+J, D-L, A-H). The best results are usually obtained in L+J topology. The most common methods used to reconstruct m_{top} are template methods and matrix element methods. In the former case, the method is based on distributions of an observable sensitive to m_{top} (signal templates) for different m_{top} values. Data distribution of this sensitive observable is compared to a combination of the signal and background templates and the best agreements defines the mass (see further for an example). In the latter case, a dependence of the top pair production cross section on top quark mass is used to extract m_{top}. In addition, any variable correlated with top quark mass can be used for determination of m_{top}, e.g. mean lepton p_{T}. An interesting example of an application of the template method is the ATLAS measurement of m_{top} carried out for the $t\bar{t}$ lepton+jets channel using the data sample of 4.7 fb^{-1} at 7 TeV. It is so-called 3-D template method using an approach based on observables $m_{\text{top}}^{\text{reco}}$, $m_{\text{W}}^{\text{reco}}$ and $R_{\text{lb}}^{\text{reco}}$ [23]. The reconstructed top quark mass is found to be

$$m_{\text{top}} = 172.31 \pm 0.75 \text{ (stat+JSF)} \pm 1.35 \text{ (syst) GeV}$$

The first uncertainty corresponds to a combined uncertainty of the statistics, jet energy scale and b-jet energy scale. In ATLAS the analyses on the top quark mass determination are carried out not only in the L+J channel but also in the D-L and A-H channels (see in Ref. [4]). The results of the ATLAS measurements are compared with the CMS and Tevatron results in Figure 5.
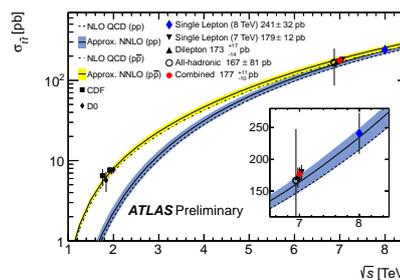

Figure 4: Summary of ATLAS measurements of the $t\bar{t}$ production cross-section at 7 and 8 TeV compared to an approximate NNLO QCD calculations as a function of $\sqrt{s}$.
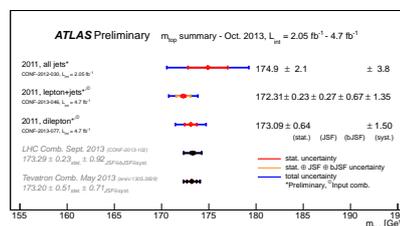

Figure 5: Summary of the ATLAS top quark mass measurements compared with the LHC and Tevatron averages.

5.1 Single top quark results

The single top-quark production occurs via EW interaction. There are three sub-processes contributing to this production: the exchange of a virtual W boson in the t-channel, or in the s-channel, and the associated production of a top quark and an on-shell W boson. The process with the highest expected cross section at the LHC is the t-channel mode.

Among the virtues of the single top quark production are: (1) its cross section is proportional to $\mid V_{tb} \mid^2$, where V_{tb} is an element of the Cabbibo-Kobayashi-Maskawa (CKM) matrix [24] so it enables a direct measurement of this CKM matrix element, (2) charge asymmetry in production of t with respect to $\bar{t}$ is sensitive to the proton u- and d-quark PDFs, and (3) is sensitive to many models of new physics [25]. In addition, the single top quark processes are an important background for Higgs boson studies.
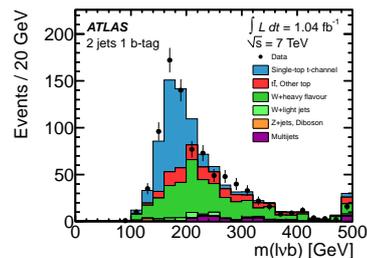

Figure 6: The invariant mass $m(\ell\nu b)$ distribution for the 2-jet b-tagged sample - the signal and different backgrounds are compared.

An example of the ATLAS single top quark studies is the analysis of the t-channel process [26] using 1.04 fb^{-1} of pp collision data at $\sqrt{s} = 7$ TeV and using 5.8 fb^{-1} at $\sqrt{s} = 8$ TeV [27]. The study is based on event selection requiring one charged lepton candidate, e or μ, two or three hadronic high-p_{T} jets; and missing transverse momentum $E_{\mathrm{T}}^{\mathrm{miss}}$. The measurement of the cross section, σ_t, is based on a fit to a multivariate discriminant constructed with a neural network (NN) to separate signal from background. The most significant background comes from from W-boson production in association with jets .

Other significant backgrounds comes from multijet events and $t\bar{t}$ production. Figure 6 shows the invariant mass of the b-tagged jet, the charged

Energy	σ_t [pb]	$\mid V_{tb} \mid$
7 TeV	$83.0 \pm 4(\text{stat}) \, ^{+20}_{-19}(\text{syst})$	$1.13^{+0.14}_{-0.13}(\text{exp}) \pm 4(\text{syst})$
8 TeV	$95.1 \pm 2.4(\text{stat.}) \, \pm 18(\text{syst.})$	$1.04^{+0.10}_{-0.11}(\text{exp.})$

Table 2: Single top quark production cross sections (σ_t) measured by ATLAS at 7 and 8 TeV and the extracted CKM element $\mid V_{tb} \mid$.

lepton, and the neutrino, $m(\ell\nu b)$, for the 2-jet b-tagged sample at 7 TeV. Table 2 shows the t-channel cross sections at $\sqrt{s} = 7$ and 8 TeV inferred from simultaneous measurements in the 2-jet and 3-jet channels applying a NN-based analysis. Even at 7 TeV the significance of the observed signal corresponds to 7.2σ. The lower limit of $\mid V_{tb} \mid$ at 95% C.L. is 0.75 at 7 TeV and $\mid V_{tb} \mid > 0.80$ at 95% C.L. at 8 TeV.

Measurement of the separate t and $\bar{t}$-quark cross sections, $\sigma_t(t)$ and $\sigma_t(\bar{t})$, was carried out by ATLAS using the data sample of 4.7 fb^{-1} at 7 TeV [28]. The separate cross sections are sensitive to the u- and d-quark PDFs an the SM expectations are $\sigma_t(t) = 41.9^{+1.8}_{-0.8}$ pb and $\sigma_t(\bar{t}) = 22.7^{+0.9}_{-1.0}$ pb. The multivariate technique combining several kinematic variables into one neural network discriminant was used. The obtained cross sections $\sigma_t(t)$ and $\sigma_t(\bar{t})$ are:

$$\sigma_t(t) = 53.2 \pm 1.7(\text{stat.}) \pm 10.7(\text{syst.}) \text{ pb}, \quad \sigma_t(\bar{t}) = 29.5 \pm 1.5(\text{stat.}) \pm 7.3(\text{syst.}) \text{ pb}.$$

The cross sections are, within uncertainties, compatible with the SM expected ones and give the ratio $R_t = \sigma_t(t)/\sigma_t(\bar{t}) = 1.81 \pm 0.10(\text{stat.}) \, ^{+0.14}_{-0.13}(\text{syst.})$.

5.2 Top quark properties

Study of the top quark properties enables a test of the SM predictions and search for new physics which can modify the top quark production mechanisms, the Wtb coupling, the top quark decays, etc.

W **boson helicity fractions.** In the SM (NNLO) the W boson helicity fractions are predicted to be [29]:

$$F_0 = 0.687 \pm 0.005, F_L = 0.311 \pm 0.005 \text{ and } F_R = 0.0017 \pm 0.0001.$$

The fractions F_0, F_L and F_R are extracted from angular distributions of top quark decay products:

$$\frac{1}{\sigma}\frac{d\sigma}{d\theta^\star} = \frac{3}{4}\left(1 - cos^2\theta^\star\right)F_0 \\ + \frac{3}{8}\left(1 - cos\theta^\star\right)^2 F_L + \frac{3}{8}\left(1 + cos\theta^\star\right)^2 F_R, \quad (3)$$

where $\theta^\star$ is the angle between the lepton and b-quark reversed momentum in the W boson rest frame. The ATLAS measurement of the W helicity fractions carried out using the data of 1.04 fb^{-1} at 7 TeV and taking into account L+J and D-L events [30] resulted in

$$F_0 = 0.67 \pm 0.03 \pm 0.06, F_L = 0.32 \pm 0.02 \pm 0.02,$$
$$F_R = 0.01 \pm 0.01 \pm 0.04 \; (\pm\text{stat} \pm \text{syst}).$$

Figure 7: Overview of the measurements included in the combination as well as the results of the combination (see text).

The ATLAS W boson helicity result is compared with other results (CMS, ATLAS dilepton and LHC combination [31]) in Figure 7 giving good agreement of the LHC data with the SM.

Anomalous Wtb couplings. Any deviation of F_0, F_L and F_R from their SM values is a sign of a new physics. In general the new physics contributing to the Wtb coupling can be generally expressed through an effective lagrangian:

$$L_{Wtb} = \frac{g}{\sqrt{(2)}}\bar{b}\gamma^\mu \left(V_L P_L + V_R P_R\right) t \cdot W_\mu^- \\ + \frac{g}{\sqrt{(2)}}\bar{b}\frac{i\sigma^{\mu\nu}q_\nu}{M_W}\left(g_L P_L + g_R P_R\right) t \cdot W_\mu^+ + h.c.,$$

Figure 8: Allowed regions at 68% and at 95% C.L. for the couplings g_R and g_L.

In the SM at tree level $V_L = V_{tb} \approx 1$ and $V_R = g_L = g_R = 0$. The limits on the anomalous coupling are inferred from measurement of the helicity fractions using their dependence on the couplings. The ATLAS limits on the anomalous couplings obtained using the data sample of 1.04 fb^{-1} recorded at 7 TeV [30] are shown in Figure 8.

Spin correlation in $t\bar{t}$ events. While the polarization of the t and $\bar{t}$ quarks in $t\bar{t}$ production is predicted to be very small, their spins are predicted be correlated [32]. The analysis carried out by ATLAS [33] uses a data sample of 2.1fb^{-1} collected at 7 TeV. The search was performed in the dilepton topology ($t\bar{t} \to \ell^+\nu\ell^-\bar{\nu}b\bar{b}$) with large E_T^{miss} and at least two jets. The observable studied was the azimuthal angle between two leptons, $\Delta\phi$. The measured degree of correlation is found in the helicity and the maximal bases (see details in Ref. [33]):

$$A_{\text{helicity}} = 0.40 \pm 0.04(\text{stat.})^{+0.08}_{-0.07}, \text{ the SM expected: } A_{\text{helicity}}^{\text{SM}} = 0.31$$
$$A_{\text{maximal}} = 0.57 \pm 0.06(\text{stat.})^{+0.12}_{-0.10}, \text{ the SM expected: } A_{\text{maximal}}^{\text{SM}} = 0.44$$
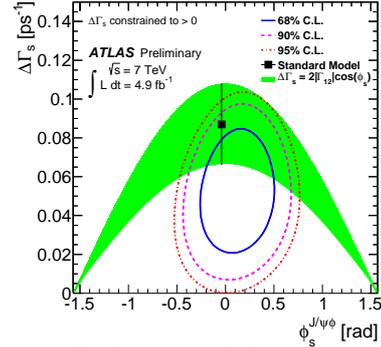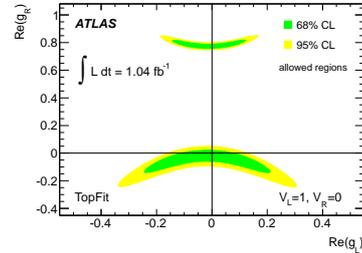
The measured values are compatible within uncertainties with the SM expectations.

Top quark charge. The main issue in the top quark charge study is determination between the SM scenario with decaying top quark having the electric charge of 2/3 (in units of the electron charge magnitude), $t \rightarrow W^+ b$, and the exotic one with an exotic quark having the charge of -4/3, $t_{\mathrm{X}} \rightarrow W^- \bar{b}$. The study carried out by ATLAS, using the data of 2.05 fb^{-1} at $\sqrt{s} = 7$ TeV [34], is based on exploiting of the charges of the top quark decay products (W boson and b-quark). The charge of the W boson is determined through charge of the lepton from its leptonic decay ($W^{\pm} \rightarrow \ell^{\pm} \nu_{\ell}$). The b-quark charge cannot be determined directly, but it should be correlated with an effective charge of b-jet found using a charge weighting procedure. Within this procedure the charges of tracks belonging to a b-jet cone are weighted using their momentum projection into the b-jet axis giving finally an effective b-jet charge. The observable which is used to distinguish between the SM top quark and the exotic one is $Q_{\mathrm{comb}} = Q_{\ell} \times Q_{b-\mathrm{jet}}$, where Q_{ℓ} and $Q_{b-\mathrm{jet}}$ are the charge of lepton and effective charge of b-jet. The lepton and b-jet should come from the same decaying quark, what is provided by fulfilling a lepton b-jet pairing condition based on the lepton–b-jet invariant mass ($m(\ell, b-\mathrm{jet})$ which should be (within resolution) less than m_{top}, if lepton and b-jet are top quark decay products. The analysis was performed in the L+J channel and the experimentally observed value is $Q_{\mathrm{comb}}^{\mathrm{obs}}$ = -0.077 $\pm$ 0.005, which is in excellent agreement with the SM expected value: $Q_{\mathrm{comb}}^{\mathrm{SM}}$ = -0.075 $\pm$ 0.004. For the exotic model a positive value is expected: $Q_{\mathrm{comb}}^{\mathrm{XM}}$ = +0.069 $\pm$ 0.004. Taking into account all statistical and systematic uncertainties, the statistical analysis excluded the exotic model with more than 8σ C.L.

From the value of $Q_{\mathrm{comb}}^{\mathrm{obs}}$ assuming the b-quark charge of -1/3, the value of the top quark charge was inferred: $Q_{\mathrm{top}} = 0.64 \pm 0.02$ (stat.) ± 0.08 (syst.)

6 Study of b-quark results

Study of B-physics is interesting from many respects but the most attractive are processes connected with the violation of CP symmetry and with the physics beyond the SM.

Dimuon decay of B_{S}^0 meson. The decay $B_{\mathrm{S}}^0 \rightarrow \mu^+ \mu^-$ is highly suppressed in the SM and its branching ratio $BR(B_{\mathrm{S}}^0 \rightarrow \mu^+ \mu^-) = (3.5 \pm 0.3) \times 10^{-9}$. To observe a deviation from the SM branching would mean a manifestation of a new physics. The ATLAS analysis of this decay is based on a dimuon trigger using a data sample of 4.9 fb^{-1} at 7 TeV [35]. The branching $BR(B_{\mathrm{S}}^0 \rightarrow \mu^+ \mu^-)$ is measured with respect to the well-known reference decay $B^{\pm} \rightarrow J/\psi K^{\pm}$.

The main background comes from $b\bar{b} \rightarrow \mu^+ \mu^- X$ and from b-hadron decay with one or two hadrons misidentified as muons. Multivariate technique using a Boosted Decision Tree (BDT) was applied to select candidate events. The discriminating variable used by the BDT takes into account that the decay vertex of $B_{\mathrm{S}}^0 \rightarrow \mu^+ \mu^-$ is separated from event primary vertex and that it is two body decay. Using the full data sample at 7 TeV the extracted limits are:

$$BR(B_{\mathrm{S}}^0 \rightarrow \mu^+ \mu^-) < 1.5 \times 10^{-8} \text{ at } 95\% \text{ C.L.}$$

After inclusion of the data sample of 21 fb^{-1} at 8 TeV a comparable result with those obtained by LHCb [36] and CMS [37], i.e. to see a value of the branching not only a limit, is expected.

Cross section of b-hadron production. The b-hadron cross section was measured by ATLAS using the data sample of 3.3 pb^{-1} collected at collision energy of 7 TeV. The events were selected using the single muon trigger with a p_{T} threshold of 6 GeV [38]. The analysis is based on partially reconstructed b-hadron decay final state $D^{*+} \mu^- X$ with $D^{*+} \rightarrow \pi^+ D^0 (\rightarrow K^- \pi^+)$. The measured integrated b-hadron cross section for $p_{\mathrm{T}}(H_b) > 9$ GeV and $|\eta(H_b)| < 2.5$ is

$$\sigma(pp \to H_b X) = 32.7 \pm 0.8(\text{stat.})$$
$$\pm\, 3.1(\text{syst.}) \; {}^{+2.1}_{-5.6}(\alpha) \pm 2.3(\text{BR}) \pm 1.1(\text{lumi.}) \; \mu\text{b},$$

where in addition to the statistical and systematic uncertainties are explicitly shown the uncertainties connected with the decay acceptance (α), the branching ratio (BR) and the luminosity (lumi.).
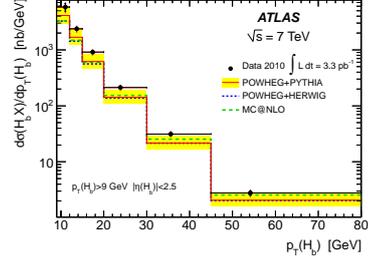

Figure 9: Differential b-hadron cross section as a function of its $p_T(H_b)$ and $|\eta(H_b)|$, the cross section is compared with those of the theoretical approaches.

Comparison with the theoretical calculation shows good agreement as is demonstrated in figure 9. The measured cross section is slightly higher than that of the theoretical model, but still within the uncertainties (for details see ref. [38]).

Angular analysis of $B_d^0 \to K^{*0}\mu^+\mu^-$. The decay $B^0 \to K^{*0}\mu^+\mu^-$ with $K^{*0} \to K^+\pi^-$ is a FCNC decay which in the SM is forbidden at tree level and goes only through loops, giving the branching BR=$(1.06 \pm 0.1)\times10^{-6}$ [1]. The analysis of this decay takes into account the invariant mass of $\mu^+\mu^-$-pair (q^2) and three angles θ_L, θ_K and ϕ (θ_L is the angle between the μ^+ and the direction opposite to the B_d^0 in the di-muon rest frame, θ_K is the angle between the K^+ and the direction opposite to the B_d^0 in the K^{*0} rest frame, and ϕ is the angle between the plane defined by the two muons and the plane defined by the kaon-pion system in the B_d^0 rest frame). The result of analysis is K^{*0} longitudinal polarisation fraction, F_L, and the lepton forward-backward asymmetry, A_{FB}, extracted from the angular distribution of the decay products:

$$\frac{1}{\Gamma}\frac{d^2\Gamma}{dq^2 d\cos\theta_L} = \frac{3}{4}F_L\left(1-\cos^2\theta_L\right) + \frac{3}{8}F_L\left(1+\cos^2\theta_L\right) + A_{FB}\cos\theta_L, \qquad (4)$$

where Γ is the decay length and a similar distribution can be written also for the angle θ_K. The analysis was carried out using the data sample of 4.9 fb^{-1} recorded at 7 TeV [39]. A likelihood fit was applied to the angular distributions and the quantities F_L and A_{FB} were found for six q^2 bins. Table 3

q^2 bin (GeV^2)	A_{FB}	F_L
$2.00 < q^2 < 4.30$	$0.22 \pm 0.28 \pm 0.14$	$0.26 \pm 0.18 \pm 0.06$
$4.30 < q^2 < 8.68$	$0.24 \pm 0.13 \pm 0.01$	$0.37 \pm 0.11 \pm 0.02$
$10.09 < q^2 < 12.86$	$0.09 \pm 0.09 \pm 0.03$	$0.50 \pm 0.09 \pm 0.04$
$14.18 < q^2 < 16.00$	$0.48 \pm 0.19 \pm 0.05$	$0.28 \pm 0.16 \pm 0.03$
$16.00 < q^2 < 19.00$	$0.16 \pm 0.10 \pm 0.03$	$0.35 \pm 0.08 \pm 0.02$
$1.00 < q^2 < 6.00$	$0.07 \pm 0.20 \pm 0.07$	$0.18 \pm 0.15 \pm 0.03$

Table 3: Summary of the fit results: the extracted asymmetry A_{FB} and longitudinal polarisation F_L for different bins in q^2 including the statistical and systematic uncertainties.

shows the measured ATLAS values of F_L and A_{FB} as a function of q^2. The values are in good agreement with the BaBar, Belle, CDF and LHCb experiments (for details see ref. [39]) as well as with the theoretical predictions.

Study of CP violation in $B_S^0 \to J/\psi\phi$.

In the decay $B_S^0 \to J/\psi(\mu^+\mu^-)\phi \to K^+K^-$ the CP violation is a result of interference between the $B_S - \bar{B}_S$ mixing followed by $\bar{B}_S$ decay and the direct $B_S(\to J/\psi\phi)$ decay. The CP violation phase ϕ_S is a phase difference between the mention amplitudes. The SM expectation is $\phi_S^{SM} \approx -0.0363^{+0.0016}_{-0.0015}$ [40]. The ATLAS study was carried out at 7 TeV using the data sample of 4.9 fb^{-1} [41]. The trigger used to select events requires two opposite charge muons identifying a $J/\psi \to \mu^+\mu^-$ decay.

The final state of B_S^0 decay was analyzed with the aim to disentangle CP-even states (CP = 1) corresponding to an orbital momentum $L = 0$ or 2 and CP-odd states (CP = -1). The analysis was performed in the transversity coordinate system (for details see ref. [41]) and resulted in extraction of several physical parameters among them ϕ_S and $\Delta\Gamma_S$ (the width difference between the heavy and light mass eigenstates of B_S^0 meson). The extracted values are:

$\phi_S = 0.12 \pm 0.25$(stat.) ± 0.11(syst.) rad,

$\Delta\Gamma_S = 0.053 \pm 0.021$(stat.) ± 0.009(syst.) ps^{-1}.

Figure 10 shows that the obtained values for ϕ_S and $\Delta\Gamma_S$ are consistent, within uncertainties, with the SM expectations.
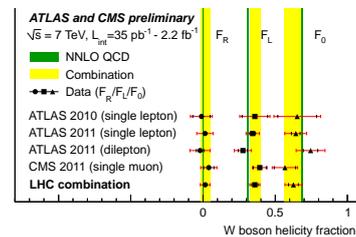

Figure 10: Likelihood contours in ϕ_S - $\Delta\Gamma_S$ plane. The blue and red contours show the 68% and 95% likelihood contours, respectively. The green band is the SM prediction of mixing-induced CP violation.

Production cross section of upsilonia. Study of Υ(nS), $b\bar{b}$ bound states, is an important test of QCD. The dominant production mechanism is gluon fragmentation. The ATLAS measurement is carried out using the data of 1.5 fb^{-1} at 7 TeV [42]. The analysis is based on reconstruction of the dimuon decay mode. Total production cross sections for Υ(1S), Υ(2S), Υ(3S) and differential cross sections as a function of upsilonium p_T and η are measured. The measured integrated cross sections are summarized in Table 4. The study also provides the differential cross sections of Υ(1S), Υ(2S) and Υ(3S) as functions of p_T for $\mid \eta \mid< 1.2$ (see for details in ref. [42]).

State	$\sigma(pp \to \Upsilon) \times \mathrm{Br}(\Upsilon \to \mu^+\mu^-)$
Υ(1S)	$8.01 \pm 0.02 \pm 0.36 \pm 0.31$ [nb]
Υ(2S)	$2.05 \pm 0.01 \pm 0.12 \pm 0.08$ [nb]
Υ(3S)	$0.92 \pm 0.01 \pm 0.07 \pm 0.04$ [nb]

Table 4: The integrated production cross section of upsilonia for the kinematic range: $p_T <$ 70 GeV and $\mid \eta \mid< 2.25$, with the statistical, systematic and luminosity uncertainties.

7   Bibliography

References

[1] J. Beringer et al., Phys. Rev. D**86**, 010001 (2012).

[2] The ATLAS Experiment at the CERN Large Hadron Collider, 459 JINST **3**, (2008) S08003.

[3] ATLAS Collaboration, ATLAS-CONF-2013-012.

[4] ATLAS public web page, https://twiki.cern.ch/twiki/bin/view/AtlasPublic

[5] CMS public web page, http://cms.web.cern.ch/org/cms-papers-and-results

[6] B. de Carlos and J. A. Casas, Phys. Lett. B309(1993) 320328

[7] A. Djouadi, Physics Reports **459**, 1-241 (2008).

[8] P. Fayet and S. Ferrara, Physics Reports **32**, 249 (1977).

[9] N. Arkani-Hamed, S. Dimopoulos, G. Dvali, Physics Letters **B429**, 263 (1998).

[10] ATLAS Collaboration, PRD 88, 072001 (2013), arXiv.1308.4075v1.

[11] E. Eichten, K. Lane, A. Martin, and E. Pilon, Phys.Rev. D86 (2012) 074015

[12] ATLAS Collaboration, Search for a dijet resonance produced in association with a leptonically decaying W or Z boson with the ATLAS detector at $\sqrt{s}$ = 8 TeV, ATLAS-CONF-2013-074.

[13] M. Czakon, P. Fiedler and A.Mitov, Phys.Rev.Lett. 110 (2013) 252004, arXiv:1303.0693 [hep/ph]

[14] Phys.Rev.D 83, 091503(R) (2011), Phys.Rev.D 82, 054028 (2010), Phys.Rev.D 82, 054028 (2010)

[15] Czarnecki et al., Nucl. Phys. B544 (1999) 520.

[16] ATLAS Collaboration, ATLAS-CONF-2012-149.

[17] ATLAS Collaboration, arXiv:1012.1792 [hep-ex], Eur. Phys. J. C71 (2011), 1577.

[18] CMS collaboration, CMS PAS TOP-12-006

[19] CMS collaboration, CMS PAS TOP-12-007

[20] ATLAS Collaboration, ATLAS-CONF-2012-024, ATLAS Collaboration, ATLAS-CONF-2012-131, ATLAS Collaboration, EPJ C73 (2013) 2328, ATLAS Collaboration, PLB717 (2012) 89, ATLAS Collaboration, ATLAS-CONF-2012-031.

[21] M. Aliev et al., Comput.Phys.Commun. 182 (2011) 1034-1046.

[22] ATLAS Collaboration, Eur. Phys. J. C (2013) 73: 2261.

[23] ATLAS Collaboration, ATLAS-CONF-2013-046.

[24] M. Kobayashi, T. Maskawa, Prog. Theor. Phys. 49 (1973).

[25] T. M. P. Tait, C. P. Yuan, Phys. Rev. D 63 (2000) 014018, [arXiv:hepph/0007298].

[26] ATLAS Collaboration, Physics Letters B 717 (2012) 330-350.

[27] ATLAS Collaboration, ATLAS-CONF-2012-132.

[28] ATLAS Collaboration, ATLAS-CONF-2012-056.

[29] A. Czarnecki, J. Korner, J. Piclum, Phys. Rev. D 81 (2010)111503, ArXiv:10005.2625[hep-ph].

[30] ATLAS Collaboration, JHEP 1206(2012) 088.

[31] ATLAS and CMS Collaborations, Combination of the ATLAS and CMS measurements of the W-boson polarization in top-quark decays, ATLAS-CONF-2013-033, CMS PAS TOP-12-025

[32] W. Bernreuther and Z. G. Si, Nucl. Phys. B 837,90(2010).

[33] ATLAS Collaboration, Phys. Rev. Lett 108, 212001(2012)

[34] ATLAS Collaboration, arXiv:1307.4568v2, accepted to JHEP.

[35] ATLAS Collaboration, ATLAS-CONF-2013-076.

[36] LHCb collaboration, Measurement of the $B_s^0 \to \mu^+\mu^-$ branching fraction and search for $B^0 \to \mu^+\mu^-$ decays at the LHCb experiment, arXiv:1307.5024, submitted to Phys. Rev. Lett.

[37] CMS collaboration, Measurement of the $B_s^0 \to \mu^+\mu^-$ branching fraction and search for $B^0 \to \mu^+\mu^-$ with the CMS experiment, arXiv:1307.5025, submitted to Phys. Rev. Lett.

[38] ATLAS Collaboration, Nucl.Phys.B864(2012)341.

[39] ATLAS Collaboration, ATLAS-CONF-2013-038.

[40] UTfit Collaboration, M. Bona et al., Phys.Rev.Lett. 97 (2006) 151803, arXiv:hep-ph/0605213 [hep-ph].

[41] ATLAS Collaboration, ATLAS-CONF-2013-039.

[42] ATLAS Collaboration, Phys. Rev. D 87, 052004(2013)

Relativistic Corrections to Pair Charmonium Production at the LHC

A.P. Martynenko[1,2], A.M. Trunin[2,3]

[1]Samara State University, Pavlov Street 1, 443011 Samara, Russia
[2]Samara State Aerospace University, Moskovskoye Shosse 34, 443086 Samara, Russia
[3]Bogoliubov Laboratory of Theoretical Physics, JINR, 141980 Dubna, Russia

On the basis of perturbative QCD and relativistic quark model we calculate relativistic and bound state corrections to processes of a pair S-wave charmonium production at the LHC. The obtained result for J/ψ pair production at the energy $\sqrt{S} = 7$ TeV lies below the experimental value measured by LHCb collaboration. In the case of η_c pair the examined effects decrease total nonrelativistic cross section more than two times and on 20 percents in the rapidity region of LHCb detector.

1   Introduction

Relativistic corrections caused by relative motion of constituent quarks are known to bring an essential modifications to the values of pair charmonium production cross sections. For example, it was found in Ref. [1] that account of relativistic corrections in the NRQCD formalism increases the nonrelativistic result for $\sigma[e^+e^- \to J/\psi + \eta_c]$ by about 40%. Analogously, the large values of discussed corrections to cross sections of S- and P-wave charmonium production in e^+e^- annihilation were revealed in the framework of potential models and other approaches in Refs. [2] and [3]. In the current work we present the results of relativistic corrections calculation to the processes of pair J/ψ and η_c production in proton–proton collisions at the LHC relevant energies $\sqrt{S} = 7$ TeV and 14 TeV [4]. Within the quasipotential approach we consider two types of the relativistic corrections sources: quark bound state wave functions, which are described by means of the potential model based on the QCD generalization of the Breit potential, and expansions of quark and gluon propagators entering production amplitude. More detailed description of the used approach and the results obtained with it can be found in Refs. [3, 4].

2   General formalism

The differential cross section $d\sigma$ for the inclusive double charmonium production in proton–proton interaction can be presented in the form of the convolution of partonic cross section $d\sigma[g+g \to 2\,J/\psi(\eta_c)]$ with the parton distribution functions (PDF) in the initial protons [5, 6, 7]:

$$d\sigma[p + p \to 2\,J/\psi(\eta_c) + X] = \int dx_1 dx_2\, f_{g/p}(x_1,\mu) f_{g/p}(x_2,\mu)\, d\sigma[g + g \to 2\,J/\psi(\eta_c)],$$

where $f_{g/p}(x,\mu)$ is a partonic distribution function for the gluon in the proton, $x_{1,2}$ are longitudinal momentum fractions of gluons, μ is the factorization scale. Neglecting the proton mass
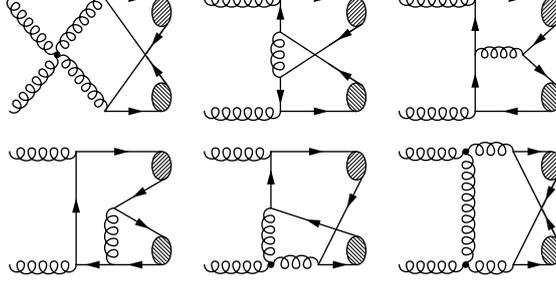
Figure 1: The typical LO diagrams contributing to the partonic process $g + g \to 2\,J/\psi(\eta_c)$. The others can be obtained by reversing the quark lines or interchanging the initial gluons.

and taking the c.m. reference frame of initial protons with the beam along the z-axis we can introduce the gluon on mass-shell momenta in the form $k_{1,2} = x_{1,2}\frac{\sqrt{S}}{2}(1,0,0,\pm 1)$. $\sqrt{S}$ is the center-of-mass energy in proton–proton collision.

In the quasipotential approach the double charmonium production amplitude for the parton subprocess $g + g \to 2\,J/\psi(\eta_c)$ can be expressed as a convolution of perturbative production amplitude of two c-quark and $\bar{c}$-antiquark pairs $\mathcal{T}(p_1, p_2; q_1, q_2)$ and the quasipotential wave functions of the final mesons Ψ [3, 4]:

$$\mathcal{M}[g + g \to 2\,J/\psi(\eta_c)](k_1, k_2, P, Q) = \int \frac{d\mathbf{p}}{(2\pi)^3} \int \frac{d\mathbf{q}}{(2\pi)^3}\, \bar{\Psi}(p, P)\bar{\Psi}(q, Q) \otimes \mathcal{T}(p_1, p_2; q_1, q_2), \quad (1)$$

where p_1 and p_2 are four-momenta of c-quark and $\bar{c}$-antiquark in the pair forming the first meson, and q_2 and q_1 are the appropriate four-momenta for quark and antiquark in the second meson. They are defined in subsequent transformations in terms of total momenta $P(Q)$ and relative momenta $p(q)$ as follows: $p_{1,2} = \frac{1}{2}P \pm p$, $(pP) = 0$; $q_{1,2} = \frac{1}{2}Q \pm q$, $(qQ) = 0$. Here $p = L_P(0, \mathbf{p})$ and $q = L_Q(0, \mathbf{q})$ are the relative four-momenta obtained by the Lorentz transformation of four-vectors $(0, \mathbf{p})$ and $(0, \mathbf{q})$ to the reference frames moving with the four-momenta P and Q.

At leading order of perturbation theory in strong coupling constant α_s there are 31 Feynman diagrams contributing to the amplitude of pair J/ψ production due to gluon fusion. The typical diagrams from this set are presented in Fig. 1. In the case of η_c pair there are also 8 additional diagrams shown in Fig. 2. The calculation of the diagrams and subsequent analytical transformations are performed by means of the package FeynArts [8] for the system Mathematica and FORM [9]. Then, the production amplitude (1) has the following structure:

$$\mathcal{M}[g + g \to 2\,J/\psi(\eta_c)](k_1, k_2, P, Q) = \frac{1}{9}M\pi^2\alpha_s^2 \int \frac{d\mathbf{p}}{(2\pi)^3} \int \frac{d\mathbf{q}}{(2\pi)^3}\big[\mathrm{Tr}\,\mathfrak{M} + 3\,\tau\Delta\mathfrak{M}\big], \quad (2)$$

$$\mathfrak{M} = \mathcal{D}_1\gamma_\beta \bar{\Psi}_{q,Q}\Gamma_1^\beta \bar{\Psi}_{p,P}\,\hat{\varepsilon}_2 \frac{m - \hat{k}_2 + \hat{p}_1}{(k_2 - p_1)^2 - m^2} + \mathcal{D}_2\gamma_\beta \bar{\Psi}_{q,Q}\Gamma_2^\beta \bar{\Psi}_{p,P}\,\hat{\varepsilon}_1 \frac{m - \hat{k}_1 + \hat{p}_1}{(k_1 - p_1)^2 - m^2} +$$

$$\mathcal{D}_3\bar{\Psi}_{q,Q}\Gamma_3^\beta \bar{\Psi}_{p,P}\,\gamma_\beta + \mathcal{D}_4\bar{\Psi}_{p,P}\Gamma_4^\beta \bar{\Psi}_{q,Q}\,\gamma_\beta + \mathcal{D}_1\bar{\Psi}_{q,Q}\Gamma_5^\beta \bar{\Psi}_{p,P}\,\gamma_\beta \frac{m + \hat{k}_2 - \hat{q}_1}{(k_2 - q_1)^2 - m^2}\hat{\varepsilon}_2 +$$

$$\mathcal{D}_2\bar{\Psi}_{q,Q}\Gamma_6^\beta \bar{\Psi}_{p,P}\,\gamma_\beta \frac{m + \hat{k}_1 - \hat{q}_1}{(k_1 - q_1)^2 - m^2}\hat{\varepsilon}_1,$$

where inverse denominators of gluon propagators are defined as $\mathcal{D}_{1,2}^{-1} = (k_2 - p_{1,2} - q_{1,2})^2$ and $\mathcal{D}_{3,4}^{-1} = (p_{1,2} + q_{1,2})^2$, $\varepsilon_{1,2}$ and $k_{1,2}$ are polarization vectors and four-momenta of the initial gluons, m is c-quark mass, M is observable $J/\psi(\eta_c)$ mass, and the hat symbol means a contraction of the four-vector with the Dirac gamma matrices. The amplitude (2) contains wave functions $\Psi_{p,P}$ and $\Psi_{q,Q}$ of the mesons taken in the reference frame moving with four momenta P and Q. The transformation law of the bound state wave function from the rest frame to the moving one was derived in the Bethe–Salpeter approach in Ref. [10] and in the quasipotential method in Ref. [11]. The $\Delta\mathfrak{M}$ integrand contribution corresponds to the 8 additional diagrams from Fig. 2, so the parameter τ in (2) equals zero in

Figure 2: The additional LO diagrams contributing to the partonic process $g + g \to 2\,\eta_c$.

the case of J/ψ and $\tau = 1$ for η_c pair. Explicit expressions for $\Delta\mathfrak{M}$ and vertex functions Γ_i entering (2) can be found in Refs. [4].

In order to calculate relativistic corrections to the amplitude (2) we expand the inverse denominators of gluon and quark propagators as series in relative quark momenta p and q:

$$\frac{1}{(p_1 + q_1)^2} = \frac{4}{s} - \frac{16}{s^2}\left[(p+q)^2 + pQ + qP\right] + \cdots,$$

$$\frac{1}{(k_2 - q_2)^2 - m^2} = \frac{2}{t - M^2} - \frac{4}{(t - M^2)^2}\left[q^2 + 2(k_2 q) + \frac{1}{4}M^2 - m^2\right] + \cdots,$$

where $s = (k_1 + k_2)^2$ and $t = (P - k_1)^2$ are Mandelstam variables of the partonic subprocess. Preserving in the expanded amplitude terms up to the second order in the relative momenta p and q, we can perform angular integration and calculate the squared modulus of the amplitude summed over polarizations of the initial gluons and, if necessary, over polarizations of the final charmonium states. Then, we obtain the following result for the pair production cross sections:

$$\frac{d\sigma}{dt}[g + g \to 2\,J/\psi(\eta_c)](s,t) = \frac{\pi M^2 \alpha_s^4}{9216\,s^2}\,|\tilde{R}(0)|^4 \sum_{i=0}^{3} \omega_i F^{(i)}(s,t). \qquad (3)$$

The auxiliary functions $F^{(i)}$ entering the cross sections (3) are written explicitly in Refs. [4]. Note that the function $F^{(0)}$ describes non-relativistic result, which coincides in the limit $M = 2m$ with the corresponding function obtained in Refs. [12, 13, 14] for the case of pair J/ψ production and in Ref. [13] for η_c pair production in the approach of NRQCD. Relativistic corrections in (3) are determined by a number of relativistic parameters ω_i:

$$\omega_0 = 1, \quad \omega_1 = \frac{I_1}{I_0}, \quad \omega_2 = \frac{I_2}{I_0}, \quad \omega_3 = \omega_1^2,$$

$$I_0 = \int_0^\infty \frac{m + \epsilon(p)}{2\epsilon(p)}R(p)p^2 dp, \quad I_{1,2} = \int_0^m \frac{m + \epsilon(p)}{2\epsilon(p)}\left(\frac{m - \epsilon(p)}{m + \epsilon(p)}\right)^{1,2}R(p)p^2 dp,$$

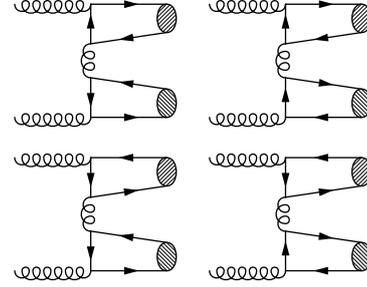$$\tilde{R}(0) = \sqrt{\frac{2}{\pi}}\int_0^\infty \frac{m + \epsilon(p)}{2\epsilon(p)}R(p)p^2 dp,$$

Table 1: The comparison of relativistic and nonrelativistic cross sections of a pair S-wave charmonium production in proton–proton collisions obtained for different sets of partonic distribution functions.

Energy $\sqrt{S}$	Meson pair, cross section type	σ(total), nb		$\sigma(2 < y_{P,Q} < 4.5)$, nb	
		CTEQ5L	CTEQ6L1	CTEQ5L	CTEQ6L1
$\sqrt{S} = 7$ TeV	$J/\psi\,J/\psi$, relativistic	9.6	7.4	1.6	1.2
	$J/\psi\,J/\psi$, nonrelativistic	23.0	17.7	3.8	2.9
	$\eta_c\,\eta_c$, relativistic	23.7	19.9	1.3	1.0
	$\eta_c\,\eta_c$, nonrelativistic	56.3	48.1	1.5	1.2
$\sqrt{S} = 14$ TeV	$J/\psi\,J/\psi$, relativistic	17.1	13.2	3.0	2.1
	$J/\psi\,J/\psi$, nonrelativistic	41.0	31.6	7.1	5.1
	$\eta_c\,\eta_c$, relativistic	47.8	39.3	2.4	1.7
	$\eta_c\,\eta_c$, nonrelativistic	116.5	94.7	2.8	2.0

where $\epsilon(p) = \sqrt{m^2 + \mathbf{p}^2}$ is quark energy and $R(p)$ is the radial charmonium wave function. All parameters, which contain the meson wave functions and describe the transition of $(c\bar{c})$ pairs to the bound state, are calculated in the framework of relativistic quark model. This model is based on the Schrödinger equation with the Breit Hamiltonian in QCD and the nonperturbative confinement terms. Using the program of numerical solution of the Schrödinger equation, we obtain relativistic wave functions and bound state energies of S-wave charmonia. The additional details on our relativistic quark model can be found in Refs. [3, 4].

3 Numerical results and discussion

The numerical results of our calculation of the pair S-wave charmonium production cross sections in the case of non-relativistic approximation as well as with the account of relativistic corrections of order v^2 are presented in Table 1. Along with total cross section values, we have also included there the cross section predictions corresponding to the rapidity interval $2 < y_{P,Q} < 4.5$ of the LHCb experiment [15] calculated with two different sets of linear PDFs: CTEQ5L [16] and CTEQ6L1 [17]. At the current moment, the only known experimental result for the cross section of pair S-wave charmonium production in proton–proton collisions is the result measured by LHCb collaboration for the pair J/ψ production at the energy $\sqrt{S} = 7$ TeV [15]: $\sigma_{LHCb}^{exp} = 5.1 \pm 1.0 \pm 1.1$ nb. The corresponding relativistic result obtained in our model with CTEQ5L partonic function is $\sigma_{rel}^{theor} = 1.6$ nb. It is evident that this results lies below the experimental value measured by LHCb collaboration. Nevertheless, despite the difference between σ_{rel}^{theor} and σ_{LHCb}^{exp}, we consider that at present it is difficult to state that there is the discrepancy between the theory and experiment in double charmonium production. Along with the possibility of large contribution from NLO α_s corrections (as in the case of e^+e^- production [7, 18]), there exists an additional mechanism through the double parton scattering, which gives the contribution comparable with the standard nonrelativistic result [19]: $\sigma_{DPS}[p + p \rightarrow 2\,J/\psi + X] = 2$ nb. Accounting for this result and our value of the cross section σ_{rel}^{theor}, we obtain the summary value $\sigma[p + p \rightarrow 2\,J/\psi + X] = 3.6$ nb. Then,

taking into account the experimental error, the difference with the LHCb result does not look so significant. A new experimental data as well as theoretical exploration of NLO α_s corrections and other uncertainties are desirable to clarify the situation.

Recently, the NRQCD calculation of relativistic corrections to pair J/ψ production cross section was performed [20]. Contrary to our results, relativistic effects were found to be much smaller in that approach. The authors of [20] investigate only one part of relativistic corrections to the production amplitude, so direct comparison of our results with [20] is difficult. Moreover, the choice of numerical value $\langle 0|O^{J/\psi}(^3S_1^{[1]})|0\rangle$ in [20] is at variance with quark model calculations.

Acknowledgements

References

[1] G.T. Bodwin, J. Lee, and C. Yu, Phys. Rev. **D77**, 094018 (2008).

[2] J.P. Ma and Z.G. Si, Phys. Rev. **D70**, 074007 (2004);
A.E. Bondar and V.L. Chernyak, Phys. Lett. **B612**, 215 (2005);
V.V. Braguta, A.K. Likhoded, and A.V. Luchinsky, Phys. Rev. **D72**, 074019 (2005).

[3] D. Ebert and A.P. Martynenko, Phys. Rev. **D74**, 054008 (2006);
D. Ebert, R.N. Faustov, V.O. Galkin, and A.P. Martynenko, Phys. Lett. **B672**, 264 (2009);
E.N. Elekina and A.P. Martynenko, Phys. Rev. **D81**, 054006 (2010);
A.P. Martynenko and A.M. Trunin, PoS QFTHEP2011 051 (2011).

[4] A.P. Martynenko and A.M. Trunin, Phys. Rev. **D86**, 094003 (2012);
A.P. Martynenko and A.M. Trunin, Phys. Lett. **B723**, 132 (2013).

[5] V.V. Kiselev, A.K. Likhoded, S.R. Slabospitsky, and A.V. Tkabladze, Sov. J. Nucl. Phys. **49**, 682 (1989).

[6] E. Braaten, S. Fleming, and T.C. Yuan, Annu. Rev. Nucl. Part. Sci. **46**, 197 (1996).

[7] N. Brambilla, S. Eidelman, B.K. Heltsley *et al.*, Eur. Phys. J. **C71**, 1534 (2011).

[8] J. Kublbeck, M. Böhm, and A. Denner, Comp. Phys. Comm. **60**, 165 (1990);
T. Hahn, Comp. Phys. Comm. **140**, 418 (2001).

[9] J.A.M. Vermaseren, FORM, arXiv:math-ph/0010025 (2000).

[10] S.J. Brodsky and J.R. Primack, Ann. Phys. **52**, 315 (1969).

[11] R.N. Faustov, Ann. Phys. **78**, 176 (1973).

[12] A.V. Berezhnoy, A.K. Likhoded, A.V. Luchinsky, and A.A. Novoselov, Phys. Rev. **D84**, 094023 (2011);
A.V. Berezhnoy, A.K. Likhoded, A.V. Luchinsky, and A.A. Novoselov, Phys. Rev. **D86**, 034017 (2012).

[13] R. Li, Y.-J. Zhang, and K.-T. Chao, Phys. Rev. **D80**, 014020 (2009).

[14] C.-F. Qiao, Phys. Rev. **D66**, 057504 (2002);
C.-F. Qiao, L.-P. Sun, and P. Sun, J. Phys. **G37**, 075019 (2010).

[15] R. Aaij *et al.* (LHCb Collaboration), Phys. Lett. **B707**, 52 (2012).

[16] H.L. Lai, J. Huston, S. Kuhlmann *et al.*, Eur. Phys. J. **C12**, 375 (2000).

[17] J. Pumplin, D.R. Stump, J. Huston *et al.*, J. High Energy Phys. **07** (2002) 012.

[18] J. Campbell, F. Maltoni, and F. Tramontano, Phys. Rev. Lett. **98**, 252002 (2007);
B. Gong and J.-X. Wang, Phys. Rev. Lett. **100**, 232001 (2008).

[19] S.P. Baranov, A.M. Snigirev, and N.P. Zotov, Phys. Lett. **B705**, 116 (2011);
A. Novoselov, arXiv:1106.2184 [hep-ph] (2011).

[20] Y.-J. Li, G.-Z. Xu, K.-Y. Liu, and Y.-J. Zhang, J. High Energy Phys. **07** (2013) 051.

The rise and fall of the fourth quark-lepton generation

M.I. Vysotsky[1]

[1]ITEP, 117218 Moscow, Russia

The existence of the fourth quark-lepton generation is not excluded by the electroweak precision data. However, the recent results on the 126 GeV higgs boson production and decay do not allow an extra generation at least as far as the perturbation theory can be used.

1 Prehistory

In the course of 1974 November Revolution J/ψ particle was discovered, and soon it was understood that it consists of $c\bar{c}$-quarks. In this way the second quark-lepton generation (ν_μ, μ, s, c) was completed. Two years later τ-lepton was found, and in 1978 $\Upsilon(b\bar{b})$-meson was discovered as well. t-quark was found only in 1994, however, already in the 1980s people started to plan finding the particles of the next, fourth, quark-lepton generation. And the main question, of course, was: How heavy are U, D, and E?

2 SLC, LEP

In the year 1989 e^+e^- colliders SLC and LEP started to work at $\sqrt{s} = M_Z$, and from the determination of Z invisible width it soon became clear that only three neutrino exist. According to the final data $\Gamma(\text{invisible}) = 499 \pm 1.5$ MeV, while according to the theory it equals $166 \cdot 3 = 498$ MeV, so there is no space for extra neutrinos. However the possibility of the heavy fourth generation neutrino with the mass $m_N > M_Z/2$ is not excluded.

3 Electroweak precision data

Since the fourth generation quarks and leptons contribute to the W- and Z-boson polarization operators and since these contributions do not decouple in the limit of heavy new generation (which is the essence of the electroweak theory and quite opposite to the case of QED, where, say, the top quark contribution to the anomalous magnetic moment of muon is suppressed as $(g-2)_\mu \sim (m_\mu/m_t)^2$) one can get the constraints on the 4th generation from the precision measurements of M_W, m_t, and Z-boson parameters.

Indeed, in 1998 volume of the Review of Particle Properties Erler and Langacker wrote: "An extra generation is excluded at the 99.2% CL"[1]. The statement of the published in the year 2000 paper [2] is: "One extra generation is still allowed".

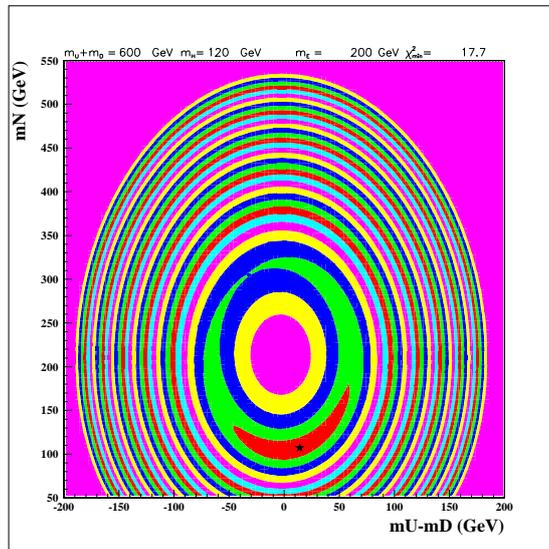The following two points were missed by Erler and Langacker:

Figure 1: $M_H = 120$ GeV, $m_E = 200$ GeV, $m_U + m_D = 600$ GeV, $\chi^2/d.o.f. = 17.7/11$, the quality of fit is the same as in SM.

1. S, T, and U parametrization is valid only when the masses of all the new particles are much larger than M_Z;

2. Instead of making a global fit they studied S, T, and U separately, while these quantities are correlated. The evolution of RPP analysis of extra quark-lepton generation in the years 1998 - 2010 is described in detail in paper [3].

The results of the fit of the electroweak precision observables in the presence of the fourth generation just before LHC started obtaining data are shown in Figures 1 and 2 [4]. Fig. 1 corresponds to the light higgs boson, $m_H = 120$ GeV, while Fig. 2 corresponds to heavy higgs, $m_H = 600$ GeV. In both cases the values of the fourth generation quark and lepton masses are determined, for which the quality of the fit is practically the same as for the Standard Model with three generations. In Figures 1 and 2 we put $m_E = 200$ GeV, $m_U + m_D = 600$ GeV, and the values of m_N and $m_U - m_D$ at which $\chi^2/$d.o.f. is minimal (and the same as in SM) are shown by star.

4 LHC direct bounds

Since the search of heavy quarks is a relatively easy task for LHC; the first lower bounds on their masses appeared soon after the start of LHC. The last ATLAS bounds are: $m_{t'} > 656$ GeV at 95% CL if $t' \to Wb$ decay dominates [5] and $m_{b'} > 480$ GeV if $b' \to Wt$ decay dominates. CMS has similar bounds. These bounds push heavy quarks out of the perturbative unitarity domain: $m_{q'} < 500$ GeV, so if such quarks exist, their interaction with the higgs doublet is described by strong dynamics (let us remind that even for a top quark the coupling with higgs is not small: $\lambda_t = m_t/(\eta/\sqrt{2}) = 172/(246/\sqrt{2}) \approx 1$.

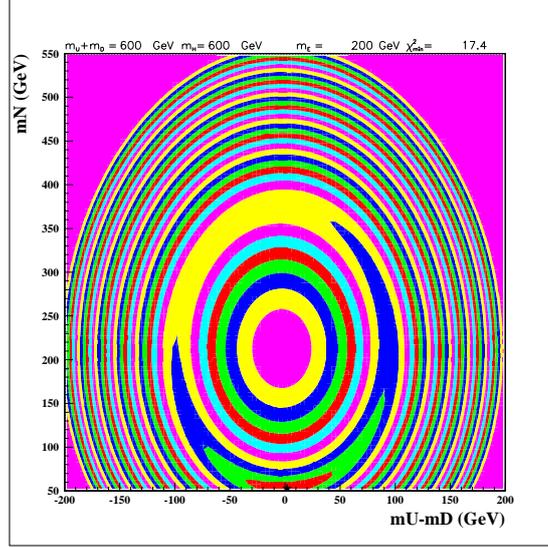However, these bounds depend on the pattern of heavy quark decays and are not univer-

Figure 2: $M_H = 600\text{GeV}$, $m_E = 200$ GeV, $m_U + m_D = 600$ GeV, $\chi^2/d.o.f. = 18.4/11$, the quality of fit is the same as in SM.

sal. Much more interesting indirect bounds follow from higgs boson production and decay probabilities measured at LHC.

5 Higgs data

In the following Table the values of μ measured by ATLAS and CMS collaborations are given. μ is equal to the ratio of the measured product of the cross section of H production at LHC and branching ratio of H decay to a specific final state to the value of this product calculated in Standard Model. Thus, if there are no heavy quarks or any other kind of New Physics, μ equals one for any decay mode. The data in the Table are taken from papers [6, 7] and correspond to the summer 2013. $H \to bb$ decay was observed only for the associative production of the higgs boson with Z- or W-boson.

Table

decay mode	ATLAS	CMS
$H \to \gamma\gamma$	1.6 ± 0.3	0.77 ± 0.27
$H \to ZZ^*$	1.5 ± 0.4	0.92 ± 0.28
$H \to WW^*$	1.0 ± 0.3	0.68 ± 0.20
$H \to \tau\tau$	0.8 ± 0.7	1.10 ± 0.41
$VH \to Vbb$	0.2 ± 0.5	1.00 ± 0.49

The values of $\mu_i \equiv (\sigma_H \cdot \text{Br}_i)_{\exp}/(\sigma_H \cdot \text{Br}_i)_{\text{SM3}}$. A new ATLAS result is $\mu_{\tau\tau} = 1.4 \pm 0.5$.
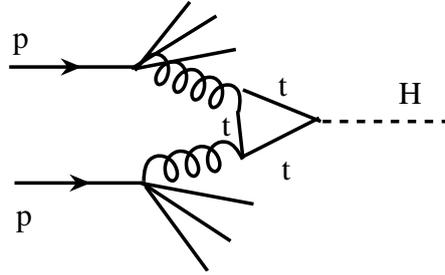
Figure 3: $t \longrightarrow t, t', b'$. $\sigma(gg \longrightarrow H)_{SM4} \approx 9\sigma(gg \longrightarrow H)_{SM3}$.

The dominant diagram which describes the higgs boson production at LHC is shown in Fig. 3. In case of the fourth generation the amplitude triples since the contributions of heavy $U(t')$ and $D(b')$ quarks are the same as that of t-quark. As a result, the cross-section of H production in the case of 4 generations is nine times bigger than in the Standard Model:

$$\sigma(gg \longrightarrow H)_{SM4} \approx 9\sigma(gg \longrightarrow H)_{SM3} \qquad (1)$$

Analogously the width of $H \to gg$ decay which in the Standard Model for $M_H = 126$ GeV is about 0.3 MeV in SM4 becomes 2.7 MeV. Taking into account that in the Standard Model $\Gamma_H \approx 4.2$ MeV, we get that the branching ratios of $H \to ZZ^*$ and $H \to WW^*$ decays in the case of SM4 are multiplied by factor $4.2/6.6 \approx 0.7$, which becomes 0.6 when the modification of other higgs decay probabilities are taken into account. However, the electroweak radiative corrections to the $H \to VV$ decay amplitude being enhanced by factor $(G_F m_{t',b'}^2)$ are big and according to [8] the factor 0.6 is changed to 0.2 (for $m_{t'} \approx 600$ GeV) when they are taken into account. It demonstrates that with such heavy new quarks we leave the domain of masses generated by Higgs mechanism where the perturbation theory is applicable. For the value of μ in case of $H \to WW^*, ZZ^*$ decays we get the enhancement by factor 2 in the case of the fourth generation. Such an enhancement is excluded by the experimental data from the Table. For the lighter fourth generation quarks the electroweak radiative corrections which diminish $H \to WW^*, ZZ^*$ decay widths are smaller, so exclusion will be even stronger.

There is a possibility to diminish $Br(H \to WW^*, ZZ^*)$ by choosing $M_H/2 > m_N > M_Z/2$, which makes $H \to NN$ a dominant higgs decay mode (N is a neutral lepton of the fourth generation). ¿From the ATLAS search of $ZH \to l^+l^-$ + invisible decay mode the 95% CL upper bound $Br(H \to$invisible)< 0.65 follows [9]. According to CMS $Br(H \to$invisible)< 0.52. Thus, for light N the values of μ for visible final states can be diminished by factor 2 and for $H \to WW^*$ and ZZ^* decay modes μ approaches its SM3 values. Up to now we present the result of the 4th generation electroweak loop corrections for the moderate values of the masses of new leptons. If their masses approach 600 GeV, then factor 0.2 in the suppression of $Br(H \to VV^*)$ becomes 0.15 [10] and the value of μ approaches its value for the 3 generation case.

6 $H \rightarrow \gamma\gamma$

In SM3 this decay is described by two one-loop diagrams shown in Fig. 4. In the limit $M_H <<$ $2m_t, 2M_W$ for the decay amplitude we have:

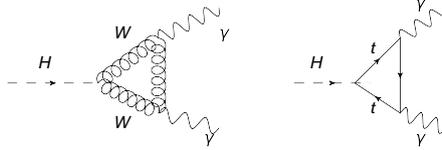$$A_3 \sim 7 - 4/3 * 3 * (2/3)^2 = 7 - 16/9 \ . \tag{2}$$

Figure 4: $H \rightarrow 2\gamma$ decay in SM3.

The numbers 7 and 16/9 are one-loop QED β - function coefficients; the signs correspond to asymptotic freedom and zero charge behavior, respectively. Number 7 for the first time appears in 1965 paper of V.S. Vanyashin and M.V. Terentiev [11]. Nowadays it could be derived from the following equation:

$$7 = 22/3 - 1/6 - 1/6 \ , \ \ 22/3 = 11/3 * 2 \ , \tag{3}$$

where the factors 1/6 originate from the higgs doublet contribution into running of SU(2) and U(1) couplings g and g', while 22/3 is a vector boson contribution into the running of g.

For $M_W = 80.4$ GeV 7 should be substituted by 8.3, while 16/9 has 3% accuracy for $m_t = 172$ GeV. So, in SM3 $A_3 \sim 8.3 - 16/9 = 6.5$, while in the case of the fourth generation a strong compensation occurs:

$$A_4 \sim 8.3 - 16/9 - 16/9 - 4/9 - 4/3 = 3.0 \tag{4}$$

and taking into account the enhancement of $gg \rightarrow H$ production cross-section and the modification of Higgs decay probabilities (mainly the enhancement of $H \rightarrow gg$ decay), we obtain the same $\sigma * Br \ (H \rightarrow 2\gamma)$ as in SM3:

$$\mu_{2\gamma} = 9 * 0.6 * (3/6.5)^2 \approx 1.2 \ . \tag{5}$$

But the electroweak radiative corrections greatly diminish $\sigma * \mathrm{Br}(H \rightarrow 2\gamma)$; according to [8] it equals 1/3 of SM3 result or even less, while the average of ATLAS and CMS data is 1.2 ± 0.2, so the 4th generation is excluded at 4-5 σ level. It would be good to calculate 3 loop electroweak corrections to the $\Gamma(H \rightarrow 2\gamma)$ in the case of the fourth generation.

7 $H \rightarrow \tau\tau$, $H \rightarrow bb$

μ for the $(\tau\tau)$ mode at tree level equals approximately

$$\mu_{\tau\tau} \approx 9 \ (\text{from } H \text{ production cross section}) * 0.6 \ (\text{enchancement of } H \text{ width in SM4}) \approx 5 \ , \tag{6}$$

and the electroweak loop corrections make the decay width larger by 30% [8]. The experimental data exclude this huge enhancement.

The consideration differs for $H \rightarrow b\bar{b}$ mode: it is seen only in the associative higgs boson production $VH \rightarrow Vbb$, which unlike gluon fusion is not enhanced in the 4th generation case, and there is no contradiction with the LHC experimental data.

8 Conclusions

- LHC data on 126 GeV higgs boson production and decays exclude the Standard Model with the sequential fourth generation in the perturbative domain: too small $gg \to H \to \gamma\gamma$ probabilitiy, too big $gg \to H \to \tau\tau$ probability;

- If we are out of the perturbative domain ($m4 \sim 1$ TeV) extra generation cannot be excluded, but we are unable to understand why all the experimentally measured μ's are close to one and SM3 works so well;

- In two higgs doublets model the fourth generation is still allowed [12];

- Since the vector generation has SU(2)×U(1) invariant masses it is not excluded by higgs data.

9 Acknowledgments

References

[1] C. Caso *et al.*, Eur. Phys. J. **C3** 1 (1998).

[2] M. Maltoni *et al.*, Phys. Lett. **B476** 107 (2000).

[3] A. Lenz, Adv. High Energy Phys. **2013** 910275 (2013).

[4] V.A. Novikov, A.N. Rozanov, M.I. Vysotsky, Yad. Fiz. **73** 662 (2010).

[5] ATLAS Collaboration, Phys. Lett. B **718** (2013) 1284.

[6] ATLAS-Conf-2013-034.

[7] CMS-PAS-MIG-13-005, 13-012.

[8] A. Denner *et al.*, Eur. Phys. J. **C72** 1992 (2012).

[9] ATLAS-CONF-2013-011.

[10] A. Djouadi, A. Lenz, Phys. Lett. **B715** 310 (2012).

[11] V.S. Vanyashin, M.V. Terentiev, ZhETF **48** 565 (1965).

[12] M. Geller *et al.*, Phys. Rev. **D86** 115008 (2012).

List of Authors

Participants

Ahmadov, Azad (JINR, Dubna)
Ali, Ahmed (DESY, Hamburg)
Alvarez Castillo, David Edwin (Wroclaw Uni., Wroclaw; JINR, Dubna)

Barreiro, Fernando (ATLAS Coll.) (Uni. Autonoma, Madrid)
Bastian, Niels-Uwe (Rostock Uni., Rostock)
Bean, Alice (CMS Coll.) (Kansas Uni.)
Blaschke, David (Wroclaw Uni., Wroclaw; JINR, Dubna)
Bystritskiy, Yury M. (JINR, Dubna)
Bytev, Vladimir (JINR, Dubna)

Chesnokov, Petr (MSU, Moscow)
Cirilo-Lombardo, Diego (JINR, Dubna)
Colangelo, Pietro (Bari Uni., Bari)

Deka, Mridupawan (JINR, Dubna)
Dzyuba, Alexey (LHCb Coll.) (PNPI, St. Petersburg)

El-Bennich, Bruno (Cruzeiro do Sul Uni., St. Paolo)

Fajfer, Svjetlana (Ljubljana Uni., Ljubljana)
Faustov, Rudolf N. (Dorodnicyn Computing Centre RAS, Moscow)
Friesen, Alexandra V. (Scientific Secretary; JINR, Dubna)
Frolov, Ivan (Yaroslavl Uni., Yaroslavl)

Galkin, Vladimir O. (Dorodnicyn Computing Centre RAS, Moscow)
Gerasimov, Sergo B. (JINR, Dubna)
Gevorgyan, Narine (Yerevan Uni., Yerevan)
Ghandilyan, Yeranuhi (Yerevan Uni., Yerevan)
Godunov, Sergey (ITEP, Moscow)
Grozin, Andrey G. (INP, Novosibirsk)

Hambrock, Christian (Dortmund Uni., Dortmund)
Hartmann, Florian (Siegen Uni., Siegen)

Ilgenfritz, Ernst Michael (JINR, Dubna)
Ivanov, Michail A. (JINR, Dubna)
Ivanytskyi, Oleksii (BITP, Kiev)
Ivashyn, Sergiy (NSC KIPT, Kharkiv)

Jäh, Christian (TU Bergakademie, Freiberg)

Kazakov, Dmitri I. (JINR, Dubna)
Khodjamirian, Alexander (Siegen Uni., Siegen)
Kidonakis, Nikolaos (Kennesaw State Uni., Kennesaw)
Koerner, Juergen G. (Mainz Uni., Mainz)
Khvorostukhin, Andrey S. (JINR, Dubna)
Kotikov, Anatoly V. (JINR, Dubna)
Kuraev, Eduard A. (JINR, Dubna)

Lange, Jens Soeren (Giessen Uni., Giessen)
Liebing, Simon (TU Bergakademie, Freiberg)
Liventsev, Dmitri (Belle Coll.) (ITEP, Moscow)
Lyubovitskij, Valery E. (Tuebingen Uni., Tuebingen)

Makhaldiani, Nugzar (JINR, Dubna)
Malyshev, Maxim (SINP, MSU, Moscow)
Massimo, Masera (ALICE Coll.) (Turin)
Mitselmakher, Guenakh (CMS Coll.) (Florida)
Mkrtchyan, Hripsime (Yerevan Uni., Yerevan)

Nedelko, Sergey N. (JINR, Dubna)
Nefedov, Maxim (Samara Uni., Samara)
Nesterenko, Vladimir V. (JINR, Dubna)
Novikova, Valentina K. (JINR, Dubna)

Olakunle, Oluwaleye(Uni. of Johannesburg, Johannesburg)

Parkhomenko, Alexander Ya. (Yaroslavl Uni., Yaroslavl)
Pena, Carlos (Wroclaw Uni., Wroclaw)
Pozdeeva, Ekaterina (SINP, MSU, Moscow)

Rivasplata, Antonio (Uni. Na. De Trujilio; JINR, Dubna)
Rosenthal, Denis (Siegen Uni., Siegen)
Rusov, Aleksey (Yaroslavl State Uni., Yaroslavl)

Sagun, Violetta (BITP, Kiev)
Saleev, Vladimir A. (Samara Uni., Samara)
Santorelli, Pietro (Napoli Uni., Napoli)
Shipilova, Alexandera (Samara Uni., Samara)
Straub, David (Mainz Uni., Mainz)
Surovtsev, Yuri S. (JINR, Dubna)

Tetlalmatzi-Xolocotzi, Gilberto (IPPP, Durham)
Tokar, Stanislav (ATLAS Coll.)(Bratislava Uni., Bratislava)
Tretyakov, Petr V. (JINR, Dubna)
Trunin, Anton (Samara Uni., Samara)

Vysotsky, Mikhail I. (ITEP, Moscow)

Yargina, Kseniya (Yaroslavl Uni., Yaroslavl)
Yeletskikh, Ivan (JINR, Dubna)

Zhuravlev, Vyacheslav I. (JINR, Dubna)